The University of Hull

Synthesis and validation of novel chelates for gallium-68 PET imaging

Being a thesis submitted for the Degree of Doctor of Philosophy in the University of Hull

by

Thomas Price

MSc (University of York)

MA (University of Cambridge)

February 2019

Abstract

Background:

The use of gallium-68 (^{68}Ga) in positron emission tomography (PET) imaging is currently of great interest. This radionuclide can be produced from a small generator allowing easy access to this imaging tool. Recently, [^{68}Ga][Ga(DOTATATE)] has been approved for clinical application for the diagnosis of neuroendocrine tumours (NETs) highlighting the value of ^{68}Ga PET imaging.

The standard macrocyclic chelators that are radiolabelled with ^{68}Ga require acidic conditions, and often also require heating to high temperatures, to achieve high radiochemical yields (RCYs) in short times. Recent developments in ^{68}Ga radiolabelling have sought to achieve high RCYs without the need for heating and at neutral pH. To this end, recent chelator designs have been open chain ligands rather than the more traditional macrocyclic designs.

Aims:

The aims of this thesis are to develop new acyclic chelators for Ga(III); to synthesise their Ga(III) complexes, to radiolabel these chelators with ^{68}Ga, and to assess the stability of these complexes.

Results:

Six novel chelators, and nine novel Ga(III) systems, were prepared and investigated.

The hexadentate ligand, H_3Dpaa, along with 3 bifunctional derivatives, was shown to form a complex with Ga(III) in which only 5 of the coordinating sites are occupied by the ligand. The remaining site is occupied by water. These chelators could be radiolabelled efficiently with ^{68}Ga, achieving RCYs of 85-95% at pH 7.4. The resulting complexes were assessed for their thermodynamic stabilities with log$K_{Ga\text{-}L}$ of 16.13-18.53. Decomplexation was complete within 30 minutes incubation with foetal bovine serum (FBS).

Complexation of Ga(III) by the heptadentate chelator H_3Tpaa saturated the coordination sphere of Ga(III). This chelator was radiolabelled with an RCY >95% at pH 7.4. When assessed for stability to FBS, 32% of this system remained intact after 30 minutes. However, decomplexation was complete within 2 hours. Further derivatives were prepared; while they could be radiolabelled, the complexes formed were not stable to FBS.

The novel chelator, H_3Bn_2DT3A, complexes Ga(III) in a hexadentate manner, forming a *mer* complex with log$K_{Ga\text{-}L}$ = 18.25. H_3Bn_2DT3A was radiolabelled with RCYs >80% across a wide pH range. This system showed a pH dependent speciation. No decomplexation of the species formed above pH 5.5 was seen over 2 hours when incubated with FBS. Formation of this species was promoted at pH 6-8, by high temperature, high ligand concentration, and with a long reaction time. A bifunctional analogue was prepared but the resulting ^{68}Ga complex formed was not stable to FBS.

Conclusions:

While capable of being radiolabelled efficiently across a wide pH range, tripodal picolinate Ga(IIII) complexes have poor FBS stability making them unsuitable for application *in vivo*. This is likely due to the rigid nature of the picolinate arms preventing the optimal coordination geometry being achieved; this is highlighted in the case of the H_3Dpaa family due to the unsaturated coordination sphere and bound water molecule.

The use of a more flexible chelator, H_3Bn_2DT3A, allowed for the formation of a serum stable ^{68}Ga complex, although the flexibility also resulted in multiple species being formed. This system has a number of sites that can be varied in the future for further optimisation of the radiolabelling conditions and for development of bifunctional derivatives. The site tested here for conjugation; the central acetate arm, resulted in a less kinetically stable system and future work should investigate alternate sites of conjugation.

Acknowledgements

Firstly I would like to thank my supervisor, Dr Graeme Stasiuk, for all of his help and guidance throughout this project. I would also like to thank my second supervisor Prof. John Greenman for his continued support and advice.

I would like to acknowledge all of the assistance that has been provided to me throughout this project; in particular Dr Timothy Prior for his assistance in the collection and analysis of the X-ray crystallography data, along with the EPSRC service at the University of Southampton for collection of data. I would like to thank Prof. Petr Hermann, Dr Vojtéch Kubíćek and Zuzanna Böhomová from Charles University, Prague, for their assistance in the potentiometric studies; for both teaching me how to conduct the studies and for assistance in collection of the data, and for their assistance in analysis of the resulting data. I would like to thank Gonçalo Clemente for his help when learning how to do radiochemistry, and to Prof. Phil Blower, Dr Michelle Ma, and Jennifer Young for providing me with the opportunity to perform radiochemistry studies at KCL. I would like to thank Isaline Renard for conducting the *in vivo* PET studies, Dr Juozas Domarkas for his advice regarding preparation of the administered probes, Prof. Steve Archibald and Prof. Anne-Marie Seymour for supervision of these experiments. Thanks also to the staff members within the University of Hull Chemistry department who provided assistance with collection of data; in particular Carol Kennedy and Daniel Mackenzie for elemental analysis, and Dr Kevin Welham and Dean Moore for collection of high resolution mass spectrometry data. I would also like to thank Linsey Malcolm for training me in tissue culture techniques.

All members of the Stasiuk group, the C222 lab and the 3rd floor Allam office deserve thanks for their support and friendship.

I would like to thank my family, especially my parents, for their love and support throughout my PhD.

Finally I would like to thank the University of Hull for funding for this project.

Declaration

I hereby declare that all the work presented within this thesis is original to the best of my knowledge, except where stated, and has not been submitted or published for other degrees.

Portions of this work have been published as papers with the references below:

Current advances in ligand design for inorganic positron emission tomography tracers ^{68}Ga, ^{64}Cu, ^{89}Zr and ^{44}Sc. T. W. Price, J. Greenman and G. J. Stasiuk, ***Dalton Trans.***, 2016, 45, 15702-15724

Amino acid based gallium-68 chelators capable of radiolabeling at neutral pH. T. W. Price, J. Gallo, V. Kubíček, Z. Böhmová, T. J. Prior, J. Greenman, P. Hermann and G. J. Stasiuk, ***Dalton Trans.***, 2017, 46, 16973-16982

Selective radiolabelling with ^{68}Ga under mild conditions: a route towards a porphyrin PET/PDT theranostic agent. S. Y. Yap, T. W. Price, H. Savoie, R. W. Boyle and G. J. Stasiuk, ***Chem. Commun.***, 2018, 54, 7952-7954

Thomas Price

Abbreviations

$[Et_4NO4PA]^+$	Tetraethyl 6,6',6'',6'''-((1λ4,4,7-triazonane-1,1,4,7-tetrayl)tetrakis(methylene))tetrapicolinate
^1H	Proton
Å	Angstrom
AAZTA	2,2'-((1,4-Bis(carboxymethyl)-6-methyl-1,4-diazepan-6-yl)azanediyl)diacetic acid
Abs	Absorbance
acac	Acetylacetonoate
Arb. U.	Arbitrary Units
ATSM	(1Z,1'Z)-N',N''''-((2E,3E)-butane-2,3-diylidene)bis(N-methylcarbamohydrazonothioic acid)
azapa	6,6'-((Ethane-1,2-diylbis(((1-benzyl-1H-1,2,3-triazol-4-yl)methyl)azanediyl))bis(methylene))dipicolinic acid
β^+	Positron
BFC	Bifunctional chelator
BSA	Bovine serum albumin
CCK2	Cholecystokinin receptor 2
CHX-A''-DTPA	2,2'-((2-(((1S,2S)-2-(bis(carboxymethyl)amino)cyclohexyl)(carboxymethyl)amino)ethyl)azanediyl)diacetic acid
CHX-dedpa	6,6'-((Cyclohexane-1,2-diylbis(azanediyl))bis(methylene))dipicolinic acid
CHX-octapa	6,6'-((Cyclohexane-1,2-diylbis((carboxymethyl)azanediyl))bis(methylene))dipicolinic acid
cm	Centimeters
CT	Computed Tomography
CyAAZTA	2,2'-((1,5-Bis(carboxymethyl)-3-methyldecahydro-1H-benzo[b][1,4]diazepin-3-yl)azanediyl)diacetic acid
DATA	2,2'-(6-((Carboxymethyl)amino)-1,4-diazepane-1,4-diyl)diacetic acid
dedpa	6,6'-((Ethane-1,2-diylbis(azanediyl))bis(methylene))dipicolinic acid
DO3Am	2,2',2''-(10-(2-Amino-2-oxoethyl)-1,4,7,10-tetraazacyclododecane-1,4,7-triyl)triacetic acid
DOTA	1,4,7,10-Tetraazacyclododecane-N,N',N'',N'''-tetraa acetic acid
DOTAGA	2-(4,7,10-Tris(carboxymethyl)-1,4,7,10-tetraazacyclododecan-1-yl)pentanedioic acid
DTPA	Diethylenetriamine-N,N,N',N'',N''-pentaacetic acid
e^-	Electron
EDTA	Ethylenediamine-N,N,N',N'-tetraacetic acid
ESI	Electron spray ionisation
Et_2MeDpaa.dab(Boc)	Diethyl 6,6'-(((4-((tert-butoxycarbonyl)amino)-1-methoxy-1-oxobutan-2-yl)azanediyl)bis(methylene))(S)-dipicolinate
Et_2tBuDpaa.lys(Z)	Diethyl 6,6'-(((6-(((benzyloxy)carbonyl)amino)-1-(tert-butoxy)-1-oxohexan-2-yl)azanediyl)bis(methylene))(S)-dipicolinate
Et_3Dpaa	Diethyl 6,6'-(((2-ethoxy-2-oxoethyl)azanediyl)bis(methylene))dipicolinate
Et_3Dpaa.cys(Tr)	Diethyl 6,6'-(((1-ethoxy-1-oxo-3-(tritylthio)propan-2-yl)azanediyl)bis(methylene))(R)-dipicolinate
Et_3NO3PA	Triethyl 6,6',6''-((1,4,7-triazonane-1,4,7-triyl)tris(methylene))tripicolinate
Et_3Tpaa	Triethyl 6,6',6''-(nitrilotris(methylene))tripicolinate

Et_4Dpaa.ga	Diethyl N,N-bis((6-(ethoxycarbonyl)pyridin-2-yl)methyl)-L-glutamate
Et_4DPAP	Diethyl 6,6'-((((diethoxyphosphoryl)methyl)azanediyl)bis(methylene))dipicolinate
Et_6DPPP	Diethyl ((bis((6-(diethoxyphosphoryl)pyridin-2-yl)methyl)amino)methyl)phosphonate
FBS	Foetal bovine serum
FC	Ferricrocin
FDG	Fluorodeoxyglucose
FDOPA	2-Fluoro-4,5-dihydroxyphenylalanine
FET	Fluoroethyl tyrosine
FLT	3'-Deoxy-3'-fluorothymidine
FOXE	Ferrioxamine E
FSC	Fusarine C
γ	Gamma
GBq	Gigabecquerels
Gd	Gadolinium
h	Hours
H_2Dpaa.ga.anh	6,6'-(((2,6-Dioxotetrahydro-2H-pyran-3-yl)azanediyl)bis(methylene))dipicolinic acid
H_3Bn_2DT3A	2,2'-((((Carboxymethyl)azanediyl)bis(ethane-2,1-diyl))bis(benzylazanediyl))diacetic acid
H_3Bn_2DT3A.ga.PSMA	2-Benzyl-5-(2-(benzyl(carboxymethyl)amino)ethyl)-9,16,24-trioxo-2,5,10,17,23,25-hexaazaoctacosane-1,6,22,26,28-pentacarboxylic acid
H_3Dpaa	6,6'-(((Carboxymethyl)azanediyl)bis(methylene))dipicolinic acid
H_3Dpaa.ala	6,6'-(((1-Carboxyethyl)azanediyl)bis(methylene))dipicolinic acid
H_3Dpaa.cys	6,6'-(((1-Carboxy-2-mercaptoethyl)azanediyl)bis(methylene))dipicolinic acid
H_3Dpaa.dab	6,6'-(((3-Amino-1-carboxypropyl)azanediyl)bis(methylene))dipicolinic acid
H_3Dpaa.ga.PSMA	1-(6-Carboxypyridin-2-yl)-2-((6-carboxypyridin-2-yl)methyl)-6,13,21-trioxo-2,7,14,20,22-pentaazapentacosane-3,19,23,25-tetracarboxylic acid
H_3Dpaa.lys	6,6'-(((5-Amino-1-carboxypentyl)azanediyl)bis(methylene))dipicolinic acid
H_3NO3PA	6,6',6''-((1,4,7-Triazonane-1,4,7-triyl)tris(methylene))tripicolinic acid
H_3Tpaa	6,6',6''-(Nitrilotris(methylene))tripicolinic acid
H_4Bn_2DT3A.ga	N,N-bis(2-(benzyl(carboxymethyl)amino)ethyl)glutamic acid
H_4Dpaa.ga	N,N-bis((6-carboxypyridin-2-yl)methyl)glutamic acid
H_4DPAP	6,6'-(((Phosphonomethyl)azanediyl)bis(methylene))dipicolinic acid
H_6DPPP	((Bis((6-phosphonopyridin-2-yl)methyl)amino)methyl)phosphonic acid
HBED	2,2'-(Ethane-1,2-diylbis((2-hydroxybenzyl)azanediyl))diacetic acid
Hno1pa2py	6-((4,7-Bis(pyridin-2-ylmethyl)-1,4,7-triazonan-1-yl)methyl)picolinic acid
HPLC	High performance liquid chromatography
HRMS	High resolution mass spectrometry
ID/g	Injected dose / gram
K	Kelvin
K_{222}	Kryptofix-222
keV	Kiloelectronvolts

MBq	Megabecquerel
Me	Methyl
mg	Milligram
MHz	Megahertz
mm	Millimeters
mM	Millimolar
MRI	Magnetic Resonance Imaging
MS	Mass spectrometry
mSv	Millisieverts
n	Neutron
NAAG	N-Acetyl L-Aspartyl-L-Gllutamate
^{Nap}ATSM	(1Z,1'Z)-N',N''''-((1E,2E)-acenaphthylene-1,2-diylidene)bis(N-methylcarbamohydrazonothioic acid)
ng	Nanogram
NMR	Nuclear Magnetic Resonance
NO2AP	2,2'-(7-(((2-Carboxyethyl)(hydroxy)phosphoryl)methyl)-1,4,7-triazonane-1,4-diyl)diacetic acid
NODAGA	2-(4,7-Bis(carboxymethyl)-1,4,7-triazonan-1-yl)pentanedioic acid
NODIA-Me	2-(4,7-Bis((1-methyl-1H-imidazol-2-yl)methyl)-1,4,7-triazonan-1-yl)-N-methylacetamide
NOPA	2-(4,7-Bis((hydroxyhydrophosphoryl)methyl)-1,4,7-triazonan-1-yl)acetic acid
NOPO	3-(((4,7-Bis((hydroxy(hydroxymethyl)phosphoryl)methyl)-1,4,7-triazonan-1-yl)methyl)(hydroxy)phosphoryl)propanoic acid
NOTA	1,4,7-Triazacyclononane-N,N',N''-triacetic acid
NOTI-Me	1,4,7-Tris((1-methyl-1H-imidazol-2-yl)methyl)-1,4,7-triazonane
NOTThia	1,4,7-Tris(thiazol-2-ylmethyl)-1,4,7-triazonane
OAc	Acetyl
^{o}C	Degrees centigrade
ORTEP	Oak Ridge Thermal Ellipsoid Plot Program
OTf	Triflate
Oxo	2,2',2''-(1-Oxa-4,7,10-triazacyclododecane-4,7,10-triyl)triacetic acid
p	Proton
PBS	Phosphate buffered saline
PCa	Prostate cancer
PCTA	2,2',2''-(3,6,9-triaza-1(2,6)-pyridinacyclodecaphane-3,6,9-triyl)triacetic acid
pD	-log[D]
PET	Positron Emission Tomography
pH	$-\log_{10}[H^+]$
p*M*	$-\log_{10}[M^+]$
pmol	Picomole
PSMA	Prostate specific membrane antigen
RCY	Radiochemical Yield
s	Seconds
Sar	3,6,10,13,16,19-Hexaazabicyclo[6.6.6]icosane-1,8-diamine
SPECT	Single Photon Emission Computed Tomography
$t_{1/2}$	Half life
TACN	1,4,7-Triazacyclononane
TAFC	Triacetylfusarine

$^{t}Bu_4Bn_2DT3a.ga$	Di-*tert*-butyl N,N-bis(2-(benzyl(2-(*tert*-butoxy)-2-oxoethyl)amino)ethyl)-L-glutamate
TeMP	4,4',4'',4'''-(Porphyrin-5,10,15,20-tetrayl)tetrakis(1-methylpyridin-1-ium)
TETA	1,4,8,11-Tetraazacyclotetradecane-N,N',N'',N'''-tetraacetic acid
TEtOHB-DAZA	6,6'-((6-((2-Hydroxy-4-ethoxybenzyl)amino)-1,4-diazepane-1,4-diyl)bis(methylene))bis(3-ethoxyphenol)
TFPP	5,10,15,20-Tetrakis(perfluorophenyl)porphyrin
THP	4-Amino-N1,N7-bis((3-hydroxy-1,6-dimethyl-4-oxo-1,4-dihydropyridin-2-yl)methyl)-4-(3-(((3-hydroxy-1,6-dimethyl-4-oxo-1,4-dihydropyridin-2-yl)methyl)amino)-3-oxopropyl)heptanediamide
TLC	Thin layer chromatography
TMeOHB-DAZA	6,6'-((6-((2-Hydroxy-4-methoxybenzyl)amino)-1,4-diazepane-1,4-diyl)bis(methylene))bis(3-methoxyphenol)
TRAP	((1,4,7-Triazonane-1,4,7-triyl)tris(methylene))tris(phosphinate)
TriMP	4,4',4''-(20-(4-(2-(2-(2-Azidoethoxy)ethoxy)ethyl)phenyl)porphyrin-5,10,15-triyl)tris(1-methylpyridin-1-ium)
µg	Microgram
µm	Micrometer
µM	Micromolar

Table of Contents

Table of Figures

Table of Schemes

Table of Tables

Table of Equations

Chapter 1 Introduction

1.1. Medical Imaging

A key part of medical treatment is diagnosis and monitoring of the affliction. Imaging techniques play a large role in the diagnosis of physical maladies as well as diseases. Imaging techniques can be used to identify the location and extent of physical injuries, such as broken bones or internal bleeding, or to identify abnormal behaviour in tissues such as tumours, heart conditions, or mental illness. Over 42 million imaging procedures were performed by the NHS in 2016/7 – and this number has increased year on year (data available since 2012).[1]

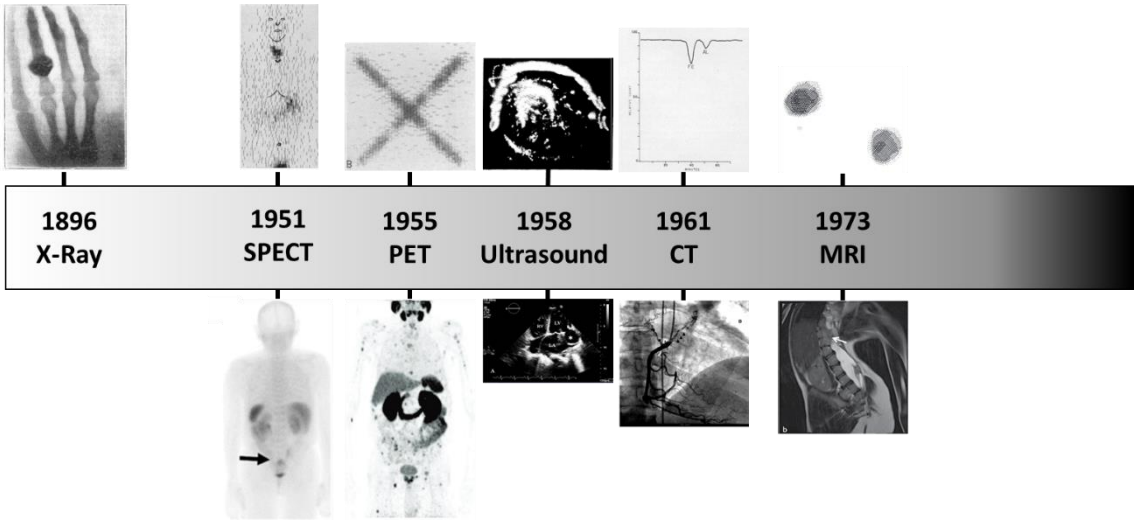

Figure 1.1: Timeline of development of key techniques in medical imaging. Above: Initial experiments demonstrating imaging properties.[2–7] Below: Modern examples demonstrating imaging modalities.[8–12]

Since the discovery of X-rays in 1896 medical imaging has progressed significantly in terms of the variety of techniques that are available (Figure 1.1), the quality of images obtained (Figure 1.1), and the range of maladies that can be imaged.

The key imaging techniques used in modern medicine are X-rays, Ultrasound, Computed Tomography (CT), Magnetic Resonance Imaging (MRI), Optical imaging and radionuclide imaging (Single Photon Emission Computed Tomography (SPECT) and Positron Emission Tomography (PET)).

X-rays are the most commonly used imaging modality[1] with a high tissue penetration, resolution (0.05-0.2 mm)[13,14] and short imaging time. X-rays are typically used for diagnosis of bone damage, dental work, and for detection of breast cancers in the form of mammograms.[15] Collection and simultaneous analysis of a high number of X-ray attenuation measurements, in the form of CT, can improve the soft tissue contrast allowing for the diagnosis of a greater range of maladies, including cancers. However, as X-rays are a form of ionising radiation, increasing the exposure increases the danger to the patient. A standard chest X-ray exposes a patient to

0.01 mSv of radiation[7] whereas a chest CT scan exposes a patient to 7-10 mSv radiation,[16,17] a much greater burden.

Ultrasound can be used to provide images with good resolution (0.05-0.5 mm)[13,14] without exposing the patient to ionising radiation.

MRI can obtain high quality images with excellent resolution (0.004-0.1 mm)[13,14] with good tissue contrast, particularly when contrast agents are used. MRI suffers from poor sensitivity, and is unable to detect biological events on the molecular level. As MRI derives its signal from water molecules, and these are in a high concentration in the body, molecular level changes are difficult to detect. This leads to longer scanning times and a high dose of contrast agent (µg-mg)[13] being required for contrast agent enhanced MRI. MRI is a non-ionising imaging technique and as such is suitable for repeated scans of the same patient.

Optical imaging can have a high sensitivity, however the light used for both exciting the fluorophore used and that is emitted is strongly absorbed by tissue limiting the penetration of this technique. Thus, optical imaging has proven to be popular for imaging of cells (where this technique's high resolution (1 µm)[13,14] is a particular benefit) or during image guided surgery when this penetration depth is not a significant issue.

The radionuclide imaging techniques, PET and SPECT, have a high tissue penetration, high sensitivity and low background signal, but do expose the patient to ionising radiation (6-7 mSv, [^{18}F]-fluorodeoxyglucose (FDG) scan).[7] Furthermore, an external imaging agent must be introduced and this has a very limited shelf life due to nuclear decay. Unlike MRI, this contrast agent is administered in very low concentrations (ng) reducing toxicity concerns. The main drawback of nuclear imaging is the relatively poor resolution (1-2 mm).[13,14]

1.2. Molecular Imaging

Molecular imaging is a subsection of medical imaging. It allows for the imaging of molecular and cellular processes in contrast to anatomical imaging.[18,19] This allows molecular imaging to provide information that would otherwise be unattainable. When disease occurs, the biochemical activity of cells begins to change. Over time, this progresses to anatomical or structural changes. As molecular imaging strives to detect the change in biochemical activity, it can be used to detect disease before other techniques that rely upon the later structural changes.

This early detection can have enormous relevance for patient care; it can allow for earlier diagnosis and treatment, more precise monitoring of disease progression, and personalised therapy.[18]

Molecular imaging typically involves the introduction of an imaging agent, such as a radiotracer. This tracer can accumulate in target tissues within the body and then be detected by an external imaging device. The pattern of this accumulation yields the information that can lead to diagnosis.

The selection of the imaging technique to be used is highly dependent on the condition being investigated. The high tissue penetration and sensitivity of PET imaging are invaluable for functional imaging of processes within the body. This has been particularly exploited for imaging brain function and for oncological purposes, where the presence of a disease may already be determined but the specific nature and extent is not yet known.

1.3. Positron Emission Tomography (PET)

1.3.1 How PET works

Positron Emission Tomography (PET) is a medical diagnostic technique that is dependent on the decay of neutron deficient nuclei that are introduced into the body as a radiotracer. Neutron deficient nuclei can undergo two different decay processes – electron capture (Equation 1) and positron emission (Equation 2).

Equation 1: Nuclear decay by electron capture.

$$ {}^{A}_{Z}X + e^{-} \rightarrow {}^{A}_{Z-1}Y + \nu $$

Equation 2: Nuclear decay by positron emission.

$$ {}^{A}_{Z}X \rightarrow {}^{A}_{Z-1}Y + \nu + \beta^{+} $$

PET exploits the second of these – the emitted positron travels a short distance (the positron range) and then undergoes an annihilation interaction with an electron nearby.[20] The distance travelled by the positron before annihilation is dependent upon the characteristic kinetic energy of the positron (Table 1.1);[21] the average positron emitted by fluorine-18 (^{18}F) travels 0.6 mm whereas one emitted by gallium-68 (^{68}Ga) travels 2.9 mm due to its higher energy.[22] The annihilation interaction results in two γ photons, each with an energy of 511 keV,[13,20] being emitted simultaneously in opposite directions to each other.[20] These two photons can be detected by a pair of detectors 180° apart and a "line of coincidence" constructed to localise their source. The collection of millions of such events allows for the construction of a PET image (Figure 1.2).[21] The requirement for two 511 keV photons to be detected simultaneously reduces the background signal; this results in PET having a very high sensitivity.

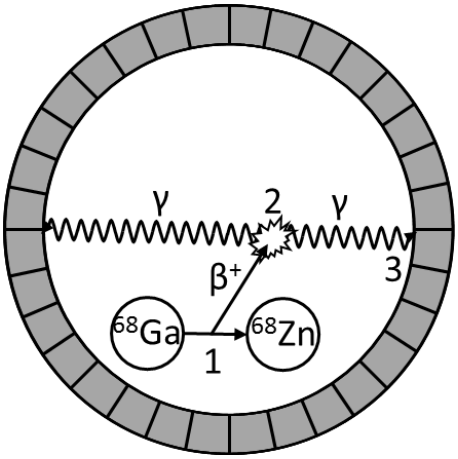

Figure 1.2: Schematic of a PET imaging process. 1. Positron emitted from radionuclide. 2. Positron and electron undergo annihilation interaction and emit two photons. 3. Emitted photons detected.[8]

PET is typically used in combination with another imaging technique, such as CT, to provide both structural and functional information (Figure 1.3). The high contrast obtained through PET imaging (Figure 1.3 d, e) can be co-registered with the full anatomical information obtained with the secondary imaging modality (Figure 1.3 b, c) to provide more precise information regarding the location of diseased tissue. In the example reported by Wagner *et al.*[23] (Figure 1.3) colorectal cancer metastases can be seen clearly in the whole body maximum intensity projection acquired 60 minutes post-administration of [^{18}F]FDG. When transverse images are obtained, the metastasis in the liver can be seen in the CT scan of the abdomen (Figure 1.3 b), but is seen more clearly in the corresponding PET image (Figure 1.3 d). This is more prominent in the transverse pelvis image, in which the tumour is difficult to distinguish from the surrounding tissue in the CT image (Figure 1.3 c) but is clearly indicated in the corresponding PET scan (Figure 1.3 e).

Table 1.1: Properties of a selection of PET radionuclides.

Nucleus	Halflife [21,24]	Production	Decay Modes	Mean positron energy / keV
^{11}C	20 minutes	$^{14}N(p, \alpha)^{11}C$ Cyclotron[21]	β^+ 100%[24]	390[25,26]
^{13}N	10 minutes	$^{16}O(p, \alpha)^{13}N$[21]	β^+ 100%[27]	492[27]
^{18}F	110 minutes	$^{18}O(p, n)^{18}F$ Cyclotron[21]	β^+ 100%[24]	252,[25] 250[26,27]
^{44}Sc	4.0 hours	$^{44}Ti/^{44}Sc$ generator,[28] $^{44}Ca(p, n)^{44}Sc$ Cyclotron[28]	β^+ 100%[24]	632[28]
^{52}Mn	5.6 days	$^{52}Cr(p,n)^{52}Mn$ Cyclotron[29]	β^+ 30%[29–33] β^+ 100%[24,33,34]	575[29]
^{64}Cu	12.7 hours	$^{64}Ni(p, n)^{64}Cu$ Cyclotron[35]	β^+ 19% EC 41% β^- 40%[8]	278[28]
^{68}Ga	68 minutes	$^{68}Ge/^{68}Ga$ Generator[35]	β^+ 90% EC 10%[8]	830,[26,28] 844[25]
^{89}Zr	3.3 days	$^{89}Y(p, n)^{89}Zr$[35]	β^+ 23% EC 77%[8]	397[36]

As an imaging technique, PET has a number of advantages over other modalities – chief amongst these is its high sensitivity.[37,38] A key advantage of the high sensitivity of PET is that this leads to a very small dose of the tracer being required – for the imaging of adults, a dosage of 370-740 MBq of [^{18}F]FDG is typical,[39] this corresponds to approximately 6 pmol of the radiotracer. This is beneficial as it reduces any toxicity concerns and ensures that PET tracers do not saturate biological receptors.[40] PET can also be used as a quantitative technique allowing for in depth study of physiological processes.[41] Furthermore, as gamma rays can pass through tissue, PET has a very high tissue penetration. This allows for imaging within the body (i.e. PET is not limited to imaging near to the skin or to *ex vivo/in vitro* imaging).

However, PET involves the use of ionising radiation. In a typical [^{18}F]FDG scan, the patient will be exposed to 6-7 mSv of radiation.[42] This may limit the frequency or number of scans a patient can have.

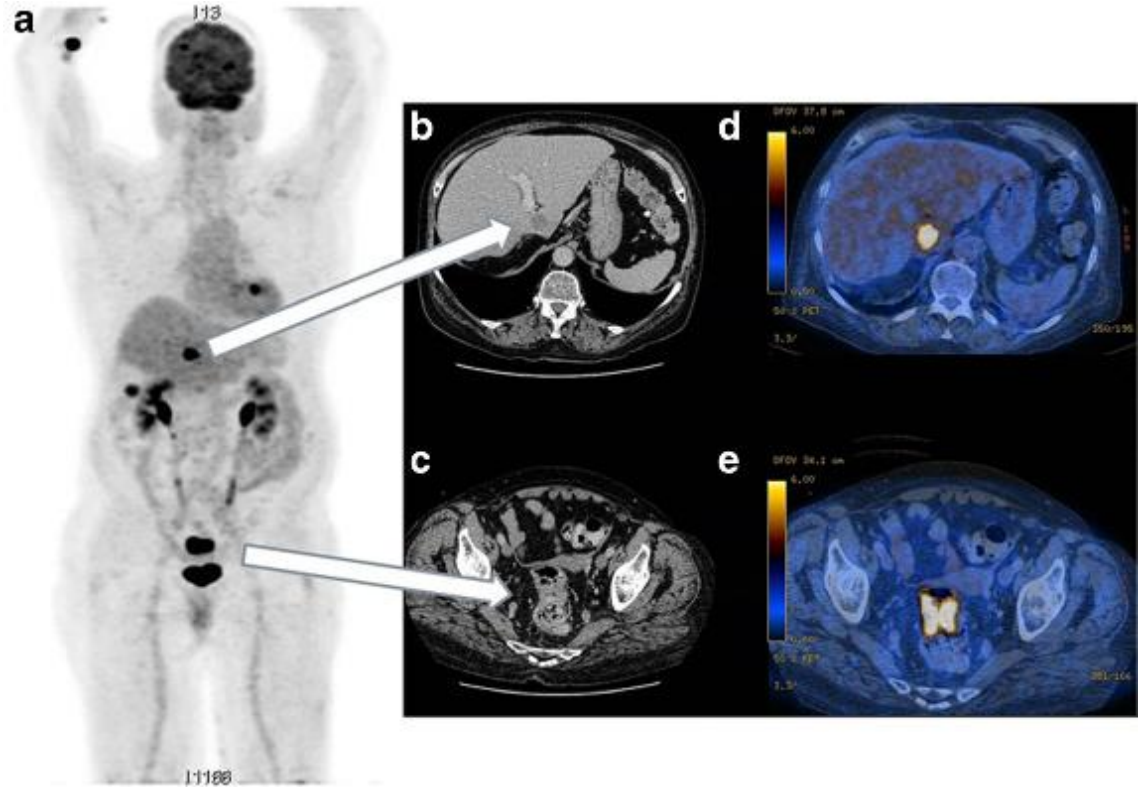

Figure 1.3: [^{18}F]FDG PET/contrast enhanced CT scan of patient with histologically proven adeno-carcinoma of the intestine with liver metastases. a) Maximum intensity projection PET scan of patient. b) Contrast enhanced CT scan of abdomen. c) Contrast enhanced CT scan of pelvis. d) PET/CT image of abdomen. e) PET/CT image of pelvis. Image adapted from reference.[23]

Unlike MRI or fluorescence, the signal produced by a PET radiotracer during imaging does not depend on the identity of the molecule – this means that metabolites will be indistinguishable from the original tracer in a PET scan. This can be an advantage; if the metabolic pathway of a drug is being followed throughout a body for example. Indeed, this is the principal behind the application of [^{18}F]FDG – the metabolite [^{18}F]fluorodeoxyglucose-6-phosphate accumulates within cells and is not further metabolised within the imaging timeframe (Figure 1.4).[21] However, this could also be seen as a disadvantage: if the radionuclide is cleaved from the targeting group then the signal will no longer be associated with the target.

[^{18}F]FDG is the most commonly used clinical PET tracer.[21] [^{18}F]FDG is taken into cells by glucose transporters where it undergoes partial metabolisation. The hexokinase enzyme is able to metabolise [^{18}F]FDG into [^{18}F]fluorodeoxyglucose-6-phosphate (Figure 1.4). However, further metabolism by glucose-6-phosphate isomerase does not occur due to the absence of the alcohol group in the 2 position. This results in [^{18}F]fluorodeoxyglucose-6-phosphate accumulating in cells in which [^{18}F]FDG is taken up as it cannot be broken down and the negative charge prevents it from crossing the cell membrane. As such, the PET signal obtained from an [^{18}F]FDG scan is essentially a map of glucose uptake; this has been applied to a wide variety of disease models where glucose uptake misregulation is an indicator of diseased tissue. [^{18}F]FDG is particularly used in oncology due to the increased metabolic activity of cancer cells.

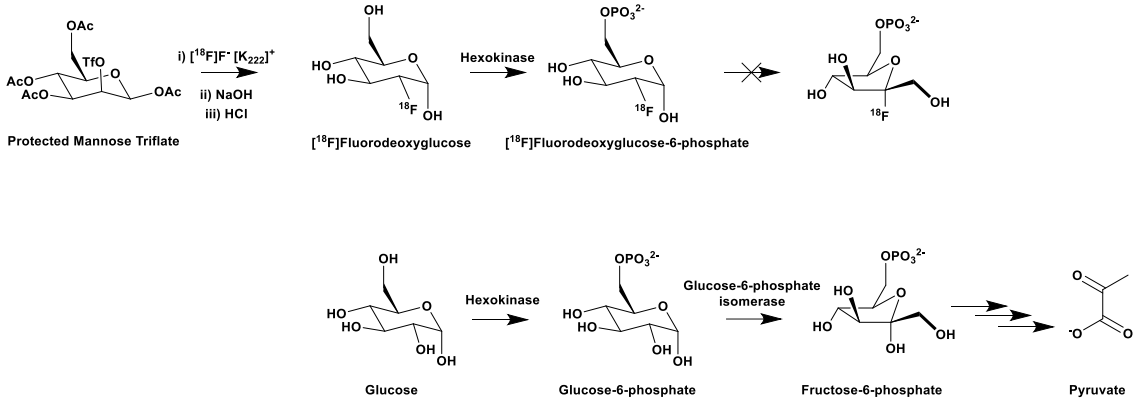

Figure 1.4: Synthesis of [^{18}F]FDG and subsequent metabolisation, glucose metabolisation for comparison.

1.3.2 PET radionuclides

There are a number of radionuclides that can be used for PET imaging (Table 1.1). Some, such as carbon-11 (^{11}C) and fluorine-18 (^{18}F), can be covalently incorporated into the radiotracer. Others, including gallium-68 (^{68}Ga), require an alternative means of incorporation, typically through the formation of coordination complexes.

^{11}C has a short half-life ($t_{1/2}$(^{11}C) = 20 minutes) – this has resulted in the development of highly specialised chemistry to produce the desired radiotracer in a short time period.[21] ^{11}C is particularly valuable as its incorporation in place of an existing carbon atom in the radiotracer means that the biodistribution is undisturbed; this gives a perfect model for the biodistribution and metabolism of drugs and other molecules of interest.[40,43,44] [^{11}C]Thymidine, [^{11}C]methionine and [^{11}C]choline are examples where the isotopic labelling of a substance allows its metabolism to be monitored directly. Labelling of these compounds allows for imaging of DNA synthesis, protein synthesis,[45] and cell membrane synthesis respectively[46] – each of these has been used in the diagnosis of cancers. [^{11}C]Thymidine and [^{11}C]methionine have been shown to be useful for imaging of brain tumours. [^{11}C]Choline has been shown to have increased uptake in prostate cancer tissues compared to normal prostate tissues, and prostate tissues displaying benign prostate hyperplasia and focal prostatitis.[47] Alternatively, [^{11}C] labelling can be used to study uptake of a compound with high affinity for diseased tissue, as seen for Pittsburgh Compound B for the diagnosis of Alzheimer's disease.[48–50]

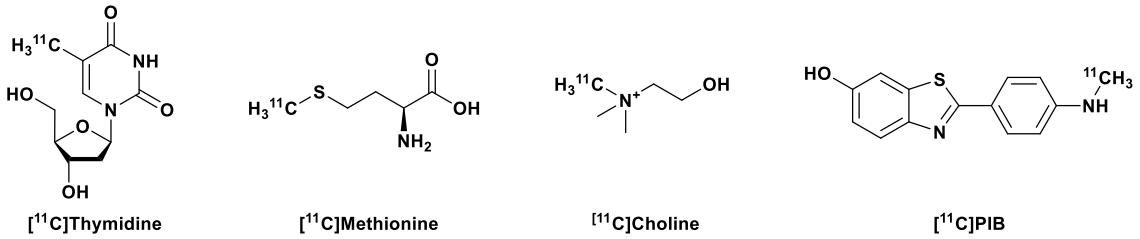

Figure 1.5: Structures of some clinically relevant ^{11}C radiotracers, with site of radiolabelling indicated.

^{18}F has been extremely popular for the development of PET radiotracers.[21] The 110 minute half-life of ^{18}F allows for more complex syntheses to be performed. Incorporation of ^{18}F

into molecules that do not already feature a fluorine atom will impact the biodistribution and metabolism.

[^{18}F]3'-deoxy-3'-fluorothymidine (FLT) is a thymidine analogue that has a fluorine atom substituted for an alcohol group. This results in an unnatural DNA base that is taken up by cells and phosphorylated by thymidine kinase 1.[51] This uptake is closely tied to cellular proliferation, thus [^{18}F]FLT can be used to image increased proliferation.[51] The [^{11}C]thymidine analogue is rapidly degraded *in vivo* (half-life 3-5 minutes)[52] and this coupled with the short half-life of ^{11}C ($t_{1/2}$(^{11}C) = 20 minutes) limits the application of this radiotracer. [^{18}F]FLT increases both the radioactive half-life ($t_{1/2}$(^{18}F) = 110 minutes) and the *in vivo* half-life as it is not as readily degraded.

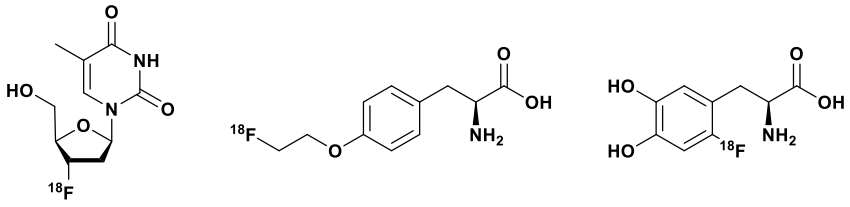

[^{18}F]FLT [^{18}F]FET [^{18}F]FDOPA

Figure 1.6: Structures of some clinically relevant ^{18}F radiotracers, with site of radiolabelling indicated.

Amino acids do not naturally contain fluorine atoms – [^{18}F] labelled amino acids are therefore different to their natural analogues. This can be seen in [^{18}F]fluoroethyltyrosine (FET) in which the phenol of tyrosine has been converted into an ether by addition of a short alkyl chain containing the ^{18}F label. [^{18}F]2-fluoro-4,5-dihydroxyphenylalanine (FDOPA) incorporates the radiolabel directly on the aryl ring of dopamine – a metabolite of tyrosine. These two ^{18}F amino acid analogues have been applied to imaging brain tumours,[53,54] where the longer half-life of ^{18}F allows for increased uptake time compared to the ^{11}C amino acid analogues.

The other nuclei on this list (Table 1.1) are metals and require special consideration; they cannot be directly incorporated into a radiotracer through covalent bonding but have a wide variety of properties that make them worth considering for PET imaging.

1.3.3 Metals in PET imaging

In order to successfully apply these metal radionuclei to PET imaging they must typically be incorporated into a targeting motif. This is often achieved through coordination of the metal by a chelator, typically through donation of electrons from the lone pairs of the ligand to the metal ion to form a coordinate bond. This chelate is then covalently attached to a targeting motif such as a peptide or antibody (Figure 1.7).

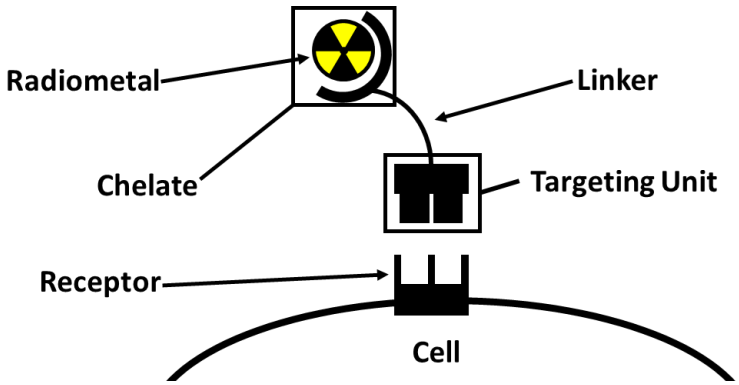

Figure 1.7: Schematic of a metal based PET radiotracer comprising of a radiometal, chelator, linker unit and targeting unit.

The coordination of the metal is important; if the metal is not incorporated into a radiotracer then it will not target the diseased tissue. Instead the metal will be picked up by competing biomolecules in the body and follow the typical biodistribution for that metal; e.g. copper-64 (^{64}Cu) will accumulate in the liver,[55] and ^{68}Ga will be picked up by *apo*-transferrin[56] and accumulate in the lungs, liver and bones. As a result, careful selection of the chelate used is a key part of designing a metal based PET radiotracer.

The chelator-metal complex must fulfil several key requirements:

- **Rapid preparation:** Due to the transient nature of radionuclides, the overall preparation time of a radiotracer should be appropriate considering the radionuclide's half-life. Ideally, purification following radiolabelling will be avoided. The 68 minute half-life of ^{68}Ga requires the tracer synthesis to be rapid to allow time for quality control and, if necessary, purification of the resultant radiotracer prior to its use. Rapid formation, purification and formulation of the chelator-metal complex is one of the key areas being developed in this field.[57]
- **Mild complexation conditions:** Many peptide targeting vectors are susceptible to decomposition under the harsh conditions often required for rapid chelation.[58] As such, high temperatures and extreme pH values should be avoided. While it is possible to conjugate the complex to the targeting vector after radiolabelling,[59] this is typically not favoured as it results in a longer synthetic period overall.
- **High *in vivo* stability:** This is essential if the radiometal is to have any specific targeting ability. The metal-chelator complex must be stable to transmetallation by biochelators (e.g. metalloproteins)[56] for the duration of the imaging experiment. If the radiometal is displaced from the chelate complex it will no longer be specifically targeted. Weakly coordinated Ga(III) is seen to accumulate in the skeleton and liver.[60,61]
- **Readily conjugated to targeting motifs:** In order to be used efficiently as imaging agents the radiotracers will need to specifically target biomarkers that indicate the

disease state that is being studied. Whilst there are examples of chelates that will target disease states automatically,[62,63] it is more common to use a bifunctional chelator (BFC) that can be conjugated to a targeting vector. Care must be taken during this step to avoid disrupting the chelation properties of the BFC.

Other methods of combining the radionuclei and targeting motif have been explored; such as direct incorporation of the radionuclide into nanoparticles,[64–67] temporarily coordinating the metal to allow for uptake into cells that are then used for cell tracking,[30,68–70] or incorporation into systems that degrade under specific conditions resulting in the metal radionuclide becoming trapped in tissues that exhibit these conditions (e.g. [^{64}Cu][Cu(ATSM)]).[71]

The decision of which radiometal to use and how to direct it *in vivo* will depend upon the requirements of the application. Zirconium-89 (^{89}Zr) has been found to have favourable properties for imaging using antibodies as targeting agents.[72] The long half-life of zirconium-89 ($t_{1/2}$(^{89}Zr) = 3.3 days) and the high *in vivo* stability of the common [Zr(deferoxamine)]$^{+}$ complex make imaging with antibodies with long blood pool residencies feasible.[72] Alongside the longer lived manganese-52 (^{52}Mn, $t_{1/2}$(^{52}Mn) = 5.7 d),[31,68] ^{89}Zr has also been applied to long term imaging of liposomal medicines[68] and for cell tracking.[69] ^{64}Cu has also found application to antibody targeted PET imaging,[73] its shorter half-life ($t_{1/2}$(^{64}Cu) = 12.7 hours) also makes it more suitable for imaging with peptides and other targeting agents that clear more rapidly from the body.[73]

The focus of this thesis is on the application of ^{68}Ga to PET imaging. With a much shorter half-life than the other PET emitting metal radionuclides discussed above, application of ^{68}Ga requires rapid localisation of the tracer to its target and efficient clearance of non-bound tracer. Thus, the majority of ^{68}Ga imaging applications use small peptides or other small molecule targeting groups.[74]

1.4. Gallium-68

1.4.1 Production of ^{68}Ga

$$^{68}\text{Ge} \xrightarrow[t_{1/2} = 271 \text{ days}]{\text{Electron Capture}} {}^{68}\text{Ga} \xrightarrow[t_{1/2} = 68 \text{ minutes}]{\beta^{+} \text{ Emission}} {}^{68}\text{Zn}$$

Figure 1.8: Decay pathway for the production and decay of ^{68}Ga.

The popularity of ^{68}Ga as a radiotracer for PET can be attributed to the development of the germanium-68(^{68}Ge)/^{68}Ga generator which produces ^{68}Ga through the decay of ^{68}Ge (Figure 1.8).[61] This generator combines a long lived "parent" radionuclide (^{68}Ge(IV), $t_{1/2}$(^{68}Ge) = 271 days) with a "daughter radionuclide" which has very different chemical properties and a half-life suitable for medical imaging (^{68}Ga(III) – $t_{1/2}$(^{68}Ga) = 68 minutes).[61] Over time the ^{68}Ge and ^{68}Ga population will reach an equilibrium (Figure 1.9) when the ^{68}Ga population decays at the same rate as it is produced by ^{68}Ge decay.

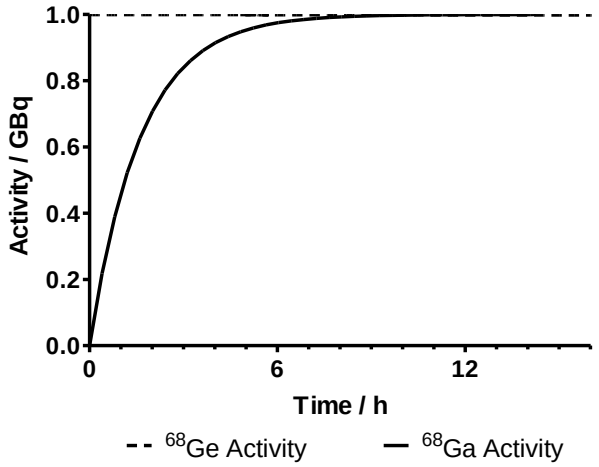

Figure 1.9: Production of ^{68}Ga within a ^{68}Ge/^{68}Ga generator of nominal ^{68}Ge activity at time = 0, $A_{0,Ge}$, of 1 GBq. ^{68}Ge activity, $A_{t,Ge}$, calculated using $A_{t,Ge} = A_{0,Ge}e^{-\lambda(Ge)t}$. ^{68}Ga activity, $A_{t,Ga}$, calculated using $A_{t,Ga} = A_{0,Ge}\lambda_{Ga}/(\lambda_{Ga}-\lambda_{Ge})(e^{-\lambda(Ge)t}-e^{-\lambda(Ga)t})$. The decay constant, λ, = $\ln 2/t_{1/2}$ for a given radionuclide.

Due to the differing chemical properties of Ge(IV) and Ga(III), ^{68}Ga(III) can be selectively eluted from commercially available generators. In these generators, the parent radionuclide, ^{68}Ge(IV), remains trapped on the generator column.[61] The column material and eluent varies, but is typically SnO_2 or TiO_2 eluted with 0.1-0.6 N HCl.[75,76] Organic resin columns are also available, and are eluted with lower acid concentrations.[75] The eluent, containing ^{68}Ga, can be used directly from the generator or purified and concentrated prior to use for radiochemistry.[76,77]A number of purification techniques have been explored,[78] including fractionation,[79] anionic exchange,[80] and cationic exchange.[81,82] These procedures concentrate the ^{68}Ga activity as well as removing impurities – such as ^{68}Ge breakthrough (should be less than 0.001%), materials from the production of the ^{68}Ge and the column (Ti(IV), Sn(IV)),[79,82] the eluent (Fe(III))[82] and ^{68}Zn(II)[82] produced by decaying ^{68}Ga within the generator.

Thus, the ^{68}Ge/^{68}Ga generator provides a non-cyclotron based route to a positron emitter, allowing for research and diagnosis to be undertaken at sites lacking access to the specialist cyclotron-based equipment normally required for ^{11}C or ^{18}F PET. This development of ^{68}Ga based PET imaging has the potential to be extremely beneficial to the field of medical imaging as the generator based production of ^{68}Ga would be suitable for implementation in hospitals.[83] Successful application of a generator produced radionuclide to diagnostic imaging

has already been seen with the highly popular ^{99m}Tc SPECT radionuclide;[84] repeating this success with ^{68}Ga would lead to a readily available PET imaging radionuclide.

The generator production of ^{68}Ga does have some limitations that are not apparent with cyclotron production of radionuclides; principally the limited activity (typically around 1.8 GBq)[85] produced in an elution and the decrease of this activity over time. This limits the number of patient doses that can be prepared simultaneously. An alternative source of ^{68}Ga is production in a cyclotron by bombarding ^{68}Zn with protons. This has been reported to produce activities of ^{68}Ga in the range of 40-60 GBq from both solid[85] and solution[86] targets.

1.4.2 Radiochemistry with ^{68}Ga

In aqueous solutions the only stable oxidation state of gallium is Ga(III) which is present as the hydrate complex under acidic conditions.[61] In the pH range 3-7, this readily forms the complex $Ga(OH)_3$ which is highly insoluble in water.[61] The formation of $Ga(OH)_3$ is a concern during the chelation step, which must be rapid due to the short half-life of ^{68}Ga, as the transchelation of Ga(III) from $Ga(OH)_3$ is slow.[60] At physiological pH $[Ga(OH)_4]^-$ is formed instead, which is soluble in water[61] but still displays slow chelation kinetics due to the strong coordination of hydroxyl ligands to Ga(III).[60] As such, chelation studies are usually undertaken under conditions that prevent the formation of $Ga(OH)_3$[61] or in the presence of a "trapping" ligand such as citrate or acetate.[60,61]

Table 1.2: Selected properties of Ga(III) and Fe(III) ions.

Property	Ga(III)	Fe(III)
Ionic Configuration	[Ar] $3d^{10}$	[Ar] $3d^5$
Ionic Radius (6 coordinate)	62[60]	65[60]
$\log K_{\text{Transferrin-M-1}}$	20.3[56,60]	22.8[60]
$\log K_{\text{Transferrin-M-2}}$	19.3[56,60]	21.5[60]

Many of the properties of six coordinate Ga(III) are very similar to high spin Fe(III) (summarised in Table 1.2) - this is the source of a number of issues *in vivo* as metalloproteins that typically chelate Fe(III) will also chelate Ga(III) strongly. Ga(III) shows a strong affinity for *apo*-transferrin,[56] an important Fe(III) transporter in humans. This affinity defines much of the work that has been undertaken in the field of Ga(III) chelation as it provides a standard against which a successful chelate must positively compare. Transchelation of ^{68}Ga by transferrin would result in a loss of specificity and an accumulation of ^{68}Ga in the liver, lungs and bone.[60,61]

1.4.3 Ga(III) coordination chemistry

Ga(III) typically has a coordination number of 6 and complexes that fulfil this should have an octahedral coordination geometry.[87] Due to its high charge and small ionic

radius, the Ga(III) ion is classified as a hard Lewis acid.[60] Therefore, it is expected that Ga(III) will display a high thermodynamic stability in complexes with hard Lewis basic sites containing atoms such as oxygen and nitrogen which can donate a lone pair of electrons to the Ga(III) ion. Carboxylate, [88] phosphonate,[88] and amine[89,90] groups are ideal, and phenolate[89] and thiol[88,91,92] groups have shown some success at chelating Ga(III) as well.

1.4.4 Current status of ^{68}Ga PET imaging

The use of ^{68}Ga for radiochemistry has increased rapidly over the last decade, with annual publications increasing from 87 in 2008 to 886 in 2018.[93] A number of factors have caused this, including increased commercial availability of ^{68}Ga/^{68}Ge generators[93,94] and development of successful, clinically relevant ^{68}Ga radiotracers. In particular, the FDA approval of [^{68}Ga][Ga(DOTATATE)] for the diagnosis of neuroendocrine tumours (NETs) and the introduction and success of [^{68}Ga][Ga(HBED-PSMA)] for the diagnosis of prostate cancer have spurred on this developing interest in ^{68}Ga as a clinical imaging tool.

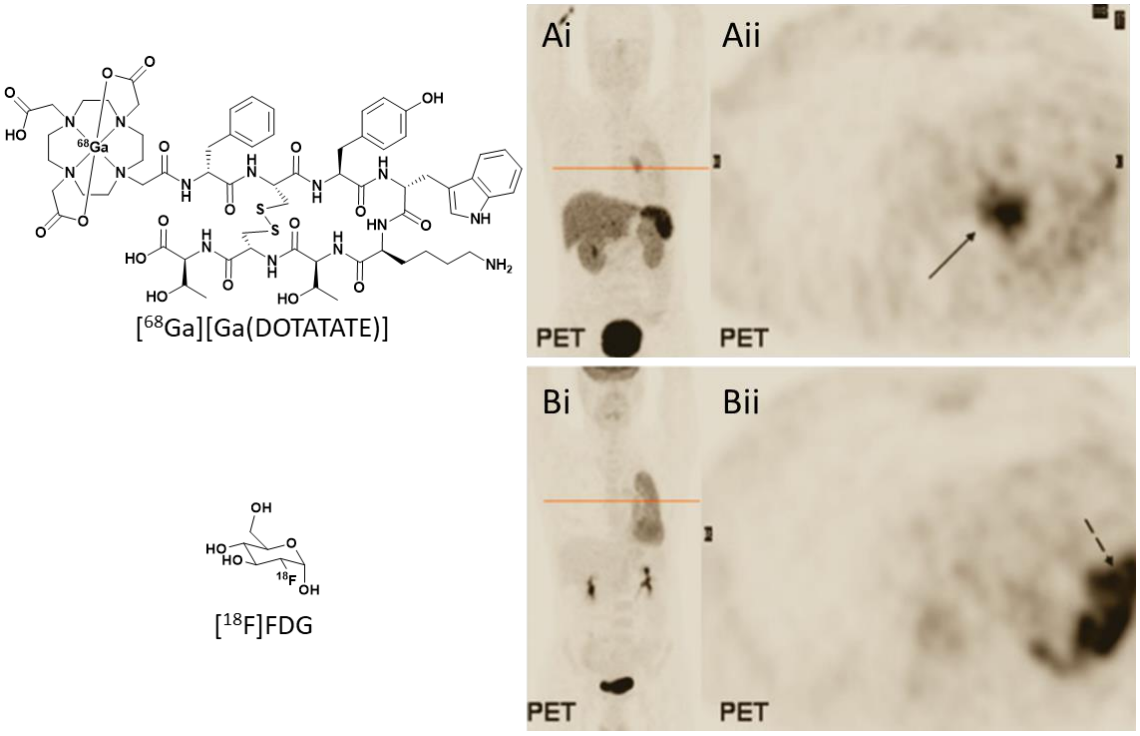

Figure 1.10: PET images of a patient with well-differentiated bronchial NET. Primary tumour indicated by solid arrow. Region of post collapse pneumonitis in left lung indicated by broken arrow. A) image collected when [^{68}Ga][Ga(DOTATATE)] was administered. B) Image collected when [^{18}F]FDG administered. i) Whole body maximum intensity projection. ii) Axial projection at position indicated by red line. Image adapted from reference [95].

NETs are rare tumours (accounting for approximately 0.5% of newly diagnosed malignancies);[96] diagnosis is complicated as well differentiated NETs are poorly imaged by [^{18}F][FDG due to their "near normal" glucose turnover.[95,97] However, many NETs overexpress somatostatin receptors (SSTRs).[95,97] Somatostatin derivatives have been used to image NETs, radiolabelling of an 8 amino acid peptide yielded [^{111}In][In(DTPA-Octreotide)] for SPECT

imaging.[98] The development of a ^{68}Ga SSTR targeting tracer, [^{68}Ga][Ga(DOTATATE)], resulted in a superior imaging agent with improved detection sensitivity.[98] [^{68}Ga][Ga(DOTATATE)] was approved by the FDA for use in diagnosis for NETs under the market name "NETSPOT".

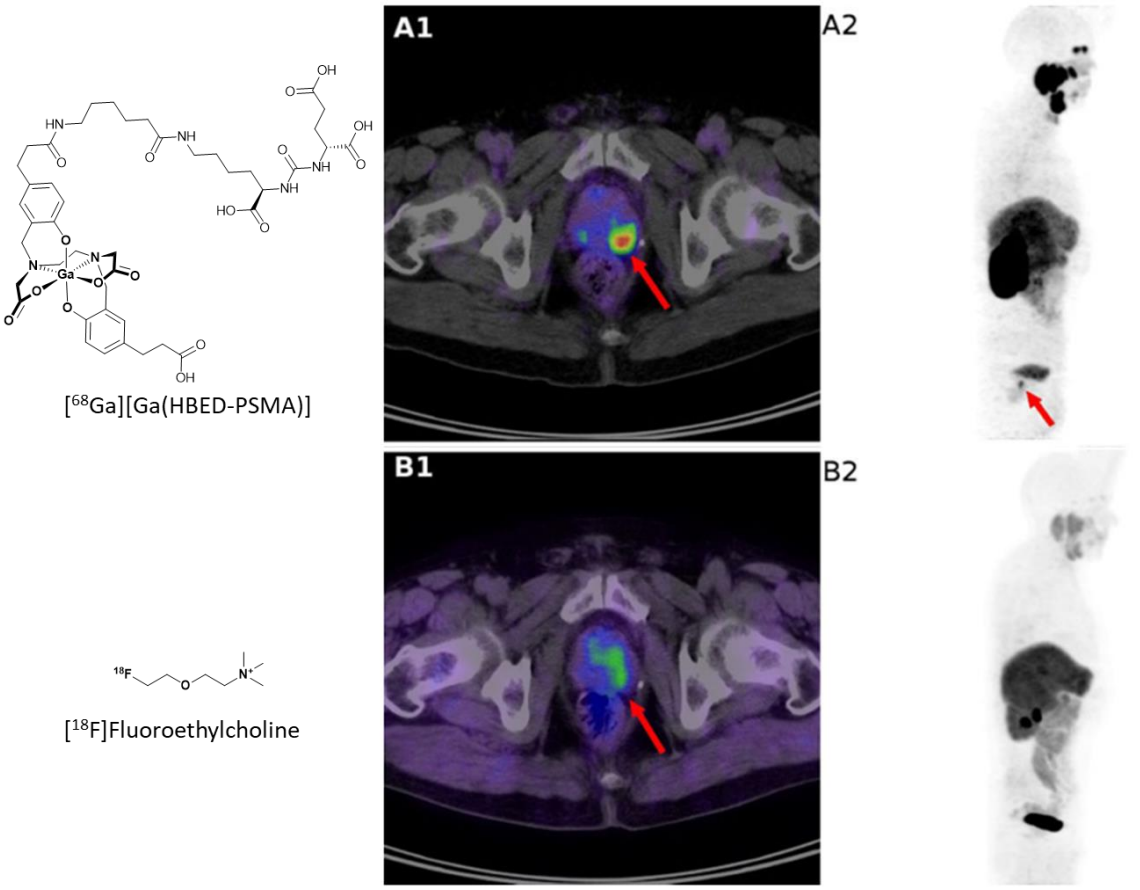

[^{68}Ga][Ga(HBED-PSMA)]

[^{18}F]Fluoroethylcholine

Figure 1.11: PET images of patient who had undergone previous radiotherapy of the prostate due to carcinoma, and was presenting elevated PSA levels. A: Images collected following administration of [^{68}Ga][Ga(HBED-PSMA)]. B: Images collected following administration of [^{18}F]fluoroethylcholine. 1: Axial projection. 2: Whole body maximum intensity projection. Red arrow indicates lesion detected by [^{68}Ga][Ga(HBED-PSMA)]. Image adapted from reference [99].

The development of [^{68}Ga][Ga(HBED-PSMA)] as a prostate cancer (PCa) targeting agent gave ^{68}Ga a "killer application";[93] targeting of PCa carcinoma cells *via* the prostate specific membrane antigen (PSMA) allowed for imaging of a highly abundant cancer (19% of new male cancer cases in the US in 2017)[100] with high sensitivity and specificity. PSMA is highly upregulated in all stages of PCa with nearly no expression in healthy tissues.[101]

1.5. Chelators for ^{68}Ga

1.5.1 Macrocyclic chelators for ^{68}Ga

A number of cyclic chelators have been studied with ^{68}Ga – particularly those based on the 1,4,7,10-tetraazacyclododecane-N,N',N'',N'''-tetraacetic acid (DOTA)[102] and 1,4,7-triazacyclononane-N,N',N''-triacetic acid (NOTA)[103] frameworks. These systems have shown a high kinetic inertness, but exhibit poor chelation kinetics – requiring either a long complexation time or harsh conditions, neither of these are ideal for the development of radiotracers

containing biomolecules. Development of these cyclic systems has aimed to improve the chelation kinetics without squandering the kinetic inertness of the resulting complex.[104,105]

1.5.1.1 Chelators based on DOTA

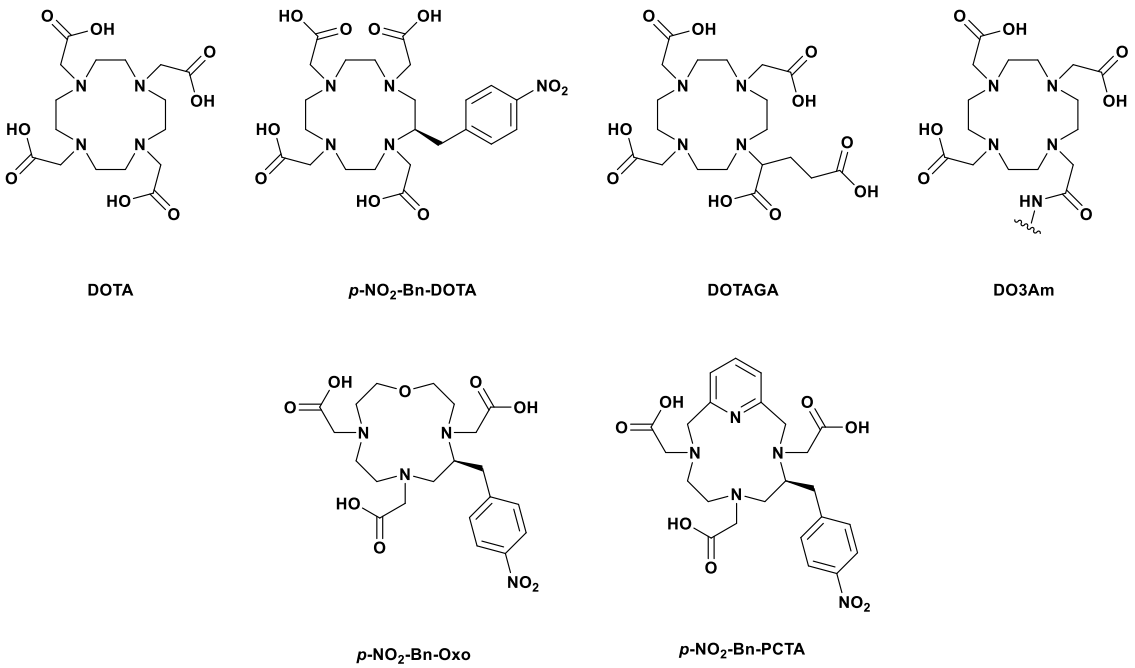

Figure 1.12: Structure of DOTA and derivatives.

The macrocyclic chelator DOTA (Figure 1.12) is one of the most popular chelators for ^{68}Ga. DOTA requires harsh conditions for efficient radiolabelling with ^{68}Ga – heating 1 µM DOTA to 80 °C at pH 4 for 10 minutes in the presence of ^{68}Ga(III) gives [^{68}Ga][Ga(DOTA)] in 93% yield.[106] The resulting complex is quite stable (log$K_{[Ga(DOTA)]}$ =26.1),[9] although some decomplexation is seen in serum challenge experiments – Weekes and co-workers report that only 80% of the activity was retained in the complex after 2 hours incubation in serum.[107]

Despite these shortcomings, conjugates of DOTA have been widely applied for imaging with ^{68}Ga. Conjugation can be undertaken *via* modification of the macrocyclic ring carbon backbone, yielding bifunctional chelators such as *p*-NO_2-Bn-DOTA,[106] through modification of one of the acetic acid arms to yield DOTAGA, or directly through one of the acetic acid arms to yield DO3Am.[108] As DOTA has 8 coordinating atoms, and Ga(III) will ideally form an octahedral complex, this last route should have limited impact on the complex in terms of formation or stability, although a reduction in the thermodynamic stability of the formed complex is reported (log$K_{[Ga(DO3Am)]}$ = 24.6).[9] As no modification of the chelator is required prior to performing this conjugation it is much simpler and as such has proven to be popular for the production of peptides labelled with ^{68}Ga (Figure 1.13).

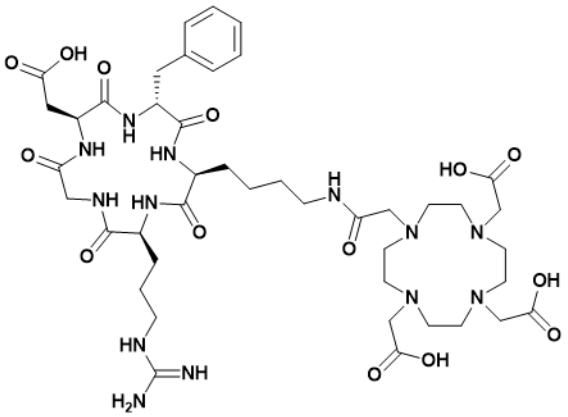

DOTA-RGD

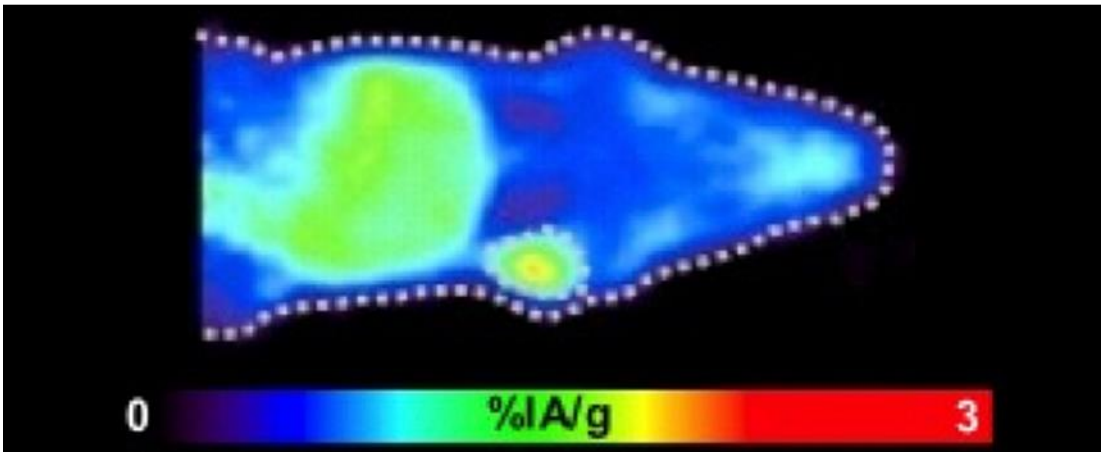

Figure 1.13: Coronal small-animal PET image of [^{68}Ga][Ga(DOTA-RGD)] in nude mouse bearing U87MG tumour at 1 hour after injection. Image adapted from reference [109].

An advantage of using DOTA over other chelators is that its coordination with a wide range of metals has been extensively explored[102] – this opens up the possibility to translate the conjugates prepared for ^{68}Ga complexation to other applications, such as MRI imaging or targeted radionuclide therapy.[110]

Currently, DOTA can only be applied to imaging with peptides that are stable to the harsh conditions that are required for radiolabelling;[111–114] this limits ^{68}Ga PET imaging to a degree. The use of more sensitive targeting motifs, such as antibodies (particularly if modified to have a biological half-life relevant for ^{68}Ga imaging),[115,116] or nanoparticles, or even some temperature sensitive peptides, may be desirable in the future. While DOTA can be radiolabelled at lower temperature, this is accompanied by much longer reaction times (10 µM *p*-NO_2-Bn-DOTA was labelled with ^{68}Ga at room temperature in 30 minutes with an 88% RCY).[106] Microwave heating can significantly reduce the incubation time required for efficient radiolabelling of DOTA – Velikyan *et al*. report quantitative radiolabelling within 1 minute when heated to 90 °C *via* microwave; in comparison they report approximately 35% yields using conventional heating at 95 °C, with 5 minutes incubation being required for >95% radiolabelling.[117] While this reduces the reaction time, it does not significantly change the

conditions required for efficient labelling. Pérez-Malo and co-workers demonstrated the beneficial effects of organic solvents on DOTA radiolabelling with ^{68}Ga; at 70 ^{o}C the radiolabelling reaction proceeded more rapidly with the addition of up to 40% ethanol. In aqueous solution the radiochemical yield was 14% after 3 minutes, rising to 66% after 15 minutes; however in 40% ethanol yields of 43% and 84% were achieved after 3 and 15 minutes, respectively.[118] This trend was also seen with acetonitrile and isopropanol as the co-solvent, with radiochemical yields of 51% and 63%, respectively, after 3 minutes and 84% and 87%, respectively, after 15 minutes.[118] This provides an alternative route to radiolabelling DOTA conjugates at slightly lower temperatures; however this also incorporates an impurity that must be removed or diluted prior to *in vivo* application. This alternative radiolabelling methodology could be particularly powerful if combined with ethanol-based processing of the ^{68}Ge/^{68}Ga generator eluent.[119]

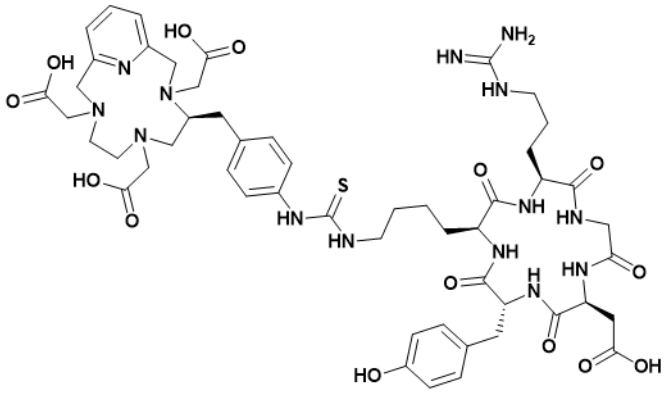

PCTA-RGD

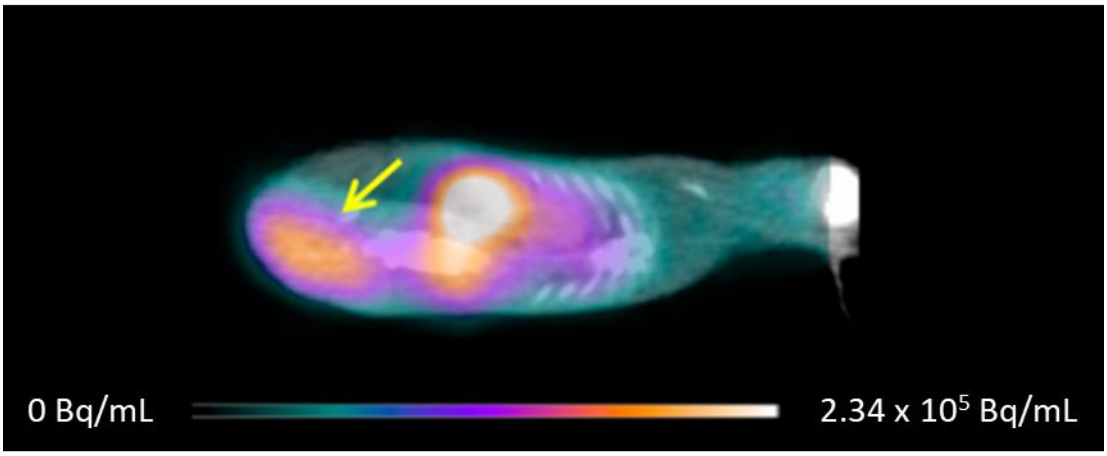

Figure 1.14: PET image of HT-29 xenograft Rag2M mouse anesthetized with isoflurane 2 hours after injection with [^{68}Ga][Ga(PCTA-RGD)]. Yellow arrows indicate the location of the tumour. Image adapted from reference [120].

Ferreira and co-workers explored the effect that substitution of one of the azamacrocyclic nitrogens of a bifunctional DOTA derivative, *p*-NO_2-Bn-DOTA, had on radiolabelling yields and stability.[106] Replacing the nitrogen with an oxygen atom yielded a ligand, *p*-NO_2-Bn-Oxo (Figure 1.12), that was capable of being radiolabelled with ^{68}Ga at room temperature under acidic conditions; a 98% yield was achieved by 1 µM *p*-NO_2-Bn-Oxo in 10

minutes.[106] Replacement of the secondary amine with a pyridine ring yielded the ligand *p*-NO_2-Bn-PCTA (Figure 1.12) which achieved a 99% radiochemical yield under the same conditions.[106] As a comparison, 10 µM *p*-NO_2-Bn-DOTA achieved only an 88% yield after 30 minutes at room temperature.[106] [^{68}Ga][Ga(*p*-NO_2-Bn-Oxo)] was found to be insufficiently stable for application to imaging with less than 20% of the complex remaining intact after 15 minutes incubation with *apo*-transferrin.[106] [^{68}Ga][Ga(*p*-NO_2-Bn-PCTA)] was more stable –7% of the activity was associated with the protein after 4 hours incubation.[106,120] Ferreira *et al*. applied a c(RGDyK) peptide conjugate of this system to imaging a colon cancer mouse model. The [^{68}Ga][Ga(PCTA-RGD)] radiotracer showed similar tumour uptake to [^{68}Ga][Ga(NOTA-RGD)] but had lower kidney uptake (Figure 1.14).[120]

1.5.1.2 Chelators based on NOTA

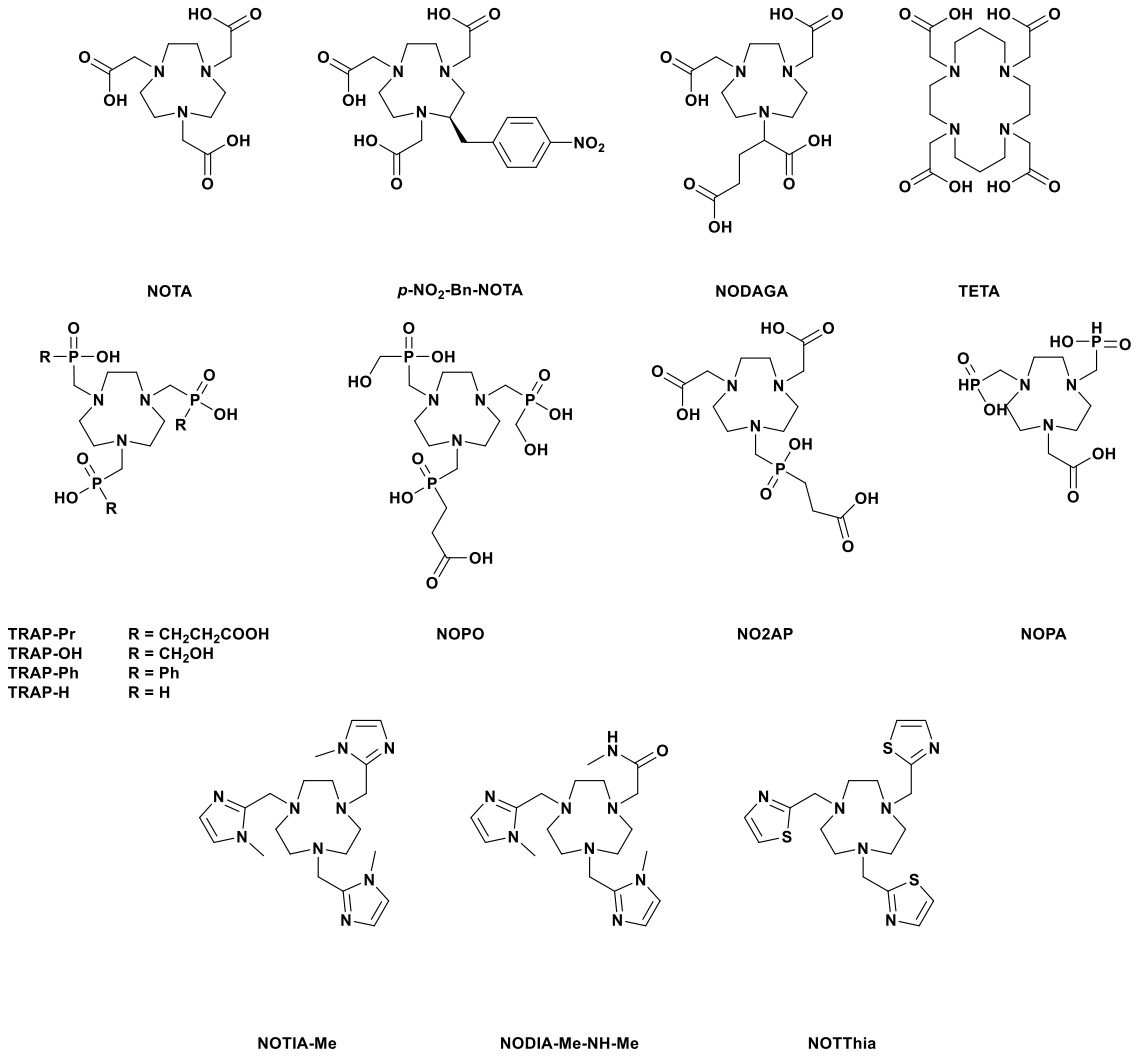

Figure 1.15: Structure of NOTA and derivatives.

1,4,7-Triazacyclononane-N, N', N''-triacetic acid (NOTA) is a smaller macrocyclic ligand than DOTA, with only 3 amines and three acetic acid arms (Figure 1.15). This ligand has a better size match for the small Ga(III) cation and the resulting complex, [Ga(NOTA)], has a greater stability than that of DOTA ($\log K_{[Ga(NOTA)]}$ = 29.60, $\log K_{[Ga(DOTA)]}$ = 26.1).[105,121,122] This difference in stability is highlighted if a larger macrocycle, 1, 4, 8, 11-tetraazacyclotetradecane-N,N',N'',N'''-

tetraacetic acid (TETA, Figure 1.15), is considered; TETA has a lower thermodynamic stability than either DOTA or NOTA upon complexing Ga(III) ($\log K_{[Ga(TETA)]}$ = 19.7). The more favourable pairing of Ga(III) and NOTA is reflected in the conditions required for efficient radiolabelling; Ferreira and co-workers report that 1 µM of NOTA can achieve a radiochemical yield of 99% after 5 minutes incubation at room temperature at pH 4; however 1 µM DOTA required heating to 80 °C for 10 minutes to achieve a 93% radiochemical yield. Furthermore, NOTA is more tolerant of the pH at which ^{68}Ga radiolabelling is undertaken than DOTA is, NOTA achieves >95% yields across the pH range of 3-5 whereas DOTA performs optimally at pH 4, with yields being reduced to 80% at either pH 3 or pH 5.[106] The complex formed by NOTA complexing Ga(III) is very stable; Weekes *et al*. report that only 2% of the activity was dissociated from the complex after 2 hours incubation in serum[107] whereas Velikyan and co-workers report no decomplexation over 4.5 hours incubation in serum.[123]

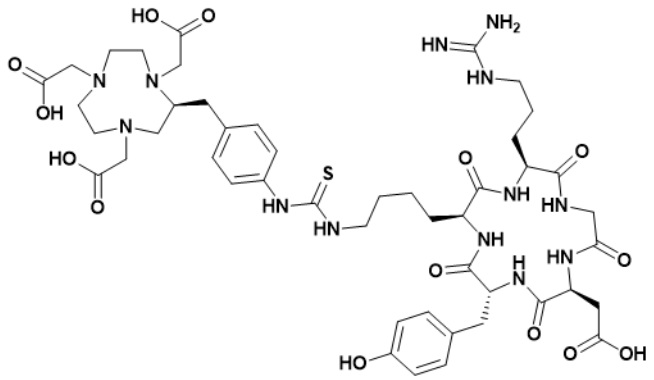

NOTA-RGD

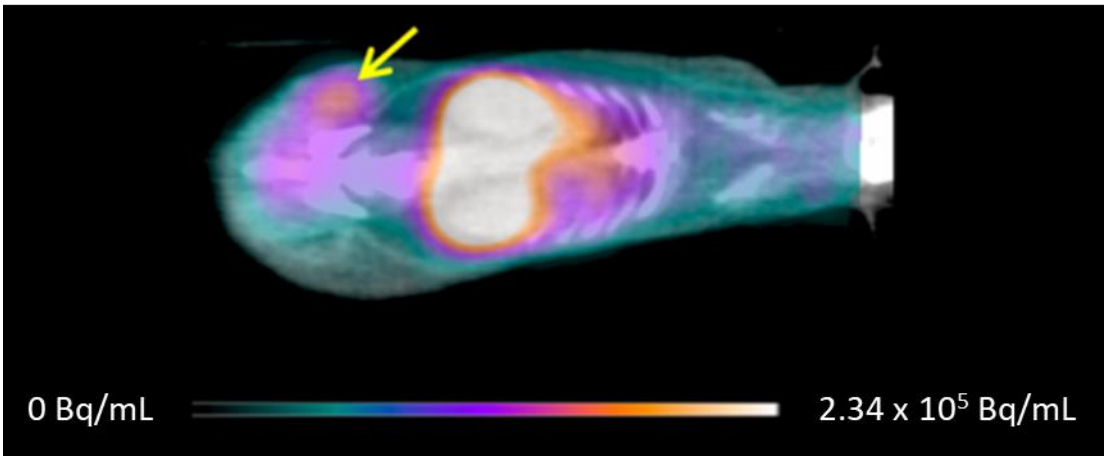

Figure 1.16: PET images of HT-29 xenograft Rag2M mouse anesthetized with isoflurane 2 hours after injection with [^{68}Ga][Ga(NOTA-RGD)]. Yellow arrows indicate the location of the tumour. Image adapted from reference [120].

Conjugation of NOTA to a targeting motif is typically achieved through modification of the carbon backbone – either through the macrocyclic ring (Figure 1.16),[103,106,124] or through one of the acetic acid arms to form 2-(4,7-bis(carboxymethyl)-1,4,7-triazonan-1-yl)pentanedioic acid (NODAGA, Figure 1.17).[108,125,126] In a direct comparison, Fani *et al.* report a 10 fold greater affinity

of a [Ga(NODAGA)]-conjugated somatostatin antagonist for the somatostatin receptor subtype 2 compared to a [Ga(DO3Am)] analogue; this also translates *in vivo* where the [^{68}Ga][Ga(NODAGA)] conjugate has greater tumour uptake and lower kidney uptake than the [^{68}Ga][Ga(DO3Am)] conjugate.[108] It is evident that, as well as changing the radiolabelling properties of the conjugate, changing the chelator can modify its targeting and biodistribution properties.

A number of groups have varied the coordinating arms of NOTA modify its complexing properties.

Notni and co-workers have extensively explored a family of NOTA derivatives in which the carboxylate arms are replaced by phosphinic acid units to yield ((1,4,7-triazonane-1,4,7-triyl)tris(methylene))tris(phosphinate) (TRAP) type ligands (Figure 1.15).[127] These derivatives have been shown to be highly capable of coordinating ^{68}Ga across a range of conditions. In particular they are able to coordinate ^{68}Ga at pH values as low as 0.5[128] (95% radiochemical yield achieved by 10 μM TRAP-Pr and TRAP-OH in 5 minutes at pH 0.5, 95 ^{o}C)[128]– this potentially allows for radiolabelling in the ^{68}Ge/^{68}Ga generator eluent without adjusting the pH. Furthermore, high radiochemical yields have been achieved under conventional ^{68}Ga radiolabelling conditions (pH 3.3, 95 ^{o}C, 5 minutes) with low ligand concentrations – radiochemical yields greater than 95% were achieved by TRAP-Pr, TRAP-OH, TRAP-Ph and TRAP-H at ligand concentrations as low as 0.5 μM whereas NOTA required 5 μM and DOTA 10 μM concentrations to achieve equivalent levels of radiolabelling.[128] This increases the molar activity of the resulting radiolabelled species.

An asymmetric derivative of TRAP has also been developed. This ligand, NOPO (Figure 1.15), has two methanolic and one propionic acid phosphinite substituents. This allows for monomeric radiotracers to be developed by conjugation of the carboxylate arm (Figure 1.18). This chelator retains the impressive ^{68}Ga complexing abilities of the symmetric analogues, with near quantitative labelling with ^{68}Ga in 5 minutes at pH 2.8 at 95 ^{o}C by just 0.1 μM NOPO.[129] Efficient radiolabelling was demonstrated across a wide pH range (0.5-7) when heated at 90 ^{o}C ([NOPO] = 30 μM, t = 5 minutes);[130] however at room temperature the effective radiolabelling pH window was much narrower with near quantitative yields only achieved in the range of pH 3-4 ([NOPO] = 30 μM, t = 5 minutes).[130]

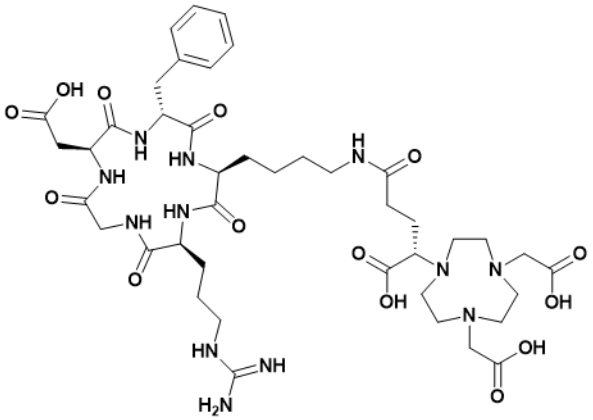

NODAGA-RGD

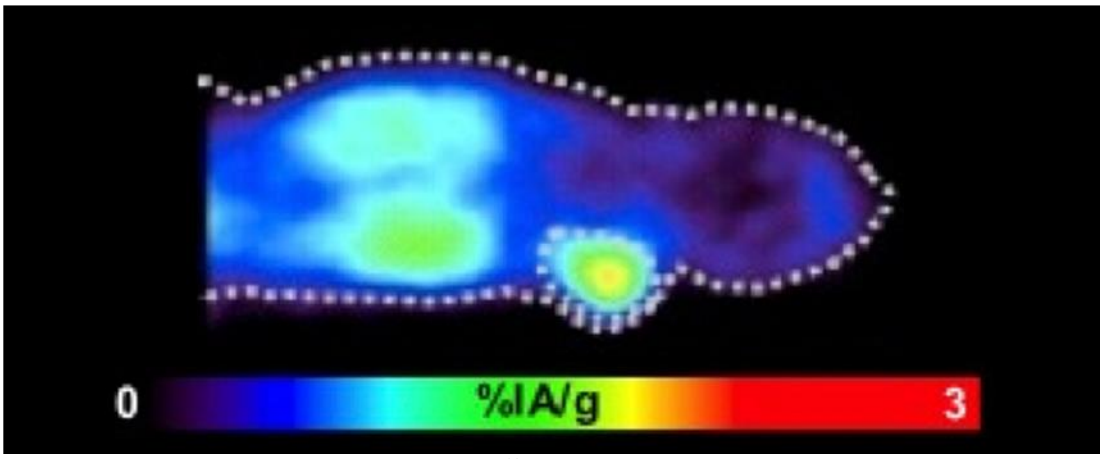

Figure 1.17: Coronal small-animal PET image of [^{68}Ga][Ga(NODAGA-RGD)] in nude mouse bearing U87MG tumour at 1 hour after injection. Image adapted from reference [109].

^{68}Ga complexation by the TRAP ligands is more tolerant towards metal contaminants that may be in the ^{68}Ga eluent such as Zn(II), Cu(II) or Fe(III) than complexation by NOTA[131] When one equivalent of Zn(II) is present during radiolabelling under acidic conditions (pH 3.3, 95 °C) NOPO and TRAP-Pr still achieved >95% radiochemical yields, whereas NOTA only achieved approximately 70% radiochemical yield.[131] In the presence of 1 equivalent Cu(II), NOPO and TRAP again performed much better than NOTA, with TRAP-Pr achieving near quantitative radiolabelling, and NOPO achieving approximately 85% radiochemical yields. In contrast, NOTA radiolabelling was approximately 20% in the presence of 1 equivalent Cu(II).[131] In the presence of Fe(III), all three ligands were able to achieve quantitative radiolabelling in the presence of one equivalent of the metal ion. However, higher Fe(III) concentrations (3 equivalents) reduced NOTA radiolabelling to approximately 20% whereas NOPO and TRAP-Pr still performed well with >90% radiolabelling.[131] This is thought to be due to the large difference in the stability of the complexes formed with these metals ($\log K_{[Cu(TRAP\text{-}Pr)]}$ = 16.85, $\log K_{[Zn(TRAP\text{-}Pr)]}$ = 16.88, $\log K_{[Cu(TRAP\text{-}OH)]}$ = 15.53, $\log K_{[Zn(TRAP\text{-}OH)]}$ = 16.12)[105] and those formed with Ga(III) ($\log K_{[Ga(TRAP\text{-}Pr)]}$ = 26.24, $\log K_{[Ga(TRAP\text{-}OH)]}$ = 23.3).[105] However, the relevant NOTA complexes also have the same trend in stability ($\log K_{[Zn(NOTA)]}$ = 22.32,[132] $\log K_{[Cu(NOTA)]}$ = 23.33,[132] $\log K_{[Ga(NOTA)]}$ = 29.60)[105,122,133] so this is

unlikely to be the sole explanation. Notni and co-workers demonstrated that ^{68}Ga is able to displace Zn(II) from preformed [Zn(TRAP-Pr)] and [Zn(NOPO)] complexes under the above conditions with near quantitative radiolabelling achieved.[131] This does not occur for [Zn(NOTA)] complexes with <50% radiochemical yield being achieved under these conditions.[131]

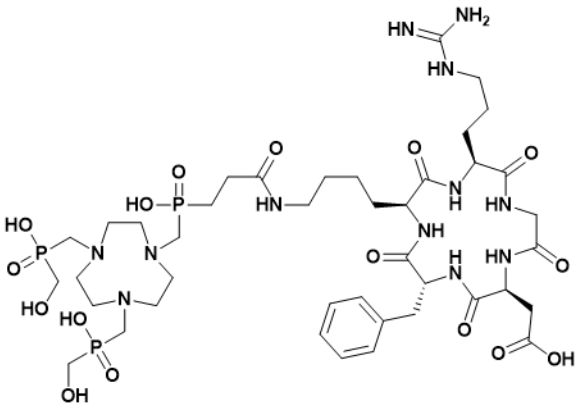

NOPO-RGD

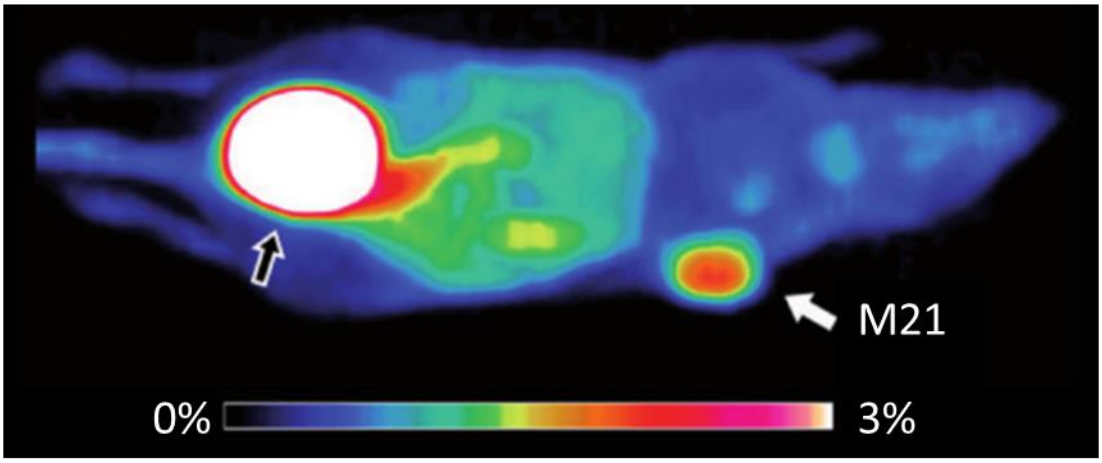

Figure 1.18: PET image of nude mouse with M21 human melanoma tumour xenografts (indicated by white arrow) injected with [^{68}Ga][Ga(NOPO-RGD)] 75 minutes post injection. Image adapted from reference [129].

The phosphinate groups of TRAP can be functionalised with a variety of groups – amongst the most reported are carboxylate and hydroxyl functionalised which provide additional functionalities for conjugation. The trimeric radiotracers formed by conjugation of the three pendant carboxylate groups of TRAP-Pr display improved affinity when compared to monomeric analogues.[134,135] A trimeric RGD conjugate, TRAP-$(RGD)_3$ (Figure 1.19), had an affinity 7.5 times better than NODAGA(RGD) (IC_{50} = 44 nM and 336 nM respectively).[134] A similar trend was seen when the PSMA targeting DUPA-PEP unit was used; TRAP$(DUPA\text{-}Pep)_3$ showed an 18 fold better affinity in LNCaP cells than DOTAGA(DUPA-PEP) (IC_{50} – 2 nM and 36 nM respectively) and this is reflected also in a greater tumour uptake *in vivo*.[135]

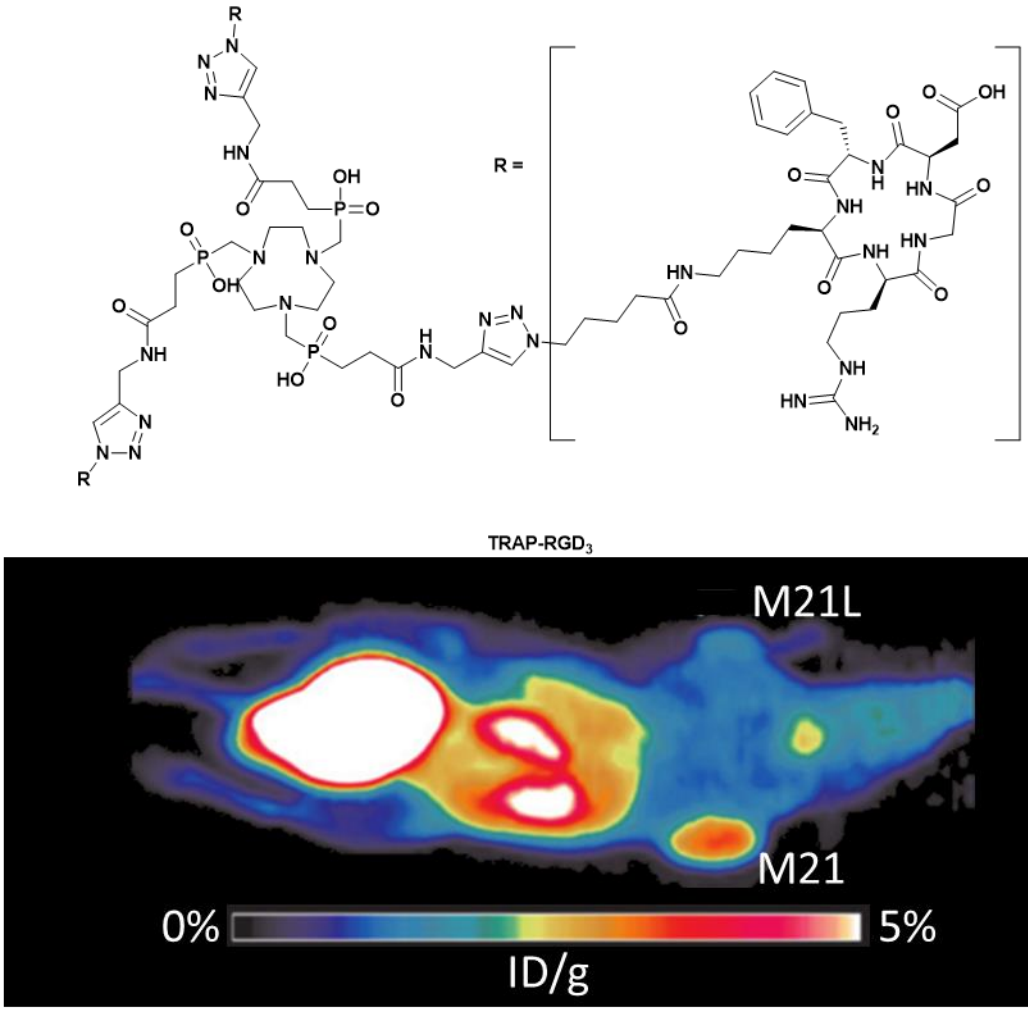

Figure 1.19: MicroPET scan of nude mouse bearing tumour xenografts on both shoulders (left: M21L, Right: M21). Image collected 75 minutes post injection of [^{68}Ga][Ga(TRAP-RGD$_3$)]. Image adapted from reference [128].

Functionalisation of TRAP-Pr with three DOTA units produced a ligand that has 4 coordinating pockets.[136] Incubation with excess Gd(III) resulted in all four macrocycles coordinating Gd(III). However, incubation of this tetra-Gd(III) system with excess Ga(III) resulted in selective replacement of the Gd(III) ion from the TRAP moiety whilst Gd(III) was not displaced from the DOTA units. [136] This could be due to the difference in thermodynamic stabilities for the Gd(III) and Ga(III) complexes of these ligands ($\log K_{[Gd(TRAP\text{-}Pr)]}$ = 13.46, $\log K_{[Ga(TRAP\text{-}Pr)]}$ = 26.24, $\log K_{[Gd(DO3A)]}$ = 21.29, $\log K_{[Ga(DO3A)]}$ = 24.64)[121,136,137] but the selectivity is likely dictated by the kinetics of metal exchange for these two ligands. TRAP is reported to undergo rapid metal exchange.[131] The Gd(III) ion was removed from the TRAP moiety with diethylenetriamine-N,N,N',N'',N''-pentaacetic acid (DTPA) prior to radiolabelling with ^{68}Ga.[136] To compensate for the difference in sensitivities of PET and MRI, the radiotracer was coinjected with a ^{nat}Ga analogue; the resulting images showed a high colocalisation of PET and MRI signal in the kidneys of a rat model after 25 minutes.[136]

Varying the ratio of phosphinite and acetate arms attached to the 1,4,7-triazacyclononane (TACN) ring changes the coordination properties of the ligand.[138] As the

number of phosphinate arms increases, the lowest pH at which radiolabelling proceeds efficiently decreases; at 95 °C, 3 µM NOPO is capable of labelling nearly quantitatively at pH 0.5, NOPA requires a pH of 2 to achieve the same result, and NOTA achieves near quantitative radiolabelling at pH 3.[138] At room temperature, the radiolabelling efficiency at high pH decreases with increasing number of phosphinate arms; at pH 6, 30 µM NOTA incorporates approximately 70% of the activity, whereas 2,2'-(7-(((2-carboxyethyl)(hydroxy)phosphoryl)methyl)-1,4,7-triazonane-1,4-diyl)diacetic acid (NO2AP) complexes 60%, 2-(4,7-bis((hydroxyhydrophosphoryl)methyl)-1,4,7-triazonan-1-yl)acetic acid (NOPA) complexes 45% and NOPO complexes 40% of the activity.[138]

Bartholomä and co-workers used imidazole based arms to prepare a TACN based chelator that resulted in a positively charged complex upon complexation of Ga(III).[139] The ligand 1,4,7-tris((1-methyl-1H-imidazol-2-yl)methyl)-1,4,7-triazonane (NOTI-Me) (Figure 1.15) was capable of ^{68}Ga complexation under acidic conditions with a 95% RCY achieved by 10 µM NOTI-Me at room temperature and the same RCY achieved by 1 µM when heated to 95 °C.[139] Similar results were also reported for a conjugate analogue, 2-(4,7-bis((1-methyl-1H-imidazol-2-yl)methyl)-1,4,7-triazonan-1-yl)-N-methylacetamide (NODIA-Me), in which one of the imidazole rings is replaced by an amide for conjugation. A thioimidazole based chelator, 1,4,7-tris(thiazol-2-ylmethyl)-1,4,7-triazonane (NOTThia) (Figure 1.15), was also tested but proved to be a poor chelator for ^{68}Ga with less than 30% yield achieved whilst heating at pH 4.[139] A radiolabelled conjugate, [^{68}Ga][Ga(NODIA-Me-NH-PSMA)] was not seen to undergo decomplexation (<1% after 4 hours) by serum, although some degradation was reported.[139] A similar conjugate with a different linker between the chelator and targeting unit has also been reported, this shows good stability to serum after 1 hour (94% intact), although a greater decomplexation was seen over 4 hours with only 85% of the complex remaining intact.[140]

1.5.1.3 Other macrocyclic chelators

Ma and co-workers used 3,6,10,13,16,19-hexaazabicyclo[6.6.6]icosane-1,8-diamine (Sar) with ^{68}Ga to some success.[141] Radiolabelling required heating, with a 98% RCY achieved after 30 minutes heating at 80 °C in ethanol.[141] The resultant complex was relatively stable to transferrin, with only 11% of the complex degrading after incubation for 2 hours incubation.[141] *In* vivo, the RGD conjugated compound displayed 6.30 ± 0.45 % ID g^{-1} tumour uptake 2 hours post-injection and uptake in the excretion pathway through the kidneys (Figure 1.20).[141]

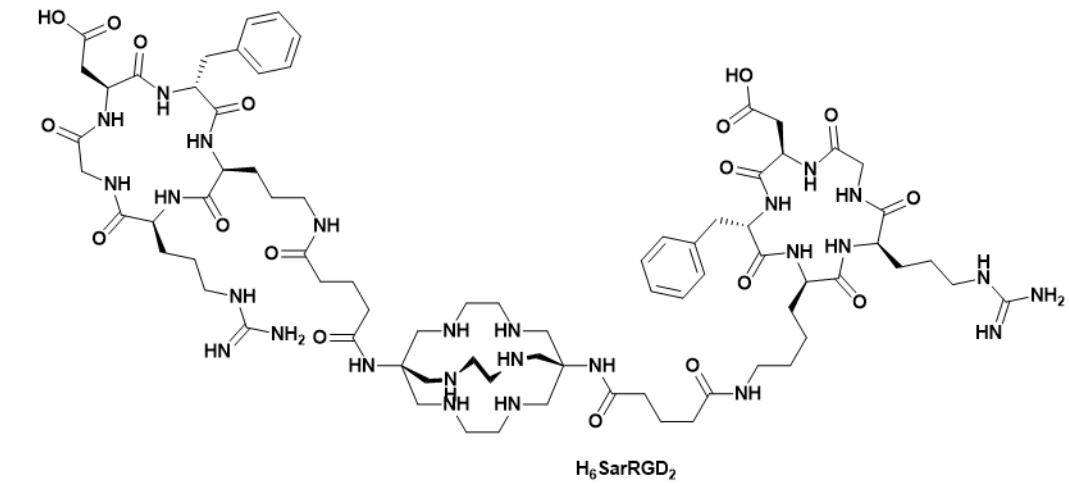

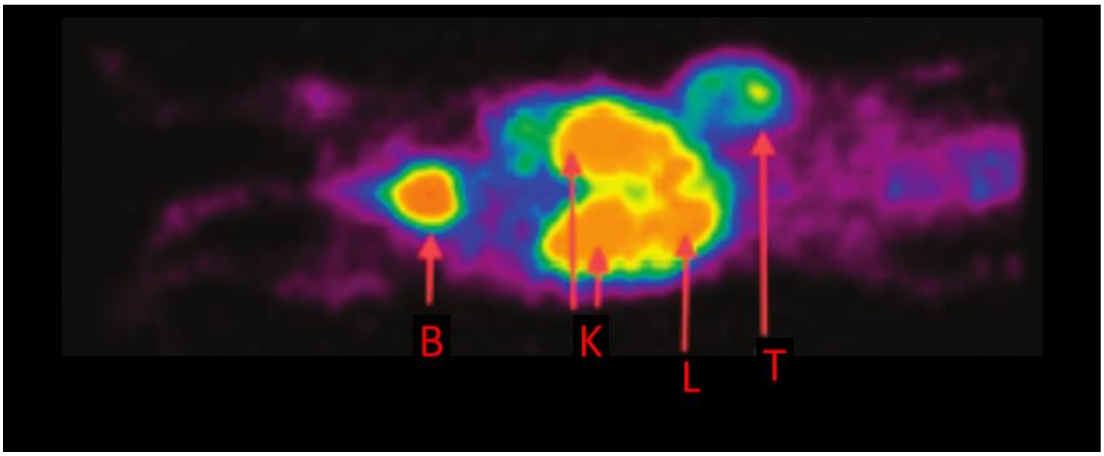

Figure 1.20: Micro-PET scan of a Balb/c mouse with selective uptake of $[^{68}Ga][Ga(SarRGD_2)]^{3+}$ in a 66cl4β3 tumour. PET images were obtained 2 hours post injection of $[^{68}Ga][Ga(SarRGD_2)]$. Image adapted from reference [141].

Zoller and co-workers used a series of tetrapyrrole porphyrins to chelate ^{68}Ga.[63] Although radiolabelling using conventional heating methods was poor (<20% after 30 minutes), microwave assisted radiolabelling was more successful, with two water soluble porphyrins, L_1 and L_2 (Figure 1.21), being labelled with a 69% and 49% yield in 5 and 7 minutes respectively. Extending the reaction time resulted in a reduced yield due to degradation of the ligand. Three lipophilic porphyrins were also tested, with radiolabelling being undertaken from $[^{68}Ga][Ga(acac)_3]$ in chloroform. Microwave heating was again required, with L_3 achieving an 82% yield and L_4 an 83% yield in 5 minutes. L_5 only achieved a 42% yield after 7 minutes microwave irradiation. L_1, L_3 and L_4 were assessed for their *in vitro* stability with little transchelation by transferrin being reported. However, in serum only the lipophilic porphyrins were stable – L_1 degraded with half of the activity being displaced in 72 minutes. This was speculated to be due to metabolism of the radiotracer. Despite this, $[^{68}Ga][Ga(L_1)]$ was applied *in vivo*; the maximum tumour to tissue ratio was achieved after only 7 minutes; following this the activity accumulated in the kidneys and bladder.

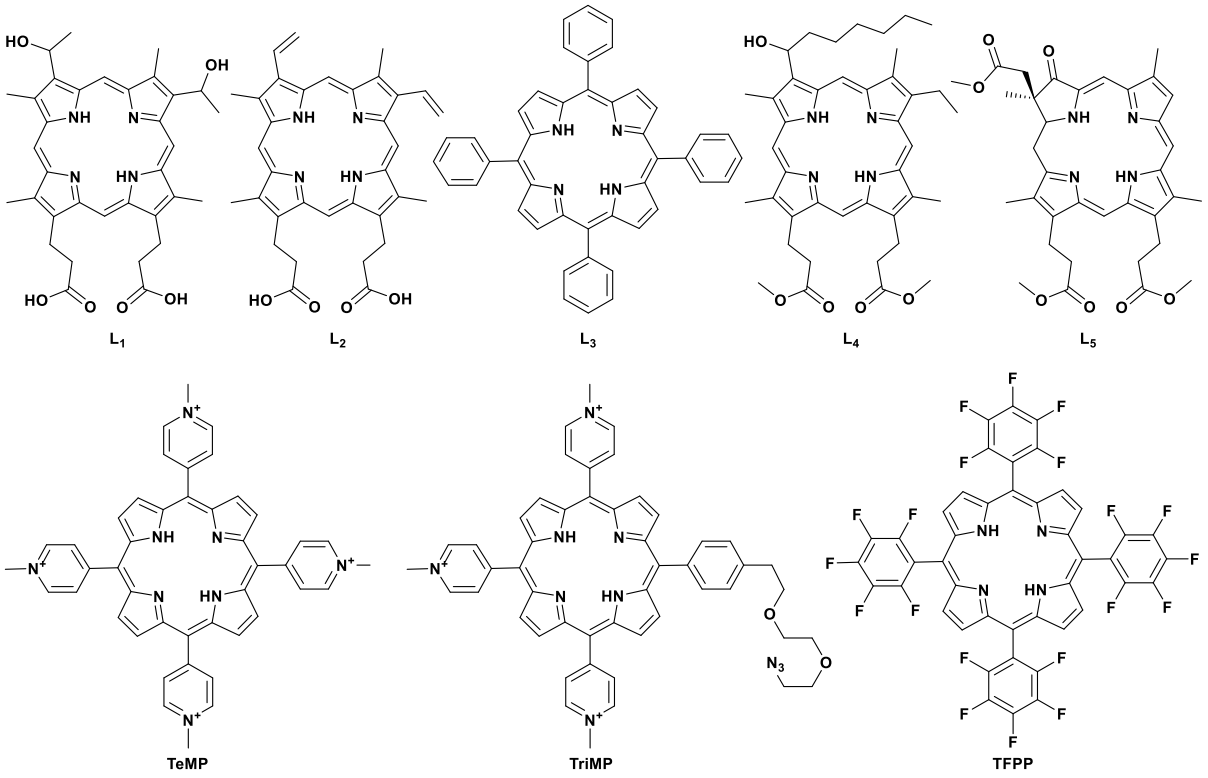

Figure 1.21: Structures of porphyrins.

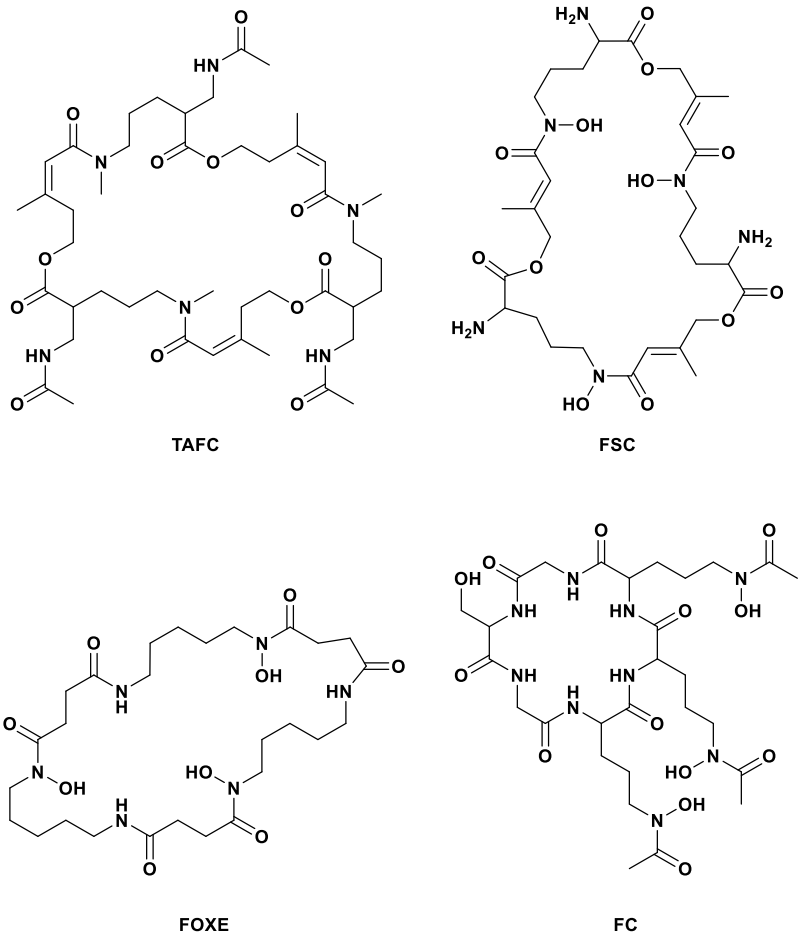

Figure 1.22: Structures of siderophores.

Bhadwel and co-workers demonstrated that 4,4',4'',4'''-(porphyrin-5,10,15,20-tetrayl)tetrakis(1-methylpyridin-1-ium) (TeMP, Figure 1.21) was capable of complexing ^{68}Ga at pH 4; a 90% yield was achieved after 45 minutes with conventional heating at 90 ^{o}C.[142] Bryden

and co-workers radiolabelled a bifunctional analogue, 4,4',4''-(20-(4-(2-(2-(2-azidoethoxy)ethoxy)ethyl)phenyl)porphyrin-5,10,15-triyl)tris(1-methylpyridin-1-ium) (TriMP, Figure 1.21), with >95% radiochemical yield in just 5 minutes through microwave irradiation; longer reaction times resulted in increased levels of impurities.[143] Fazaeli and co-workers radiolabelled a similar system; 5,10,15,20-tetrakis(perfluorophenyl)porphyrin (TFPP, Figure 1.21) was radiolabelled with ^{68}Ga in 10% ethanol at pH 5.5 by refluxing for 60 minutes, achieving a 97% yield.[144] Both [^{68}Ga][Ga(TeMP)] and [^{68}Ga][Ga(TFPP)] were shown to be stable to serum for over 2 hours.[142,144]

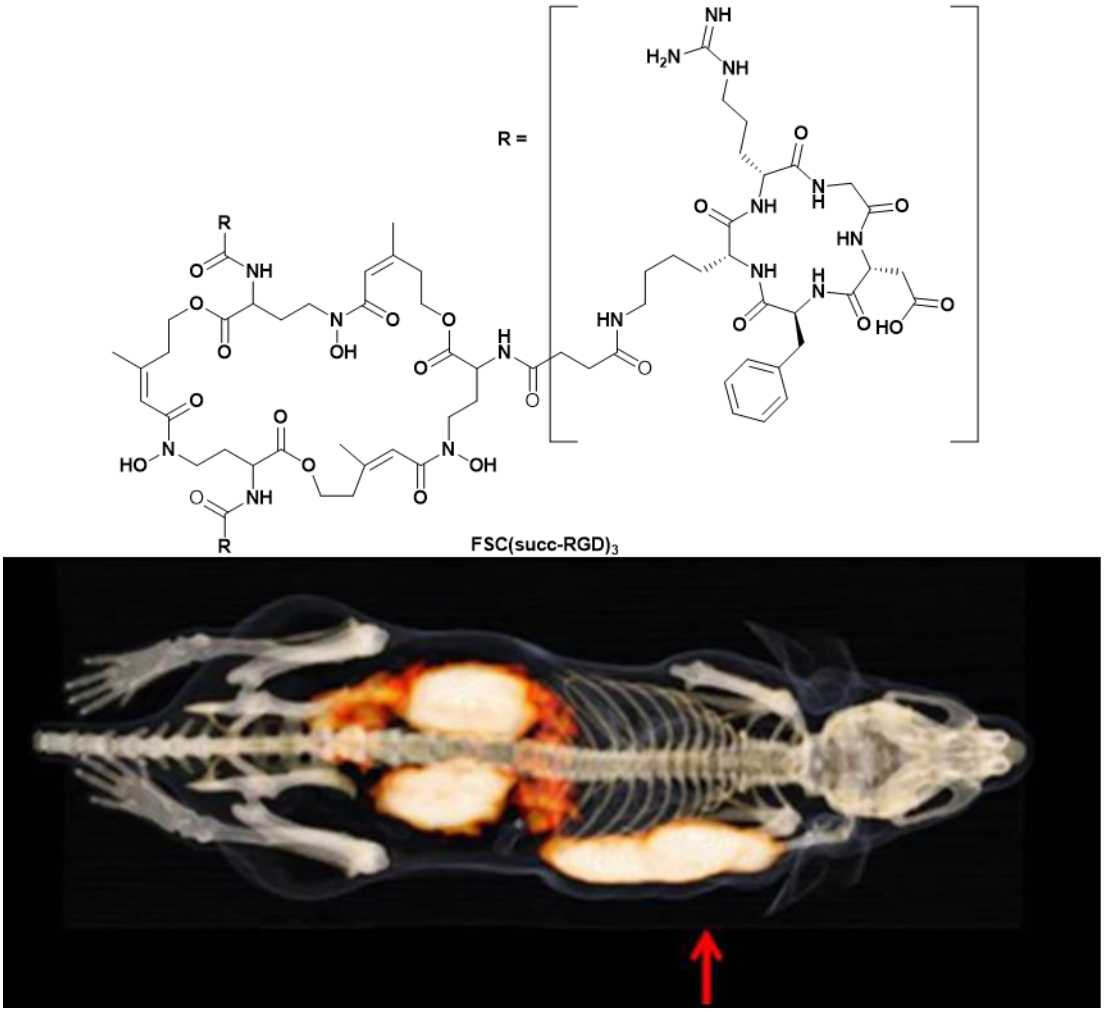

Figure 1.23: Three-dimensional volume projections of fused microPET/CT static images of a nude mouse bearing a M21 xenograft tumours at 1 hour post injection of [^{68}Ga][Ga(FSC(succ-RGD)$_3$)]. Red arrow indicates integrin $\alpha_v\beta_3$-positive M21 tumour. Image adapted from reference [145].

A number of siderophores (Figure 1.22), have been tested for their suitability as Ga(III) chelators by Decristoforo and co-workers.[146–148] As Fe(III) binding compounds it can be expected that these chelators will also bind Ga(III) efficiently due to their similar properties (Table 1.2). Triacetylfusarine (TAFC) was labelled with ^{68}Ga at room temperature in 15 minutes,[148] and was shown to be stable to serum over 2 hours.[127,148,131] Ferrioxamine E (FOXE) required more strenuous conditions for efficient radiolabelling, with heating to 80 ^{o}C for 20 minutes required for 95% complexation; however the resulting complex was more than 99% stable in serum over 2 hours.[148] Ferricrocin (FC) was radiolabelled at pH 3.9, achieving a 95% yield in 10 minutes at

room temperature.[146] The resulting complex was stable to serum, but 20% of the ^{68}Ga was displaced by excess Fe(III) after 2 hours.[146] Fusarine C (FSC) was shown to be a versatile chelator – with effective labelling of a trimeric RGD conjugate, FSC(RGD)$_3$, from pH 3 to 8 at room temperature by 45 μM siderophore (Figure 1.23).[151] [^{68}Ga][Ga(FSC)] was demonstrated to be stable to serum over 2 hours.[147]

1.5.1.4 Development of macrocycles for ^{68}Ga complexation

Much of the development of ^{68}Ga as a PET imaging tool has been undertaken using conjugates of DOTA as chelating agents. This has resulted in approval of [^{68}Ga][Ga(DOTATATE)] as a somatostatin receptor targeting agent for the diagnosis of neuroendocrine tumours and highlights the viability of ^{68}Ga PET imaging as a clinical technique.

[^{68}Ga][Ga(DOTA)] conjugates have been applied to imaging a wide variety of targets, this demonstrates the versatility of metal based PET imaging as a technique, with minimal modification required for preliminary studies into imaging a given target once an inhibitor has been identified.

The versatility of DOTA as a chelating agent is a further advantage of this system;[102] the same conjugate can be applied to imaging with other metals if the half-life of ^{68}Ga proves to be too short, a therapeutic metal radionuclide (such as β^- emitter ^{177}Lu)[152,153] can be substituted in to give a diagnostic/therapeutic pair, and many previously developed DOTA conjugates that have been applied to other metals can be applied to ^{68}Ga imaging.

These properties make DOTA a useful chelator for ^{68}Ga imaging, and it will likely continue to be employed in this role. However, DOTA is not the ideal chelator for ^{68}Ga. The complexation conditions required for efficient radiolabelling with ^{68}Ga are harsh, requiring heating under acidic conditions. The resulting complex is sufficiently stable for imaging purposes, but the reported instability to serum is not ideal.

The application of NOTA to ^{68}Ga complexation is a simple development that optimises the chelator size for Ga(III). This chelator has proven to be capable of radiolabelling with ^{68}Ga without the requirement for heating. Furthermore, the resulting complex is reported to be more stable to serum challenges. However, NOTA is more difficult to conjugate to peptides than DOTA as it does not have an excess of coordinating arms upon complexation of Ga(III). As such, bifunctional derivatives must be prepared for conjugation to targeting motifs.

Further refinement of the NOTA chelator, yielding the phosphonate based TRAP and NOPO ligands, has produced highly specific chelators for Ga(III). This is reflected in the thermodynamic stabilities of the resulting Ga(III) complexes in comparison to other metals. In terms of radiolabelling, the TRAP chelators were shown to be more tolerant of metal impurities; however the importance of this is reduced as ^{68}Ge/^{68}Ga generator technology improves. A key advantage

of the TRAP chelators is that the phosphonate units can be modified to incorporate additional functionalities. This results in bifunctional chelators that can be conjugated without requiring extensive protecting strategies and still retain their coordinating core.

Incorporation of ^{68}Ga into other macrocycles, such as porphyrins and siderophores, has not been as widely explored. The highly constrained porphyrin core is difficult to radiolabel, with microwave heating required for efficient radiolabelling with ^{68}Ga. Radiolabelling porphyrins through conjugation to chelators that are more suitable for ^{68}Ga has been shown to be a more effective route to radiolabelling these species.[154,155] While a number of siderophores have been radiolabelled with ^{68}Ga, they are not widely applied, possibly due to their complex structures. The high affinity of the siderophores for Fe(III) remains an issue, with transmetallation of ^{68}Ga seen in the presence of excess Fe(III).

Overall, the use of macrocyclic chelators for ^{68}Ga will likely continue to favour DOTA due to its widespread availability and use. The improved characteristics of NOTA in terms of radiolabelling conditions and stability will be hampered by the more difficult conjugation of this chelate to a targeting motif – however the phosphinate derivatives will likely find increased use as they overcome this issue.

1.5.2 Non-macrocyclic Chelators

In recent years there has been a shift towards acyclic ligands for the chelation of ^{68}Ga. This movement away from macrocyclic chelators is due to the aims of rapid radiolabelling under mild conditions – room temperature and neutral pH – and at a low ligand concentration.[156]

1.5.2.1 HBED

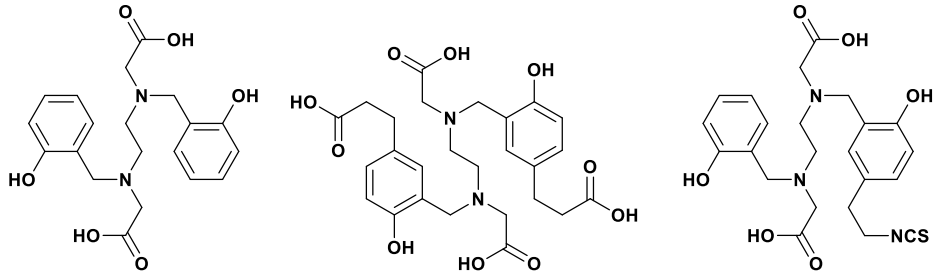

Figure 1.24: Structure of HBED chelators.

2,2'-(Ethane-1,2-diylbis((2-hydroxybenzyl)azanediyl))diacetic acid (HBED) has proven effective for the complexation of Ga(III) due to the hard oxygen donors of its phenol arms; the resulting complex has a high thermodynamic stability ($\log K_{[Ga(HBED)]}$ = 39.57),[157] even greater than macrocycles such as DOTA ($\log K_{[Ga(DOTA)]}$ = 26.1)[9] and NOTA ($\log K_{[Ga(NOTA)]}$ = 29.60).[105,122] This stability is further realised *in vitro* with no release of ^{67}Ga seen from the [^{67}Ga][Ga(HBED)] complex in 48 hours; and less than 1% over 7 days.[158] Under the same

conditions [^{67}Ga][Ga(NOTA)] released 3% of the activity over 7 days.[158] Whilst these time points are excessively long for ^{68}Ga imaging they highlight the kinetic stability of the [Ga(HBED)] complexes.

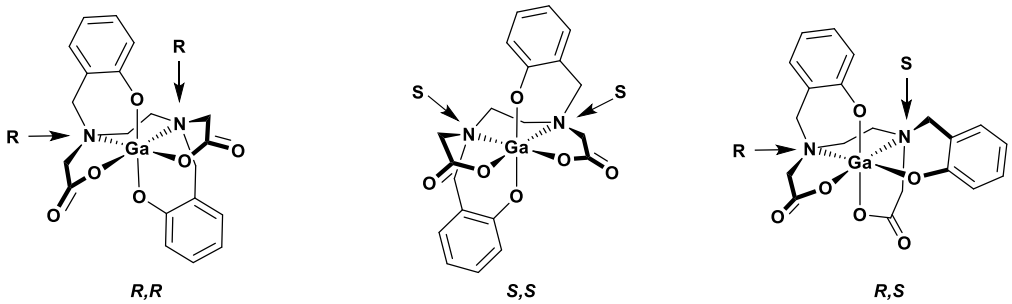

R,R *S,S* *R,S*

Figure 1.25: Proposed structures of [Ga(HBED)] diastereomers.

Whilst HBED has been labelled efficiently with ^{68}Ga at room temperature,[158–163] questions have been raised regarding the formation of diasteromers upon complexation (Figure 1.25).[158,164–166] Three NMR distinguishable diastereomers were identified by Schuhmacher and co-workers upon complexation of Ga(III) by HBED-Cl;[165] the conditions for complex formation had an impact upon the ratio of the diastereomers formed.[164] Preparation of [Ga(HBED)] at ligand concentrations below 2 mM under acidic conditions (pH 3-3.5) followed by neutralisation yielded a single diastereomer whereas higher ligand concentrations and at pH 7.0 all three diastereomers were formed.[164]

The absolute configuration may affect the affinity of the radiolabelled conjugate for the target receptor. Eder *et al*. explored this; radiolabelling a prostate specific membrane antigen (PSMA) targeting conjugate, (Glu-urea-Lys-Ahx)-HBED-CC at room temperature and at 95 °C yielded different ratios of diastereomers (48% and 89% the thermodynamically favoured product, respectively), however no difference was seen in the receptor uptake when the different ratios were used.[158] Whilst this suggests that the different diastereomers do not negatively affect the radiotracer it is would still be preferable to form only a single species.

1.5.2.2 Dedpa

The Orvig group have developed an acyclic chelator, 6,6'-((ethane-1,2-diylbis(azanediyl))bis(methylene))dipicolinic acid (dedpa), for ^{68}Ga based on ethylenediamine with two picolinic acid arms added.[37] This chelator was shown to be highly capable for the complexation of ^{68}Ga; quantitative labelling was achieved at room temperature in 10 minutes at pH 4, even at low ligand concentrations (10^{-7} M).[37] The resulting species was reported to be stable to *apo*-transferrin with no decomplexation seen over 2 hours;[37] however later studies revealed that [^{68}Ga][Ga(dedpa)] is partially decomplexed in serum with only 78% remaining intact after 2 hours incubation.[167]

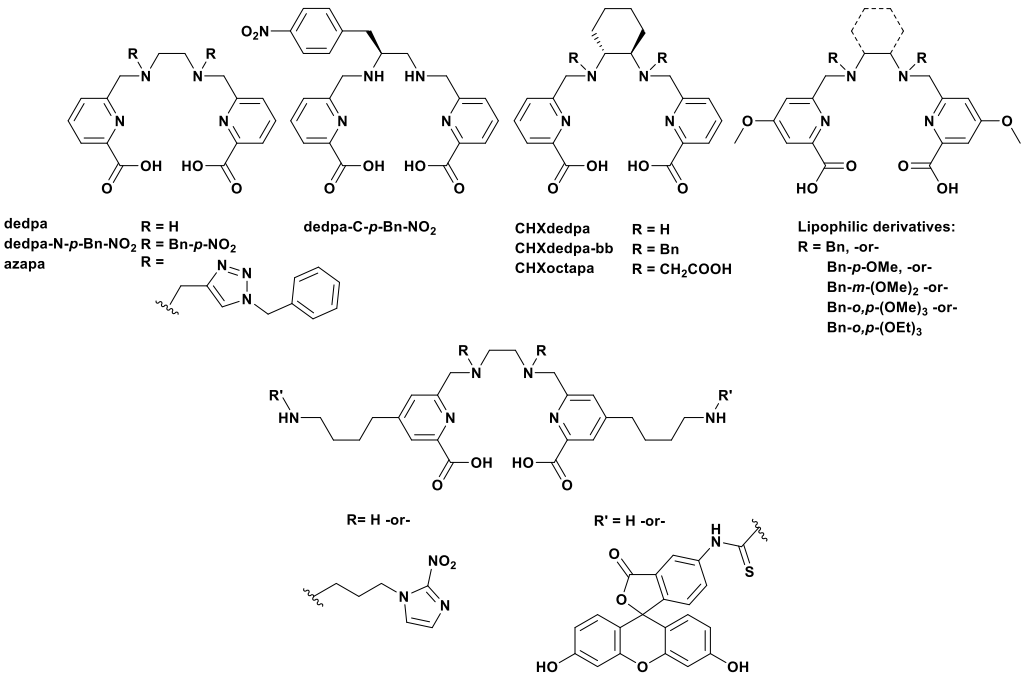

Figure 1.26: Structure of dedpa chelators.

Attempts to develop bifunctional derivatives of dedpa had mixed results – the site of functionalisation was shown to be critical to the stability of the resulting ^{68}Ga complex.[37] When functionalised through the secondary amines, the resulting complex was much less stable to transferrin, with 49% of the activity being displaced from the [^{68}Ga][Ga(dedpa-N-*p*-Bn-NO_2)] complex.[37] Functionalisation through the carbon backbone was more successful – with only 3% of the activity being decomplexed by *apo*-transferrin after 2 hours incubation.[37] When the chelator is conjugated to c(RGDfK) (Figure 1.27) this trend is again seen; functionalisation through the backbone results in a complex with 92% stability to transferrin over 2 hours whereas functionalisation *via* the coordinating nitrogen (Figure 1.28) results in a complex with only 73% stability over 2 hours.[168] Despite incorporating two targeting units, the amine functionalised dedpa derivative (Figure 1.28) did not show significantly enhanced tumour uptake compared to the backbone functionalised derivative. When alkynes were incorporated into the dedpa scaffold by addition to the secondary amines, the chelator could undergo azide-alkyne reactions.[169] The resulting triazole functionalised dedpa ligand, 6,6'-((ethane-1,2-diylbis(((1-benzyl-1H-1,2,3-triazol-4-yl)methyl)azanediyl))bis(methylene))dipicolinic acid (azapa), was readily radiolabelled, however the complex formed was poorly stable with only 52% of activity being retained after 2 hours incubation in serum at room temperature.[169]

This is not a general rule however; when lipophilic derivatives were prepared by adding benzyl units to the secondary amines and further modifying the structure with methoxy groups the resulting complexes had differing stabilities.[170] Whilst the least modified structures had poor stability to transferrin, with as little as 66% of the activity being retained, the most lipophilic had much greater stability with 93% of the activity being retained despite the functionalisation of the secondary amine.[170] This was speculated to be due to repulsion from the polar binding

pocket of transferrin preventing effective competition.[170] When nitroimidazole derivatives were prepared for hypoxia imaging the nature of the nitroimidazole and the length of the linker was shown to impact the stability. Despite all compounds tested being functionalised through the secondary amine sites those with propyl linkers were more stable than those in with shorter ethyl linkers; two of the propyl linked nitroimidazole dedpa derivatives were stable to transferrin with no decomplexation seen over 2 hours.[62] Orvig and co-workers also explored functionalisation *via* the pyridyl ring; incorporation of an alkyl chain in the 4 position of the two pyridine arms did not hamper radiochemistry with >99% yields reported in 10 minutes at room temperature.[171] The resulting complex was reasonably stable to transferrin, with 93% of the activity being retained in the complex after 2 hours incubation.[171] However, when these chains were conjugated to fluorescein no radiolabelling was observed, even after heating at 85 °C for an extended period of time (1 hour).[171]

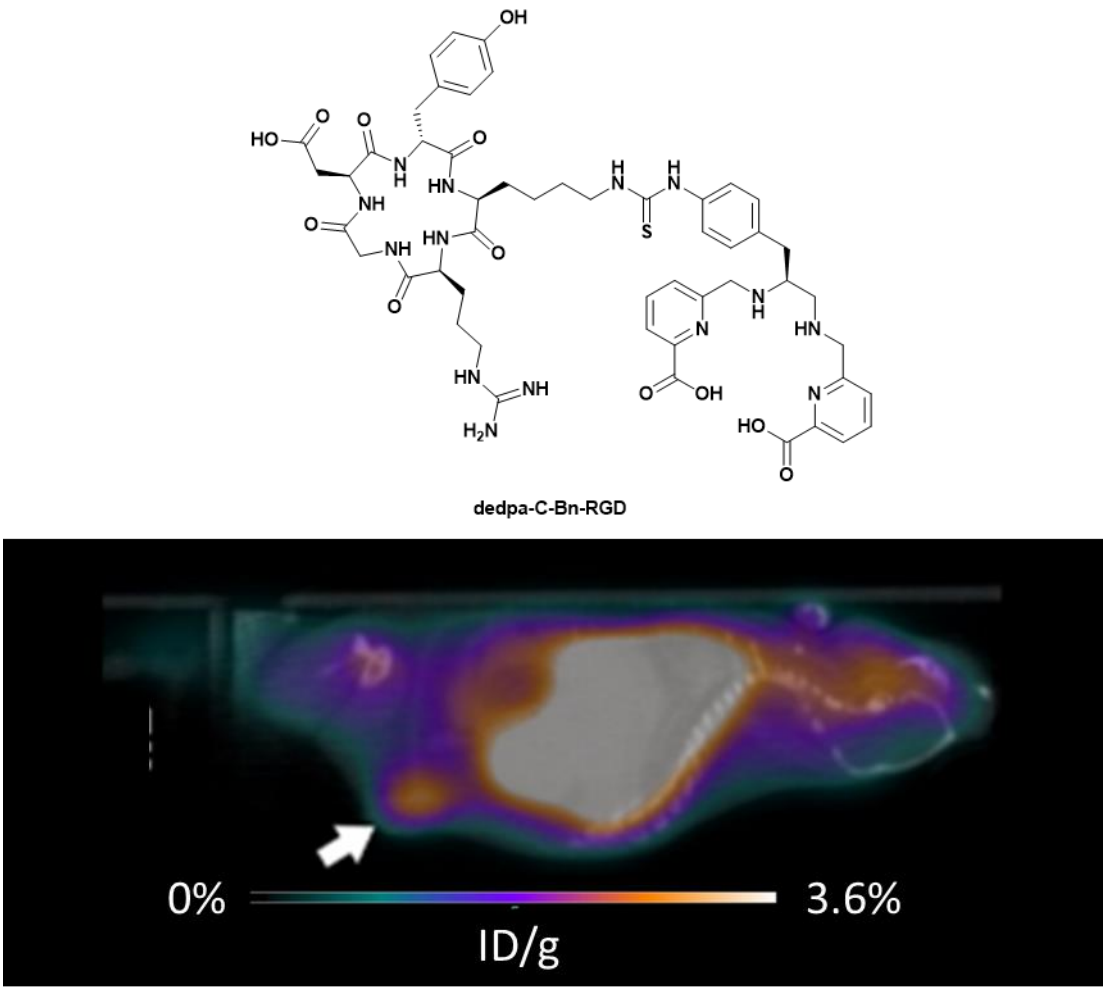

Figure 1.27: PET/CT overlaid images of RAG2M mice bearing U87MG human glioblastoma xenographs. 1.5 – 2 hours post injection with [^{68}Ga][Ga(dedpa-C-Bn-RGD)]. Tumour masses are indicated by white arrows. Image adapted from reference [168].

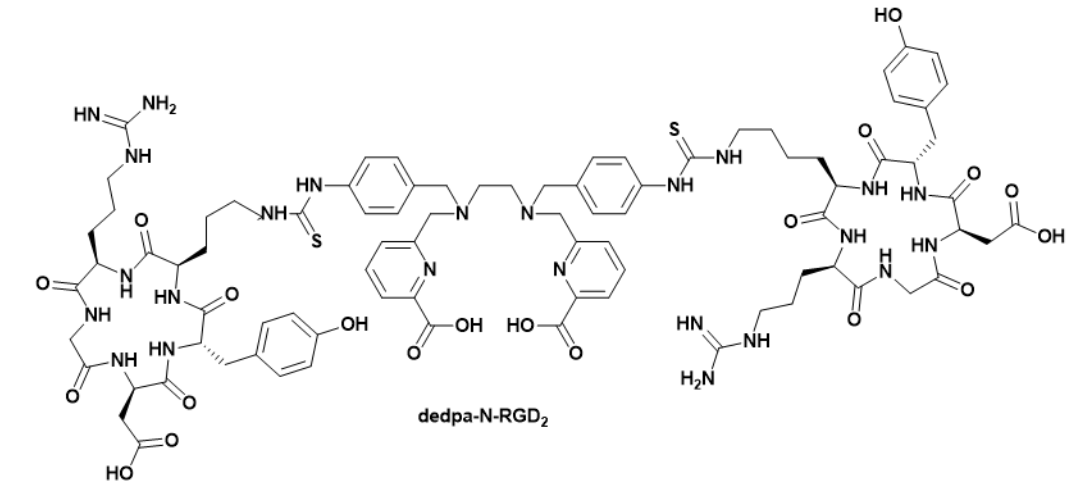

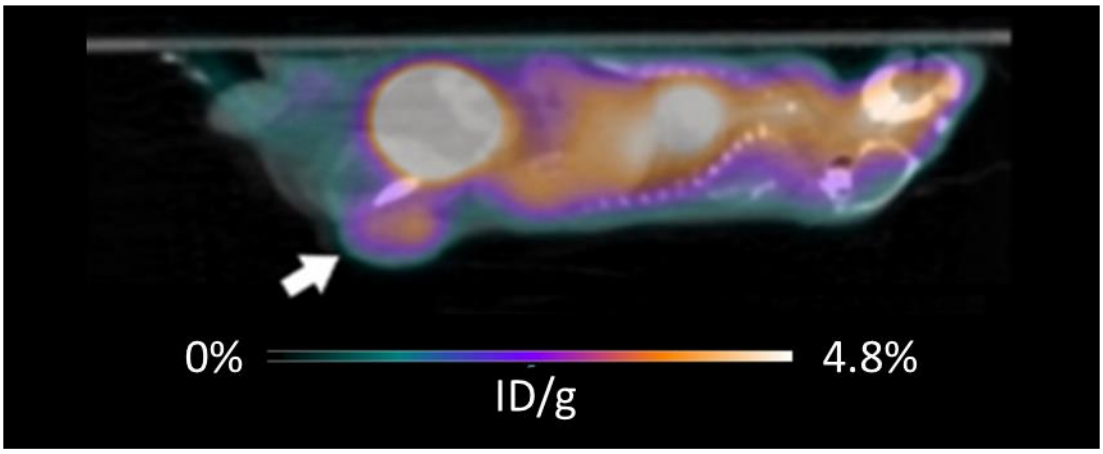

Figure 1.28: PET/CT overlaid images of RAG2M mice bearing U87MG human glioblastoma xenographs. 1.5 – 2 hours post injection with [^{68}Ga][Ga(dedpa-N-RGD$_2$)]. Tumour masses are indicated by white arrows. Representative intensity scales are indicated. Image adapted from reference [168].

Seeking to improve the serum stability of [^{68}Ga][Ga(dedpa)], Orvig and co-workers increased the rigidity of the ligand by incorporating a cyclohexane unit into the ethylenediamine backbone.[167] The resulting chelator, 6,6'-((cyclohexane-1,2-diylbis(azanediyl))bis(methylene))dipicolinic acid (CHX-dedpa), was capable of complexing ^{68}Ga at room temperature, with quantitative radiolabelling being reported by 10^{-5} M ligand in 10 minutes.[167] The serum stability was improved; 91% of the activity was retained in the complex after 2 hours incubation at 37 °C. Again; functionalisation through the secondary amines reduced the stability of the resulting complex. Addition of benzyl units reduced the stability to 83% and addition of acetate arms resulted in a stability of just 73%. The acetate functionalised ligand, 6,6'-((cyclohexane-1,2-diylbis((carboxymethyl)azanediyl))bis(methylene))dipicolinic acid (CHX-octapa), also displayed worse radiolabelling kinetics than CHX-dedpa; 10^{-6} M CHX-dedpa was able to achieve 96% radiochemical yields after 30 minutes heating at 60 °C whereas H_4CHX-octapa was only able to achieve 72% yields when heated to 70 °C for 1 hour at this concentration.[167] Nitroimidazole derivatives of CHX-dedpa were shown to produce more stable ^{68}Ga complexes than those with non-cyclic backbones; the least stable example reported was 86% stable to transferrin with a linear backbone but 92% stable with the cyclic backbone.[62]

Lipophilic derivatives of CHX-dedpa have also been reported; again functionalisation through the secondary amine reduced the complex stability with 15-20% decomposition by transferrin. The most functionalised derivatives formed multiple species in the radiolabelling mixture; this was shown to not be due to radiolysis but the identity of these species could not be determined.[172]

1.5.2.3 AAZTA

Waldron *et al*. applied 2,2'-((1,4-bis(carboxymethyl)-6-methyl-1,4-diazepan-6-yl)azanediyl)diacetic acid (AAZTA, Figure 1.29) to the complexation of ^{68}Ga;[173] they found that the chelator rapidly complexed ^{68}Ga with >95% incorporation of the activity within 1 minute at room temperature.[173] This high yield was achieved under both acidic (pH 4.0) and neutral conditions (pH 6.8).[173] However, multiple species were formed; this is likely due to the excess number of coordinating arms of AAZTA relative to 6 coordinate Ga(III). When Waldron and co-workers assessed the stability of [^{68}Ga][Ga(AAZTA)] in a competition study with transferrin they found that the minor products were less stable than the main product.[173] Despite this instability, the attractive complexation kinetics of AAZTA have prompted further investigation; Manzoni *et al* applied a bifunctional derivative of AAZTA to cholecystokinin receptor 2 (CCK2) imaging by conjugating it to a tricyclic RGD derivative, DB58.[174] Following radiolabelling under acidic conditions, the pH was adjusted to 7.4 with no degradation observed.[174] In contrast, an analogous radiotracer with DTPA as the coordinating unit was shown to be completely demetallated upon neutralisation.[174] The [^{68}Ga][Ga(AAZTA-DB58)] radiotracer was applied *in vivo* with greater uptake in CCK2 expressing tumours at later time points (40-150 minutes) than [^{68}Ga][Ga(AAZTA)].[174] Pfister and co-workers have also applied an AAZTA conjugate to CCKR2 imaging;[175] the selected minigastrin motif is readily degraded[176] leading to loss of receptor binding. As a result the use of [^{68}Ga][Ga(DOTA)] would be unsuitable; however AAZTA is a potential chelator for this targeting motif as heating is not required for efficient radiolabelling.[173] The AAZTA-minigastrin conjugate was radiolabelled at pH 4.5 in 10 minutes at room temperature achieving a 95% radiochemical yield.[175] In contrast to the report by Waldron *et al*., no additional radiolabelled products were seen.[173,175] The resulting radiotracer was found to be reasonably stable to serum – 81% of the activity was retained within the complex after 2 hours incubation;[175] this is comparable to reports for [^{68}Ga][Ga(DOTA)] systems.[107]

In a bid to improve the stability of the resulting ^{68}Ga complex, Vágner and co-workers increased the rigidity of the chelator by incorporating a cyclohexane motif into the backbone.[177] The resulting chelator, 2,2'-((1,5-bis(carboxymethyl)-3-methyldecahydro-1H-benzo[b][1,4]diazepin-3-yl)azanediyl)diacetic acid (CyAAZTA, Figure 1.29), was found to have a similar thermodynamic stability with Ga(III) to AAZTA ($\log K_{[Ga(AAZTA)]}$ = 22.2,[178] $\log K_{[Ga(CyAAZTA)]}$ = 21.4[177]). However, when incubated with serum no transmetallation was observed over 90 minutes demonstrating an improved kinetic stability.[177] Unfortunately, the increased rigidity

reduced the radiolabelling kinetics of the system; radiochemical yields greater than 95% were only achieved by CyAAZTA when the system was heated to 90 °C.[177] At lower temperature (25 °C and 37 °C) 80% radiochemical yields were achieved by 10 µM of CyAAZTA.[177]

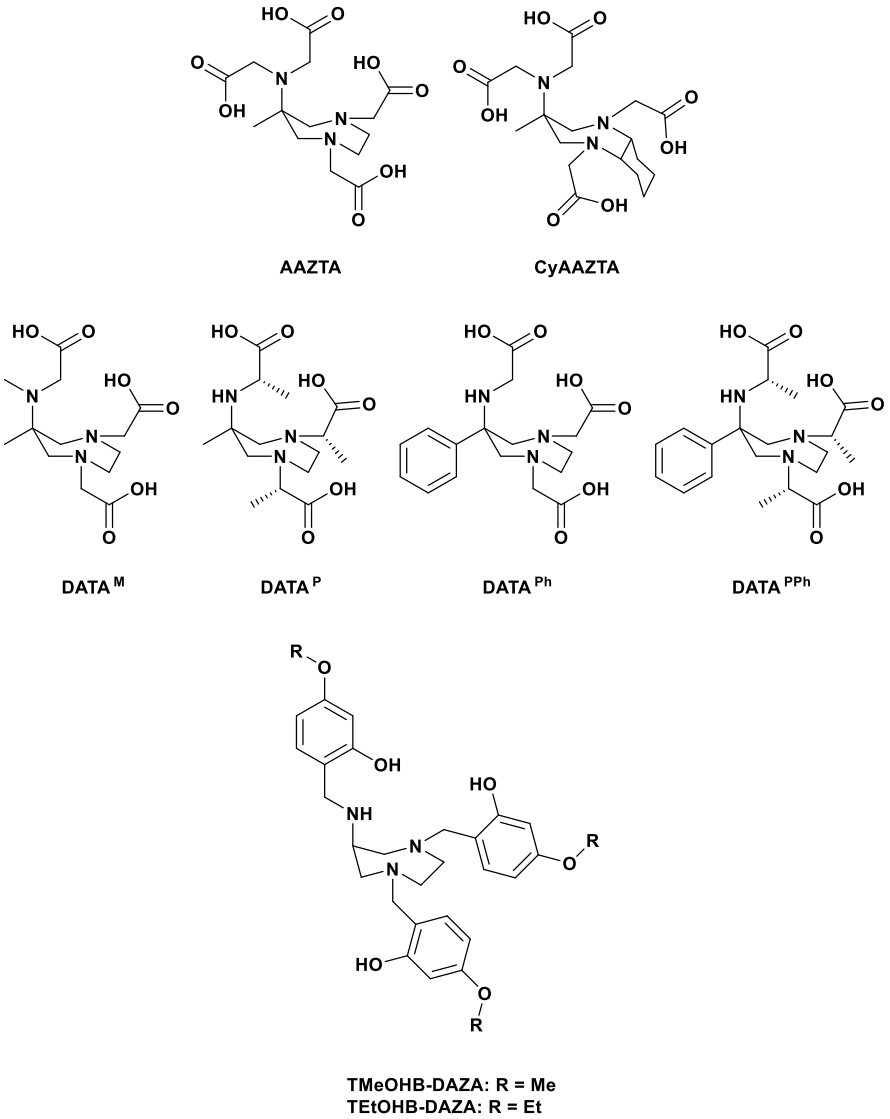

Figure 1.29: Structure of AAZTA-like ligands.

Waldron and co-workers reduced the number of coordinating arms of AAZTA to produce a tailored system of chelators with a 2,2'-(6-((carboxymethyl)amino)-1,4-diazepane-1,4-diyl)diacetic acid (DATA) core (Figure 1.29). By varying the substituents of the quarternary carbon the rigidity of the chelator was changed; importantly this modified the favoured geometry. Whilst the methyl substituent of AAZTA, DATA^{M} and DATA^{P} is insufficiently sterically bulky to promote the ideal geometry for Ga(III) coordination, the bulkier phenyl group of DATA^{Ph} and DATA^{PPh} improves the preorganisation of the chelator for metal coordination. All four DATA chelators were able to be radiolabelled efficiently with ^{68}Ga under a range of conditions.[173,179] Seemann and co-workers thoroughly explored the radiolabelling conditions required with a view to developing a "kit-type" system for ^{68}Ga radiolabelling. They found that the bulkier systems, DATA^{Ph} and DATA^{PPh}, had a reduced radiochemical yield (95-96%) compared to the methyl substituted systems (98-99%) at very short reaction times (1 minute).[179] However when the

reaction was allowed to proceed at pH 5 at 25 °C all four chelators achieved >98% radiochemical yields after 10 minutes.[179] The substituents also affected the radiolabelling of the DATA chelators at different pHs. At pH 4 $DATA^{P}$ achieved a radiochemical yield >95% within 1 minute, however the other 3 chelators required a reaction time of 15 minutes under these conditions to achieve the same radiochemical yield.[179] In contrast, at pH 7 only $DATA^{PPh}$ achieved a radiochemical yield >95% after 10 minutes.[179] $DATA^{M}$, $DATA^{P}$ and $DATA^{Ph}$ only achieved a radiochemical yield of 85% after 15 minutes.[179] All four chelates were stable to transferrin,[179] however when incubated with foetal bovine serum Waldron *et al* report some instability of $DATA^{M}$ but $DATA^{P}$, $DATA^{Ph}$ and $DATA^{PPh}$ were all seen to be completely stable after 2 hours.[173] Waldron and co-workers also reported that $DATA^{M}$ formed two species when radiolabelled;[173] however this was not seen by Seemann *et al*.[179] This may contribute to the instability seen by Waldron *et al*, mirroring that seen with [^{68}Ga][Ga(AAZTA)].[173] The $DATA^{M}$ system has been developed to form a bifunctional chelator and conjugated to the TOC targeting unit.[180,181] Waldron and co-workers demonstrated that high radiochemical yields could be achieved by the conjugated system under acidic conditions (pH 4-5).[181] 13 nmol of DATA-TOC was able to achieve radiochemical yields >95% rapidly, although the time required for this was dependent on the ^{68}Ga post-processing technique achieved all methods tested allowed for production of the radiotracer with 10 minutes incubation.[181] The resulting system was stable to serum, with 98% of the activity being retained after 2 hours in contrast to the previous report by Waldron *et al*.[173,181]

Greiser and co-workers report a pair of chelators based on the same scaffold as DATA that incorporate phenolic arms instead of acetic acid arms.[182] These chelators, 6,6'-((6-((2-hydroxy-4-methoxybenzyl)amino)-1,4-diazepane-1,4-diyl)bis(methylene))bis(3-methoxyphenol) (TMeOHB-DAZA) and 6,6'-((6-((2-hydroxy-4-ethoxybenzyl)amino)-1,4-diazepane-1,4-diyl)bis(methylene))bis(3-ethoxyphenol) (TEtOHB-DAZA, Figure 1.29), formed more than one diastereomer upon complexation of Ga(III). Following radiolabelling with ^{68}Ga under relatively harsh conditions (pH 3.8-4.0, 100 °C, 5 minutes), the radiolabelled complexes were applied to *in ovo* imaging and showed rapid liver uptake in an ostrich egg model.[182] The complexes were reported to be highly stable, with more than 99% radiochemical purity after 4 hours incubation in serum.[182]

1.5.2.4 THP

Inspired by iron scavengers such as deferiprone, the 4-amino-N1,N7-bis((3-hydroxy-1,6-dimethyl-4-oxo-1,4-dihydropyridin-2-yl)methyl)-4-(3-(((3-hydroxy-1,6-dimethyl-4-oxo-1,4-dihydropyridin-2-yl)methyl)amino)-3-oxopropyl)heptanediamide (THP, Figure 1.30) ligand combines three hydroxypyridinone motifs into a single structure.[183,184] The hydroxypyridinone units have long been recognised as effective iron complexing agents and due to the similar coordinating properties of Fe(III) and Ga(III) they translate readily into Ga(III) complexing agents.[183] The THP ligands have been shown to radiolabel with ^{68}Ga very rapidly at high pH –

Berry and co-workers reported quantitative complexation in under 5 minutes at pH 6.5 by 10 μM of THP-Ac.[184] The radiolabelled conjugate [^{68}Ga][Ga(THP-TATE)] complex had a high kinetic stability with <2% transchelation seen in serum after 5 hours.[185]

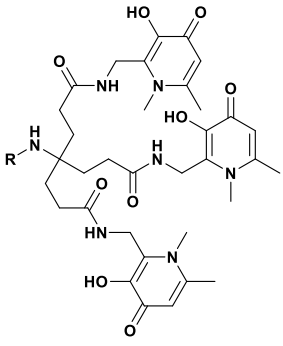

Figure 1.30: Structure of THP chelators.

The branching nature of the THP ligands has been expanded to form the multimeric conjugates THP-RGD$_3$, featuring one chelating unit and three $\alpha_v\beta_3$ binding motifs, and THP$_3$-RGD$_3$, featuring three chelators and three $\alpha_v\beta_3$ binding motifs.[186] Comparison of these multimers to the monomeric THP-PhNCS-RGD (Figure 1.31)[187] gave mixed results; whilst a higher specific activity was achieved by THP$_3$-RGD$_3$ than the mono-chelator analogues this had a much greater non-target uptake *in vivo* in the liver, muscle, spleen and lung. Whilst the multimers had worse receptor bindings (IC_{50}(THP-Ph-NCS-RGD) = 46 nM, IC_{50}(THP-RGD$_3$) = 73 nM, IC_{50}(THP$_3$-RGD$_3$) = 79 nM), the multimers had improved tumour uptake *in vivo* (2.9%, 4.3%, 4.7% of the injected dose, respectively).

The mild radiolabelling conditions required when using THP for ^{68}Ga complexation has been exploited by conjugation to a single chain fragment variant of the anti-PSMA monoclonal antibody J591.[188] This antibody fragment was then labelled under at neutral pH and room temperature with a 97% radiochemical yield after 5 minutes.[188] The resulting product was not pure; 81% of the activity was associated with the desired protein and 14% with its dimer.[188] A further 2% was unidentified product. However, the species formed were stable; no change in speciation was seen after 6 hours incubation in serum.[188] This radiolabelled protein was applied to *in vivo* imaging of a prostate cancer modelling; whilst the uptake in a PSMA expressing tumour was 10 fold greater than in a PSMA negative tumour, the radiotracer also exhibited a high liver uptake and Nawaz *et al.* concluded that overall there was no advantage using this radiotracer when compared to [^{68}Ga][Ga(THP-PSMA)] (*vida infra*) and [^{68}Ga][Ga(HBED-CC-PSMA)].[188] Nonetheless, this represents an exciting development in the potential application of ^{68}Ga radiolabelling to proteins – although care must be taken to ensure that the biological half-life of the selected protein matches the relatively short half-life of ^{68}Ga.

The conjugate of THP with a Glu-Urea-Lys motif has been explored for PET imaging of prostate cancer, targeting PSMA. Young *et al*. reported that the radiolabelled conjugate has a reduced affinity for PSMA than [^{68}Ga][Ga(HBED-CC-PSMA)];[189] however [^{68}Ga][Ga(THP-PSMA)] has been applied *in human*[190–192] due to the favourable labelling properties of THP compared to other chelators. Young and co-workers demonstrated the viability of using THP-PSMA for "kit-type" radiolabelling – preparation of a ^{68}Ga labelled tracer by addition of the raw generator eluent directly to a pre-prepared, dried, vial of reagents.[189] After incubation, the radiolabelling mixture was sufficiently pure and at an appropriate pH for further use *in vitro* and *in vivo* without further manipulation.[189]

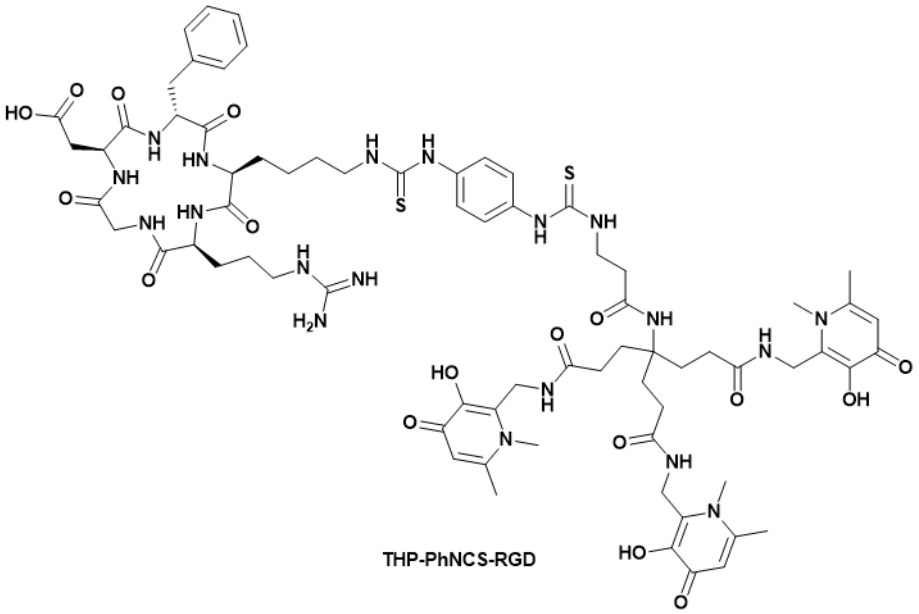

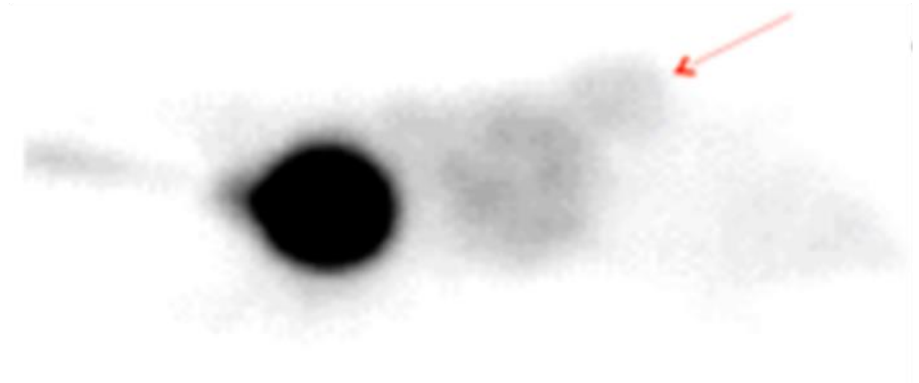

Figure 1.31: Representative PET maximum intensity projection of Balb/c nu/nu mouse bearing a U87MG tumour on right flank, 1 hour post-injection of [^{68}Ga][Ga(THP-RGD)]. Red arrow indicates position of tumour on animal. Image adapted from reference [186].

1.5.2.5 Other non-macrocyclic chelators

Silva *et al*. developed a pair of chelators based on a linear polyamine with additional phenol and heterocyclic coordinating arms.[193] The pyrazole functionalised chelator, $H_2L^{pz*,NH}$ (Figure 1.32), was found to form predominantly the *fac* isomer in solution and in solid state structures.[193] However, this system performed poorly when radiolabelled with ^{67}Ga; radiochemical yields of only 25% were achieved at pH 5 after 15 minutes when high concentrations (1 mM) of ligand were used at high temperature (85 °C).[193] In contrast, $H_2L^{py,NH}$ (Figure 1.32) was more successfully

radiolabelled, achieving yields >95% when 62.5 µM were heated to 85 °C at pH 5.[193] However, when complexed to Ga(III), this ligand produced three species in solution – a mixture of *fac* and *mer* isomers and a 5 coordinate species.[193] When analysed by HPLC only a single species was seen for [^{67}Ga][Ga($L^{py,NH}$)]; this species was found to be stable to *apo*-transferrin with no transmetallation seen over 48 hours.[193] *In vivo* this system was shown to have rapid blood clearance, with excretion *via* the kidneys and hepatobiliary pathways.[193] The complex was shown to be stable *in vivo* by analysis of serum and blood samples and negligible bone uptake.[193]

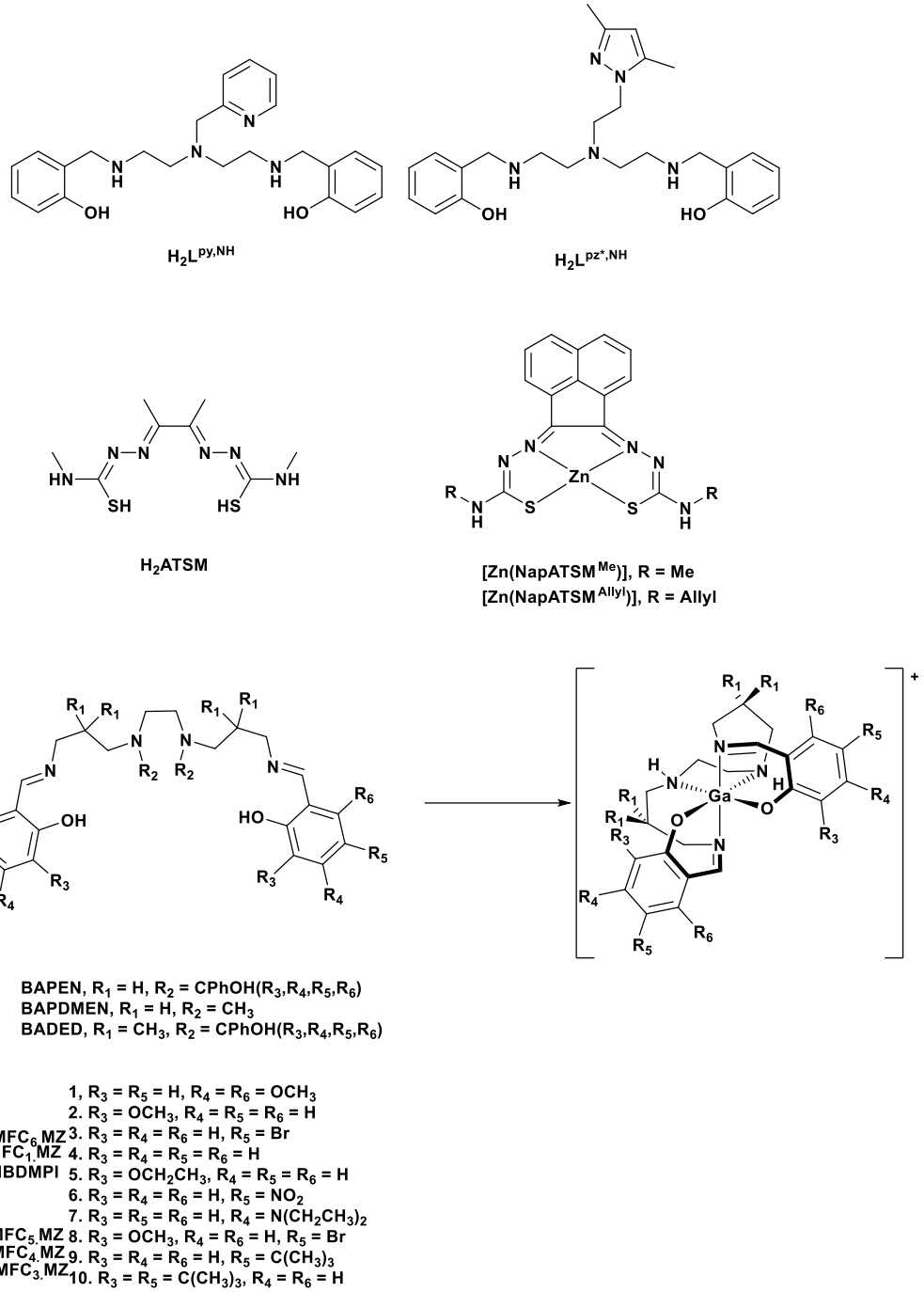

Figure 1.32: Structures of other acyclic chelators.

Arrowsmith and co-workers assessed the thiosemicarbazone (1Z,1'Z)-N',N''''-((2E,3E)-butane-2,3-diylidene)bis(N-methylcarbamohydrazonothioic acid) (ATSM, Figure 1.32) for its Ga(III) complexing abilities.[194] Whilst the complex [Ga(Cl)(ATSM)] could be formed, it was found to decompose within 6 hours in a 10% water/DMSO solution and within 5 minutes in FBS.[194]

Drawing on previous experience with Cu(II) and Zn(II) systems, Arrowsmith and co-workers increased the rigidity of the ligand by incorporating a naphthalene unit into the backbone to yield (1Z,1'Z)-N',N''''-((1E,2E)-acenaphthylene-1,2-diylidene)bis(N-methylcarbamohydrazonothioic acid) (NapATSM, Figure 1.32) ligands; this has previously been observed to increase kinetic stability of the formed complexes.[194] While the ligand could not be isolated, the Zn(II) complex was prepared and transmetallated with Ga(III).[194] The two derivatives tested, [Zn(NapATSM^{Me})] and [Zn(NapATSM^{Allyl})], formed two 5 coordinate species in solution upon complexing Ga(III), [Ga(Cl)(NapATSM$^{Me/Allyl}$)].[194] The complexes formed differ in the identity of the nitrogen atoms coordinated to the Ga(III) cation.[194] The resulting complexes showed an increased stability when compared to [Ga(Cl)(ATSM)], although some decomposition of the complex was reported over 18 hours in FBS.[194] 200 µM [Zn(NapATSM^{Allyl})] was radiolabelled with ^{68}Ga in an ethanolic solution; heating at 90 °C for 30 minutes yielded two radiolabelled products in a 71% radiochemical yield.[194] These products interconverted upon isolation and were assigned to the different isomers previously seen.[194] More recent work by Alam *et al*. resulted in the free ligand being obtained and applied to ^{68}Ga complexation.[195] H_2NapATSM^{Et} achieved similar radiochemical yields to the equivalent Zn(II) complex (58% and 50% respectively after 30 minutes heating at 90 °C in ethanol); however H_2NapATSM^{Allyl} performed significantly worse than [Zn(NapATSM^{Allyl})] under these conditions (36% vs 89%).[195] Importantly, the radiochemical yield achieved by [Zn(NapATSM^{Et})] could be greatly improved through the use of microwave heating; Alam and co-workers report a 96% yield after a 10 minute reaction time under these conditions.[195] The effect of microwave heating on the free ligand was not reported. The resulting complexes were assessed for their stability *in vitro* – with a 75% stability to citrate over 1 hour and 40% to an ethylenediamine-N,N,N',N'-tetraacetic acid (EDTA) solution observed.[195] When applied *in vivo* the activity was rapidly excreted within an hour and a slight liver accumulation reported after 4 hours; this is similar to the distribution seen for non-complexed ^{68}Ga(III).[195] In *in vitro* assays a 53% increased uptake of activity in hypoxic cells compared to normoxic cells when [^{68}Ga][Ga(Cl)(NapATSM^{Allyl})] was applied.[195] This is typically seen for [Cu(ATSM)] type systems[196] but is surprising for the Ga(III) analogue due to the difference in redox behaviour of Ga(III) and Cu(II). As this trend was not seen when [^{68}Ga]$GaCl_3$ was applied to the same assay, this suggests that the ligand, NapATSM^{Allyl}, may have some capacity for targeting hypoxic cells.[195]

The Rösch research group assessed a series of Schiff base ligands (Figure 1.32)– initial assessments by heating 35 µM ligand at 80 °C for 10 minutes in organic or aqueous solutions of ^{68}Ga gave radiochemical yields greater than 87%.[197] Further assessment of a small selection of the ligands (BADED-3, -4, -5, -8, -9, -10) achieved 92% yields by reducing the acetone content of the radiolabelling mixture and increasing the concentration used to 75 µM.[198] The ^{68}Ga complexes formed were generally stable to transferrin and serum competition studies, with >92% stability reported over 1 hour.[197] BAPEN-2 and -3 were exceptions to this; although

stability could evidently be improved by changing the substitution or backbone (BAPEN-1, BAPDMEN-2, -3).[197] These radiotracers were applied to myocardial imaging[197] and to imaging of the p-glycoprotein;[198] the Schiff bases investigated have previously been identified as targeting p-glycoprotein and retain this property upon complexing ^{68}Ga.[198]

1.5.2.6 Summary of development of non-macrocyclic chelators for ^{68}Ga coordination

The more flexible acyclic chelators have generally been radiolabelled with ^{68}Ga under milder reaction conditions than the macrocyclic chelators. However, this often comes at the expense of stability of the resulting complex.

The linear chelator, dedpa, was reported by Orvig *et al.* to be capable of achieving 99% radiochemical yields, without heating, at very low ligand concentrations (10^{-7} M). This results in a radiolabelled complex with high molar activity. However, the stability of the resulting complex was questionable; whilst stable to transferrin, later studies showed that the complex was unstable when subjected to a serum challenge. Furthermore, the design of bifunctional derivatives was not straightforward: conjugation through the secondary amines reduced the complex stability, but conjugation through the carbon backbone was more successful, although more synthetically challenging. Increasing the rigidity of the chelator by incorporating a cyclohexane unit into the carbon backbone improved the stability, but hampered the radiolabelling with higher ligand concentrations (10^{-5} M) required for effective labelling. Overall this chelator system showed some improvement over the macrocyclic chelators in terms of chelator concentration required, but the acidic conditions required for radiolabelling are similar to these used for NOTA labelling whilst the resulting complex is less stable.

The AAZTA ligand has a more rigid structure, based around a cycloheptane ring, but coordinates Ga(III) in an open facing pocket. This results in very rapid complexation of ^{68}Ga (<1 minute reaction times) and the ability to be radiolabelled close to neutral pH (pH 6.8). However, the resulting complex shows some instability to serum challenges (19% decomplexed after 2 hours incubation). This is comparable to DOTA, but worse than NOTA, however the radiolabelling conditions are much milder. This system forms multiple species upon coordination of ^{68}Ga, this is another issue that is faced by the more flexible non-macrocyclic systems that can form multiple conformations upon complexation of Ga(III). Further optimisation of the system reduced the number of products formed and improved the stability of the resulting complex by reducing the number of chelating arms and locking the 7-membered ring with sterically bulky units. Increasing the rigidity by incorporating a cyclohexane ring improved the stability of the Ga(III) complex, but significantly hampered the radiolabelling effectiveness of the system.

HBED has been shown to form highly stable ^{68}Ga complexes. This chelator has not been widely explored, although it has recently been shown to produce PSMA targeting conjugates with high specificity when conjugated to a glu-urea-lys motif (*vida infra*). While this chelator has

been reported to be capable of being radiolabelled with ^{68}Ga at neutral pH, it is more typically radiolabelled at acidic pH with heating. This is due to multiple species being formed when complexing Ga(III); under the harsher radiolabelling conditions one species is favoured. Therefore, HBED does not significantly improve upon the radiolabelling conditions used for DOTA or NOTA, but future optimisation of this chelator could result in an acyclic system that can be readily radiolabelled under mild conditions with the resulting complex having high stability.

As seen previously for siderophores, the adaptation of iron scavengers such as deferiprone can yield effective Ga(III) chelators. THP is an example of this – the branching structure gives the flexibility to rapidly complex ^{68}Ga at high pH (pH 6.5, 10 minutes) whilst the hydroxypyridinone units form a complex with high stability. The branching, aromatic structure results in a more lipophilic chelator than DOTA or NOTA – this has resulted in off target uptake within the liver when conjugated to somatostatin targeting TATE, however careful design of the conjugate may be able to overcome this drawback to take advantage of the mild radiolabelling conditions.

Overall, the developments in non-macrocyclic chelator design have resulted in a number of chelators capable of complexing ^{68}Ga under mild conditions. However, the resulting complexes are often of lower stability or require rigorous optimisation to prevent the formation of multiple species and to further improve the stability. The inclusion of cyclohexyl units into carbon backbones often improves the stability of the resulting complex but hampers the radiolabelling process. HBED is currently being employed for PSMA imaging, demonstrating the viability of using acyclic chelators for ^{68}Ga PET imaging. However, it remains to be seen whether this will translate to imaging of other targets. THP is also being employed, with its mild radiolabelling conditions making kit-type preparation of ^{68}Ga feasible.

1.6. Prostate cancer

Prostate cancer (PCa) is the second most common cancer worldwide for males, with >161 000 new cases reported in the United States of America in 2017.[100] Diagnosis of PCa involves measurement of serum levels of prostate specific antigen, with invasive biopsies used for more precise staging. Recently, imaging of PCa using PET has been shown to be a viable method of diagnosing this disease.[49,199]

Glutamate-Urea targeting units have found wide use in the development of imaging probes for the diagnosis and management of PCa.[200] These small molecular targeting motifs bind to prostate specific membrane antigen (PSMA) *via* the cytoplasmic S1' domain and can be internalised into the cell.[200] ^{68}Ga has been applied to PET imaging of prostate cancer using glutamate-urea motifs through HBED-[163,201,202] and DOTA-conjugates.[110,152,153,203]Recently, a THP

conjugate has been developed that can be radiolabelled with ^{68}Ga at room temperature at pH 6-7.[189,192]

Eder *et al*. reported a conjugate of HBED, Glu-Urea-Lys-(Ahx)-HBED-CC, which had improved affinity for PSMA when compared to a DOTA analogue ($K_{i(\text{Glu-Urea-Lys-(Ahx)-[Ga(HBED-CC)]})}$ = 12.0 nM, $K_{i(\text{Glu-Urea-Lys-(Ahx)-[Ga(DOTA)]})}$ = 37.6 nM), and significantly improved PSMA specific cell internalisation (~9% internalised vs <1% internalised at 37 ^{o}C).[163] These differences were also reflected *in vivo* with the HBED conjugate having greater tumour uptake (~3% injected dose per gram (ID/g) compared to the DOTA analogue (~1% ID/g) in a mouse model.[163] This increased affinity was shown to be due to the lipophilic nature of HBED advantageously binding to part of the PSMA pocket.[158,163] Modification of the linker between the chelator and glu-urea-lys unit to include a lipophilic motif improved the affinity of the DOTA analogue ($K_{i(\text{Glu-Urea-Lys-Ahx-KFF-[Ga(DOTA)]})}$ = 11.1 nM).[163]

Comparison of DOTA, NOTA and HBED conjugates of PSMA was undertaken by Banerjee and co-workers, however, the linkers of each chelator to the targeting unit are different making direct comparison of the effect of the chelator on biodistribution more difficult. They showed that all three chelates were taken up by the PSMA^{+} tumour, with no significant difference at late time points (2 and 3 hours post injection). However, the NOTA conjugate showed faster clearance from tissues and an improved tumour uptake after 1 hour (

Figure 1.33) compared to the other conjugates.

Baranyai and co-workers used click chemistry to prepare a triply conjugated TRAP chelator which they compared to the singly conjugated DOTAGA chelator. The TRAP conjugate had a much better affinity for PSMA, and this was reflected *in vivo* (Figure 1.34). This increased tumour uptake is likely due to the increased number of targeting units and affinity for PSMA, although Baranyai *et al* also suggest that it may be due to *in vivo* degredation of the linker used in this study – this would be masked by the presence of additional targeting units in the trimeric TRAP complex.

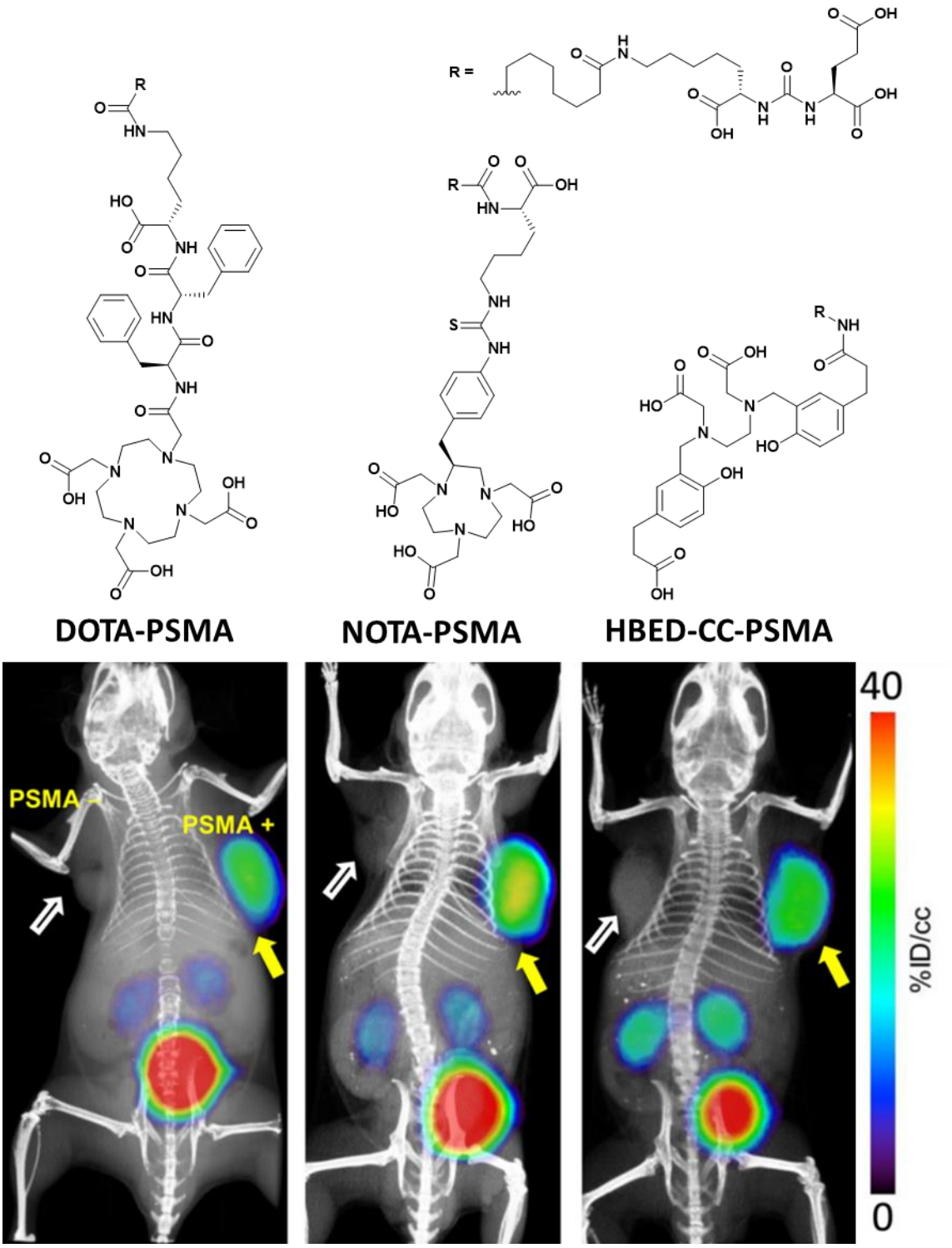

Figure 1.33: PET-CT image 1 hour post-injection using NOD-SCID male mice bearing both $PSMA^+$ PC3 PIP (right) and $PSMA^-$ flu (left) tumour xenografts within the upper flanks. Left to right: [^{68}Ga][Ga(DOTA)] conjugate, [^{68}Ga][Ga(NOTA)] conjugate, [^{68}Ga][Ga(HBED-CC)] conjugate. Image adapted from reference [161].

Young and co-workers applied a THP conjugate to PSMA imaging. They reported a 10 fold lower affinity for PSMA than the HBED conjugate, although *in vivo* there was little difference in the tumour uptake of the radiotracer.

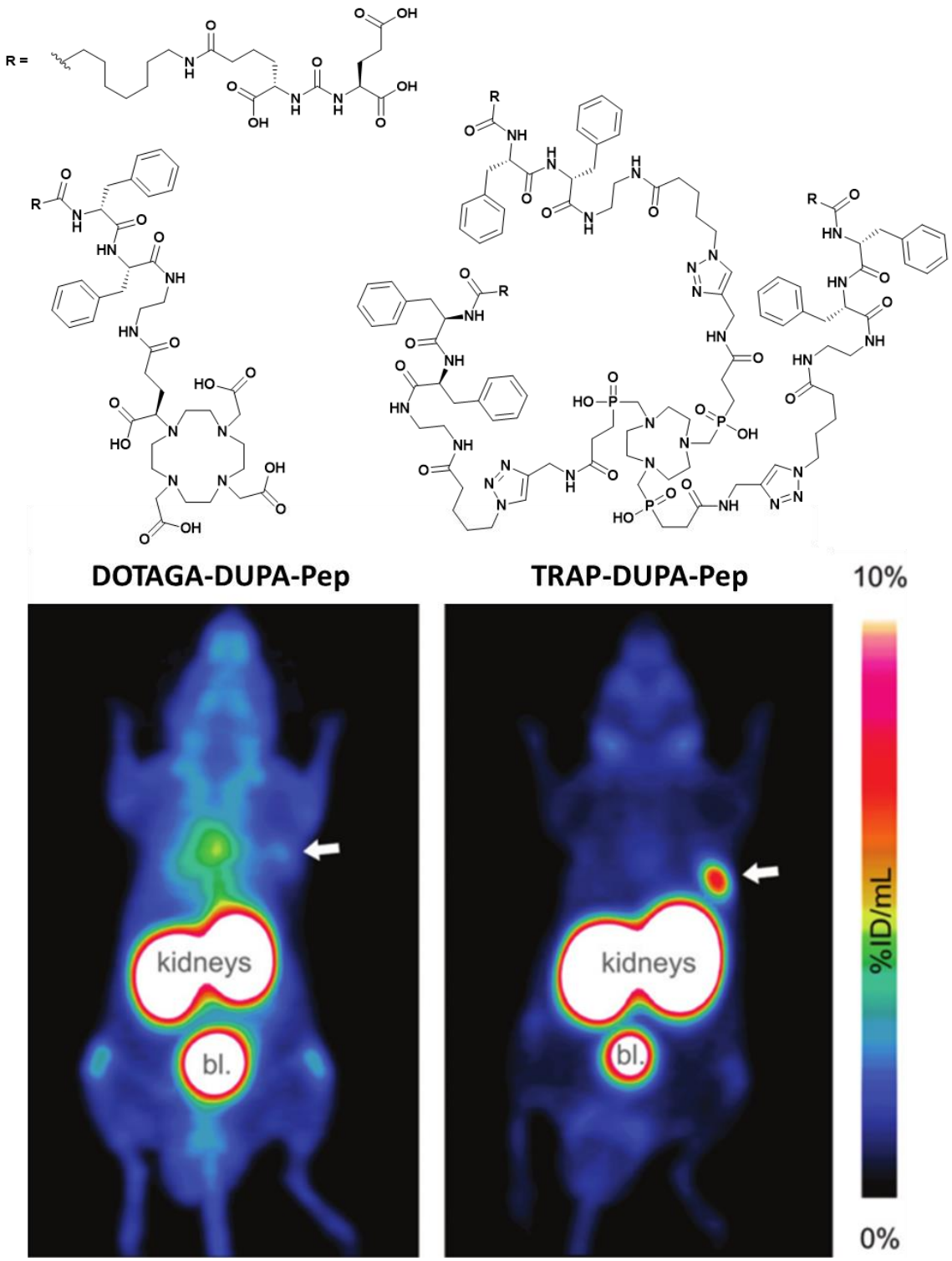

Figure 1.34: PET images of CD-1 athymic nude mice bearing LNCaP tumour xenografts on the right shoulder acquired 90 minutes after injection of [^{68}Ga][Ga(DOTAGA-DUPA-Pep)] (Left) and [^{68}Ga][Ga(TRAP-(DUPA-Pep)$_3$)] (Right). Tumour positions are indicated by arrows.Image adapted from reference [135].

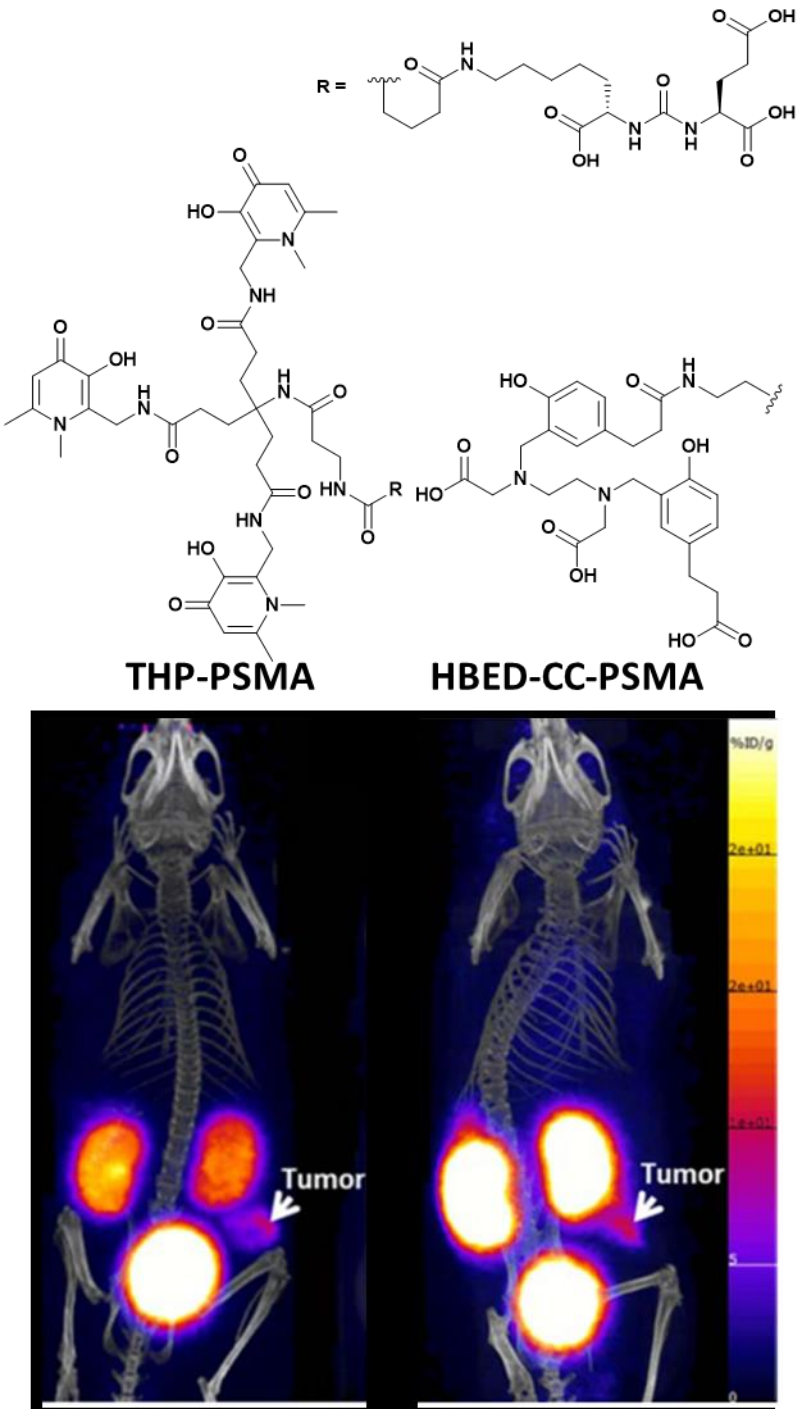

Figure 1.35: Representative PET.CT image of mouse bearing DU145-PSMA xenografts at 40-60 minutes post injection with (left) [^{68}Ga][Ga(THP-PSMA)], (right) [^{68}Ga][Ga(HBED-CC-PSMA)]. PET images scaled from 0%-25% ID/cm^3. Image adapted from reference [189].

It is evident that the nature of the chelator can have a direct impact upon the affinity of a radiotracer for its target. In some cases this can be overcome by modification of the linker between the chelator and the targeting unit to fulfil a second binding pocket or to otherwise improve the pharmacological properties of the radiotracer. The general successful application of a wide number of chelators to imaging of PSMA with the same targeting unit and minimal

modification of the linker unit demonstrates that metal based PET imaging can be readily used to image new targets once a targeting motif has been identified.

1.7. Conclusions

Table 1.3: Selected properties of macrocyclic ^{68}Ga chelators. [a] Stability of ^{68}Ga complex to serum after 2 hours incubation. [b] Stability of ^{68}Ga complex to *apo*-transferrin after 2 hours incubation.

Chelator	log$K_{Ga\text{-}L}$	Stability / %	Conditions required to achieve > 95% radiochemical yield
DOTA	26.1[9]	80[a,107]	*[L]* = 1 μM, *T* = 80 °C, *pH* = 4.0, *t* = 10 minutes[106]
p-NO_2-Bn-Oxo		20[b,106]	*[L]* = 1 μM, *T* = RT, *pH* = 4.0, *t* = 10 minutes[106]
p-NO_2-Bn-PCTA		93[b,106]	*[L]* = 1 μM, *T* = RT, *pH* = 4.0, *t* = 10 minutes[106]
NOTA	31.0[122]	>98[a,107]	*[L]* = 1 μM, *T* = RT, *pH* = 4.0, *t* = 5 minutes[106]
TRAP-Pr	26.2[105]		*[L]* = 0.5 μM, *T* = 95 °C, *pH* = 3.3, *t* = 5 minutes[128]
NOPO	25.0[130]		*[L]* = 10 μM, *T* = 90 °C, *pH* = 0.5 - 7, *t* = 5 minutes[130] *[L]* = 30 μM, *T* = RT, *pH* = 3.5, *t* = 5 minutes[130]
NOTI-Me		>99[a,139]	*[L]* = 10 μM, *T* = RT, *pH* = 4, *t* = 10 minutes[139]
Sar		89[b,141]	*[L]* = 13 μM, *T* = 85 °C, *pH* = 4, EtOH, *t* = 30 minutes[141]
TeMP		98[a,142]	*[L]* = 77 μM, *T* = 100 °C, *pH* = 4, *t* = 45 minutes
TFPP		>99[a,144]	*[L]* = 871 μM, *T* = 100 °C, *pH* = 5.5, 10% EtOH, *t* = 60 minutes[144]
TAFC		>99[a,148]	*[L]* = 3 μM, *T* = RT, *pH* = 3.9, *t* = 10 minutes[146]
FOXE		>99[a,148]	*T* = 80 °C, *pH* = 4, *t* = 20 minutes[148]
FC		>99[a,146]	*[L]* = 45 μM, *T* = RT, *pH* = 3.9, *t* = 10 minutes[146]
FSC		>99[a,147]	*[L]* = 1.5 μM, *T* = RT, *pH* = 4.5, *t* = 5 minutes[151]

Overall the improvements made in the field of cyclic chelators for ^{68}Ga are relatively mild – the promising TRAP and NOPO systems being comparable to NOTA for labelling efficiency, although the remote carboxylic functionalities of TRAP-Pr allow for easier conjugation to a targeting moiety. These chelators are however a significant improvement over the widely used DOTA for complexation of ^{68}Ga, in terms of complexation kinetics and the stability of the resulting complex. The increased affinity seen for [^{68}Ga][Ga(TRAP-$(RGD)_3$)][134] when compared to [^{68}Ga][Ga(DOTA-RGD)] is promising for the future of this system - if this increase in affinity is transferable to other bioconjugates then the use of TRAP chelators instead of DOTA chelators would be highly favourable. Indeed, this increased affinity is also seen for [Ga(TRAP(DUPA-$pep)_3$)] compared to [Ga(DOTA-DUPA-pep)].[135] The separation of conjugation functionality from

the binding core also makes it easier to create a variety of different tracers with specific applications without increasing transchelation.

The adaption of Fe(III) scavengers such as siderophores is an encouraging route to selection of an initial design although further work is required to specify ^{68}Ga complexation over Fe(III) complexation *in vivo* to prevent transmetallation.

Table 1.4: Selected properties of non-macrocyclic ^{68}Ga chelators. [a] Stability of ^{68}Ga complex to serum after 2 hours incubation. [b] Stability of ^{68}Ga complex to *apo*-transferrin after 2 hours incubation.

Chelator	log$K_{Ga\text{-}L}$	Stability[a] / %	Conditions required to achieve >95% radiochemical yield
HBED	39.6[157]	100[a,158]	*[L]* = 17 μM, *T* = 85 °C, *pH* = 4.0, *t* = 10 mins[204]
dedpa	28.1[37]	78[a,167]	*[L]* = 0.1 μM, *T* = RT, *pH* = 4.0, *t* = 10 mins[37]
CHX-dedpa	27.6[167]	91[a,167]	*[L]* = 10 μM, *T* = RT, *pH* = 4.0, *t* = 10 mins[167]
AAZTA	22.2[178]	81[a,175]	*[L]* = 10 μM, *T* = RT, *pH* = 5.3, *t* = 1 min[173]
CyAAZTA	21.4[177]	100[a,177]	*[L]* = 10 μM, *T* = 90 °C, *pH* = 3.8, *t* = 5 mins[177]
DATA^{M}	21.5[205]	98[a,181]	*[L]* = 3.6 μM,*pH* = 5, *T* = RT, *t* = 5 mins[179]
DATA^{PPh}		100[a,173]	*[L] = 3.6 μM*, *pH* = 7, *T* = RT, *t* = 15 mins[179]
TMeOHB-DAZA		99[a,182]	*pH* = 4.0, *t* = 100 °C, *t* = 5 mins[182]
THP		>98[a,185]	*[L]* = 10 μM, *pH* = 6.5, *T* = RT, *t* = 5 mins[184]
$H_2L^{Py,NH}$		>99[b,193]	*[L]* = 62.5 μM, *pH* = 5, *T* = 85 °C, *t* = 15 mins[193]
[Zn(NapATSM)]			*[L]* = 50 μM, *pH* = N/A, THF, *T* = 90 °C, *t* = 9 min[195]
BADED-3, -4, -5, -8, -9, -10		>92[a,197]	*[L]* = 75 μM, *pH* = 4.3 , *T* = 80 °C, *t* = 10 mins, RCY > 92%[198]

The field of acyclic ^{68}Ga chelators has developed significantly in recent years – with the success of HBED proving that stable complexes can be formed by acyclic chelators with ^{68}Ga. The DATA family of ligands show great promise, forming stable complexes with ^{68}Ga under very mild conditions – efficiently coordinating ^{68}Ga at neutral pH and room temperature.[179] THP has also been able to radiolabel under mild conditions, approaching neutral pH, and has high stability to common biological competitors such as transferrin.[184] Kit type development of conjugates of these three chelators may prove to be the future of ^{68}Ga PET.

The use of preformed coordinating centers appears to be key to the production of an inert metal-chelator complex as shown by the kinetic stability of NOTA, tetrapyrrole and DATA complexes, and the improved stability of the more rigid [^{68}Ga][Ga(CHX-dedpa)] complex in comparison to the complex formed from the linear dedpa system in human serum. The use of a preformed coordinating face in the DATA ligands offers an inert alternative to the

macrocyclic systems, such as NOTA, that can withstand transferrin competition and also rapidly complex ^{68}Ga. Incorporation of this style of preformed core into future chelators may allow for improved retention of ^{68}Ga *in vivo* without negatively impacting upon radiolabelling kinetics. While THP does not have a rigid structure, the branched nature of this chelator may act to preorganise the coordinating arms, improving stability of the resulting complex.

The work undertaken in recent years has moved Ga(III) chelates much closer to widespread use. The acceptance and application of [^{68}Ga][Ga(DOTA)] derivatives to medical studies is promising and demonstrates the value of this radionuclide as a diagnostic tool. However, progress towards a simple, easy to conjugate chelator that can be radiolabelled with ^{68}Ga under mild conditions and is stable *in vivo* is still ongoing. Further work is required to allow simple production of ^{68}Ga radiotracers without the need for heating, and ideally without the need for adjustment of pH post-radiolabelling. Achieving this goal will allow for more widespread application of ^{68}Ga radiotracers for diagnosis.

1.8. Aims

The aim of this project was to develop new chelators for ^{68}Ga capable of being radiolabelled under mild conditions.

The majority of chelators for ^{68}Ga require harsh conditions – acidic pH and elevated temperature. Recent advances in chelator design have been towards developing chelators that can be radiolabelled without heating and at neutral pH. Achieving this goal will allow for the application of ^{68}Ga radiolabelling to pH or temperature sensitive targeting units. Furthermore, achieving this will aid in the development of ^{68}Ga radiolabelling kits akin to those used for ^{99m}Tc facilitating widespread application of ^{68}Ga PET imaging by simplifying and standardising the radiolabelling procedure. The development of new chelators is also required to provide additional options for optimisation of biodistribution and pharmacological properties of new imaging agents. Having an increased pool of chelators to select from will make it easier to overcome issues in the future – specific conjugation routes, unexpected incompatibilities, or biodistributions distorted by the chelator could all be avoided by changing chelator.

The standard chelators for ^{68}Ga are macrocyclic chelators, such as DOTA, NOTA and TRAP. The rigid nature of these chelators results in slow radiolabelling kinetics and as such acidic conditions are required to prevent the formation of kinetically inert $Ga(OH)_3$ and $[Ga(OH)_4]^-$. Non-macrocyclic chelators should be more flexible and able to complex ^{68}Ga more rapidly, potentially allowing for radiolabelling at higher pH, and this has been seen through the developments of HBED, THP and DATA chelators for ^{68}Ga. When this project was begun in 2015, the state of the art macrocyclic chelators for ^{68}Ga were NOTA and TRAP. In the field of acyclic chelators for ^{68}Ga, Dedpa had been shown to be radiolabelled with ^{68}Ga at low ligand

concentrations and was sufficiently stable to *apo*-transferrin for application *in vivo*. However, the serum stability assessment had not yet been reported. While AAZTA had been radiolabelled with ^{68}Ga, the more constrained derivatives, the DATA family, had not yet been radiolabelled. THP had been shown to be capable of being radiolabelled at pH 6.5 and was also applied *in vivo*.

The target chelators for this project will be acyclic in nature – this should allow for radiolabelling under mild conditions. In particular, the target chelators will include picolinic acids, amines and carboxylic acids. Amines and carboxylic acids have been selected for their hard basic nature; a combination of the two can also be found in amino acids allowing for a library of chelators to be prepared from a readily available starting material. Picolinic acids combine a hard base with a soft base, furthermore the picolinate unit can act as a bidentate ligand forming a 5-membered ring upon metal coordination; this should be favourable for complexation. These functional groups should be deprotonated at neutral pH; this will make radiolabelling rapid reducing the requirement for heating of the reaction.

The chelator H_3Dpaa has a simple, modular synthesis, with a central amino acid residue that can readily be substituted to develop bifunctional chelators or to tune the coordinating properties of the chelator. Following initial assessment, modification of this chelator system will be undertaken with a view to improving its ^{68}Ga coordinating properties.

Polyaminocarboxylate ligands have been applied to complexation of a wide number of metal ions. The chelator H_3Bn_2DT3A combines amine and carboxylate functionalities to produce a ligand with 6 coordinating atoms and a number of groups that can be substituted for further development of the chelator system.

The potential application of the described chelators will be investigated through the synthesis of bifunctional derivatives and conjugation to a PSMA targeting unit. This will allow for *in vitro* assessment of these systems for future application to the imaging of prostate cancer.

Chapter 2 H_3Dpaa Ligands for Gallium-68

2.1. Introduction

2.1.1 Ligand design considerations

To facilitate the acceptance of ^{68}Ga as an imaging radionuclide further development towards rapid, simple radiolabelling is required. ^{99m}Tc is currently widely used for medical imaging as a SPECT tracer; application of ^{99m}Tc is achieved through simple, kit based radiolabelling.[206,207] This produces a radiotracer ready for use without any requirement for purification or additional formulation. ^{68}Ga radiochemistry is not yet at this stage, with most procedures requiring reformulation due to the acidic radiolabelling conditions used.[156] Advances have been made towards the goal of "kit-type" radiolabelling recently, in particular with development of the DATA and THP chelators for ^{68}Ga.[179,181,189,192] Further development of new chelators that can achieve rapid radiolabelling under biologically acceptable conditions is still required for wider future application of ^{68}Ga.

The majority of ^{68}Ga radiolabelling is performed at pH 4-5 to prevent the formation of kinetically inert hydroxide species that will hinder the radiolabelling process.[60] To achieve radiolabelling at a higher pH the radiolabelling must be rapid; with the complex being formed faster than the hydroxide species. A flexible chelator could provide a template that would achieve this. However, the design of the chelator should be such that the resulting complex is kinetically stable to allow for effective *in vivo* application; displacement of ^{68}Ga from the chelator within the imaging window is to be avoided. Therefore, some preorganisation of the chelator to match the complex geometry should be considered.

Overall this suggests a flexible chelator with some preorganisation. A tripodal chelator in which the coordinating arms are held in close proximity due to a central node, but are free moving could potentially provide the combination of preorganisation and flexibility to achieve rapid complexation and kinetic stability.

The coordinating units should also be deprotonated in the pH range being applied – thus pyridyl and carboxyl units are preferred to alcohol and thiol units.

2.1.2 H_3Dpaa

The ligand 6,6'-(((carboxymethyl)azanediyl)bis(methylene))dipicolinic acid (H_3Dpaa) (Figure 2.1) is made up of two picolinic acid groups attached to a central amine through a methylene bridge. An acetic acid group is also attached to the central amine, forming a tripodal ligand with 6 potential coordinating atoms. It has been applied to the complexation of lanthanide metals[208,209] as well as transition metals.[107,210,211]

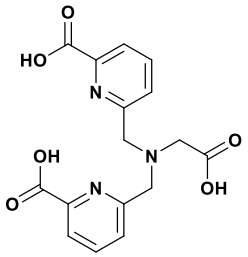

Figure 2.1: Structure of H_3Dpaa

Nonat *et al*. first reported the synthesis of H_3Dpaa, applying it to the complexation of lanthanides to produce a MRI contrast agent through the chelation of Gd(III).[208] The resulting complex was 9 coordinate, with 6 coordination sites being occupied by Dpaa and the remaining 3 by bound water molecules. [Gd(Dpaa)$(H_2O)_3$] is a neutral complex, with a thermodynamic stability constant (for the equilibrium Gd^{3+} + $Dpaa^{3-}$ ↔ [Gd(Dpaa)]), log$K_{[Gd(Dpaa)]}$ = 10.6.[208] This is relatively low when compared to the stability constants reported for macrocyclic complexes (log$K_{[Gd(DOTA)]}$ = 25.3).[102]

The high number of bound water molecules resulted in a relaxivity (r_1 = 11.64 mM^{-1} s^{-1}, 200 MHz, *pD* = 7.4),[208] higher than that of the clinical Gd(III) based contrast agents (r_1 = 4.0 mM^{-1} s^{-1}, [Gd(DOTA)(H_2O)]).[212]

In the presence of 200 equivalents of either acetate, lactate, bisphosphonate, bicarbonate or oxalate the relaxivity drops significantly (r_1 = 9.19-6.15 mM^{-1} s^{-1} in the presence of these anions);[208] this is reported to be due to coordination of the anions in either a monodentate or bidentate manner, reducing the number of bound water molecules and therefore the relaxivity of the complex. In the presence of excess citrate the relaxivity drops to 2.97 mM^{-1} s^{-1} suggesting that all three bound water molecules are replaced by the citrate anion.[208] In the presence of BSA the relaxivity increases; however the number of coordinated water molecules drops.[208] The measured number of coordinated water molecules falls from *q* = 3.1 to *q* = 1.5 in the presence of BSA; this suggests that side chain carboxylate arms of the protein are coordinating to the Gd(III) metal centre, displacing water molecules. The increased molecular weight due to the coordination of BSA to the complex results in the increased r_1 value due to slower tumbling in solution.

Stasiuk *et al*. developed a dual modal MRI/fluorescence imaging probe by appending a high number of bifunctional H_3Dpaa based chelators to InP/ZnS quantum dots through a thiol linker.[209] To synthesise this bifunctional derivative of H_3Dpaa, the central glycine residue was replaced with a diaminobutyric acid residue; the resulting chelator, 6,6'-(((3-amino-1-carboxypropyl)azanediyl)bis(methylene))dipicolinic acid (H_3Dpaa.dab), has an additional amine group for conjugation.[209]

More recently, H_3Dpaa has been applied to the complexation of transition metals.[107,210] Forgács *et al*. used H_3Dpaa to complex Mn(II), resulting in another MRI contrast agent $[Mn(Dpaa)(H_2O)]^-$.[210] The H_3Dpaa ligand again coordinates to the metal ion in a hexadentate manner, with one water molecule bound in the axial position of the pentagonal bipyramidal complex.[210] This complex showed greater stability than the other aminebis(picolinic acid) ligands investigated ($\log K_{[Mn(Dpaa)]}$ = 13.19, *pMn* = 8.98) and had a relaxivity of r_1 = 3.6 mM^{-1} s^{-1} (25 °C, 20 MHz, *pH* = 7.4).[210] The relaxivity of this complex was constant across a wide pH range (pH 2.5-11.5), increasing at acidic pH due to dissociation of the complex and a slight decrease at pH > 11.5 due to formation of a hydroxide complex in agreement with the reported potentiometry.[210] A modification of this complex, $[Mn(Dpaa.ala)(H_2O)]^-$, with alanine used as the central amino acid, was reported by Khannam *et al*. with slightly improved stability (*pMn* = 9.29).[211] $[Mn(Dpaa.ala)(H_2O)]^-$ was reported to have a similar relaxivity (r_1 = 3.02 mM^{-1} s^{-1}, 25 °C, 60 MHz, pH 4-9) to $[Mn(Dpaa)(H_2O)]$.[211] The relaxivity was reduced at high pH (r_1 = 2.22 mM^{-1} s^{-1}, 25 °C, 60 MHz, pH = 10) likely due to deprotonation of the bound water molecule to give a hydroxyl ligand; this occurs at a lower pH than reported by Forgács *et al*.[210,211] The complex retained its relaxivity in the presence of 200 equivalents of competitive anions HCO_3^-, PO_4^{3-} and F^-, suggesting that the complex remains intact and the coordinated water molecule is not displaced by these competing anions.[211]

During the course of this work, Weekes *et al.* applied H_3Dpaa to the complexation of La(III) and Ga(III).[107] The La(III) complexes tested by Weekes *et al*. were designed to be used as orally administered osteoporosis drugs. [La(Dpaa)] ($\log K_{[La(Dpaa)]}$ = 13.6) was more stable than the dipicolylamine complex, 6,6'-(azanediylbis(methylene))dipicolinic acid ($\log K_{[La(L)]}$ = 9.72), and had similar stability to the phosphonate derivative, (6,6'-{[(2-phosphonoethyl)-azanediyl]dimethylene}dipicolinic acid ($\log K_{[La(L)]}$ = 13.99).[107] However, [La(Dpaa)] showed poor hydroxyapatite uptake making it a unsuitable for the target application; directing La(III) to bone tissue. Surprisingly, it was found that in the Ga(III) complex H_3Dpaa only coordinated to the Ga(III) ion through 5 atoms – the central tertiary amine was not coordinated.[107] The vacant coordination site was instead occupied by a bound water atom.[107] The resulting complex showed improved thermodynamic stability ($\log K_{[Ga(Dpaa)]}$ = 18.70, *pGa* = 22.0) in comparison to the La(III) complex.[107] Weekes *et al*. showed that H_3Dpaa could be radiolabeled with ^{67}Ga across a wide pH range (pH 2 – 6.5) and at ligand concentrations as low as 10^{-5} M at room temperature.[107] After radiolabeling with ^{67}Ga, the complex was tested for stability against human serum – 60% of the activity was retained within the complex over 1 hour, and 58% over 2 hours.[107]

Table 2.1: Thermodynamic stability of H_3Dpaa complexes reported in the literature.

Metal Ion	$\log K_{ML}$	pM
Gd(III) [208]	10.6(2)	12.3
Tb(III) [208]	10.4(2)	-
La(III) [107]	13.6(2)	14.3
Ga(III) [107]	18.70(1)	22.0
Mn(II) [210]	13.19(5)	8.98

The promising thermodynamic stability of [Ga(Dpaa)(H_2O)], the potential for rapid development of bifunctional derivatives by changing the amino acid used in the synthesis of the ligand, and the acyclic nature of H_3Dpaa along with the N_3O_3 donor atoms make H_3Dpaa an exciting lead compound for the development of novel chelators for rapid complexation of ^{68}Ga. The acyclic nature of the chelator should allow for rapid complexation of ^{68}Ga, and the tripodal structure may lead to some preorganisation of the chelator for complexation of the metal ion improving the stability of the resulting complex. The picolinate units are readily deprotonated, giving bidentate sites that should be able to coordinate to Ga(III) across a wide pH range, potentially enabling radiolabelling under a variety of conditions.

2.2. Synthesis of H_3Dpaa ligand and Ga(III) complex

2.2.1 Synthesis of ligand

H_3Dpaa was synthesised in 5 steps from 2,6-pyridinedicarboxylic acid (**1**, Scheme 2.1) as outlined by Nonat *et al*.[208] Protection of the two carboxylic units as ethyl esters was achieved in an 85% yield under acidic conditions yielding **2**. Reduction of a single carboxylic arm was achieved by sodium borohydride in ethanol to yield **3**. This reaction was not selective, with the doubly reduced product also being formed; however, purification was readily achieved by column chromatography to give the desired product with a 60% yield. The reactivity of **3** was increased by reaction with thionyl chloride to yield **4** quantitatively. Reaction with glycine ethyl ester hydrochloride yielded the proligand, diethyl 6,6'-(((2-ethoxy-2-oxoethyl)azanediyl)bis(methylene))dipicolinate (Et_3Dpaa), with a lower yield (34%) than that previously reported by Nonat *et al*. (58%) or Weekes *et al*. (84%). Weekes *et al*. quenched the reaction mixture with water followed by extraction prior to concentration, this may reduce side reactions during concentration improving yield or ease of purification. Deprotection under acidic conditions yielded H_3Dpaa as a hydrochloride salt quantitatively, an improvement on the previously reported 65% by Nonat *et al.* and 91% reported by Weekes *et al.* The overall yield of H_3Dpaa from the glycinate ester was 34% - comparable to the 38% reported by Nonat *et al*, but approximately half of that reported by Weekes *et al*. (76%) principally due to the lower yield in the proligand formation step.

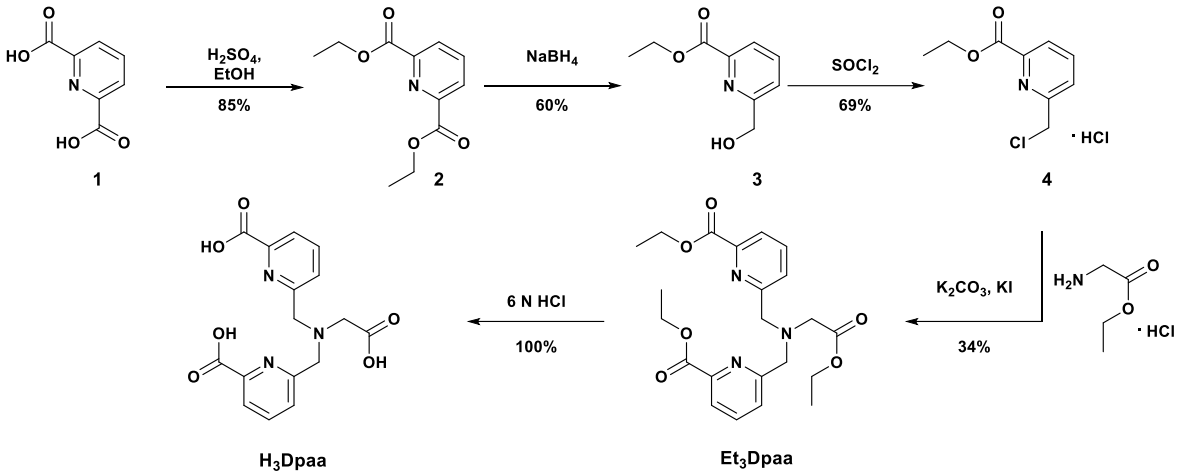

Scheme 2.1: Synthesis of H_3Dpaa.

2.2.2 Protonation constants of H_3Dpaa

The protonation constants for the ligand H_3Dpaa were determined by potentiometry (Figure 2.2, Table 2.2). These values closely match those previously reported.[107,208] The first protonation constant (pK_1 = 7.38) can be assigned to the central tertiary amine, and the two acidic protonation constants (pK_2 = 3.73, pK_3 = 2.82) can be assigned to the picolinate arms. The protonation constant of the acetic acid arm could not be elucidated as it is outside the experimental range.

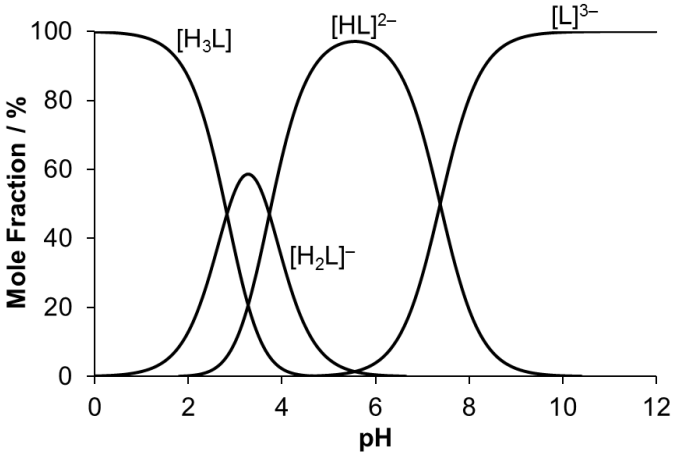

Figure 2.2: Speciation diagram for H_3Dpaa system. (*[L]* = 0.004 M, *T* = 25 °C, *I* = 0.1 M (NMe_4)Cl).

These protonation constants suggest that complexation of Ga(III) should be undertaken above pH 4 to ensure that the two picolinate arms and the carboxylate arm are deprotonated to make complexation more favourable.

Table 2.2: Stepwise protonation constants obtained for H_3Dpaa by potentiometry. (*[L]* = 0.004 M, *T* = 25 ^oC, *I* = 0.1 M (NMe_4)Cl).

logK_a	H_3Dpaa
logK_1	7.38(2)
logK_2	3.73(2)
logK_3	2.82(2)

2.2.3 Synthesis of [Ga(Dpaa)(H_2O)]

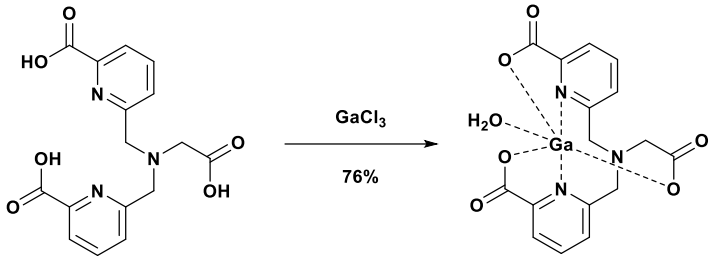

H_3Dpaa [Ga(Dpaa)]

Scheme 2.2: Synthesis of [Ga(Dpaa)(H_2O)].

H_3Dpaa was reacted with $GaCl_3$ in a water-methanol solution at pH 4 (Scheme 2.2). The solution was heated to reflux for 16 hours, with a white precipitate forming. Isolation by centrifugation and drying under high vacuum yielded a white powder, [Ga(Dpaa)(H_2O)].3HCl in a 64% yield. The increased rigidity of the complex is reflected by characteristic changes in the proton (^{1}H) nuclear magnetic resonance (NMR) spectrum (Figure 2.3). The proton resonance corresponding the methylene linkers between the picolinates and the central tertiary amine shifts downfield ($\Delta_{\delta H}$ = + 0.56-0.70) indicating a decrease in shielding. The two protons in each bridge are equivalent in the ligand (δ_H = 3.92), but in the Ga(III) complex are no longer equivalent with distinct resonances (δ_H = 4.62, 4.48) displaying a strong geminal coupling ($^2J_{HH}$ = 16 Hz).

2.2.4 Thermodynamic stability of [Ga(Dpaa)(H_2O)]

The Ga(III)-Dpaa system was further characterised through potentiometry. The obtained association constants are given in Table 2.4 with a speciation diagram given in Figure 2.4.

The speciation diagram shows that Ga(III) will be complexed by H_3Dpaa across a wide pH range, up to pH 8. The obtained value (log$K_{[Ga(Dpaa)]}$ = 18.53(5)) is comparable to that previously reported by Weekes *et al*. (log$K_{[Ga(Dpaa)]}$ = 18.70(1)).[107] Unsurprisingly, this value is lower than that obtained for macrocyclic chelators DOTA (log$K_{[Ga(DOTA)]}$ = 26.05(3))[121] and NOTA (log$K_{[Ga(NOTA)]}$ = 29.60(3)),[105] as expected due to the macrocylic nature of these chelators. This value is significantly higher than that reported for the complex formed by other metals with H_3Dpaa (Table 2.1). This increased stability is likely due to the better match between the hard

Lewis bases of the ligand oxygen donors and the hard Lewis acid of the Ga(III) cation. In addition, H_3Dpaa has the potential to occupy all of the coordination sites of Ga(III) whereas this ligand does not have sufficient denticity to fully coordinate the 8- and 9- coordinate lanthanides or the 7-coordinate Mn(II) and therefore the thermodynamic stability should be greater for the Ga(III) species.

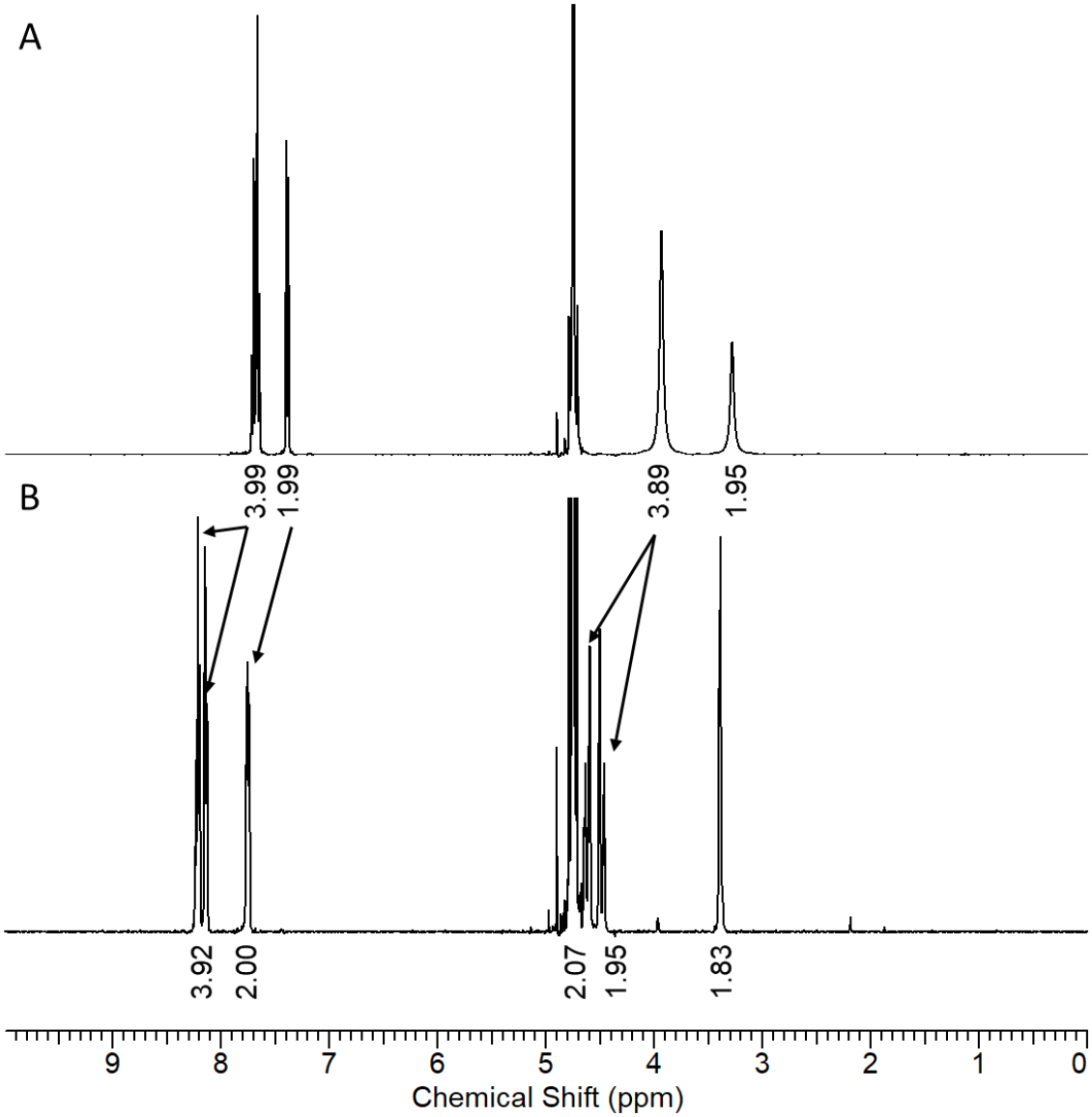

Figure 2.3: Change in ^{1}H NMR of H_3Dpaa upon complexation of $GaCl_3$. A) ^{1}H NMR of H_3Dpaa (D_2O, 298 K, *pD* = 8.8), B) ^{1}H NMR of [Ga(Dpaa)(H_2O)] (D_2O, 298 K, *pD* = 8.8).

Further analysis of the speciation diagram for the Ga(III)-H_3Dpaa system reveals that the species formed in solution is different at acidic pH (pH 2.0-3.5) to that formed at pH approaching neutral (pH 6-8). While the exact nature of these species cannot be determined by potentiometery, the difference between them is equivalent to a deprotonation. This deprotonation event, beginning around pH 3.5, is surprising. It is possible that this could be accounted for due to deprotonation of the ligand, however this would suggest that one of the carboxylate arms is not coordinated to Ga(III). Alternatively, this could be assigned to deprotonation of a Ga(III) bound water molecule. Deprotonation of $[Ga(H_2O)_6]^{3+}$ begins at pH 3

so this is not unreasonable.[213–215] Other examples of Ga(III) complexes in which a ligand with six coordinating atoms is only pentacoordinate are known in the literature including the acyclic N,N,N',N'-tetrakis-(2-hydroxy-3,5-dimethylbenzyl)ethylenediamine and macrocyclic NODIA-Me.[139,216]

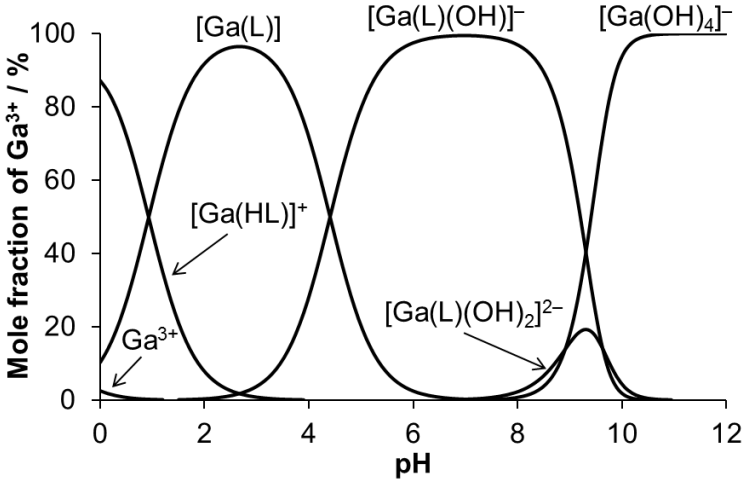

Figure 2.4: Speciation diagram for Ga(III)-Dpaa system as assessed by potentiometry. (*[L]* = [Ga(III)] =0.004 M, *T* = 25 °C, *I* = 0.1 M (NMe_4)Cl)

Table 2.3: Stability constants (logK_{ML}) obtained for [M(Dpaa)] complexes. [a] Determined by UV-VIS titration *[L]* = *[M]* = 0.1 mM, *T* = 25 °C, *pH* = 2-7 [b] Determined by potentiometric titration (*[L]* = *[M]* = 0.004 M, *T* = 25 °C, *I* = 0.1 M (NMe_4)Cl). *pM* calculated for pH 7.4, [M] = 1 x 10^{-6} M, [L] = 1 x 10^{-5} M. Free Ga(III) is present as both $[Ga(H_2O)_6]^{3+}$ and $[Ga(OH)_4]^-$, Cu^{2+} and Zn^{2+} are present as their aqua ions.

Metal Ion	logK_{ML}	*pM*
Ga(III)	18.53(5)[a]	8.91
Cu(II)	10.85(1)[b]	12.60
Zn(II)	11.93(3)[b]	12.60

Overall, the deprotonated species formed at pH 6-8 has log$K_{[Ga(Dpaa)(OH)]}$= 22.94 (Table 2.4), this is comparable to other non-macrocyclic ligands such as EDTA (log$K_{[Ga(EDTA)]}$ = 22.01)[217] and AAZTA (log$K_{[Ga(AAZTA)]}$ = 22.18)[178] and greater than the iron transport protein *apo*-transferrin (log$K_{[Ga(Transferrin)]}$ = 20.3),[56] an important biological competitor for Ga(III). The calculated value for *pGa* is 8.91 (*pH* = 7.4, [Ga(III)] = 10^{-6} M, [Dpaa] = 10^{-5} M).

The stability constants for Cu(II) and Zn(II) were also assessed as these are likely to be competitors *in vivo* due to the high concentration of these ions in human tissues (Table 2.3). The Ga(III) complex is more stable than either the Cu(II) or Zn(II) species which is promising for future application. The speciation diagrams for the Cu(II) and Zn(II) systems are given in Appendix 1. This preference for Ga(III) is likely due to the harder nature of Ga(III) than Cu(II) and Zn(II), matching well with the high negative charge of the deprotonated ligand.

Table 2.4: Equilibrium constants (log*K*) obtained for complexes. [a] Determined by potentiometric titration. (*[L]* = *[M]* = 0.004 M, *T* = 25 °C, *I* = 0.1 M (NMe_4)Cl), [b] Determined by UV-VIS titration. (*[L]* = *[M]* = 0.1 mM, *T* = 25 °C, pH = 2-7)

Equilibrium (Charges are omitted)	Ga(III)[a,b]	Cu(II)[a]	Zn(II)[a]
M + L ↔[M(L)]	18.53(5)	10.85(1)	11.93(3)
[M(HL)] ↔ [M(L)] + H	1.0(2)	3.38(1)	2.33(4)
[M(L)] + H_2O ↔ [M(L)(OH)] + H	4.41(2)	9.86(2)	11.27(3)
[M(L)(OH)] + H_2O ↔ [M(L)$(OH)_2$] + H	9.63(8)	12.00(2)	-

2.2.5 Crystal structure

A crystal of suitable quality for single crystal X-ray diffraction was grown by slow evaporation of an acidic solution containing [Ga(Dpaa)(H_2O)] in water. Ga(III) is in a six coordinate, distorted octahedral environment. The Dpaa ligand occupies five of the coordination sites, with the sixth occupied by a water molecule. The central tertiary amine is not coordinated to the Ga(III) atom as the distance (N2···Ga1 = 2.488 Å) is greater than their combined covalent radius. The bonds between the Ga(III) atom and the nitrogen donors are longer than those between the Ga(III) atom and the oxygen donors (Table 2.5). This may be due to the preference of Ga(III) for hard donor atoms, like oxygen, over softer ones, like nitrogen.

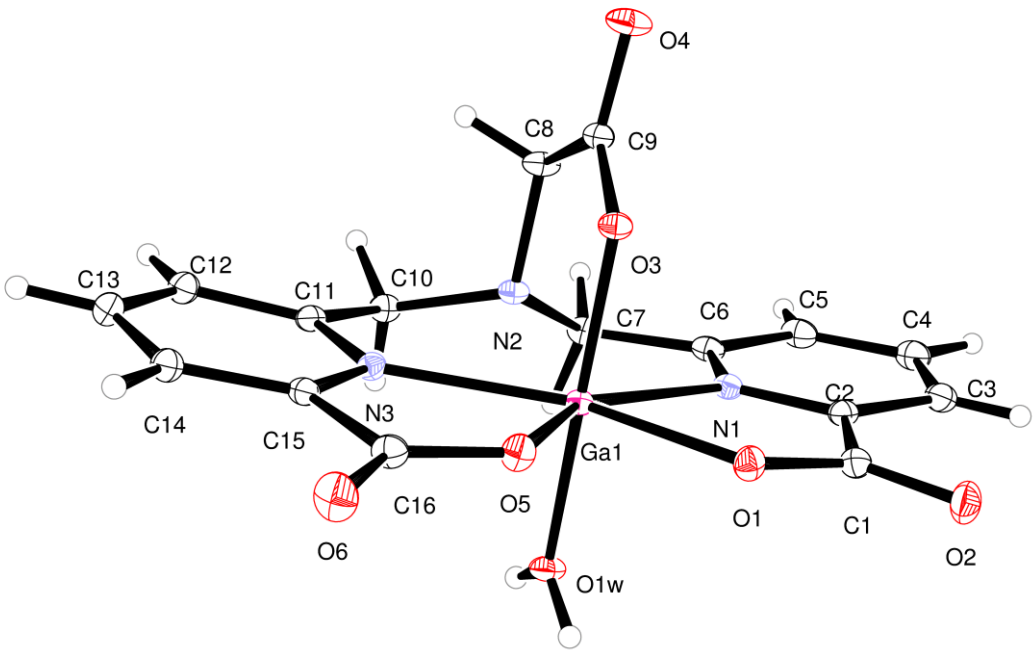

Figure 2.5: ORTEP representation of structure obtained by single crystal X-ray diffraction of [Ga(Dpaa)(H_2O)]. Thermal ellipsoids set at 30% certainty.

Alternatively, this may be due to the strain induced in the structure by the rigid ligand. This strain is highlighted in the bond angles in the pseudo plane of the picolinate arms. The N1-Ga1-N3 angle (135.16°) is significantly greater than the N-Ga-O angles (73.97°, 74.95°). Indeed, the N1-Ga1-N3 angle is significantly greater than the 90° dictated by an ideal octahedral geometry, and the N-Ga-O angles significantly smaller than 90°. Overall, the complex is fairly symmetric with a pseudo-mirror plane present in the complex (through O3, N2 and O1w). The picolinate arms are slightly distorted away from the perpendicular plane, with a total angle between them of 9.53(3)°. Full crystallographic data is included in Appendix 2.

Table 2.5: Selected crystallographic parameters for [Ga(Dpaa)(H_2O)].

Bond Length / Å		Bond Angle / °	
Bond	**[Ga(Dpaa)(H_2O)]**	**Angle**	**[Ga(Dpaa)(H_2O)]**
O1-Ga1	2.0441(10)	O1-Ga1-N1	73.97(4)
N1-Ga1	2.2354(11)	N1-Ga1-N3	135.16(4)
N2···Ga1	2.4880(11)	N3-Ga1-O5	74.95(4)
N3-Ga1	2.2017(12)	O5-Ga1-O1	75.92(4)
O5-Ga1	2.0229(10)	O3-Ga1-O1	90.08(4)
O3-Ga1	1.9173(10)	O3-Ga1-N1	88.09(4)
O1W-Ga1	1.9109(10)	O3-Ga1-N3	91.36(4)
		O3-Ga1-O5	92.23(4)
		O3-Ga1-O1W	175.40(4)

The presence of a coordinated water molecule in the crystal structure supports the conclusions drawn from the potentiometric titrations. The deprotonation event that begins to occur at pH 3.5 can reasonably be assigned to the deprotonation of this bound water molecule and not to a deprotonation of the Dpaa ligand.

2.2.6 Radiolabelling H_3Dpaa

2.2.6.1 Initial radiolabelling studies –HPLC and TLC

The extent of radiolabelling of H_3Dpaa with [^{68}Ga]$GaCl_3$ could be assessed by either radio-thin layer chromatography (TLC) or radio-high performance liquid chromatography (HPLC). A single species was seen by radio-HPLC following radiolabelling at pH 4.0 of 100 µM H_3Dpaa. In contrast, Weekes *et al*. report the formation of multiple species upon radiolabelling with [^{67}Ga]$GaCl_3$ under similar conditions,[107] with the formation of these species being pH dependent. It is likely that these reported species are the different protonation states of the formed [^{67}Ga][Ga(Dpaa)(H_2O)] complex. As both the radiolabelling reported here and previously by Weekes *et al*. is undertaken in acetate buffer, from a starting material of [$^{68/67}$Ga]$GaCl_3$, these differences are surprising. Regardless, the species formed is clearly distinct from free

[^{68}Ga]Ga(III) as indicated by radio-HPLC and radio-TLC and has the same retention time as the cold complex [Ga(Dpaa)(H_2O)] (Figure 2.6d).

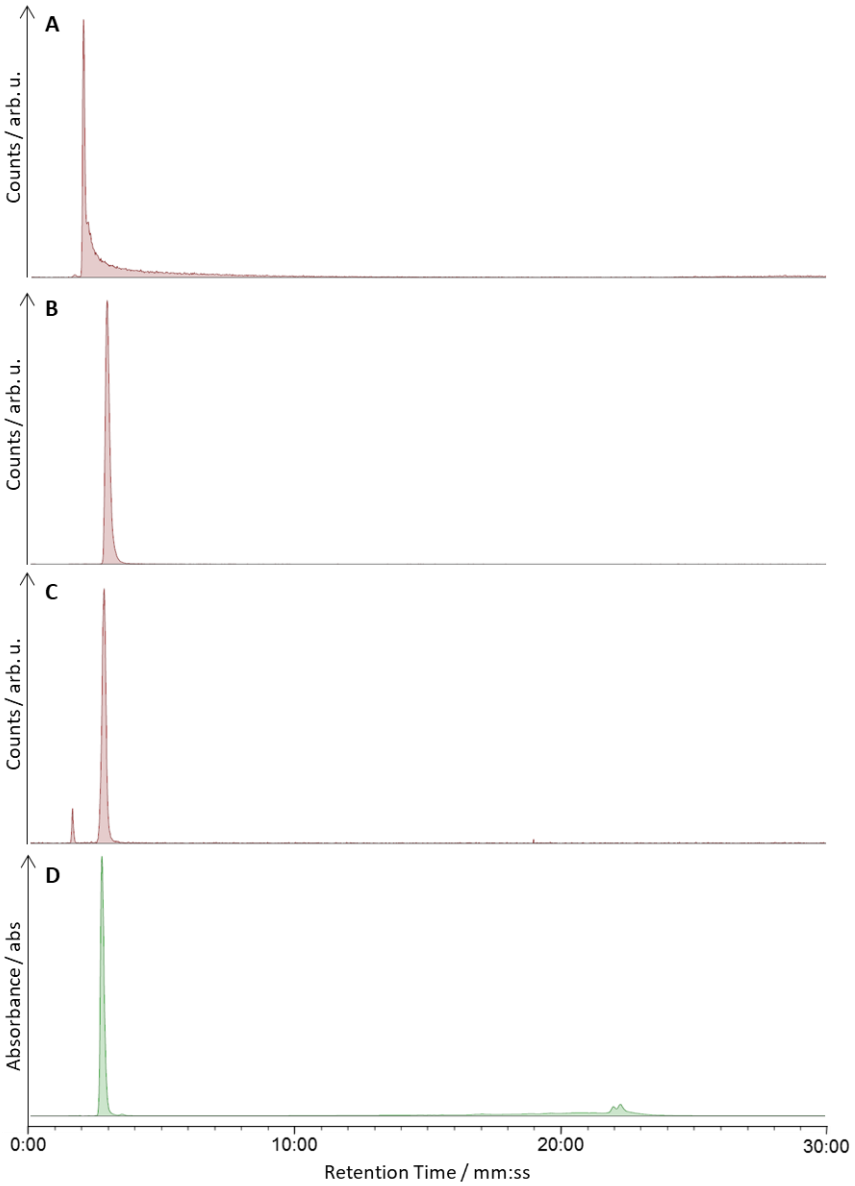

Figure 2.6: HPLC Chromatograms for the radiolabelling of H_3Dpaa with [^{68}Ga]$GaCl_3$. A) Radio-HPLC chromatogram of non-complexed [^{68}Ga]Ga(III). B/C) Radio-HPLC of crude radiolabelling mixture containing H_3Dpaa and [^{68}Ga]Ga(III) B) (*[L]* = 100 µM,*t* = 15 minutes, *pH* = 4.0, *T* = 25 °C, *I* = 0.1 M Acetate buffer). C) (*[L]* = 100 µM,*t* = 15 minutes, *pH* = 7.5, *T* = 37 °C, *I* = 0.1 M Phosphate buffer). D) UV-HPLC chromatogram of isolated [Ga(Dpaa)(H_2O)]. **HPLC Gradient A.**

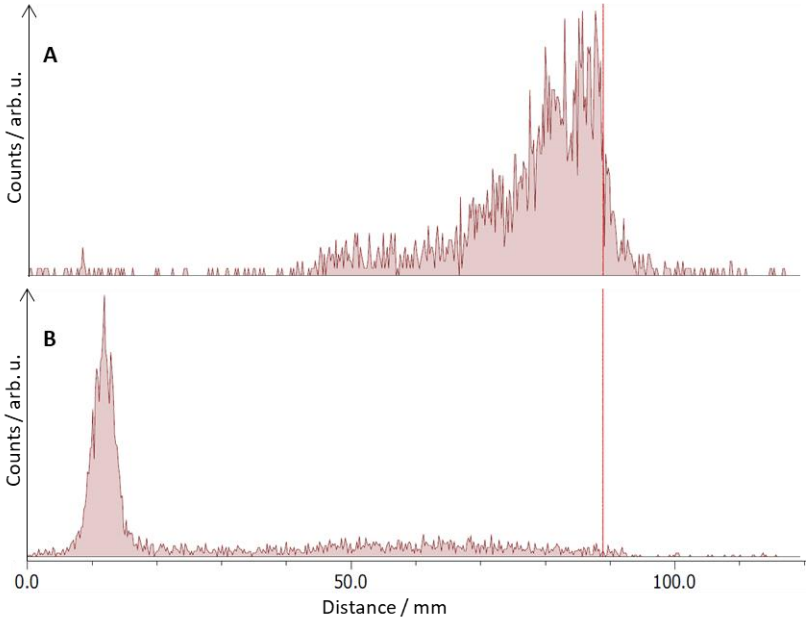

Figure 2.7: TLC Chromatograms for the radiolabelling of H_3Dpaa with [^{68}Ga]$GaCl_3$. A) Radio-TLC chromatogram of non-complexed [^{68}Ga]Ga(III). B) Radio-TLC of crude radiolabelling mixture containing H_3Dpaa and [^{68}Ga]Ga(III) (*[L]* = 100 µM,*t* = 15 minutes, *pH* = 4.0, *T* = 25 °C, *I* = 0.1 M Acetate buffer).

2.2.6.2 The effect of pH on H_3Dpaa radiolabelling

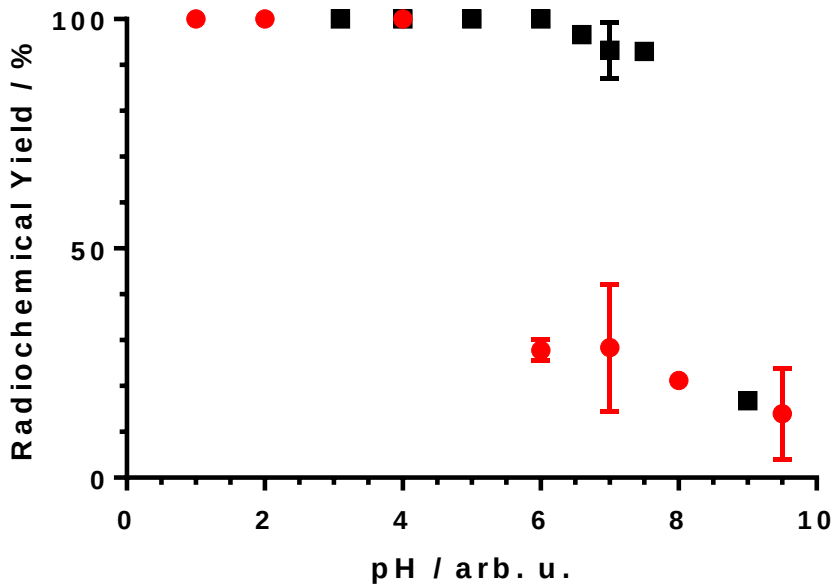

Figure 2.8: Effect of pH on the RCY achieved by H_3Dpaa in the presence of [^{68}Ga]$GaCl_3$. Red circles indicate radiolabelling in aqueous media, with pH adjusted by addition of HCl or NaOH. Black squares indicate radiolabelling in buffered solutions (*I* = 0.1 M Acetate or Phosphate). (*[L]* = 100 µM, *t* = 15 minutes, *T* = 25 °C)

The radiolabelling of H_3Dpaa with [^{68}Ga]$GaCl_3$ was found to have a distinct pH dependence – in aqueous solutions RCY was high (>95%) up to approximately pH 4. Above this pH the RCY is significantly lower, with only 30% RCY being achieved at pH 6 and above (Figure 2.8). This is likely due to the formation of kinetically inert Ga(III) hydroxide species above pH 4, hampering radiochemical incorporation.

However, when a buffered solution (0.1 M acetate or phosphate) is used as the radiolabelling medium the pH dependence of this reaction changes. The high RCY (>95%) is maintained up to pH 8 before rapidly falling to 20% at pH 9. This difference is postulated to be due to the formation of a "pre-coordination" complex in which the Ga(III) ion is coordinated by acetate or phosphate anions, hindering the rate of formation of gallium hydroxide species and allowing for displacement of the weakly bound acetate and phosphonate ions by the multidentate H_3Dpaa ligand. The poor radiolabelling above pH 8 correlates with the speciation determined *via* potentiometry – above pH 8 $[Ga(OH)_4]^-$ begins to form instead of a $[Ga(Dpaa)(H_2O)]$ species.

2.2.6.3 The effect of ligand concentration on H_3Dpaa radiolabelling

Radiolabelling of H_3Dpaa at pH 4.0 was rapid at ligand concentrations as low as 10^{-6} M, with >95% RCYs being achieved in 15 minutes. Radiolabelling was ineffective at lower concentrations, with no radiolabelling being seen below 10^{-7} M.

At pH 7.4, radiolabelling was less tolerant of lower ligand concentrations. Significantly reduced RCYs were achieved at concentrations less than 10^{-4} M, with no radiolabelling seen below 10^{-6} M ligand concentration.

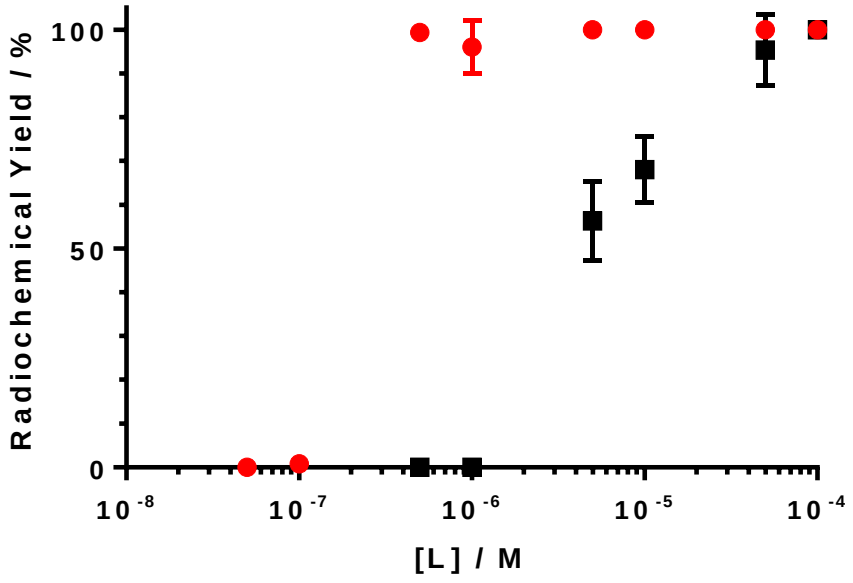

Figure 2.9: Radiochemical yield for formation of $[^{68}Ga][Ga(Dpaa)(H_2O)]$ at varying ligand concentrations. Red circles = pH 4.0, *I* = 0.1 M acetate buffer. Black squares = pH 7.4, *I* = 0.1 M phosphate buffer. (*T* = 25 ^oC, *t* = 15 minutes)

This difference in radiolabelling behaviour with pH is likely an effect of kinetics; with radiolabelling at pH 7.4 happening before the formation of kinetically inert hydroxide species. At lower ligand concentrations, the rate of formation of $[^{68}Ga][Ga(Dpaa)(H_2O)]$ will be slower. Therefore more ^{68}Ga will be found as hydroxide species.

2.2.6.4 Radiolabelling of H_3Dpaa in saline, phosphate buffered saline (PBS)

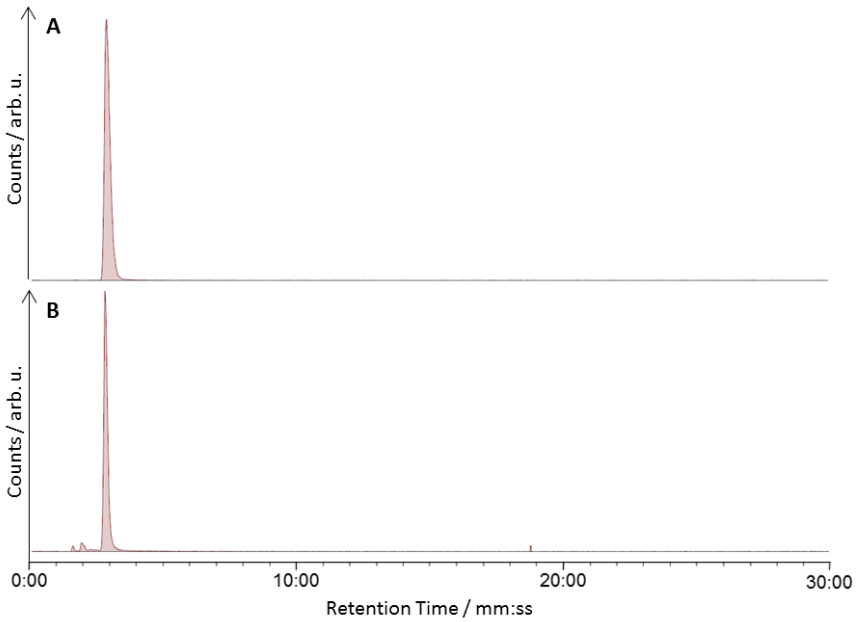

Figure 2.10: HPLC Chromatograms for the radiolabelling of H_3Dpaa with [^{68}Ga]$GaCl_3$. A) (*[L]* = 100 µM, *t* = 5 minutes, *pH* = 5.5, *T* = 25 °C, *I* = saline). B) (*[L]* = 100 µM,*t* = 5 minutes, *pH* = 7.4, *T* = 37 °C, *I* = PBS). **HPLC Gradient A.**

While high RCYs can be achieved at neutral pH by H_3Dpaa in buffered solutions, the buffer content of these reactions is quite high (0.1 M). To make this reaction more biocompatible, radiolabelling in saline and phosphate buffered saline (PBS) was explored. While radiolabelling proceeded readily in both media, the poorly buffered saline solution was acidified (pH = 5.5) by the addition of the acidic ligand and acidic [^{68}Ga]$GaCl_3$. However, PBS has sufficient buffering capacity to maintain its pH (pH = 7.4) and still allowed for high RCYs (94%) at room temperature. Mild heating resulted in slightly improved RCYs (T = 37 °C, RCY = 95%, t = 5 minutes). These results suggest that radiolabelling of H_3Dpaa bioconjugates may be achieved in a biocompatible solution at neutral pH; this would simplify the production of radiotracers by reducing the reconstitution required post-labelling.

2.2.6.5 Stability to apo-Transferrin

An important consideration in the design of new radiotracers is the stability of the radiolabelled complex to biological competitors. The iron transport protein *apo*-transferrin is often used as a competitor for Ga(III) ($\log K_{[Ga(Transferrin)]}$ = 20.3).[56] Due to the similarities between Ga(III) and Fe(III) ($\log K_{[Fe(Transferrin)]}$ = 22.8),[56] transmetallation of Ga(III) by *apo*-transferrin is a useful indicator of *in vivo* stability. [^{68}Ga][Ga(Dpaa)(H_2O)] was found to be stable to *apo*-transferrin; after 1 hour incubation in a carbonate buffered transferrin solution, only 5% of the activity had been dissociated from the [^{68}Ga][Ga(Dpaa)(H_2O)] complex, and only 8% after 2 hours.

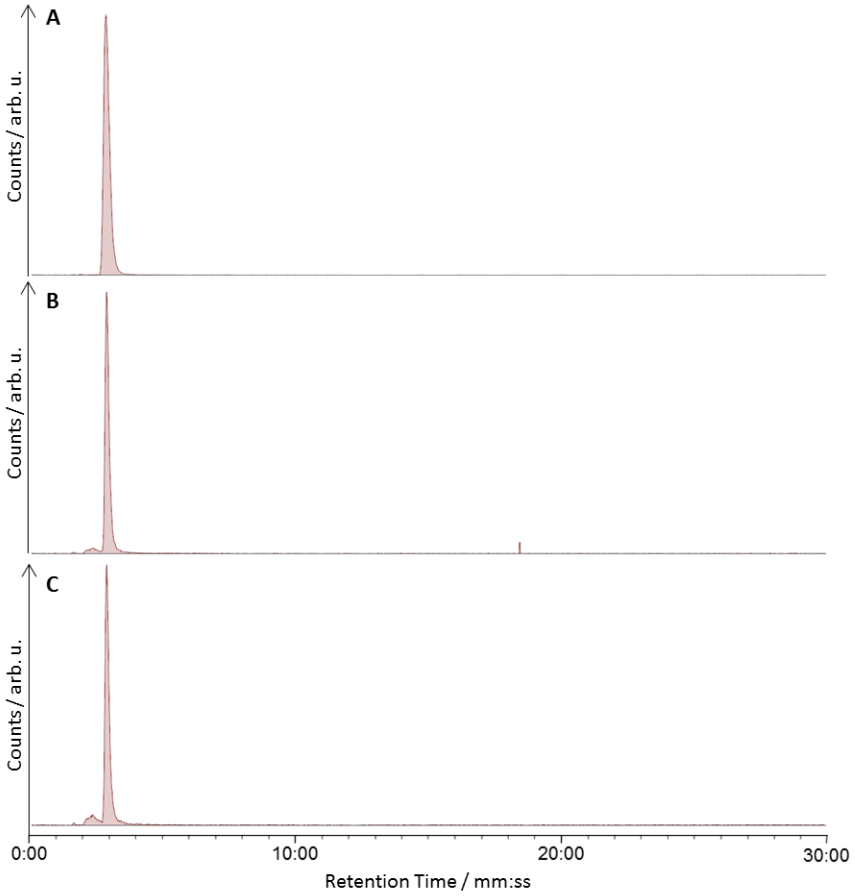

Figure 2.11: HPLC Chromatograms for the assessment of stability of [^{68}Ga][Ga(Dpaa)(H_2O)] to *apo*-transferrin. A) Crude radiolabelling mixture. B) Crude mixture after incubation with *apo*-transferrin for 60 minutes. C) Crude mixture after incubation with *apo*-transferrin for 120 minutes. **HPLC Gradient A.**

2.2.6.6 Semi-preparative HPLC and specific activity

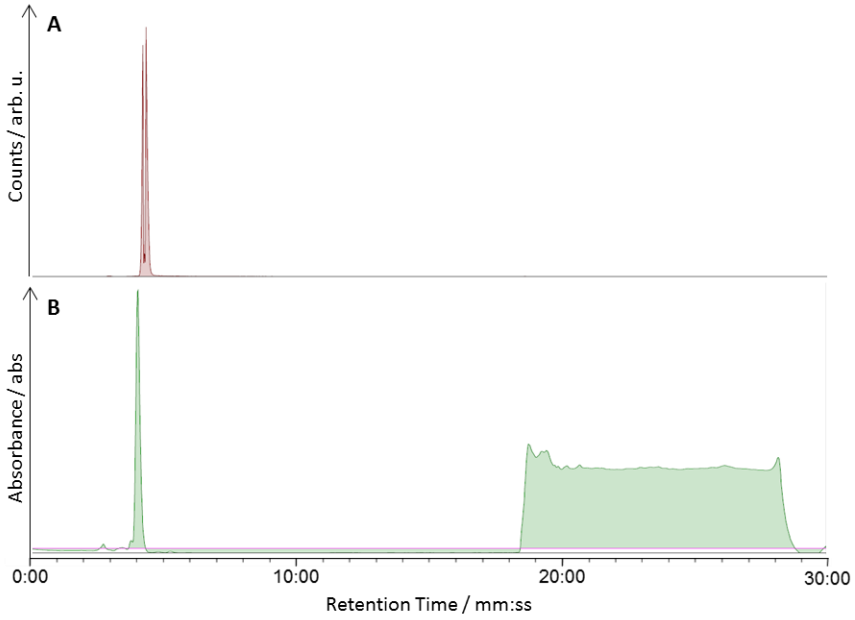

Figure 2.12: A) Radio-HPLC and B) UV-HPLC of [^{68}Ga][Ga(Dpaa)(H_2O)] on a semi-preparative column. Peak splitting seen in radio-HPLC trace due to saturation of the detector. Difference in retention times between radio- and UV-HPLC due to serial detection. **HPLC Gradient B.**

Isolation of the radiolabelled species by semi-preparative HPLC gave a molar activity of 3.9 GBq µmol^{-1}. Whilst semi-preparative HPLC would provide a route to isolation of the radiolabelled complex from free ligand/peptide conjugate and also free [^{68}Ga]Ga(III), purification in this way would negate many of the benefits of radiolabelling at a higher pH as concentration and reconstitution of the isolated peak would be required. This is also a slow procedure, which is not ideal for the production short lived ^{68}Ga radiotracers.

2.3. Synthesis of bifunctional chelators

2.3.1 Synthesis of ligands

To apply the [^{68}Ga][Ga(Dpaa)(H$_2$O)] system to diagnostic imaging, a targeting unit is likely to be required. Bifunctional derivatives of H$_3$Dpaa can be made readily from the same precursor (**4**) by substituting the amino acid used in the synthesis (Scheme 2.3).

Three bifunctional chelators, H$_3$Dpaa.dab, N,N-bis((6-carboxypyridin-2-yl)methyl)glutamic acid (H$_4$Dpaa.ga), and 6,6'-(((5-amino-1-carboxypentyl)azanedi-yl)bis(methylene))dipicolinic acid (H$_3$Dpaa.lys), have been synthesised from the commercially available protected amino acid hydrochloride salts, methyl (*S*)-2-amino-4-((*tert*-butoxycarbonyl)amino)butanoate hydrochloride, diethyl *L*-glutamate dihydrochloride, and *tert*-butyl N$_6$-((benzyloxy)carbonyl)-*L*-lysinate hydrochloride respectively.

A thiol functionalised chelator, 6,6'-(((1-carboxy-2-mercaptoethyl)azanediyl)bis(methylene))dipicolinic acid (H$_3$Dpaa.cys), could not be obtained – although the protected proligand, diethyl 6,6'-(((1-ethoxy-1-oxo-3-(tritylthio)propan-2-yl)azanediyl)bis(methylene))(R)-dipicolinate (Et$_3$Dpaa.cys(Tr)), could be prepared from ethyl *S*-trityl-*L*-cysteinate.

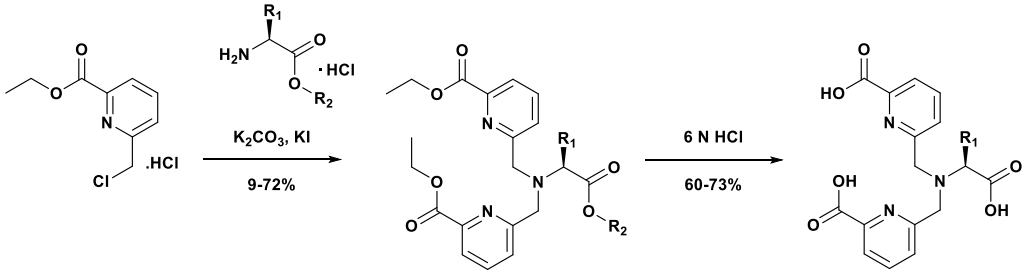

Et_4Dpaa.ga, $R_1 = CH_2CH_2C(=O)OCH_2CH_3$, $R_2 = CH_2CH_3$ → H_4Dpaa.ga, $R_1 = CH_2CH_2C(=O)OH$

Et_2MeDpaa.dab(Boc), $R_1 = CH_2CH_2NHC(=O)OC(CH_3)_3$, $R_2 = CH_3$ → H_3Dpaa.dab, $R_1 = CH_2CH_2NH_2$

$Et_2{}^tBu$Dpaa.lys(Z), $R_1 = CH_2CH_2CH_2CH_2NHC(=O)OCH_2C_6H_5$, $R_2 = C(CH_3)_3$ → H_3Dpaa.lys, $R_1 = CH_2CH_2CH_2CH_2NH_2$

Et_3Dpaa.cy(Tr), $R_1 = CH_2SC(C_6H_5)_3$, $R_2 = CH_2CH_3$ → ✕ H_3Dpaa.Cys, $R_1 = CH_2SH$

Scheme 2.3: Synthesis of bifunctional chelators.

The protected chelators, diethyl 6,6'-(((4-((tert-butoxycarbonyl)amino)-1-methoxy-1-oxobutan-2-yl)azanediyl)bis(methylene))(S)-dipicolinate (Et$_2$MeDpaa.dab(Boc)), diethyl N,N-

bis((6-(ethoxycarbonyl)pyridin-2-yl)methyl)-L-glutamate (Et_4Dpaa.ga), diethyl 6,6'-(((6-(((benzyloxy)carbonyl)amino)-1-(tert-butoxy)-1-oxohexan-2-yl)azanediyl)bis(methylene))(S)-dipicolinate (Et_2^{t}BuDpaa.lys(Z)), and Et_3Dpaa.cys(Tr) were prepared by reaction of the protected amino acids with **4** before giving the desired products in 37%, 72%, 44%, and 9% yields respectively. These differences in yields may be due to the stability of the side arms or due to the different purification methods used.

The methylene bridge between the central amine and pyridine groups of the short side arm bifunctional proligands is composed of two inequivalent protons – this is evidenced in Et_2MeDpaa.dab(Boc), Et_4Dpaa.ga and Et_3Dpaa.lys(Tr) as a pair of doublets ($\Delta\delta$ = 0.6 ppm) with strong geminal coupling ($^2J_{HH}$ = 15.1-15.5 Hz). When the side arm is longer, as in Et_2^{t}BuDpaa.lys(Z) this inequivalence is not seen, instead a broad singlet is observed for these protons. Aside from this, the common proton environments have similar resonances in all four bifunctional proligands investigated and closely match those of Et_3Dpaa.

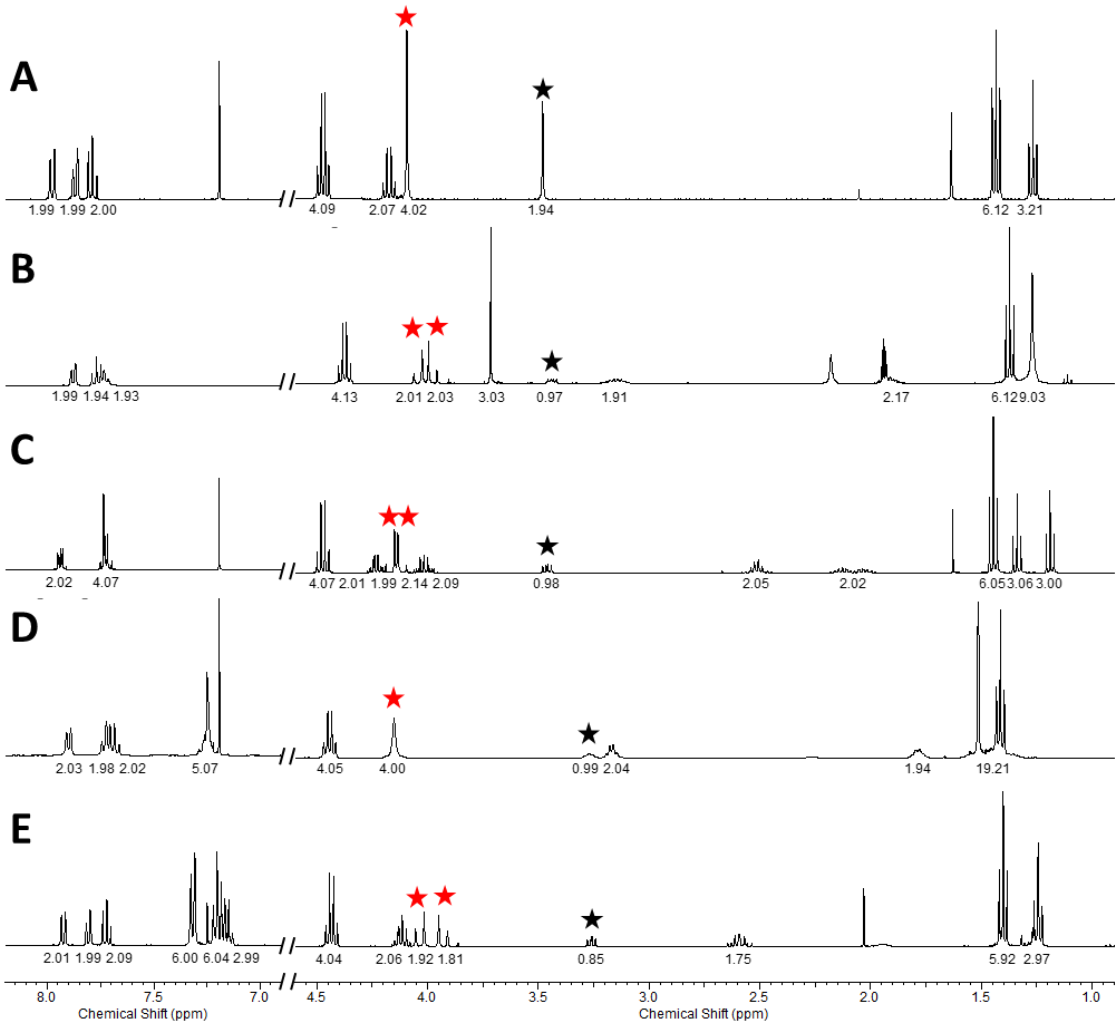

Figure 2.13: ^{1}H NMR of A) Et_3Dpaa in $CDCl_3$, B) Et_2MeDpaa.dab(Boc) in d_3-MeCN, C) Et_4Dpaa.ga in $CDCl_3$, D) Et_2^{t}BuDpaa.lys(Z) in $CDCl_3$, E) Et_3Dpaa.cys(Tr) in $CDCl_3$. Red stars indicate methylene linker between pyridyl and central amine units. Black stars indicate the protons attached to the alpha carbon of the amino acid unit (400 MHz, 298 K).

Deprotection of Et_2MeDpaa.dab(Boc), Et_4Dpaa.ga and $Et_2{}^t$BuDpaa.lys(Z) under acidic conditions yielded the desired bifunctional chelator which could be isolated by precipitation.

In the case of Et_3Dpaa.cys(Tr), significant decomposition of the ligand was seen under the acidic deprotection conditions – including cleavage of C-N bond at the chiral centre as evidenced by the presence of this fragment in the mass spectrum (*m/z* = 288.1). This decomposition route was also reported for the aspartic acid analogue by Nonat *et al*.[218]

2.3.2 Protonation constants of H_4Dpaa.ga and H_3Dpaa.dab

The bifunctional chelators H_3Dpaa.dab and H_4Dpaa.ga were investigated by potentiometry to assess the effect additional functional groups would have on the ligand and the viability of using these bifunctional chelators for coordination of Ga(III).

The picolinate arms for both bifunctional ligands (logK_3 = 3.77/3.92, logK_4 = 2.69/2.75, Table 2.6) had comparably logK_a values to those of H_3Dpaa (logK_2 = 3.73, logK_3 = 2.82 Table 2.2). This is to be expected as these sites are distant from the structural changes due to changing the amino acid used. The terminal amine of H_3Dpaa.dab (logK_1 = 11.35) is similar to that of the free amino acid (logK_a = 10.44),[219,220] as is the terminal acid of H_4Dpaa.ga (logK_2 = 4.67, free amino acid logK_a = 4.33).[219]

In contrast, the central amine of H_3Dpaa.dab is significantly less basic (logK_2 = 5.39) than in H_3Dpaa (logK_1 = 7.38) or H_4Dpaa.ga (logK_1 = 7.17). This is likely due to an intramolecular hydrogen bond between this central amine and the protonated terminal amine, and a similar trend is seen for the alpha amines of the amino acids (logK_{glycine} = 9.86, log$K_{\text{diaminobutyric acid}}$ = 8.24, log$K_{\text{glutamic acid}}$ = 9.92).[219] The effect that this will have on complexation of Ga(III) is unclear, as this central amine does not form a covalent bond with the Ga(III) cation in the solid state [Ga(Dpaa)(H_2O)] structure it is possible that the effect will be minimal.

Table 2.6: Stepwise protonation constants of H_3Dpaa.dab and H_4Dpaa.ga. (*[L]* = 0.004 M, *T* = 25 °C, *I* = 0.1 M (NMe_4)Cl).

	H_3Dpaa.dab	**H_4Dpaa.ga**
logK_1	11.35(1)	7.17(1)
logK_2	5.39(2)	4.67(2)
logK_3	3.77(3)	3.92(2)
logK_4	2.69(3)	2.75(2)

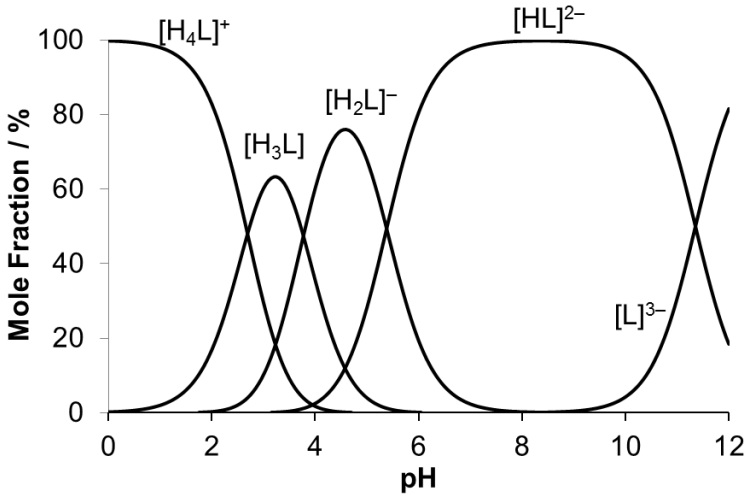

Figure 2.14: Speciation diagram of H_3Dpaa.dab.

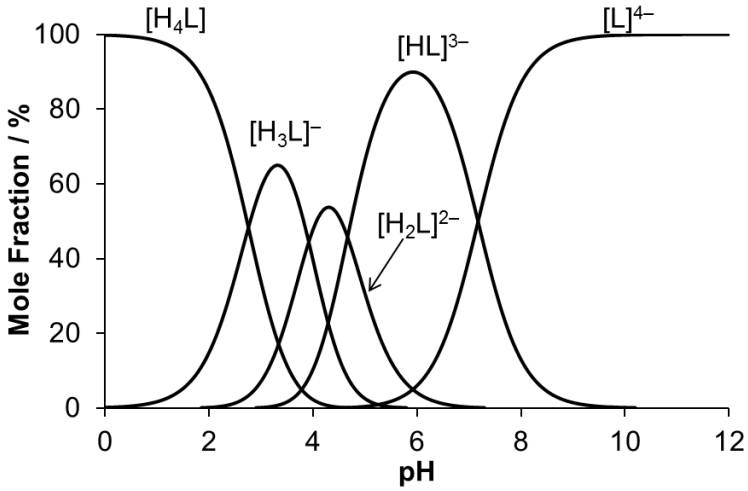

Figure 2.15: Speciation diagram of H_4Dpaa.ga.

2.3.3 Crystal structure of H_4Dpaa.ga

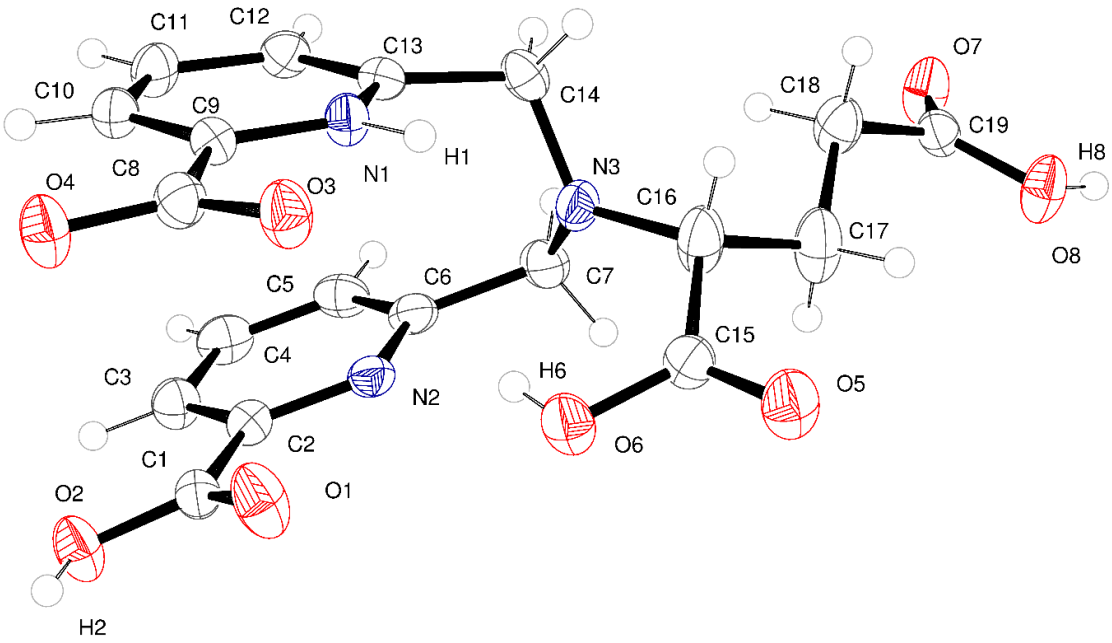

Figure 2.16: ORTEP representation of structure obtained by single crystal X-ray diffraction of H_4Dpaa.ga. Thermal ellipsoids set at 30% certainty.

Single crystals of suitable quality for X-ray diffraction were grown from a solution of H_4Dpaa.ga in acidic water. The obtained structure is asymmetric due to the chiral carbon center (C16). This promotes an intramolecular hydrogen bond (N2···H6-O6) between the acetic acid arm and one of the picolinate rings. The remaining picolinate ring is in the tautomeric form with the nitrogen protonated and a carboxylate anion. A cyclic hydrogen bonding network is seen ($R_2^2(8)$) between this protonated pyridine and the terminal carboxylate group of an adjacent molecule (N1-H1···O7i, where i = x−½, ½−y, z+½). Full crystallographic details are available in Appendix 2.

2.3.4 Synthesis of complexes

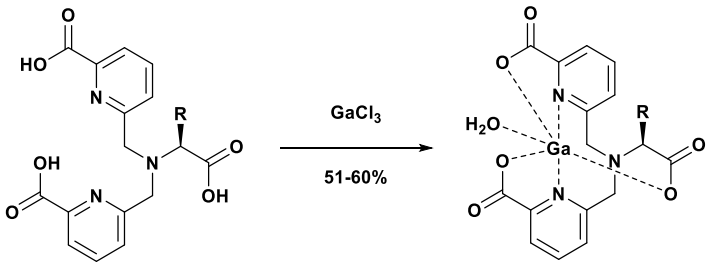

H_3Dpaa.aa **[Ga(Dpaa.aa)(H_2O)]**

Scheme 2.4: Synthesis of bifunctional chelator complexes.

The Ga(III) complexes of the bifunctional chelators were prepared in an analogous manner to [Ga(Dpaa)(H_2O)] (Scheme 2.4). Similar changes are seen in the ^{1}H NMR of the bifunctional chelates upon complexation of Ga(III) as are seen for H_3Dpaa (Figure 2.17, Figure

2.18, Figure 2.19). In all cases the protons of the methylene bridge between the central amine and the picolinate groups become inequivalent. This is evident through the increased number of resonances and the geminal coupling ($^2J_{HH}$ = 16-17 Hz).

Upon complexation the expected increase in molecular weight is observed by mass spectrometry, in addition to the loss of three protons (likely from the coordinating acid groups). The isotopic splitting due to the two naturally abundant radionuclides of gallium (^{69}Ga/^{71}Ga in a 3:2 ratio) is also seen.

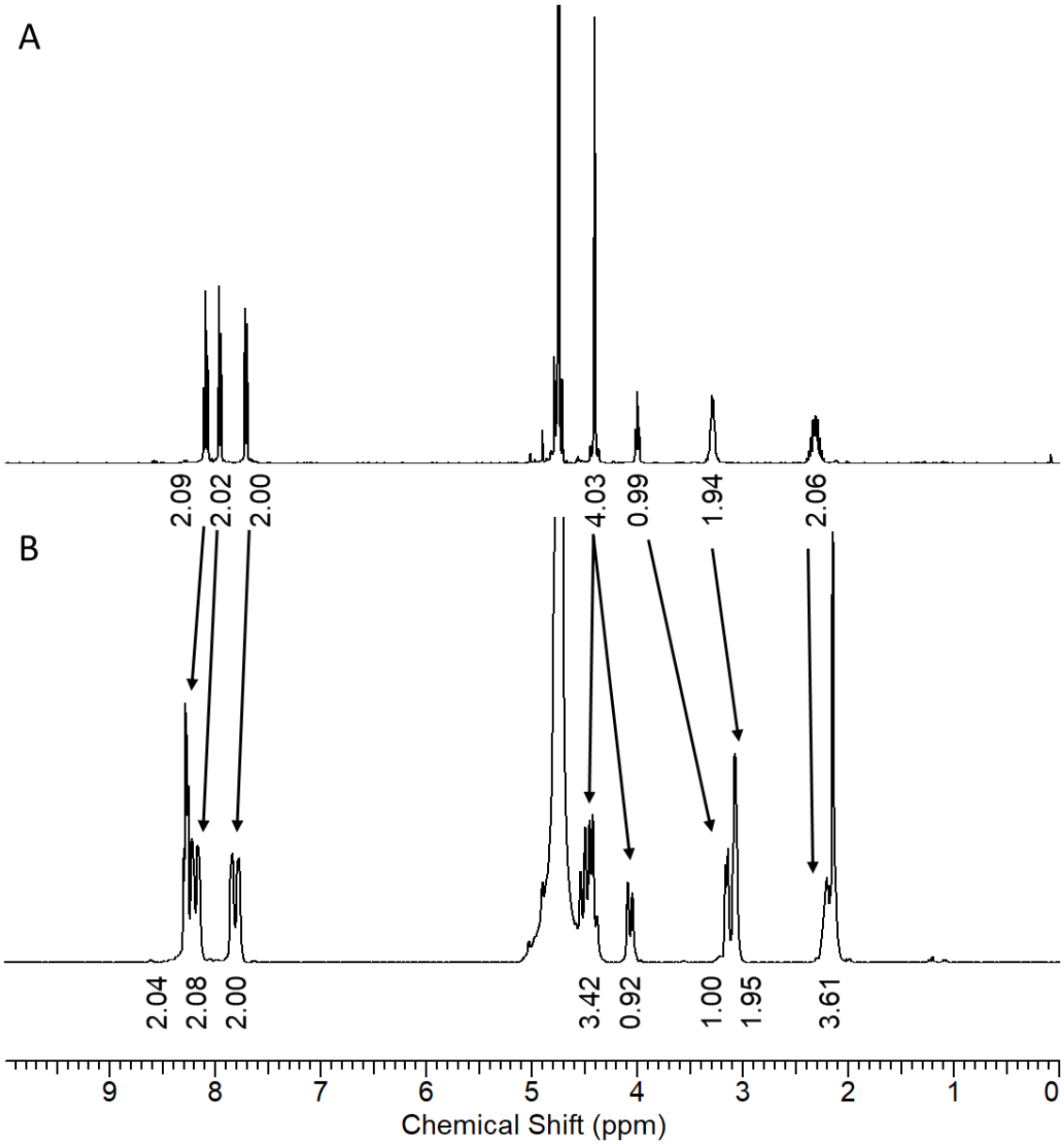

Figure 2.17: ^{1}H NMR of A) H_3Dpaa.dab (D_2O, 298 K, pD = 1.6) B) [Ga(Dpaa.dab)(H_2O)] (D_2O, 298 K, pD = 1.1).

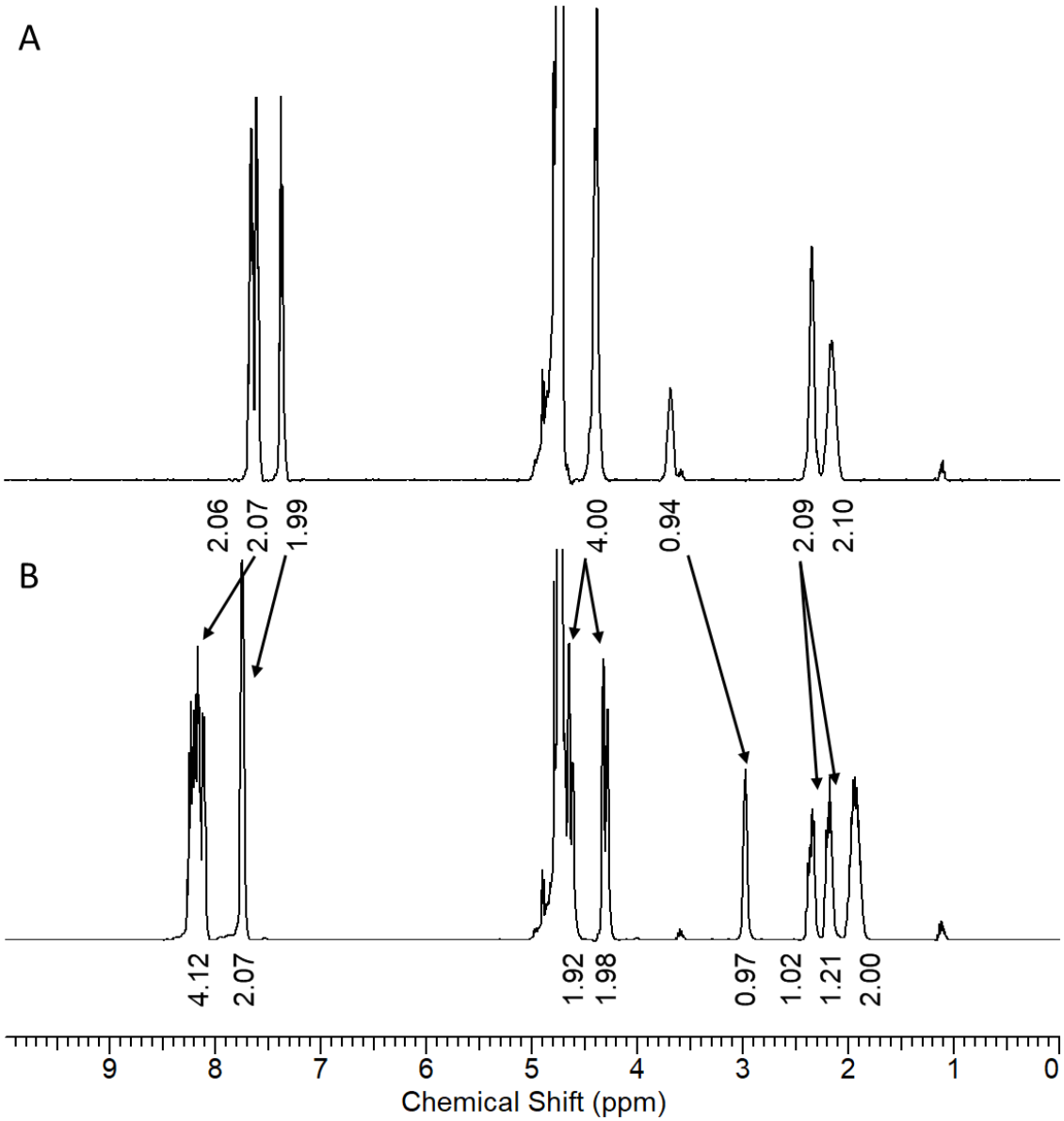

Figure 2.18: ^{1}H NMR of A) $H_4Dpaa.ga$ (D_2O, 298 K, pD = 7.1) B) [Ga(Dpaa.ga)(H_2O)] (D_2O, 298 K, pD = 6.0).

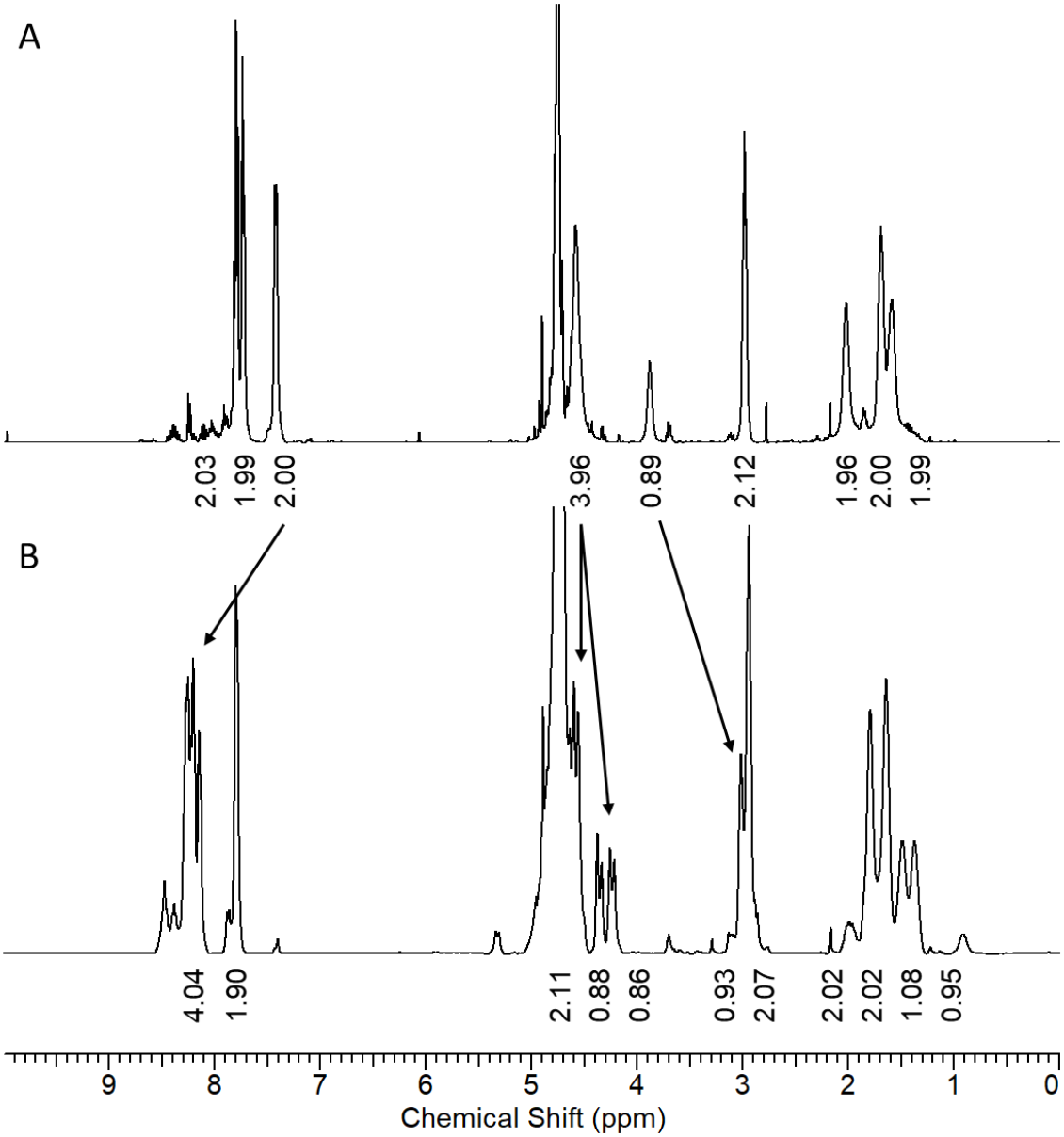

Figure 2.19: ^{1}H NMR of A) H_4Dpaa.lys (D_2O, 298 K, pD = 4.6) B) [Ga(Dpaa.lys)(H_2O)] (D_2O, 298 K, pD = 4.8).

2.3.5 Thermodynamic stability of H_3Dpaa.dab and H_4Dpaa.ga complexes

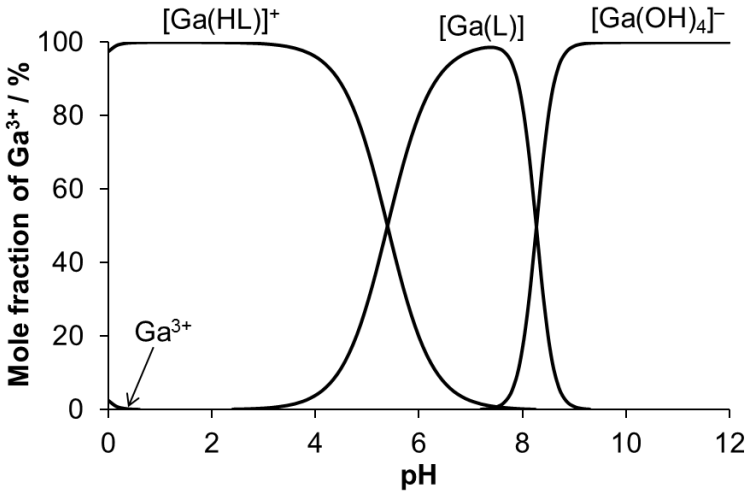

Figure 2.20: Speciation diagram of [Ga(Dpaa.dab)(H_2O)].

Table 2.7: Equilibrium constants (log*K*) obtained for complexes. L = H_3Dpaa.dab [a] Determined by potentiometric titration (*[L]* = *[M]* = 0.004 M, *T* = 25 °C, *I* = 0.1 M (NMe_4)Cl), [b] Determined by UV-VIS titration *[L]* = *[M]* = 0.01 mM, *T* = 25 °C, pH = 0-2)

Equilibrium (Charges are omitted)	Ga(III)[a]	Cu(II)[a, b]	Zn(II)[a, b]
M + L ↔[M(L)]	22.08(1)	19.1(1)	15.8(1)
[M(HL)] ↔ [M(L)] + H	5.40(2)	5.0(1)	6.8(1)
[M(H_2L)] ↔ [M(HL)] + H		2.8(1)	1.8(1)
[M(L)] + H_2O ↔ [M(L)(OH)] + H		12.5(1)	12.2(1)

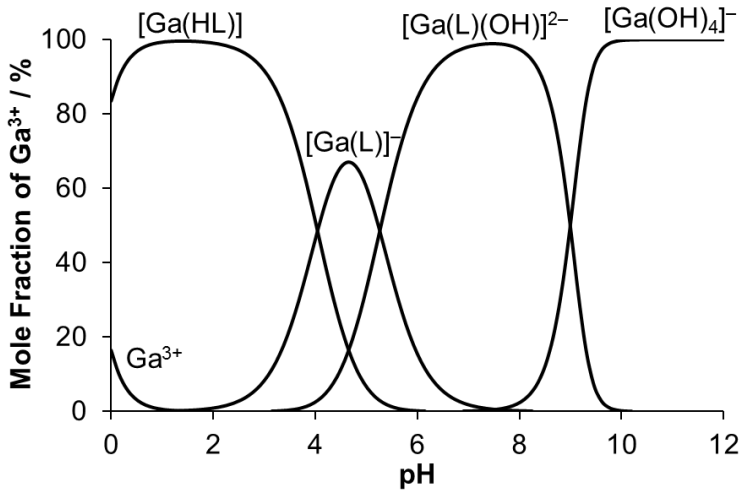

Figure 2.21: Speciation diagram of [Ga(Dpaa.ga)(H_2O)].

Table 2.8: Equilibrium constants (log*K*) obtained for complexes. L = H_4Dpaa.ga [a] Determined by potentiometric titration (*[L]* = *[M]* = 0.004 M, *T* = 25 °C, *I* = 0.1 M (NMe_4)Cl), [b] Determined by UV-VIS titration *[L]* = *[M]* = 0.01 mM, *T* = 25 °C, pH = 0-2)

Equilibrium (Charges are omitted)	Ga(III)[a]	Cu(II)[a, b]	Zn(II)[a, b]
M + L ↔[M(L)]	18.36(3)	14.52(7)	13.38(7)
[M(HL)] ↔ [M(L)] + H	4.04(3)	4.54(7)	4.65(7)
[M(H_2L)] ↔ [M(HL)] + H	-	3.10(7)	1.77(8)
[M(L)] + H_2O ↔ [M(L)(OH)] + H	5.27(1)	10.52(7)	12.24(7)

The Ga(III)-H_3Dpaa.dab and Ga(III)-H_4Dpaa.ga systems were investigated by potentiometry. The equilibrium constants are given in Table 2.7 and Table 2.8 and speciation diagrams in Figure 2.20 and Figure 2.21.

The association constant for the H_3Dpaa.dab system ($logK_{[Ga(Dpaa.dab)]}$ = 22.08) is significantly higher than that of the H_3Dpaa system ($logK_{[Ga(Dpaa)]}$ = 18.53). However, when the additional protonated site (of the terminal amine) is considered, the lower equilibirium constant ($logK_{[Ga(Dpaa.dab)(OH)]}$ = 16.13) is more directly comparable to the H_3Dpaa system. This lower constant suggests that the Ga(III)-H_3Dpaa.dab complex is less stable than the Ga(III)-H_3Dpaa complex – this is likely due to the less basic central amine (*vida supra*). Although this amine isn't

definitively involved in bonding, it likely plays some role in stabilising the charged Ga(III) ion and the significant change in basicity will affect binding.

The association constant for the H_4Dpaa.ga system ($logK_{[Ga(Dpaa.ga)]}$ = 18.36) is very comparable to that of the H_3Dpaa system. In addition, the protonation of the complex ($logK_{[Ga(Dpaa.ga)(H)]}$ = 4.04) is close to that of the pendant carboxylic acid of the ligand ($logK_2$ = 4.67). These values suggest that the coordination environment of Ga(III) is similar in both complexes, and that the terminal carboxylate of the glutamic acid is not involved in complexation of Ga(III) as it is deprotonated at a similar pH. This is further supported by the obtained crystal structure (*vida infra*).

Table 2.9: Stability constants (log*K*) obtained for M-L complexes. [a] Determined by UV-VIS titration *[L]* = *[M]* = 0.1 mM, *T* = 25 °C, pH = 2-7 [b] Determined by potentiometric titration (*[L]* = *[M]* = 0.004 M, *T* = 25 °C, *I* = 0.1 M (NMe_4)Cl), [c]Constant ($logK_{GaHL}$) describing equilibrium Ga(III) + $(HL)^{2-} \leftrightarrow [Ga(HL)]^+$ where the amine group deprotonation and hydroxido species formation are not considered. [d] Determined by UV-VIS titration ([L] = [M] = 0.01 mM, *T* = 25 °C, pH = 0-2)

	H_3Dpaa	H_3Dpaa.dab	H_4Dpaa.ga
Ga(III)	18.53(5)[a]	22.08(1)[b]	18.36(3)[b]
		(16.13(1))[b,c]	
Cu(II)	10.85(1)[b]	19.1(1)[b,d]	14.52(7)[b,d]
Zn(II)	11.93(3)[b]	15.8(1)[b,d]	13.38(7)[b,d]

Both the H_3Dpaa.dab ($logK_{[Cu(Dpaa.dab)]}$ = 19.1, $logK_{[Zn(Dpaa.dab)]}$ = 15.8) and H_4Dpaa.ga ($logK_{[Cu(Dpaa.ga)]}$ = 14.52, $logK_{[Zn(Dpaa.ga)]}$ = 13.38) systems show greater affinity for Cu(II) and Zn(II) than the H_3Dpaa system ($logK_{[Cu(Dpaa)]}$ = 10.85, $logK_{[Zn(Dpaa)]}$ = 11.93). This may be due to the additional coordinating atoms of the pendant amine and carboxylate groups increasing the complex stability – however this is speculative as the exact coordination environment of these complexes is still unknown. Regardless, the Ga(III) complexes are more stable than the Cu(II) and Zn(II) complexes in all cases.

Table 2.10: pM values. pH = 7.4. *[M]* = 1 x 10^{-6} M, *[L]* = 1 x 10^{-5} M. Ga(III) is present as $[Ga(OH)_3]$ and $[Ga(OH)_4]^-$, Cu(II) and Zn(II) are present as free aqua anions.

	H_3Dpaa	H_3Dpaa.dab	H_4Dpaa.ga
Ga(III)	8.91	6.34	6.21
Cu(II)	12.60	16.06	15.27
Zn(II)	12.60	12.90	14.14

The *pM* values for all three ligands are less promising. The *pGa* values are significantly lower than the obtained *pCu* and *pZn* values. The *pGa* value accounts for the strong affinity of the hydroxide anion for Ga(III). In contrast to the association constants, these values suggest that the bifunctional chelators form less stable complexes with Ga(III) than H_3Dpaa.

2.3.6 Crystal structure

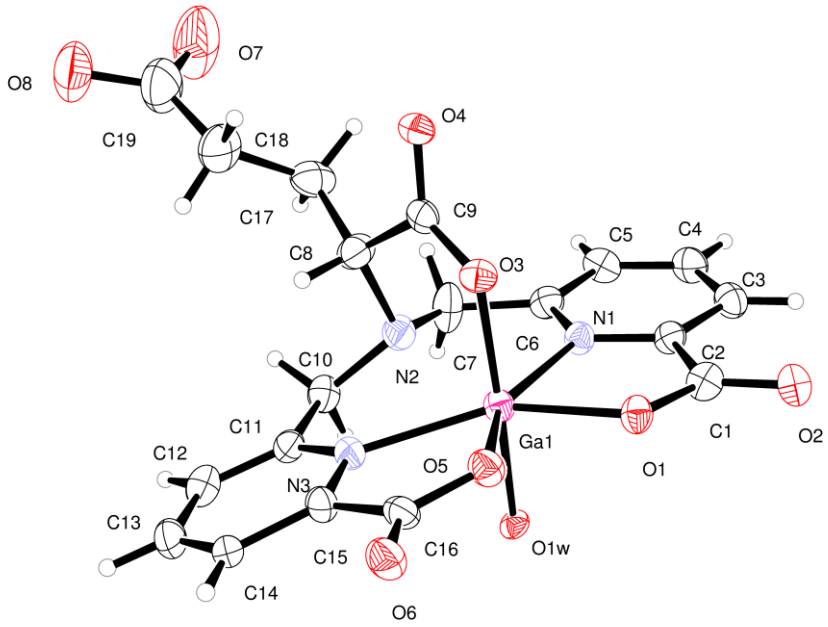

Figure 2.22: ORTEP representation of structure obtained by single crystal X-ray diffraction of [Ga(Dpaa.ga)(H_2O)]. Thermal ellipsoids set at 30% certainty.

Single crystals of suitable quality for X-ray diffraction were obtained by slow evaporation of an acidic water solution containing [Ga(Dpaa.ga)(H_2O)]. The obtained structure has a similar coordination environment to that obtained for [Ga(Dpaa)(H_2O)]. The central tertiary amine is not covalently bonded to the Ga(III) atom, and a water molecule occupies the vacant coordination site. The angles in the plane of the picolinate arms are heavily distorted away from the ideal octahedral geometry, with N1-Ga1-N3 (133.8°) being significantly greater than the ideal 90°, and N1-Ga1-O1 (76.2°) and N3-Ga1-O5 (75.1°) being significantly smaller than the ideal 90°. The additional carboxylate of the glutamic acid residue is not involved in coordinating the Ga(III) atom. Full crystallographic details are available in Appendix 2.

In contrast to the structure for [Ga(Dpaa)(H_2O)], the asymmetry caused by the chiral carbon centre (C8) induces a large twist in the structure of [Ga(Dpaa.ga)(H_2O)]. This is evident in the angle between the mean planes of the picolinate arms – for [Ga(Dpaa.ga)(H_2O)] this angle is 15.85(3)°, much greater than for [Ga(Dpaa)(H_2O)].

Table 2.11: Selected crystallographic parameters for [Ga(Dpaa.ga)(H_2O)].

Bond	Bond Length / Å	Angle	Bond Angle / °
O1-Ga1	2.000(6)	O1-Ga1-N1	76.2(3)
N1-Ga1	2.180(8)	N1-Ga1-N3	133.8(3)
N2···Ga1	2.510(9)	N3-Ga1-O5	75.1(3)
N3-Ga1	2.192(7)	O5-Ga1-O1	75.4(3)
O5-Ga1	2.028(7)	O3-Ga1-O1	93.7(3)
O3-Ga1	1.939(7)	O3-Ga1-N1	85.8(3)
O1W-Ga1	1.958(6)	O3-Ga1-N3	96.5(3)
		O3-Ga1-O5	90.9(3)
		O3-Ga1-O1W	172.7(3)

2.3.7 Radiolabelling

2.3.7.1 Radiolabelling of bifunctional chelators

The bifunctional derivatives of H_3Dpaa retain their ability to complex [^{68}Ga]Ga(III) under mild reaction conditions (Table 2.12). H_3Dpaa.dab was a less effective chelator than H_3Dpaa at neutral pH; this suggests that the pendant amine has a negative effect on radiolabelling. However, when this amine is further from the central amine, the radiochemical yield at neutral pH is high as demonstrated by H_3Dpaa.lys. This may be due to intramolecular hydrogen bonding between the terminal amine and the α-carboxylate of H_3Dpaa.dab (forming a 7 membered ring) preventing efficient chelation of ^{68}Ga under neutral pH conditions, whereas H_3Dpaa.lys does not have a significant hydrogen bonding between these two units due to the increased length of the alkyl chain. This is evidenced in the parent amino acids as an increased acidity of the α-carboxylate of diaminobutyric acid (pK_a = 1.85) than that of glycine (pK_a = 2.22) or lysine (pK_a = 2.18).[219] The radiochemical yield achieved by H_4Dpaa.ga is comparable to that of the parent ligand; this supports the conclusion that the pendant acid arm is not involved in complexation of Ga(III). This acid is a viable site for functionalisation, and conjugation at this site should not affect the radiolabelling ability of the ligand.

These results compare very favourably to those obtained with other acyclic chelators radiolabelled at neutral pH. HBED is reported to achieve radiochemical yields of approximately 90% at pH 7 (25 °C, 5 μM, 10 minutes), however multiple radiolabelled species were formed during this radiolabelling.[221] While DATA^{PPh} was able to achieve radiochemical yields >95% at pH 7 (23 °C, 5 μM, 5 minutes) the three other DATA chelators reported by Seemann *et al.* failed to reach 85% radiochemical yields under these conditions.[179] These chelators are not bifunctional – radiolabelling of the conjugated analogue DATATOC has not been reported under neutral conditions.[181] THP has been reported to achieve radiochemical yields of 97% at pH 6.5 (5 μM, 25

°C, 10 minutes).[221] The high radiochemical yields achieved by H_3Dpaa, H_4Dpaa.ga and H_3Dpaa.lys with ^{68}Ga at pH 7.4 are promising for further development; however, the concentration of ligand required is higher than for THP and DATA^{PPh}.

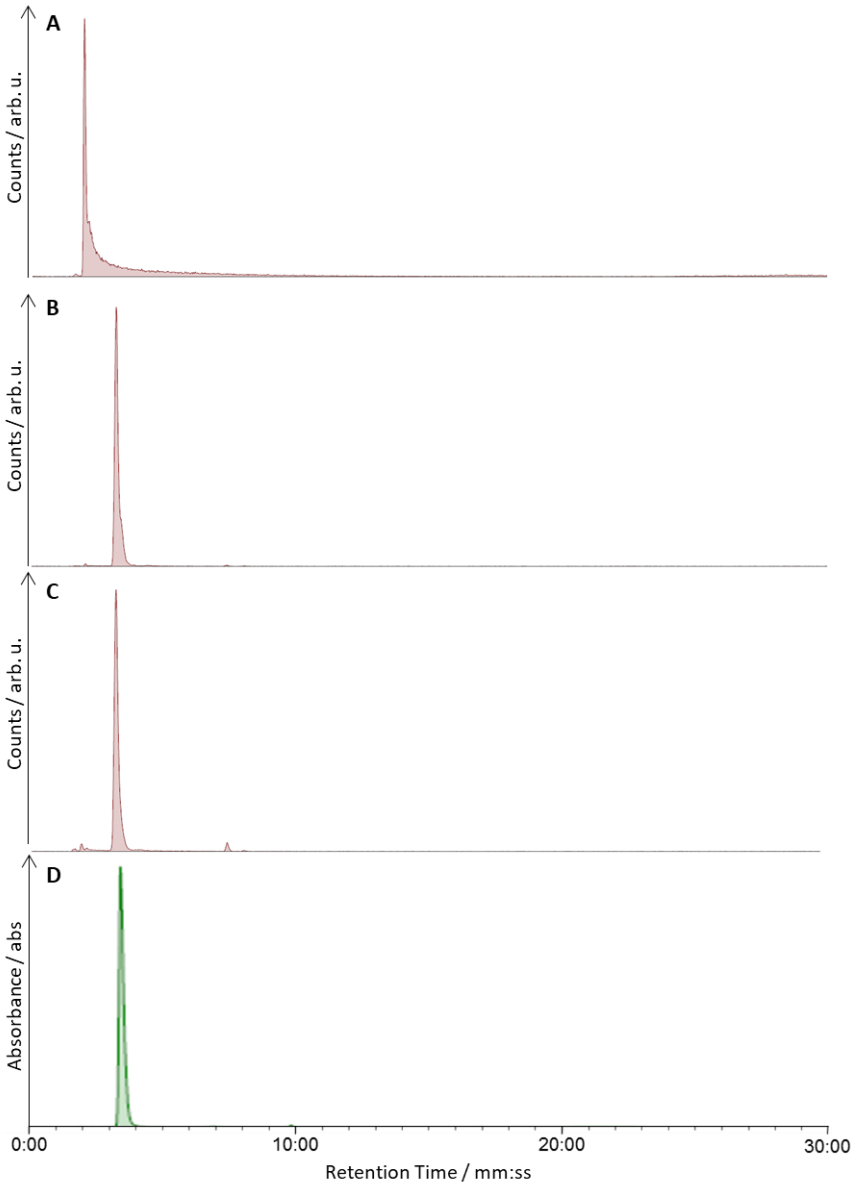

Figure 2.23: HPLC Chromatograms for the radiolabelling of H_3Dpaa.dab with [^{68}Ga]$GaCl_3$. A) Radio-HPLC chromatogram of non-complexed [^{68}Ga]Ga(III) B/C) Radio-HPLC of crude radiolabelling mixture containing H_3Dpaa.dab and [^{68}Ga]Ga(III) B) (*[L]* = 100 µM, *t* = 5 minutes, *pH* = 4.0, *T* = 25 °C, *I* = 0.1 M Acetate buffer). C) (*[L]* = 100 µM, *t* = 5 minutes, *pH* = 7.5, *T* = 37 °C, *I* = PBS). D) UV-HPLC chromatogram of isolated [Ga(Dpaa.dab)(H_2O)]. **HPLC Gradient A.**

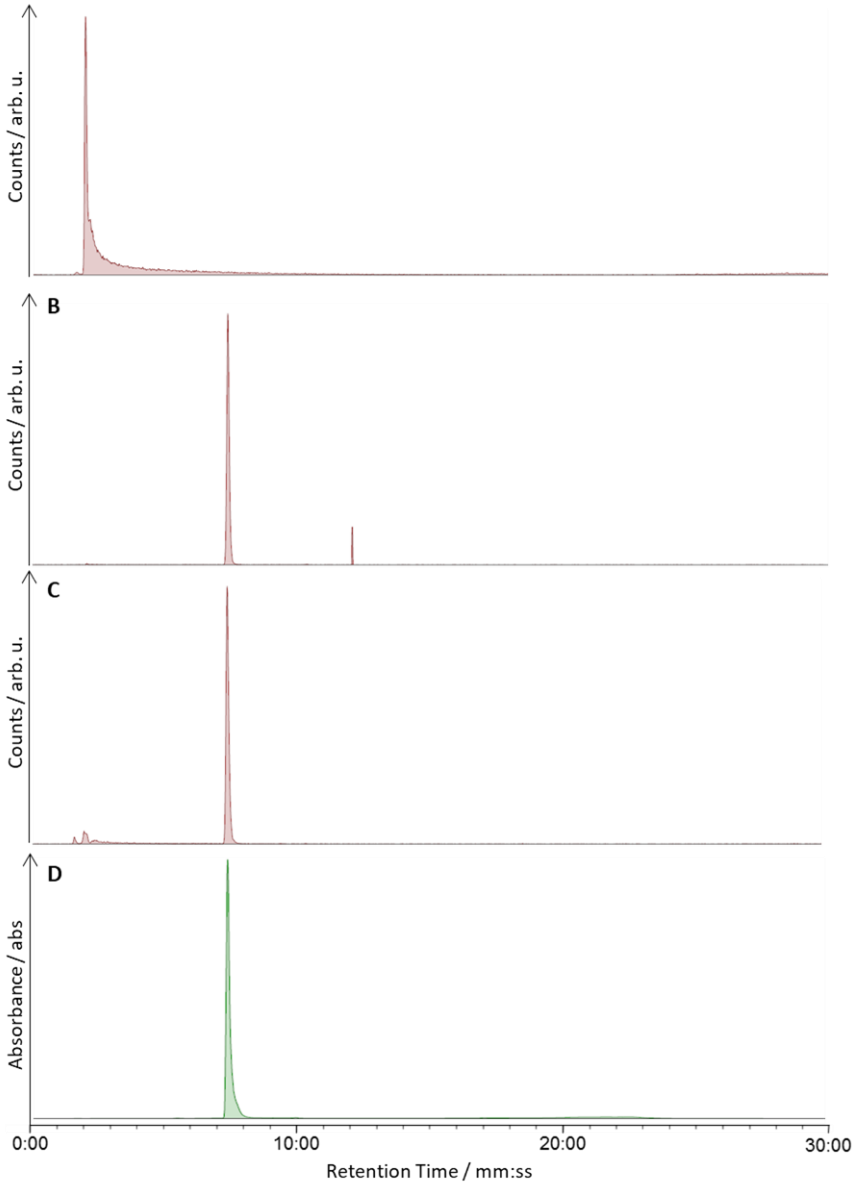

Figure 2.24: HPLC Chromatograms for the radiolabelling of H_4Dpaa.ga with [^{68}Ga]$GaCl_3$. A) Radio-HPLC chromatogram of non-complexed [^{68}Ga]Ga(III) B/C) Radio-HPLC of crude radiolabelling mixture containing H_4Dpaa.ga and [^{68}Ga]Ga(III) B) (*[L]* = 100 µM, *t* = 5 minutes, *pH* = 4.0, *T* = 25 °C, *I* = 0.1 M Acetate buffer). C) (*[L]* = 100 µM, *t* = 5 minutes, *pH* = 7.5, *T* = 37 °C, *I* = PBS). D) UV-HPLC chromatogram of isolated [Ga(Dpaa.ga)]. **HPLC Gradient A.**

Table 2.12: Summary of radiolabelling with bifunctional H_3Dpaa.aa chelators. [a] pH = 4.0, *I* = 0.1 M Acetate, *T* = 25 °C, *t* = 5 minutes. [b] pH = 7.4, *I* = PBS, *T* = 37 °C, *t* = 5 minutes.

	H_3Dpaa	**H_3Dpaa.dab**	**H_4Dpaa.ga**	**H_3Dpaa.lys**
pH 4.0[a] / %	99	99	99	95
pH 7.4[b] / %	95	84	94	95
Molar Activity[b] / GBq µmol^{-1}	3.9	20.0	28.9	3.4

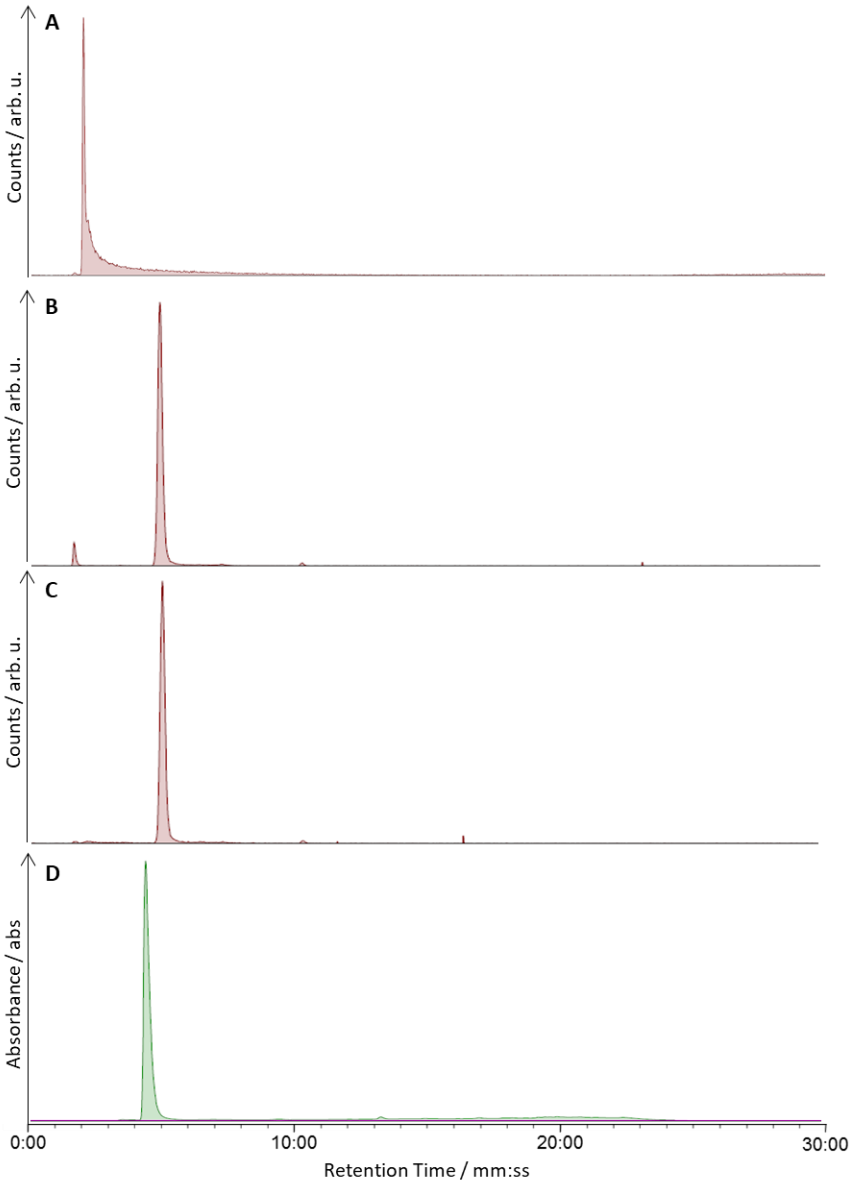

Figure 2.25: HPLC Chromatograms for the radiolabelling of H_3Dpaa.lys with [^{68}Ga]$GaCl_3$. A) Radio-HPLC chromatogram of non-complexed [^{68}Ga]Ga(III) B/C) Radio-HPLC of crude radiolabelling mixture containing H_3Dpaa.lys and [^{68}Ga]Ga(III) B) (*[L]* = 100 µM,*t* = 5 minutes, *pH* = 4.0, *T* = 25 °C, *I* = 0.1 M Acetate buffer). C) (*[L]* = 100 µM, *t* = 5 minutes, *pH* = 7.5, *T* = 37 °C, *I* = PBS). D) UV-HPLC chromatogram of isolated [Ga(Dpaa.lys)(H_2O)]. **HPLC Gradient A.**

2.4. Conjugation to PSMA

2.4.1 Synthesis of PSMA urea

The PSMA targeting Glu-Urea-Lys-$(CH_2)_6NH_2$, **9**, was synthesised according to Felber *et al*. in 5 steps (Scheme 2.5).[222]

Urea coupling of di *tert*-butyl-L-glutamic acid to *tert*-butyl Nε-((benzyloxy)carbonyl)-L-lysinate to give **6** was achieved in a 25% yield – lower than the reported yield of 69% obtained by Felber and co-workers.[222] This was due to the formation of the double lysine product (*m/z* = 700.3) which could be separated by silica gel chromatography allowing isolation of the desired product (*m/z* = 622.8). Selective deprotection of the benzoyl protected amino group was

achieved by hydrogenation in a good yield (97%) to give **6**. This deprotection is evident through the absence of aromatic peaks in the NMR and the retention of the other peaks; in particular the alpha carbon hydrogen peaks (δ_H = 4.37-4.30) and the *tert*-butyl ester peaks (δ_H = 1.47, 1.44).

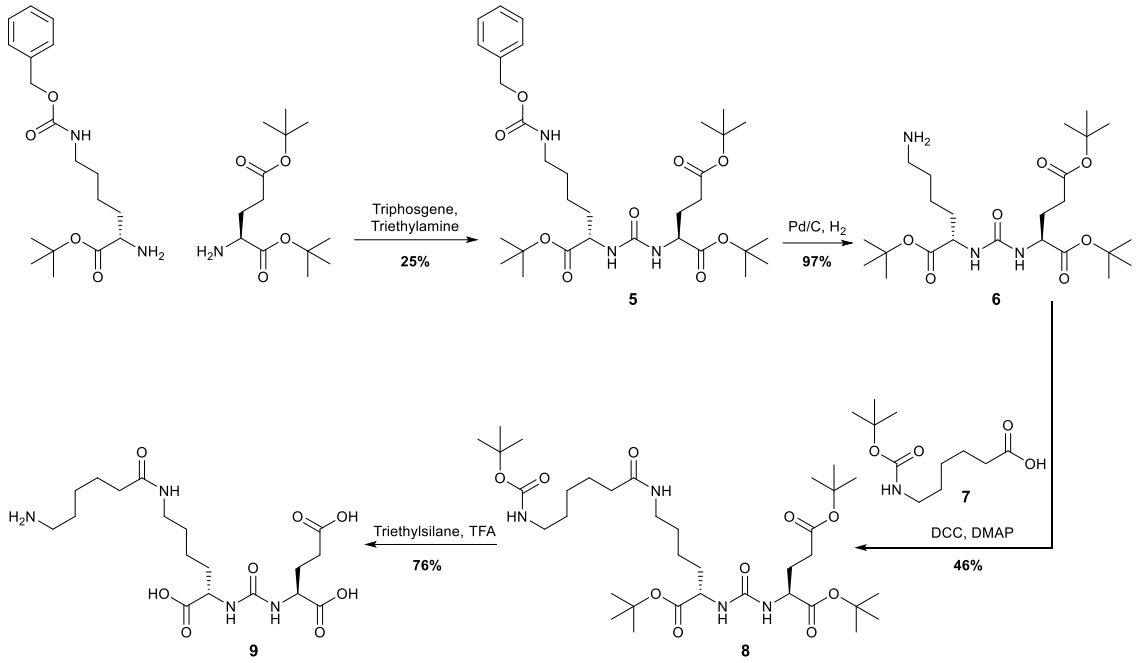

Scheme 2.5: Synthesis of Glu-Urea-Lys-$(CH_2)_6NH_2$, **9**.

Coupling to *tert*-butyl carbamate protected aminohexanoic acid (**7**) was achieved through a carbodiimide coupling, giving **8** in a 46% yield. Evidence for this coupling can be seen in the ^{1}H NMR shift of the protons alpha to the terminal amine; upon coupling these protons are deshielded and the resonance corresponding to them increases to 3.38-3.06 ppm from 2.68 ppm. A slight increase in shielding is seen for the protons adjacent to the terminal acid (δ_H = 2.35) once it is converted into an amide (δ_H = 2.22-2.15).

8 was fully deprotected by trifluoroacetic acid in dichloromethane to yield the deprotected species, **9**; deprotection was evidenced by the loss of peaks corresponding to the –$C(CH_3)_3$ environments.

2.4.2 Synthesis of H_3Dpaa.ga.PSMA

The reactivity of H_4Dpaa.ga was increased by formation of a cyclic anhydride in the glutamate backbone (Scheme 2.6) to yield 6,6'-(((2,6-dioxotetrahydro-2H-pyran-3-yl)azanediyl)bis(methylene))dipicolinic acid (H_2Dpaa.ga.anh). Addition of acetic anhydride in acetonitrile in the presence of pyridine resulted in the condensation of the two carboxylic acids. This is evidenced through a reduction in molecular weight (*m/z* = 400, $[M + H]^+$). While the ligand H_4Dpaa.ga is not soluble in acetonitrile, even in the presence of pyridine, in the presence of both pyridine and acetic anhydride the reaction solution becomes clear as the reaction progresses. Analysis of the crude reaction mixture by NMR (Figure 2.26) shows the presence of excess

pyridine and acetic anhydride, along with the acetic acid byproduct. The remaining peaks correspond to the anhydride; the increased rigidity of the glutamate backbone results in the geminal protons along this backbone and in the methylene bridges becoming inequivalent.

The excess pyridine and acetic anhydride can be removed by precipitating the product, H_2Dpaa.ga.anh, by addition of diethyl ether. Following drying it is evident that the excess acetic anhydride has been removed (Figure 2.26). Some additional aromatic resonances remain, possibly due to pyridinium salt formation. Removal of the excess acetic anhydride is key to prevent unwanted acylation of the amine in the next step. The precipitate formed was used without further purification.

Under the strongly basic conditions required for conjugation of **9** to H_2Dpaa.ga.anh, H_2Dpaa.ga.anh rapidly hydrolyses back to H_4Dpaa.ga. The N-hydroxysuccinimide-ester of H_2Dpaa.ga.anh is more stable under these conditions and can be readily prepared by addition of N-Hydroxysuccinimide and pyridine in acetonitrile.

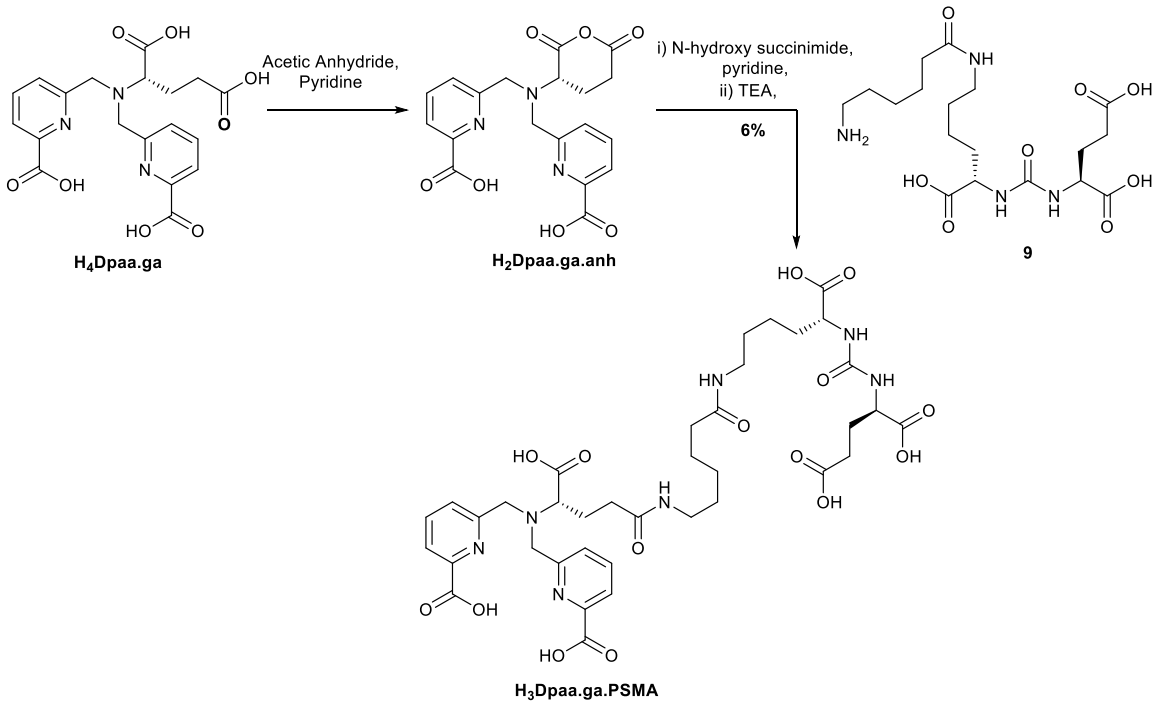

Scheme 2.6: Conjugation of H_4Dpaa.ga to **9**.

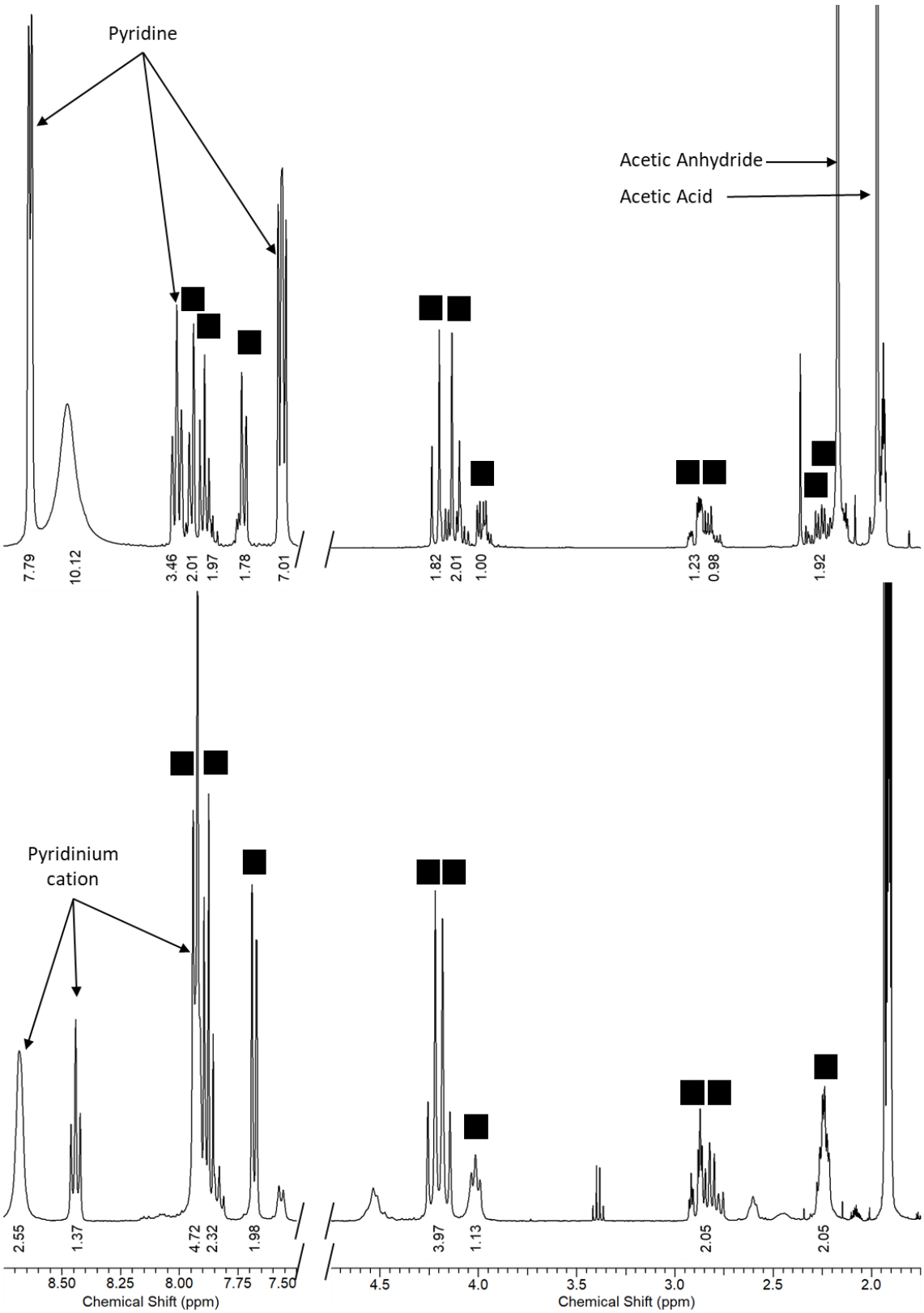

Figure 2.26: ^{1}H NMR of H_2Dpaa.ga.anh. Top: Crude reaction mixture containing H_4Dpaa.ga, acetic anhydride and pyridine in acetonitrile after incubation at room temperature. Bottom: Dried precipitate from crude reaction mixture. (400 MHz, d_3-MeCN, 298 K)

Following formation of the N-hydroxysuccinimide ester, **9** in dimethylformamide was added directly to the reaction mixture, along with triethylamine. The desired product was purified by semi-preparative HPLC to give 1-(6-carboxypyridin-2-yl)-2-((6-carboxypyridin-2-

yl)methyl)-6,13,21-trioxo-2,7,14,20,22-pentaazapentacosane-3,19,23,25-tetracarboxylic acid (H_3Dpaa.ga.PSMA) in a 6% yield.

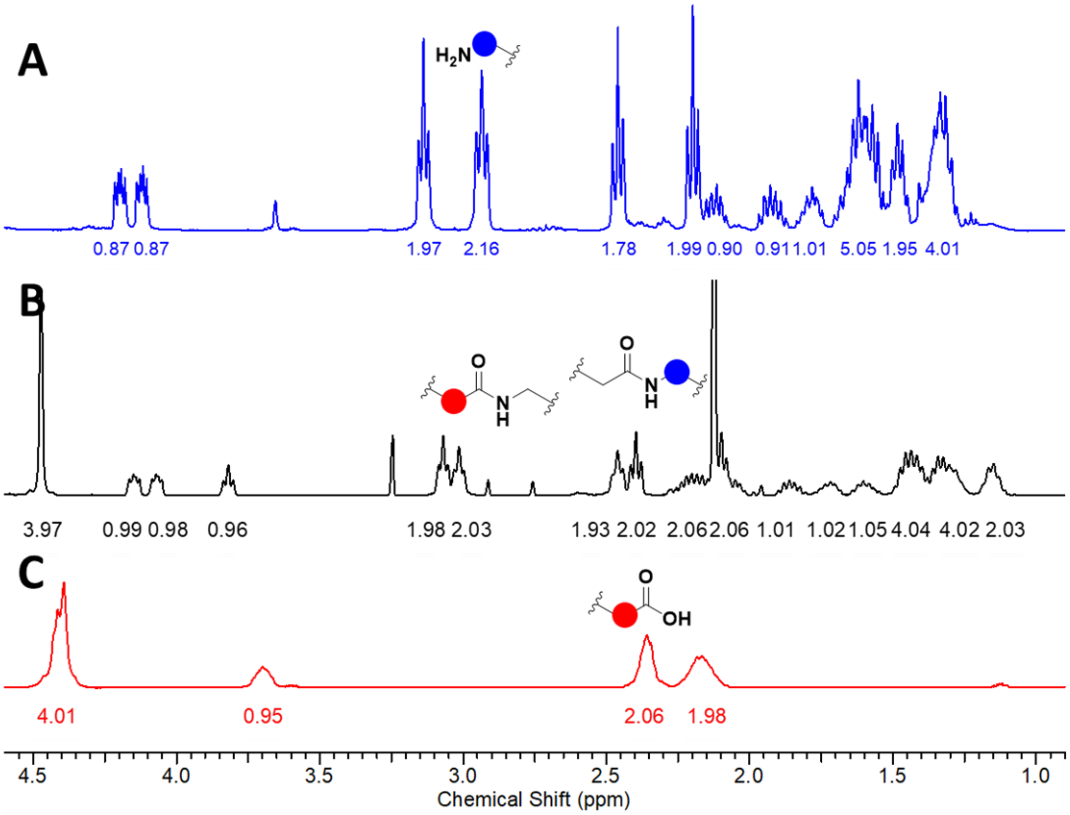

Figure 2.27: ^{1}H NMR of A) **9**, B) H_3Dpaa.ga.PSMA, C) H_4Dpaa.ga. Resonances adjacent to the amide linkage are highlighted. Blue circles indicate resonances of protons that have been translated from **9** into H_3Dpaa.ga.PSMA, Red circles indicate resonances of protons that have been translated from H_4Dpaa.ga. (400 MHz, D_2O, 298 K)

The conjugate has ^{1}H NMR resonances corresponding to both the ligand, H_4Dpaa.ga, and the urea, **9** (Figure 2.27). Most of the protons are in a similar environment in the conjugate as they are in the starting materials, as such there is no significant difference in their chemical shift or splitting patterns. The protons adjacent to the newly formed amide bond are in a different environment following the coupling reaction. The protons of H_4Dpaa.ga that are adjacent to the carboxylic acid are deshielded upon coupling; the resonance corresponding to these protons moves downfield from δ_H = 2.43 to δ_H = 3.01. The protons adjacent to the amine of **9** have an increased shielding upon conjugation, with the resonance corresponding to these protons shifting from δ_H = 2.93 to δ_H = 2.46.

2.4.3 Radiolabelling of H_3Dpaa.ga.PSMA

2.4.3.1 Radiolabelling

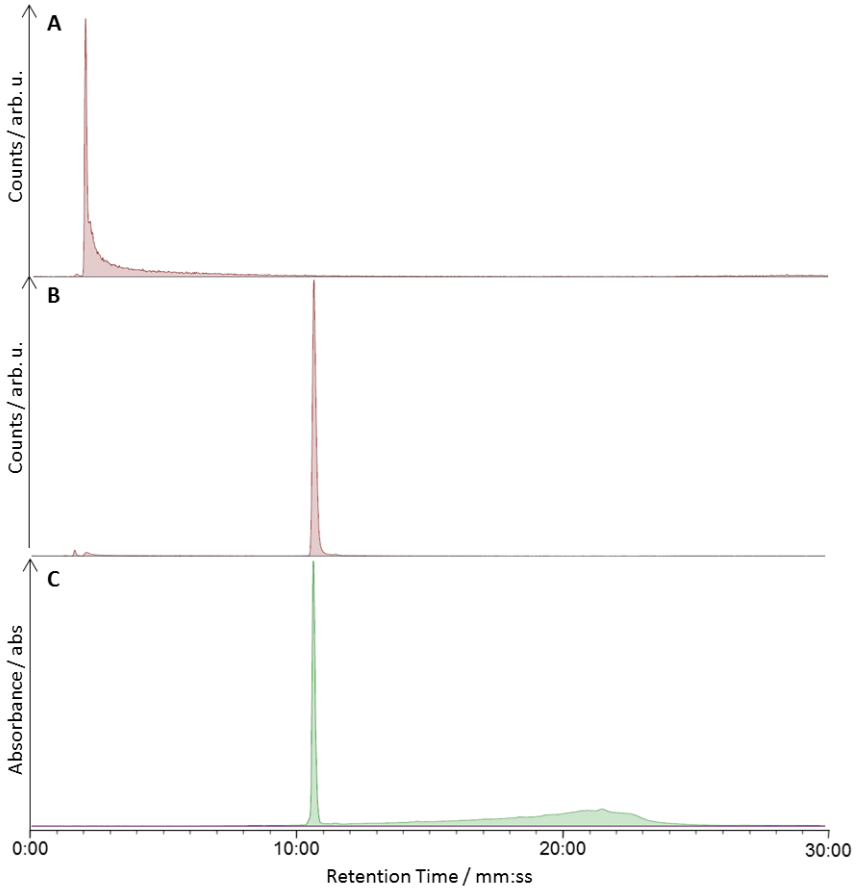

Figure 2.28: Radio-HPLC of [^{68}Ga][Ga(Dpaa.ga.PSMA)] and UV HPLC of [Ga(Dpaa.ga.PSMA)] HPLC Chromatograms for the radiolabelling of H_3Dpaa.ga.PSMA with [^{68}Ga]$GaCl_3$. A) Radio-HPLC chromatogram of non-complexed [^{68}Ga]Ga(III) B) Radio-HPLC of crude radiolabelling mixture containing H_3Dpaa.ga.PSMA and [^{68}Ga]Ga(III) ([L] = 139 µM,*t* = 15 minutes, *pH* = 7.0, *T* = 25 °C, *I* = 0.015 M Acetate buffer). C) UV-HPLC chromatogram of isolated [Ga(Dpaa.ga.PSMA)]. **HPLC Gradient A**

H_3Dpaa.ga.PSMA was radiolabelled at pH 7, producing only a single radiolabelled species (95% RCY). Furthermore, radiolabelling at a second site (King's College London) further confirmed the rapid radiolabelling of this conjugate. In radiolabelling studies designed to act as preliminary tests prior to *in vivo* application, radiolabelling of 4 ng of conjugate achieved a 95% RCY at approximately pH 7.

2.4.3.2 Hot uptake

When the radiolabelled conjugate, [^{68}Ga][Ga(Dpaa.ga.PSMA)] was applied to *in vitro* hot uptake studies, the results were unexpected. The radiolabelled conjugate was diluted to 50 nM before being incubated with PSMA +ve and PSMA –ve DU145 cells at 37 °C for 30 minutes. No significant difference in uptake was seen between the two cell lines. In contrast, uptake of [^{68}Ga][Ga(THP.PSMA)] was over 50 fold greater in PSMA +ve DU145 cells than in PSMA –ve cells under the same conditions. [^{68}Ga][$GaCl_3$] performed similarly to [^{68}Ga][Ga(Dpaa.ga.PSMA)], with

little uptake in either PSMA +ve or –ve cells suggesting that the complex stability may be an issue.

Table 2.13: Uptake of ^{68}Ga radiotracers by DU145 cells. (*[Radiotracer]* = 5 x 10^{-9} M, incubation time = 30 minutes, *T* = 37 °C.)

	Activity associated with cells / %	
Radiotracer	**PSMA +ve**	**PSMA -ve**
[^{68}Ga][Ga(THP.PSMA)]	2.67	0.04
[^{68}Ga][Ga(Dpaa.ga.PSMA)]	0.67	0.61
[^{68}Ga]$GaCl_3$	0.66	0.72

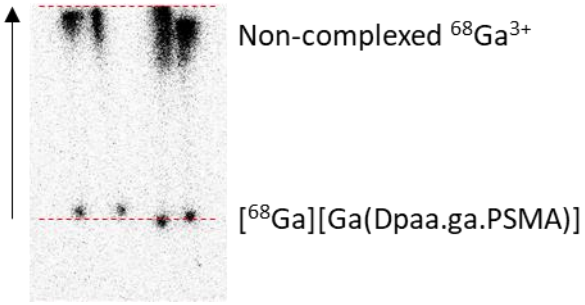

Figure 2.29: Radiolabelling mixture containing [^{68}Ga][Ga(Dpaa.ga.PSMA)] diluted to 200 nM in PBS after 30 minutes incubation. 10-15% intact.

Indeed, when the radiolabelling mixture was diluted to 200 nM and incubated in PBS for 30 minutes 85-90% of the activity was released from the complex. *In vivo* the radiotracer will be significantly diluted, as well as being in the presence of competitors that may promote decomplexation. This instability makes [^{68}Ga][Ga(Dpaa.ga.PSMA)] unsuitable for *in vivo* application.

2.5. Assessment of stability of [^{68}Ga][Ga(Dpaa)(H_2O)]

2.5.1 Stability to dilution

To confirm the results seen with [^{68}Ga][Ga(Dpaa.ga.PSMA)], a radiolabelling solution containing 100 µM of H_3Dpaa and [^{68}Ga]$GaCl_3$ was diluted with PBS. Significant release of the [^{68}Ga]Ga(III) was seen at ligand concentrations of 1 µM and below after 30 minutes. Further dilution was prevented by the detection limit of the radio-TLC reader

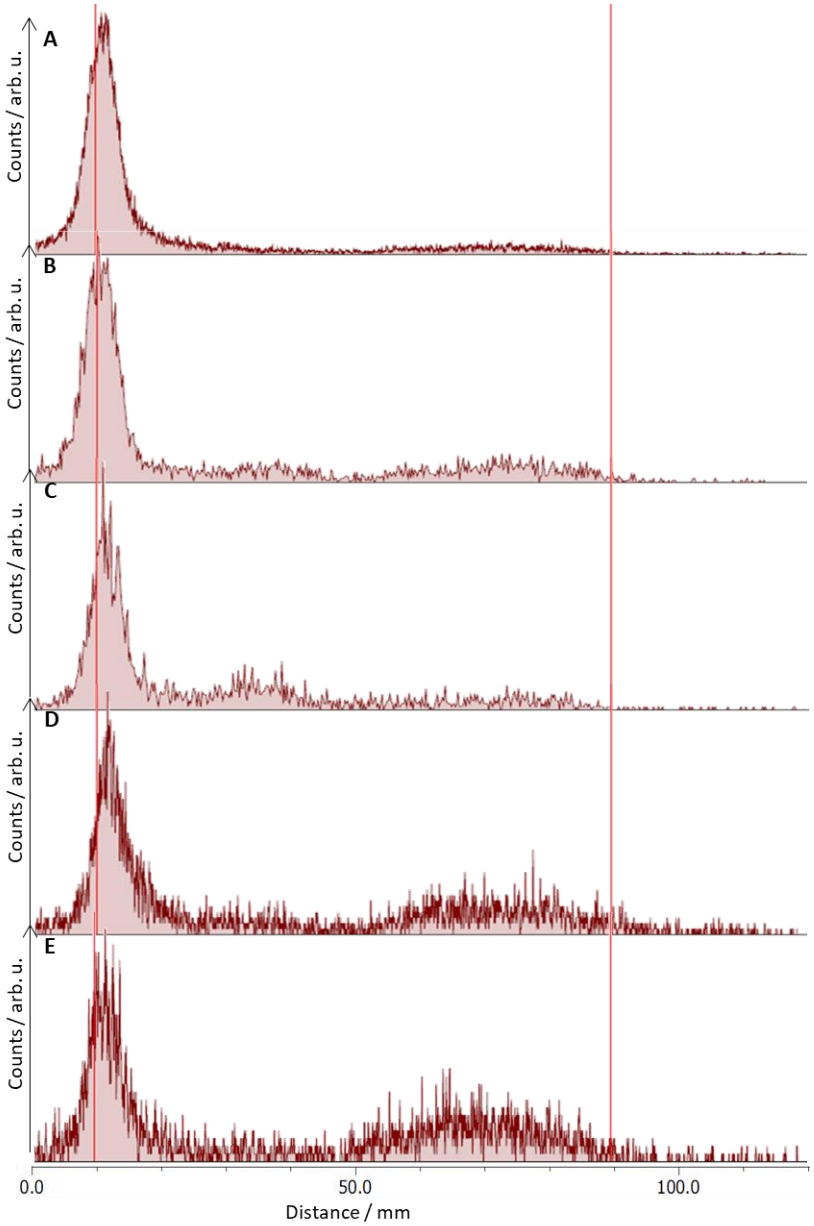

Figure 2.30: Effect of dilution on [^{68}Ga][Ga(Dpaa)(H_2O)] A) Radiolabelling mixture containing [^{68}Ga][$GaCl_3$] and 100 µM H_3Dpaa. B) Radiolabelling solution diluted to a ligand concentration of 10 µM C) 5 µM D) 1 µM E) 0.5 µM.

2.5.2 Serum Stability of [^{68}Ga][Ga(Dpaa)(H_2O)]

Incubation of an aliquot of radiolabelling solution containing [^{68}Ga][Ga(Dpaa)(H_2O)] in foetal bovine serum revealed that the [^{68}Ga]Ga(III) was rapidly dissociated from the complex. This result shows that this family of ligands is unsuitable for *in vivo* application as ^{68}Ga radiotracers. This assessment is more stringent than that conducted by Weekes *et al*.[107] (in which 58% of the activity was retained in the complex after 2 hours); this stability assessment was designed to closely match *in vivo* experiments in terms of injection volume and serum volume and concentration to provide an accurate conclusion of the radiolabelled complex stability. Unfortunately, [^{68}Ga][Ga(Dpaa)(H_2O)] is not stable under these stringent conditions. Therefore, this system is not suitable for *in vivo* application.

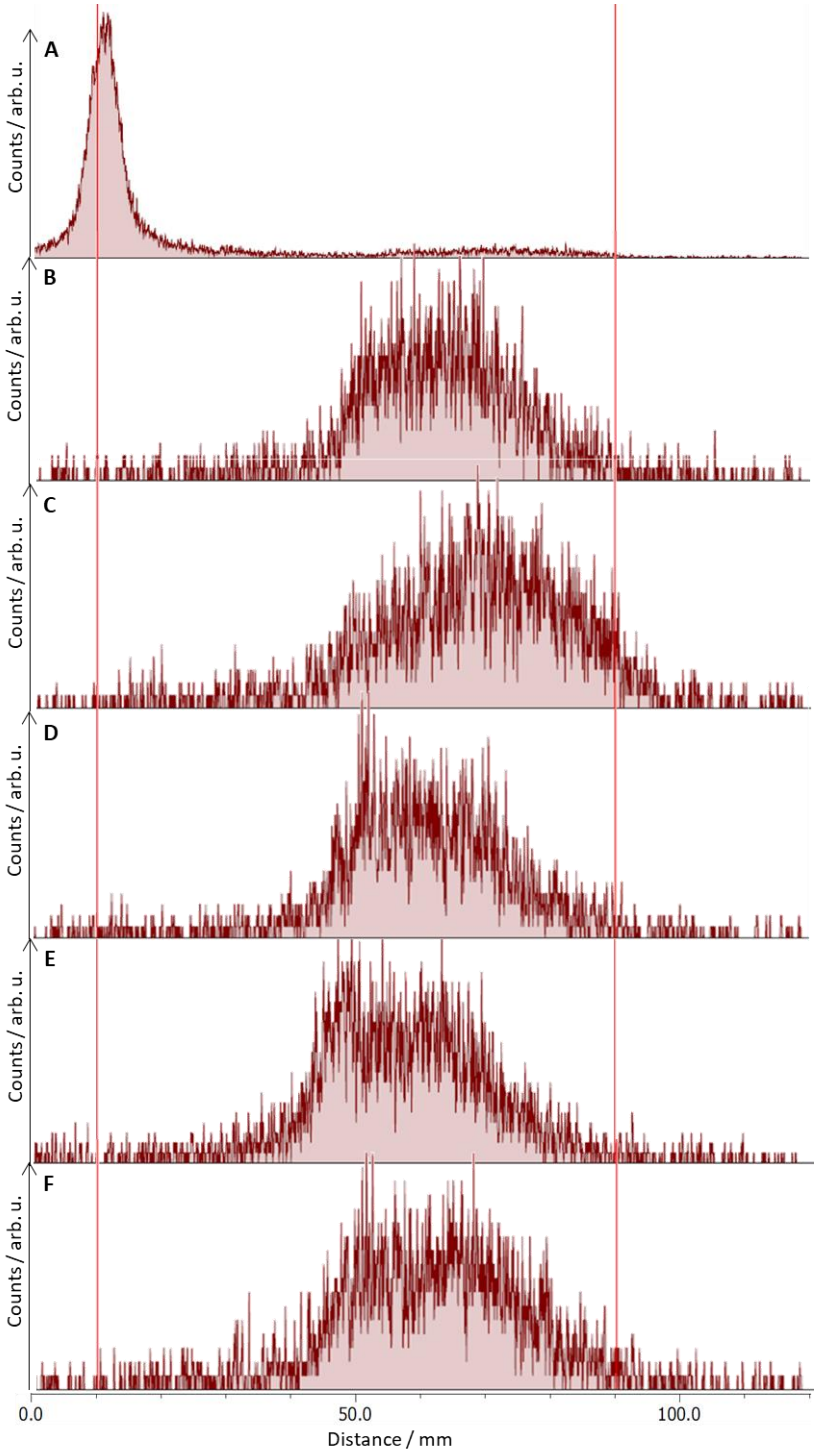

Figure 2.31: Stability of [^{68}Ga][Ga(Dpaa)(H_2O)] to foetal bovine serum (FBS). T = 37 °C. A) Crude reaction mixture. B) After 15 minutes incubation C) 30 minutes D) 60 minutes E) 90 minutes F) 120 minutes. Method development for TLC analysis is shown in appendix 4.

2.6. Conclusions

The ligand H_3Dpaa can be readily modified to incorporate additional functionalities for conjugation by changing the amino acid used in the penultimate step of the ligand synthesis.

This family of ligands is capable of complexing [^{68}Ga]Ga(III) over a wide pH range– from pH 2 up to pH 8 – at room temperature. This development is promising for the development of acyclic chelators for ^{68}Ga complexation; few chelators have been reported that are capable of

rapid complexation of ^{68}Ga at neutral pH and examples of bifunctional chelators that can achieve this are rare.

H_3Dpaa and the bifunctional derivatives H_4Dpaa.ga and H_3Dpaa.lys were able to complex ^{68}Ga in PBS with >94% radiochemical yields achieved in 5 minutes. This is significantly better than the standard chelators, DOTA and NOTA, and comparable to recently developed chelators such as THP and DATA.[179,184]

The molar activities achieved by these chelators varies from 3.4 to 28.9 GBq μmol^{-1}; this is an 19-106 fold lower than that achieved by the dipicolinate ligand H_2dedpa[37] and 24-260 fold lower than that reported for TRAP analogues.[128] H_2dedpa and TRAP are both capable of achieving high radiochemical yields at low ligand concentrations (0.1 μM, 0.7 μM respectively) under optimised conditions allowing for high molar activities without isolation. As H_3Dpaa requires a higher ligand concentration to achieve > 95% radiochemical yields it is to be expected that the resulting product has a lower molar activity.

The conjugate H_3Dpaa.ga.PSMA was synthesised through an anhydride reaction to activate H_4Dpaa.ga followed by ring opening with **9**. The conjugate was successfully radiolabelled with ^{68}Ga under mild conditions (pH 7.4, T = 37 ^{o}C, t = 15 mins) achieving a high radiochemical yield (>95%).

Unfortunately, the resulting radiolabelled species are not stable in serum. This significantly limits their application as ^{68}Ga radiotracers and makes further assessment of their biological properties impractical. The stability of [^{68}Ga][Ga(Dpaa)(H_2O)] to *apo*-transferrin does not truly reflect its stability to biological competitors – this highlights the importance of thorough *in vitro* assessment of novel radiotracers prior to *in vivo* application.

Application of this system to PET imaging could be continued in the future through assessment of ^{64}Cu(II) or ^{52}Mn(II) complexation. The *pCu* values obtained for the ligands presented here are significantly higher than the *pGa* values obtained; this indicates a greater stability of the complex at physiological pH and is a promising first result in the development of a Cu(II) based radiotracer. The parent ligand H_3Dpaa has been applied to Mn(II) complexation recently, with promising results as an MRI agent; application to ^{52}Mn has not yet been reported. Successful application to the complexation of ^{52}Mn would allow for this system to be used as a dual-modal probe for both PET and MRI imaging.

Chapter 3 Picoline based ligands for ^{68}Ga

3.1. Ligand design

The rapid complexation of ^{68}Ga by H_3Dpaa across a range of conditions is very promising for the application of picolinate arms to ^{68}Ga complexation. However, the resulting complex [^{68}Ga][Ga(Dpaa)(H_2O)] is insufficiently stable for application to *in vivo* imaging.[223] The chelator does not fulfil the 6-coordinate environment of Ga(III) due to strain preventing coordination of the central amine.

Further optimisation of this chelator design should retain the promising ^{68}Ga complexation properties whilst improving upon the stability of the resulting complex to *in vivo* competitors.

One potential route to improving the stability of the Ga(III) complex would be to increase the number of coordinating arms. Increasing the number of potential coordinating atoms in the chelator should allow for the 6-coordinate environment of Ga(III) to be fulfilled without requiring the central amine to coordinate to the gallium atom.

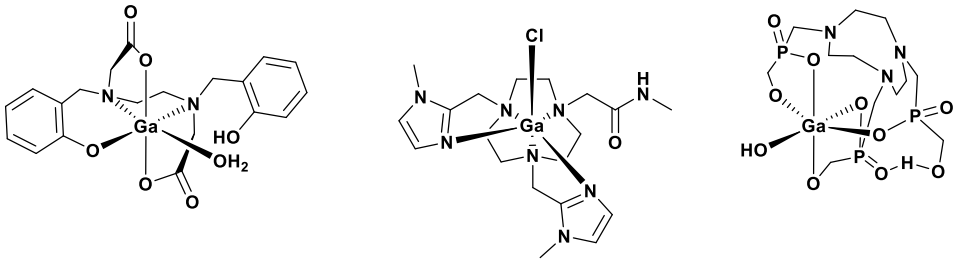

Figure 3.1: Proposed structures of [Ga(HBED)(OH_2)],[221] [Ga(NODIA-Me)(Cl)][139] and [Ga(TRAP-OH)(OH)][105] in which the hexadentate ligand fulfils only 5 coordination sites of Ga(III).

However, stable complexes in which the Ga(III) coordination sphere is not saturated by the chelator have also been reported(Figure 3.1). Due to its favourable properties for imaging PSMA,[158] conjugates of HBED have recently become increasingly popular. However, HBED has been reported to form a number of species upon radiolabelling with ^{68}Ga.[164,165,221] A recent report by Tsionou *et al*. implicates a pentadentate ligand in the varied speciation of [^{68}Ga][Ga(HBED)] with the sixth coordination site occupied by a water molecule (Figure 3.1).[221] Despite this the system continues to be applied successfully to *in vivo* imaging,[164] and its *in vitro* stability to serum is reported to be >99% over 7 days.[158]

Schmidtke *et al.* reported a TACN derivative, NODIA-Me, which coordinates Ga(III) in a 5 coordinate manner with the sixth coordination site occupied by either chloride or an as yet unidentified ligand (Figure 3.1).[139] While the sixth coordination site is reportedly labile, the overall complex retains ^{68}Ga when incubated with serum (~1% decomplexed over 4 hours).

TRAP-OH is also reported to form a complex with Ga(III) in which a hydroxide anion is also coordinated to the metal ion.[105] The "out-of-cage" complex formed at high pH (pH > 8,

Figure 3.1) has 5 coordinating atoms from the ligand and one coordinating hydroxide anion. A similar structure has been reported for the related NOPO ligand.[130] Despite this, TRAP ligands have been successfully applied to *in vivo* imaging with no degradation reported.[104,130] This may be due to the "in-cage" complex being the dominant species at pH 7 – in this species all six coordinating atoms are provided by the TRAP ligand with the three amines from the macrocycle and the three phosphonate arms coordinating Ga(III).

Thus, the 5 coordinate nature of the H_3Dpaa family need not prevent application of similar ligands to ^{68}Ga complexation; however the kinetic stability of the Ga(III) complex must be improved. Varying the nature of the coordinating arms will change the stability of the resulting complex, potentially resulting in a sufficiently stable complex that can be applied to *in vivo* imaging.

3.1.1 Increasing the number of coordinating arms

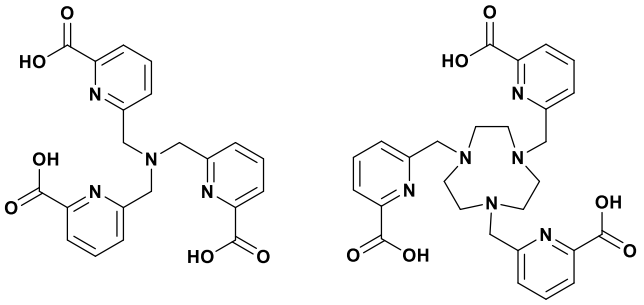

Figure 3.2: Structures of picolinate ligands, with increased number of potential coordinating atoms, discussed in this chapter.

Two chelators that increase the number of coordinating atoms, whilst retaining the picolinate motif, are 6,6',6''-(nitrilotris(methylene))tripicolinic acid (H_3Tpaa) and 6,6',6''-((1,4,7-triazonane-1,4,7-triyl)tris(methylene))tripicolinic acid (H_3NO3PA, Figure 3.2). Increasing the coordination number should improve the stability of the resulting complex by satisfying the 6 coordinate environment of Ga(III). This will remove the bound water from the coordination sphere, and this will remove a readily substituted ligand that is vulnerable to attack by competing ligands.

H_3Tpaa is an acyclic chelator that incorporates three picolinate arms into a tripodal structure. This chelator has previously been reported for the complexation of lanthanides, including Gd(III),[224] in which it acted in a heptadentate manner. H_3Tpaa has also been applied to complexation of Ca(II)[225] and Pb(II).[225] The ligand picolinate arms are reported to have pK_a values of 2.5, 3.3 and 4.11 and the central amine has a pK_a of 6.78.[224] Thus, at neutral pH all three picolinate arms should be fully deprotonated and the central amine may be partially deprotonated. This will promote rapid coordination of ^{68}Ga.

When Tpaa was applied to the coordination of lanthanide ions the remaining coordination sites were occupied by water.[224] In solution both Eu(III) and Tb(III) were reported to have solvation state, *q*, of 2.[224] The corresponding Gd(III) complex had a high relaxativity, r_1 = 13.3 mM^{-1} s^{-1} (25 °C, 60 MHz).[224] This relaxivity is greater than that reported for other Gd(III) systems with a solvation state of 2; $[Gd(DO3A)(H_2O)_2]$ (r_1 = 6.1 mM^{-1} s^{-1}) and $[Gd(PCTA)(H_2O)_2]$ (r_1 = 6.9 mM^{-1} s^{-1}); Bretonnière and co-workers suggested a flexible coordination environment with exchange between a 9 and 10 coordinate Gd(III) metal centre. This would correlate to *q* = 2.5.[224] The thermodynamic stability of this system was lower than that of other Gd(III) complexes with a similar solvation state ($\log K_{[Gd(Tpaa)(H2O)2]}$ = 10.2[224], $\log K_{[Gd(DTPA\text{-}bma)(H2O)2]}$ = 15.8), this may be due to the exchange between a 9 and 10 coordinate structure resulting in a greater average solvation state.

In the solid state crystal structures obtained for this system, the complex formed by La(III) and $Tpaa^{3-}$ had 3 additional coordinating atoms (one water molecule and two carboxylate arms of an adjacent complex) giving a total coordination number of 10.[224] The Lu(III) complex had a total coordination number of 8, with only one additional coordinating water molecule.[224] The remaining lanthanides had a coordination number of 9; with one coordinating water molecule and one neighbouring carboxylate coordinating.[224] This structural flexibility may explain the exchange between a 9 and 10 coordinate system producing a solvation number between 2 and 3. The structure formed by Tpaa with the lanthanide ions has an exposed metal face;[224] this is reflected in the crystal structures by coordination of an adjacent carboxylate but may be a source of instability in solution.

In the crystal structure for the Pb(II)-Tpaa system, Tpaa is only pentacoordinate.[225] Under acidic conditions (pH = 1.6), two of the carboxylate arms are not coordinated, remaining protonated.[225] An additional coordination site is occupied by a chloride anion leaving an open face in the complex that is likely occupied by the Pb(II) ion lone pair.[225] At higher pH, the ligand is again pentacoordinate.[225] However, coordination at pH 5.6 is fulfilled by the central amine and two picolinate arms, with one arm remaining uncoordinated.[225] The Pb(II) lone pair is reported to be sterically hindering this arm, preventing coordination.[225] In solution this system is symmetric with only one environment seen for the methylene bridges and one set of three resonances for the picolinate arms.[225] When coordinating Ca(II) a multimeric crystal structure is reported, $[Ca(Tpaa)(H_2O)]_2[Ca(H_2O)_4]$.[225] Two of the Ca(II) ions are coordinated by Tpaa in a heptadentate manner, with an eighth coordinating site fulfilled by a water molecule.[225] The third Ca(II) ion acts as a bridge between the other two complexes and is coordinated by four water molecules and two carboxylates from each complex.[225] The Tpaa system was poorly selective for Pb(II) ($\log K_{[Pb(Tpaa)]}$ = 10.0) over Ca(II) ($\log K_{[Ca(Tpaa)]}$ = 8.5).[225]

Assuming that strain precludes coordination of Ga(III) by the central amine, as seen for the Ga(III)-Dpaa system, the three picolinate arms should provide 6 coordinating atoms (N_3O_3)

to bind Ga(III). This will fully satisfy the 6-coordinate environment of Ga(III) producing a more stable system than [Ga(Dpaa)(H_2O)].

H_3NO3PA is a macrocyclic chelator based on the TACN scaffold with three picolinate arms. H_3NO3PA has been applied to the complexation of lanthanides (Tb(III) ($\log K_{[Tb(NO3PA)]}$ = 17.4),[226] Nd(III),[227] Eu(III),[227–229] Gd(III)[227]and Lu(III)[227]) and recently for complexation of Cu(II) and Zn(II) ($\log K_{[Cu(NO3PA)]}$ = 16.21, $\log K_{[Zn(NO3PA)]}$ = 15.95).[230] The ligand picolinate arms are reported to have pK_a values of 1.86, 2.51 and 2.81 with the macrocycle amines having pK_a values of 3.85, 5.62 and 10.72.[230] Thus, at pH 4 the picolinate arms should be fully deprotonated allowing for rapid Ga(III) coordination. Furthermore, at pH 7.4 the macrocyclic ring should be partially deprotonated; this will aid in complexation of Ga(III) in an "in-cage" manner, although fully deprotonating the macrocyclic ring may be slow under these conditions.

When coordinating the lanthanides a series of isostructural crystal structures were reported in which the coordination sphere was saturated by the 9 coordinating atoms of NO3PA.[227] Despite the absence of a coordinated water molecule, [Gd(NO3PA)] was still able to increase the relaxation rate of water, with a reported r_1, of approximately 2 mM^{-1} s^{-1} (298 K, 60 MHz).[227] This is likely through an outer sphere mechanism and is lower than the values reported for systems in which water is directly coordinated to the Gd(III) center ($[Gd(DOTA)(H_2O)]^-$ r_1 = 4.0 mM^{-1} s^{-1}).[212]

NO3PA showed little selectivity for Cu(II) over Zn(II) ($\log K_{[Cu(NO3PA)]}$ = 16.21, $\log K_{[Zn(NO3PA)]}$ = 15.95).[230] Guillou *et al.* reported a greater selectivity by substituting the picolinate arms for pyridyl arms ($\log K_{[Cu(NO3Py)]}$ = 27.4, $\log K_{[Zn(NO3Py)]}$ = 17.25) principally due to the increase in stability of the resulting Cu(II) complex.[230] DFT modelling suggests that in the trispyridyl complex all three pyridine arms are coordinated to the Cu(II) center; however in the tripicolinate complex one arm is uncoordinated, a second is coordinated through only the pyridyl unit, and a third through both the pyridyl and carboxyl moieties.[230] This is reported to induce a significant steric constraint in the complex and may be a source of instability.[230]

This chelator has 9 potential coordinating atoms; this should be sufficient to satisfy the 6 coordinate environment of Ga(III). However, chelators with an excess of coordinating atoms are not necessarily ideal - the high number of potential coordinating atoms may result in a variety of products being formed due to different coordination modes. The macrocyclic backbone of H_3NO3PA should increase the stability of the resulting complex due to an increased preorganisation of the ligand before complexation.

3.1.2 Phosphonate ligands

The use of phosphinate arms in the TRAP ligands, instead of the carboxylate arms of NOTA, results in a ligand that is capable of complexing ^{68}Ga at lower concentrations. This results in a radiotracer with higher molar activity. Notni and co-workers report that NOTA required

ligand concentrations of 3 µM to achieve radiochemical yields of 95% (pH 3.3, 95 °C, 5 minutes), TRAP-Pr was able to achieve the same yields with ligand concentrations of just 0.3 µM.[128] Thus, the molar activity of the radiolabelled TRAP species will be 10 fold greater. The TRAP ligands are also able to tolerate a greater concentration of other metal ions (Cu(II), Zn(II), Fe(III)) in the radiolabelling solution whilst still attaining high radiochemical yields (>95%) than NOTA is.[131] This may be a contributing factor to the high molar activities obtained by the TRAP ligands when radiolabelled with ^{68}Ga as less excess ligand is required to overcome any metal contaminants. This tolerance of other metals is in part due to the high selectivity of the TRAP ligands for Ga(III); Whilst [Ga(NOTA)] has a greater thermodynamic stability than [Ga(TRAP-Pr)], the TRAP system has a greater difference in stability between the Ga(III) complex and the Cu(II) and Zn(II) complexes (For TRAP-Pr, $\log K_{[Ga(L)]} - \log K_{[Cu(L)]} = 9.4$, $\log K_{[Ga(L)]} - \log K_{[Zn(L)]} = 9.3$. For NOTA, $\log K_{[Ga(L)]} - \log K_{[Cu(L)]} = 7.6$ and $\log K_{[Ga(L)]} - \log K_{[Zn(L)]} = 7.8$).[105,127,231,232]

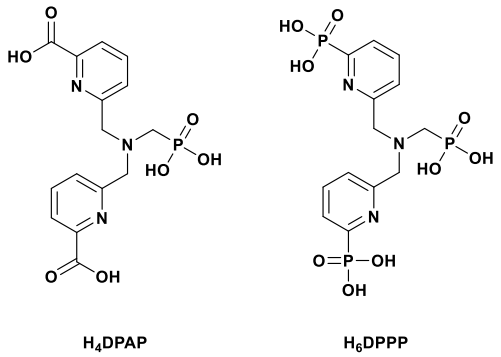

Figure 3.3: Structures of picolinate ligands with carboxylic acid arms replaced by phosphonic acids.

Two derivatives of H_3Dpaa, 6,6'-(((phosphonomethyl)azanediyl)bis(methylene))-dipicolinic acid (H_4DPAP) and ((bis((6-phosphonopyridin-2-yl)methyl)amino)methyl)phosphonic acid (H_6DPPP), were designed to harness this increased selectivity for Ga(III). H_4DPAP substitutes a phosphonic acid for the carboxylic acid in the amino acid back bone of H_3Dpaa. H_6DPPP has the same substitution, but also replaces the picolinic acid motifs with pyridyl phosphonic acid arms. These ligands should produce ^{68}Ga complexes with a greater molar activity than H_3Dpaa and potentially with greater stability.

3.2. H_3Tpaa

3.2.1 Ligand synthesis - H_3Tpaa

H_3Tpaa was prepared through a synthetic route similar to that of H_3Dpaa (Scheme 3.1). The proligand, triethyl 6,6',6''-(nitrilotris(methylene))tripicolinate (Et_3Tpaa), was synthesised in a manner analogous to Et_3Dpaa – however, instead of using ethyl glycinate hydrochloride as a building block, ammonium chloride was used instead. An additional equivalent of the building block **4** was also required due to the increased number of picolinate arms in the desired product. This produced the proligand Et_3Tpaa in a 16% yield. The picolinate arms are equivalent on the

NMR time scale, with only a single environment seen for the methylene bridge (δ_H = 4.06), two environments for the ethyl esters (δ_H = 4.61, 1.48) and three environments for the pyridyl protons (δ_H = 8.02, 7.90, 7.74). The presence of three picolinate arms is confirmed by mass spectrometry (*m/z* = 507.8, $[M + H]^+$). Higher yields of ester protected H_3Tpaa proligands have been reported using analogous routes,[233,234] with an 82% yield being achieved by Zeng *et al.* using gaseous ammonia bubbled into tetrahydrofuran as the nitrogen source.[235] Deprotection of Et_3Dpaa under acidic conditions yielded H_3Tpaa in a 69% yield.

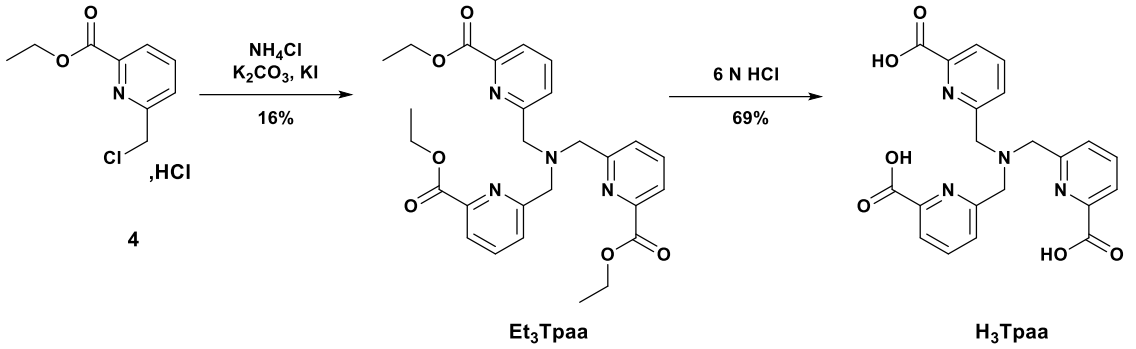

Scheme 3.1: Synthetic route for the preparation of H_3Tpaa.

This synthetic route to H_3Tpaa differs from that reported previously by Bretonnière *et al*. who produced an amide protected proligand by reacting N,N-diethyl 2-(chloromethyl) pyridine-2-carboxamide with N,N-diethyl 2-(aminomethyl)pyridine-2-carboxamide under similar conditions. This produced an amide protected proligand in a 66% yield.[224,236,237] Production of the N,N-diethyl 2-(aminomethyl)pyridine-2-carboxamide starting material from N,N-diethyl 2-(hydroxymethyl)pyridine-2-carboxamide (analogous to **3**) requires 2 further synthetic steps.[237] The use of a single picolinate starting material makes the route reported here simpler, but with a reduced yield.

3.2.2 Complexation [Ga(Tpaa)]

Complexation of Ga(III) by H_3Tpaa was undertaken at pH 4.5 (Scheme 3.2). As shown in Figure 3.4, upon complexation a significant deshielding of the picolinate units is seen ($\Delta\delta_H$ = 0.64-0.75 ppm). Importantly, only one set of peaks is seen for the picolinate arms, indicating that these are equivalent. This suggests that the Ga(III) ion is coordinated equally by all three picolinate arms. The protons in the methylene linker between the picolinate units and the central amine are also deshielded ($\Delta\delta_H$ = 1.54-2.01 ppm) and, as with [Ga(Dpaa)(H_2O)], the two protons in each linker are no longer equivalent with a strong geminal coupling ($^2J_{HH}$ = 17 Hz) being seen. The carboxylate resonance shows an increase in shielding ($\Delta\delta_C$ = -5.67 ppm) as do resonances in the 2 and 6 positions of the pyridine ring ($\Delta\delta_C$ = -2.29 and -6.59 ppm respectively). In the case of the pyridine ring resonances, the decrease in shielding in the 3, 4 and 5 positions suggests that the electron density is being donated through the pyridine nitrogen to the Ga(III) atom.

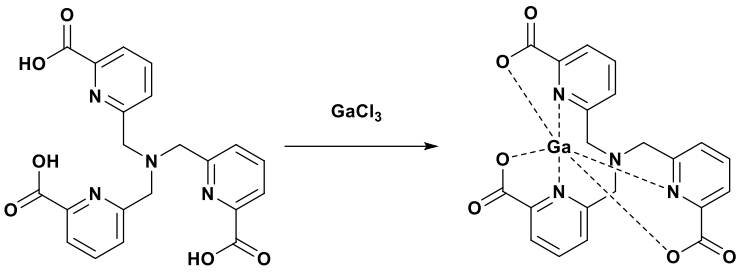

H_3Tpaa [Ga(Tpaa)]

Scheme 3.2: Proposed complexation of Ga(III) by H_3Tpaa.

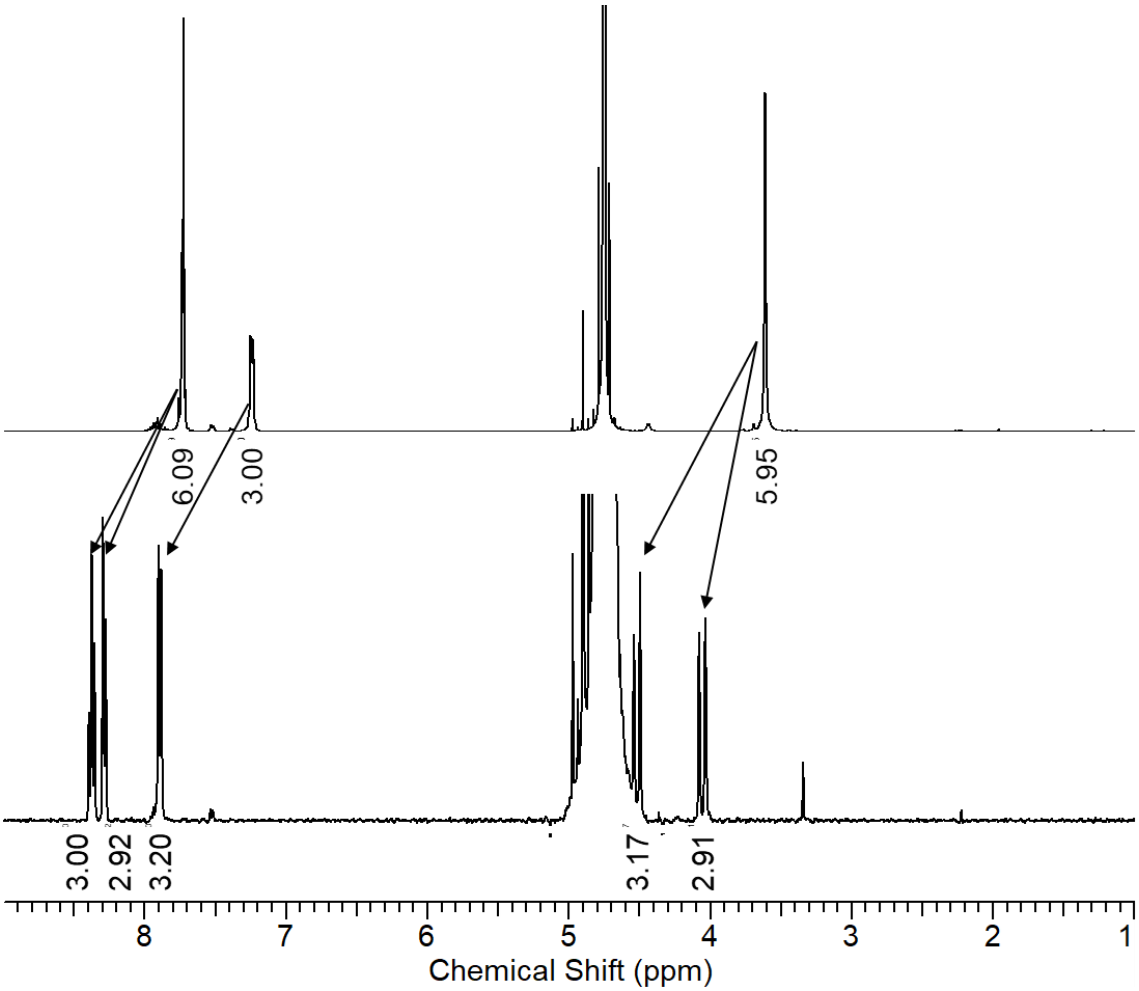

Figure 3.4: ^1H NMR of A) H_3Tpaa and B) [Ga(Tpaa)] (D_2O, pD = 9.45, 298 K).

A crystal of suitable quality for X-ray diffraction analysis was obtained by slow evaporation of an acidic solution of the complex. The unit cell obtained contains two symmetry-unique [Ga(Tpaa)] complexes and 7 water molecules. In both complexes the Ga(III) centre is coordinated by three chelating picolinate arms of the ligand; the overall coordination geometry is that of a distorted octahedron. The central amine is not involved in complexation in this structure (Ga1···N2 distance = 2.641(3) Å, Ga2···N6 distance = 2.670(3) Å, Figure 3.5). This is in agreement with the previously reported structures for [Ga(Dpaa)(H_2O)] in which the central amine is not involved in coordination of the Ga(III) ion (Ga-N distance = 2.4880(11) Å).[107,223] The Ga-N bond length of the coordinating picolinate arms is decreased (mean Ga-N bond length = 2.08 Å) when compared to the bond length reported for [Ga(Dpaa)(H_2O)] (mean Ga-N bond length= 2.22 Å)[223] suggesting an improved binding interaction; the Ga-O distance does not

significantly change (mean Ga-O = 2.01 vs 2.03 Å). This suggests that overall there is an improved bonding character between the picolinate arms and the Ga(III) centre. Furthermore, the mean picolinate bite angle is increased (78.66 ° compared to 74.46 °)[223] – this is closer to the ideal 90° for an octahedral geometry; this suggests reduced strain in the [Ga(Tpaa)] complex than in [Ga(Dpaa)(H_2O)].

Table 3.1: Selected bond lengths from the obtained crystal structure of [Ga(Tpaa)].

Bond Length / Å			
Ga(1)-N(1)	2.068(3)	Ga(2)-N(5)	2.081(3)
Ga(1)-N(3)	2.083(3)	Ga(2)-N(7)	2.093(3)
Ga(1)-N(4)	2.054(3)	Ga(2)-N(8)	2.080(3)
Ga(1)-O(1)	2.022(3)	Ga(2)-O(7)	2.023(2)
Ga(1)-O(3)	2.012(3)	Ga(2)-O(9)	2.006(3)
Ga(1)-O(5)	2.013(2)	Ga(2)-O(11)	1.985(2)

Table 3.2: Selected bond angles from the obtained crystal structure of [Ga(Tpaa)].

Bond Angle / °			
O(1)-Ga(1)-N(1)	78.77(11)	O(7)-Ga(2)-N(5)	78.24(10)
O(3)-Ga(1)-N(3)	78.91(12)	O(9)-Ga(2)-N(7)	78.09(10)
O(5)-Ga(1)-N(4)	78.72(10)	O(11)-Ga(2)-N(8)	79.20(12)
N(1)-Ga(1)-N(3)	103.22(11)	N(5)-Ga(2)-N(7)	104.49(11)
N(4)-Ga(1)-N(3)	104.91(12)	N(8)-Ga(2)-N(7)	104.75(11)
N(4)-Ga(1)-N(1)	107.52(11)	N(8)-Ga(2)-N(5)	105.00(12)
O(3)-Ga(1)-O(1)	83.93(11)	O(11)-Ga(2)-O(7)	85.30(10)
O(3)-Ga(1)-O(5)	84.78(10)	O(9)-Ga(2)-O(7)	85.26(10)
O(5)-Ga(1)-O(1)	86.36(10)	O(11)-Ga(2)-O(9)	85.11(10)

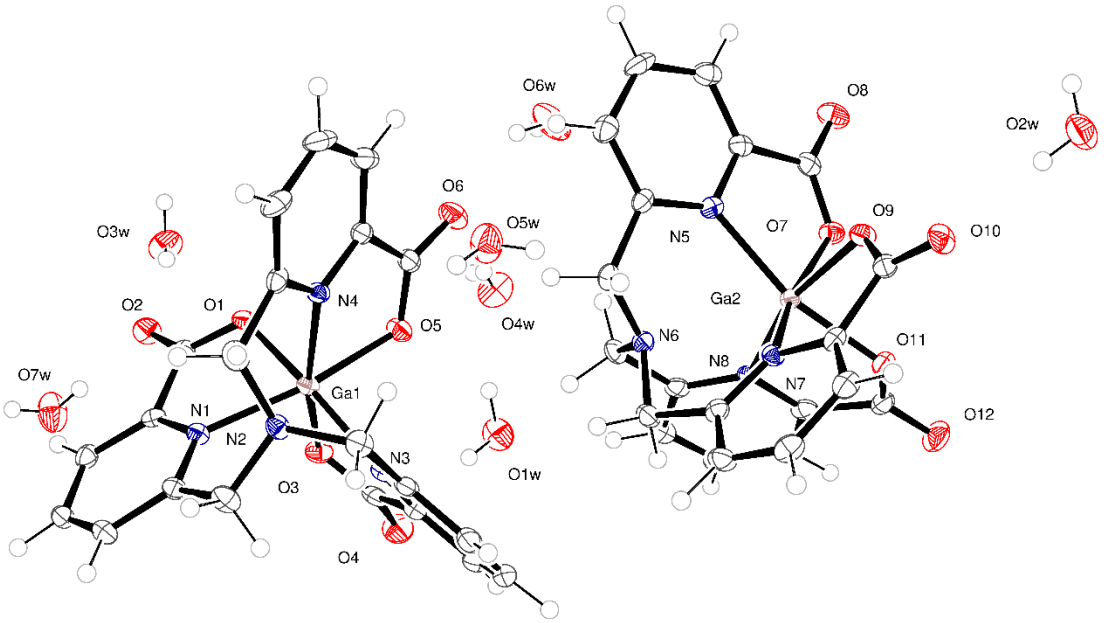

Figure 3.5: ORTEP representation of structure obtained by single crystal X-ray diffraction of [Ga(Tpaa)]. Thermal ellipsoids set at 30% certainty.

3.2.3 [^{68}Ga][Ga(Tpaa)]

H_3Tpaa was able to rapidly complex ^{68}Ga under both acidic (pH 4) and neutral (pH 7.4) conditions, achieving yields of over 99% under both conditions (Figure 3.6). This result further confirms those discussed in Chapter 2 supporting picolinate arms as rapid chelators of ^{68}Ga. Isolation of the radiolabelled species gave the product with a molar activity of 3.1 GBq µmol^{-1}.

The resulting complex was assessed for its stability to FBS (Figure 3.7). A greater stability was seen than for [^{68}Ga][Ga(Dpaa)(H_2O)], with 32% of the complex remaining intact after 30 minutes. However, the ^{68}Ga had been fully decomplexed after 120 minutes and as such this chelator is not suitable for further application towards a targeted ^{68}Ga radiotracer. This improvement in kinetic stability of [^{68}Ga][Ga(Tpaa)] relative to [^{68}Ga][Ga(Dpaa)(H_2O)] confirms that fulfilling the coordination geometry of Ga(III) improves the stability of the resulting radiolabelled complex.

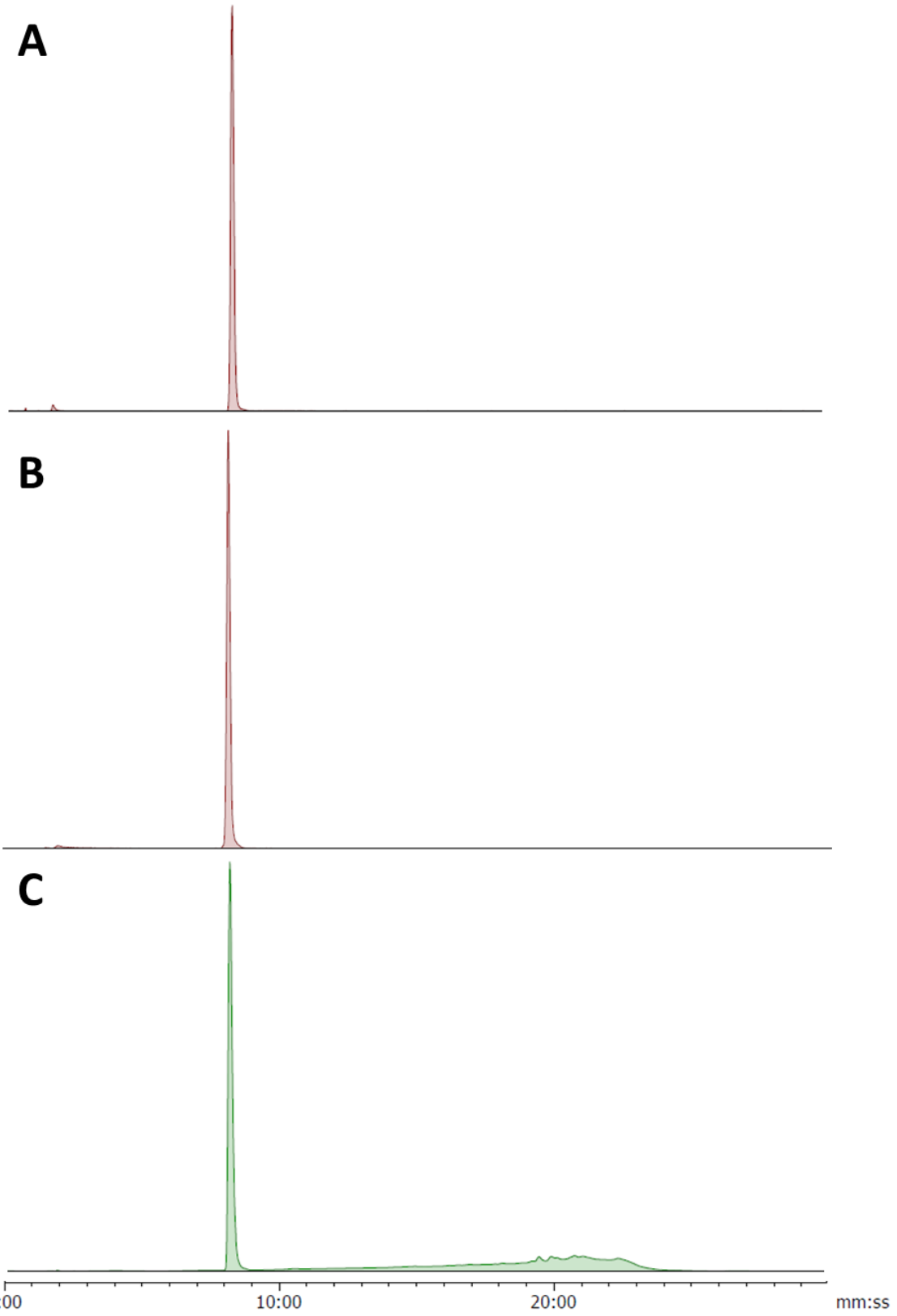

Figure 3.6: HPLC chromatograms of crude radiolabelling mixtures and cold standard. A) *[L]* = 100 µM, *pH* = 4, *I* = 0.1 M Acetate, *T* = 25 °C, *t* = 15 minutes, B) *[L]* = 100 µM, *pH* = 7.4, *I* = PBS, *T* = 37 °C, *t* = 15 mins C) cold UV trace of standard [Ga(Tpaa)]. **HPLC gradient A.**

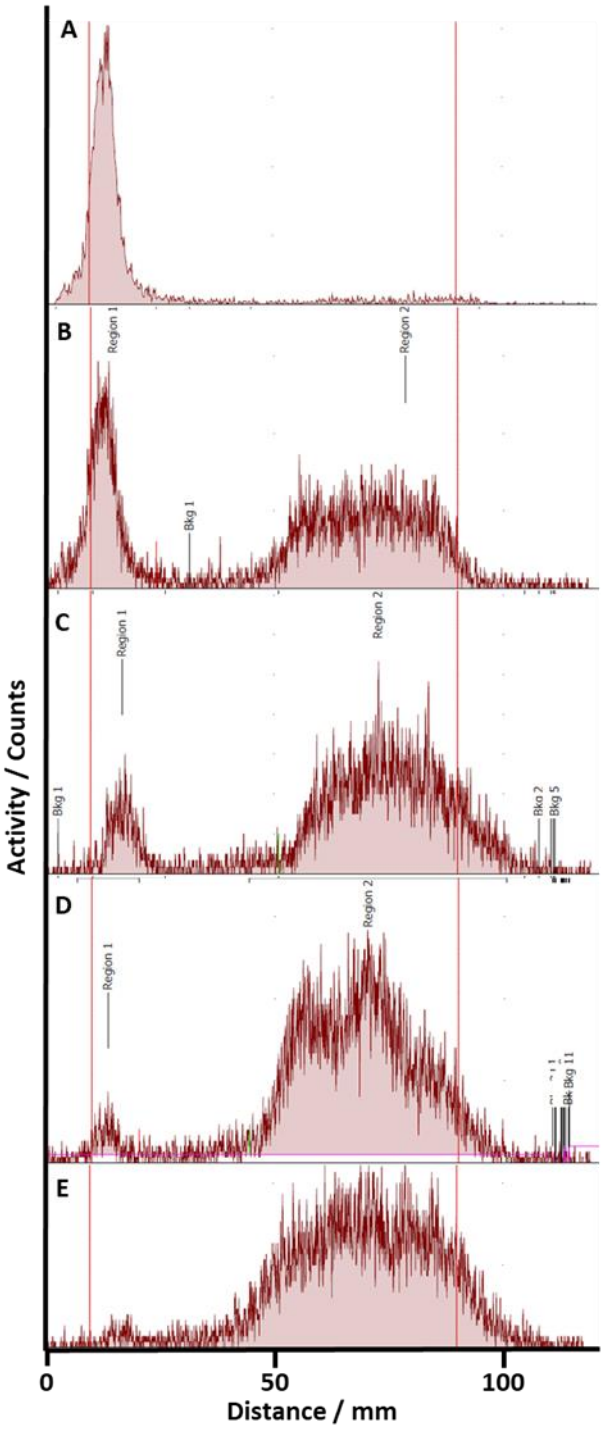

Figure 3.7: Assessment of stability of [^{68}Ga][Ga(Tpaa)] to FBS at 37 ^{o}C by TLC (silica, 0.1 M Citrate). Free ^{68}Ga is eluted with R_f = 0.9, complexed ^{68}Ga has R_f = 0. A) Crude radiolabelling mixture B) 30 minutes incubation with FBS C) 60 minutes D) 90 minutes E) 120 minutes. Method development for TLC analysis is shown in appendix 4.

3.3. H_3NO3PA

3.3.1 Ligand synthesis – H_3NO3PA

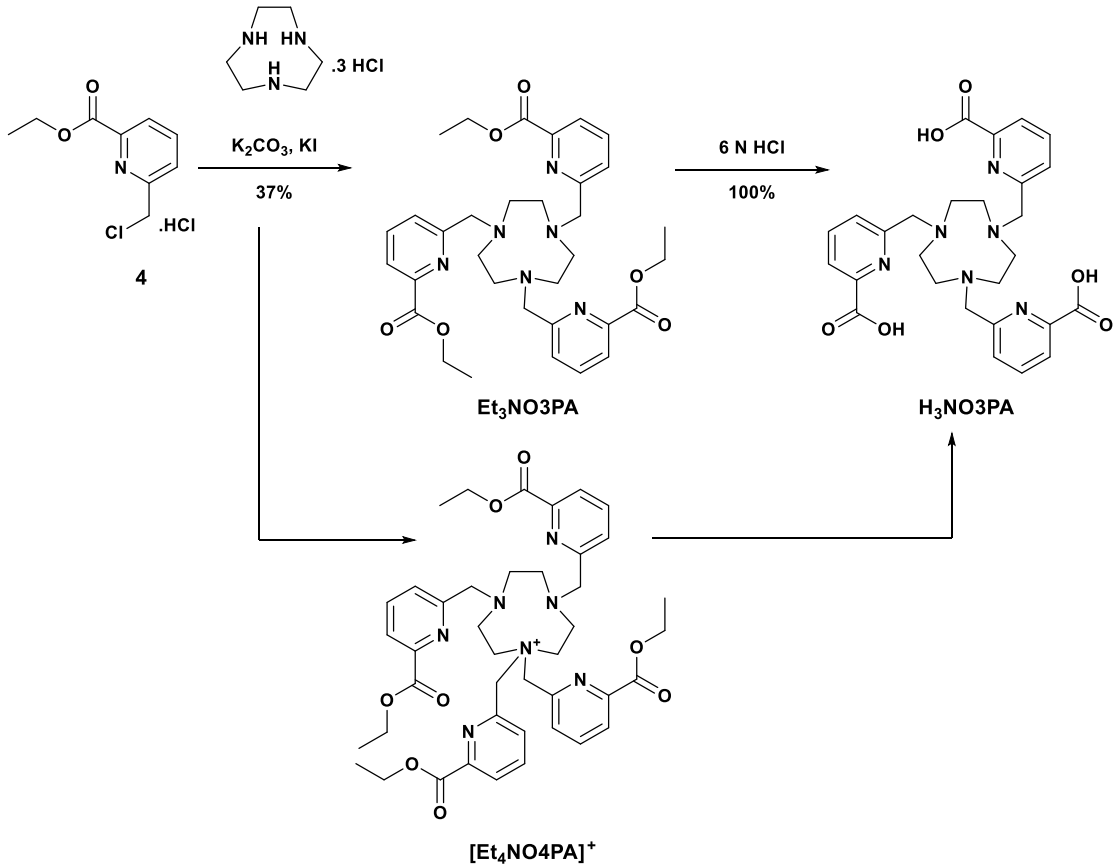

Scheme 3.3: Synthetic scheme for the preparation of H_3NO3PA.

Macrocyclic chelators are widely regarded to produce more stable complexes than the equivalent acyclic chelators.[58,156,37] To improve the stability of Ga(III) complexes produced with picolinate based chelators, three picolinic acid arms were incorporated into a macrocyclic structure, H_3NO3PA (Scheme 3.3).

TACN.3HCl was used as the amine source for the proligand synthesis, yielding both the desired product, triethyl 6,6',6''-((1,4,7-triazonane-1,4,7-triyl)tris(methylene))tripicolinate (Et_3NO3PA, 22% yield), and also the quarternised product, tetraethyl 6,6',6'',6'''-((1λ_4,4,7-triazonane-1,1,4,7-tetrayl)tetrakis(methylene))tetrapicolinate ($[Et_4NO4PA]^+$, 37% yield). The two products were resolved using column chromatography and could be distinguished through both mass spectrometry and NMR spectroscopy (Figure 3.8).

Et_3NO3PA has a simple NMR due to the symmetric nature of the ligand, however, $[Et_4NO4PA]^+$ has an increased number of signals due to the reduction of symmetry (loss of C_3 rotational symmetry). The picolinate arms of Et_3NO3PA have pyridine resonances (δ_H = 7.99-7.49) that are analogous to those of Et_3Dpaa (δ_H = 8.01-7.83) and Et_3Tpaa (δ_H = 8.02-7.74). $[Et_4NO4PA]^+$ has two sets of signals, in a 1:1 ratio, suggesting a pair of picolinate arms attached to tertiary amines (δ_H = 7.95-7.78) and a pair of arms attached to the same, quarternary, amine (δ_H = 8.40-7.93). The arms attached to the quarternary amine are significantly deshielded

($\Delta\delta_{H(R2N+(CH2pyC(=O)OEt)2)}$) = 0.62 ppm) as expected due to the electronegative nature of the charged amine.

The loss of symmetry is also evident in the methylene bridges – those attached to the quarternised amine are significantly deshielded (δ_H = 5.23) compared to those attached to the tertiary amine centers (δ_H = 4.15), which also correspond well with Et_3Dpaa (δ_H = 4.08) and Et_3Tpaa (δ_H = 4.06) and Et_3NO3PA (δ_H = 3.78).

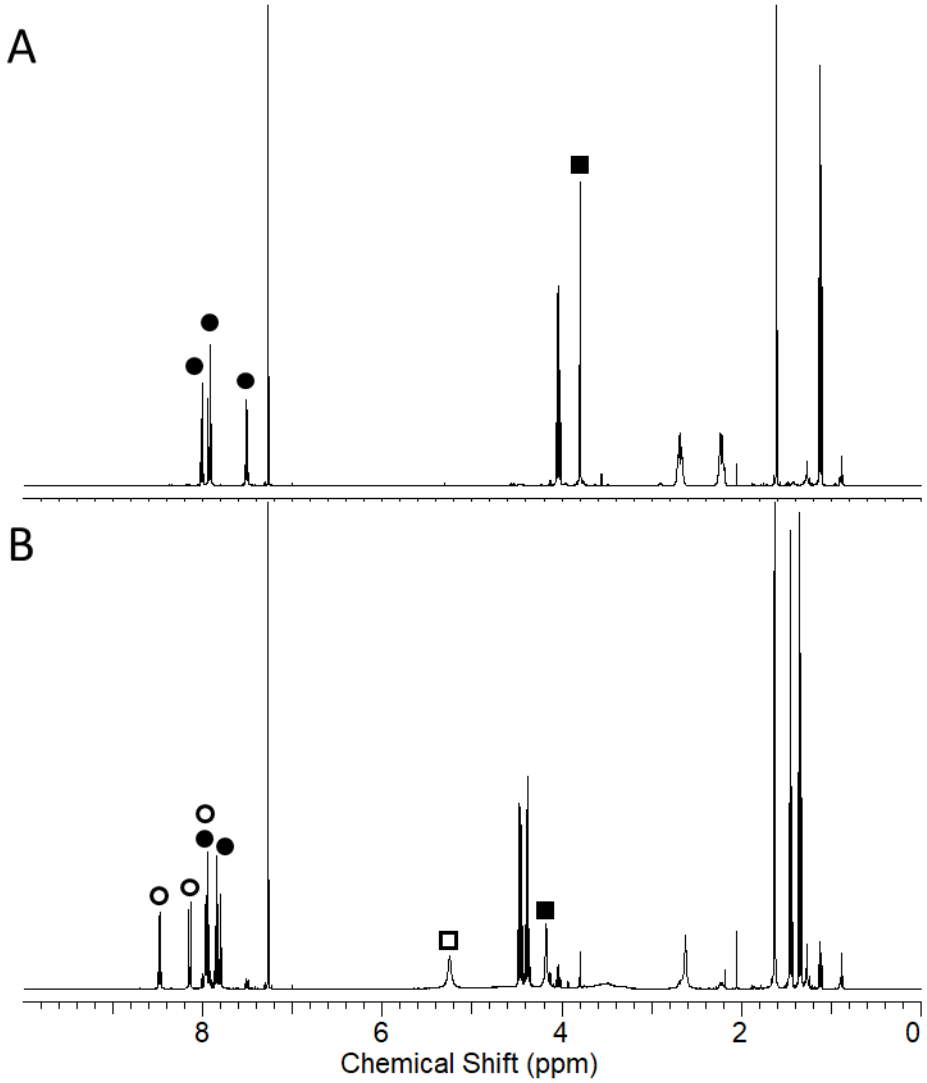

Figure 3.8: ^{1}H NMR of A) Et_3NO3PA and B) $[Et_4NO4PA]^+$. (400 MHz, $CDCl_3$, 298 K). Circles indicate picolinate resonances. Squares indicate the methylene linker. Filled symbols indicate arms attached to tertiary amines, empty symbols indicate arms attached to quarternary amines.

Deprotection of both Et_3NO3PA and $[Et_4NO4PA]^+$ under acidic conditions yielded the same product, H_3NO3PA.

H_3NO3PA has been previously prepared – Gateau *et al*. prepared this chelator in a 51% yield from **4** following the same procedure as reported here to produce the proligand.[227] However, purification of the proligand was not undertaken; instead the crude product was subjected to basic hydrolysis followed by precipitation of the deprotected ligand.[227] This may explain the higher yield reported; deprotection of both the trimeric and quarternised proligands will likely produce the same ligand. Guillou *et al.* reported a 57% yield when preparing H_3NO3PA

from methyl 6-(chloromethyl)pyridine-2-carboxylate; formation of the proligand Me_3NO3PA was performed at room temperature over 5 days in a 68% yield.[230] The lower temperature of this reaction may reduce the formation of the quarternised byproduct, however the crude product was still purified by column chromatography.

3.3.2 Complexation [Ga(NO3PA)]

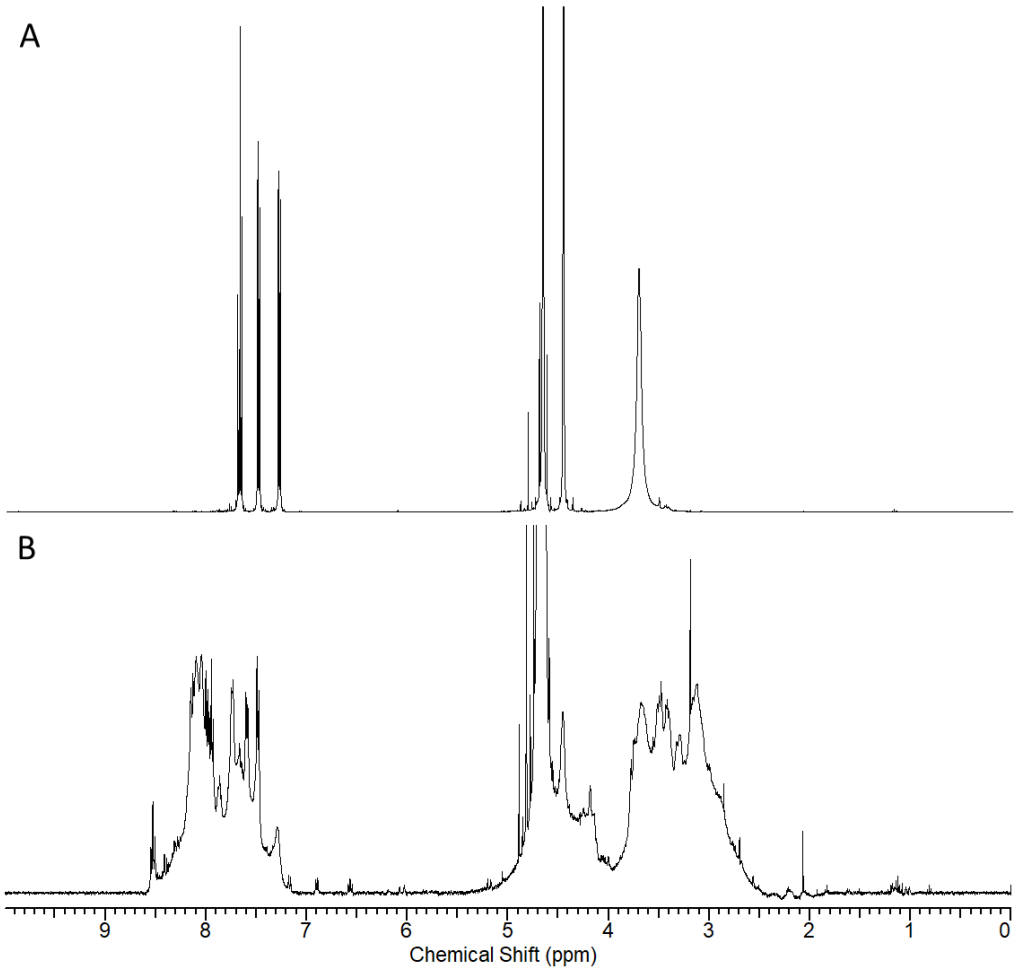

Figure 3.9: ^{1}H NMR of A) H_3NO3PA (*pD* = 3.14) and B) [Ga(NO3PA)] (*pD* = 3.07) (400 MHz, D_2O, 298 K).

Whilst most of the ^{1}H NMR signals for H_3NO3PA are sharp and well defined, the resonance corresponding to the macrocyclic ring is broad (Figure 3.9, δ_H = 3.84). This is in agreement with the previously reported data for this ligand,[240] and a similar broadening of the macrocyclic ring resonances has been reported for DOTA.[241,242]

The formation of the Ga(III) complex can be confirmed by high resolution mass spectrometry (HRMS, m/z = 601.1321). The NMR spectrum for [Ga(NO3PA)] shows a significant increase in complexity with numerous broad overlapping peaks. The increase in number of peaks points towards a loss of symmetry – as has been seen previously upon Ga(III) complexation by the picolinate ligands H_3Dpaa and H_3Tpaa. However, the broad signals suggest a high fluxionality of the system which was not previously observed.

Variable temperature NMR of this system was undertaken. Reducing the temperature had little effect on the NMR spectrum – the signals were still broad, suggesting that exchange was still rapid at 5 °C. Increasing the temperature of the NMR sample resulted in averaging of the NMR resonances, giving broad peaks for each environment. In particular, the methylene groups between the macrocyclic amines and the picolinic acids give rise to two resonances. This suggests that there is at least 2 environments for these arms – possibly a mixture of coordinated and non-coordinated as reported for similar ligands with Cu(II).[230]

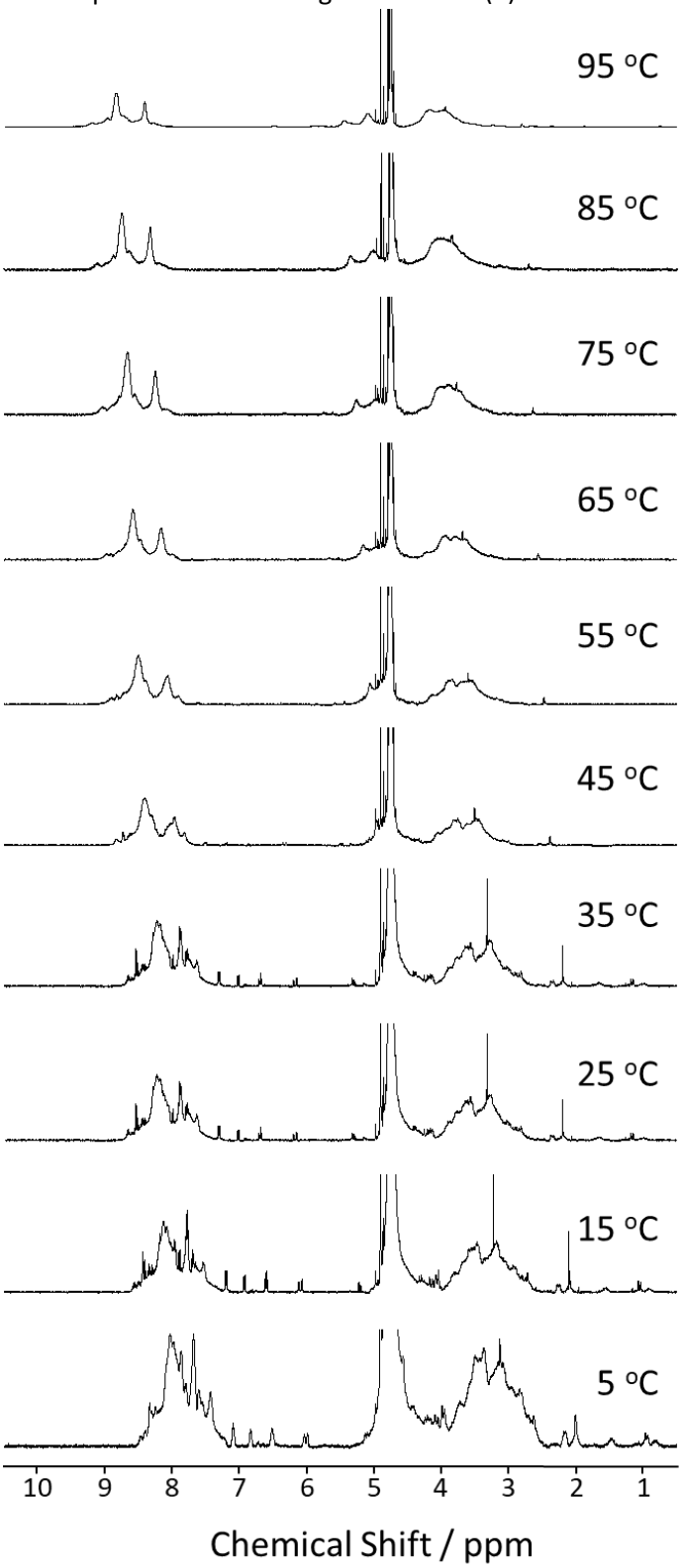

Figure 3.10: Variable Temperature ^{1}H NMR of [Ga(NO3PA)] (400 MHz, D_2O, p*D* = 3.07).

3.3.3 [^{68}Ga][Ga(NO3PA)]

H_3NO3PA was shown to be less efficient than H_3Dpaa or H_3Tpaa at complexing ^{68}Ga. Incorporation of ^{68}Ga was incomplete even when heated to 90 °C (Figure 3.11, Figure 3.12, Table 3.3). Furthermore, a number of species were formed in the radiolabelling mixture and the ratios of these species were dependent on the radiolabelling conditions. The major product formed at pH 4.0 (retention time = 2.9 minutes, Figure 3.11 A) has a similar retention time to the very broad peak of the [Ga(NO3PA)] standard. An additional product, with a later retention time, is also formed at room temperature – however when heated only the major product is formed. This can also be seen in the TLC analysis – after heating the product is a single, sharp peak whereas after reaction at room temperature there is an additional peak (R_f = 0.75, Figure 3.12). The reduced radiochemical yield of this system with ^{68}Ga can be attributed to the increased rigidity of the macrocyclic chelator when compared to the acyclic chelators previously discussed. This may also be the source of the multiple products formed – these can be attributed to different coordination modes with formation of the most thermodynamically favourable being promoted by heating. This thermodynamic product is likely "in-cage" – with coordination of the Ga(III) center by the macrocyclic nitrogens and some of the pendant arms.

When the radiolabelling reaction is undertaken at pH 7.4 an additional product is formed (retention time = 6-7.5 minutes, Figure 3.11 B). This product was not seen in the radiolabelling reactions at pH 4.0. The identity of this product is unclear. At this pH there will be increased competition from hydroxide anions – this may prevent the formation of the thermodynamically favoured product instead forming the kinetic product. This kinetic product may be the "out of cage" species in which the Ga(III) center is coordinated by the picolinic acid without contribution from the macrocycle.

Table 3.3: Summary of radiolabelling results when incubating 100 µM H_3NO3PA with $^{68}GaCl_3$ for 15 minutes.

Conditions		**RCY (HPLC) / %**		**RCY (TLC) / %**	
pH / Arb. U.	**T / °C**	**Major product**	**Total**	**Major product**	**Total RCY**
4.0	25	40.4	86.3	37.6	83.9
7.4	37	50.9	86.2	66.1	85.6
4.0	90	49.4	78.8	63.2	63.2

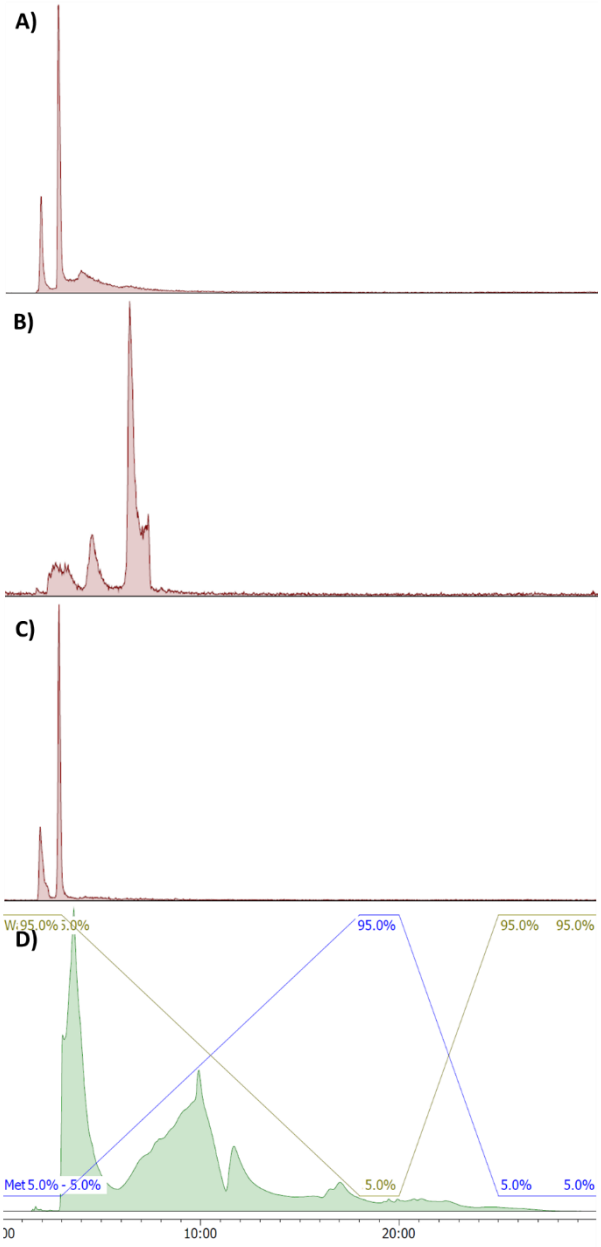

Figure 3.11: HPLC chromatograms of A-C) Crude radiolabelling mixtures containing $^{68}GaCl_3$ and 100 µM H_3NO3PA. D) [Ga(NO3PA)] cold standard. A) *pH* = 4.0, *T* = 25 °C, *I* = 0.1 M Acetate, *t* = 15 mins B) *pH* = 7.4, *T* = 37 °C, *I* = PBS, *t* = 15 mins C) *pH* = 4.0, *T* = 90 °C, *I* = 0.1 M Acetate, *t* = 15 mins. **HPLC Gradient C.**

Roger and co-workers reported the formation of 3 radiolabelled species when using the chelator 6-((4,7-bis(pyridin-2-ylmethyl)-1,4,7-triazonan-1-yl)methyl)picolinic acid (Hno1pa2py) for the complexation of ^{64}Cu.[243] One of these products was assigned to being a radiolysis product, and the remaining two to different coordination geometries. Thus, the formation of multiple species by H_3NO3PA is not unexpected.

When assessed for stability to serum, the products formed at pH 4.0 and at pH 7.4 were found to be rapidly decomposed, with none of the activity being retained on the base line after 30 minutes incubation in serum (Figure 3.12). Thus, regardless of the coordination mode, H_3NO3PA does not produce a kinetically stable product upon complexing ^{68}Ga

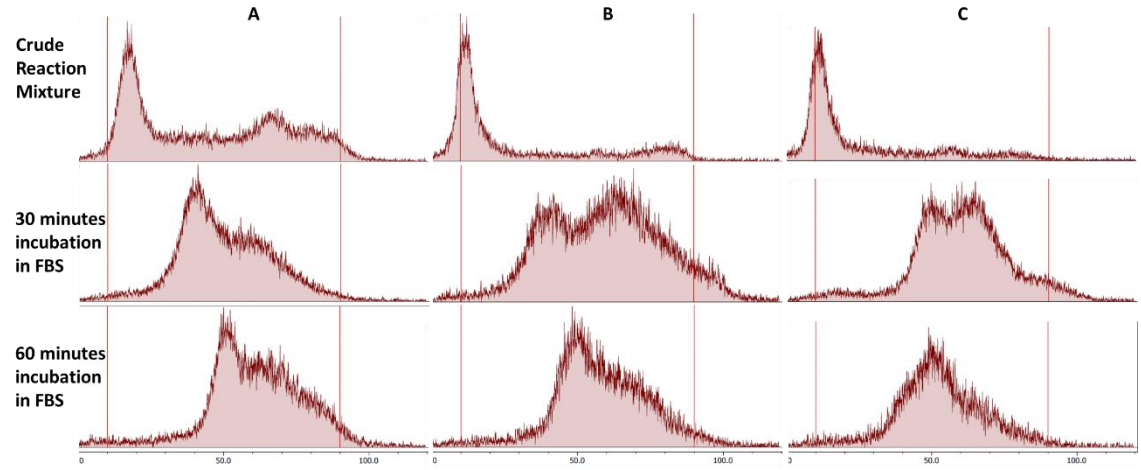

Figure 3.12: Radio-TLCs of: Top: Crude radiolabelling mixtures containing $^{68}GaCl_3$ and 100 µM H_3NO3PA. Middle: Crude radiolabelling mixture after incubation with FBS for 30 minutes at 37 °C. Bottom: Crude radiolabelling mixture after incubation with FBS for 60 minutes at 37 °C. A) *pH* = 4.0, *T* = 25 °C, *I* = 0.1 M Acetate, *t* = 15 mins B) *pH* = 7.4, *T* = 37 °C, *I* = PBS, *t* = 15 mins C) *pH* = 4.0, *T* = 90 °C, *I* = 0.1 M Acetate, *t* = 15 mins. Method development for TLC analysis is shown in appendix 4.

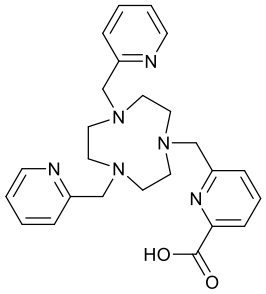

Figure 3.13: Structure of Hno1pa2py.

3.4. Phosphonates

3.4.1 Synthesis of diethyl phosphonate analogue of ethyl glycinate

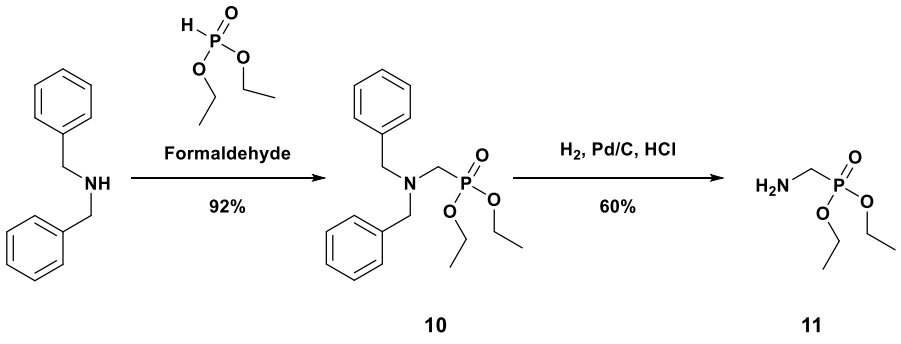

Scheme 3.4: Synthetic scheme for the production of diethyl (aminomethyl)phosphonate, **11**.

A diethyl phosphonate analogue of ethyl glycinate, diethyl (2-aminomethyl)phosphonate (**11**), was prepared in a 2 step process (Scheme 3.4)– addition of the phosphonate group to dibenzylamine through a Kabichinik-Fields reaction[244,245] followed by deprotection of the amine to yield the phosphonate ester.[244]

Initial attempts at the Kabichinik-Fields reaction using alternative protected amines, *tert*-butyl carbamate and benzylamine, were unsuccessful. *Tert*-butyl carbamate did not react due to the deactivating nature of the carbamate group. Benzylamine was sufficiently active to react; however the reaction progressed to form the double phosphonate ester product. Using dibenzylamine yielded the mono-addition product, **10**, as desired, in a 92% yield. Deprotection was straightforward, with **11** obtained in a 60% yield being obtained through hydrogenation in a Parr reactor.

3.4.2 Synthesis of diethyl phosphonate analogue of ethyl 6-(chloromethyl)picolinate ester

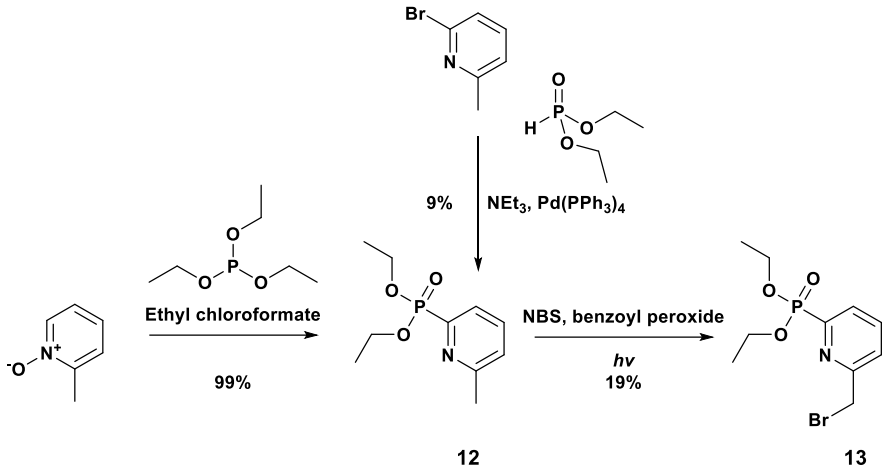

Scheme 3.5: Synthetic scheme for the preparation of diethyl (6-(bromomethyl)pyridine-2-yl)phosphonate, **13**.

Preparation of a diethyl phosphonate analogue of ethyl picolinate was achieved in a two step process – addition of the diethyl phosphonate unit to picoline followed by bromination of the methyl group to yield diethyl (6-(bromomethyl)pyridine-2-yl)phosphonate (**13**, Scheme 3.5).

Diethyl (6-methylpyridin-2-yl)phosphonate, **12**, was prepared *via* two different routes – a palladium catalysed cross coupling between diethyl phosphonate and 2-bromo-6-methylpyridine[246] and a deoxylative phosphorylation reaction[247] between 2-picoline-N-oxide and triethylphosphite. The palladium catalysed coupling of 2-methyl-6-bromopyridine with diethyl phosphonate was low yielding (9%), difficult to purify and required expensive starting materials. In contrast, the phosphorylation of 2-picoline-N-oxide had a much higher yield (99%), and a simpler synthetic procedure and purification.

Bromination of the methyl unit of **12** was achieved through a light initiated radical bromination.[246] The reaction was not selective for the mono-brominated product; the crude reaction mixture contained unreacted starting material, the desired mono-brominated product and the doubly brominated side product. This reduced the overall yield, with only 19% **13** being obtained with 20% remaining as starting material and 7% as the doubly brominated product. Isolation of the desired product, diethyl (6-(bromomethyl)pyridine-2-yl)phosphonate, was achieved through column chromatography.

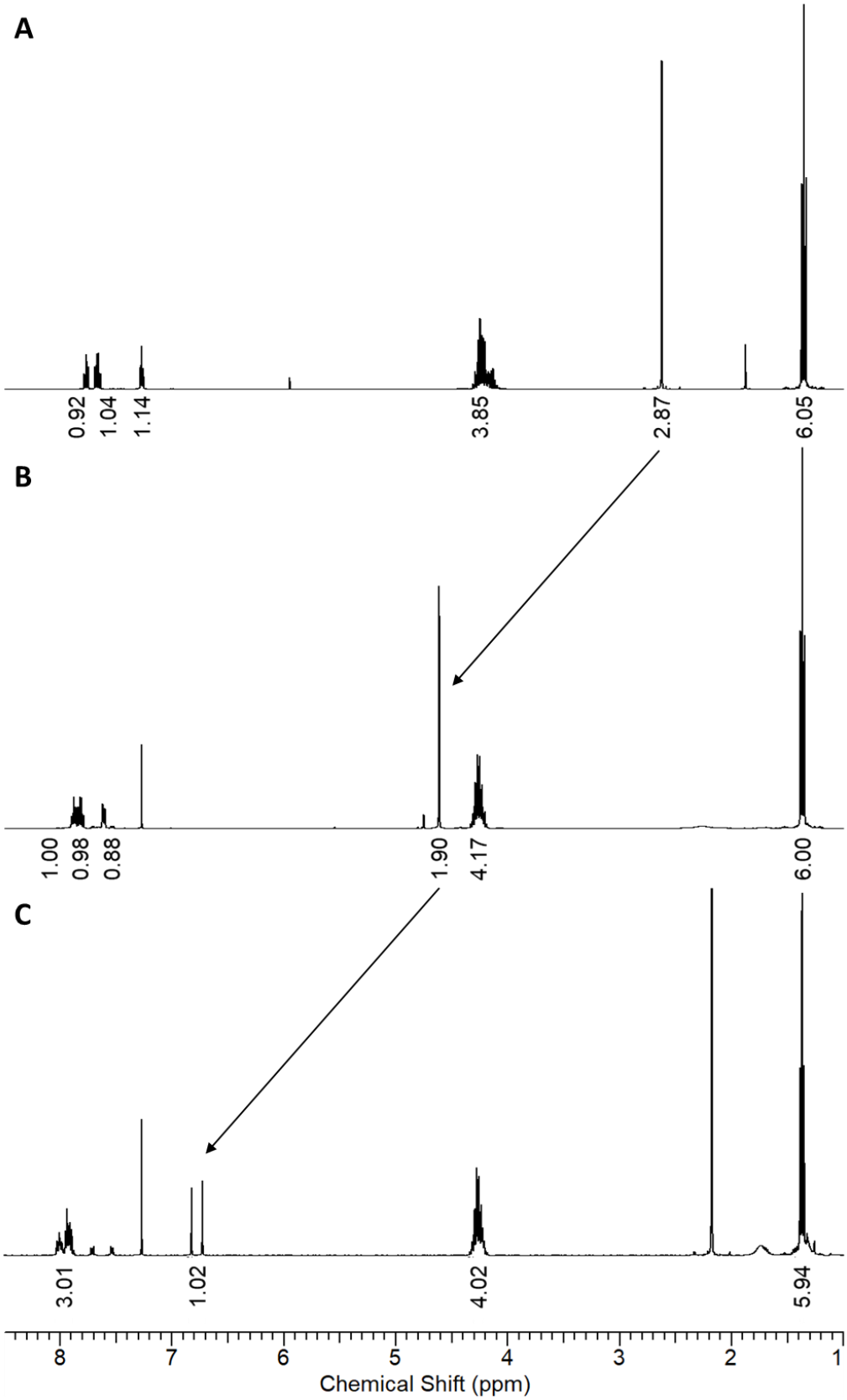

Figure 3.14: 1H NMR spectra of A) **12** B) **13** C) diethyl (6-(dibromomethyl)pyridine-2-yl phosphonate. (400 MHz, $CDCl_3$, 298 K).

The bromination of **12** is evident through both mass spectrometry and NMR spectroscopy. The molecular ion peak of **12** is a single peak (*m/z* = 230.1), the product **13** is a pair of peaks (*m/z* = 308.2 and 310.2, 1:1 ratio) and the doubly brominated species, diethyl (6-

(dibromomethyl)pyridin-2-yl) phosphonate, comprises of three peaks (*m/z* = 386.1, 388.1 and 390.1, 1:2:1 ratio). These additional peaks are due to the two isotopes of bromine.

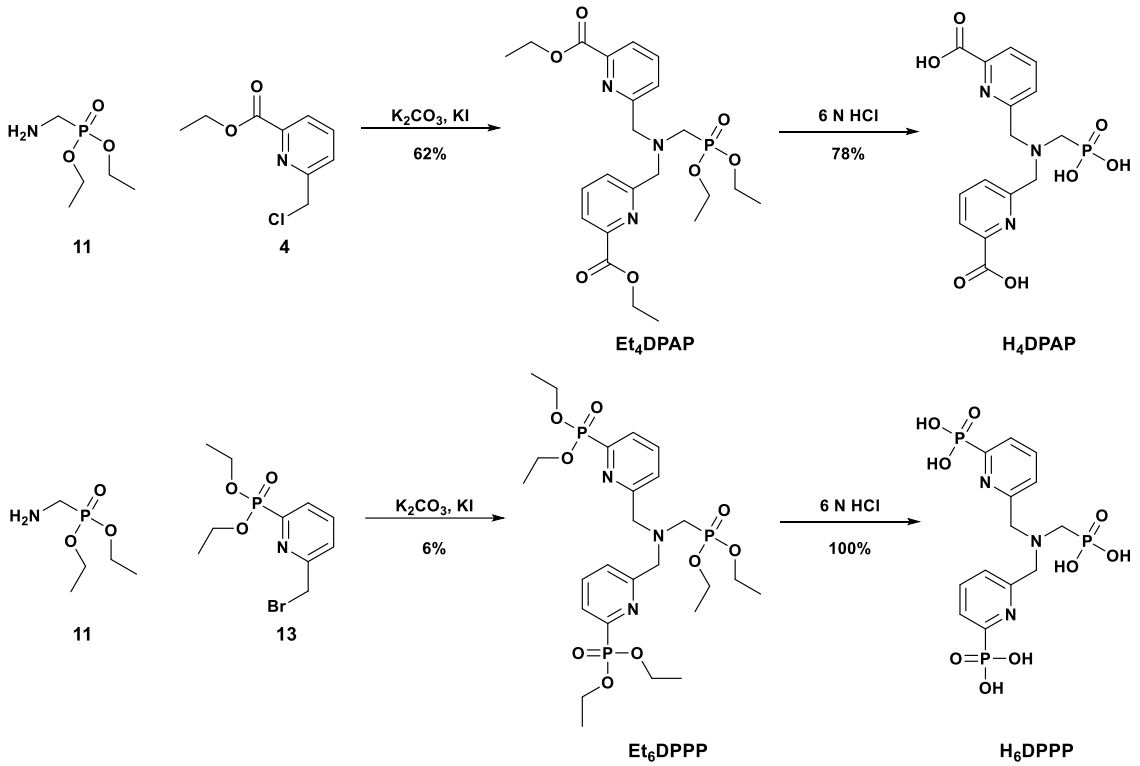

Scheme 3.6: Synthesis of phosphonated H_3Dpaa analogues – H_4DPAP and H_6DPPP.

The alkyl environment is also increasingly deshielded, and depopulated, upon bromination. The methyl unit of **12** (δ_H = 2.55. δ_C = 24.86) corresponds to 3 protons. Upon bromination, this environment corresponds to only 2 protons (δ_H = 4.64, δ_C = 34.46) and in the dibrominated byproduct it corresponds to only 1 proton and is strongly deshielded (δ_H = 6.73, δ_C = 42.70) relative to the starting material.

3.4.3 Synthesis of H_4DPAP and H_6DPPP

H_4DPAP was synthesised by reaction of **11** with **4** to give diethyl 6,6'-((((diethoxyphosphoryl)methyl)azanediyl)-bis(methylene))dipicolinate (Et_4DPAP) in a 62% yield followed by deprotection under acidic conditions (Scheme 3.6). H_6DPPP was prepared by reaction of **11** with **13** to give diethyl ((bis((6-(diethoxyphosphoryl)pyridin-2-yl)methyl)amino)methyl)phosphonate (Et_6DPPP) followed by deprotection under acidic conditions.

The proligands, Et_4DPAP and Et_6DPPP, have similar ^{1}H NMR spectra to the carboxylate analogue Et_3Dpaa. One principle difference is the upfield shift of the resonance of the "amino acid" backbone. In the phosphonated analogues this resonance has an increased shielding, with a chemical shift of 3.04-3.05 ppm in comparison to 3.47 ppm for the equivalent protons in Et_3Dpaa. Furthermore, these resonances are doublets due to coupling to the adjacent phosphorous nucleus ($^2J_{PH}$ = 10.4 Hz).

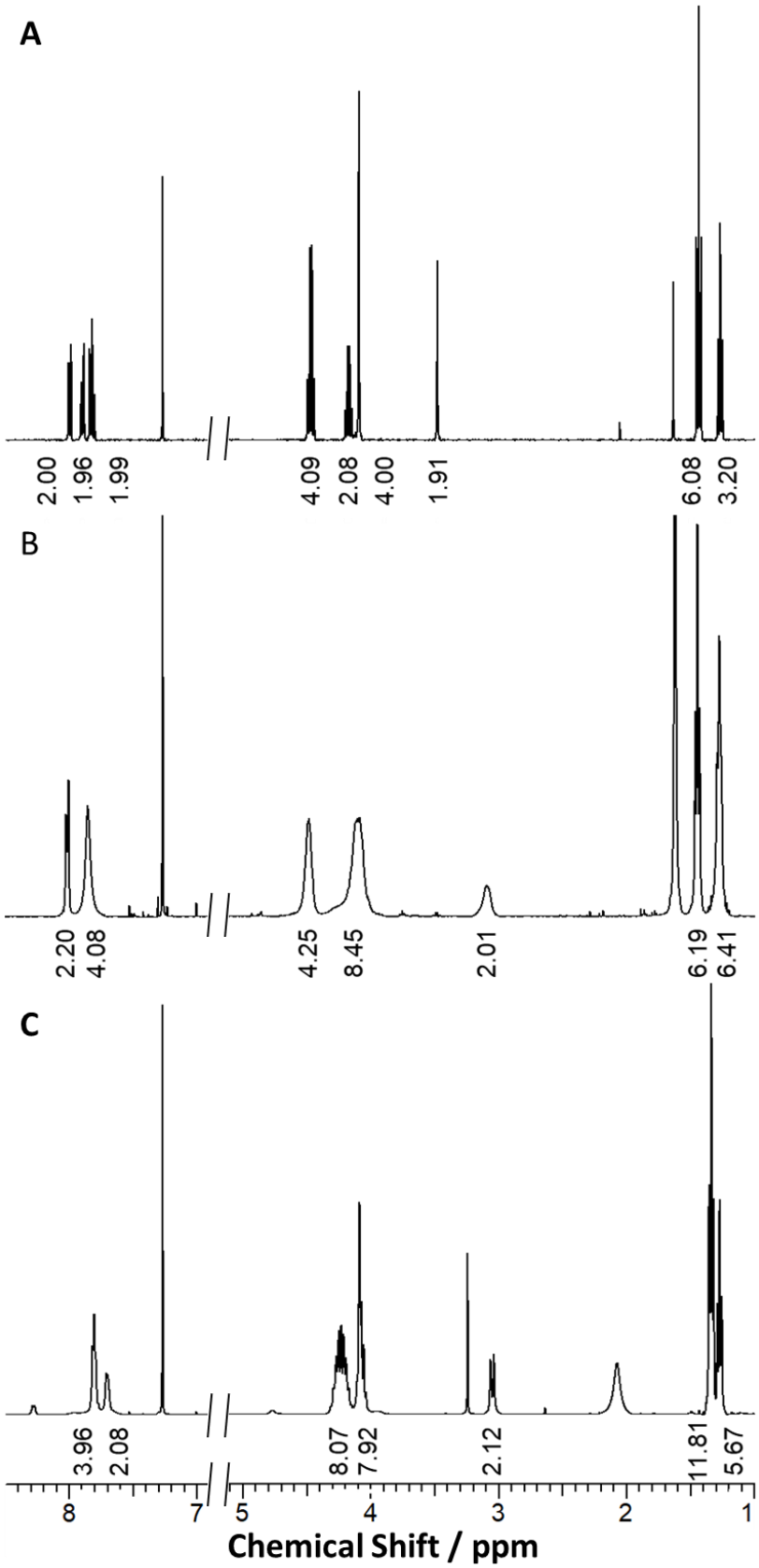

Figure 3.15: ^{1}H NMR of A) Et_3Dpaa ($CDCl_3$), B) Et_4DPAP (d_6-DMSO), C) Et_6DPPP ($CDCl_3$) (400 MHz, 298 K)

Upon deprotection the complex peaks due to the phosphonate esters (δ_H = 4.30-3.96 and 1.34-1.14) are no longer present. The alkyl phosphonate ester of Et_4DPAP (δ_P = 25.50) is significantly shielded upon deprotection to H_4DPAP (δ_P = 8.60). A similar trend is seen for

Et_6DPPP (δ_P = 25.91) upon deprotection to H_6DPPP (δ_P = 10.15), and the aryl phosphonate (δ_P = 11.53) is also deshielded as it hydrolysed to an aryl phosphonic acid (δ_P = 7.11)

3.4.4 Complexation [Ga(DPAP)] and [Ga(DPPP)]

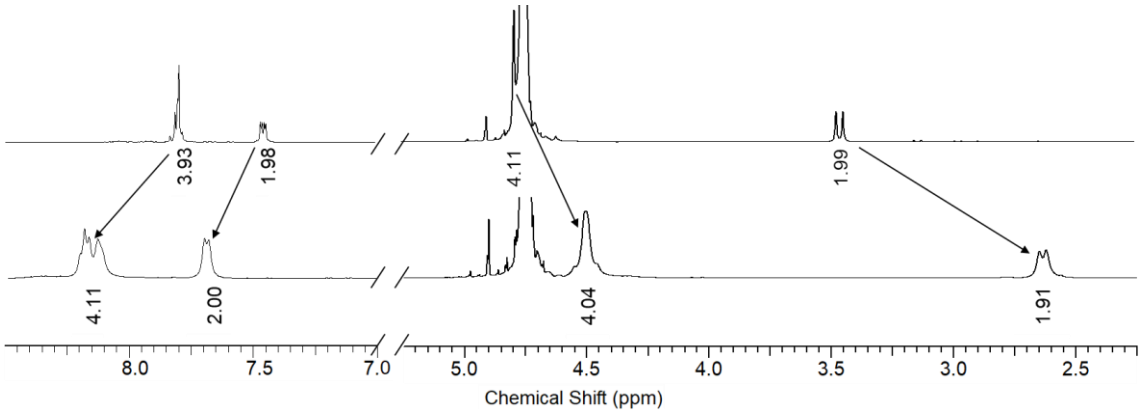

Figure 3.16: ^{1}H NMR spectra of A) H_4DPAP B) [Ga(DPAP)] (400 MHz, D_2O, *pD* = 7.14, 298 K)

Upon complexation of Ga(III) the aromatic protons of H_4DPAP are deshielded ($\Delta\delta_H$ = 0.2-0.3). Unusually, the methylene bridge protons of the Ga(III) complex are equivalent on the NMR timescale – only a single peak is observed at δ_H = 4.51 and no geminal coupling is observed (Figure 3.16). This peak is also shielded compared to the equivalent peak in the free ligand (δ_H = 4.77) in contrast to the results seen for H_3Dpaa and H_3Tpaa upon complexation of Ga(III).

3.4.5 Radiolabelling [^{68}Ga][Ga(DPAP)] and [^{68}Ga][Ga(DPPP)]

Due to the highly acidic nature of phosphonic acids, it is likely that even in the acidic HPLC eluate the non-coordinating oxygen will be deprotonated. This results in a charged complex which will be very hydrophilic. As a result, there is little separation in the retention time of non-complexed ^{68}Ga and [^{68}Ga][Ga(DPAP)] (Figure 3.17) as both of these species elute close to the solvent front; this makes it difficult to determine precise radiochemical yields although analysis of the shape of the peak shape suggests that complexation has occurred. A similar retention time is seen for [^{68}Ga][Ga(DPPP)] (Figure 3.18) – although complexation is evidently not complete under these reaction conditions due to the overlapping peaks at the solvent front of the HPLC chromatogram. Qualitatively it can be said that the pH of the radiolabelling solution has an effect on the complexation of ^{68}Ga by H_6DPPP, with radiolabelling being lower at neutral pH than under acidic conditions. TLC analysis of the radiolabelling reactions of H_4DPAP and H_6DPPP with ^{68}Ga is hampered by the coelution of the radiolabelled products with free ^{68}Ga.

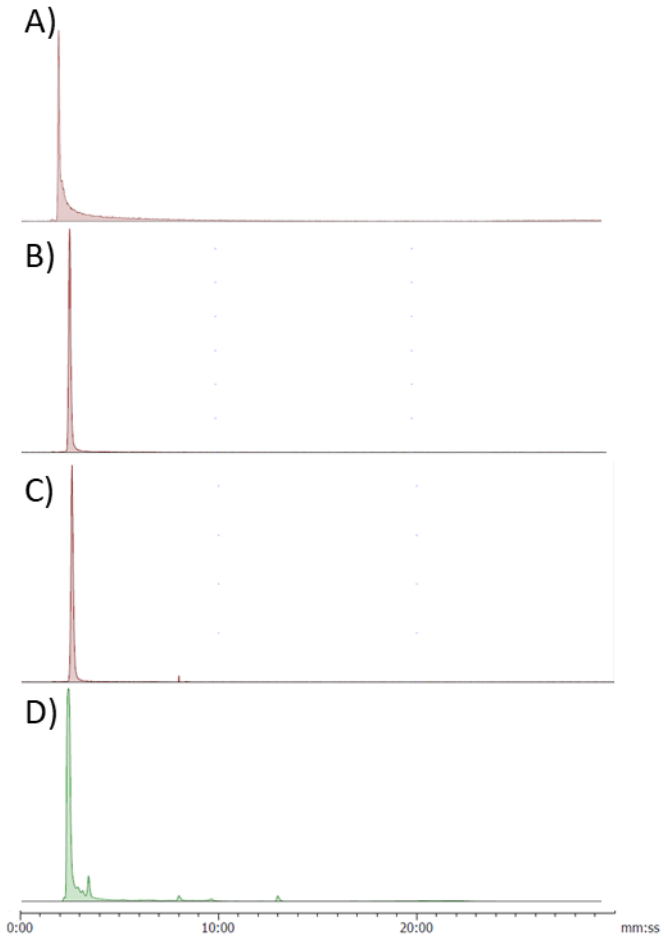

Figure 3.17: HPLC chromatograms for A) non-complexed ^{68}Ga B) ^{68}Ga incubated with 100 µM H_4DPAP, *pH* = 4.0, *I* = 0.1 M Acetate, *T* = 25 °C, *t* = 15 mins C) ^{68}Ga incubated with 100 µM H_4DPAP, *pH* = 7.4, *I* = PBS, *T* = 37 °C, *t* = 15 mins, D) [Ga(DPAP)] UV trace. **HPLC Gradient A.**

To further confirm these radiolabelling results, H_4Dpaa.ga was used to chelate any non-complexed ^{68}Ga to increase its retention time. Incubation of the crude radiolabelling solution, containing ^{68}Ga and H_4DPAP, with H_4Dpaa.ga resulted in 4% of the activity being associated with [^{68}Ga][Ga(Dpaa.ga)(H_2O)] and the remaining 96% with the peak at the solvent front (Figure 3.19). In the absence of H_4DPAP, H_4Dpaa.ga achieved 99% RCY under the same conditions. Incubation of this radiolabelled product with H_4DPAP resulted in transchelation of 9% of the activity. Therefore the radiochemical yield achieved by H_4DPAP can be considered to be >95% after 30 minutes (the original incubation time and the incubation with H_4Dpaa.ga).

Applying the same methodology to H_6DPPP reveals that the radiolabelling is significantly lower; after incubation of a solution of ^{68}Ga and H_6DPPP with H_4Dpaa.ga only 22% of the activity was associated with the solvent front (Figure 3.20). None of the activity was transferred from H_4Dpaa.ga to H_6DPPP in 15 minutes. This suggests that either the RCY of H_6DPPP is much lower than that of H_4DPAP, or that significant transchelation to H_4Dpaa.ga is occurring. In either case, this is not suitable for further application.

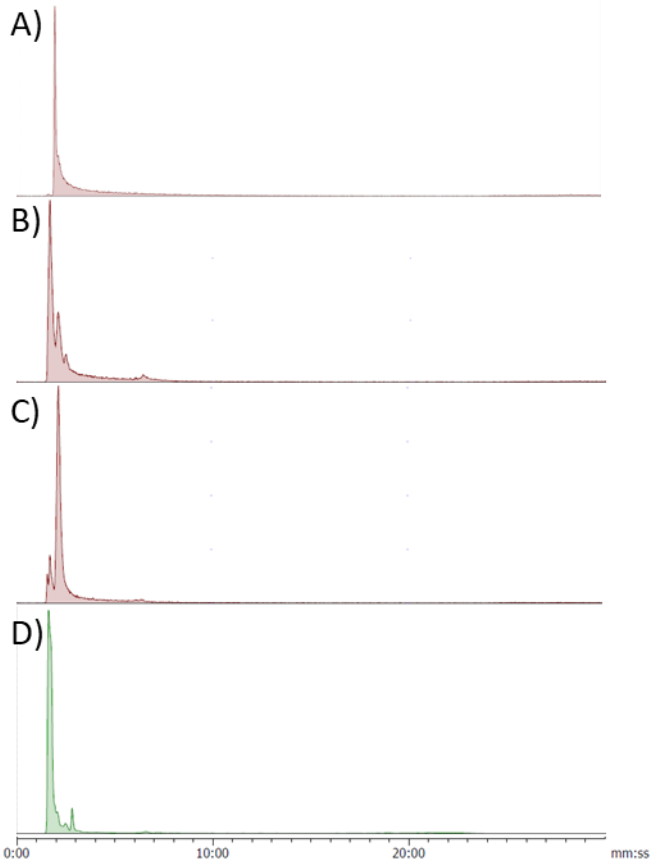

Figure 3.18: HPLC chromatograms for A) non-complexed ^{68}Ga B) ^{68}Ga incubated with 100 µM H_4DPPP, *pH* = 4.0, *I* = 0.1 M Acetate, *T* = 25 °C, *t* = 15 mins C) ^{68}Ga incubated with 100 µM H_4DPAP, *pH* = 7.4, *I* = PBS, *T* = 37 °C, *t* = 15 mins, D) [Ga(DPPP)] UV trace. **HPLC Gradient A**.

As the radiochemical yield of the reaction between H_4DPAP and ^{68}Ga is high, serum stability can be assessed by TLC, despite the coelution of [^{68}Ga][Ga(DPAP)] and non-chelated ^{68}Ga. There is some overlap between the complex peak and that of serum bound ^{68}Ga; despite this it is evident that the activity shifts from R_f = 0.5-1.0 in the reaction mixture to R_f = 0.3-0.7 upon being challenged by serum (Figure 3.21). This shows that the complex formed is not stable to FBS and therefore unsuitable for application to *in vivo* studies.

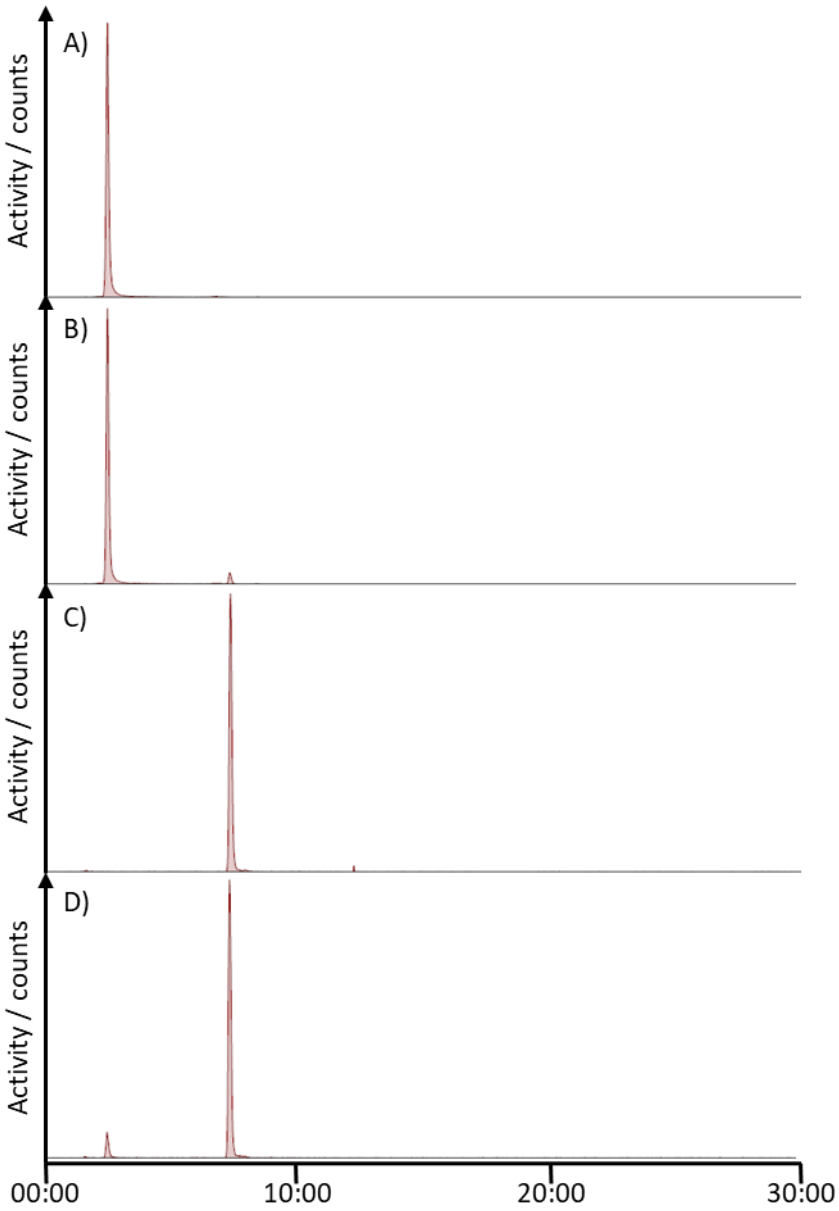

Figure 3.19: Radio HPLC chromatograms for A) ^{68}Ga incubated with H_4DPAP. *[H_4DPAP]* = 100 µM, *I* = 0.1 M Acetate, *pH* = 3.5, *T* = 25 °C, *t* = 15 minutes. B) A + H_4Dpaa.ga, *[H_4Dpaa.ga]* = 100 µM, *t* =15 minutes. C) ^{68}Ga incubated with H_4Dpaa.ga. *[H_4Dpaa.ga]* = 100 µM, *I* = 0.1 M Acetate, *pH* = 3.5, *T* = 25 °C, *t* = 15 minutes. D) C + H_4DPAP. *[H_4DPAP]* = 100 µM, *t* = 15 minutes. **HPLC Gradient A.**

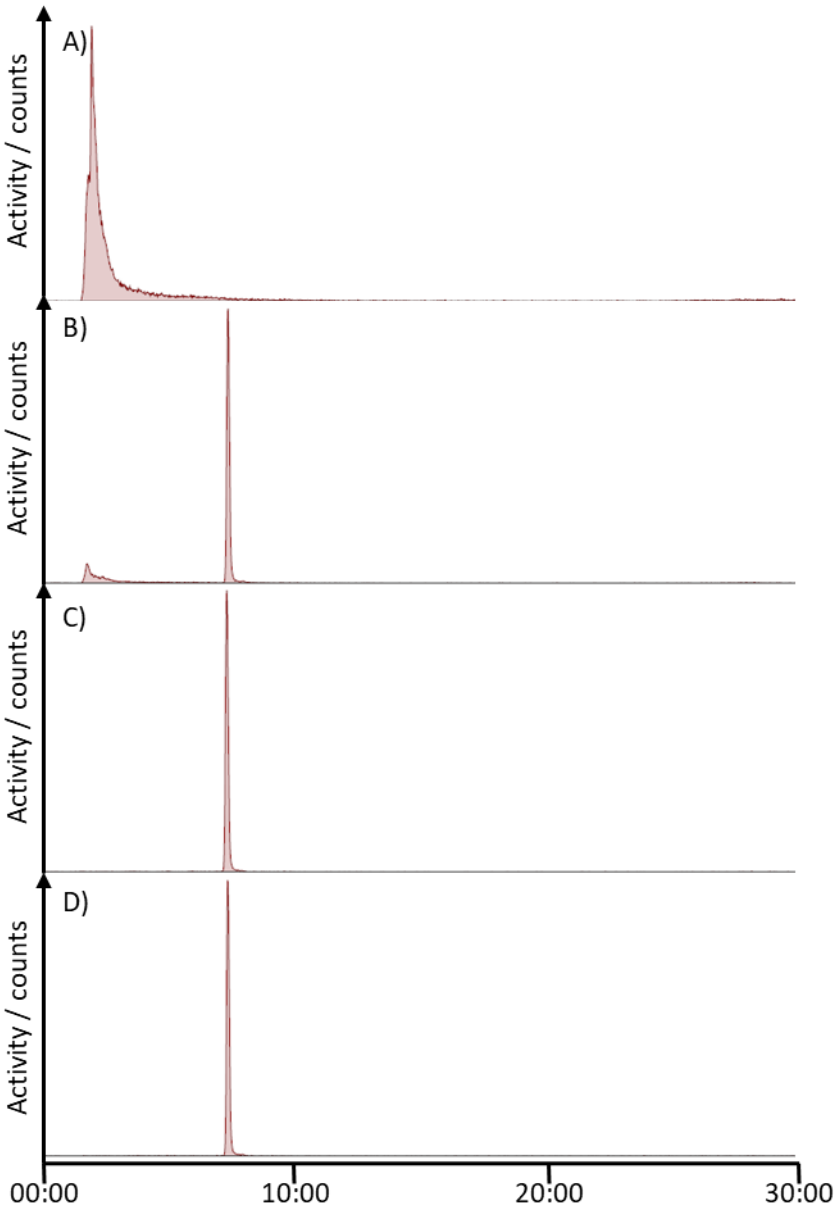

Figure 3.20: Radio HPLC chromatograms for A) ^{68}Ga incubated with H_6DPPP. *[H_6DPPP]* = 100 µM, *I* = 0.1 M Acetate, *pH* = 3.5, *T* = 25 °C, *t* = 15 minutes. B) A + H_4Dpaa.ga, *[H_4Dpaa.ga]* = 100 µM, *t* =15 minutes. C) ^{68}Ga incubated with H_4Dpaa.ga. *[H_4Dpaa.ga]* = 100 µM, *I* = 0.1 M Acetate, *pH* = 3.5, *T* = 25 °C, *t* = 15 minutes. D) C + H_6DPPP. *[H_6DPPP]* = 100 µM, *t* = 15 minutes. **HPLC Gradient A.**

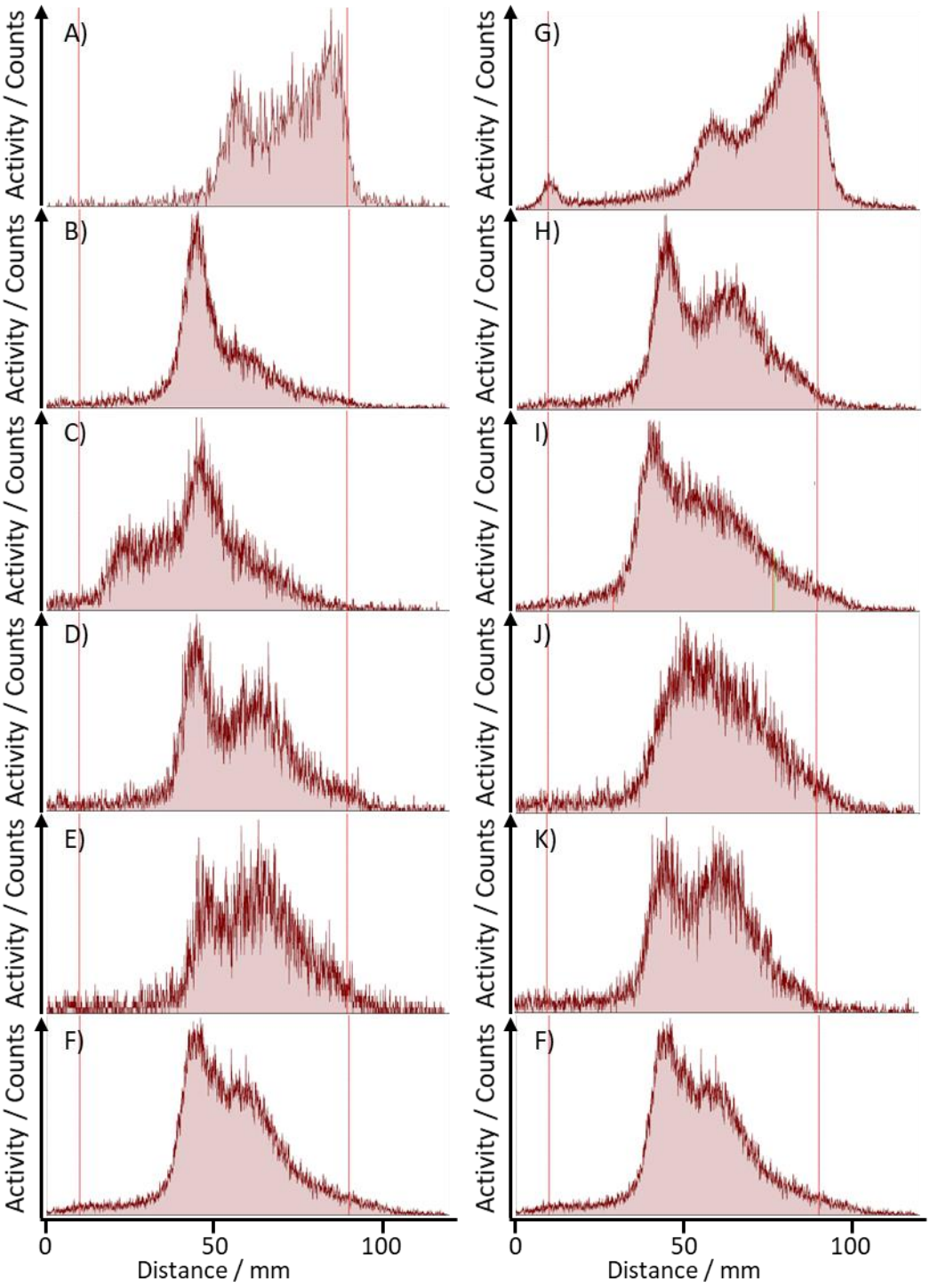

Figure 3.21: Radio TLC for A) ^{68}Ga incubated with H_4DPAP. *[H_4DPAP]* = 100 µM, *I* = 0.1 M Acetate, *pH* = 4.0, *T* = 25 °C, *t* = 15 minutes. B-E) A + FBS. *T* = 37 °C. F) ^{68}Ga incubated with FBS. *T* = 37 °C, *t* = 60 minutes. G) ^{68}Ga incubated with H_4DPAP. *[H_4DPAP]* = 100 µM, *I* = PBS, *pH* = 7.4, *T* = 37 °C, *t* = 15 minutes. H-K) G + FBS. *T* = 37 °C. B + H) *t* = 30 minutes. C+I) *t* = 60 minutes. D + J) *t* = 90 minutes. E + K) *t* = 120 minutes. Method development for TLC analysis is shown in appendix 4.

3.5. Conclusions

Incorporation of an additional picolinate arm into the tripodal picolinate design resulted in the chelator H_3Tpaa. The single crystal X-ray structure obtained for the Ga(III) complex confirms this heptadentate chelator fulfils the six coordinate environment of Ga(III). This

chelator was able to complex ^{68}Ga rapidly at both acidic and neutral pH, with greater than 99% yields in both cases. The radiolabelled complex was prepared with a molar activity of 3.1 GBq µmol^{-1}; this is comparable to that obtained by H_3Dpaa. The resulting radiolabelled complex was found to be more stable than that formed by H_3Dpaa with ^{68}Ga, with 32% of the complex remaining intact after 30 minutes incubation with serum. However, the complex did not show sufficient kinetic stability for further studies as it was fully decomplexed in serum within 2 hours.

The macrocyclic chelator, H_3NO3PA, formed multiple species upon complexation of ^{68}Ga – this is most likely due to alternative coordination modes due to its high number of potential coordinating atoms relative to the ideal coordination geometry of Ga(III). This finding is corroborated by the ^{1}H NMR of the complex; multiple species were present that rapidly exchanged at higher temperatures. Both temperature and pH had an influence on the ratio of the products formed when radiolabelling with ^{68}Ga; however, the radiolabelled products formed were not stable when challenged by serum.

Incorporation of phosphonic acids into the picolinate and carboxylate arms of H_3Dpaa resulted in the chelators H_4DPAP and H_6DPPP. The complexes formed by radiolabelling these chelators with ^{68}Ga were not sufficiently distinguishable from free ^{68}Ga for a full study to be undertaken. Initial studies show that H_4DPAP can be radiolabelled with ^{68}Ga at both acidic and neutral pH, however the resulting complex is not stable to FBS, with complete decomplexation within 30 minutes. Future work with these chelators should strive to increase their lipophilicity to improve the quality of the results obtained by allowing for separation from non-complexed ^{68}Ga. This could be achieved by using phenyl phosphonates instead of phosphonic acids; the replacement of an ionisable oxygen atom with a phenyl group would reduce the overall charge of the complex and add a lipophilic aromatic group. To improve the stability of the resulting complex, the pyridylphosphonate arms could be incorporated into a H_3Tpaa type structure.

Overall, the results presented here confirm those of Chapter 2 – picolinate arms are able to rapidly complex ^{68}Ga at both acidic and neutral conditions. By incorporating additional coordinating sites into the ligands the kinetic stability of the resulting ^{68}Ga complexes has been improved but further work is needed to develop a picolinate based chelator for ^{68}Ga that is sufficiently stable for *in vitro* application.

While H_3Tpaa was able to fully coordinate Ga(III), the radiolabelled complex [^{68}Ga][Ga(Tpaa)] was insufficiently stable for *in vivo* application. This result, along with similar results reported for H_3Dpaa and H_2dedpa, suggest that picolinic acids are not the ideal chelating units for ^{68}Ga. This may be due to the rigid nature of the picolinic acid preventing the optimal coordination geometry being obtained (N-Ga-O = 74-79^o in the solid state crystal structures; smaller than the ideal 90^o). To further develop these tripodal systems for complexation of ^{68}Ga

the coordinating arms should be varied to increase the hard basic nature of the coordinating atoms or to make the arms more flexible.

Chapter 4 Polyaminocarboxylate chelators for ^{68}Ga

4.1. Ligand design

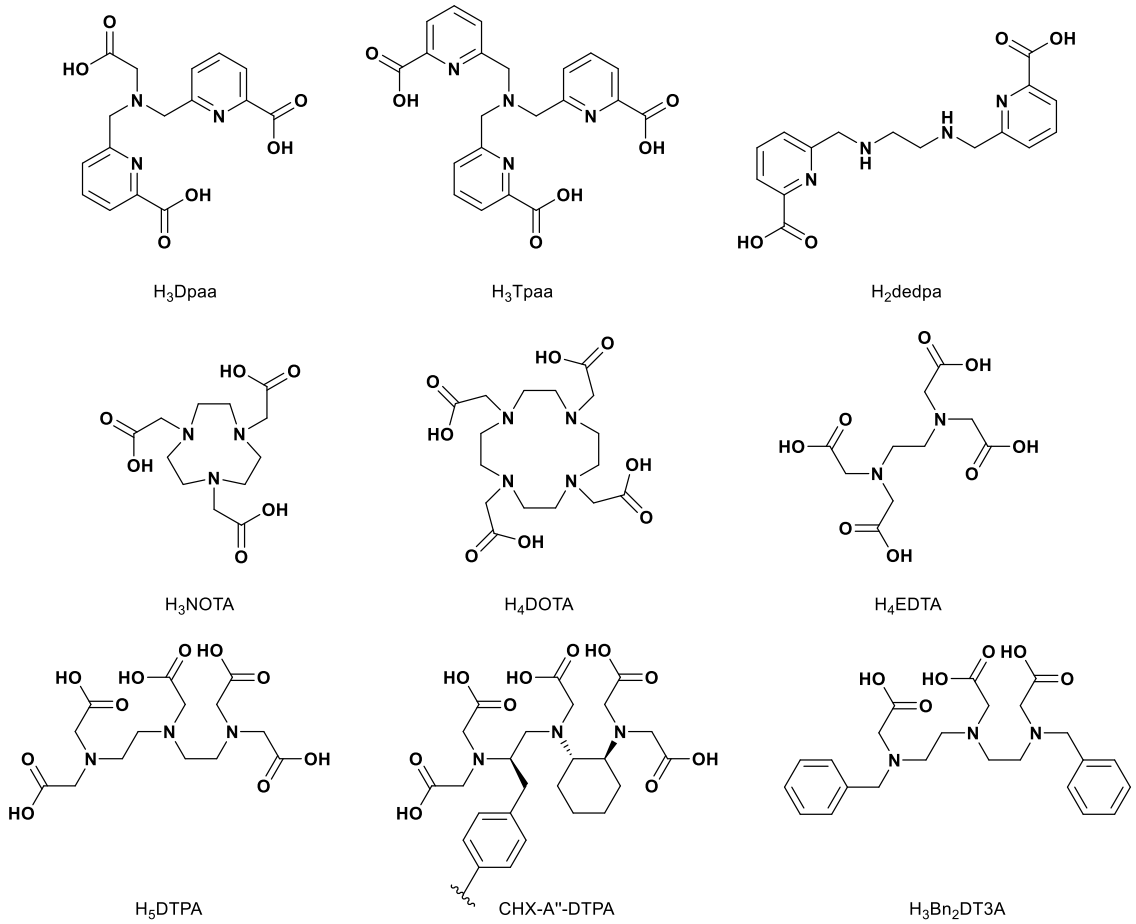

Figure 4.1: Structures of ligands discussed in this chapter.

It has become apparent that ligands based on picolinic acid arms are capable of rapidly complexing ^{68}Ga under mild conditions. However, the resulting complexes do not have sufficient stability for *in vivo* application. This result has been seen for H_3Dpaa,[107,223] H_3Tpaa and dedpa[167] and bifunctional derivatives of these ligands. Analysis of the solid state crystal structures of these ligands reveals that the five-membered ring formed by the picolinic acid motif distorts the complex away from the ideal octahedral geometry preferred by Ga(III). The N-Ga-O bond angle of the picolinate unit is consistently below the ideal 90° for an octahedral complex ([Ga(Dpaa)(OH)] average bond angle = 74.5°, [Ga(Tpaa)] average bond angle = 80.0°, [Ga(dedpa)] average bond angle = 79.9°) [37,207]. This suggests that the complexes have strain inherently built into the coordinating units that will negatively impact on their stability.

Chelators such as EDTA, DTPA, NOTA and DOTA, which have been widely applied to a complexing a number of metals, contain amino and acetate units. These also form five-membered rings when complexing Ga(III). However these rings have a slightly larger bite angle ([Ga(EDTA)] average bond angle = 82.93°,[249] [Ga(NOTA)] average bond angle = 83.41°,[250] [Ga(DOTA)$^{2-}$] average bond angle = 83.71°).[251] Whilst this is still smaller than the ideal 90° it is closer to this ideal than the angle seen for picolinate complexes and the more flexible amino-

acetate arm allows for twisting of the structure to reduce strain. These chelators have also been shown to have a greater stability when complexing ^{68}Ga.[252,253]

Lee *et al.* reported that 200 μM EDTA was capable of quantitative radiolabelling with ^{68}Ga at acidic pH (pH 4.5) in 10 minutes at room temperature.[252] When DTPA was heated to 100 ^{o}C under the same conditions only a 31% yield was achieved.[252] The [^{68}Ga][Ga(EDTA)] complex was stable to serum with < 3% protein bound activity after 1 hour whereas the [^{68}Ga][Ga(DTPA)] complex had 44% protein bound activity.[252] Chakravarty and co-workers reported that 155 μM DTPA-Ph-NCS was able to achieve 95% yield at room temperature under acidic conditions (pH 3.5) whereas heating (80 ^{o}C) allowed lower concentrations (62 μM) to achieve a 98% RCY.[253] They also reported that <60% of the radiolabelled complex was intact after 2 hours incubation in serum.[253]

The more constrained chelator, 2,2'-((2-(((1S,2S)-2-(bis(carboxymethyl)amino)cyclohex-yl)(carboxymethyl)amino)ethyl)azanediyl)diacetic acid (CHX-A''-DTPA) has also been applied to ^{68}Ga complexation; Bauer *et al.* reported >95% RCYs after incubation of 36 μM at room temperature and at pH 7.4; however this required long incubation times of 1 hour.[201] Wei *et al.* achieved >95% yields when incubating 29 μM CHX-A''-DTPA with ^{68}Ga in only 20 minutes, however this required heating to 85 ^{o}C.[254] Whilst requiring more strenuous radiolabelling conditions than DTPA, CHX-A''-DTPA produced complexes that showed no exchange with serum.[201]

These mixed results suggest that acyclic polyaminocarboxylate chelators are capable of forming stable complexes with ^{68}Ga, but further refinement is required to improve their suitability for the production of ^{68}Ga radiotracers. While EDTA was able to form stable complexes, it lacks a clear site for conjugation to a targeting agent. Both DTPA and the bifunctional DTPA-Ph-NCS ligands were able to form complexes with ^{68}Ga and still have additional functional groups that can be used for conjugation; however these complexes are not stable in serum challenges and are therefore not suitable for imaging application. The more rigid CHX-A''-DTPA ligand is shown to form stable complexes, but requires long reaction times or heating; under these conditions the proven macrocyclic chelators may prove more popular.

Further development of this family of chelators may allow for the preparation of a chelator that is capable of complexation under mild conditions, whilst retaining the stability of EDTA and CHX-A''-DTPA, in addition to being readily conjugated to targeting agents.

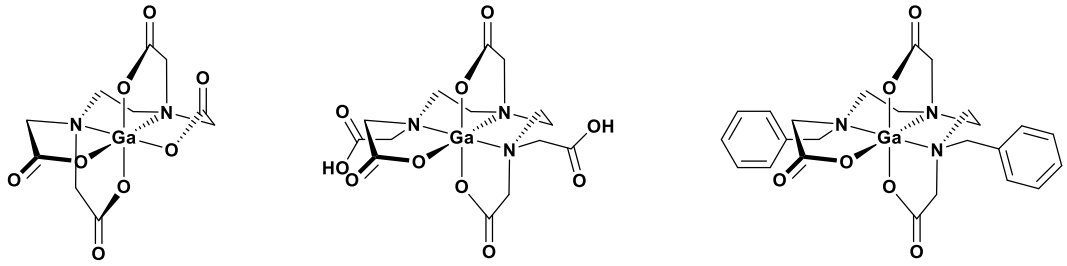

Figure 4.2: Proposed coordination of Ga(III) by EDTA, DTPA and H_3Bn_2DT3A

The proposed chelator, 2,2'-((((carboxymethyl)azanediyl)bis(ethane-2,1-diyl))bis(benzylazanediyl))diacetic acid (H_3Bn_2DT3A), has a reduced number of coordinating arms when compared to DTPA. Two of the potentially coordinating acetate arms are replaced with benzyl units to provide a UV-active group to make purification easier. This reduced number of coordinating arms will provide a more precise match for the hexadentate Ga(III) (Figure 4.2). Furthermore, this will match the coordinating sites of NOTA; three tertiary amines and three carboxylates (N_3O_3). This should provide a stable complex that is capable of rapid radiolabelling with ^{68}Ga. The terminal amines could potentially be used for conjugation, or the functional groups could be varied to optimise the steric and electronic properties for complexation. This structure also features a central glycine motif that could be substituted for other amino acids as an alternative route to formation of a bifunctional chelator.

4.2. Synthesis

4.2.1 Ligand synthesis

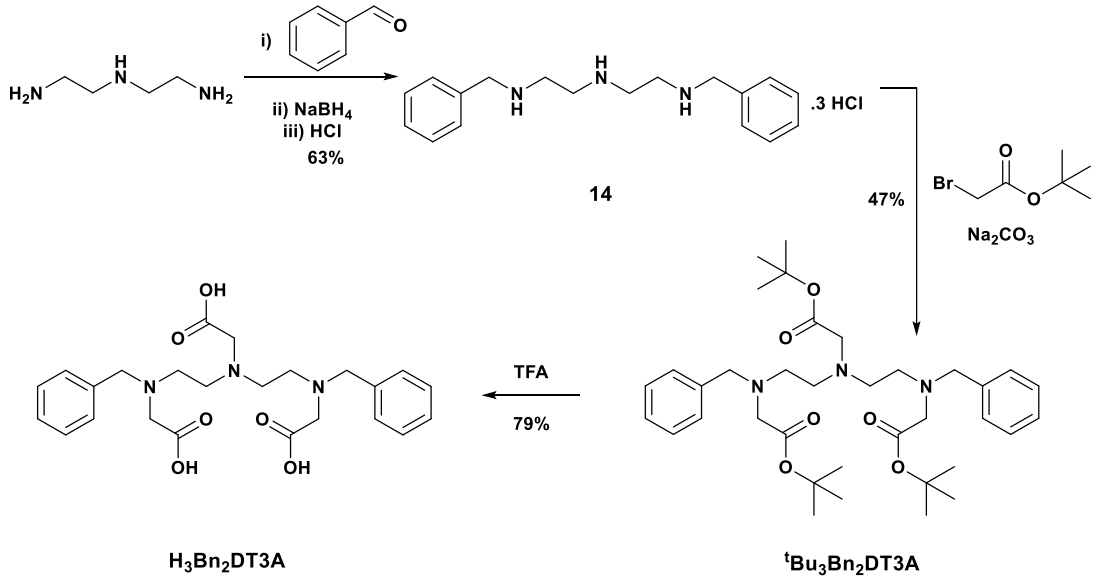

Scheme 4.1: Synthetic scheme for the preparation of H_3Bn_2DT3A

The ligand H_3Bn_2DT3A was prepared in a 3 step process (Scheme 4.1). The terminal amine groups of diethylenetriamine were selectively protected through a one pot, two step reductive amination with benzaldehyde to yield N1-benzyl-N2-(2-(benzylamino)ethyl)ethane-

1,2-diamine.[255] The resulting product was precipitated as a hydrochloride salt, **14**, in a 63% yield and used without further purification. The selective protection of the terminal amines was confirmed through ^{1}H NMR (Figure 4.3) as only a single peak was seen for the methylene linker of the benzyl units and the ratio of protons in these units (δ_H = 4.21) with the diethylenetriamine chain (δ_H = 3.38-3.18) was 4:8 as expected. The carboxylate functionality was introduced by addition of 3 equivalents of *tert*-butyl bromoacetate to give di-tert-butyl 2,2'-((((2-(tert-butoxy)-2-oxoethyl)azanediyl)bis(ethane-2,1-diyl))bis(benzylazanediyl))diacetate (^{t}Bu$_3$Bn$_2$DT3A) in a 47% yield,[256] followed by deprotection under acidic conditions to hydrolyse the *tert*-butyl esters whilst retaining the benzyl units. This yielded H_3Bn_2DT3A in a 79% yield; 23% overall from the diethylenetriamine starting material. Whilst the two acetate arm environments are similar in the protected ligand (δ_H = 3.32, 3.23), in the deprotected ligand the central arm is significantly more shielded (Figure 4.3, δ_H = 3.12) than the terminal arms (δ_H = 3.90).

4.2.2 Potentiometry

H_3Bn_2DT3A was studied using potentiometric titration; the obtained pK_a values are given in Table 4.1. By comparison to similar ligands, DTPA and diethylenetriamine, the first three constants can be assigned to protonation of the nitrogen atoms; the remaining two constants are assigned to the carboxylate arms with the third carboxylate protonation constant being too acidic to determine using this method.

The amines of H_3Bn_2DT3A (pK_1 = 9.70, pK_2 = 7.48) are more acidic than those of H_5dien (pK_1 = 9.84, pK_2 = 9.02)[257] or DTPA (pK_1 = 10.79, pK_2 = 8.64).[257–259] A comparison of glycine (pK_a = 9.8)[260] and benzylamine (pK_a = 9.35)[261] reveals the same trend; the carboxylate arm of glycine stabilises the protonated amine more than the benzyl arm of benzylamine resulting in a more basic amine.

The acidic pK_a values of H_3Bn_2DT3A, pK_3 (3.34), pK_4 (1.50) and pK_5 (1.40), are reasonably similar to those of NOTA (3.22, 1.96 and 0.7 respectively);[105,132] with the more flexible H_3Bn_2DT3A resulting in the two carboxylate arms being protonated independently with a similar pK_a whereas in the more constrained NOTA the arms likely interact more resulting in more diverse pK_a values. It is surprising that the pendant acid arms of H_3Bn_2DT3A are approximately 1 pK_a unit more acidic than those of DTPA – this may again be due to stabilisation of the protonated arms by internal hydrogen bonding from the remaining deprotonated arms of DTPA.

Complexation of metal ions by H_3Bn_2DT3A should be undertaken above pH 3.3 to ensure that the carboxylate arms are deprotonated. This will result in the ligand being pre-prepared for complexation allowing the reaction to proceed more efficiently.

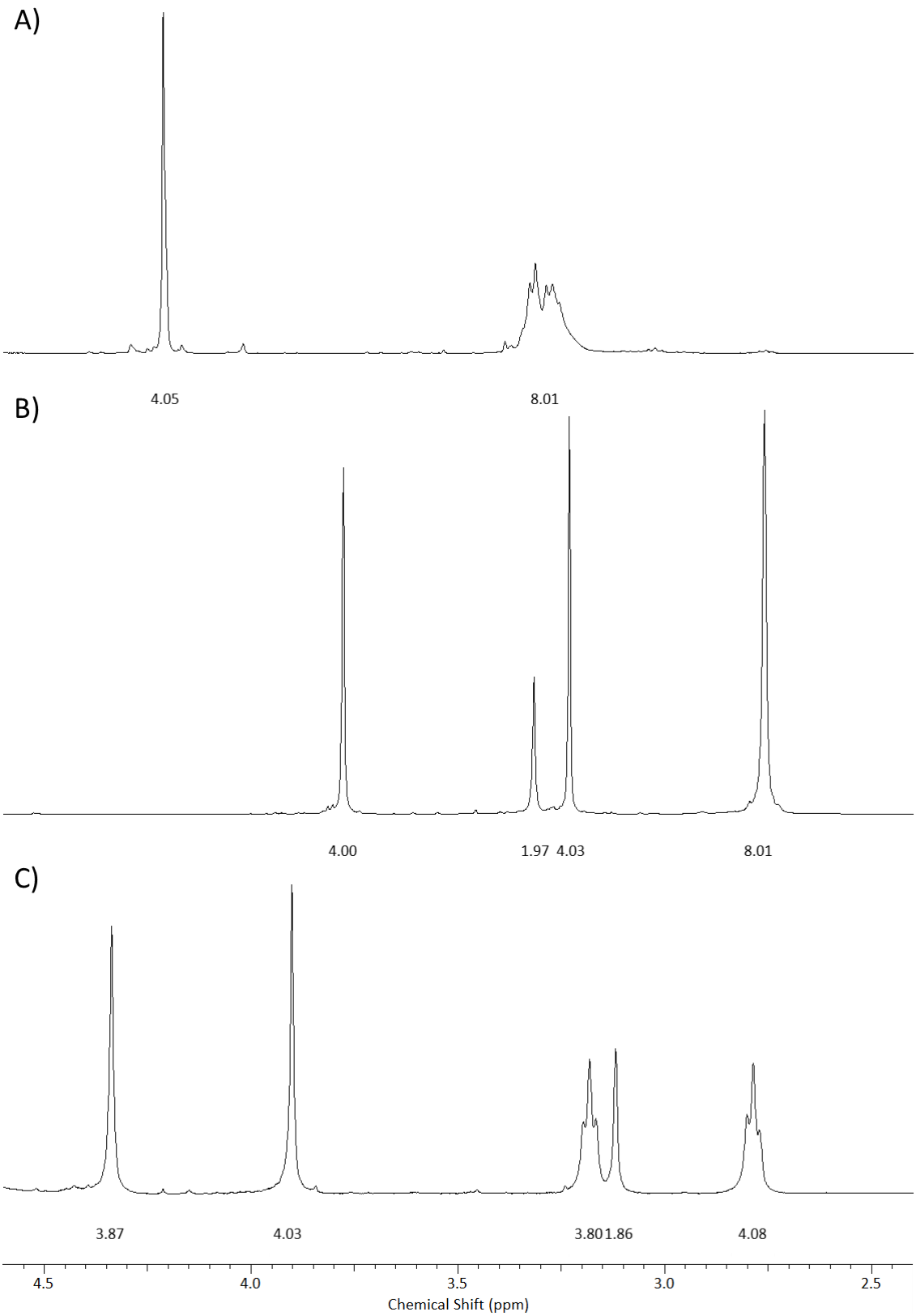

Figure 4.3: ^{1}H NMR spectra of A) **14** (400 MHz, D_2O, 298 K), B) $^{t}Bu_3Bn_2DT3A$ (400 MHz, $CDCl_3$, 298 K) C) H_3Bn_2DT3A (400 MHz, D_2O, 298 K).

Table 4.1: Protonation constants of the discussed ligands. [a] This work, T = 25 °C, I = 0.1 M NMe_4Cl; [b] Ref.[257]; [c] Refs. [105,132,262]

	H_3Bn_2DT3A[a]	Diethylenetriamine[b]	DTPA[b]	NOTA[c]
pK_1	9.70(1)	9.84	10.79	13.17
pK_2	7.48(1)	9.02	8.64	5.74
pK_3	3.34(1)	4.25	4.28	3.22
pK_4	1.50(2)	-	2.70	1.96
pK_5	1.40(2)	-	2.0	0.7

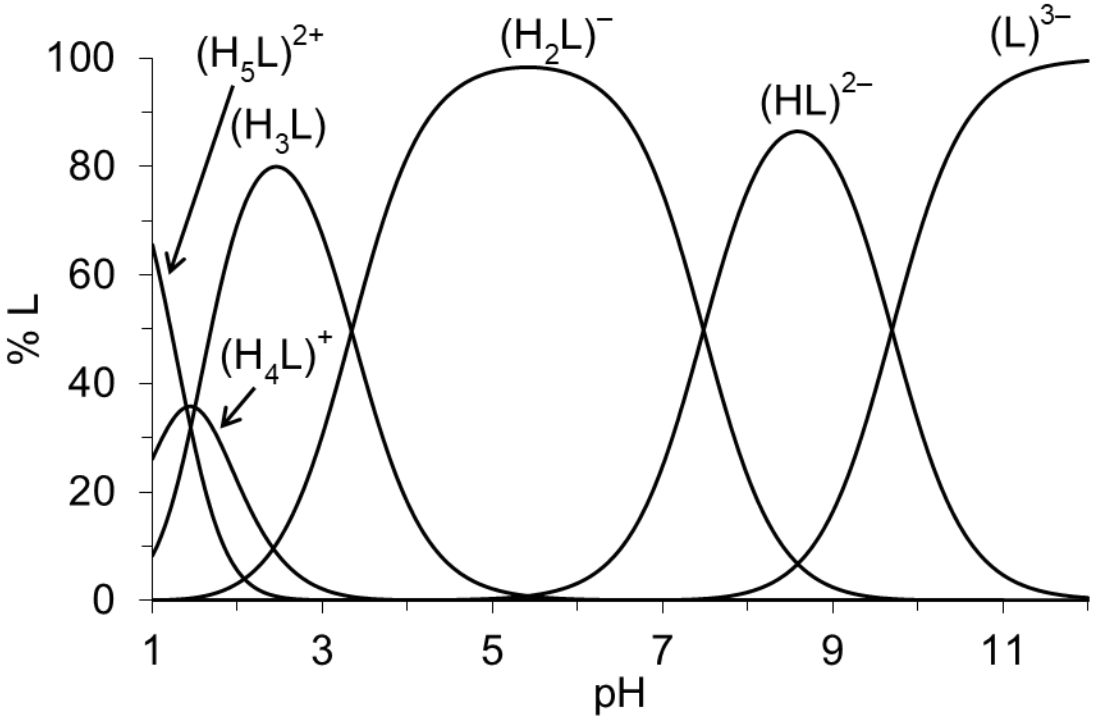

Figure 4.4: Speciation diagram of H_3Bn_2DT3A obtained by potentiometric titration. (T = 25 °C, I = 0.1 M NMe_4Cl, *[H_3Bn_2DT3A]* = 4 mM.)

4.2.3 Complexation

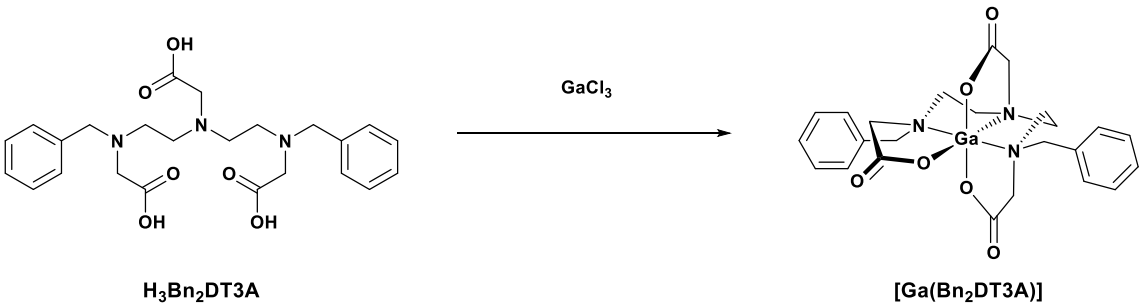

Scheme 4.2: Complexation of Ga(III) by H_3Bn_2DT3A

Upon complexation of Ga(III) by H_3Bn_2DT3A a 1:1 complex is formed (Scheme 4.2). As with the H_3Dpaa ligands discussed previously, a deprotonation event (indicated as $[Ga(L)(OH)]^-$ in Figure 4.5) occurs in the mildly acidic region ($pK_a = 5.32$). This may be due to the deprotonation of already bound water or addition of hydroxide to the Ga(III) ion.

The ligand H_3Bn_2DT3A has a slightly greater affinity for Cu(II) than Ga(III); the affinity for both of these ions is greater than for Zn(II). If the deprotonated species is taken into account (giving $\log K_{[Ga(Bn2DT3A(OH)]} = 23.57$) then the affinity for Ga(III) is much higher than for Cu(II).

The thermodynamic stability of the $[Ga(Bn_2DT3A)]$ complex formed by H_3Bn_2DT3A is lower than that of the similar systems [Ga(DTPA)] ($\log K_{[Ga(DTPA)]} = 24.3$)[257] and [Ga(NOTA)] ($\log K_{[Ga(NOTA)]} = 29.60$)[92] – this is unsurprising in the case of the NOTA complex due to the macrocyclic nature of NOTA resulting in improved thermodynamic stability due to preorganisation of the ligand prior to complexation. The difference between H_3Bn_2DT3A and DTPA is more surprising – both ligands likely bind Ga(III) in an N_3O_3 manner. However this can be rationalised by considering the ligand basicity; each basic site of DTPA is more basic than the equivalent of H_3Bn_2DT3A. This is expected to result in an increase in stability of the formed complex.[92]

Analysis of this system by UV-Vis spectrophotometry and Ga(III) titration further confirms the 1:1 system formed by Ga(III) and H_3Bn_2DT3A at both pH 3.8 and pH 8.3.

Table 4.2: Stability constants, $\log K$, of H_3Bn_2DT3A complexes (T = 25 °C, I = 0.1 M NMe_4Cl). Charges are omitted.

	Ga(III)	**Cu(II)**	**Zn(II)**
M + L = [M(L)]	18.25(3)	18.9(1)	14.12(3)
[M(HL)] = [M(L)] + H	2.73(3)	2.8(1)	4.16(1)
[M(L)] = [M(L)(OH)] + H	5.32(2)	-	12.06(4)
[M(L)(OH)] = $[M(L)(OH)_2]$ + H	8.21(2)	-	-

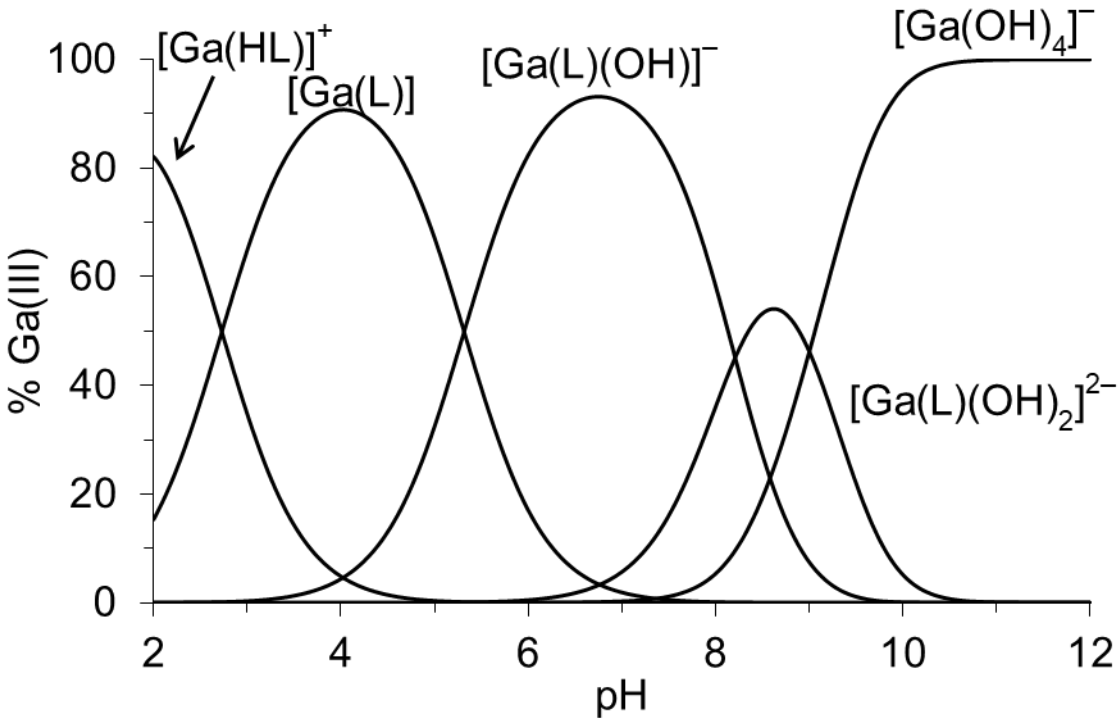

Figure 4.5: Speciation diagram of Ga(III)-H_3Bn_2DT3A system. (25 °C, *I* = 0.1 M NMe_4Cl, *[H_3Bn_2DT3A]* = 4 mM, *[Ga(III)]* = 2 mM).

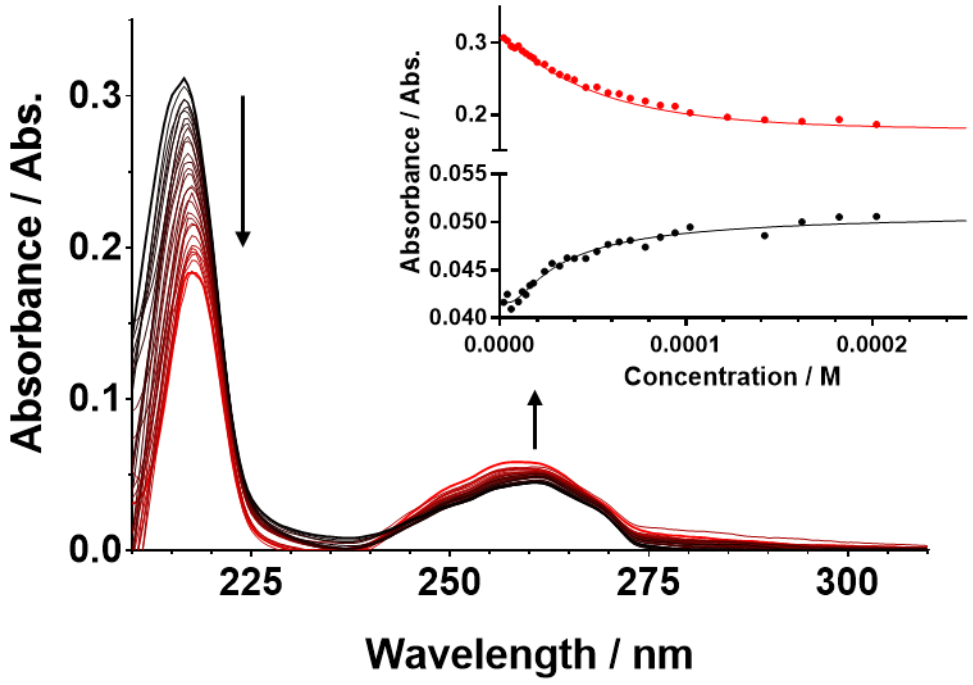

Figure 4.6: UV absorption spectra upon addition of $GaCl_3$. *[I]* = 0.1 M HEPES, *[L]* = 100 µM, *[Ga(III)]* = 0 – 200 µM, pH = 3.8. Arrows indicate direction of change upon addition of Ga(III). Inset: Binding curves fit with asymmetric sigmoidal 5PL non-linear regression using GraphPad. Red: Absorption at 217 nm, Black: Absorption at 263 nm.

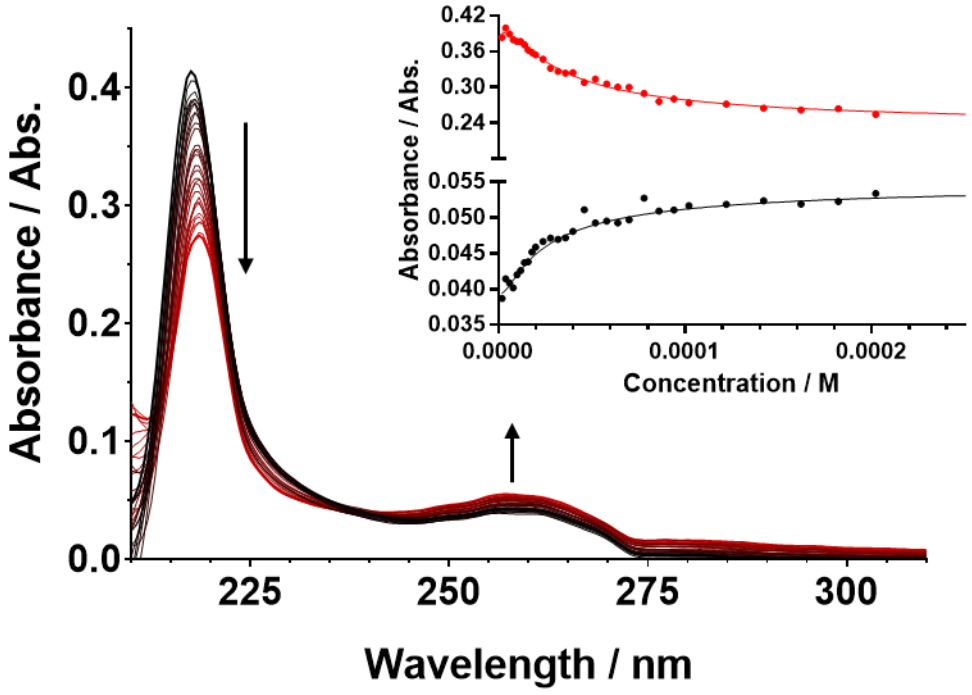

Figure 4.7: UV absorption spectra upon addition of $GaCl_3$. *[I]* = 0.1 M HEPES, *[L]* = 100 µM, *[Ga(III)]* = 0 – 200 µM, pH = 8.3. Arrows indicate direction of change upon addition of Ga(III). Inset: Binding curves fit with asymmetric sigmoidal 5PL non-linear regression using GraphPad. Red: Absorption at 217 nm, Black: Absorption at 260 nm.

The ^{1}H NMR spectrum of [Ga(Bn_2DT3A)] is pH dependent; there are clear changes in peak shift and shape between the spectra at pD = 4.0 and 6.8 (Figure 4.8, Figure 4.9). The changes in chemical shift are abrupt indicating slow exchange between the different species in solution (Figure 4.10). Integration of the peaks allows the relative ratios of species to be analysed – this allows for some changes in species to be observed (Figure 4.10 c). This is particularly true for the formation of free ligand at high pH with the proportion of free ligand determined from the aromatic region being in good agreement with the previously obtained speciation diagram (Figure 4.10 c). Following the transition from [Ga(Bn_2DT3A)] to [Ga(Bn_2DT3A)(OH)] by ^{1}H NMR is ineffective due to the high number of overlapping peaks in the alkyl region.

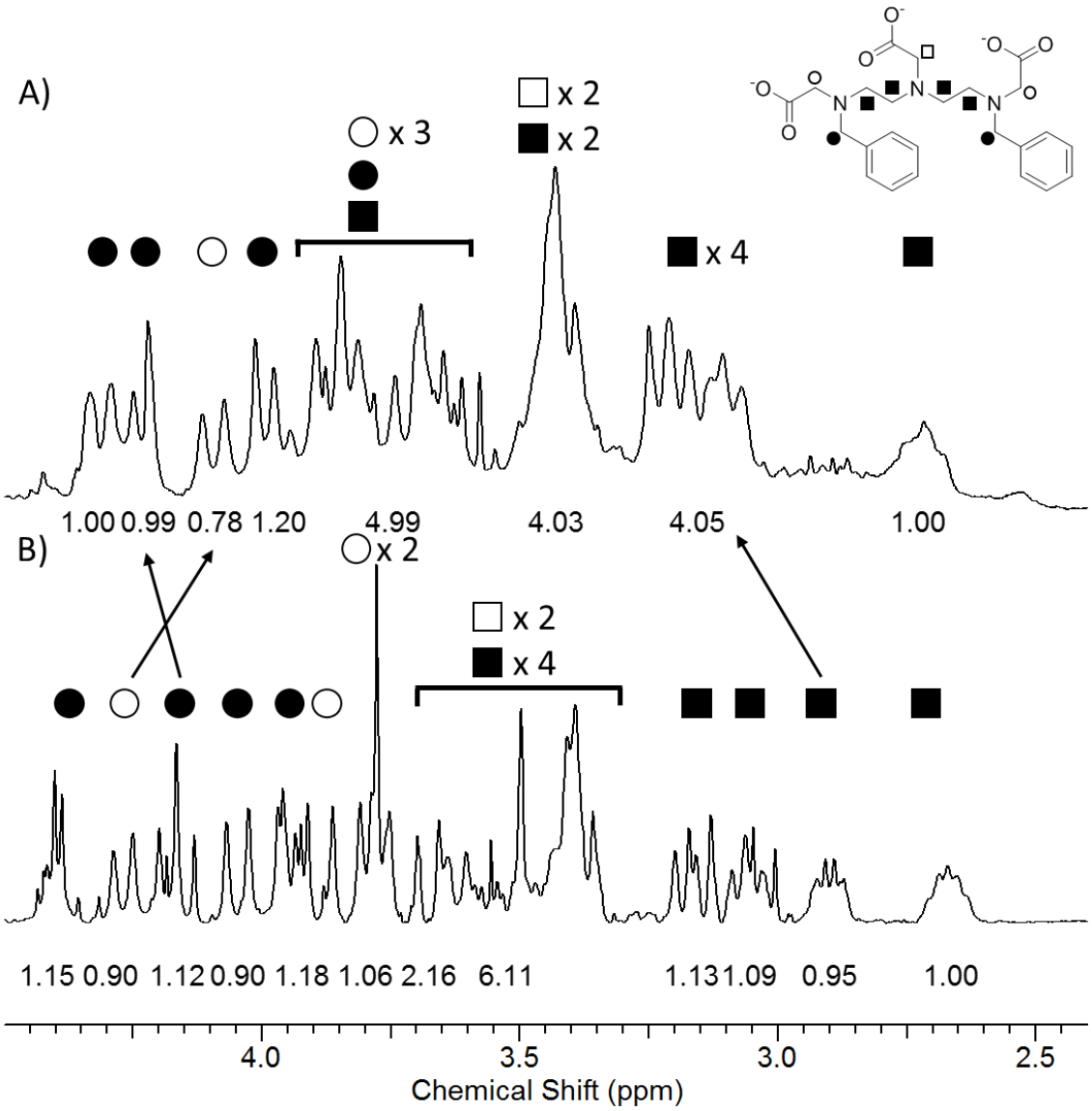

Figure 4.8: Alkyl region of ^{1}H NMR of [Ga(Bn$_2$DT3A)]. A) pD = 6.8. B) pD = 4.0. Black circles indicate -NC**H$_2$**Ph protons. White circles indicate BnNC**H$_2$**C(=O)O- protons. White squares indicate –NC**H$_2$**C(=O)O- protons. Black squares indicate –NC**H$_2$**C**H$_2$**N- protons (400 MHz, D$_2$O, 298 K).

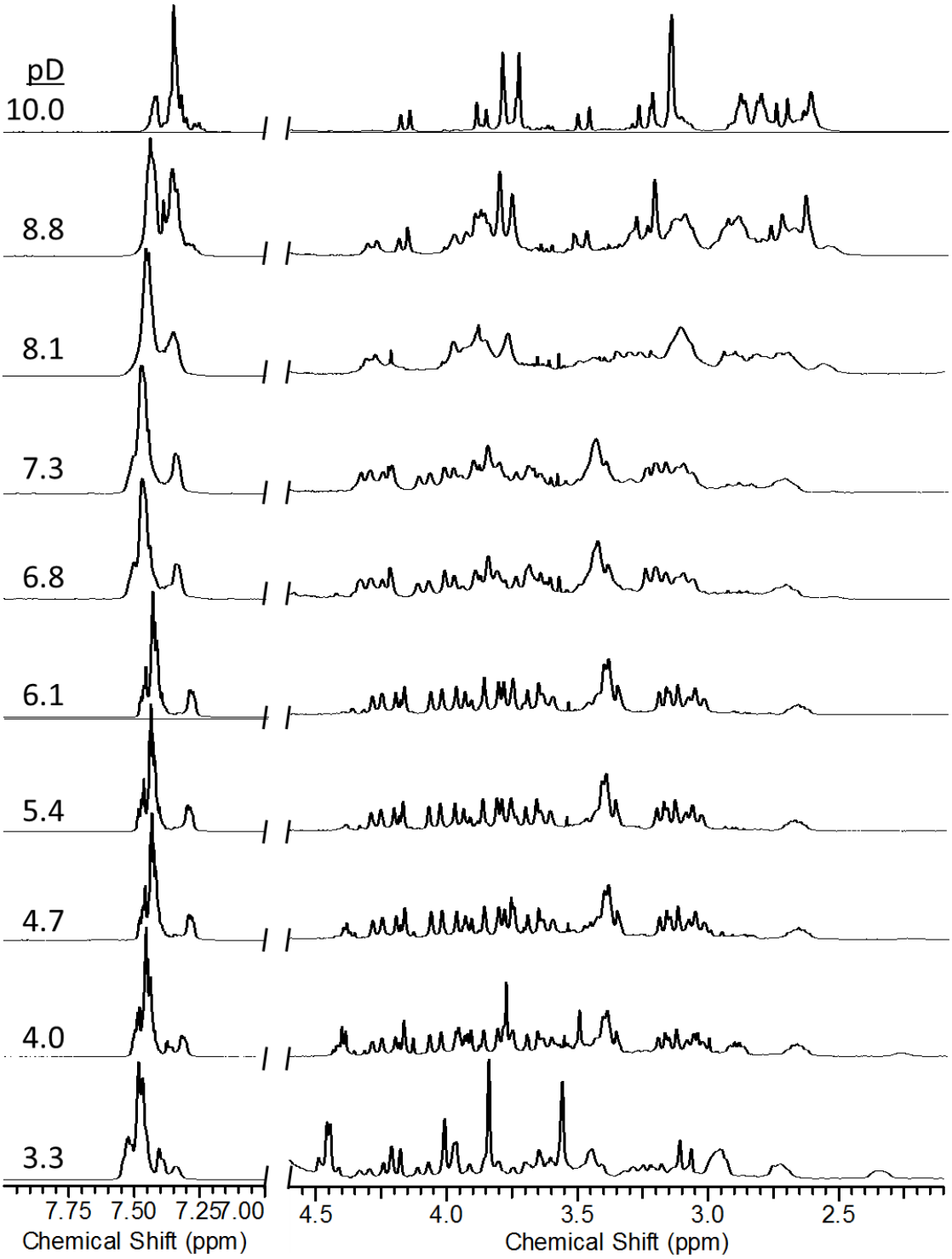

Figure 4.9: ^{1}H NMR spectra of [Ga(Bn_2DT3A)] recorded at indicated pD values (400 MHz, D_2O, 298 K).

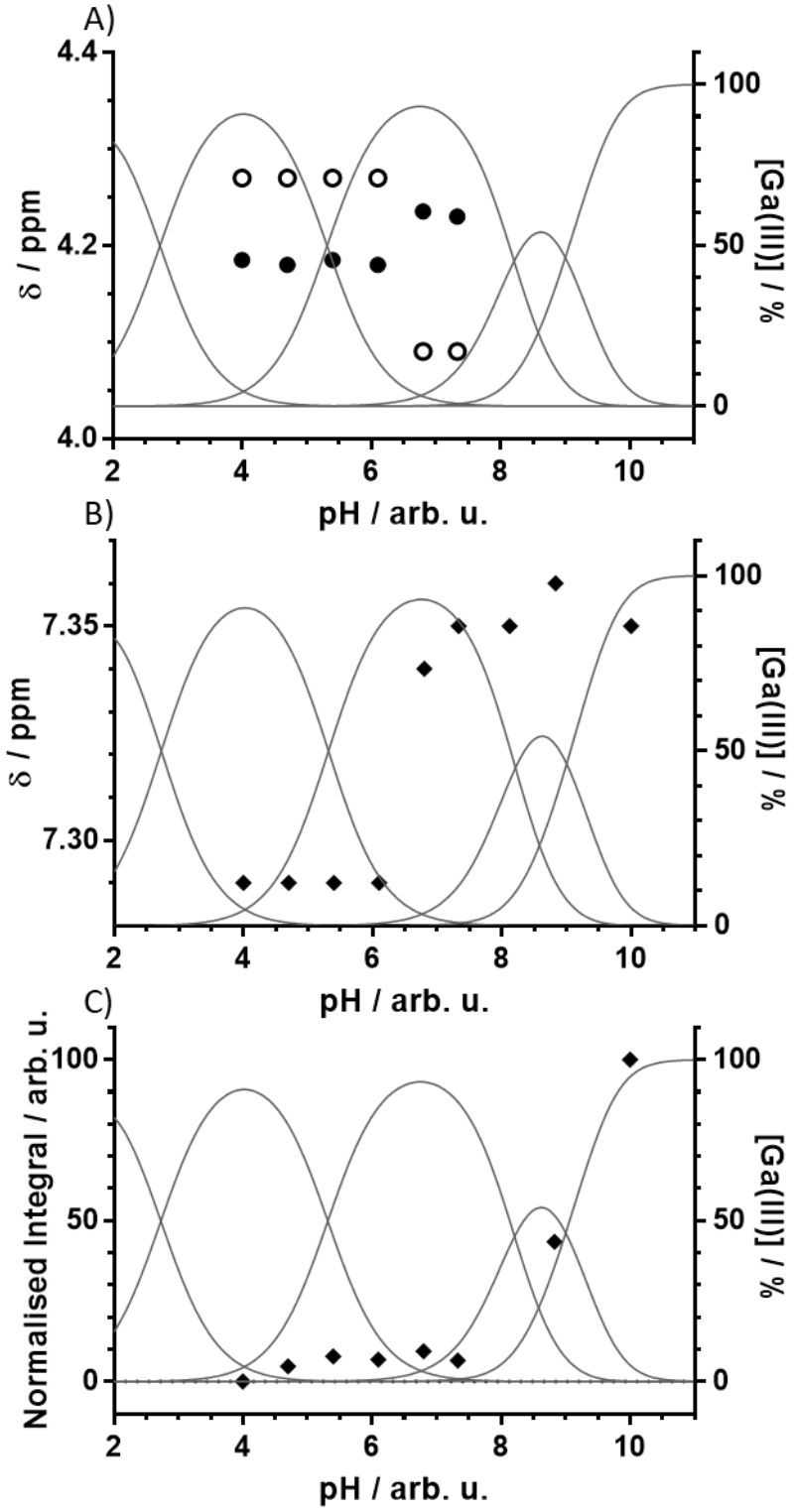

Figure 4.10: Comparison of ^{1}H NMR results with speciation diagram obtained by potentiometry for [Ga(Bn_2DT3A)]. A, B) Chemical shift of peaks indicated by symbols in Figure 4.9. C) Relative integral of aromatic peak indicated by black diamond.

4.2.4 Crystal structure

Crystals of suitable quality for X-ray diffraction were obtained by slow evaporation in acidic water. The crystal structure obtained at acidic pH is of the complex in the S,S conformation, with the nitrogen atoms in a *mer* arrangement. The hexadentate chelator fulfils

the six coordinate environment of Ga(III) with a distorted octahedral geometry. The largest distortion from the ideal geometry around the Ga(III) centre is the angle between N(1) and O(3) (108.6°); the remaining angles are between 81.9° and 99.4° (Table 4.4), within 10° of the ideal 90°

The Ga-O bonds are shorter than the Ga-N bonds, this reflects the more electronegative nature of the oxygen atoms and the preference of Ga(III) for hard donor ligands. The sum of the *trans* bond lengths decreases with increasing number of oxygen atoms. i.e. O(1)-Ga(1)-O(5) (3.98 Å) < N(2)-Ga(1)-O(3) (4.07 Å) < N(1)-Ga(1)-N(3) (4.24 Å). The Ga-O bonds formed by the terminal carboxylate arms (Ga(1)-O(5) = 1.95(2) Å and Ga(1)-O(3) = 1.95(3) Å) are comparable to those reported for [Ga(DOTA)] (1.926-1.934 Å),[251] [Ga(NOTA)] (1.927-1.934 Å)[250] and [Ga(EDTA)] (1.932-1.972 Å).[249] The central carboxylate arm has a longer Ga-O bond length (Ga(1)-O(1) = 2.03(3) Å) suggesting that the bonding for this arm is less effective; possibly due to the constraint induced by the bonding of the central amine to Ga(III). The bonds between the amines and Ga(III) (Ga(1)-N(1) = 2.09(3) Å, Ga(1)-N(2) = 2.12(3) Å, Ga(1)-N(3) = 2.15(3) Å) are comparable to those reported for [Ga(DOTA)] (2.115-2.147 Å),[251] [Ga(NOTA)] (2.079- 2.099 Å),[250] and [Ga(EDTA)] (2.081-2.109 Å).[249]

The angles formed by the amine and carboxylate around Ga(III) of each bidentate unit (O(5)-Ga(1)-N(1) = 81.9(12)°, O(3)-Ga(a)-N(3) = 82.2(11)°, O(1)-Ga(1)-N(2) = 82.3(13)°) are comparable to those formed by DOTA (83.25-84.17°),[251] NOTA (83.18- 83.55°)[250] and EDTA (82.42-83.47°)[249] upon complexation of Ga(III). The angles formed by the ethylenediamine bidentate units are also comparable ([Ga(Bn_2DT3A)] N(2)-Ga(1)-N(3) = 85.9(12)°, N(1)-Ga(1)-N(2) = 85.3(13)°, [Ga(DOTA)] N-Ga-N = 82.3-83.6°,[251] [Ga(NOTA)] N-Ga-N = 84.3-84.6°,[250] [Ga(EDTA)] N-Ga-N = 85.42°).[249]

The angles formed by different carboxylate arms around the central Ga(III) ion are quite different. In the crystal structure reported for [Ga(DOTA)] the O-Ga-O angle is 84.95°,[251] in [Ga(NOTA)] the three O-Ga-O angles are very similar to each other (94.21-95.51°).[250] However in the acyclic chelator complexes the bond angles are asymmetric; in [Ga(EDTA)] the angles between carboxylates attached to the same amine are larger (95.53°)[249] than those on different carboxylates (87.30-87.52°)[249] and in [Ga(Bn_2DT3A)] the two angles are substantially different (86.5(13)° and 99.4(11)°). This results in an open face between the two terminal carboxylates that may be a site of attack by hydroxide or other anions *in vivo*.

The same coordination geometry is seen in crystal structures obtained from crystals grown at pH 5.3 and 6.8 (Appendix 2) – this may be due to the preferential crystallisation of the neutral [Ga(Bn_2DT3A)] species over the charged [Ga(Bn_2DT3A)(OH)]$^-$ species.

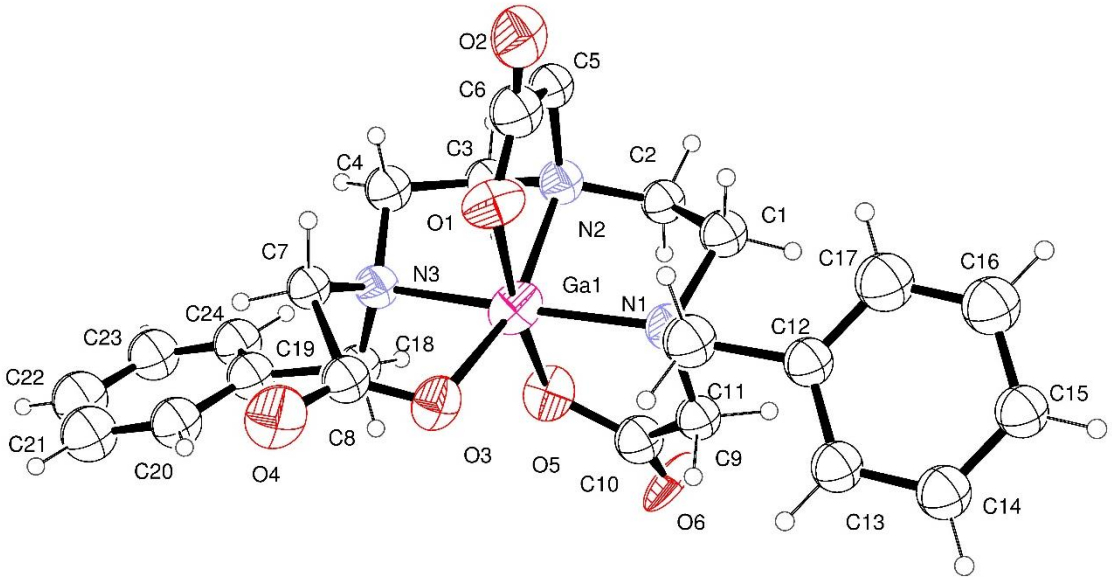

Figure 4.11: ORTEP representation of structure obtained by single crystal X-ray diffraction of [Ga(Bn_2DT3A)]. Thermal ellipsoids set at 30% certainty.

Table 4.3: Selected bond lengths obtained from crystal structure of [Ga(Bn_2DT3A)].

Bond	Bond Length / Å
Ga(1)-O(3)	1.95(3)
Ga(1)-O(5)	1.95(2)
Ga(1)-O(1)	2.03(3)
Ga(1)-N(1)	2.09(3)
Ga(1)-N(2)	2.12(3)
Ga(1)-N(3)	2.15(3)

Table 4.4: Selected bond angles obtained from crystal structure of [Ga(Bn_2DT3A)].

Angle	Angle / °	Angle	Angle / °
O(1)-Ga(1)-N(1)	93.3(12)	O(5)-Ga(1)-N(2)	92.7(11)
O(1)-Ga(1)-N(2)	82.3(13)	O(5)-Ga(1)-N(3)	87.3(11)
O(1)-Ga(1)-N(3)	96.7(11)	N(1)-Ga(1)-N(2)	85.3(13)
O(1)-Ga(1)-O(3)	86.5(13)	N(2)-Ga(1)-N(3)	85.9(12)
O(3)-Ga(1)-N(1)	108.6(12)	O(1)-Ga(1)-O(5)	173.3(13)
O(3)-Ga(1)-N(3)	82.2(11)	O(3)-Ga(1)-N(2)	162.6(12)
O(3)-Ga(1)-O(5)	99.4(11)	N(1)-Ga(1)-N(3)	165.7(12)
O(5)-Ga(1)-N(1)	81.9(12)		

4.3. Radiolabelling

4.3.1 Initial Studies

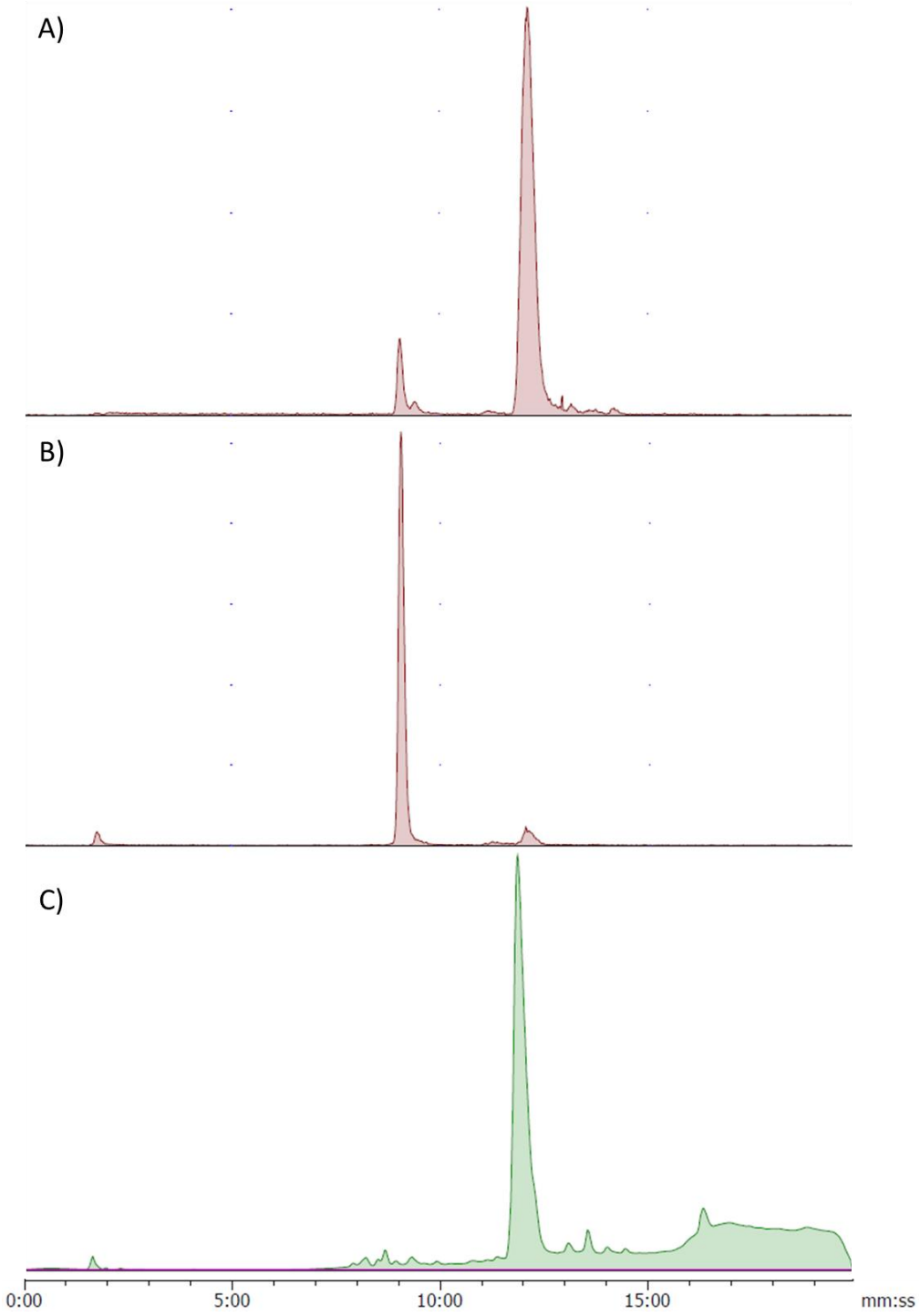

Figure 4.12: HPLC chromatograms of A) radiolabelling reaction of H_3Bn_2DT3A with $^{68}GaCl_3$. *I* = 0.1 M Acetate, *pH* = 4.0, *t* = 15 minutes, *T* = 25 °C, *[H_3Bn_2DT3A]* = 100 µM. B) *I* = PBS, *pH* = 7.4, *t* = 15 minutes, *T* = 37 °C, *[H_3Bn_2DT3A]* = 100 µM. C) Cold complexation reaction between $GaCl_3$ and H_3Bn_2DT3A. **HPLC Gradient D.**

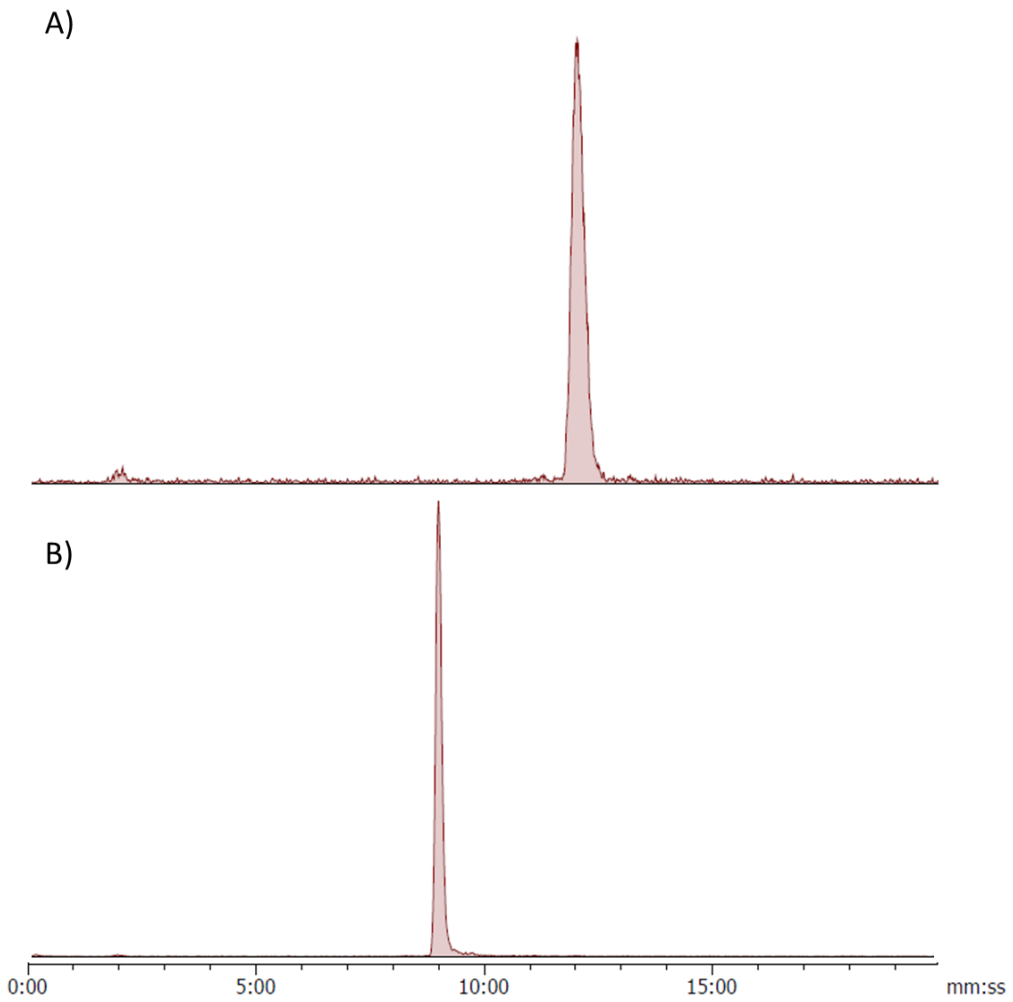

Figure 4.13: HPLC chromatograms of reinjected fractions isolated from crude radiolabelling mixture containing both species. **HPLC Gradient D.**

H_3Bn_2DT3A was applied to the complexation of ^{68}Ga under both acidic and neutral conditions. At pH 4 a major product was formed with high radiochemical yields; this product had the same retention time as the cold complex (12 minutes, Figure 4.12). However, at pH 7.4 a second product was also formed with an earlier retention time (9 minutes, Figure 4.12). This product was not seen when analysing the cold complex.

The two species could be isolated by semipreparative HPLC (Figure 4.13) with molar activities of 18.4 GBq μmol^{-1} and 5.2 GBq μmol^{-1}. No interconversion was seen at acidic pH after 30 minutes.

4.3.2 Stability

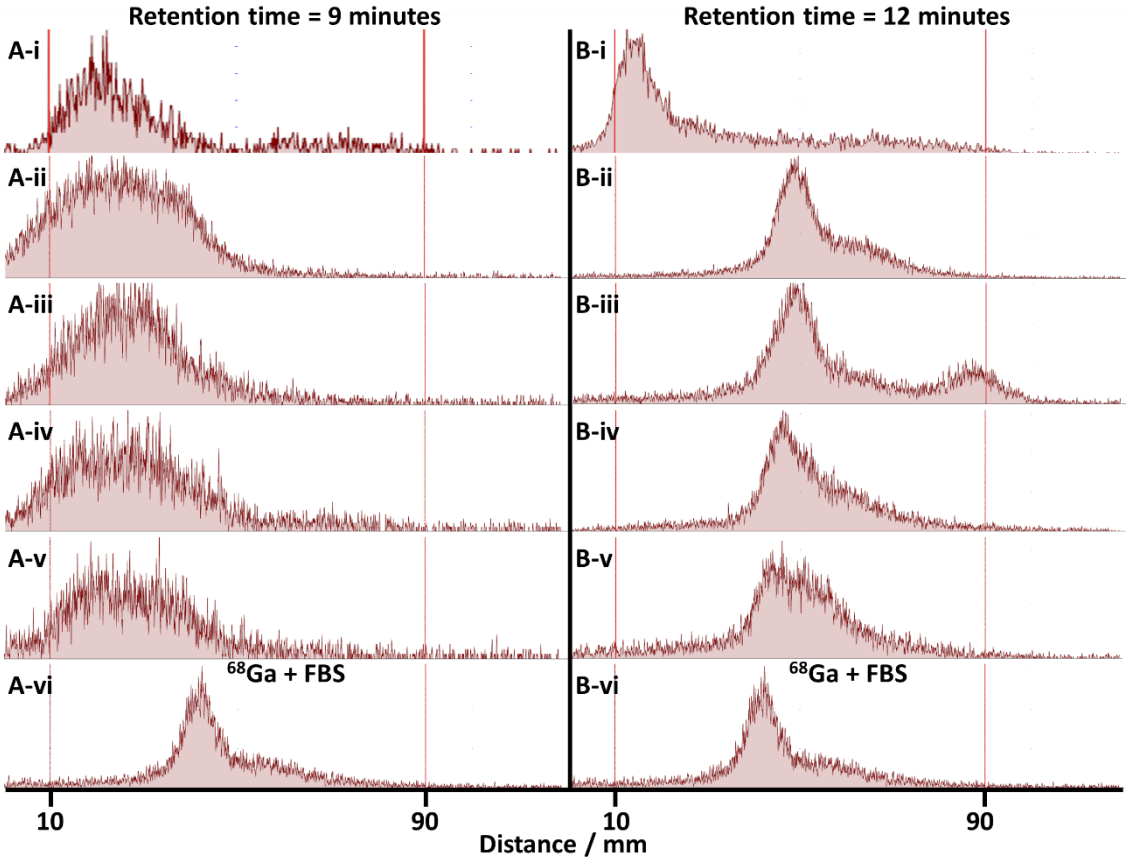

Figure 4.14: Stability of species formed in radiolabelling of H_3Bn_2DT3A with ^{68}Ga. A) species with retention time = 9 mins, B) species with retention time = 12 mins. i) isolated species. ii) After 30 minutes incubation with FBS at 37 ^{o}C. iii) after 60 minutes incubation. iv) 90 minutes incubation. v) 120 minute incubation. vi) ^{68}Ga incubated with FBS at 37 ^{o}C. Method development for TLC analysis is shown in appendix 4.

The isolated species were analysed for stability to serum; when incubated with foetal bovine serum at 37 ^{o}C the product with a retention time of 9 minutes was stable to serum for over 2 hours (Figure 4.14). The product with a retention time of 12 minutes was not stable to serum under these conditions with decomplexation seen within 30 minutes (Figure 4.14).

4.3.3 pH dependence

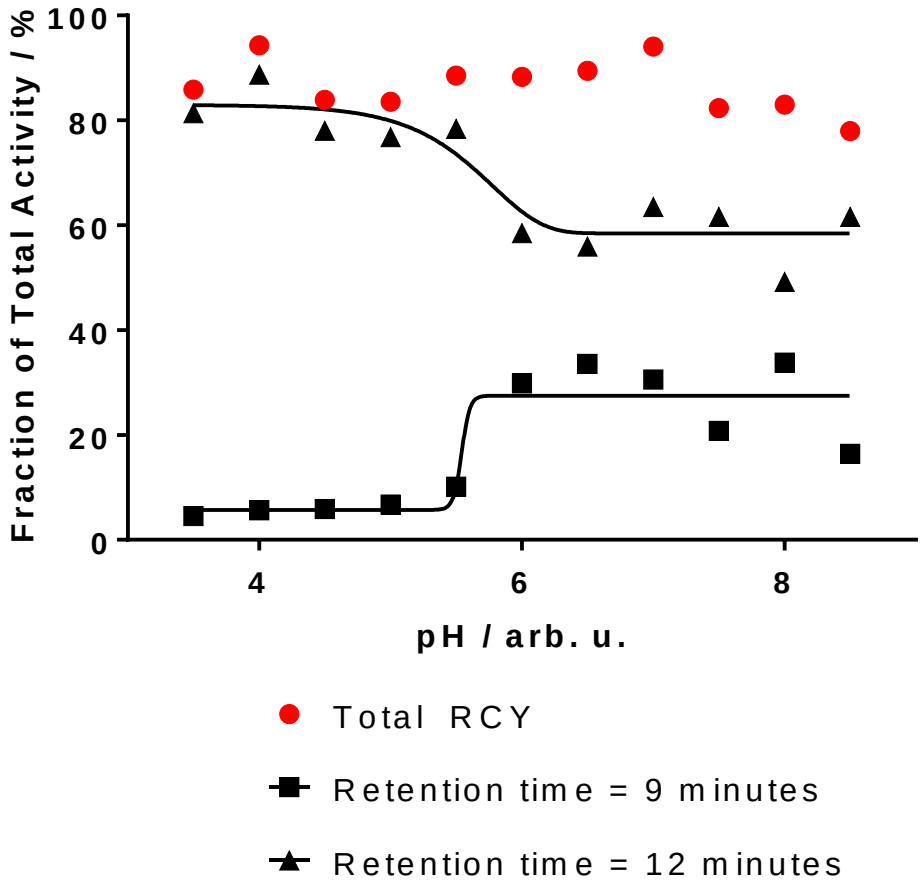

Figure 4.15: pH dependence of H_3Bn_2DT3A radiolabelling with ^{68}Ga. (*[H_3Bn_2DT3A]* = 100 µM, *t* = 15 minutes, *T* = RT, *I* = 0.1 M Acetate buffer)

The pH of the radiolabelling solution has only a minor effect on the radiochemical yield achieved by H_3Bn_2DT3A complexing ^{68}Ga at room temperature in 15 minutes. Across the pH range 3.5 to 8.5 the radiochemical yield is consistently between 80% and 90% (Figure 4.15, red circles). This is promising for the future development of this chelator as precise pH control should not be necessary to achieve high radiochemical yields, and the radiolabelling conditions can be chosen to match the targeting unit being used.

However, pH has a distinct effect on the species formed in the radiolabelling reaction. The serum-stable species (retention time = 9 minutes) is only seen in a significant amount above pH 5.5 (Figure 4.15). Above this pH the proportion of product that is the serum-stable product does not significantly improve, with only 33% of the product being the stable product at 25 °C.

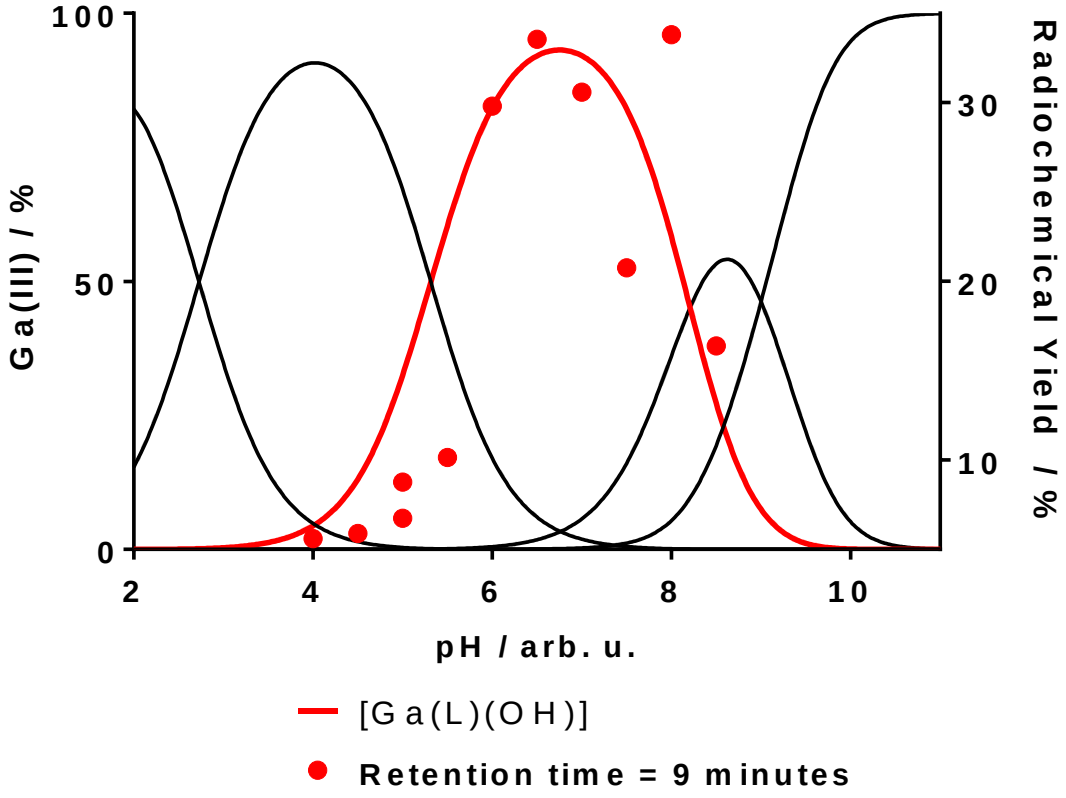

Figure 4.16: Overlay of RCY of species formed between ^{68}Ga and H_3Bn_2DT3A with retention time of 9 minutes (red circles) and speciation diagram of [Ga(Bn_2DT3A)] obtained *via* potentiometry (solid lines); [Ga(L)(OH)] is highlighted as a red line.

This switch in radiolabelling behaviour can be compared to the speciation of the Ga(III)-H_3Bn_2DT3A complex (Figure 4.16). The overall trend in the formation of the serum-stable product agrees with the formation of the [Ga(L)(OH)] species.

4.3.4 Concentration dependence

Concentration has an important effect on the radiolabelling efficiency; whilst radiolabelling at pH 7.4 is efficient at concentrations greater than 50 µM it is reduced at lower concentrations (Figure 4.17). Below 1 µM no radiolabelling is seen at pH 7.4 at room temperature.

The ratio of products formed changes with increasing concentration; at higher concentrations a greater proportion of the formed products are the desired serum-stable product.

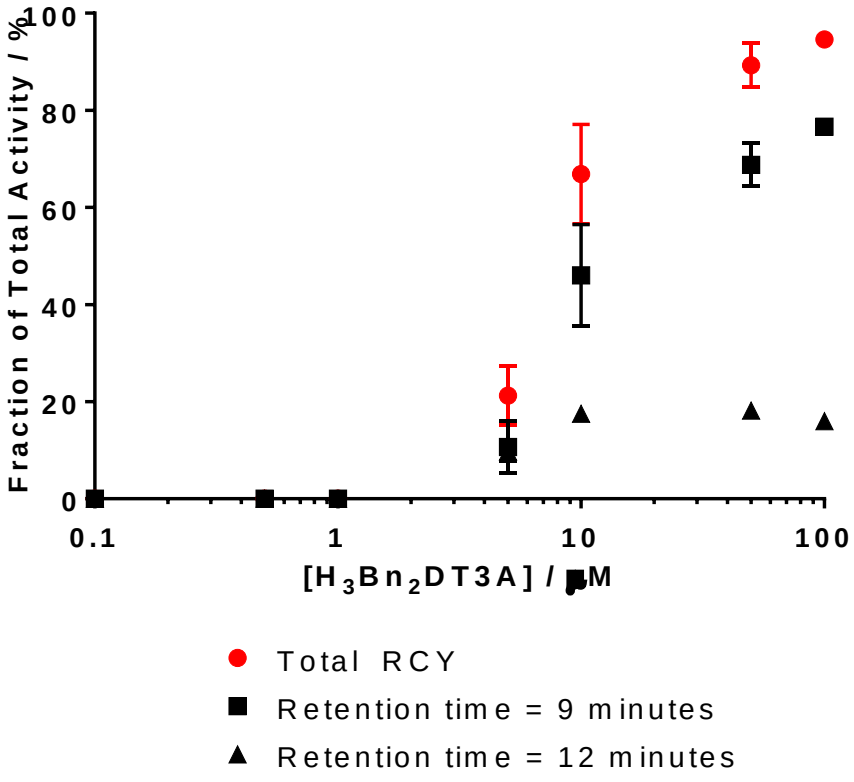

Figure 4.17: Effect of ligand concentration on speciation and radiochemical yield (*t* = 15 minutes, *T* = RT, *I* = PBS, p*H* = 7.4).

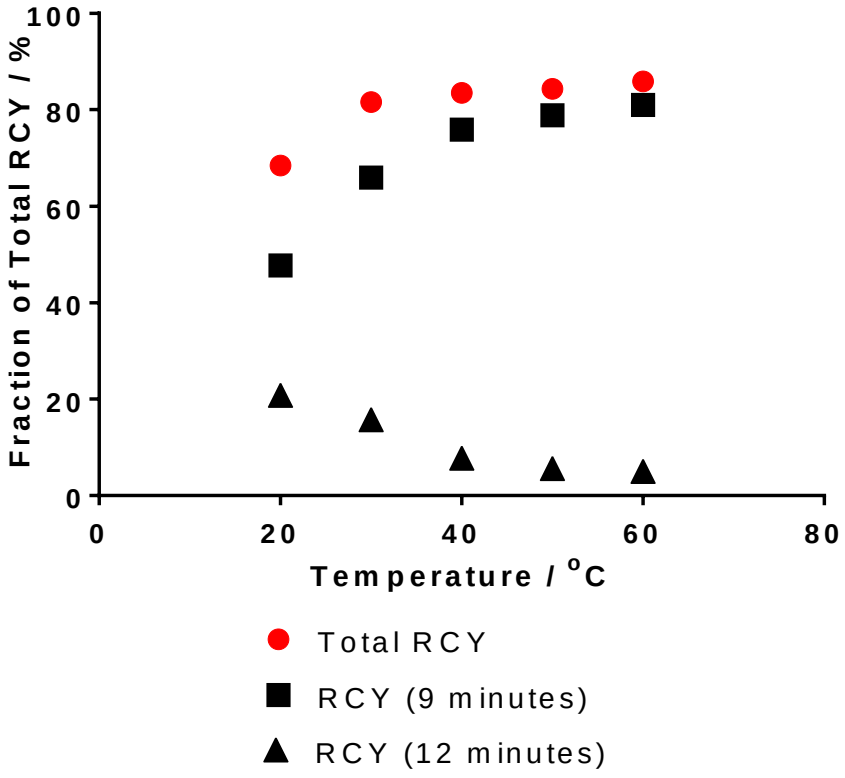

Figure 4.18: Effect of reaction temperature on radiochemical yield ([*H₃Bn₂DT3A*] = 100 µM, *t* = 5 minutes, *I* = PBS, p*H* = 7.4).

4.3.5 Temperature dependence

The effect of temperature on radiolabelling of H_3Bn_2DT3A with ^{68}Ga was investigated after 5 minutes incubation (Figure 4.18) – as the radiochemical yield has been shown to be high at room temperature after 15 minutes a shorter time point was selected to allow a meaningful comparison to be made at higher temperatures. At 20 °C only a 65% radiochemical yield is achieved in 5 minutes. At higher temperatures the radiochemical yield increases, plateauing above 30 °C. Furthermore, a greater proportion of the radiolabelled species is the serum-stable product at higher temperatures.

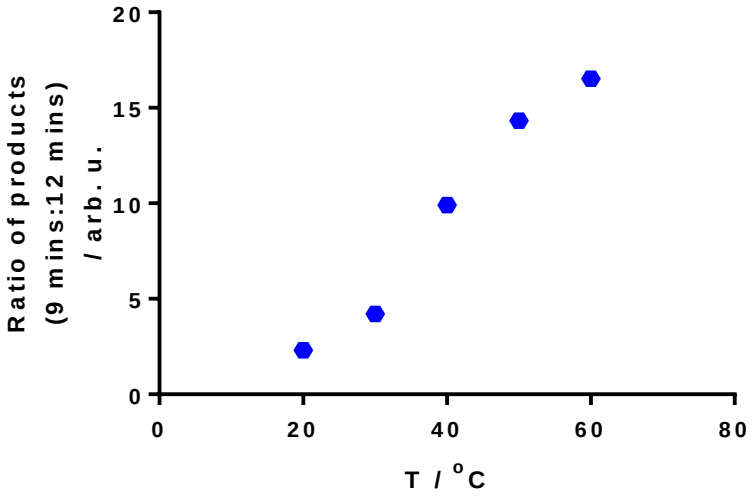

Figure 4.19: Effect of temperature on the ratio of products formed during radiolabelling of H_3Bn_2DT3A with ^{68}Ga.

The ratio of products also depends on the temperature; higher temperatures improve the ratio. At 20 °C the ratio of serum stable product:non-serum stable product is only 2, whereas at 60 °C it is 20 (Figure 4.19). Thus, higher temperatures promote the formation of the serum stable product in the radiolabelling reaction.

4.3.6 Time dependence

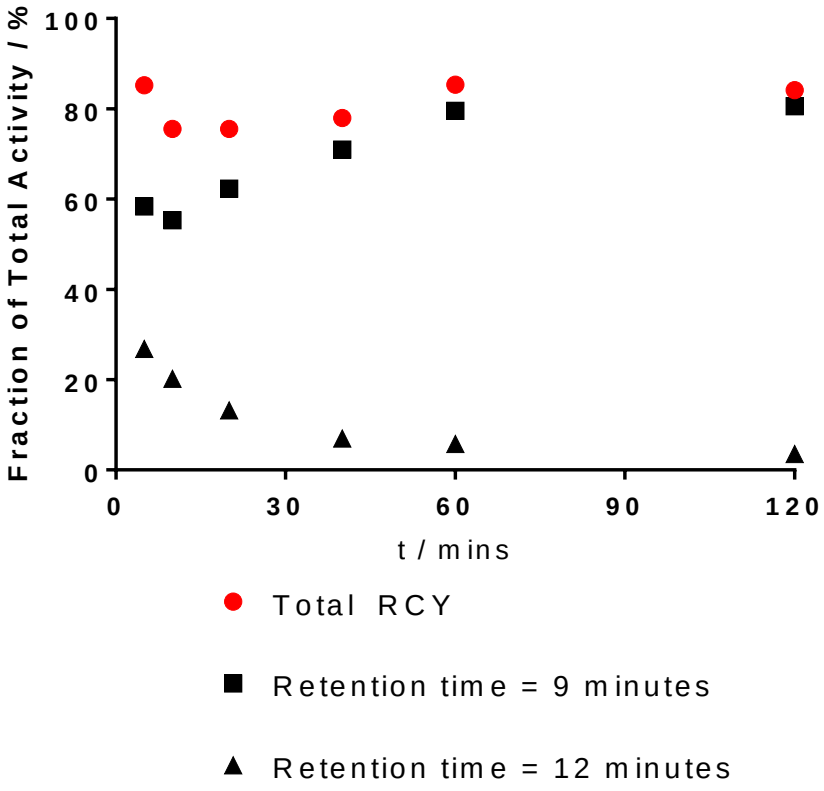

Figure 4.20: Effect of reaction time on radiolabelling of H_3Bn_2DT3A with ^{68}Ga. ([*H_3Bn_2DT3A*] = 100 µM, *T* = RT, *I* = PBS, p*H* = 7.4)

The radiochemical yield achieved by H_3Bn_2DT3A improves with extended incubation times; after 15 minutes the radiochemical yield is 78% but this increases to 83% when the incubation time is extended to 1 hour (Figure 4.20). More importantly, the proportion of the radiolabelled product that is the serum-stable product also increases with increasing reaction time, plateauing after 1 hour.

Thus, the formation of the serum-stable radiolabelled product is promoted by high pH (> 5.5), high ligand concentration, high temperature and longer reaction times. Furthermore, the use of phosphate buffered saline instead of 0.1 M acetate buffer significantly improves the ratio of serum-stable:non-serum-stable product.

4.3.7 *H_3Bn_2DT3A summary*

H_3Bn_2DT3A can produce a serum stable ^{68}Ga complex – however a second, unstable, product is also formed in the radiolabelling process. Selectively producing the stable product requires careful control of the pH of the radiolabelling solution, and can be enhanced by heating the reaction and longer reaction times.

The exact identity of this stable complex is unclear – however, the pH dependent behaviour is in agreement with a change in speciation seen during potentiometric studies of this system. This suggests that deprotonation of the complex leads to the production of a more stable product. This deprotonation may occur at one of the coordinating atoms or at a bound water molecule, as has been reported for H_3Dpaa.[107,223] The solid state crystal structure obtained does not have a bound water molecule; this suggests that it is deprotonation of the ligand that is occurring, although the solid state structure may not represent the speciation in solution. H_3Bn_2DT3A is capable of producing multiple coordination geometries upon complexation of Ga(III), pH may promote formation of different geometries as is seen for HBED.[164,165,221] If a change in pD were to promote formation of a different geometry significant changes would be expected in the ^{1}H NMR. While there is some change across the pD range of interest it is not clear due to the overlapping peaks.

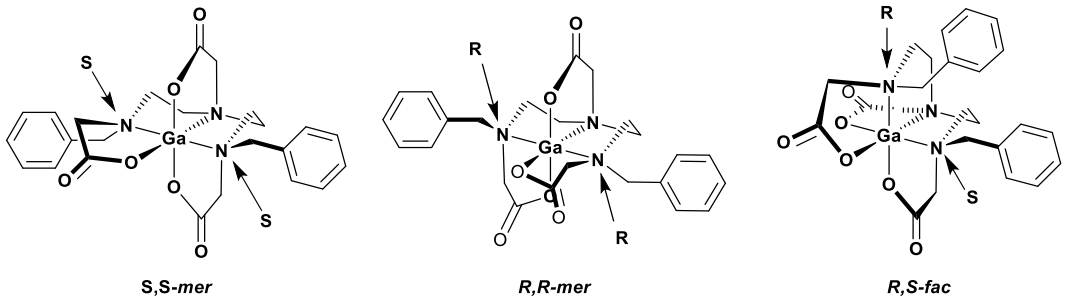

Figure 4.21: Different coordination geometries of [Ga(Bn_2DT3A)] with assigned stereochemistry of nitrogen atoms.

4.4. Bifunctional Derivative

4.4.1 Synthesis

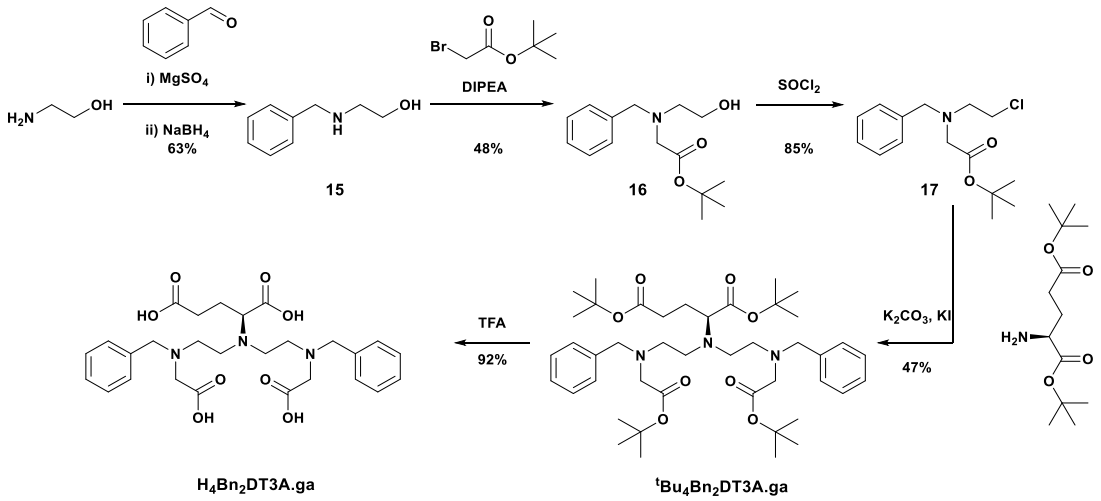

Scheme 4.3: Synthetic scheme for the preparation of H_3Bn_2DT3A.ga.

To prepare a bifunctional derivative of H_3Bn_2DT3A an alternate synthetic route was devised (Scheme 4.3). As with bifunctional derivatives of H_3Dpaa, a protected amino acid, di-*tert*-butyl glutamate ester, was used as the source of the additional functionality. This will allow

further derivatives based on other amino acids to be prepared in the future, incorporating alternate functional groups.

The activated side arm, *tert*-butyl N-benzyl-N-(2-chloroethyl)glycinate (**17**), was prepared in 3 steps from ethanolamine. Reductive amination with benzaldehyde incorporated a single benzyl unit onto the amine to give 2-(benzylamino)ethan-1-ol (**15**).[263] The protected carboxylate functionality was incorporated through an S_N2 reaction with *tert*-butyl bromoacetate yielding tert-butyl N-benzyl-N-(2-hydroxyethyl)glycinate (**16**).[264] Thionyl chloride was used to replace the alcohol with a chlorine atom yielding **17**.[265]

Reaction of di-*tert*-butyl glutamate ester with two equivalents of *tert*-butyl N-benzyl-N-(2-chloroethyl)glycinate yielded the proligand, di-*tert*-butyl N,N-bis(2-(benzyl(2-(*tert*-butoxy)-2-oxoethyl)amino)ethyl)-L-glutamate ($^{t}Bu_4Bn_2DT3A.ga$).

The protons adjacent to the terminal alcohol group of **15** become more shielded at each step (Figure 4.22); this is particularly significant upon reaction with di-*tert*-butyl glutamate ester as the ^1H NMR resonance shifts from $\delta_H = 3.54$ to $\delta_{H(tBu4Bn2DT3A.ga)} = 2.78\text{-}2.61$.

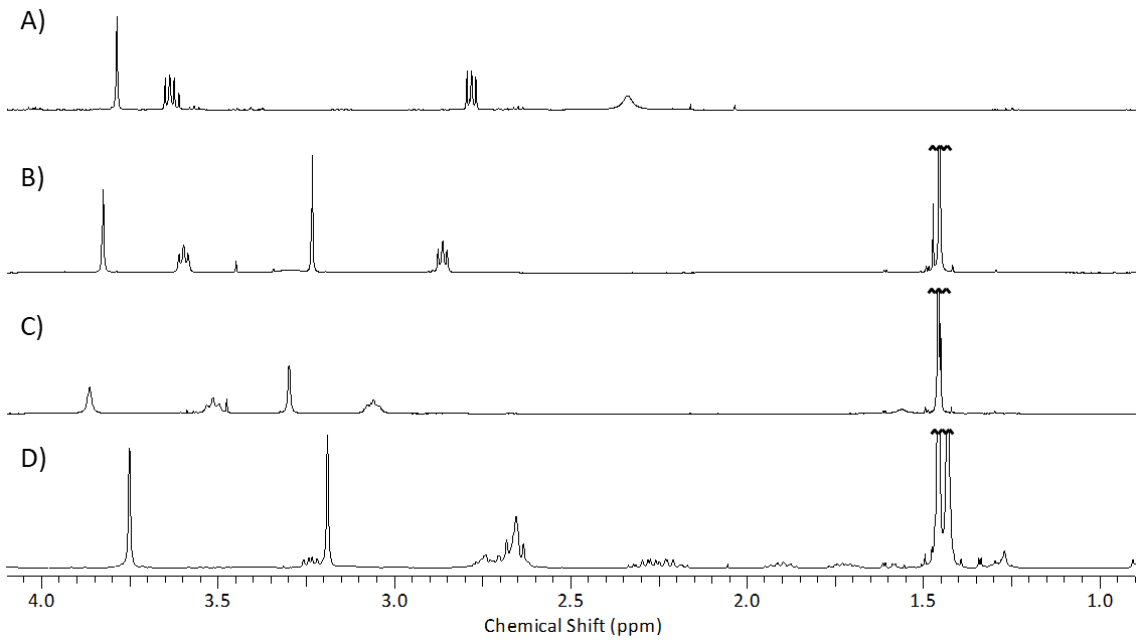

Figure 4.22: ^1H NMR of alkyl region of A) **15** B) **16** C) **17** D) $^{t}Bu_4Bn_2DT3A.ga$. Resonances at 1.4 ppm are truncated. (400 MHz, $CDCl_3$, 298 K).

Deprotection of $^{t}Bu_4Bn_2DT3A.ga$ with trifluoroacetic acid in dichloromethane yielded the ligand N,N-bis(2-(benzyl(carboxymethyl)amino)ethyl)glutamic acid ($H_4Bn_2DT3A.ga$) in a 92% yield.

4.4.2 Complexation

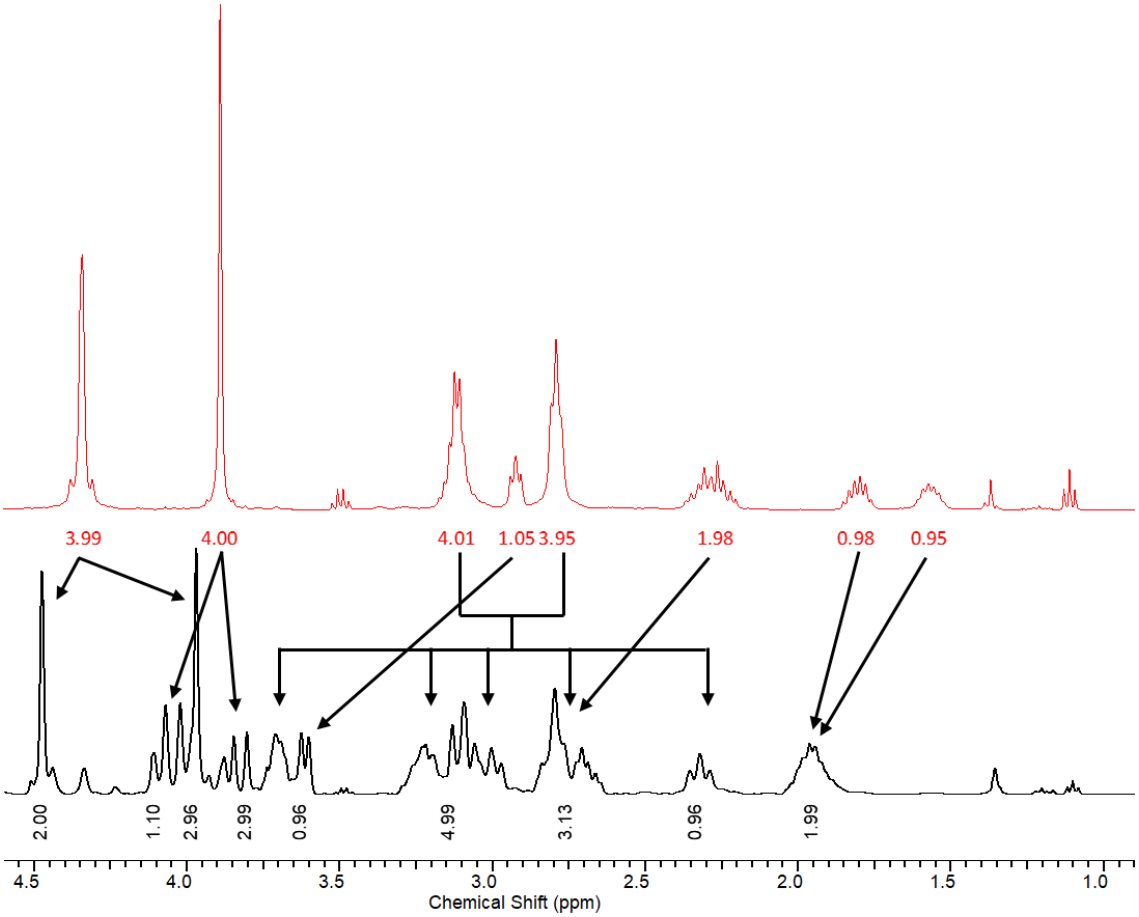

Figure 4.23: ^{1}H NMR of A) $H_3Bn_2DT3A.ga$ (pD = 4.1), B) [$Ga(Bn_2DT3A.ga)$] (pD = 3.8). (400 MHz, D_2O, 298 K)

Upon complexation of Ga(III) the number of proton resonances increases significantly due to the increased rigidity of the complex reducing symmetry when compared to the more flexible ligand (Figure 4.23).

The ^{1}H NMR resonance corresponding to the alpha proton of the glutamate residue is significantly deshielded upon complexation of Ga(III) ($\delta_{H(H3Bn2DT3A.ga)}$ = 2.93, $\delta_{H[Ga(Bn2DT3A.ga)]}$ = 3.61) suggesting a significant change in environment for this proton. This will partially be due to electron density being drawn away from the carboxylate and amine units by complexation to Ga(III), but this large change is not evident for the equivalent protons of the terminal carboxylates. This may be due to the benzyl side arms donating electron density into the terminal amines mitigating the reduction in shielding caused by complexation.

The protons adjacent to the terminal glutamate carbonate are also deshielded – this was not seen for $H_4Dpaa.ga$ upon complexation of Ga(III); this may indicate some role of this carboxylate in complexation of the metal ion.

4.4.3 Radiolabelling

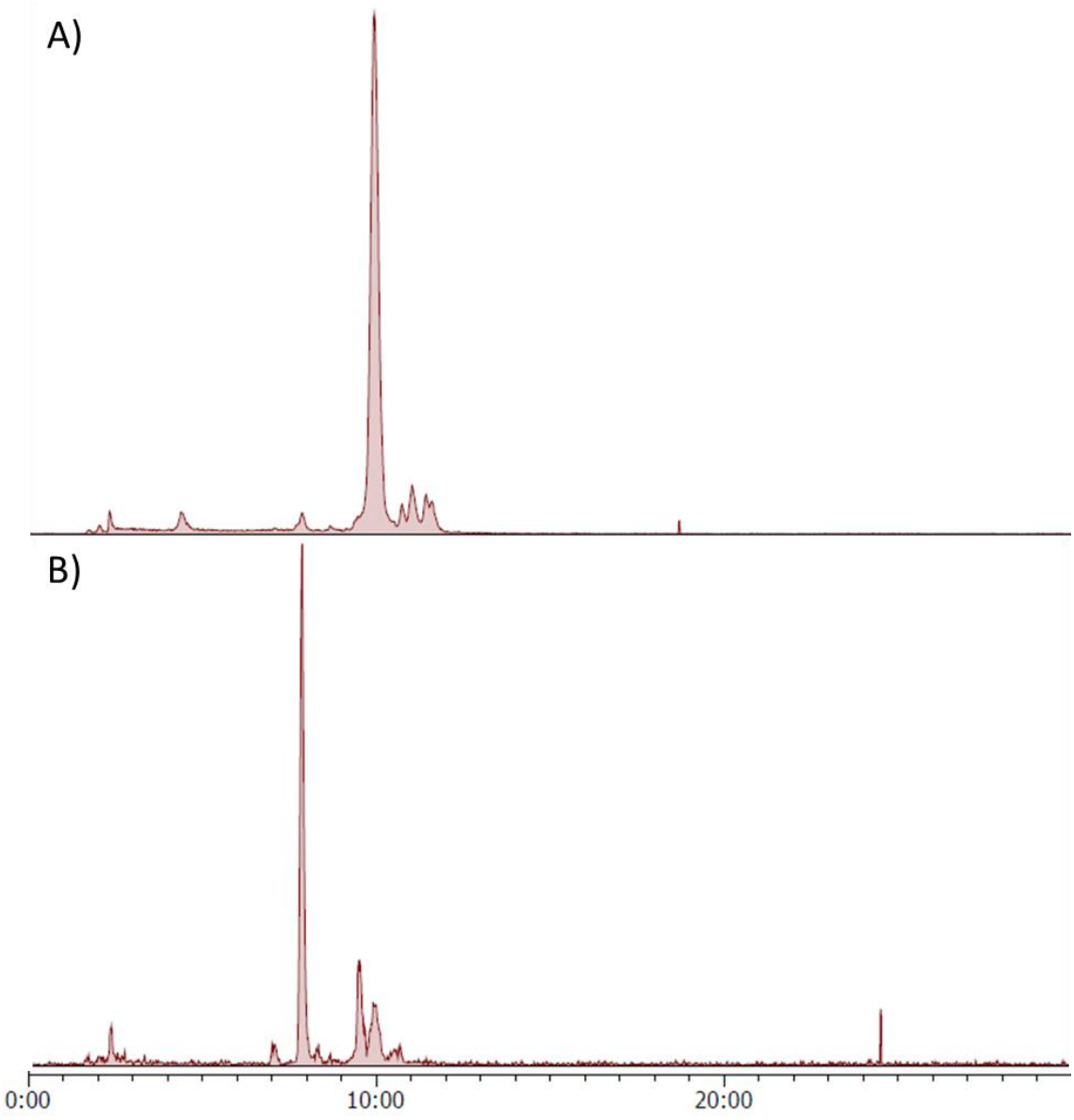

Figure 4.24: HPLC Chromatograms of ^{68}Ga incubated with H_4Bn_2DT3A.ga A) *[$H_4Bn_2DT3A.ga$]* = 100 µM, I = 0.1 M Acetate, *pH* = 4.0, *T* = 25 °C, *t* = 15 mins. B) *[$H_4Bn_2DT3A.ga$]* = 200 µM, *I* = PBS, *pH* = 7.4, *T* = 37 °C, *t* = 15 mins. **HPLC Gradient A.**

Radiolabelling of H_4Bn_2DT3A.ga with ^{68}Ga also produces different products depending on the pH of the radiolabelling reaction (Figure 4.24). At pH 4.0 a product with retention time of 10 minutes is the predominant product; with a 74% RCY achieved by 100 µM ligand in 15 minutes at room temperature. This yield increases to 78% as the concentration is increased to 200 µM. At pH 7.4 the major product formed has retention time of 8 minutes, however the RCY is much lower at 100 µM. After 15 minutes only 20% of the activity was associated with this product. Increasing the concentration of ligand to 200 µM increased the yield to 53%. At both pH values a number of minor impurities were seen; purification will likely be necessary for further application of this ^{68}Ga complex.

4.4.4 Stability

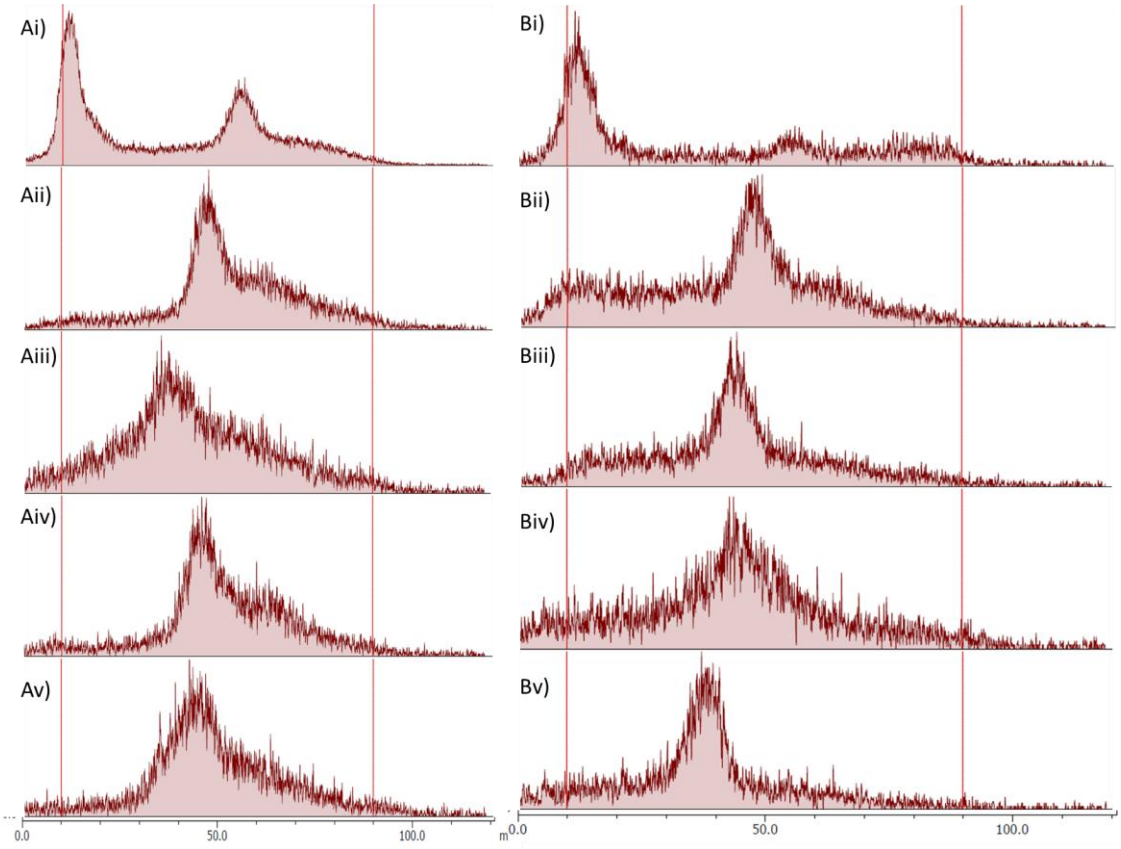

Figure 4.25: Radio-TLC to assess serum stability of ^{68}Ga complexes formed by $H_4Bn_2DT3A.ga$. A) Products formed under the conditions *[$H_4Bn_2DT3A.ga$]* = 100 µM, *I* = 0.1 M Acetate, *pH* = 4.0, *T* = 25 °C, *t* = 15 mins. B) Products formed under the conditions *[$H_4Bn_2DT3A.ga$]* = 100 µM, *I* = PBS, *pH* = 7.4, *T* = 37 °C, *t* = 15 mins. Products were incubated in FBS at 37 °C for various time points. i) Crude reaction mixture. ii) 30 minutes incubation. iii) 60 minutes incubation. iv) 90 minutes incubation. v) 120 minutes incubation. Method development for TLC analysis is shown in appendix 4.

The products of the radiolabelling reaction between $H_4Bn_2DT3A.ga$ and ^{68}Ga were assessed for their stability in serum by incubating in FBS (Figure 4.25). As was seen for H_3Bn_2DT3A the product formed at pH 4.0 was not stable to serum, with all of the activity being associated with serum after 30 minutes. However, unlike the non-functionalised chelator, the product formed by $H_4Bn_2DT3A.ga$ and ^{68}Ga at pH 7.4 also dissociates when incubated with serum.

This may be due to the side chain attached to one of the coordinating arms causing increased steric hinderance, preventing the ideal coordination environment from forming, or inducing additional strain in the complex. Alternatively, it may be due to involvement of the additional carboxylate in coordination of ^{68}Ga as suggested by NMR. These effects could be deconvoluted by using a non-coordinating side arm (e.g. methyl). Future application of this system to targeted ^{68}Ga PET imaging will likely require alternative conjugation sites to be explored to allow for the production of a serum stable conjugatable ^{68}Ga complex.

4.5. PSMA-Conjugate

4.5.1 Synthesis

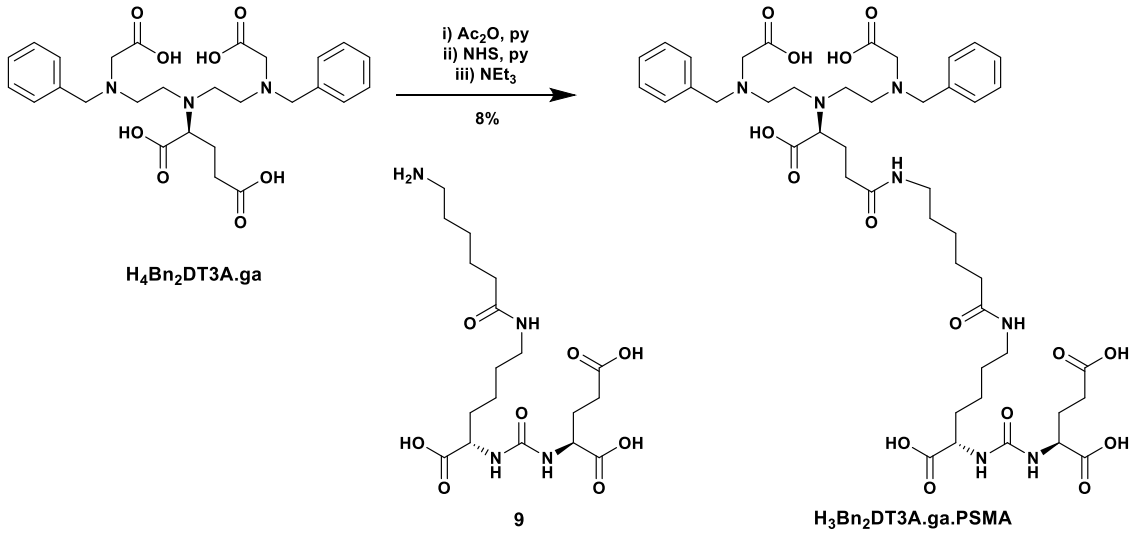

Scheme 4.4: Synthetic scheme for the conjugation of **9** to $H_4Bn_2DT3A.ga$ to yield $H_3Bn_2DT3A.ga.PSMA$.

While the ^{68}Ga complex of this bifunctional chelator is unstable when challenged by FBS, this system may find future application to PET imaging through application to a different radiometal. To confirm that this system can be successfully conjugated to a targeting agent the bifunctional $H_4Bn_2DT3A.ga$ was conjugated to the PSMA targeting urea, **9**. This conjugation will also change the glutamate carboxylate into an amide; this may impact upon radiolabelling or stability.

The bifunctional chelator, $H_4Bn_2DT3A.ga$, was activated through the formation of a cyclic anhydride within the glutamic acid arm by addition of acetic anhydride (Scheme 4.4). The reaction progress could be followed by mass spectrometry ($m/z_{(H2Bn2DT3A.ga.anh)}$ = 512.4 **[M + H]**$^+$). The reaction proceeded at room temperature and could be purified by precipitation of the product using diethyl ether. N-Hydroxysuccinimide was added to form the NHS-ester to improve the resistance of the activated bifunctional chelator to hydrolysis. This NHS ester was added to a solution of **9** to produce the conjugated chelator 2-benzyl-5-(2-(benzyl(carboxymethyl)amino)ethyl)-9,16,24-trioxo-2,5,10,17,23,25-hexaazaoctacosane-1,6,22,26,28-pentacarboxylic acid ($H_3Bn_2DT3A.ga.PSMA$) (Scheme 4.4). The conjugate was purified by semi-preparative HPLC to afford the product as a clear oil in a 7.6% yield.

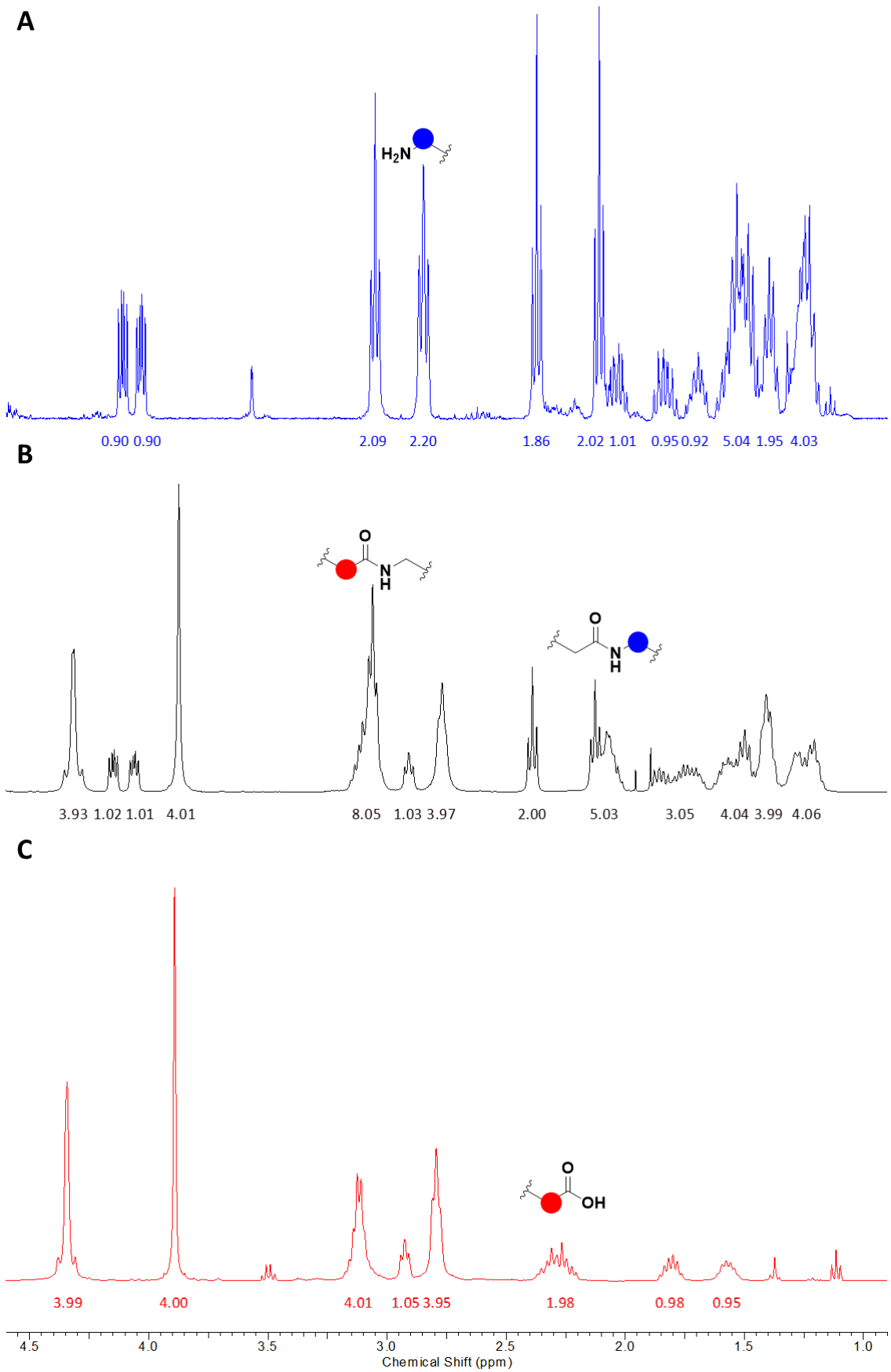

Figure 4.26: ^{1}H NMR of A) **9**, B) $H_3Bn_2DT3A.ga.PSMA$, C) $H_4Bn_2DT3A.ga$. Resonances adjacent to the amide linkage are highlighted. Blue circles indicate resonances of protons that have been translated from **9** into $H_3Bn_2DT3A.ga.PSMA$, Red circles indicate resonances of protons that have been translated from $H_4Bn_2DT3A.ga$. (400 MHz, D_2O, 298 K)

Analysis of the ^{1}H NMR spectrum of the conjugate (Figure 4.26) shows that it retains the resonances associated with both $H_4Bn_2DT3A.ga$ and **9**. The chemical shifts of the protons attached to carbons adjacent to the newly formed amide bond have shifted; those adjacent to the carboxylic acid of $H_4Bn_2DT3A.ga$ are more shielded in the conjugate ($\delta_{H4Bn2DT3A.ga}$ = 2.33-2.24, $\delta_{H3Bn2DT3A.ga.PSMA}$ = 3.16-3.02) whereas those adjacent to the amine of **9** have become more shielded in the conjugate ($\delta_{\mathbf{9}}$ = 2.83, $\delta_{H3Bn2DT3A.ga.PSMA}$ = 2.16-2.00). The resonances associated with the protons adjacent to the other carboxylic acids of $H_4Bn_2DT3A.ga$ ($\delta_{H(H4Bn2DT3A.ga)}$ = 3.89, 2.93) remain unchanged ($\delta_{H(H3Bn2DT3A.ga.PSMA)}$ = 3.87, 2.91), confirming the site of conjugation.

4.5.2 Uptake/inhibition of PSMA

Urea based inhibitors of PSMA have been applied to PET imaging.[161] The radiometal based imaging agents with the greatest affinity for PSMA link the chelator to the urea through a short linker featuring a lipophilic moiety at the end (either within the linker or the chelator).[266] The urea unit occupies the active site in a reversible manner, and the lipophilic residues promote binding by occupying a lipophilic pocket, the S1 domain, slowing the dissociation kinetics.[267] Thus, [Ga(Bn_2DT3A.ga.PSMA)] is expected to be an inhibitor of PSMA with the urea motif binding to the active site and the benzyl units of the chelator providing the lipophilic units that can occupy the S1 domain. The ability of [Ga(Bn_2DT3A.ga.PSMA)] to inhibit PSMA hydrolysis of N-acetyl aspartyl glutamate (NAAG) was assessed through a fluorometric assay, Amplex Red (Figure 4.27).

LNCaP cell lysates containing PSMA were incubated with N-Acetyl L-Aspartyl-L-Glutamate (NAAG), following incubation the Amplex Red assay was added. In the absence of an inhibitor, NAAG is hydrolysed to form L-glutamic acid by PSMA. The glutamate oxidase in the assay oxidises L-glutamic acid to form oxoglutarate and hydrogen peroxide; this hydrogen peroxide is then used by horseradish peroxidase to oxidise the Amplex Red reagent to form resorufin.[268] Due to the extended conjugated network, resorufin has an increased fluorescence when excited at 563 nm than Amplex Red thus allowing for the concentration of hydrogen peroxide to be determined.[268] As the concentration of hydrogen peroxide is dependent on the concentration of L-glutamic acid, this can be used to assess the extent of NAAG hydrolysis. In the presence of an inhibitor, NAAG is prevented from binding to the PSMA receptor; this prevents its hydrolysis and therefore a reduced signal will be observed following the addition of the assay.

In the presence of high concentrations of [Ga(Bn_2DT3A.ga.PSMA)] the hydrolysis is reduced (Figure 4.28), whereas at low concentrations hydrolysis remains uninhibited. Fitting of this data gives an IC_{50} of $10^{-8.49}$ M; conversion of this using the Cheng-Prusoff equation (Equation 3)[269] gives a K_I of 0.37 nM.

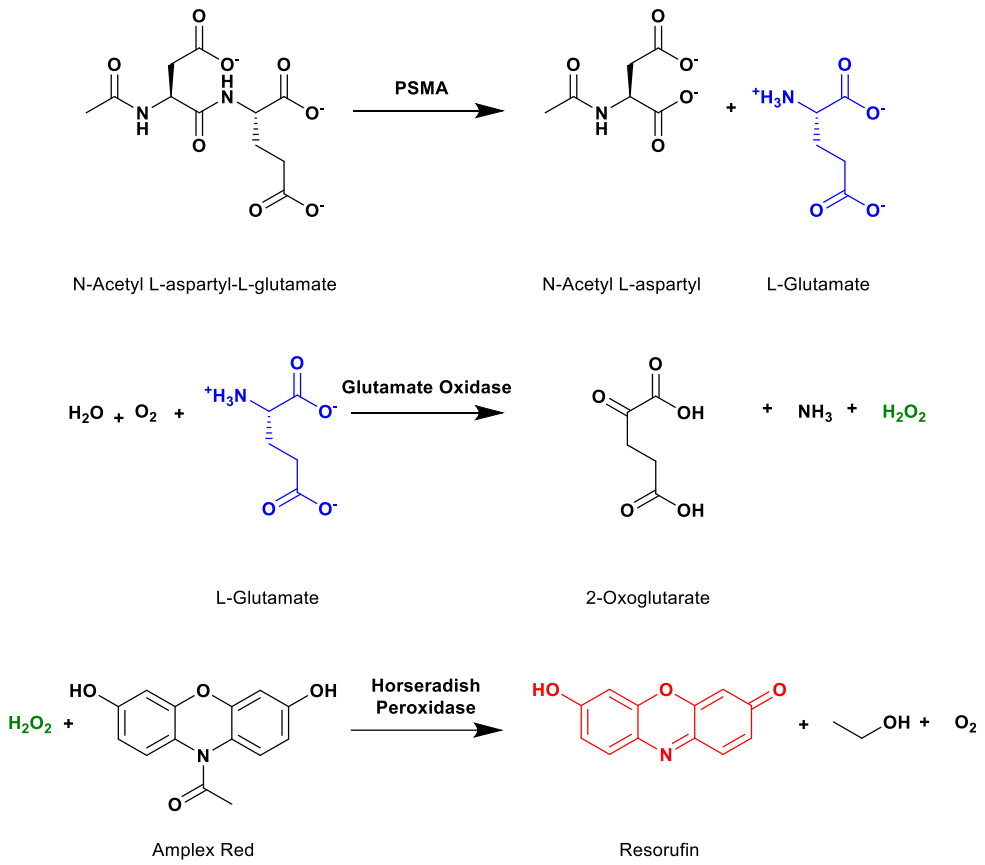

Figure 4.27: Schematic of Amplex Red detection of NAAG hydrolysis by PSMA.

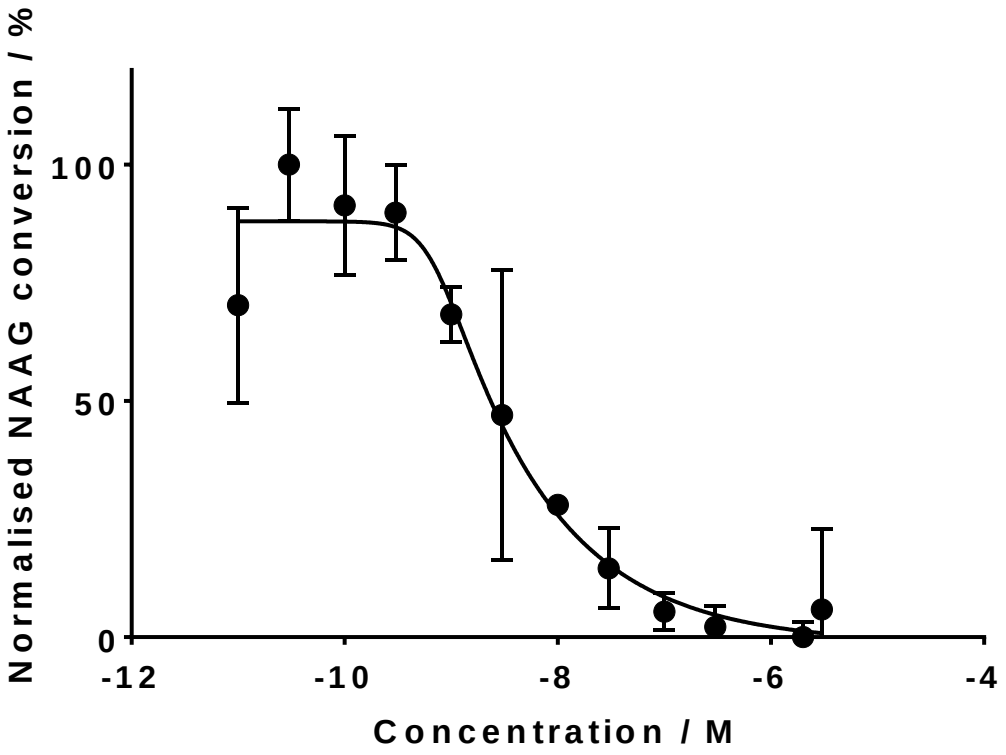

Figure 4.28: Inhibition of PSMA activity by [Ga(Bn_2DT3A.ga.PSMA)].

Equation 3: Cheng-Prusoff equation. IC_{50} = concentration of inhibitor which reduces enzyme activity by half. K_I = Inhibitory constant. S = substrate concentration (1 μM). K_M = Michalis constant of enzyme and substrate, for PSMA and NAAG this is 130 x 10^{-9} M.[270]

$$IC_{50} = K_I(1 + \frac{S}{K_M})$$

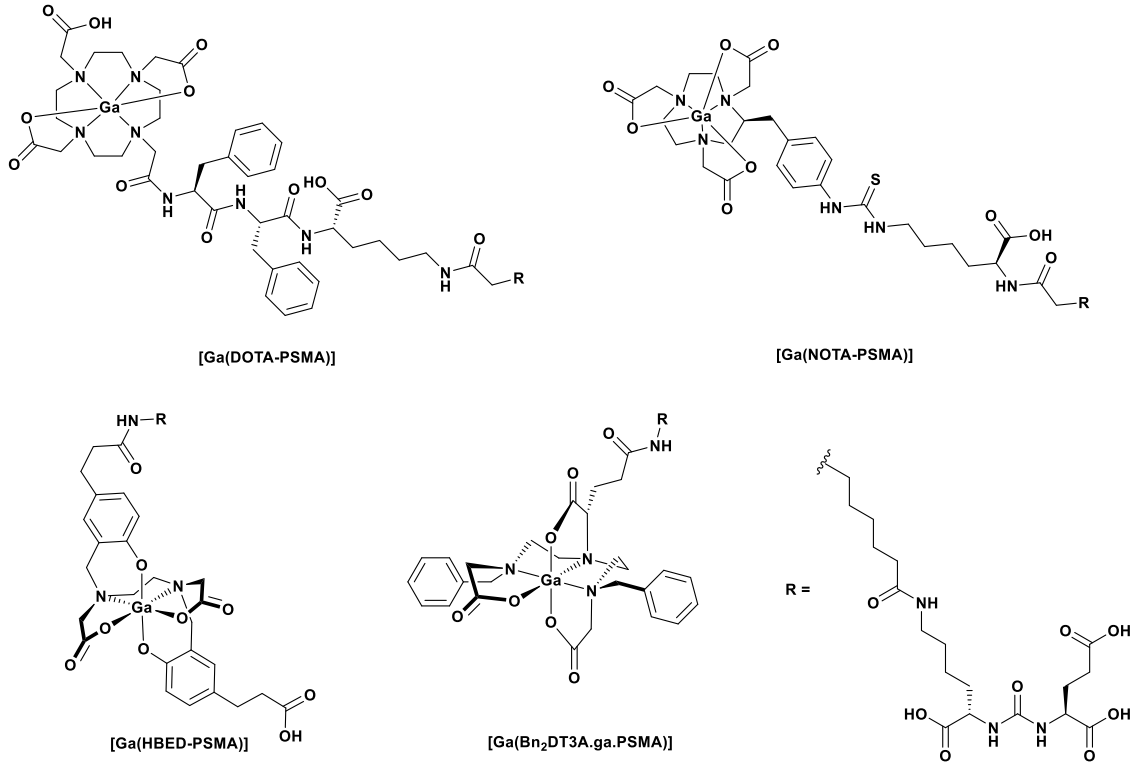

Figure 4.29: Structures of PSMA inhibitors discussed in this chapter

This value is comparable to the inhibition constants obtained for [Ga(DOTA-PSMA)][161] and [Ga(NOTA-PSMA)][161] complexes with the same targeting motif; however these were modified with lipophilic linkers to improve their affinity. However, this value is approximately an order of magnitude worse than that obtained for a HBED analogue, HBED-PSMA, with the same linker and targeting unit as [Ga(Bn_2DT3A.ga.PSMA)].[161]

Table 4.5: Selected inhibition constants of chelators and Ga(III) complexes targeting PSMA.

Chelator	Conjugate K_i / nM	Complex K_i / nM
DOTA-PSMA[161]	0.70	0.33
NOTA-PSMA[161]	0.81	0.38
HBED-PSMA[161]	0.03	-
H_3Bn_2DT3A.ga.PSMA	-	0.37

4.5.3 Radiolabelling

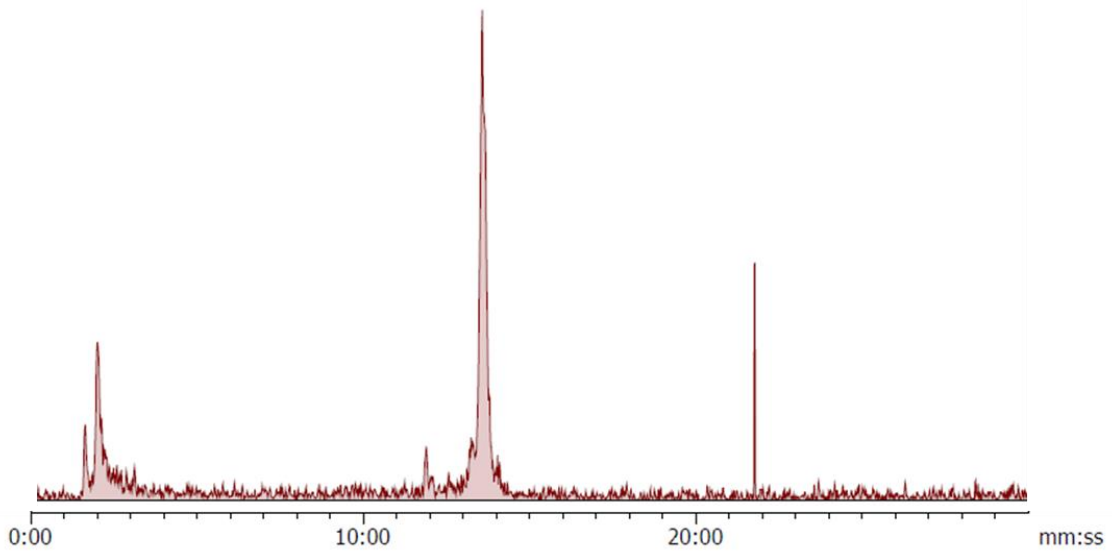

Figure 4.30: Radio HPLC of ^{68}Ga incubated with H_3Bn_2DT3A.ga.PSMA. *[H_3Bn_2DT3A.ga.PSMA]* = 400 µM, *I* = PBS, *pH* = 7.4, *T* = 37 °C, *t* = 15 mins. **HPLC Gradient A.**

Radiolabelling of H_3Bn_2DT3A.ga.PSMA with ^{68}Ga was less efficient than radiolabelling of the ligand H_3Bn_2DT3A or bifunctional chelator H_4Bn_2DT3A.ga; high concentrations of conjugate were required to achieve acceptable radiochemical yields. 400 µM conjugate only achieved a 62% yield when heated to 37 °C at pH 7.4. A single product was formed under these conditions (Figure 4.30). Attempts to radiolabel lower concentrations of H_3Bn_2DT3A.ga.PSMA resulted in significantly reduced radiochemical yields. Due to the instability of the products formed by H_3Bn_2DT3A and H_4Bn_2DT3A.ga under acidic conditions, these conditions were not assessed with H_3Bn_2DT3A.ga.PSMA.

When assessed for stability to serum it was found that the radiolabelled species were not stable to serum; the activity was all associated with serum within 30 minutes incubation (Figure 4.31). This confirms the result seen for the bifunctional chelator H_4Bn_2DT3A.ga and the need to investigate alternative sites for conjugation of this chelator before application to targeted *in vivo* imaging.

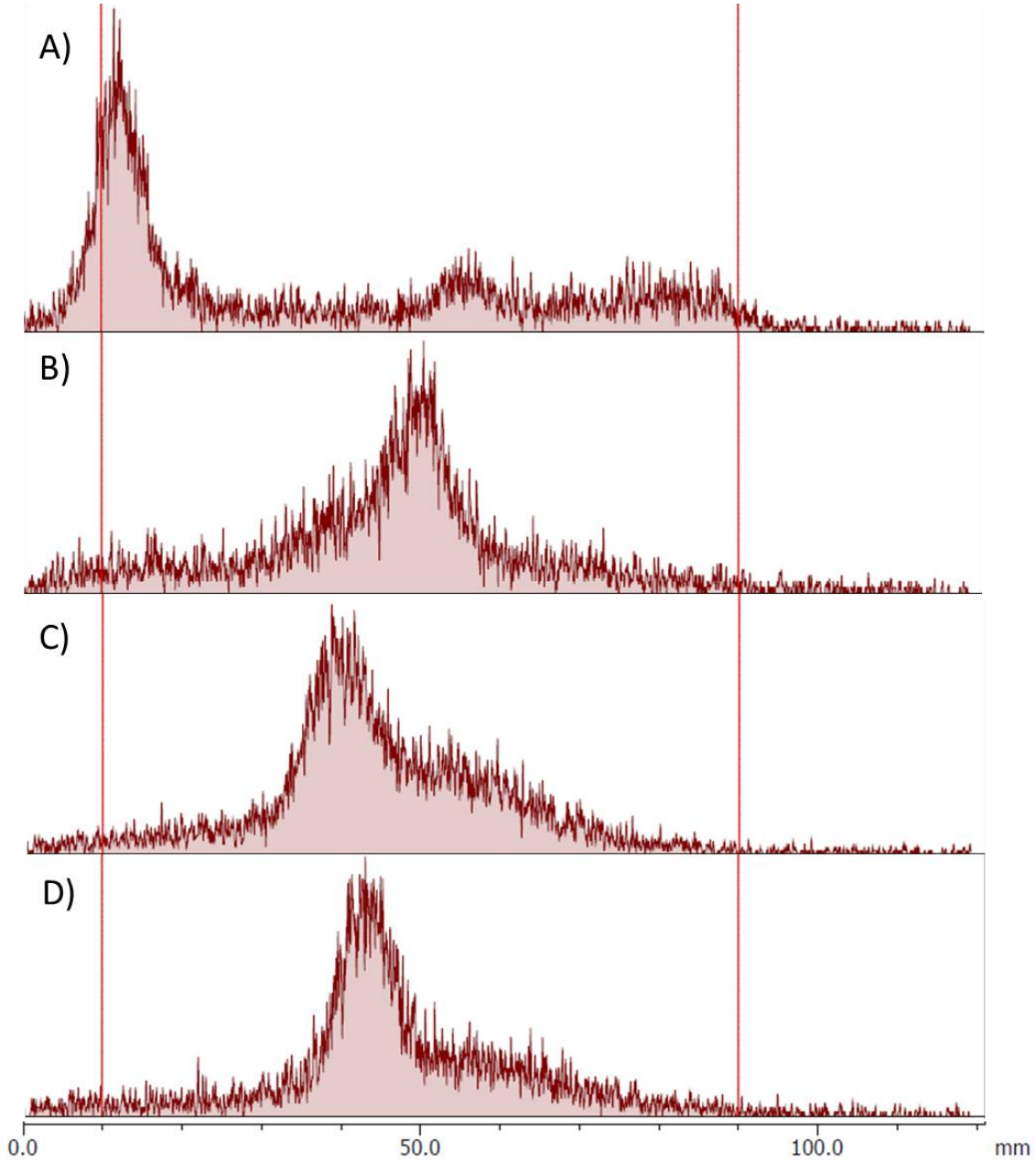

Figure 4.31: Assessment of serum stability of [^{68}Ga][Ga(Bn_2DT3A.ga.PSMA)]. A) Crude radiolabelling solution. B-D) Incubation with FBS at 37 °C for B) 30 mins, C) 90 mins, D) 120 mins. Method development for TLC analysis is shown in appendix 4.

4.6. Conclusions

A novel chelator, H_3Bn_2DT3A, has been developed and assessed for its potential to coordinate ^{68}Ga. This chelator fulfils the octahedral coordination geometry of Ga(III) as evidenced by the solid state crystal structure. The thermodynamic stability ($\log K_{[Ga(Bn2DT3A)]}$ = 18.25) is lower than that of other similar acyclic chelators; however when a deprotonated species, $[Ga(Bn_2DT3A)(OH)]^-$, is considered H_3Bn_2DT3A has a similar thermodynamic stability with Ga(III) as DTPA. This deprotonation event is observed through potentiometric titration and in the species formed when radiolabelling this chelator with ^{68}Ga. When radiolabelling with ^{68}Ga the species formed is dependent on a variety of conditions; in particular pH has an effect with

two species being observed. The species that is formed at higher pH is more stable to serum with no decomplexation seen over 2 hours. In contrast, the species formed at lower pH is unstable when incubated with serum. As such, future studies applying this chelator to ^{68}Ga complexation should be performed above pH 6.5 for *in vivo* application.

A bifunctional derivative of H_3Bn_2DT3A has been prepared by incorporating an amino acid into the synthetic procedure. This chelator, $H_4Bn_2DT3A.ga$, can complex ^{68}Ga, although the RCYs are lower than those obtained with H_3Bn_2DT3A, with 100 µM achieving only a 74% RCY at pH 4.0 and 200 µM achieving only a 53% yield at pH 7.4. The resulting complex, [^{68}Ga][Ga($Bn_2DT3A.ga$)], is less stable to serum than [^{68}Ga][Ga(Bn_2DT3A)], with decomplexation seen within 30 minutes of incubation with FBS. This system has also been successfully conjugated to a PSMA inhibiting motif; this has been shown to inhibit the hydrolysis of NAAG *in vitro* with an IC_{50} of 3.2 nM and a K_I of 0.37 nM. Future developments of this system should investigate alternative sites for functionalisation to incorporate a site that can be conjugated without disrupting the binding pocket of the chelator. Possible sites of functionalisation are through the carbon backbone, as reported for CHX-A''-DTPA (Figure 4.1), or through the terminal benzyl units. Functionalisation through the backbone will be synthetically taxing and may also impact upon the binding pocket of the chelator. The terminal benzyl units could be replaced with other units by varying the aldehyde used in first step of the synthesis. Varying this terminal functional group may also allow for further optimisation of this system for ^{68}Ga complexation.

Chapter 5 Conclusions and future work

In this thesis a number of new chelators and Ga(III) complexes have been described, along with the assessment of physical properties and radiolabelling ability of these systems.

In chapter 2, a series of chelators based upon the H_3Dpaa scaffold were described. H_3Dpaa and bifunctional derivatives were prepared by reaction of a protected amino acid with **4** followed by hydrolysis of the proligand.

This chelator scaffold has been previously applied to the complexation of trivalent lanthanide ions, Mn(II), and during the course of this project the complexation of Ga(III). The thermodynamic stability of the Ga(III) complexes were investigated, with stability constants $\log K_{[Ga(Dpaa)]}$ = 18.53, $\log K_{[Ga(Dpaa.dab)]}$ = 16.13, $\log K_{[Ga(Dpaa.ga)]}$ = 18.36 being determined through potentiometry. These much lower than that of the picolinate based chelator dedpa ($\log K_{[Ga(dedpa)]}$ = 28.1),[37] likely due to the pentadentate nature of the Dpaa chelators upon complexation of Ga(III). The novel bifunctional chelator, H_4Dpaa.ga, was conjugated to a urea based PSMA targeting unit through cyclisation of the glutamic acid residue as an anhydride, followed by ring opening to yield the desired amide conjugate.

The single crystal X-ray structures obtained for [Ga(Dpaa)(H_2O)] and [Ga(Dpaa.ga)(H_2O)] reveal the chelator coordinates Ga(III) in a pentadentate manner with the vacant coordination site being occupied by a water molecule. This is corroborated by an observed deprotonation event in the potentiometry with pK_a = 4.41 for [Ga(Dpaa)(H_2O)]. This likely corresponds to deprotonation of the bound water or to the non-coordinated amine.

Radiolabelling with these picolinate chelators was facile, with radiochemical yields >95% achieved by all four chelators at pH 4 without requiring heating. H_3Dpaa, H_4Dpaa.ga and H_3Dpaa.lys were able to achieve radiochemical yields >95% at pH 7.4 with only mild heating (37 ^oC). This is comparable to the results reported for THP[184] and DATA^{PPh},[179] although the ligand concentration used is 10-30 fold greater. The radiolabelling efficiency was found to be highly dependent on ligand concentration at pH 7.4, with the RCY dropping significantly at ligand concentrations below 50 µM. The achieved molar activities were low, in part because they were determined by isolation of the radiotracer.

The radiolabelled complexes, of the type [^{68}Ga][Ga(Dpaa)(H_2O)], were found to be resilient to transchelation by *apo*-transferrin but were not stable to challenge by serum. This makes this system unsuitable for PET imaging using ^{68}Ga.

The current interest in using this system for Mn(II) complexation for MRI application suggests a route forwards for these chelators; application of the bifunctional systems to the

development of targeted Mn(II) MRI contrast agents. Furthermore this could be paired with the PET radionuclide ^{52}Mn to produce a PET/MRI pair for dual modal imaging.

Despite the poor stability of the [^{68}Ga][Ga(Dpaa)(H_2O)] family in serum, the high radiochemical yields achieved at pH 7.4 encouraged further exploration of picolinate based chelators for ^{68}Ga complexation in chapter 3.

Incorporation of another picolinate arm into the structure yields the heptadentate H_3Tpaa. A simplified synthetic strategy was investigated in comparison to that previously reported by Bretonnière *et al*.[236] Synthesis of the proligand by direct reaction with ammonium hydrochloride yielded the proligand in a single step from **4** without the need to prepare the aminomethyl picolinate starting material separately. However, the yield (16%) was reduced following this method. The additional coordinating atom allows this chelator to fulfil the coordination sphere of Ga(III). This is confirmed by a highly symmetric ^{1}H NMR of the complex [Ga(Tpaa)] and the single crystal X-ray structure. High radiochemical yields were achieved, even at high pH, although the molar activity was similar to that obtained with H_3Dpaa. The resulting complex, [^{68}Ga][Ga(Tpaa)] was found to be more stable to serum than [^{68}Ga][Ga(Dpaa)(H_2O)], with 32% of the activity being retained in the complex after 30 minutes incubation. However as further degradation occurred over 2 hours this is insufficient for application to ^{68}Ga PET imaging.

Expanding the chelator through the use of TACN as a scaffold for three picolinate arms yielded H_3NO3PA. The synthesis of this system was hampered by the formation of [Et_4NO4PA]$^+$ as a byproduct during the proligand synthesis reducing the overall yield. Complexation of Ga(III) by the nonadentate H_3NO3PA resulted in a number of species being formed in solution; this was reflected in both the ^{1}H NMR and during radiolabelling. The products obtained by reaction of H_3NO3PA with ^{68}Ga were found to be unstable when challenged with serum.

The glycine residue of H_3Dpaa was replaced with an aminomethylphosphonic acid unit prepared from benzylamine by condensation with formaldehyde and diethyl phosphite followed by hydrogenation. The resulting chelator, H_4DPAP, was able to complex ^{68}Ga at acidic pH, with RCYs of 96% determined by co-incubation with H_4Dpaa.ga. When assessed for serum stability, this system as found to be poorly stable. Although the single crystal X-ray structure was not obtained, the [Ga(DPAP)] complex likely contains a bound water molecule and this may be a source of instability.

Further replacement of the picolinate arms with pyridylphosphonic acid arms yielded H_6DPPP. Preparation of the precursor, **13**, was achieved in two steps from N-picoline oxide. The initial step, reaction with triethyl phosphite in the presence of ethyl chloroformate, was found to be significantly higher yielding (99%) than synthesis through a palladium catalysed cross coupling of 2-bromo-6-methyl pyridine (9%). Light mediated radical bromination of **12** produced

the desired bromide as well as a double bromination product. Alternative synthesis methods have been reported that avoid this by formation of ethyl (6-(hydroxymethyl)pyridin-2-yl)(methyl)phosphinate followed by activation of the alcohol group.[246] H_6DPPP was found to be a poor chelator for ^{68}Ga, with low radiochemical yields obtained at both pH 4 and pH 7.4.

Future development of these chelators for ^{68}Ga complexation should focus on the H_3Tpaa core instead of H_3Dpaa. Incorporation of phosphonic residues into this would allow for a true comparison between picolinate and pyridylphosphonate arms for ^{68}Ga complexation. Phosphinates should also be explored as replacement of the –OH group with an alkyl or aryl group should increase lipophilicity making detailed assessment of the radiolabelled complex easier. This system could be further modified by replacing the picolinate arms for other groups – the small bite angle of the picolinic residues with Ga(III) may be inducing strain into the complex that causes the observed instability. Phenols have been shown to be effective coordinating units for Ga(III) through the success and high thermodynamic stability of HBED; potential developments of this system could be hydroxyquinoline or pyridyl-phenol based.

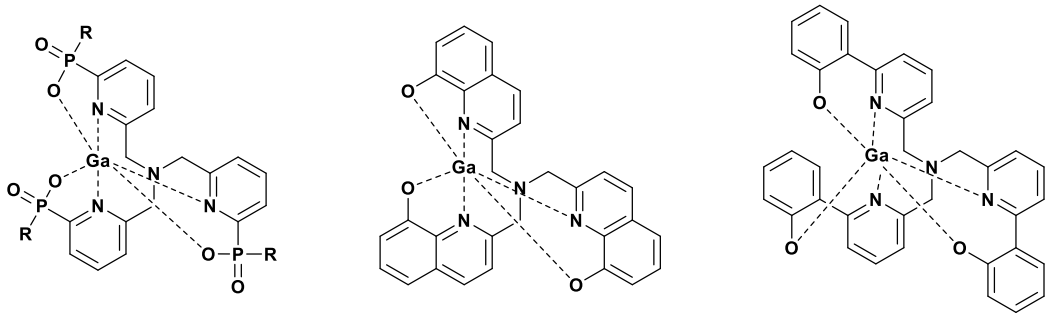

Figure 5.1: Potential future H_3Tpaa based Ga(III) complexes.

In chapter 4 the hexadentate linear polyaminocarboxylate chelator H_3Bn_2DT3A was prepared by reductive amination of diethylenetriamine with benzaldehyde followed by alkylation by *tert*-butyl bromoacetate and hydrolysis. Complexation of Ga(III) by this ligand resulted in a complex with thermodynamic stability $\log K_{[Ga(Bn2DT3A)]}$ = 18.25. Potentiometry revealed a deprotonation event with pK_a = 5.32; this is similar to the deprotonation event seen for [Ga(Dpaa)(H_2O)] (pK_a = 4.41). However, the single crystal X-ray structure obtained reveals that the coordination sphere of Ga(III) is fully satisfied by H_3Bn_2DT3A, with no bound water observed. The ^{1}H NMR is highly asymmetric with each alkyl proton having its own environment, making analysis of the pH dependent speciation difficult.

When radiolabelling with ^{68}Ga two major species are seen; the populations of these species is pH dependent in agreement with the determined by potentiometric titration. These two species can be isolated by semipreparative HPLC and the isolated species were not seen to interconvert. Only one of these radiolabelled species is stable to serum, with no decomplexation seen after 2 hours. The other species is rapidly decomposed by serum. Optimisation of the

radiolabelling conditions show that formation of the stable product is promoted by high radiolabelling temperatures, high ligand concentrations and longer reaction times with a pH in the range of 6-8. This species was prepared in an 77% yield and 18.4 GBq μmol^{-1} molar activity following 15 minutes reaction of 100 μM H_3Bn_2DT3A with 297 MBq ^{68}Ga at pH 7.4 in phosphate buffered saline at 37 °C. The total synthesis time was 66 minutes from elution of the generator.

To apply this system to targeted PET imaging a bifunctional derivative, $H_4Bn_2DT3A.ga$, was prepared with the same strategy as was applied to H_3Dpaa. An activated side arm, **17**, was prepared in three steps from aminoethanol and reacted with a protected amino acid residue. This will allow for variation of the central amino acid to vary the additional functional groups to tailor the conjugation method as required. Following deprotection, conjugation was achieved through anhydride formation followed by ring opening by the amine of the targeting unit **9** to yield $H_3Bn_2DT3A.ga.PSMA$. The Ga(III) complex of this conjugate had a similar inhibition constant for the hydrolysis of N-acetyl aspartyl glutamate by PSMA, K_I = 0.37 nM, as was reported for Ga(III) complexes of NOTA (0.38 nM) and DOTA (0.33 nM); however the macrocyclic systems required modification of the linker unit to include lipophilic residues whereas [$Ga(Bn_2DT3A.ga.PSMA)$] did not have this modification. Radiolabelling of the bifunctional chelator and conjugate with ^{68}Ga was less efficient, with high ligand concentrations (200 μM $H_4Bn_2DT3A.ga$) required for mediocre RCYs (53% at pH 7.4). The resulting complexes were not stable to serum with decomplexation seen within 30 minutes.

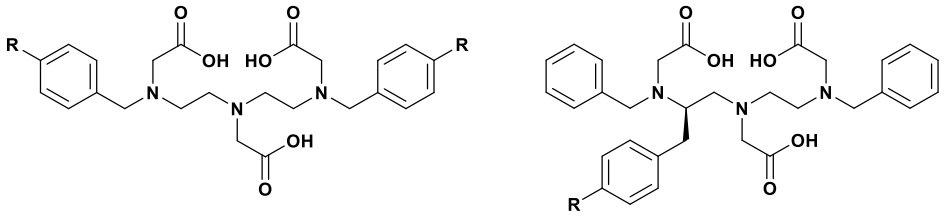

Figure 5.2: Alternative sites for conjugation of the H_3Bn_2DT3A core.

While the H_3Bn_2DT3A core is able to form stable ^{68}Ga complexes, the introduction of a bulkier amino acid into the chelator results in reduced stability. This should be further explored by using non-coordinating amino acids to confirm that this instability is induced by the steric bulk of a side group; if this is the case then alternate conjugation routes will be required. One route to achieving this would be through the modification of the diethylenetriamine backbone as has been previously reported for DTPA – this would also introduce steric bulk into the coordination center and so may not be ideal. Modification of the benzyl units would be a simpler method to introduce additional functional groups into the H_3Bn_2DT3A chelator scaffold. Incorporation of an amine or acid into the para position of the benzaldehyde used would allow for conjugation at a site distant to the coordination pocket.

Substitution of the benzyl units for other groups, such as methyl, cyclohexyl, or substituted benzyl units, could give insight into the coordination geometry at different pHs by

simplifying the alkyl region of the ^{1}H NMR. This may also change the electronics of the amine which could give insight into the role of these atoms in the coordination of Ga(III) at various pHs.

An improved understanding of the coordination modes seen in solution will allow for more intelligent design of future generations of the H_3Bn_2DT3A scaffold with regards to placement of functional groups and optimisation for the coordination of the target metal ion.

While investigating the Ga(III)-H_3Bn_2DT3A system the stability of the Cu(II)- and Zn(II)-systems were also investigated. The Zn(II) system ($\log K_{[Zn(Bn2DT3A)]}$ = 14.12) is less stable than that of Ga(III), whereas the Cu(II) system ($\log K_{[Cu(Bn2DT3A)]}$ = 18.9) is of a similar stability to that of Ga(III). This is the same as the reported stability for [Cu(EDTA)][271] but significantly lower than that reported for macrocyclic compounds[156] and likely insufficient for application to ^{64}Cu radiochemistry. The H_3Bn_2DT3A ligand has not been reported to be applied to any other metal ions, but the versatile nature of polyaminocarboxylates such as EDTA and DTPA make such an application feasible.

Overall, application of the chelators reported here to complexation of Ga(III) and to radiolabelling with ^{68}Ga has had mixed success. The target of rapid radiolabelling under mild conditions has been achieved, but the stability of the resulting radiolabelled picolinate complexes leaves much to be desired whilst the formation of multiple species complicates radiolabelling of H_3Bn_2DT3A with ^{68}Ga. Future development of ^{68}Ga radiotracers should take heed of the instability of picolinate chelators with ^{68}Ga; in particular to the potential for the rigid nature of the picolinate units to prevent coordination by other atoms resulting in unanticipated coordinated water. Future work into the application of polyaminocarboxylate chelators should consider the potential for the formation of multiple complex species due to different coordination geometries; this could be avoided by introducing increased rigidity into the chelator to promote a specific coordination geometry.

Chapter 6 Experimental Methods

6.1. Materials and Methods

Unless otherwise stated all chemicals were purchased from Sigma Aldrich (Dorset, UK), and all solvents were purchased from VWR (Leicestershire, UK). Triazacyclononane.3HCl was purchased from Chematech (Dijon, France). Diethyl glutamate hydrochloride, di-*tert*-butyl glutamate hydrochloride, and *tert*-butyl N_6-((benzyloxy)carbonyl)lysinate were purchased from Flurochem (Derbyshire, UK). All commercially available starting materials were used without further purification. Unless otherwise stated all reactions that required anhydrous conditions or involved moisture sensitive compounds were performed under an atmosphere of dry argon.

NMR spectra were recorded on a JEOL ECP 400 MHz/JEOL Lambda 400 MHz spectrometer using the residual protic solvent signal as an internal reference. Chemical shifts (δ) are reported in parts per million (ppm). Coupling constants (J) were measured in hertz (Hz) and NMR multiplicity are abbreviated as follows: s = singlet, d = doublet, t = triplet, q = quartet, quin = quintet, m = multiplet, br = broad.

ESI Mass spectra were recorded on Advion MS SOP electrospray ionisation spectrometer. High resolution mass spectra were collected by the University of Hull Mass Spectrometry service on a maXis impact instrument. Elemental analysis was performed by the University of Hull Elemental analysis service. UV-Vis absorption spectra were recorded on a Thermo Scientific Evolution 300 UV-Vis spectrometer using quartz cuvettes. pH measurements were carried out using a Jenway model 3520 pH/mV/temperature meter with a three point calibration.[272]

TLC was performed on Kieselgel 60 F_{254} plates (Merck, Kenilworth, USA) and the spots were visualised in UV (254 and 366 nm) or I_2 vapour. Column chromatography was carried out with silica gel (0.040 – 0.063 mm, Merck, Kenilworth, USA).

Analytical HPLC was performed using an Agilent Zorbax Eclipse XDB-C18 column (4.6 × 150 mm with 4.6 × 12.5 mm guard column) and the indicated solvents and gradient. Semi-preparative HPLC was performed using an Agilent Zorbax Eclipse XDB-C18 column (9.4 × 250 mm).

6.1.1 HPLC Gradients

HPLC Gradient A:

Flow Rate: 1 ml min^{-1}. Solvent A: Methanol. Solvent B: Water + 0.1% trifluoroacetic acid.

Gradient, ([Time / minutes] Solvent A: Solvent B): [0] 5:95, [3] 5:95, [18], 95:5, [20] 95:5, [25] 5:95, [30] 5:95

HPLC Gradient B:

Flow Rate: 3 ml min^{-1}. Solvent A: Methanol. Solvent B: Water + 0.1% trifluoroacetic acid.

Gradient, ([Time / minutes] Solvent A: Solvent B): [0] 5:95, [3] 5:95, [18], 95:5, [20] 95:5, [25] 5:95, [30] 5:95

HPLC Gradient C:

Flow Rate: 1 ml min^{-1}. Solvent A: Methanol. Solvent B: Water

Gradient, ([Time / minutes] Solvent A: Solvent B): [0] 5:95, [3] 5:95, [18], 95:5, [20] 95:5, [25] 5:95, [30] 5:95

HPLC Gradient D:

Flow Rate: 1 ml min^{-1}. Solvent A: Methanol. Solvent B: Water + 0.1% trifluoroacetic acid.

Gradient, ([Time / minutes] Solvent A: Solvent B): [0] 5:95, [3] 5:95, [12] 60:40, [13], 95:5, [16] 95:5, [17] 5:95, [20] 5:95

Attempts were made to optimise HPLC gradients, but no methods were obtained that achieved better separation than those reported here.

6.2. Potentiometry

Potentiometry was carried out according to previously published procedures.[273,274] Protonation and stability constants were determined in 0.1 M (NMe_4)Cl at 25.0 °C with pK_w = 13.81. Protonation constants (*[L]* = 0.004 M) were determined from data obtained in pH range 1.6–12.1 (~40 points per titration and three parallel titrations) with electrode calibrated by acid–base titration in extended pH ranges (1.7–12.2 for each titration set).Complex stability constants (*[L]* = *[M]* = 0.004 M) were determined from data obtained in pH range 1.5–12.1, 50 data points per titration, three parallel titrations. Solutions of Ga(III)-H_3Bn_2DT3A complex had to be equilibrated for 30 min before the titration start to reach the full complexation at pH 1.6. UV-VIS spectra were recorded on spectrophotometer Specord 50 Plus (Analytik Jena AG). Temperature was maintained by Peltier block. UV-VIS titration of the Ga(III)-H_3Dpaa system (*[L]* = *[M]* = 0.0001 M) was performed at pH range 2.4–6.9 in 0.1 M (NMe_4)Cl, pH was adjusted with 0.2 M(NMe_4)OH using a glass electrode. UV-VIS titrations of the Cu(II) and Zn(II) systems with H_4Dpaa.ga and H_3Dpaa.dab (*[L]* = *[M]* = 0.00001 M) were performed at pH range 0.0–2.0 without ionic strength control, pH was calculated from added amount of HCl. UV-VIS titration of Cu(II)-H_3Bn_2DT3A system (*[L]* = 0.004 M, *[M]* = 0.002 M) was performed at pH range 0.0–1.8 without ionic strength control, pH was calculated from added amount of HCl. The titration and UV-VIS data were treated simultaneously with OPIUM program package.[275,276] Calculated constants are concentration constants defined as β_{hl} = $[H_hL_l]/[H]_h\cdot[L]_l$ or β_{hlm}=$[H_hL_lM_m]/[H]_h\cdot[L]_{l'}\cdot[M]_m$ and standard deviations are given directly by the program. p*M* values were also calculated by OPIUM from determined protonation and stability constants.

6.3. Radiolabelling

6.3.1 General Procedures

^{68}Ga was obtained from either an IGG100 (Eckert & Ziegler, Berlin, Germany) or an iThemba (iThemba, Somerset West, South Africa) ^{68}Ge/^{68}Ga generator by elution with 4 mL 0.6 N HCl. This eluent was diluted with 20 mL water and the solution passed through a Strata-X-C 33 µm Cation Mixed-mode polymeric support under vacuum. The activity was trapped on the cartridge. The activity was liberated using 1 mL 98% acetone 2% 0.1 N HCl solution.

Aliquots (~30 MBq) of this solution were dried under a stream of inert gas at 90 °C and allowed to cool before use. 1 mL of ligand solution was preheated and added to the dried ^{68}Ga and shaken at the reaction temperature. 5 µL aliquots were taken for analysis by TLC and 20 µL aliquots for analysis by HPLC.

TLC analysis was performed on Kieselgel 60 F_{254} plates with an eluent of 0.1 M citric acid in water.

Isolation of the radiolabelled product was achieved by semi-preparative HPLC. The activity of the collected fraction was measured and molar activity determined for this fraction by comparison of the UV absorbance of the HPLC trace to a known standard.

6.3.2 Assessment of stability to apo-transferrin

100 µL of radiolabelling solution containing 100 µM ligand in 0.1 M acetate buffer (pH 4.5) after incubation with ^{68}Ga for 5 minutes was added to 600 µL of 1 mg mL^{-1} transferrin in 0.1 M sodium hydrogen carbonate solution to give a final pH of 7.2. This solution was incubated at 37 °C with aliquots taken at 60 and 120 minutes for HPLC analysis.

6.3.3 Assessment of stability to foetal bovine serum

100 µL of radiolabelling solution containing 100 µM ligand in PBS or 0.1 M acetate was added to 1.5 mL of foetal bovine serum and incubated at 37 °C. Aliquots were taken at 30 minute intervals for TLC analysis.

6.4. In Vitro Studies

6.4.1 Cell Culture

LNCaP cells (LNCaP clone FGC ATCC CRL-1740, ATCC, Middlesex, UK) were cultivated in RPMI-1640 media supplemented with 10% FBS. The cells were cultivated using standard techniques with a subcultivation ratio of 1:3.

PSMA-expressing DU145 cells and non-PSMA-expressing DU145 cells were provided by Professor Phil Blower and cultivated in RPMI-1640 media supplemented with 10% FBS, 1% PenStrep and 1% glutamine.

6.4.2 PSMA inhibition assay

Solutions of Amplex Red, Horseradish peroxidase, L-glutamate oxidase, L-glutamate-pyruvate and L-alanine in 1 M Tris buffer according to the manufacturer's instructions. A working solution containing 100 µM Amplex Red, 0.25 U/mL HRP, 0.08 U/mL L-glutamate oxidase, 0.5 U/mL L-glutamate-pyruvate transaminase and 200 µM L-alanine was prepared. A 4 µM solution of N-acetyl aspartyl glutamate was prepared in 1 M Tris buffer. Solutions of [Ga(Bn_2DT3a.ga.PSMA)] in 1 M Tris buffer were prepared.

LNCaP cell extracts were prepared by sonication of a pellet of cells in 50 mM Tris buffer (pH 7.4) containing 0.5% Triton-X 100. After pelleting, the supernatant (25 µL) was incubated with [Ga(Bn_2DT3A.ga.PSMA)] (12.5 µL) and NAAG (12.5 µL) in an incubator for 2 hours. The assay solution (50 µL) was added and the solutions incubated for a further hour before being read with excitation at 490 nm and emission at 642 nm. Inhibition curves were determined using semilog plots and IC_{50} values were determined at the concentration at which enzyme activity was inhibited by 50%. Assays were performed in triplicate. Data analysis was performed using Graphpad Prism 6.05 (GraphPad Software, San Diego, California).

6.4.3 Hot Uptake

24 well plates were seeded with 250,000 cells per well. The plates were incubated overnight. The media was replaced with fresh media (495 µL). The radiotracer (5 µL, 50 nM ligand concentration) was added to the cells and incubated for 30 minutes at 37 ^{o}C. The media was removed and the cells washed twice with PBS (500 µL). 1 N NaOH solution was added (500 µL). The plates were stored for 5 minutes at room temperature. The supernatant was removed. The plates were washed with PBS (500 µL). The activity in the original media and washings, and the lysate and washings were recorded using a gamma counter.

6.5. Synthesis of diethyl pyridine-2,6-dicarboxylate (**2**)[277]

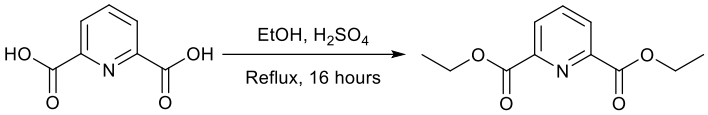

To pyridine-2,6-dicarboxylic acid (30.0 g, 180 mmol) in ethanol (360 mL) was added sulfuric acid (100 µL, 17.8 mmol, 0.1 eq). The solution was heated to reflux for 16 hours. The solvent was removed and the residue taken up in chloroform (250 mL) and washed with saturated sodium hydrogen carbonate solution (100 mL). The aqueous layer was extracted with chloroform (3 x 100 mL). The combined organic layers were dried with magnesium sulfate and concentrated to yield a white crystalline solid (34.0 g, 153 mmol, 85%).

^{1}H NMR (400 MHz, $CDCl_3$, 298 K), δ: 8.30 (d, 2 H, $CH_3CH_2OC(=O)CC\mathbf{H}CHC\mathbf{H}CC(=O)OCH_2CH_3$, $^3J_{HH}$ = 7.7 Hz), 8.01 (t, 1 H, $CH_3CH_2OC(=O)CCHC\mathbf{H}CHCC(=O)OCH_2CH_3$, $^3J_{HH}$ = 7.7 Hz), 4.50 (q, 4 H, p $CH_3C\mathbf{H_2}OC(=O)CCHCHCHCC(=O)OC\mathbf{H_2}CH_3$, $^3J_{HH}$ = 7.1 Hz), 1.47 (t, 6 H, $C\mathbf{H_3}CH_2OC(=O)CCHCHCHCC$-$(=O)OCH_2C\mathbf{H_3}$, $^3J_{HH}$ = 7.1 Hz)

^{13}C{^{1}H} NMR (100 MHz, $CDCl_3$, 298K), δ: 164.64 ($CH_3CH_2O\mathbf{C}(=O)CCHCHCHC\mathbf{C}(=O)OCH_2CH_3$), 148.62 ($CH_3CH_2OC(=O)\mathbf{C}CHCHCH\mathbf{C}C(=O)OCH_2CH_3$), 138.20 ($CH_3CH_2OC(=O)CCH\mathbf{C}HCHCC(=O)$-$OCH_2CH_3$), 127.82 ($CH_3CH_2OC(=O)C\mathbf{C}HCH\mathbf{C}HCC(=O)OCH_2CH_3$), 62.36 ($CH_3\mathbf{C}H_2OC(=O)CCHCH$-$CHCC(=O)O\mathbf{C}H_2CH_3$), 14.21 ($\mathbf{C}H_3CH_2OC(=O)CCHCHCHCC(=O)OCH_2\mathbf{C}H_3$)

MS (ESI), *m/z* = 224.2 **[M+H]$^+$**

6.6. Synthesis of ethyl 6-(hydroxymethyl)picolinate (**3**)

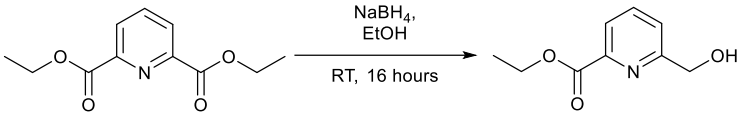

Sodium borohydride (3.15 g, 82.9 mmol, 0.6 eq) was added portionwise to a solution of **2** (31.0 g, 139 mmol, 1 eq) in anhydrous ethanol (400 mL). The solution was stirred at room temperature for 16 hours. The reaction was quenched by addition of water (400 mL) and the volume reduced by half. The solution was extracted with dichloromethane (3 x 250 mL) and the combined organic layers dried with magnesium sulfate and concentrated. The white solid was purified by column chromatography (silica, dichloromethane/ethyl acetate 3:1) to yield a white solid (15.0 g, 82.9 mmol, 60%).

^{1}H NMR (400 MHz, $CDCl_3$, 298 K), δ: 8.04 (d, 1 H, $HOCH_2CCHCHC\mathbf{H}CC(=O)OCH_2CH_3$, $^{3}J_{HH}$ = 7.8 Hz), 7.85 (t, 1 H, $HOCH_2CCHC\mathbf{H}CHCC(=O)OCH_2CH_3$, $^{3}J_{HH}$ = 7.8 Hz), 7.51 (d, 1 H, $HOCH_2CC\mathbf{H}CHCHCC(=O)OCH_2CH_3$, $^{3}J_{HH}$ = 7.8 Hz), 4.87 (s, 2 H, $HOC\mathbf{H_2}CCHCHCHCC(=O)OCH_2CH_3$), 4.47 (q, 2 H, $HOCH_2CCHCHCHCC(=O)OC\mathbf{H_2}CH_3$, $^{3}J_{HH}$ = 7.1 Hz), 1.44 (t, 3 H, $HOCH_2CCHCHCHCC(=O)OCH_2C\mathbf{H_3}$, $^{3}J_{HH}$ = 7.1 Hz)

^{13}C{^{1}H} NMR (100 MHz, $CDCl_3$, 298K), δ: 165.44 ($HOCH_2CCHCHCHC\mathbf{C}(=O)OCH_2CH_3$), 160.11 ($HOCH_2\mathbf{C}CHCHCHCC(=O)OCH_2CH_3$), 147.64 ($HOCH_2CCHCHCH\mathbf{C}C(=O)OCH_2CH_3$), 137.8 ($HOCH_2CCH\mathbf{C}HCHCC(=O)OCH_2CH_3$), 123.92 ($HOCH_2C\mathbf{C}HCHCHCC(=O)OCH_2CH_3$), 123.86 ($HOCH_2CCHCH\mathbf{C}HCC(=O)OCH_2CH_3$), 64.69 ($HOCH_2CCHCHCHCC(=O)O\mathbf{C}H_2CH_3$), 62.22 ($HO\mathbf{C}H_2CCHCHCHCC(=O)OCH_2CH_3$), 14.47 ($HOCH_2CCHCHCHCC(=O)OCH_2\mathbf{C}H_3$)

MS (ESI), *m/z*: 182.2 **$[M+H]^+$**

6.7. Synthesis of ethyl 6-(chloromethyl)picolinate hydrochloride (**4**)[208]

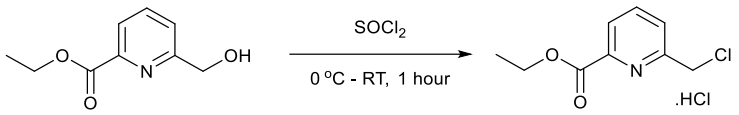

Thionyl chloride (15 mL, 207 mmol, 2.5 eq) was added slowly to **3** (14.9 g, 82.6 mmol, 1 eq) with cooling in an ice bath. The solution was allowed to warm to room temperature and stirred for 1 hour. The solution was concentrated under vacuum using a secondary trap. Toluene (40 mL) was added and a white precipitate formed. Collection of the precipitate and washing with toluene and diethyl ether yielded a white solid (13.6 g, 57.6 mmol, 69%)

^{1}H NMR (400 MHz, $CDCl_3$, 298 K), δ: 8.07 (d, 1 H, $ClCH_2CCHCHC\mathbf{H}CC(=O)OCH_2CH_3$, $^{3}J_{HH}$ = 7.7 Hz), 7.89 (t, 1 H, $ClCH_2CCHC\mathbf{H}CHCC(=O)OCH_2CH_3$, $^{3}J_{HH}$ = 7.7 Hz), 7.73 (d, 1 H, $ClCH_2CC\mathbf{H}CHCHCC(=O)OCH_2CH_3$, $^{3}J_{HH}$ = 7.7 Hz), 4.79 (s, 2 H, $ClC\mathbf{H_2}CCHCHCHCC(=O)OCH_2CH_3$), 4.49 (q, 2 H, $ClCH_2CCHCHCHCC(=O)OC\mathbf{H_2}CH_3$, $^{3}J_{HH}$ = 7.1 Hz), 1.44 (t, 3 H, $ClCH_2CCHCHCHCC(=O)OCH_2C\mathbf{H_3}$, $^{3}J_{HH}$ = 7.1 Hz)

^{13}C{^{1}H} NMR (100 MHz, $CDCl_3$, 298 K), δ: 164.81 ($ClCH_2CCHCHCHC\mathbf{C}(=O)OCH_2CH_3$), 157.24 ($ClCH_2\mathbf{C}CHCHCHCC(=O)OCH_2CH_3$), 147.73 ($ClCH_2CCHCHCH\mathbf{C}C(=O)OCH_2CH_3$), 138.07 ($ClCH_2CCH\mathbf{C}HCHCC(=O)OCH_2CH_3$), 126.01 ($ClCH_2C\mathbf{C}HCHCHCC(=O)OCH_2CH_3$), 124.33 ($ClCH_2CCHCH\mathbf{C}HCC(=O)OCH_2CH_3$), 62.10 ($ClCH_2CCHCHCHCC(=O)O\mathbf{C}H_2CH_3$), 46.33 ($Cl\mathbf{C}H_2CCHCHCHCC(=O)OCH_2CH_3$), 14.28 ($ClCH_2CCHCHCHCC(=O)OCH_2\mathbf{C}H_3$)

MS (ESI), *m/z*: 200.2 **[^{35}Cl][M+H]$^{+}$**, 202.2 **[^{37}Cl][M+H]$^{+}$**

Elemental Analysis Found, %: C, 45.54, H, 4.97, N, 5.49 (Calculated for **4**, $C_9H_{11}NO_2Cl_2$, %: C, 45.79, H, 4.70, N, 5.93).

6.8. Synthesis of diethyl 6,6'-(((2-ethoxy-2-oxoethyl)azane-diyl)bis(methylene))dipicolinate (Et_3Dpaa)[208]

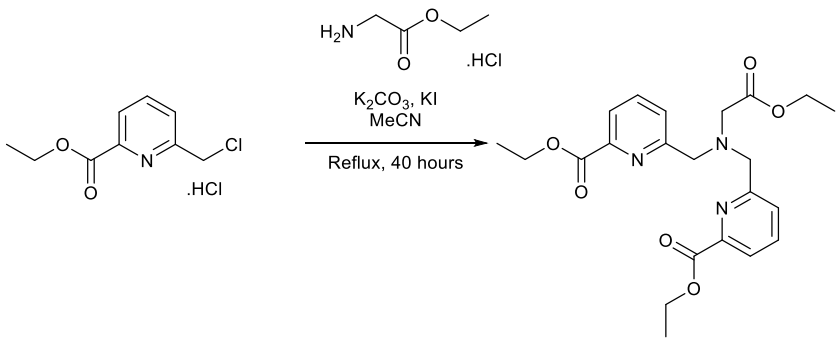

To **4** (4.58 g, 19.4 mmol, 2.2 eq), ethyl glycinate hydrochloride (1.23 g, 8.8 mmol, 1 eq) and potassium carbonate (6.86 g, 49.6 mmol, 5.6 eq) under argon was added anhydrous acetonitrile (35 mL). After 1 hour, potassium iodide (3.22 g, 19.4 mmol, 2.2 eq) was added and the solution heated to reflux under argon for 40 hours. After cooling, the solution was filtered and the solvent removed to give an orange gum. Purification by column chromatography (silica, dichloromethane:ethyl acetate:ammonia, 10:1:0.005 – 3:2:0.02) yielded an orange solid that was purified by recrystallization from diethyl ether to yield white needles (1.30 g, 3.0 mmol, 34%).

^{1}H NMR (400 MHz, $CDCl_3$, 298 K) δ: 7.98 (d, 2 H, -$NCH_2CCHCHC\mathbf{H}CC(=O)OCH_2CH_3$, $^3J_{HH}$ = 7.4 Hz), 7.88 (d, 2 H, -$NCH_2CC\mathbf{H}CHCHCC(=O)OCH_2CH_3$, $^3J_{HH}$ = 7.4 Hz), 7.81 (t, 2 H, -$NCH_2CCHC\mathbf{H}CHCC(=O)$-$OCH_2CH_3$, $^3J_{HH}$ = 7.4 Hz), 4.45 (q, 4 H, -$NCH_2CCHCHCHCC(=O)OC\mathbf{H_2}CH_3$, $^3J_{HH}$ = 7.1 Hz), 4.16 (q, 2 H, -$NCH_2C(=O)OC\mathbf{H_2}CH_3$, $^3J_{HH}$ = 7.1 Hz), 4.08 (s, 4 H,- $NC\mathbf{H_2}CCHCHCHCC(=O)OCH_2CH_3$), 3.47 (s, 2 H, -$NC\mathbf{H_2}C(=O)OCH_2CH_3$), 1.42 (t, 6 H, -$NCH_2CCHCHCHCC(=O)OCH_2C\mathbf{H_3}$, $^3J_{HH}$ = 7.1 Hz), 1.25 (t, 3 H, -$NCH_2C(=O)OCH_2C\mathbf{H_3}$, $^3J_{HH}$ = 7.1 Hz)

^{13}C{^{1}H} NMR (100 MHz, $CDCl_3$, 298 K) δ: 171.15 (-$NCH_2\mathbf{C}(=O)OCH_2CH_3$), 165.24 (-$NCH_2CCH$-$CHCHC\mathbf{C}(=O)OCH_2CH_3$), 159.86 (-$NCH_2\mathbf{C}CHCHCHCC(=O)OCH_2CH_3$), 147.64 (-$NCH_2CCHCHCH$-$\mathbf{C}C(=O)OCH_2CH_3$), 137.40 (-$NCH_2CCH\mathbf{C}HCHCC(=O)OCH_2CH_3$), 126.14 (-$NCH_2C\mathbf{C}HCHCHCC(=O)$-$OCH_2CH_3$), 123.60 (-$NCH_2CCHCH\mathbf{C}HCC(=O)OCH_2CH_3$), 61.82 (-$NCH_2CCHCHCHCC(=O)O\mathbf{C}H_2CH_3$), 60.59 (-$NCH_2C(=O)O\mathbf{C}H_2CH_3$), 59.82 (-$N\mathbf{C}H_2C(=O)OCH_2CH_3$), 55.25 (-$N\mathbf{C}H_2CCHCHCHCC(=O)$-$OCH_2CH_3$), 14.26 (- $NCH_2CCHCHCHCC(=O)OCH_2\mathbf{C}H_3$), 14.17 (-$NCH_2C(=O)OCH_2\mathbf{C}H_3$)

MS (ESI), *m/z*: 430.7 **[M + H]$^+$**

HRMS (ESI), *m/z*: 430.1984 (Calculated for **[M + H]$^+$**, $C_{22}H_{28}N_3O_6$ 430.1978)

Elemental Analysis Found, %: C, 61.69, H, 6.40, N, 9.69 (Calculated for Et_3Dpaa, %: C, 61.53, H, 6.33, M, 9.78).

6.9. Synthesis of 6,6'-(((carboxymethyl)azanediyl)bis-(methylene))dipicolinic acid (H_3Dpaa)[208]

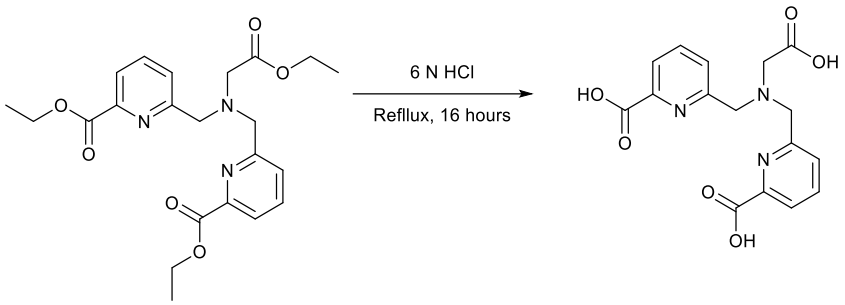

Et_3Dpaa (38 mg, 0.089 mmol) in 6 N HCl (6 mL) was heated to reflux for 16 h. The sample was concentrated, ethanol added, and the precipitate collected and washed with diethyl ether to yield a white solid (36.5 mg, 0.089 mmol, 100%)

^{1}H NMR (400 MHz, D_2O (p*D* = 8.8), 298 K), *δ*: 7.70 (br t, 2 H, -NCH_2CCHC**H**$CHCC(=O)OH$, $^3J_{HH}$ = 7.8 Hz), 7.66 (br d, 2 H, -$NCH_2CCHCHC$**H**$CC(=O)OH$, $^3J_{HH}$ = 7.8 Hz), 7.38 (br d, 2 H, -NCH_2CC**H**$CHCHCC(=O)OH$, $^3J_{HH}$ = 7.8 Hz), 3.92 (br s, 4 H, -NC**H$_2$**$CCHCHCHCC(=O)OH$), 3.27 (br s, 2 H, -NC**H$_2$**$C(=O)OH$)

^{13}C{^{1}H} NMR (100 MHz, D_2O (p*D* = 8.8), 298 K), *δ*: 179.28 (-NCH_2**C(=**$O)OH$), 173.11 (-$NCH_2CCHCHCHC$**C**$(=O)OH$), 157.79 (-NCH_2**C**$CHCHCHCC(=O)OH$), 152.72 (-$NCH_2CCHCHCH$**C**$C(=O)$-OH), 138.01 (-NCH_2CCH**C**$HCHCC(=O)OH$), 125.78 (-NCH_2C**C**$HCHCHCC(=O)OH$), 122.14 (-NCH_2CCHCH**C**$HCC(=O)OH$), 60.21 (-N**C**$H_2CCHCHCHCC(=O)OH$), 59.42 (-N**C**$H_2C(=O)OH$)

MS (ESI), *m/z* = 346.4 **[M+H]$^+$**

HRMS (ESI), *m/z*: 346.1039 (Calculated for **[M + H]$^+$**, $C_{16}H_{16}N_3O_3$: 346.1039)

Elemental Analysis Found, %: C, 49.63, H, 4.40, N, 9.94 (Calculated for $H_3Dpaa(HCl)_{1.3}$(diethyl ether)$_{0.25}$, $C_{17}H_{19.05}Cl_{1.3}N_3O_{6.25}$, %: C, 49.62, H, 4.67, N, 10.21).

6.10. Complexation of Ga(III) by H_3Dpaa

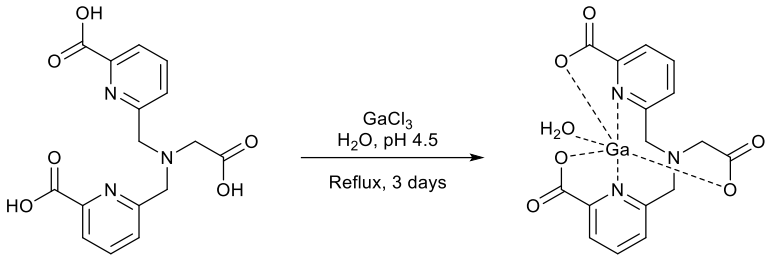

To H_3Dpaa (76 mg, 0.18 mmol) in water (5 mL) was added $GaCl_3$ (38.8 mg, 0.22 mmol, 1.2 eq) in water (3.8 mL). The pH was adjusted to 4.5 with sodium hydroxide. The solution was heated to reflux for 3 days. After cooling, the solution was filtered to give a white solid (76 mg, 0.14 mmol, 76%).

^{1}H NMR (400 MHz, D_2O (p*D* = 8.8), 298 K) *δ*: 8.20 (t, 2 H, -NCH$_2$CCHC**H**CHCC(=O)O-, $^3J_{HH}$ = 7.8 Hz), 8.11 (d, 2 H, -NCH$_2$CCHCHC**H**CC(=O)O-, $^3J_{HH}$ = 7.8 Hz), 7.72 (d, 2 H, -NCH$_2$CC**H**CHCHCC(=O)O-, $^3J_{HH}$ = 7.8 Hz), 4.59 (d, 2 H, -NC**H$_2$**CCHCHCHCC(=O)O-, $^2J_{HH}$ = 16.0 Hz), 4.45 (d, 2 H, -NC**H$_2$**CCHCHCHCC(=O)O-, $^2J_{HH}$ = 16.0 Hz), 3.37 (s, 2 H, -NC**H$_2$**C(=O)O-)

^{13}C{^{1}H} NMR (100 MHz, D_2O (p*D* = 8.8), 298 K), *δ*: 176.86 (-NCH$_2$**C**(=O)O-), 168.40 (-NCH$_2$CCHCHCHC**C**(=O)O-), 151.26 (-NCH$_2$**C**CHCHCHCC(=O)O-), 144.57 (-NCH$_2$CCHCHCH**C**C(=O)O-), 142.35 (-NCH$_2$CCH**C**HCHCC(=O)O-), 126.76 (-NCH$_2$C**C**HCHCHCC(=O)O-), 122.99 (-NCH$_2$CCHCH**C**HCC(=O)O-), 60.60 (-N**C**H$_2$CCHCHCHCC(=O)O-), 59.89 (-N**C**H$_2$COO-)

MS (ESI), *m/z*: 411.95 **[^{69}Ga][M+H]$^+$**, 413.89 **[^{71}Ga][M+H]$^+$**

HRMS (ESI), *m/z*: 412.0058 (Calculated for **[^{69}Ga][M+H]$^+$**, $^{69}GaC_{16}H_{13}N_3O_6$: 412.0060)

Elemental Analysis Found, %: C, 35.85, H, 3.09, N, 7.59 (Calculated for [Ga(Dpaa)(H_2O)](HCl)$_3$, $C_{16}H_{17}Cl_3GaN_3O_7$, %: C, 35.63, H, 3.18, N, 7.79).

6.11. Synthesis of N,N-bis((6-(ethoxycarbonyl)pyridin-2-yl)methyl)-L-glutamate (Et_4Dpaa.ga)

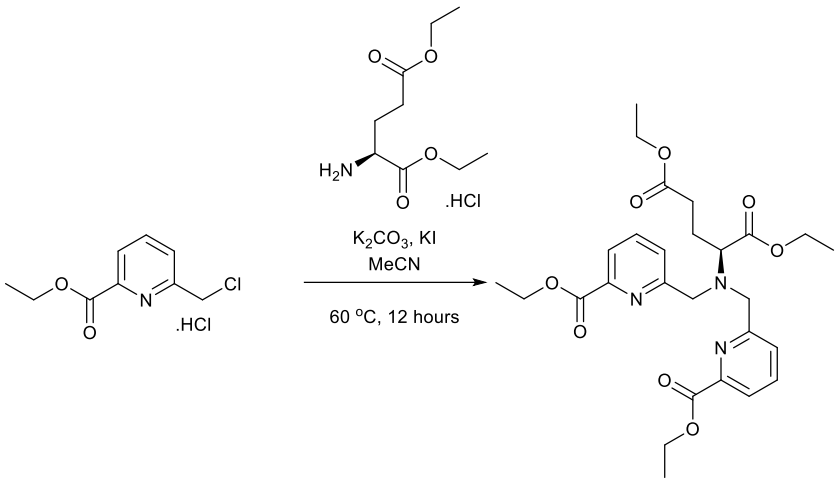

To a suspension of l-glutamic acid diethyl ester hydrochloride (1.82 g, 7.6 mmol), potassium carbonate (4.00 g, 28.9 mmol) and potassium iodide (2.64 g, 15.9 mmol) in anhydrous acetonitrile (10 mL) was added **4** (3.75 g, 15.9 mmol). The mixture was heated to 60 °C for 12 hours. The reaction was quenched with water (50 mL) and extracted with dichloromethane (3 x 100 mL). The combined organic layers were dried with magnesium sulfate and concentrated under reduced pressure. The dark orange oil was purified by column chromatography (silica, Hexane/Ethyl Acetate 20-50%) to yield an orange oil (2.91 g, 5.5 mmol, 72%)

^{1}H NMR (400 MHz, $CDCl_3$, 298 K), δ: 7.96 (dd, 2 H, -$NCH_2CCHCHC$**H**$CC(=O)OCH_2CH_3$, $^3J_{HH}$ = 6.2, $^4J_{HH}$ = 2.5 Hz), 7.79-7.73 (m, 4 H, -NCH_2CC**H**C**H**$CHCC(=O)OCH_2CH_3$), 4.47 (q, 4 H, -$NCH_2CCHCHCHCC(=O)OC$**H$_2$**CH_3, $^3J_{HH}$ = 7.1 Hz), 4.24 (dq, 1 H, -$NCH(C(=O)OC$**H$_2$**$CH_3)CH_2CH_2C(=O)$-OCH_2CH_3, $^2J_{HH}$ = 11.0 Hz $^3J_{HH}$ = 7.1 Hz), 4.23 (dq, 1 H, -$NCH(C(=O)OC$**H$_2$**$CH_3)CH_2CH_2C(=O)OCH_2CH_3$, $^2J_{HH}$ = 11.0 Hz, $^3J_{HH}$ = 7.1 Hz), 4.17 (d, 2 H, -NC**H$_2$**$CCHCHCHCC(=O)OCH_2CH_3$, $^2J_{HH}$ = 15.5 Hz), 4.11 (d, 2 H, -NC**H$_2$**$CCHCHCHCC(=O)OCH_2CH_3$, $^2J_{HH}$ = 15.5 Hz), 4.04 (dq, -$NCH(C(=O)OCH_2CH_3)CH_2$-$CH_2C(=O)OC$**H$_2$**CH_3, 1 H, $^2J_{HH}$ = 10.8, $^3J_{HH}$ = 7.1 Hz), 3.99 (dq, 1 H, -$NCH(C(=O)OCH_2CH_3)CH_2$-$CH_2C(=O)OC$**H$_2$**CH_3, $^2J_{HH}$ = 10.8, $^3J_{HH}$ = 7.1 Hz), 3.46 (dd, 1 H, -NC**H(**$C(=O)OCH_2CH_3)CH_2$-$CH_2C(=O)OCH_2CH_3$, $^3J_{HH}$ = 9.2, 6.8 Hz), 2.54 (ddd, 1 H, -$NCH(C(=O)OCH_2CH_3)CH_2$-C**H$_2$**$C(=O)OCH_2CH_3$, $^2J_{HH}$ = 16.7, $^3J_{HH}$ = 8.5, 6.8 Hz), 2.48 (ddd, 1 H, -$NCH(C(=O)OCH_2CH_3)CH_2$-C**H$_2$**$C(=O)OCH_2CH_3$, $^2J_{HH}$ = 16.7, $^3J_{HH}$ = 8.1, 7.1 Hz), 2.14 (dddd, 1 H, -$NCH(C(=O)OCH_2CH_3)C$**H$_2$**-$CH_2C(=O)OCH_2CH_3$, $^2J_{HH}$ = 14.5, $^3J_{HH}$ = 8.5, 7.1, 6.8 Hz), 2.03 (dddd, 1 H, -$NCH(C(=O)OCH_2CH_3)C$**H$_2$**-$CH_2C(=O)OCH_2CH_3$, $^2J_{HH}$ = 14.5, $^3J_{HH}$ = 9.2, 8.1, 6.8 Hz), 1.45 (t, 6 H, -$NCH_2CCHCHCHCC(=O)$-OCH_2C**H$_3$**, $^3J_{HH}$ = 7.1 Hz), 1.34 (t, 3 H, -$NCH(C(=O)OCH_2C$**H$_3$**$)CH_2CH_2C(=O)OCH_2CH_3$, $^3J_{HH}$ = 7.1 Hz), 1.19 (t, 3 H, -$NCH(C(=O)OCH_2CH_3)CH_2CH_2C(=O)OCH_2C$**H$_3$**, $^3J_{HH}$ = 7.1 Hz)

^{13}C{^{1}H} NMR (100 MHz, $CDCl_3$, 298 K), δ: 173.04 (-$NCH(C(=O)OCH_2CH_3)CH_2CH_2$**C**$(=O)OCH_2CH_3$), 172.36 (-$NCH($**C**$(=O)OCH_2CH_3)CH_2CH_2C(=O)OCH_2CH_3$), 165.28 (-$NCH_2CCHCHCHC$**C**$(=O)OCH_2CH_3$), 160.23 (-$NCH_2$**C**$CHCHCHCC(=O)OCH_2CH_3$), 147.76 (-$NCH_2CCHCHCH$**C**$C(=O)OCH_2CH_3$), 137.21 (-

$NCH_2CCH\mathbf{C}HCHCC(=O)OCH_2CH_3$), 125.93 (-$NCH_2C\mathbf{C}HCHCHCC(=O)OCH_2CH_3$, 123.35 (-$NCH_2CCHCH\mathbf{C}HCC(=O)OCH_2CH_3$), 62.33 (-$N\mathbf{C}H(C(=O)OCH_2CH_3)C(=O)OCH_2CH_3$), 61.73 (-$NCH_2CCHCHCHCC(=O)O\mathbf{C}H_2CH_3$), 60.65 (-$NCH(C(=O)O\mathbf{C}H_2CH_3)CH_2CH_2C(=O)OCH_2CH_3$), 60.25 (-$NCH(C(=O)OCH_2CH_3)CH_2CH_2C(=O)O\mathbf{C}H_2CH_3$), 57.08 (-$N\mathbf{C}H_2CCHCHCHCC(=O)OCH_2CH_3$), 30.66 (-$NCH(C(=O)OCH_2CH_3)CH_2\mathbf{C}H_2C(=O)OCH_2CH_3$), 24.79 (-$NCH(C(=O)OCH_2CH_3)\mathbf{C}H_2CH_2C(=O)$-$OCH_2CH_3$), 14.38 (-$C(=O)OCH_2\mathbf{C}H_3$), 14.25 (-$C(=O)OCH_2\mathbf{C}H_3$), 14.08 (-$C(=O)OCH_2\mathbf{C}H_3$)

MS (ESI), *m/z*: 530.7 **[M+H]**$^+$

HRMS (ESI), *m/z*: 530.2506 (Calculated for **[M+H]**$^+$, $C_{27}H_{36}N_3O_8$: 530.2502)

6.12. Synthesis of N,N-bis((6-carboxypyridin-2-yl)methyl)-L-glutamic acid (H_4Dpaa.ga)

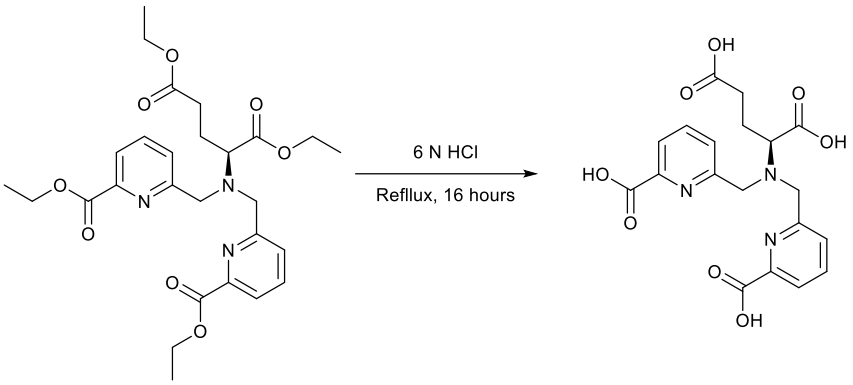

To Et_4Dpaa.ga (887 mg, 1.72 mmol) was added 6 N HCl (14 mL). The solution was heated to reflux for 16 hours and then allowed to cool to room temperature. The solvent was removed to yield a yellow oil. Acetone (10 mL) was added to yield an off-white precipitate (617 mg, 1.26 mmol, 73 %).

^{1}H NMR (400 MHz, D_2O (p*D* = 7.1), 298 K), *δ*: 7.69-7.61 (m, 2 H, -NCH_2CCHC**H**$CHCC(=O)OH$), 7.59 (d, 1 H, -$NCH_2CCHCHC$**H**$CC(=O)OH$, $^3J_{HH}$ = 7.3 Hz), 7.58 (d, 1 H, -$NCH_2CCHCHC$**H**$CC(=O)OH$, $^3J_{HH}$ = 7.3 Hz), 7.37 (d, 1 H, -NCH_2CC**H**$CHCHCC(=O)OH$, $^3J_{HH}$ = 7.3 Hz), 7.36 (d, 1 H, -NCH_2CC**H**$CHCHCC(=O)OH$, $^3J_{HH}$ = 7.3 Hz), 4.37 (br s, 4 H, -NC**H$_2$**$CCHCHCHCC(=O)OH$), 3.66 (br s, 1 H, -NC**H**$(C(=O)OH))CH_2CH_2C(=O)OH$), 2.33 (br s, 2 H, -$NCH(C(=O)OH)CH_2C$**H$_2$**$C(=O)OH$), 2.15 (br s, 2 H, -$NCH(C(=O)OH)C$**H$_2$**$CH_2C(=O)OH$)

^{13}C{^{1}H} NMR (100 MHz, D_2O (p*D* = 7.1), 298 K), *δ*: 182.78 (-$NCH(C(=O)OH)CH_2CH_2$**C**$(=O)OH$), 180.22 (-$NCH($**C**$(=O)OH)CH_2CH_2C(=O)OH$), 173.15 (-$NCH_2CCHCHCHC$**C**$(=O)OH$), 159.04 (-NCH_2**C**$CHCHCHCC(=O)OH$), 152.42 (-$NCH_2CCHCHCH$**C**$C(=O)OH$), 137.90 (-NCH_2CCH**C**$HCHCC(=O)$-OH), 125.49 (-NCH_2CCHCH**C**$HCC(=O)OH$), 121.93 (-NCH_2C**C**$HCHCHCC(=O)OH$), 68.31 (-N**C**$H(C(=O)OH)CH_2CH_2C(=O)OH$), 57.59 (-N**C**$H_2CCHCHCHCC(=O)OH$), 34.83 (-$NCH(C(=O)OH)CH_2$-**C**$H_2C(=O)OH$), 26.73 (-$NCH(C(=O)OH)$**C**$H_2CH_2C(=O)OH$)

MS (ESI), *m/z*: 418.04 **[M+H]$^+$**

HRMS (ESI), *m/z*: 418.1250 (Calculated for **[M+H]$^+$,** $C_{19}H_{20}N_3O_8$: 418.1250

Elemental Analysis Found, %: C, 46.22, H, 4.40, N, 7.99 (Calculated for H_4Dpaa.ga$(HCl)_{2.2}(Acetone)_{0.2}$, $C_{19.6}H_{22.4}N_3O_{8.2}Cl_{2.2}$, %: C, 46.23, H, 4.43, N, 8.25).

6.13. Complexation of Ga(III) by H_4Dpaa.ga

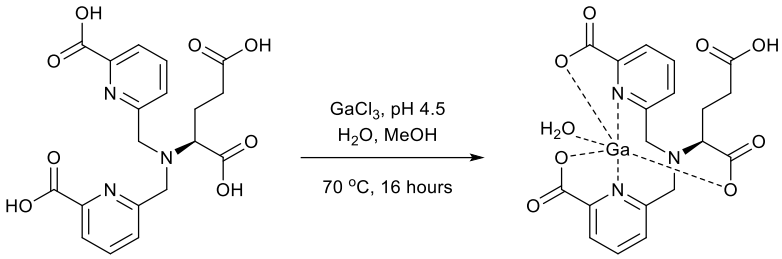

To H_4Dpaa.ga (25 mg, 0.051 mmol) in a solution of methanol (1 mL) and water (1 mL) was added $GaCl_3$ (10.9 mg, 0.062 mmol, 1.2 eq) in water (1.2 mL). The solution was heated to 70 °C for 16 hours and allowed to cool. The precipitate was collected by centrifugation (4000 rpm, 3 minutes) to give a white solid (14.6 mg, 0.026 mmol, 51%).

^{1}H NMR (400 MHz, D_2O (p*D* = 6.0), 298 K) δ: 8.24 (t, 1 H, -NCH$_2$CCHC**H**CHCC(=O)O-, $^3J_{HH}$ = 7.8 Hz), 8.20 (t, 1 H, -NCH$_2$CCHC**H**CHCC(=O)O-, $^3J_{HH}$ = 7.8 Hz), 8.16 (d, 1 H, -NCH$_2$CCHCHC**H**CC(=O)O-, $^3J_{HH}$ = 7.8 Hz), 8.12 (d, 1 H, -NCH$_2$CCHCHC**H**CC(=O)O-, $^3J_{HH}$ = 7.8 Hz), 7.76 (d, 1 H, -NCH$_2$CC**H**CHCHCC(=O)O-, $^3J_{HH}$ = 7.8 Hz), 7.75 (d, 1 H, -NCH$_2$CC**H**CHCHCC(=O)O-, $^3J_{HH}$ = 7.8 Hz), 4.67 (d, 1 H, -NC**H$_2$**CCHCHCHCC(=O)O-, $^2J_{HH}$ = 16.5 Hz), 4.64 (d, 1 H, -NC**H$_2$**CCHCHCHCC(=O)O-, $^2J_{HH}$ = 16.5 Hz), 4.31 (d, 2 H, -NC**H$_2$**CCHCHCHCC(=O)O-, $^2J_{HH}$ = 16.5 Hz), 2.99 (tt, 1 H, -NC**H(**C(=O)O-)CH$_2$CH$_2$C(=O)OH), $^3J_{HH}$ = 8.3 Hz, $^4J_{HH}$ = 1.3 Hz)), 2.37 (dtd, 1 H, -NCH(C(=O)O-)CH$_2$C**H$_2$**C(=O)OH, $^2J_{HH}$ = 15.6 Hz, $^3J_{HH}$ = 7.3 Hz, $^4J_{HH}$ = 1.3 Hz), 2.20 (dtd, 1 H, -NCH(C(=O)O-)CH$_2$C**H$_2$**C(=O)OH, $^2J_{HH}$ = 15.6 Hz, $^3J_{HH}$ = 7.3 Hz, $^4J_{HH}$ = 1.3 Hz), 1.99 (ddt, 1 H, -NCH(C(=O)O-)C**H$_2$**CH$_2$C(=O)OH, $^2J_{HH}$ = 14.2 Hz, $^3J_{HH}$ = 8.3, 7.3 Hz), 1.91 (ddt, 1 H, -NCH(C(=O)O-)C**H$_2$**CH$_2$C(=O)OH, $^2J_{HH}$ = 14.2 Hz, $^3J_{HH}$ = 8.3, 7.3 Hz)

^{13}C{^{1}H} NMR (100 MHz, D_2O (p*D* = 6.0), 298 K) δ: 180.99 (-NCH(C(=O)O-)CH$_2$CH$_2$**C**(=O)OH), 178.13 (-NCH(**C**(=O)O-)CH$_2$CH$_2$C(=O)OH), 168.10 (-NCH$_2$CCHCHCHC**C**(=O)O-), 152.32 (-NCH$_2$**C**CHCHCHCC(=O)O-), 151.03 (-NCH$_2$**C**CHCHCHCC(=O)O-), 144.69 (-NCH$_2$CCHCHCH**C**C(=O)O-), 144.45 (-NCH$_2$CCHCHCH**C**C(=O)O-), 142.83 (-NCH$_2$CCH**C**HCHCC(=O)O-), 142.76 (-NCH$_2$CCH**C**HCHCC(=O)O-), 127.57 (-NCH$_2$CCHCH**C**HCC(=O)O-), 126.38 (-NCH$_2$CCHCH**C**HCC(=O)O-), 123.11 (-NCH$_2$C**C**HCHCHCC(=O)O-), 123.06 (-NCH$_2$C**C**HCHCHCC(=O)O-), 62.08 (-N**C**H(C(=O)O-)CH$_2$CH$_2$C(=O)OH), 58.28 (-N**C**H$_2$CCHCHCHCC(=O)O-), 52.07 (-N**C**H$_2$CCHCHCHCC(=O)O-), 34.80 (-NCH(C(=O)O-)CH$_2$**C**H$_2$C(=O)OH), 22.33 (-NCH(C(=O)O-)**C**H$_2$CH$_2$C(=O)OH)

MS (ESI), *m/z*: 483.9 **[^{69}Ga][M+H]$^+$**, 485.9 **[^{71}Ga][M+H]$^+$**.

HRMS (ESI), *m/z*: 484.0267 (Calculated for **[^{69}Ga][M+H]$^+$**, $^{69}GaC_{19}H_{17}N_3O_8$: 484.0266

Elemental Analysis Found, %: C, 41.56, H, 4.68, N, 7.42 (Calculated for [Ga(Dpaa.ga)(H_2O)](H_2O)$_{2.5}$(MeOH)$_{0.5}$, $C_{19.5}H_{25}GaN_3O_{12}$, %: C, 41.59, H, 4.47, N, 7.46).

6.14. Synthesis of diethyl 6,6'-(((4-((tert-butoxycarbonyl)amino)-1-methoxy-1-oxobutan-2-yl)azanediyl)bis(methylene))(S)-dipicolinate (Et_2MeDpaa.dab(Boc))[209]

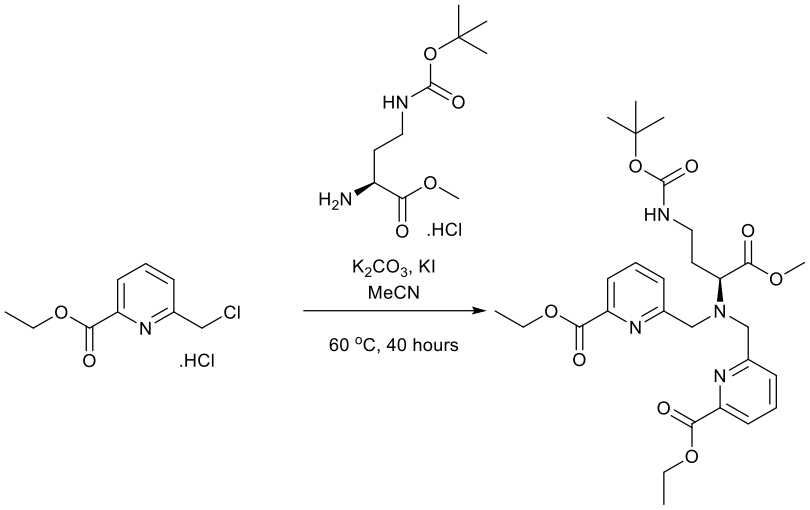

To **4** (0.504 g, 2.14 mmol, 2.2 eq), methyl (S)-2-amino-4-((tert-butoxycarbonyl)amino)butanoate (0.250 g, 0.97 mmol, 1 eq) and potassium carbonate (0.737 g, 5.34 mmol, 5.5 eq) under argon was added acetonitrile (10 mL). After stirring at room temperature for 1 hour, potassium iodide (0.354 g, 2.13 mmol, 2.2 eq) was added and the solution heated to 60 °C under argon for 40 hours. After cooling, the solution was filtered and the solvent removed. The residue was purified by column chromatography (silica, Dichloromethane/Methanol 0-3%) to yield a yellow oil (200 mg, 0.36 mmol, 37%).

^{1}H NMR (400 MHz, d_3-MeCN, 298 K), δ: 7.90 (d, 2 H, -$NCH_2CCHCHCH$**H**$CC(=O)OCH_2CH_3$, $^3J_{HH}$ = 7.5 Hz), 7.80 (t, 2 H, -NCH_2CCHC**H**$CHCC(=O)OCH_2CH_3$, $^3J_{HH}$ = 7.5 Hz), 7.76 (d, 2 H, -NCH_2CC**H**$CHCHCC(=O)OCH_2CH_3$, $^3J_{HH}$ = 7.5 Hz), 4.37 (q, 4 H, -$NCH_2CCHCHCHCC(=O)OC$**H$_2$**CH_3, $^3J_{HH}$ = 7.1 Hz), 4.04 (d, 2 H, -NC**H$_2$**$CCHCHCHCC(=O)OCH_2CH_3$, $^2J_{HH}$ = 15.2 Hz), 3.98 (d, 2 H, -NC**H$_2$**$CCHCHCHCC(=O)OCH_2CH_3$, $^2J_{HH}$ = 15.2 Hz), 3.71 (s, 3 H, -$NCH(C(=O)OC$**H$_3$**$)CH_2CH_2NHC(=O)OC(CH_3)_3$), 3.44 (dd, 1 H, -NC**H**$(C(=O)OCH_3)CH_2CH_2NHC(=O)OC(CH_3)_3$), $^3J_{HH}$ = 9.6, 5.7 Hz), 3.24-3.07 (m, 2 H, -$NCH(C(=O)OCH_3)CH_2C$**H$_2$**$NHC(=O)OC(CH_3)_3$),1.98-1.83 (m, 2 H, -$NCH(C(=O)OCH_3)C$**H$_2$**$CH_2NHC(=O)OC(CH_3)_3$),1.37 (t, 6 H, -$NCH_2CCHCHCHCC(=O)OCH_2C$**H$_3$**, $^3J_{HH}$ = 7.1 Hz), 1.27 (s, 9 H, --$NHC(=O)OC(C$**H$_3$**$)_3$)

^{13}C{^{1}H} NMR (100 MHz, d_3-MeCN, 298 K), δ: 174.34 (-$NCH($**C**$(=O)OCH_3)CH_2CH_2NHC(=O)OC(CH_3)_3$), 166.46 (-$NCH_2CCHCHCHC$**C**$(=O)OCH_2CH_3$), 161.42 ($NCH_2$**C**$CHCHCHCC(=O)OCH_2CH_3$), 157.30 (-$NCH(C(=O)OCH_3)CH_2CH_2NH$**C**$(=O)OC(CH_3)_3$), 149.04 ($NCH_2CCHCHCH$**C**$C(=O)OCH_2CH_3$), 138.91 ($NCH_2CCH$**C**$HCHCC(=O)OCH_2CH_3$), 127.81 ($NCH_2C$**C**$HCHCHCC(=O)OCH_2CH_3$), 124.65 ($NCH_2CCHCH$**C**$HCC(=O)OCH_2CH_3$), 79.13 (-$NCH(C(=O)OCH_3)CH_2CH_2NHC(=O)O$**C**$(CH_3)_3$), 62.72 (-N**C**$H(C(=O)OCH_3)CH_2CH_2NHC(=O)OC(CH_3)_3$), 62.67 ($NCH_2CCHCHCHCC(=O)O$**C**$H_2CH_3$), 58.00

(N**C**H_2CCHCHCHCC(=O)OCH_2CH_3), 52.40 (-NCH(C(=O)O**C**H_3)CH_2CH_2NHC(=O)O$C(CH_3)_3$), 38.74 (-NCH(C(=O)OCH_3)CH_2**C**H_2NHC(=O)O$C(CH_3)_3$), 30.82 (-NCH(C(=O)OCH_3)**C**H_2CH_2NHC(=O)O$C(CH_3)_3$), 28.95 (-NHC(=O)OC(**C**$H_3)_3$), 14.95 (NCH_2CCHCHCHCC(=O)OCH_2**C**H_3)

MS (ESI), *m/z*: 559.8 **[M+H]$^+$**

HRMS (ESI), *m/z*: 559.2771 (Calculated for **[M+H]$^+$,** $C_{28}H_{39}N_4O_8$: 559.2768)

6.15. Synthesis of (S)-6,6'-(((3-amino-1-carboxypropyl)azanediyl)bis(methylene))dipicolinic acid (H_3Dpaa.dab)

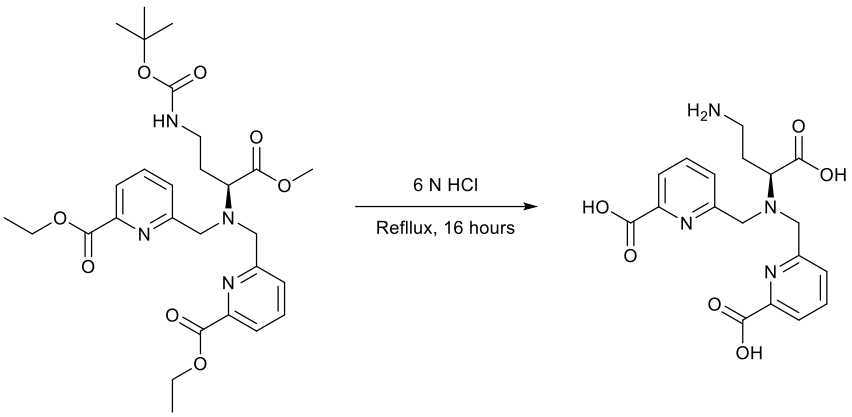

Et_2MeDpaa.dab(Boc) (676.4 mg, 1.21 mmol) was dissolved in 6 N HCl (20 mL) and heated to reflux overnight. The solvent was removed under reduced pressure to yield a yellow oil. Addition of acetone resulted in precipitation of a solid. Isolation of this precipitate yielded a yellow solid (446.3 mg, 0.84 mmol, 70%).

^{1}H NMR (400 MHz, D_2O (p*D* = 1.6), 298 K), δ: 8.07 (t, 2 H, -NCH_2CCHC**H**$CHCC(=O)OH$, $^3J_{HH}$ = 7.8 Hz), 7.93 (dd, 2 H, -$NCH_2CCHCHC$**H**$CC(=O)OH$, $^3J_{HH}$ = 7.8 Hz, $^4J_{HH}$ = 0.9 Hz), 7.68 (dd, 2 H, -NCH_2CC**H**$CHCHCC(=O)OH$, $^3J_{HH}$ = 7.8 Hz, $^4J_{HH}$ = 0.9 Hz), 4.39 (s, 4 H, -NC**H$_2$**$CCHCHCHCC(=O)OH$), 3.98 (t, 1 H, -NC**H***$C(=O)OH)CH_2CH_2NH_2$, $^3J_{HH}$ = 7.1 Hz), 3.30 (dt, 1 H, -$NCH(C(=O)OH)CH_2C$**H$_2$**NH_2, $^2J_{HH}$ = 12.8 Hz, $^3J_{HH}$ = 6.9 Hz), 3.25 (dt, 1 H, -$NCH(C(=O)OH)CH_2C$**H$_2$**NH_2, $^2J_{HH}$ = 12.8 Hz, $^3J_{HH}$ = 6.9 Hz), 2.33 (ddt, 1 H, -$NCH(C(=O)OH)C$**H$_2$**CH_2NH_2, $^2J_{HH}$ = 14.7 Hz, $^3J_{HH}$ = 7.1, 6.9 Hz), 2.27 (ddt, 1 H, -$NCH(C(=O)OH)C$**H$_2$**CH_2NH_2, $^2J_{HH}$ = 14.7 Hz, $^3J_{HH}$ = 7.1, 6.9 Hz)

^{13}C{^{1}H} NMR (100 MHz, D_2O (p*D* = 1.6), 298 K), δ: 174.50 (-$NCH($**C**$(=O)OH)CH_2CH_2NH_2$), 164.62 (-$NCH_2CCHCHCHC$**C**$(=O)OH$), 154.81 (-NCH_2**C**$CHCHCHCC(=O)OH$), 145.26 (-$NCH_2CCHCHCH$**C**$C(=O)$-OH), 143.74 (-NCH_2CCH**C**$HCHCC(=O)OH$), 128.24 (-NCH_2CCHCH**C**$HCC(=O)OH$), 124.92 (-NCH_2C**C**$HCHCHCC(=O)OH$), 64.99 (-N**C**$H(C(=O)OH)CH_2CH_2NH_2$), 55.53 (-N**C**$H_2CCHCHCHCC(=O)$-OH), 37.66 (-$NCH(C(=O)OH)CH_2$**C**H_2NH_2), 26.10 (-$NCH(C(=O)OH)$**C**$H_2CH_2NH_2$)

MS (ESI) m/z: 389.4 **[M+H]$^+$**

HRMS (ESI), *m/z*: 389.1463 (Calculated for **[M+H]$^+$,** $C_{18}H_{21}N_4O_6$: 389.1461)

Elemental Analysis Found, %: C, 42.85, H, 5.15, N, 9.93 (Calculated for H_3Dpaa.dab$(HCl)_3(Acetone)_{0.55}$, $C_{19.65}H_{28.3}Cl_3N_4O_{7.55}$, %: C, 43.09, H, 5.21, N, 10.23).

6.16. Complexation of Ga(III) by H_3Dpaa.dab

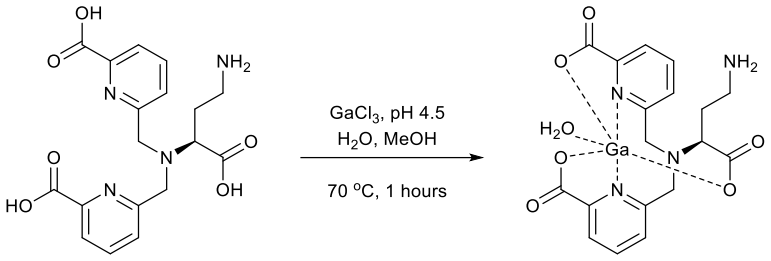

To H_3Dpaa.dab (25 mg, 0.064 mmol) in methanol (5 mL) was added $GaCl_3$ (11.3 mg, 0.064 mmol) in water (1.2 mL). This solution was heated to 70 °C for 1 hour and allowed to cool. The precipitate was collected by centrifugation (4000 rpm, 3 minutes) to give a white solid (17 mg, 0.039 mmol, 60%)

^{1}H NMR (400 MHz, D_2O (p*D* = 1.1), 298 K) δ: 8.29 (t, 2 H, -NCH$_2$CCHC**H**CHCC(=O)O-, $^3J_{HH}$ = 7.8 Hz), 8.23 (d, 1 H, -NCH$_2$CCHCHC**H**CC(=O)O-, $^3J_{HH}$ = 7.8 Hz), 8.17 (d, 1 H, -NCH$_2$CCHCHC**H**CC(=O)O-, $^3J_{HH}$ = 7.8 Hz), 7.85 (d, 1 H, -NCH$_2$CC**H**CHCHCC(=O)O-, $^3J_{HH}$ = 7.8 Hz), 7.79 (d, 1 H, -NCH$_2$CC**H**CHCHCC(=O)O-, $^3J_{HH}$ = 7.8 Hz), 4.52 (d, 1 H, -NC**H$_2$**CCHCHCHCC(=O)O-, $^2J_{HH}$ = 17.0 Hz), 4.48 (d, 1 H, -NC**H$_2$**CCHCHCHCC(=O)O-, $^2J_{HH}$ = 17.0 Hz), 4.41 (d, 1 H, -NC**H$_2$**CCHCHCHCC(=O)O-, $^2J_{HH}$ = 17.0 Hz), 4.07 (d, 1 H, -NC**H$_2$**CCHCHCHCC(=O)O-, $^2J_{HH}$ = 17.0 Hz), 3.16 (dd, 1 H, -NC**H(**C(=O)O-)CH$_2$CH$_2$NH$_2$, $^3J_{HH}$ = 9.2 Hz, $^4J_{HH}$ = 2.3 Hz), 3.08 (t, 2 H, -NCH(C(=O)O-)CH$_2$C**H$_2$**NH$_2$, $^3J_{HH}$ = 7.1 Hz), 2.28-2.09 (m, 2 H, -NCH(C(=O)O-)C**H$_2$**CH$_2$NH$_2$)

^{13}C{^{1}H} NMR (100 MHz, D_2O (p*D* = 1.1), 298 K) δ: 177.21 (-NCH(**C**(=O)O-)CH$_2$CH$_2$NH$_2$), 167.18 (-NCH$_2$CCHCHCHC**C**(=O)O-), 167.05 (-NCH$_2$CCHCHCHC**C**(=O)O-), 153.37 (-NCH$_2$**C**CHCHCHCC(=O)O-), 152.71 (-NCH$_2$**C**CHCHCHCC(=O)O-), 145.06 (-NCH$_2$CCHCHCH**C**C(=O)O-), 144.69 (-NCH$_2$CCHCHCH**C**C(=O)O-), 143.97 (-NCH$_2$CCHC**H**CHCC(=O)O-), 128.49 (-NCH$_2$CC**H**CHCHCC(=O)O-), 127.67 (-NCH$_2$CC**H**CHCHCC(=O)O-), 123.77 (-NCH$_2$CCHCHC**H**CC(=O)O-, 123.63 (-NCH$_2$CCHCHC**H**CC(=O)O-), 61.19 (-N**C**H(C(=O)O-)CH$_2$CH$_2$NH$_2$), 55.00 (-N**C**H$_2$CCHCHCHCC(=O)O-), 51.95 (-N**C**H$_2$CCHCHCHCC(=O)O-), 38.11 (-NCH(C(=O)OH)CH$_2$**C**H$_2$NH$_2$), 24.07 (-NCH(C(=O)OH)**C**H$_2$CH$_2$NH$_2$)

MS (ESI), *m/z*: 454.43 **[^{69}Ga][M+H]$^+$**, 456.39 **[^{71}Ga][M+H]$^+$**.

HRMS (ESI), *m/z*: 455.0478 (Calculated for **[^{69}Ga][M+H]$^+$**, ^{69}GaC$_{18}$H$_{18}$N$_4$O$_6$: 455.0482)

Elemental Analysis Found, %: C, 43.02, H, 3.63, N, 10.87 (Calculated for [Ga(Dpaa.dab)(H$_2$O)](HCl)$_{0.9}$, C$_{18}$H$_{19.9}$Cl$_{0.9}$GaN$_4$O$_7$, %: C, 42.73, H, 3.97, N, 11.07).

6.17. Synthesis of Diethyl 6,6'-(((6-(((benzyloxy)carbonyl)amino)-1-(tert-butoxy)-1-oxohexan-2-yl)azanediyl)bis(methylene))(S)-dipicolinate (Et_2^{t}BuDpaa.lyz(Z))

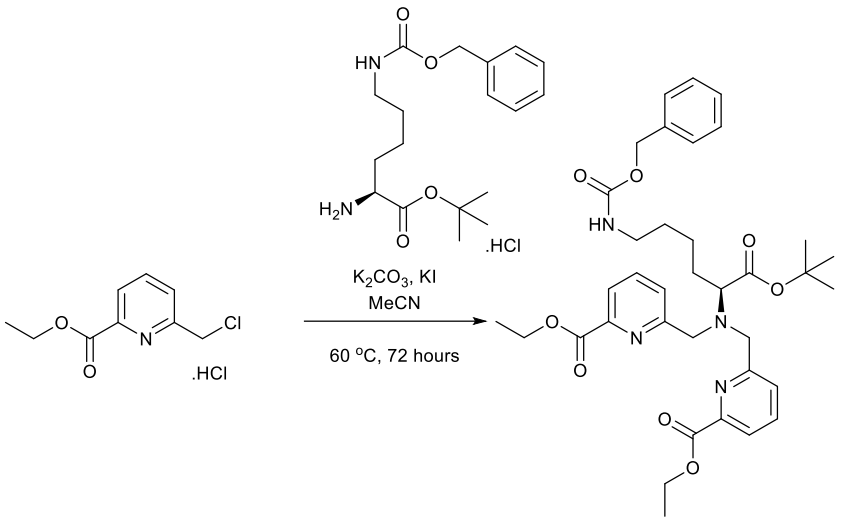

To **4** (1.50 g, 6.3 mmol, 2.1 eq) in acetonitrile (10 mL) was added *tert*-butyl N_6-((benzyloxy)carbonyl)-L-lysinate hydrochloride (1.125 g, 3.0 mmol, 1 eq) and potassium carbonate (1.50 g, 10.9 mmol, 3.6 eq). The solution was stirred under argon for 1 hour. Potassium iodide (1.05 g, 6.3 mmol, 2.1 eq) was added and the solution heated to 60 °C for 72 hours.

The solution was filtered and concentrated. The residue was purified by column chromatography (Silica, 1:1 Ethyl Acetate:Hexane) to yield a yellow oil (886.8 mg, 1.3 mmol, 44%)

^{1}H NMR (400 MHz, $CDCl_3$, 298 K), δ: 7.92 (d, 2 H, -$NCH_2CCHCHCHCC(=O)OCH_2CH_3$, $^3J_{HH}$= 7.3 Hz), 7.77 (d, 2 H, -$NCH_2CCHCHCHCC(=O)OCH_2CH_3$, $^3J_{HH}$ = 7.3 Hz), 7.72 (t, 2 H, -$NCH_2CCHCHCHCC(=O)OCH_2CH_3$, $^3J_{HH}$ = 7.3 Hz), 7.36-7.29 (m, 5 H, -$NCHCH_2CH_2CH_2CH_2NHC(=O)OCH_2C_6H_5$), 5.14-5.07 (m, 1 H, -$NCH(C(=O)OC(CH_3)_3)CH_2CH_2CH_2CH_2NHC(=O)OCH_2C_6H_5$), 5.06 (s, 2 H, -$NCH(C(=O)OC(CH_3)_3)CH_2CH_2CH_2CH_2NHC(=O)OCH_2C_6H_5$), 4.44 (q, 4 H, -$NCH_2CCHCHCHCC(=O)OCH_2CH_3$, $^3J_{HH}$ = 7.3 Hz), 4.15 (br s, 4 H, -$NCH_2CCHCHCHCC(=O)OCH_2CH_3$), 3.27 (t, 1 H, -$NCH(C(=O)OC(CH_3)_3)CH_2CH_2CH_2CH_2NHC(=O)OCH_2C_6H_5$, $^3J_{HH}$ = 6.9 Hz), 3.17 (q, 2 H, -$NCH(C(=O)OC(CH_3)_3)CH_2CH_2CH_2CH_2NHC(=O)OCH_2C_6H_5$, $^3J_{HH}$ = 6.4 Hz), 1.79 (q, 2 H, -$NCH(C(=O)OC(CH_3)_3)CH_2CH_2CH_2NHC(=O)OCH_2C_6H_5$, $^3J_{HH}$ = 6.9 Hz), 1.51 (s, 9 H, -$NCH(C(=O)OC(CH_3)_3)CH_2CH_2CH_2CH_2NHC(=O)OCH_2C_6H_5$, 1.41 (t, 6 H, -$NCH_2CCHCHCHCC(=O)OCH_2CH_3$, $^3J_{HH}$ = 7.3 Hz), 1.58-1.28 (m, 4 H, -$NCH(C(=O)OC(CH_3)_3)CH_2CH_2CH_2NHC(=O)OCH_2C_6H_5$)

^{13}C{^{1}H} NMR (100 MHz, $CDCl_3$, 298 K), δ: 171.84 (-$NCH(C(=O)OC(CH_3)_3)CH_2CH_2CH_2CH_2NHC(=O)OCH_2C_6H_5$), 165.25 (-$NCH_2CCHCHCHCC(=O)OCH_2CH_3$), 159.99 (-$NCH_2CCHCHCHCC(=O)OCH_2CH_3$), 156.40 (-$NCH(C(=O)OC(CH_3)_3)CH_2CH_2CH_2CH_2NHC(=O)OCH_2C_6H_5$), 147.68 (-$NCH_2CCHCHCH$-

CC(=O)OCH$_2$CH$_3$), 137.27 (-NCH(C(=O)OC(CH$_3$)$_3$)CH$_2$CH$_2$CH$_2$CH$_2$NHC(=O)OCH$_2$**C$_6$**H$_5$), 136.65 (-NCH$_2$CCH**C**HCHCC(=O)OCH$_2$CH$_3$), 128.44 (-NCH(C(=O)OC(CH$_3$)$_3$)CH$_2$CH$_2$CH$_2$CH$_2$NHC(=O)-OCH$_2$**C$_6$**H$_5$), 128.05 (-NCH(C(=O)OC(CH$_3$)$_3$)CH$_2$CH$_2$CH$_2$CH$_2$NHC(=O)OCH$_2$**C$_6$**H$_5$), 127.99 (-NCH(C(=O)OC(CH$_3$)$_3$)CH$_2$CH$_2$CH$_2$CH$_2$NHC(=O)OCH$_2$**C$_6$**H$_5$), 126.12 (-NCH$_2$C**C**HCHCHCC(=O)-OCH$_2$CH$_3$), 123.47 (-NCH$_2$CCHCH**C**HCC(=O)OCH$_2$CH$_3$), 81.49 (-NCH(C(=O)O**C**(CH$_3$)$_3$)-CH$_2$CH$_2$CH$_2$CH$_2$NHC(=O)OCH$_2$C$_6$H$_5$), 66.44 (-NCH(C(=O)OC(CH$_3$)$_3$)CH$_2$CH$_2$CH$_2$CH$_2$NC(=O)-O**C**H$_2$C$_6$H$_5$), 63.74 (-N**C**H(C(=O)OC(CH$_3$)$_3$)CH$_2$CH$_2$CH$_2$CH$_2$NHC(=O)OCH$_2$C$_6$H$_5$), 61.82 (-NCH$_2$CCHCHCHCC(=O)O**C**H$_2$CH$_3$), 57.04 (-N**C**H$_2$CCHCHCHCC(=O)OCH$_2$CH$_3$), 40.73 (-NCH(C(=O)OC(CH$_3$)$_3$)CH$_2$CH$_2$CH$_2$**C**H$_2$NHC(=O)OCH$_2$C$_6$H$_5$), 29.29 (-NCH(C(=O)OC(CH$_3$)$_3$)-CH$_2$**C**H$_2$**C**H$_2$**C**H$_2$NHC(=O)OCH$_2$C$_6$H$_5$), 28.68 (-NCH(C(=O)OC(CH$_3$)$_3$)CH$_2$**C**H$_2$**C**H$_2$**C**H$_2$NHC(=O)-OCH$_2$C$_6$H$_5$), 28.27 (-NCH(C(=O)OC(**C**H$_3$)$_3$)CH$_2$CH$_2$CH$_2$CH$_2$NHC(=O)OCH$_2$C$_6$H$_5$), 23.38 (-NCH(C(=O)OC(CH$_3$)$_3$)CH$_2$**C**H$_2$**C**H$_2$**C**H$_2$NHC(=O)OCH$_2$C$_6$H$_5$), 14.28 (-NCH$_2$CCHCHCHCC(=O)OCH$_2$**C**H$_3$)

MS (ESI), *m/z*: 663.9 **[M+H]$^+$**

HRMS (ESI), *m/z*: 663.3399 (Calculated for **[M+H]$^+$**, $C_{36}H_{47}N_4O_8$: 663.3394)

6.18. Synthesis of (S)-6,6'-(((5-amino-1-carboxypentyl)azanediyl)bis(methylene))dipicolinic acid (H_3Dpaa.lys)

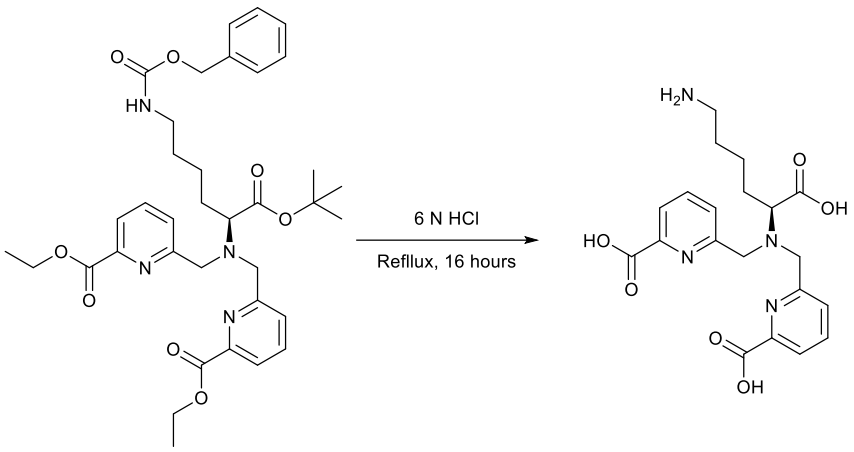

$Et_2{}^tBu$Dpaa.lys(Z) (80 mg, 0.12 mmol) was dissolved in 6 N hydrochloric acid (10 mL). The solution was heated to reflux for 16 hours before being concentrated. Acetone was added and the precipitate was collected to yield a yellow hygroscopic solid (30 mg, 0.07 mmol, 60%)

^{1}H NMR (400 MHz, D_2O (pD = 4.6), 298 K), δ: 7.80 (t, 2 H, -NCH_2CCHC**H**$CHCC(=O)OH$, $^3J_{HH}$ = 7.3 Hz), 7.73 (d, 2 H, -NCH_2CC**H**$CHCHCC(=O)OH$, $^3J_{HH}$ = 7.3 Hz), 7.42 (d, 2 H, -$NCH_2CCHCHC$**H**$CC(-O)OH$, $^3J_{HH}$ = 7.3 Hz), 4.58 (s, 4 H, -NC**H$_2$**$CCHCHCHCC(=O)OH$), 3.88 (s, 1 H, -NC**H(**$C(=O)OH)CH_2CH_2CH_2CH_2NH_2$), 2.98 (s, 2 H, -$NCH(C(=O)OH)CH_2CH_2CH_2C$**H$_2$**$NH_2$), 2.02 (s, 2 H, -C**H$_2$**-), 1.69 (s, 2 H, -C**H$_2$**-), 1.59 (s, 2 H, -C**H$_2$**-)

^{13}C{^{1}H} NMR (100 MHz, D_2O (pD = 4.6), 298 K), δ: 169.42 (-NCH(**C**$(=O)OH)CH_2CH_2CH_2CH_2NH_2$), 163.31 (-$NCH_2CCHCHCHC$**C**$(=O)OH$), 162.98 (-$NCH_2$**C**$CHCHCHCC(=O)OH$), 151.41 ($NCH_2CCHCHCH$**C**$C(=O)OH$), 140.16 ($NCH_2CCH$**C**$HCHCC(=O)OH$), 126.67 (-$NCH_2C$**C**$HCHCHCC(=O)$-OH), 123.93 (-$NCH_2CCHCH$**C**$HCC(=O)OH$), 69.49 (-N**C**$H(C(=O)OH)CH_2CH_2CH_2CH_2NH_2$), 56.60 (-N**C**$H_2CCHCHCHCC(=O)OH$), 39.19 (-$NCH(C(=O)OH)CH_2CH_2CH_2$**C**$H_2NH_2$), 28.22 (-**C**$H_2$-),26.52 (-**C**$H_2$-), 23.06 (-**C**$H_2$-),

MS (ESI), *m/z*: 417.6 **[M+H]$^+$**

HRMS (ESI), *m/z*: 417.1763 (Calculated for **[M+H]$^+$**, $C_{20}H_{25}N_4O_6$: 417.1774)

6.19. Complexation of Ga(III) by H_3Dpaa.lys

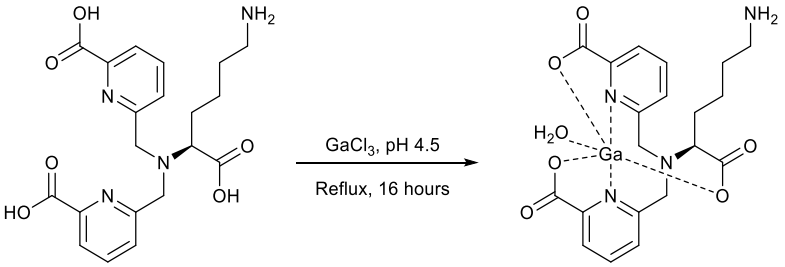

H_3Dpaa.lys (12.4 mg, 29.7 mmol) was dissolved in water (500 µL). $GaCl_3$ (5.7 mg, 32.8 mmol) was added and the pH adjusted to 4.5. The solution was heated to reflux for 16 hours and the solution was concentrated to yield a yellow oil (22 mg) that was used without further purification.

^{1}H NMR (400 MHz, D_2O (pD = 4.8), 298 K), δ: 8.33-8.11 (m, 4 H, -NCH_2CCHC**H**C**H**$CC(=O)O$-), 7.80 (d, 2 H, NCH_2CC**H**$CHCHCC(=O)O$-, $^3J_{HH}$ = 6.2 Hz), 4.68-4.48 (m, 2 H, -NC**H$_2$**$CCHCHCHCC(=O)O$-), 4.36 (d, 1 H, -NC**H$_2$**$CCHCHCHCC(=O)O$-, $^2J_{HH}$ = 16.3 Hz), 4.24 (d, 1 H, -$NCH_2CCHCHCHCC(=O)O$-, $^2J_{HH}$ = 16.0 Hz), 3.02 (br s, 1 H, $NCH(C(=O)O$-$)CH_2CH_2CH_2CH_2NH_2$), 2.99-290 (m, 2 H, $NCH(C(=O)O$-$)CH_2CH_2CH_2C$**H$_2$**NH_2), 1.80 (br s, 2 H, -C**H$_2$**-), 1.65 (br s, 2 H, -C**H$_2$**-), 1.49 (br s, 1 H, -C**H$_2$**-), 1.35 (br s, 1 H, -C**H$_2$**-)

^{13}C{^{1}H} NMR (100 MHz, D_2O (pD = 4.8), 298 K), δ: 167.51 (-**C**$(=O)O$-), 152.87 (-NCH_2**C**$CHCHCHCC(=O)O$-)), 152.02 (-$NCH_2CCHCHCH$**C**$C(=O)O$-),143.56 (-NCH_2CCH**C**$HCHCC(=O)O$-), 127.94 (-NCH_2C**C**$HCHCHCC(=O)O$-), 123.37 (-NCH_2CCHCH**C**$HCC(=O)O$-), 62.82 (-N**C**$H(C(=O)O$-$)CH_2CH_2CH_2CH_2NH_2$), 57.17 (-N**C**$H_2CCHCHCHCC(=O)O$-), 39.15 (-**C**H_2-), 26.85 (-**C**H_2-), 25.57 (-**C**H_2-), 24.50 (-**C**H_2-)

HRMS (ESI), *m/z*: 483.0801 (Calculated for **[^{69}Ga][M + H]$^+$**, $^{69}GaC_{20}H_{22}N_4O_6$: 483.0790)

6.20. Synthesis of Diethyl 6,6'-(((1-ethoxy-1-oxo-3-(tritylthio)propan-2-yl)azanediyl)bis(methylene))(R)-dipicolinate (Et_3Dpaa.cys(Tr))

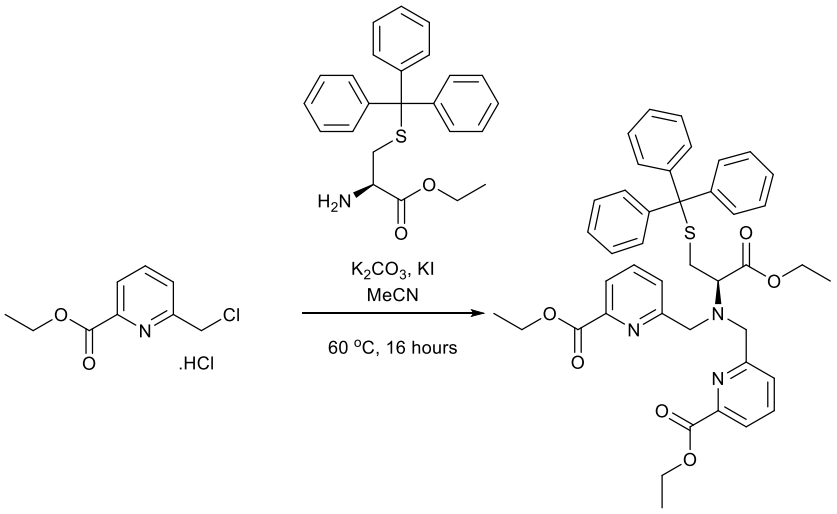

To **4** (0.49 g, 2.1 mmol, 2.1 eq), ethyl S-tritylcysteinate (0.38 g, 1 mmol, 1 eq),potassium carbonate (0.525 g, 3.8 mmol, 3.8 eq) and potassium iodide (0.349 g, 2.1 mmol, 2.1 eq) under argon was added acetonitrile (1.3 mL). The solution was heated to 60 °C for 16 hours under argon. Water (15 mL) was added and the solution extracted with dichloromethane (3 x 10 mL). The combined organic layers were dried with magnesium sulfate and concentrated to yield an orange oil. Purification by column chromatography (silica, Ethyl Acetate/Hexane, 0-100%) yielded a yellow oil (66.3 mg, 92 µmol, 9.2%).

^{1}H NMR (400 MHz, $CDCl_3$, 298 K), δ: 7.93 (d, 2 H, -$NCH_2CCHCHC$**H**$CC(=O)OCH_2CH_3$, $^3J_{HH}$ = 7.8 Hz), 7.81 (d, 2 H, -NCH_2CC**H**$CHCHCC(=O)OCH_2CH_3$, $^3J_{HH}$ = 7.8 Hz), 7.72 (t, 2 H, -NCH_2CCHC**H**$CHCC(=O)OCH_2CH_3$, $^3J_{HH}$ = 7.8 Hz), 7.32 (dt, 6 H, -$NCHCH_2SC($**C$_6$**$H_5)_3$, $^3J_{HH}$ = 6.9 Hz, $^4J_{HH}$ = 1.4 Hz), 7.20 (br t, 6 H, -$NCHCH_2SC($**C$_6$**$H_5)_3$, $^3J_{HH}$ = 6.9 Hz), 7.15 (tt, 3 H, -$NCHCH_2SC($**C$_6$**$H_5)_3$, $^3J_{HH}$ = 6.9 Hz, $^4J_{HH}$ = 1.4 Hz), 4.43 (q, 4 H, -$NCH_2CCHCHCHCC(=O)OC$**H$_2$**CH_3, $^3J_{HH}$ = 6.9 Hz), 4.12 (m, 2 H, -$NCH(C(=O)OC$**H$_2$**$CH_3)CH_2SC(C_6H_5)_3$), 4.03 (d, 2 H, -NC**H$_2$**$CCHCHCHCC(=O)OCH_2CH_3$, $^2J_{HH}$ = 15.1 Hz), 3.93 (d, 2 H, -NC**H$_2$**$CCHCHCHCC(=O)OCH_2CH_3$, $^2J_{HH}$ = 15.1 Hz), 3.26 (dd, 1 H, -NC**H**$(C(=O)OCH_2CH_3)$-$CH_2SC(C_6H5)_3$), $^3J_{HH}$ = 8.7, 6.4 Hz), 2.62 (dd, 1 H, -$NCH(C(=O)OCH_2CH_3)C$**H$_2$**$SC(C_6H_5)_3$, $^2J_{HH}$ = 12.8 Hz, $^3J_{HH}$ = 6.4 Hz), 2.56 (dd, 1 H, -$NCH(C(=O)OCH_2CH_3)C$**H$_2$**$SC(C_6H_5)_3$, $^2J_{HH}$ = 12.8 Hz, $^3J_{HH}$ = 8.7 Hz), 1.40 (t, 6 H, -$NCH_2CCHCHCHCC(=O)OCH_2C$**H$_3$**, $^3J_{HH}$ = 6.9 Hz), 1.24 (t, 3 H, -$NCH(C(=O)OCH_2C$**H$_3$**$)CH_2SC(C_6H_5)_3$, $^3J_{HH}$ = 7.3 Hz)

^{13}C{^{1}H} NMR (100 MHz, $CDCl_3$, 298 K), δ: 171.00 (-$NCH($**C**$(=O)OCH_2$**C**$H_3)CH_2SC(C_6H_5)_3$), 165.19 (-$NCH_2CCHCHCHC$**C**$(=O)OCH_2CH_3$), 159.98 (-NCH_2**C**$CHCHCHCC(=O)OCH_2CH_3$), 147.41 (-$NCH_2CCHCHCH$**C**$C(=O)OCH_2CH_3$), 133.37 (-$NCH(C(=O)OCH_2CH_3)CH_2SC($**C$_6$**$H_5)_3$), 137.29 (-

$NCH_2CCH\mathbf{C}HCHCC(=O)OCH_2CH_3$), 129.48 (-$NCH(C(=O)OCH_2CH_3)CH_2SC(\mathbf{C_6}H_5)_3$), 127.87 (-$NCH(C(=O)OCH_2CH_3)CH_2SC(\mathbf{C_6}H_5)_3$), 126.67 (-$NCH(C(=O)OCH_2CH_3)CH_2SC(\mathbf{C_6}H_5)_3$), 126.08 (-$NCH_2C\mathbf{C}HCHCHCC(=O)OCH_2CH_3$), 123.48 (-$NCH_2CCHCH\mathbf{C}HCC(=O)OCH_2CH_3$), 66.99 (-$NCH(C(=O)OCH_2CH_3)CH_2S\mathbf{C}(C_6H_5)_3$), 63.15 (-$N\mathbf{C}H(C(=O)OCH_2CH_3)CH_2SC(C_6H_5)_3$), 61.83 (-$NCH_2CCHCHCHCC(=O)O\mathbf{C}H_2CH_3$), 60.94 (-$NCH(C(=O)O\mathbf{C}H_2CH_3)CH_2SC(C_6H_5)_3$), 57.01 (-$N\mathbf{C}H_2CCHCHCHCC(=O)OCH_2CH_3$), 31.30 (-$NCH(C(=O)OCH_2CH_3)\mathbf{C}H_2SC(C_6H_5)_3$), 14.29 (-$NCH_2CCHCHCHCC(=O)OCH_2\mathbf{C}H_3$, -$NCH(C(=O)OCH_2\mathbf{C}H_3)CH_2SC(C_6H_5)_3$)

MS (ESI), *m/z*: 718.6 **[M+H]**$^+$

6.21. Synthesis of tri-*tert*-butyl 3,11-dioxo-1-phenyl-2-oxa-4,10,12-triazapentadecane-9,13,15-tricarboxylate (**5**)[222]

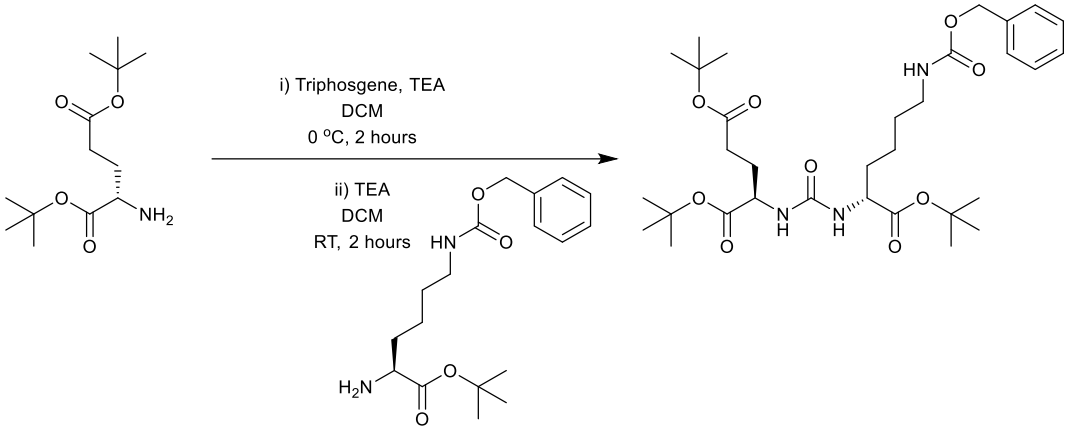

Triphosgene (0.83 g, 2.8 mmol, 1 eq) was dissolved in dry dichloromethane (10 ml) and cooled to 0 °C. To this solution a mixture of L-glutamic acid di-*tert*-butyl ester hydrochloride (2.24 g, 7.6 mmol, 2.7 eq), triethylamine (2.1 ml, 15.2 mmol, 5.4 eq) and dry dichloromethane (30 ml) was added dropwise during 2 h at 0 °C. After stirring for additional 40 min, a solution of N(ε)-benzoyloxycarbonyl-L-lysine *tert*-butyl ester hydrochloride (2.82 g, 7.6 mmol, 2.7 eq), triethylamine (2.1 ml, 15.2 mmol, 5.4 eq) and dry dichloromethane (25 ml) was added and the mixture was stirred at room temperature for 2 h. Afterwards the solution was concentrated and ethyl acetate (50 ml) was added. The organic phase was washed with 2 M $NaHSO_4$ (2 x 50 ml), brine (40 ml) and dried over magnesium sulfate. The solvent was removed under reduced pressure and the residue was purified by silica gel column chromatography (1:1 ethyl acetate / hexane) to give the product as a colorless gum (1.20 g, 1.93 mmol, 25%).

^{1}H NMR (400 MHz, $CDCl_3$, 298 K), δ: 7.36-7.23 (m, 5 H, -NC(=O)NCHCH$_2$CH$_2$CH$_2$CH$_2$NHC(=O)-CH$_2$C$_6$**H$_5$**), 5.52 (m, 2 H, (CH$_3$)$_3$COC(=O)CHN**H**C(=O)N**H**CHC(=O)OC(CH$_3$)$_3$), 5.43 (m, 1 H, -NC(=O)NCHCH$_2$CH$_2$CH$_2$CH$_2$N**H**C(=O)OCH$_2$C$_6$H$_5$), 5.14-5.00 (m, 2 H, -NC(=O)NCHCH$_2$CH$_2$CH$_2$-CH$_2$NHC(=O)OC**H$_2$**C$_6$H$_5$), 4.40-4.25 (m, 2 H, (CH$_3$)$_3$COC(=O)C**H**NHC(=O)NHC**H**C(=O)OC(CH$_3$)$_3$), 3.13 (m , 2 H, -NC(=O)NCHCH$_2$CH$_2$CH$_2$C**H$_2$**NHC(=O)OCH$_2$C$_6$H$_5$), 2.23 (m, 2 H, -NHC(=O)NHCH-CH$_2$C**H$_2$**C(=O)OC(CH$_3$)$_3$), 2.06-1.95 (m, 1 H, -NHC(=O)NHCHC**H$_2$**CH$_2$C(=O)OC(CH$_3$)$_3$), 1.84-1.63 (m, 2 H, -NHC(=O)NHCHC**H$_2$**CH$_2$C(=O)OC(CH$_3$)$_3$, -NC(=O)NCHC**H$_2$**CH$_2$CH$_2$CH$_2$NHC(=O)OCH$_2$C$_6$H$_5$), 1.61-1.44 (m, 3 H, -NC(=O)NCHC**H$_2$**CH$_2$C**H$_2$**CH$_2$NHC(=O)OCH$_2$C$_6$H$_5$), 1.42 (s, 6 H, -C(=O)OC(C**H$_3$**)$_3$), 1.40 (s, 12 H, -C(=O)OC(C**H$_3$**)$_3$), 1.39 (s, 9 H, -C(=O)OC(C**H$_3$**)$_3$), 1.34-1.20 (m, 2 H, -NC(=O)NCHCH$_2$C**H$_2$**CH$_2$CH$_2$NHC(=O)OCH$_2$C$_6$H$_5$)

^{13}C{^{1}H} NMR (100 MHz, $CDCl_3$, 298 K), δ: 172.87 (-**C**(=O)OC(CH$_3$)$_3$), 172.50 (-**C**(=O)OC(CH$_3$)$_3$), 172.26 (-**C**(=O)OC(CH$_3$)$_3$), 157.03 ((CH$_3$)$_3$COC(=O)CHNH**C**(=O)NHCHC(=O)OC(CH$_3$)$_3$), 156.59 (-NHC(=O)NHCHCH$_2$CH$_2$CH$_2$CH$_2$NHCH$_2$**C$_6$**H$_5$), 136.65 (-NHC(=O)NHCHCH$_2$CH$_2$CH$_2$CH$_2$NHCH$_2$**C$_6$**H$_5$), 128.35 (-NHC(=O)NHCHCH$_2$CH$_2$CH$_2$CH$_2$NHCH$_2$**C$_6$**H$_5$), 127.95 (-NHC(=O)NHCHCH$_2$CH$_2$CH$_2$CH$_2$NH-CH$_2$**C$_6$**H$_5$), 127.87 (-NHC(=O)NHCHCH$_2$CH$_2$CH$_2$CH$_2$NHCH$_2$**C$_6$**H$_5$), 82.08 (-C(=O)O**C**(CH$_3$)$_3$), 81.50 (-

C(=O)O**C**$(CH_3)_3$), 80.37 (-C(=O)O**C**$(CH_3)_3$), 66.37 (-NHC(=O)NHCHCH$_2$CH$_2$CH$_2$CH$_2$NH**C**H$_2$C$_6$H$_5$), 53.15 (-NHC(=O)NH**C**HCH$_2$CH$_2$CH$_2$CH$_2$NHCH$_2$C$_6$H$_5$) 52.73 (-NHC(=O)NH**C**HCH$_2$CH$_2$C(=O)OC$(CH_3)_3$), 40.81 (-NHC(=O)NHCHCH$_2$CH$_2$CH$_2$**C**H$_2$NHCH$_2$C$_6$H$_5$), 32.53 (-NHC(=O)NHCH**C**H$_2$CH$_2$CH$_2$CH$_2$NH-CH$_2$C$_6$H$_5$), 31.48 (-NHC(=O)NHCHCH$_2$**C**H$_2$C(=O)OC$(CH_3)_3$), 29.24 (-NHC(=O)NHCH-CH$_2$CH$_2$**C**H$_2$CH$_2$NHCH$_2$C$_6$H$_5$), 28.23 (-NHC(=O)NHCH**C**H$_2$CH$_2$C(=O)OC$(CH_3)_3$), 27.97 (-C(=O)O-C(**C**H$_3)_3$), 27.91 (-C(=O)OC(**C**H$_3)_3$), 22.29 (-NHC(=O)NHCHCH$_2$**C**H$_2$CH$_2$CH$_2$NHCH$_2$C$_6$H$_5$)

MS (ESI), *m/z*: 622.8 **[M+H]**$^+$

6.22. Synthesis of di-*tert*-butyl ((6-amino-1-(*tert*-butoxy)-1-oxohexan-2-yl)carbamoyl)glutamate (**6**)[222]

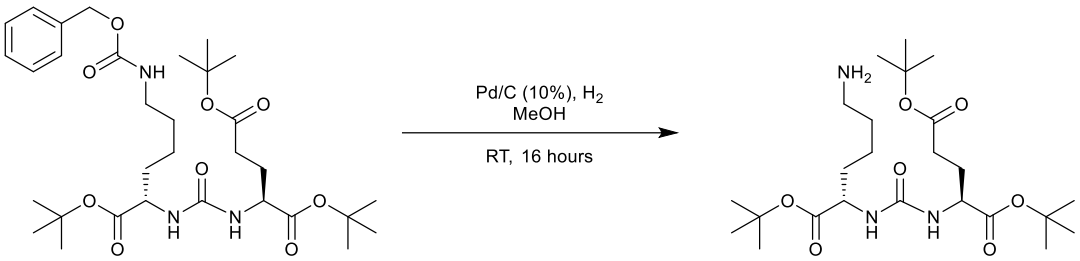

5 (600 mg, 0.97 mmol) was dissolved in dry methanol (15 ml). Palladium on carbon (10%) (50 mg) was added and the reaction stirred under atmospheric pressure hydrogen at room temperature overnight. The reaction mixture was filtered and the solution concentrated to give a colourless oil (460 mg, 0.94 mmol, 97%).

^{1}H NMR (400 MHz, $CDCl_3$, 298 K), δ: 5.08 (d, 1 H, $(CH_3)_3COC(=O)CHN\mathbf{H}C(=O)N\mathbf{H}CHC(=O)OC(CH_3)_3$, $^{3}J_{HH}$ = 3.2 Hz), 5.06 (d, 1 H, $(CH_3)_3COC(=O)CHN\mathbf{H}C(=O)N\mathbf{H}CHC(=O)OC(CH_3)_3$, $^{3}J_{HH}$ = 3.2 Hz), 4.37-4.30 (m, 2 H, $(CH_3)_3COC(=O)C\mathbf{H}NHC(=O)NHC\mathbf{H}C(=O)OC(CH_3)_3$), 2.68 (t, 2 H, -NHC(=O)NHCHCH$_2$CH$_2$CH$_2$C$\mathbf{H_2}$NH$_2$, $^{3}J_{HH}$ = 6.6 Hz), 2.40-2.23 (m, 2 H, -NHC(=O)NHCHCH$_2$C$\mathbf{H_2}$C(=O)OC$(CH_3)_3$), 2.13-2.02 (m, 1 H, -NHC(=O)NHCHC$\mathbf{H_2}$CH$_2$C(=O)OC$(CH_3)_3$), 1.91-1.73 (m, 3 H, -NHC(=O)NHCHC$\mathbf{H_2}$CH$_2$C(=O)OC$(CH_3)_3$ + -NHC(=O)NHCHC$\mathbf{H_2}$CH$_2$CH$_2$CH$_2$NH$_2$), 1.67-1.57 (m, 2 H, -NHC(=O)NHCHCH$_2$CH$_2$C$\mathbf{H_2}$CH$_2$NH$_2$), 1.47 (s, 18 H, -C(=O)OC(C$\mathbf{H_3}$)$_3$), 1.44 (s, 9 H, -C(=O)OC(C$\mathbf{H_3}$)$_3$), 1.41-1.28 (m, 2 H, -NHC(=O)NHCHCH$_2$C$\mathbf{H_2}$CH$_2$CH$_2$NH$_2$)

^{13}C{^{1}H} NMR (100 MHz, $CDCl_3$, 298 K), δ: 172.50 (-**C**(=O)OC$(CH_3)_3$), 172.46 (-**C**(=O)OC$(CH_3)_3$), 172.10 (-**C**(=O)OC$(CH_3)_3$), 156.70 ($(CH_3)_3OC(=O)CHNH\mathbf{C}(=O)NHCHC(=O)OC(CH_3)_3$), 82.05 (-C(=O)O**C**$(CH_3)_3$), 81.72 (-C(=O)O**C**$(CH_3)_3$), 80.52 (-C(=O)O**C**$(CH_3)_3$), 53.43 ($(CH_3)_3C\mathbf{C}HNHC(=O)NH\mathbf{C}HC(=O)OC(CH_3)_3$), 53.01 ($(CH_3)_3C\mathbf{C}HNHC(=O)NH\mathbf{C}HC(=O)OC(CH_3)_3$), 41.92 (-NHC(=O)NHCHCH$_2CH_2CH_2$**C**H$_2NH_2$), 33.35 (-NHC(=O)NHCHCH$_2CH_2$**C**H$_2CH_2NH_2$), 33.04 (-NHC(=O)NHCH**C**H$_2$CH$_2$CH$_2$CH$_2$NH$_2$), 31.56 (-NHC(=O)NHCHCH$_2$**C**H$_2$C(=O)OC$(CH_3)_3$), 28.39 (-NHC(=O)NHCH**C**H$_2$CH$_2$C(=O)OC$(CH_3)_3$), 28.06 (-C(=O)OC(**C**H$_3)_3$), 28.01 (-C(=O)OC(**C**H$_3)_3$), 27.99 (-C(=O)OC(**C**H$_3)_3$), 22.34 (-NHC(=O)NHCHCH$_2$**C**H$_2$CH$_2$CH$_2$NH$_2$)

MS (ESI), *m/z*: 488.8 **[M+H]$^{+}$**

6.23. Synthesis of 6-((*tert*-butoxycarbonyl)amino)hexanoic acid (**7**)[222]

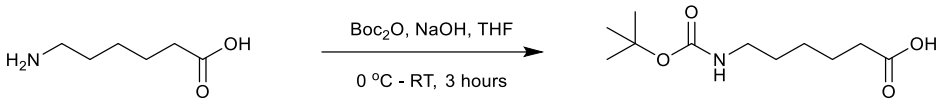

To 6-aminohexanoic acid (1.27 g, 9.7 mmol) in tetrahydrofuran (25 mL) was added 1 M NaOH (10 mL, 10 mmol). The solution was cooled in an ice bath. Di-*tert*butyl carbonate (2.8 g, 12.6 mmol, 1.3 eq) was added and stirring continued with cooling for 1 hour. The ice bath was removed and stirring continued for 3 hours.

The solvent was removed and the residue partitioned between diethyl ether (20 mL) and water (20 mL). The organic later was discarded and the aqueous phase acidified with 1 N HCl to pH 1. The aqueous layer was extracted with diethyl ether (2 x 20 mL). The combined organic phases were dried with magnesium sulfate and concentrated to yield a white solid (1.89 g, 8.1 mmol, 84%).

^{1}H NMR (400 MHz, $CDCl_3$, 298 K), δ: 4.56 (br s, 1 H, $(CH_3)_3COC(=O)N\mathbf{H}CH_2CH_2CH_2CH_2CH_2C(=O)$-OH), 3.12 (br s, 2 H, $(CH_3)_3COC(=O)NHC\mathbf{H_2}CH_2CH_2CH_2CH_2C(=O)OH$), 2.35 (br s, 2 H, $(CH_3)_3CO$-$C(=O)NHCH_2CH_2CH_2CH_2C\mathbf{H_2}C(=O)OH$), 1.70-1.59 (m, 2 H, $(CH_3)_3COC(=O)NHCH_2CH_2CH_2C\mathbf{H_2}$-$CH_2C(=O)OH$), 1.54-1.48 (m, 2 H, $(CH_3)_3COC(=O)NHCH_2C\mathbf{H_2}CH_2CH_2CH_2C(=O)OH$), 1.44 (s, 9 H, $(C\mathbf{H_3})_3COC(=O)NHCH_2CH_2CH_2CH_2CH_2C(=O)OH$), 1.41-1.32 (m, 2 H, $(CH_3)_3COC(=O)NHCH_2CH_2C\mathbf{H_2}$-$CH_2CH_2C(=O)OH$)

^{13}C{^{1}H} NMR (100 MHz, $CDCl_3$, 298 K), δ: 178.85 ($(CH_3)_3COC(=O)NHCH_2CH_2CH_2CH_2CH_2\mathbf{C}(=O)OH$), 155.99 ($(CH_3)_3CO\mathbf{C}(=O)NHCH_2CH_2CH_2CH_2CH_2C(=O)OH$), 79.17 ($(CH_3)_3\mathbf{C}OC(=O)NHCH_2CH_2$-$CH_2CH_2CH_2(=O)OH$), 40.31 ($(CH_3)_3COC(=O)NH\mathbf{C}H_2CH_2CH_2CH_2CH_2C(=O)OH$), 33.80 ($(CH_3)_3CO$-$C(=O)NHCH_2CH_2CH_2CH_2\mathbf{C}H_2C(=O)OH$), 29.69 ($(CH_3)_3COC(=O)NHCH_2CH_2CH_2\mathbf{C}H_2CH_2C(=O)OH$), 28.38 ($(\mathbf{C}H_3)_3COC(=O)NHCH_2CH_2CH_2CH_2CH_2C(=O)OH$), 26.17 ($(CH_3)_3COC(=O)NHCH_2CH_2\mathbf{C}H_2$-$CH_2CH_2C(=O)OH$), 24.29 ($(CH_3)_3COC(=O)NHCH_2\mathbf{C}H_2CH_2CH_2CH_2C(=O)OH$)

MS (ESI), *m/z*: 232.3 **$[M+H]^+$**

6.24. Synthesis of tri-*tert*-butyl 2,2-dimethyl-4,11,19-trioxo-3,18-dioxa-5,12,20-triazatricosane-17,21,23-tricarboxylate (**8**)[222]

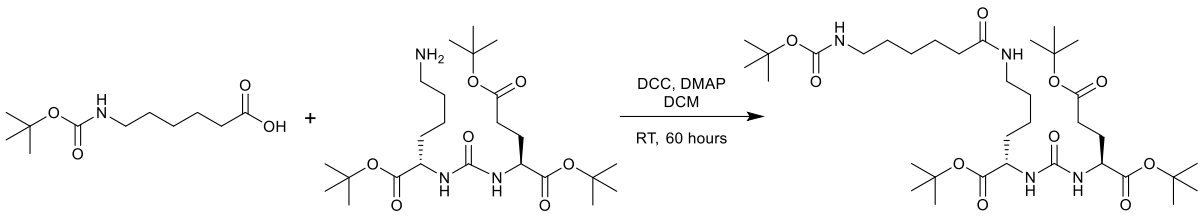

7 (157 mg, 0.678 mmol, 1.1 eq), **6** (300 mg, 0.616 mmol, 1 eq), N,N'-dicyclohexylcarbodiimide (152 mg, 0.739 mmol, 1.2 eq) and N,N-dimethyl-4-aminopyridine (152 mg, 0.739 mmol, 1.2 eq) were dissolved in anhydrous dichloromethane (10 mL) and stirred at room temperature under argon for 60 hours. After filtering, the solution was concentrated to yield a clear oil. This was purified by column chromatography (silica, Ethyl acetate/Hexane, 50-60%) to yield a clear oil (198 mg, 0.28 mmol, 46%).

^{1}H NMR (400 MHz, $CDCl_3$, 298 K), δ: 6.04 (br s, 1 H, -CH_2C(=O)N**H**$CH_2CH_2CH_2CH_2$CHNHC(=O)NH-), 5.33 (br s, 1 H, $(CH_3)_3$COC(=O)N**H**$CH_2CH_2CH_2CH_2CH_2$C(=O)NHCH_2-), 4.67 (br s, 1 H, $(CH_3)_3$COC(=O)CHN**H**C(=O)N**H**CHC(=O)OC$(CH_3)_3$), 4.33 (br s, 2 H, -$(CH_3)_3$COC(=O)CHN**H**-C(=O)N**H**CHC(=O)OC$(CH_3)_3$), 3.38-3.28 (m, 1 H, -CH_2C(=O)NHC**H$_2$**$CH_2CH_2CH_2$CHNHC(=O)NH-), 3.19-3.06 (m, 3 H, -CH_2C(=O)NHC**H$_2$**$CH_2CH_2CH_2$CHNHC(=O)NH-, $(CH_3)_3$COC(=O)NH-C**H$_2$**$CH_2CH_2CH_2CH_2$C(=O)NHCH_2-), 2.41-2.25 (m, 2 H, --NHC(=O)NHCHCH_2C**H$_2$**C(=O)OC$(CH_3)_3$), 2.22-2.15 (m, 2H, $(CH_3)_3$COC(=O)NHC$H_2CH_2CH_2CH_2$C**H$_2$**C(=O)NHCH_2-), 2.13-2.03 (m, 1 H, -NHC(=O)NHCHC**H$_2$**CH_2C(=O)OC$(CH_3)_3$), 1.90-1.76 (m, 2 H, -NHC(=O)NHCHC**H$_2$**-), 1.69-1.58 (m, 3 H, -NHC(=O)NHCHC**H$_2$**-, -C**H$_2$-**), 1.56-1.48 (m, 4 H, -C**H$_2$-**), 1,47 (br s, 9 H, -C(=O)OC(C**H$_3$**)$_3$), 1.46 (br s, 9 H, -C(=O)OC(C**H$_3$**)$_3$), 1.45-1.43 (br s, 18 H, -C(=O)OC(C**H$_3$**)$_3$), 1.43-1.23 (m, 4 H, -C**H$_2$-**)

^{13}C{^{1}H} NMR (100 MHz, $CDCl_3$, 298 K), δ: 173.18 ($(CH_3)_3$COC(=O)NHC$H_2CH_2CH_2CH_2CH_2$**C**(=O)-NHCH_2-), 172.37 ($(CH_3)_3$CO**C**(=O)-), 157.09 (-$(CH_3)_3$COC(=O)CHNH**C**(=O)NHCHC(=O)OC$(CH_{3)3})$, 82.00 (-C(=O)O**C**$(CH_3)_3$), 81.62 (-C(=O)O**C**$(CH_3)_3$), 80.55 (-C(=O)O**C**$(CH_3)_3$), 53.12 ($(CH_3)_3$OC(=O)**C**HNHC(=O)NH**C**HC(=O)OC$(CH_3)_3$), 40.42 (-CH_2C(=O)NH**C**$H_2CH_2CH_2CH_2$CHNHC(=O)-NH-), 38.82 ($(CH_3)_3$COC(=O)NH**C**$H_2CH_2CH_2CH_2CH_2$C(=O)NHCH_2-), 36.48 ($(CH_3)_3$COC(=O)-NHC$H_2CH_2CH_2CH_2$**C**H_2C(=O)NHCH_2-), 32.50 (-**C**H_2-), 31.64 (-NHC(=O)NHCHCH_2**C**H_2C(=O)O-C$(CH_3)_3$), 29.60 (-**C**H_2-), 28.69 (-**C**H_2-), 28.43 (-C(=O)OC(**C**$H_3)_3$), 28.07 (-C(=O)OC(**C**$H_3)_3$), 28.00 (-C(=O)OC(**C**$H_3)_3$), 28.23 (-**C**H_2-), 26.25 (-**C**H_2-), 25.33 (-**C**H_2-), 22.20 (-**C**H_2-)

MS (ESI), *m/z*: 701.5 **[M+H]$^+$**

6.25. Synthesis of (((5-(6-aminohexanamido)-1-carboxypentyl)oxy)carbonyl)glutamic acid (**9**)[222]

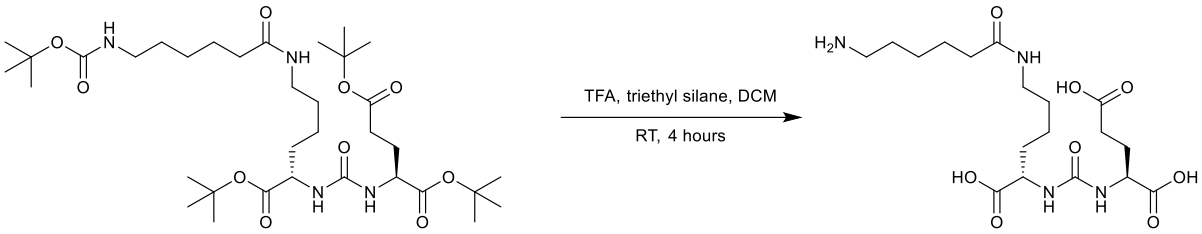

To **8** (170 mg, 0.24 mmol) was added dichloromethane (2 mL), trifluoroacetic acid (1 mL) and triethylsilane (0.4 mL, 2.5 mmol, 10 eq). The solution was stirred at room temperature for 4 hours and concentrated. The oil was triturated with diethyl ether (3x3 mL) and dried to yield a clear gum (80 mg, 0.18 mmol, 76%)

^{1}H NMR (400 MHz, D_2O, 298 K), δ: 4.20 (dd, 1 H, -NHC(=O)NHC**H**(C(=O)OH)CH_2CH_2C(=O)OH, $^3J_{HH}$ = 8.7, 5.0 Hz), 4.12 (dd, 1 H, -CH_2C(=O)NHC$H_2CH_2CH_2CH_2$C**H**(C(=O)OH)NHC(=O)NH-, $^3J_{HH}$ = 8.5, 5.3 Hz), 3.14 (t, 2 H, $H_2NCH_2CH_2CH_2CH_2$C**H_2**C(=O)NHCH_2-, $^3J_{HH}$ = 6.6 Hz), 2.93 (t, 2 H, H_2NC**H_2**$CH_2CH_2CH_2CH_2$C(=O)NHCH_2-, $^3J_{HH}$ = 7.6 Hz), 2.46 (t, 2 H, -NHC(=O)NHCH(C(=O)OH)-CH_2C**H_2**C(=O)OH, $^3J_{HH}$ = 7.3 Hz), 2.20 (t, 2 H, -CH_2C(=O)NHC**H_2**$CH_2CH_2CH_2$CH-(C(=O)OH)NHC(=O)NH-, $^3J_{HH}$ = 7.3 Hz), 2.13 (dtd, 1 H, -NHC(=O)NHCH(C(=O)OH)C**H_2**CH_2C(=O)OH, $^2J_{HH}$ = 14.5 Hz, $^3J_{HH}$ = 7.3, 5.0 Hz), 1.92 (ddt, 1 H, -NHC(=O)NHCH(C(=O)OH)C**H_2**CH_2C(=O)OH, $^2J_{HH}$ = 14.5 Hz, $^3J_{HH}$ = 8.7, 7.3 Hz), 1.79 (dtd, 1 H, -CH_2C(=O)NHC$H_2CH_2CH_2$C**H_2**CH(C(=O)-OH)NHC(=O)NH-, $^2J_{HH}$ = 13.5 Hz, $^3J_{HH}$ = 7.3, 5.3 Hz), 1.71-1.53 (m, 5 H, -CH_2C(=O)NH-$CH_2CH_2CH_2$C**H_2**CH(C(=O)OH)NHC(=O)NH-, -C**H_2**-), 1.48 (quin, 2 H, $H_2NCH_2CH_2CH_2$C**H_2**CH_2C(=O)-NHCH_2-, $^3J_{HH}$ = 6.9 Hz), 1.31-1.26 (m, 4 H, -C**H_2**-)

^{13}C{^{1}H} NMR (100 MHz, D_2O, 298 K), δ: 177.44 (-**C**(=O)OH), 176.59 (-**C**(=O)N-), 159.34 (-NH**C**(=O)NH-), 53.41 (-CH_2C(=O)NH$CH_2CH_2CH_2$C**H**(C(=O)OH)NHC(=O)NH-), 52.84 (-NHC(=O)NH**C**H(C(=O)OH)CH_2CH_2C(=O)OH), 39.28 ($H_2NCH_2CH_2CH_2CH_2$**C**H_2C(=O)NHCH_2-), 38.92 (H_2N**C**$H_2CH_2CH_2CH_2CH_2$C(=O)NHCH_2-), 35.50 (-CH_2C(=O)NH**C**$H_2CH_2CH_2CH_2$CH(C(=O)OH)-NHC(=O)NH-), 30.69 (-CH_2C(=O)NH$CH_2CH_2CH_2$**C**H_2CH(C(=O)OH)NHC(=O)NH-), 30.18 (-NHC(=O)NHCH(C(=O)OH)CH_2**C**H_2C(=O)OH), 27.75 ($H_2NCH_2CH_2CH_2$**C**H_2CH_2C(=O)NHCH_2-), 26.44 (-NHC(=O)NHCH(C(=O)OH)**C**H_2CH_2C(=O)OH, H_2NCH_2**C**$H_2CH_2CH_2CH_2$C(=O)NHCH_2-), 25.05 (-CH_2C(=O)NHCH_2**C**$H_2CH_2CH_2$CH(C(=O)OH)NHC(=O)NH-), 24.88 ($H_2NCH_2CH_2$**C**$H_2CH_2CH_2$C(=O)NH-), 22.31 (-CH_2C(=O)NHCH_2CH_2**C**H_2CH_2CH(C(=O)OH)NHC(=O)NH-)

MS (ESI), *m/z*: 433.5 **[M + H]$^+$**

6.26. Synthesis of (S)-6,6'-(((2,6-dioxotetrahydro-2H-pyran-3-yl)azanediyl)bis(methylene))dipicolinic acid (H_2Dpaa.ga.anh)

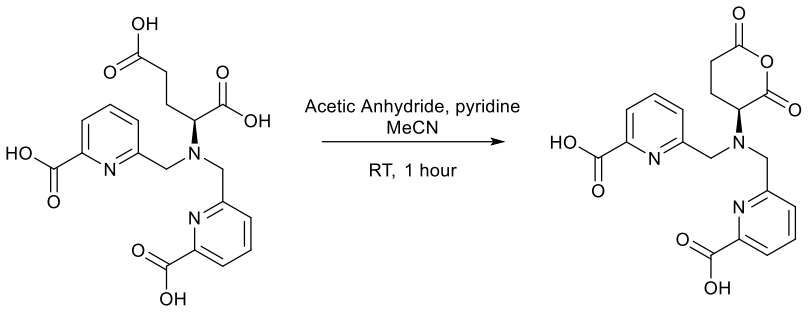

To a suspension of H_4Dpaa.ga (14 mg, 0.03 mmol, 1 eq) in acetonitrile (1.5 mL) was added acetic anhydride (5 mg, 4.7 µL, 0.05 mmol, 1.5 eq) and pyridine (7.9 mg, 8.1 µL, 0.10 mmol, 3.0 eq). The solution was stirred for 1 hour at room temperature, with the solid dissolving over time. Precipitation was induced by addition of diethyl ether (1 mL) and the suspension filtered through celite. The precipitate was washed with diethyl ether. The product was released from the celite plug with acetonitrile (1 mL) and dried under vacuum. This was used without further purification.

^{1}H NMR (400 MHz, *d_3*-MeCN, 298 K), *δ*: 7.95 (d, 2 H, -NCH$_2$CCHCHC**H**CC(=O)OH, $^3J_{HH}$ = 7.8 Hz), 7.90 (t, 2 H, -NCH$_2$CCHC**H**CHCC(=O)OH, $^3J_{HH}$ = 7.8 Hz), 7.73 (d, 2 H, -NCH$_2$CC**H**CHCHCC(=O)OH, $^3J_{HH}$ = 7.8 Hz), 4.22 (d, 2 H, -NC**H$_2$**CCHCHCHCC(=O)OH, $^2J_{HH}$ = 15.1 Hz), 4.12 (d, 2 H, -NC**H$_2$**CCHCHCHCC(=O)OH, $^2J_{HH}$ = 15.1 Hz), 3.98 (dd, 1 H, -NC**H**(C(=O)O-)CH$_2$CH$_2$C(=O)O-, $^3J_{HH}$ = 12.4, 5.5 Hz), 2.90 (ddd, 1 H, -NCH(C(=O)O-)CH$_2$C**H$_2$**C(=O)O-, $^2J_{HH}$ = 18.2 Hz, $^3J_{HH}$ = 5.5 Hz, 2.0 Hz), 2.81 (dt, 1 H, -NCH(C(=O)O-)CH$_2$C**H$_2$**C(=O)O-, $^2J_{HH}$ = 18.2 Hz, $^3J_{HH}$ = 6.0 Hz), 2.29 (dddd, 1H, -NCH(C(=O)O-)C**H$_2$**CH$_2$C(=O)O-, $^2J_{HH}$ = 18.5, $^3J_{HH}$ = 12.4, 6.0, 2.0 Hz), 2.26 (ddt, 1H, -NCH(C(=O)O-)C**H$_2$**CH$_2$C(=O)O-, $^2J_{HH}$ = 18.5 Hz, $^3J_{HH}$ = 6.0, 5.5 Hz)

^{13}C{^{1}H} NMR (100 MHz, *d_3*-MeCN, 298 K), *δ*: 169.20 (-NCH(**C**(=O)O-)CH$_2$CH$_2$C(=O)O-), 167.91 (-NCH(C(=O)O-)CH$_2$CH$_2$**C**(=O)O-), 165.90 (-NCH$_2$CCHCHCHC**C**(=O)OH), 159.73 (-NCH$_2$**C**CH-CHCHCC(=O)OH), 147.14 (-NCH$_2$CCHCHCH**C**C(=O)OH), 140.18 (-NCH$_2$CCH**C**HCHCC(=O)OH), 128.21 (-NCH$_2$C**C**HCHCHCC(=O)OH), 123.54 (-NCH$_2$CCHCH**C**HCC(=O)OH), 62.41 (-N**C**H(C(=O)O-)CH$_2$CH$_2$C(=O)O-), 57.43 (-N**C**H$_2$CCHCHCHCC(=O)OH), 30.77 (-NCH(C(=O)O-)CH$_2$**C**H$_2$C(=O)O-), 22.03 (-NCH(C(=O)O-)**C**H$_2$CH$_2$C(=O)O-)

MS (ESI), *m/z*: 400.3 **[M + H]$^+$**

6.27. Synthesis of (3S,19S,23S)-1-(6-carboxypyridin-2-yl)-2-((6-carboxypyridin-2-yl)methyl)-6,13,21-trioxo-2,7,14,20,22-pentaazapentacosane-3,19,23,25-tetracarboxylic acid (H_3Dpaa.ga.PSMA)

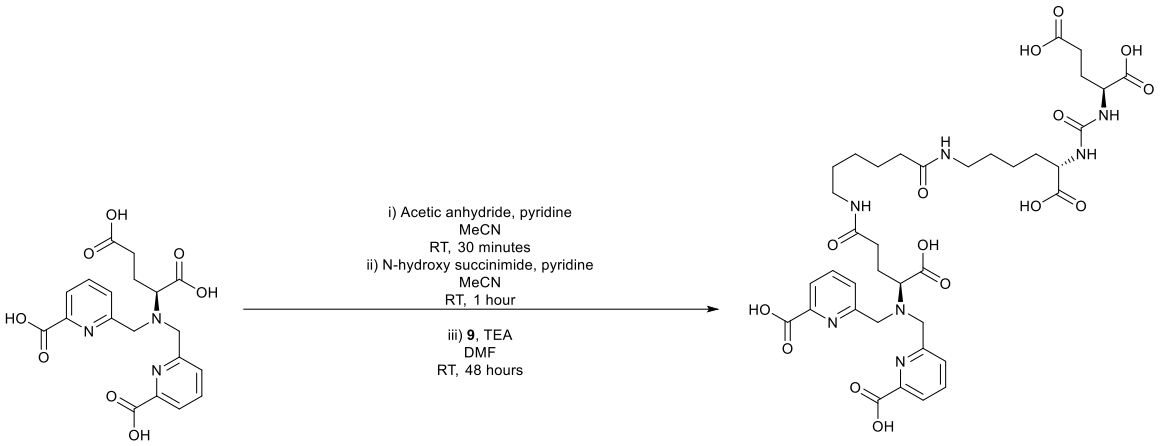

To H_4Dpaa.ga (45.0 mg, 0.11 mmol, 3 eq) was added acetic anhydride (17.3 mg, 16 µL, 0.17 mmol, 4.5 eq), pyridine (24.6 mg, 25 µL, 0.31 mmol, 9 eq) and acetonitrile (0.5 mL). The solution was stirred at room temperature for 30 minutes and diethyl ether (1.0 mL) was added. The solid was isolated and used without further purification.

N-hydroxysuccinimide (37.3 mg, 0.31 mmol, 4.7 eq), pyridine (24.6 mg, 25 µL, 0.31 mmol, 8 eq) and acetonitrile (1.2 mL) were added and stirring continued for 1 hour.

9 (30 mg, 0.07 mmol, 1 eq), triethylamine (219 mg, 0.3 mL, 2.17 mmol, 32 eq) and dimethylformamide (1.0 mL) were added and the solution stirred for 48 hours.

The solution was concentrated under vacuum and the residue purified by semi-preparative HPLC (Methanol + 0.1% TFA/Water + 0.1% TFA) to yield a clear oil (3.0 mg, 0.004 mmol, 6%).

^{1}H NMR (400 MHz, D_2O, 298 K), δ: 8.09 (t, 2 H, -NCH_2CCHCH**H**$CHCC(=O)OH$, $^3J_{HH}$ = 7.8 Hz), 7.97 (d, 2 H, -$NCH_2CCHCHCH$**H**$CC(=O)OH$, $^3J_{HH}$ = 7.8 Hz), 7.72 (d, 2 H, -NCH_2CC**H**$CHCHCC(=O)OH$, $^3J_{HH}$ = 7.8 Hz), 4.49 (d, 2 H, -NC**H$_2$**$CCHCHCHCC(=O)OH$, $^2J_{HH}$ = 16.0 Hz), 4.45 (d, 2 H, -NC**H$_2$**$CCHCHCHCC(=O)$-OH, $^2J_{HH}$ = 16.0 Hz), 4.15 (dd, 1 H, $NHC(=O)NHC$**H**$(C(=O)OH)CH_2CH_2C(=O)OH$, $^3J_{HH}$ = 8.9, 5.3 Hz), 4.07 (dd, 1 H, -$CH_2C(=O)NHCH_2CH_2CH_2CH_2C$**H**$(C(=O)OH)NHC(=O)NH$-, $^3J_{HH}$ = 7.8, 5.0 Hz), 3.82 (t, 1 H, NC**H**$(C(=O)OH)CH_2CH_2C(=O)NHCH_2$, $^3J_{HH}$ = 6.9 Hz), 3.07 (t, 2 H, -$CH_2C(=O)NHCH_2CH_2CH_2$-CH_2C**H$_2$**$C(=O)NHCH_2$-, $^3J_{HH}$ = 6.4 Hz), 3.01 (t, 2 H, $NCH(C(=O)OH)CH_2C$**H$_2$**$C(=O)NHCH_2$-, $^3J_{HH}$ = 6.9 Hz), 2.46 (t, 2 H, -$CH_2C(=O)NHC$**H$_2$**$CH_2CH_2CH_2CH_2C(=O)NHCH_2$-, $^3J_{HH}$ = 6.9 Hz), 2.40 (t, 2 H, -$NHC(=O)NHCH(C(=O)OH)CH_2C$**H$_2$**$C(=O)OH$, $^3J_{HH}$ = 7.3 Hz), 2.30-2.14 (m, 2 H, $NCH(C(=O)OH)C$**H$_2$**-$CH_2C(=O)NHCH_2$-), 2.11-2.00 (m, 2 H, -$CH_2C(=O)NHC$**H$_2$**$CH_2CH_2CH_2CH_2CH(C(=O)OH)NHC(=O)NH$-

), 1.85 (m, 1 H, -C**H$_2$**-), 1.73 (m, 1 H, -C**H$_2$**-), 1.59 (m, 1 H, -C**H$_2$**-), 1.50-1.37 (m, 4 H, -C**H$_2$**-), 1.37-1.23 (m, 4 H, -C**H$_2$**-), 1.20-1.10 (m, 2 H, -C**H$_2$**-)

^{13}C{^{1}H} NMR (100 MHz, D_2O, 298 K), *δ*: 177.54 (-NHC(=O)NHCH**C**(=O)OH), 176.81 (-NHC(=O)NHCH(C(=O)OH)CH_2CH_2**C**(=O)OH), 176.72 (-CH_2NH**C**(=O)$CH_2CH_2CH_2CH_2CH_2$NHC(=O)-CH_2-), 175.42 (-CH_2NHCHCH_2CH_2**C**(=O)NHCH_2-), 174.74 (-NCH(**C**(=O)OH)CH_2CH_2C(=O)NHCH_2-), 164.57 (-NCH_2CCHCHCHC**C**(=O)OH), 154.04 (-NCH_2**C**CHCHCHCC(=O)OH), 145.55 -NCH_2CCH-CHCH**C**C(=O)OH), 143.72 (-NCH_2CCH**C**HCHCC(=O)OH), 128.39 (-NCH_2C**C**HCHCHCC(=O)OH), 125.13 (-NCH_2CCHCH**C**HCC(=O)OH), 65.99 (-N**C**H(C(=O)OH)CH_2CH_2C(=O)NHCH_2-, 56.04 (-N**C**H_2CCHCHCHCC(=O)OH), 53.24 (-NHC(=O)NH**C**H(C(=O)OH)$CH_2CH_2CH_2CH_2$NHC(=O)CH_2-), 52.74 (-NHC(=O)NH**C**H(C(=O)OH)CH_2CH_2C(=O)OH), 38.81 (-CH_2NHC(=O)**C**$H_2CH_2CH_2CH_2CH_2$NHC(=O)-CH_2-), 35.91 (-NHC(=O)NHCH(C(=O)OH)$CH_2CH_2CH_2$**C**H_2NHC(=O)CH_2-), 34.48 (-NCH(C(=O)OH)CH_2-**C**H_2C(=O)NHCH_2-), 32.82 (-CH_2NHC(=O)$CH_2CH_2CH_2CH_2$**C**H_2NHC(=O)CH_2-), 30.13 (-NHC(=O)NH-CH(C(=O)OH)CH_2**C**H_2C(=O)OH), 28.15 (-**C**H_2-), 25.80 (-NHC(=O)NHCH(C(=O)OH)**C**H_2CH_2C(=O)OH), 25.47 (-**C**H_2-), 24.93 (-NHC(=O)NHCHCH_2CH_2**C**H_2CH_2NHC(=O)CH_2-), 24.76 (-NCH(C(=O)OH)**C**H_2-CH_2C(=O)NHCH_2-), 22.85 (-**C**H_2-)

HRMS (ESI), *m/z*: 832.3359 (Calculated for **[M+H]$^+$**, $C_{37}H_{50}N_7O_{15}$: 832.3365)

HPLC: Flow Rate: 3 ml min^{-1}. Solvent A: Methanol + 0.1% TFA. Solvent B: Water + 0.1% trifluoroacetic acid. Gradient, ([Time / minutes] Solvent A: Solvent B): [0] 5:95, [10] 5:95, [11], 10:90, [21] 10:90, [22] 20:80, [32] 20:80, [33] 30:70, [43] 30:70, [44] 50:50, [54] 50:50. Retention time: 42 minutes.

6.28. Synthesis of triethyl 6,6',6''-(nitrilotris(methylene))tripicolinate (Et_3Tpaa)

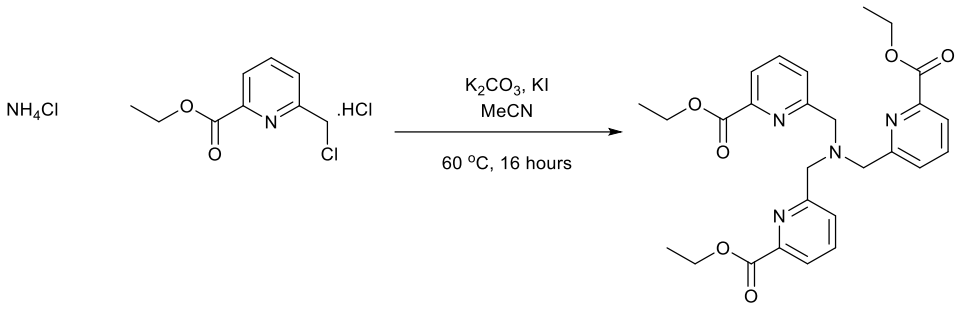

4 (790 mg, 3.30 mmol, 3.3 eq), ammonium chloride (53 mg, 1.00 mmol, 1.0 eq), potassium carbonate (1.10 g, 8.00 mmol, 8.0 eq), and potassium iodide (550 mg, 3.30 mmol, 3.3 eq) were combined in acetonitrile (10 mL) and heated to 60 °C for 16 h. Water (50 mL) was added and the solution extracted into dichloromethane (3 x 50 mL). The combined organic layers were dried with magnesium sulfate and dried to yield a dark orange oil. Purification by column chromatography (silica, dichloromethane/methanol, 0-4%) yielded a yellow/brown solid. Purification by recrystallization from ethyl acetate/dichloromethane (3:1) with hexane yielded an off white solid (80 mg, 0.16 mmol, 16%).

^{1}H NMR (400 MHz, $CDCl_3$, 298 K), δ: 8.02 (d, 3 H, -$NCH_2CCHCHC\mathbf{H}CC(=O)OCH_2CH_3$, $^3J_{HH}$ = 7.8 Hz), 7.90 (t, 3 H, -$NCH_2CCHC\mathbf{H}CHCC(=O)OCH_2CH_3$, $^3J_{HH}$ = 7.8 Hz), 7.74 (d, 3 H, -$NCH_2CC\mathbf{H}CHCHCC(=O)O$-$CH_2CH_3$, $^3J_{HH}$ = 7.8 Hz), 4.61 (q, 6 H, -$NCH_2CCHCHCHCC(=O)OC\mathbf{H_2}CH_3$, $^3J_{HH}$ = 7.1 Hz), 4.06 (s, 6 H, -$NC\mathbf{H_2}CCHCHCHCC(=O)OCH_2CH_3$), 1.48 (t, 9 H, -$NCH_2CCHCHCHCC(=O)OCH_2C\mathbf{H_3}$, $^3J_{HH}$ = 7.1 Hz)

^{13}C{^{1}H} NMR (100 MHz, $CDCl_3$, 298 K), δ: 165.75 (-$NCH_2CCHCHCHC\mathbf{C}(=O)OCH_2CH_3$), 159.29 (-$NCH_2\mathbf{C}CHCHCHCC(=O)OCH_2CH_3$), 146.95 (-$NCH_2CCHCHCH\mathbf{C}C(=O)OCH_2CH_3$), 138.84 (-$NCH_2C$-$CH\mathbf{C}HCHCC(=O)OCH_2CH_3$), 128.17 (-$NCH_2C\mathbf{C}HCHCHCC(=O)OCH_2CH_3$), 123.84 (-$NCH_2C\mathbf{C}H$-$CHCHCC(=O)OCH_2CH_3$), 62.73 (-$NCH_2CCHCHCHCC(=O)O\mathbf{C}H_2CH_3$), 58.43 (-$N\mathbf{C}H_2CCHCHCH$-$CC(=O)OCH_2CH_3$), 14.26 (- $NCH_2CCHCHCHCC(=O)OCH_2\mathbf{C}H_3$)

MS (ESI), *m/z*: 507.8 **[M + H]$^+$**

6.29. Synthesis of 6,6',6''-(nitrilotris (methylene))tripicolinic acid (H_3Tpaa)

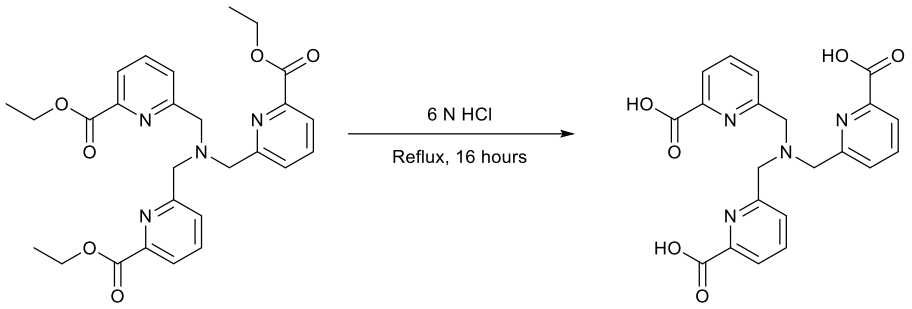

To Et_3Tpaa (56 mg, 0.11 mmol) was added 6 N HCl (8 mL) and the solution heated to reflux for 16 h. The solvent was removed and acetone added to yield an off white precipitate collected by filtration (32 mg, 0.075 mmol, 69%).

^{1}H NMR (400 MHz, D_2O, *pD* = 9.45, 298 K), *δ*: 7.73 (m, 6 H, -NCH_2CCHC**H**C**H**CC(=O)OH), 7.24 (dd, 3 H, -NCH_2CC**H**CHCHCC(=O)OH, $^3J_{HH}$ = 6 Hz, $^4J_{HH}$ = 2.8 Hz), 2.61 (s, 6 H, -NC**H_2**CCHCHCHCC(=O)OH)

^{13}C{^{1}H} NMR (100 MHz, D_2O, *pD* = 9.45, 298 K), *δ*: 172.69 (-$NCH_2CCHCHCHC$**C**(=O)OH), 157.83 (-NCH_2**C**CHCHCHCC(=O)OH), 152.71 (-$NCH_2CCHCHCH$**C**C(=O)OH), 138.30 (-NCH_2CCH**C**HCHCC(=O)-OH), 125.60 (-NCH_2C**C**HCHCHCC(=O)OH), 122.39 (-NCH_2CCHCH**C**HCC(=O)OH), 59.81 (-N**C**H_2CCHCHCHCC(=O)OH)

MS (ESI), *m/z*: 423.3 **[M + H]$^+$**, 445.3 **[M + Na]$^+$**

HRMS (ESI), *m/z*: 423.1298 (Calculated for **[M + H]$^+$**, $C_{21}H_{19}N_4O_6$: 423.1299)

6.30. Gallium (III) complexation by H_3Tpaa ([Ga(Tpaa)])

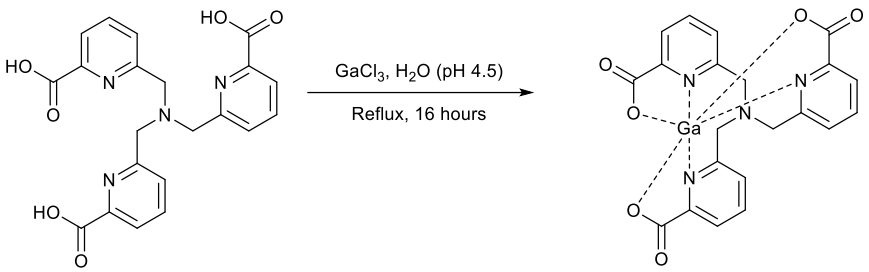

H_3Tpaa (6.3 mg, 14.9 µmol, 1 eq) was dissolved in water (4.5 mL) and $GaCl_3$ (2.6 mg, 14.7 µmol, 0.99 eq) was added. The pH was adjusted to 4.5 with NaOH and the solution heated to reflux for 16 h. Drying yielded an off white solid (12.3 mg).

^{1}H NMR (400 MHz, D_2O, *pD* = 9.44, 298 K), *δ*: 8.47 (br t, 3 H, -NCH_2CCHC**H**$CHCC(=O)O$-, $^3J_{HH}$ = 7.1 Hz), 8.37 (d, 3H, -$NCH_2CCHCHC$**H**$CC(=O)O$-, $^3J_{HH}$ = 7.1 Hz), 7.99 (d, 3 H, -NCH_2CC**H**$CHCHCC(=O)O$-, $^3J_{HH}$ = 7.1 Hz), 4.62 (d, 3 H, -NC**H$_2$**$CCHCHCHCC(=O)O$-, $^2J_{HH}$ = 17.4 Hz), 4.15 (d, 3 H, -NC**H$_2$**$CCHCHCHCC(=O)O$-, $^2J_{HH}$ = 17.4 Hz)

^{13}C{^{1}H} NMR (100 MHz, D_2O, *pD* = 9.44, 298 K), *δ*: 167.02 (-$NCH_2CCHCHCHC$**C**$(=O)O$-), 155.54 (-NCH_2**C**$CHCHCH$**C**$C(=O)O$-), 145.74 (-NCH_2**C**$CHCHCH$**C**$C(=O)O$-), 144.78 (NCH_2CCH**C**$HCHCC(=O)O$-), 128.94 (-NCH_2C**C**$HCHCHCC(=O)O$-), 124.24 (-NCH_2CCHCH**C**$HCC(=O)O$-), 53.30 (-N**C**$H_2CCHCHCH$-$CC(=O)O$-)

MS (ESI), *m/z*: 511.2 **[^{69}Ga][M + Na]$^+$**, 513.2 **[^{71}Ga][M + Na]$^+$**

HRMS (ESI), *m/z*: 489.0321 (Calculated for **[M+H]$^+$,** $C_{21}H_{16}GaN_4O_6$: 489.0320)

6.31. Synthesis of triethyl 6,6',6''-((1 ,4,7-triazonane-1,4,7-triyl)tris(methylene))tripicolinate (Et_3NO3PA)

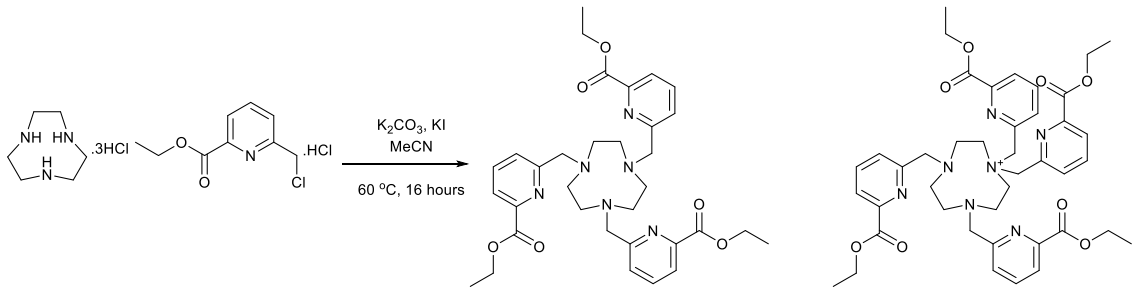

Triazacyclononane trihydrochloride (0.48 g, 2.0 mmol, 1 eq), **4** (1.51 g, 6.4 mmol, 3.2 eq), potassium carbonate (2.85 g, 20.7 mmol, 10.4 eq), and potassium iodide (1.06 g, 6.4 mmol, 3.2 eq) were combined in acetonitrile (7 mL) and the suspension heated to 60 °C for 16 h. Water (35 mL) was added and extracted with dichloromethane (3 x 70 mL). The combined organic layers were dried with magnesium sulfate and concentrated to yield a dark orange oil. This was purified by column chromatography (silica, dichloromethane/methanol, 0-5%) to yield a white solid (271 mg, 0.44 mmol, 22%). The quarternised product was also isolated as a white solid (585 mg, 0.75 mmol, 37%).

6.31.1 triethyl 6,6',6''-((1,4,7-triazonane-1,4,7-triyl)tris(methylene))tripicolinate (Et_3NO3PA)

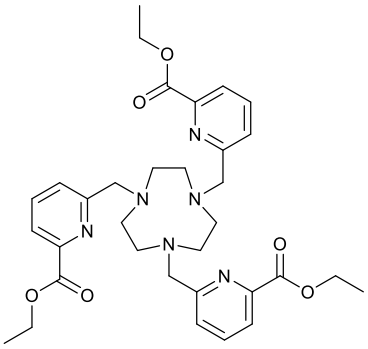

^{1}H NMR (400 MHz, $CDCl_3$, 298 K), δ: 7.99 (d, 3 H, -$NCH_2CCHCHC$**H**$CC(=O)OCH_2CH_3$, $^3J_{HH}$ = 7.8 Hz), 7.90 (t, 3 H, -NCH_2CCHC**H**$CHCC(=O)OCH_2CH_3$, $^3J_{HH}$ = 7.8 Hz), 7.49 (d, 3 H, -NCH_2CC**H**$CHCHCC(=O)OCH_2CH_3$, $^3J_{HH}$ = 7.8 Hz), 4.02 (q, 6 H, -$NCH_2CCHCHCHCC(=O)OC$**H$_2$**CH_3, $^3J_{HH}$ = 7.2 Hz), 3.78 (br s, 6 H, -NC**H$_2$**$CCHCHCHCC(=O)OCH_2CH_3$), 2.66 (m, 6 H, -NC**H$_2$**C**H$_2$**N-), 2.20 (m, 6 H, -NC**H$_2$**C**H$_2$**N-), 1.10 (t, 9 H, -$NCH_2CCHCHCHCC(=O)OCH_2C$**H$_3$**, $^3J_{HH}$ = 7.2 Hz)

^{13}C{^{1}H} NMR (100 MHz, $CDCl_3$, 298 K), δ: 164.81 (-$NCH_2CCHCHCHC$**C**$(=O)OCH_2CH_3$), 159.19 (-NCH_2**C**$CHCHCHCC(=O)OCH_2CH_3$), 147.30 (-$NCH_2CCHCHCH$**C**$C(=O)OCH_2CH_3$), 138.53 (-NCH_2C-CH**C**$HCHCC(=O)OCH_2CH_3$), 126.76 (-NCH_2**C**$CHCHCHCC(=O)OCH_2CH_3$), 123.78 (-NCH_2CCH-

CH**C**HCC(=O)OCH$_2$CH$_3$), 65.19 (-N**C**H$_2$CCHCHCHCC(=O)OCH$_2$CH$_3$), 61.81 (-NCH$_2$CCHCH-CHCC(=O)O**C**H$_2$CH$_3$), 54.04 (-N**C**H$_2$**C**H$_2$N-), 14.07 (-NCH$_2$CCHCHCHCC(=O)OCH$_2$**C**H$_3$)

MS (ESI), *m/z*: 619.7 **[M + H]$^+$**

HRMS (ESI), *m/z*: 619.3243 (Calculated for **[M+H]$^+$**, $C_{33}H_{43}N_6O_6$: 619.3239)

6.31.2 1,1,4,7-tetrakis((6-(ethoxycarbonyl)pyridin-2-yl)methyl)-1,4,7-triazonan-1-ium ([Et$_4$NO4PA]$^+$)

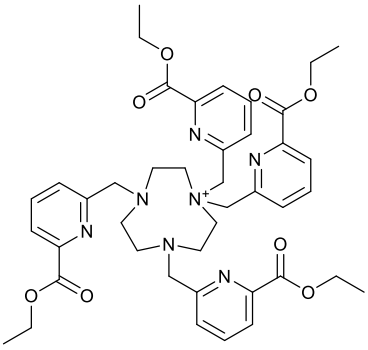

^{1}H NMR (400 MHz, CDCl$_3$, 298 K), *δ*: 8.40 (dd, 2 H, -N$^+$(CH$_2$CC**H**CHCHCC(=O)OCH$_2$CH$_3$)$_2$, $^3J_{HH}$ = 7.8 Hz, $^4J_{HH}$ = 0.9 Hz), 8.13 (dd, 2 H, -N$^+$(CH$_2$CCHCHC**H**CC(=O)OCH$_2$CH$_3$)$_2$, $^3J_{HH}$ = 7.8 Hz, $^4J_{HH}$ = 0.9 Hz), 7.95 (dd, 2 H, -NCH$_2$CCHCHC**H**CC(=O)OCH$_2$CH$_3$, $^3J_{HH}$ = 7.8 Hz, $^4J_{HH}$ = 0.9 Hz), 7.93 (t, 2 H, -N$^+$(CH$_2$CCHC**H**CHCC(=O)OCH$_2$CH$_3$)$_2$, $^3J_{HH}$ = 7.8 Hz), 7.82 (t, 2 H, -NCH$_2$CCHC**H**CHCC(=O)OCH$_2$CH$_3$, $^3J_{HH}$ = 7.8 Hz), 7.78 (dd, 2 H, -NCH$_2$CC**H**CHCHCC(=O)OCH$_2$CH$_3$, $^3J_{HH}$ = 7.8 Hz, $^4J_{HH}$ = 0.9 Hz), 5.23 (br s, 4 H, -N$^+$(C**H$_2$**CCHCHCHCC(=O)OCH$_2$CH$_3$)$_2$), 4.44 (q, 4 H, -NCH$_2$CCHCHCHCC(=O)OC**H$_2$**CH$_3$, $^3J_{HH}$ = 7.2 Hz),4.36 (q, 4 H, -NCH$_2$CCHCHCHCC(=O)OC**H$_2$**CH$_3$, $^3J_{HH}$ = 7.2 Hz), 4.15 (br s, 4 H, -NC**H$_2$**CCHCHCHCC(=O)OCH$_2$CH$_3$), 3.50 (br s, 4 H, -NC**H$_2$**C**H$_2$**N-), 2.66 (br s, 4 H, -NC**H$_2$**C**H$_2$**N-), 1.43 (t, 6 H, -NCH$_2$CCHCHCHCC(=O)OCH$_2$C**H$_3$**, $^3J_{HH}$ = 7.2 Hz), 1.33 (t, 6 H, -NCH$_2$CCHCHCHCC(=O)OCH$_2$C**H$_3$**, $^3J_{HH}$ = 7.2 Hz)

^{13}C{^{1}H} NMR (100 MHz, CDCl$_3$, 298 K), *δ*: 165.14 (-NCH$_2$CCHCHCHC**C**(=O)OCH$_2$CH$_3$), 164.27 (-N$^+$(CH$_2$CCHCHCHC**C**(=O)OCH$_2$CH$_3$)$_2$), 159.36 (-NCH$_2$**C**CHCHCHCC(=O)OCH$_2$CH$_3$), 150.26 (-N$^+$(CH$_2$**C**CHCHCHCC(=O)OCH$_2$CH$_3$)$_2$), 147.97 (-N$^+$(CH$_2$CCHCHCH**C**C(=O)OCH$_2$CH$_3$)$_2$), 147.68 (-NCH$_2$CCHCHCH**C**C(=O)OCH$_2$CH$_3$), 139.17 (-N$^+$(CH$_2$CCH**C**HCHCC(=O)OCH$_2$CH$_3$)$_2$), 137.82 (-NCH$_2$CCH**C**HCHCC(=O)OCH$_2$CH$_3$), 131.13 (-N$^+$(CH$_2$C**C**HCHCHCC(=O)OCH$_2$CH$_3$)$_2$), 127.65 (-NCH$_2$CCHCH**C**HCC(=O)OCH$_2$CH$_3$), 125.62 (-NCH$_2$C**C**HCHCHCC(=O)OCH$_2$CH$_3$), 123.96 (-N$^+$(CH$_2$CCHCH**C**HCC(=O)OCH$_2$CH$_3$)$_2$), 65.00 (-N**C**H$_2$CCHCHCHCC(=O)OCH$_2$CH$_3$), 62.13 (-NCH$_2$CCHCHCHCC(=O)O**C**H$_2$CH$_3$), 61.82 (-NCH$_2$CCHCHCHCC(=O)O**C**H$_2$CH$_3$), 61.25 (-N$^+$(**C**H$_2$CCHCHCHCC(=O)OCH$_2$CH$_3$)$_2$), 60.21 (-N**C**H$_2$**C**H$_2$N-), 57.76 (-N**C**H$_2$**C**H$_2$N-), 54.03 (-N**C**H$_2$**C**H$_2$N-) 14.43 (-NCH$_2$CCHCHCHCC(=O)OCH$_2$**C**H$_3$)

MS (ESI), *m/z*: 392.1 **[M+H]$^{2+}$**, 782.7 **[M]$^+$**

HRMS (ESI), *m/z*: 782.3864 (Calculated for **[M]$^+$**, $C_{42}H_{52}N_7O_8$: 782.3872)

6.32. Synthesis of 6,6',6''-((1,4,7-triazonane -1,4,7-triyl)tris(methylene))tripicolinic acid (H_3NO3PA)

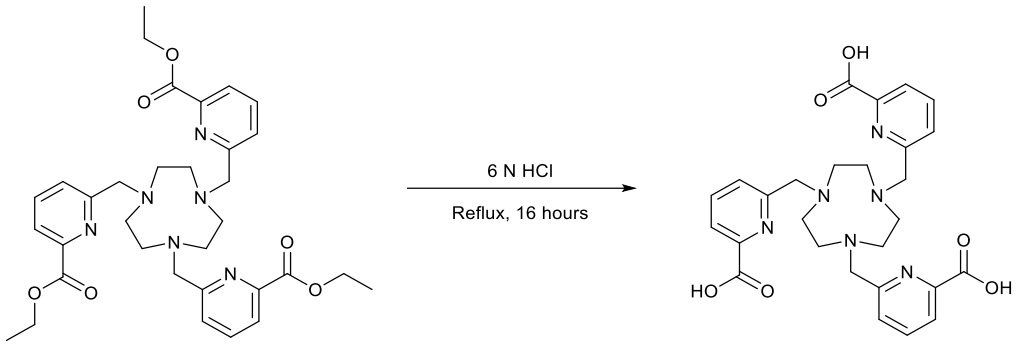

Et_3NO3PA (150 mg, 0.24 mmol) was heated to reflux in 6 M HCl (10 mL) for 16 h. The solvent was removed to yield a yellow oil. Addition of acetone yielded a yellow solid (130 mg, 0.24 mmol, 100%).

^{1}H NMR (400 MHz, D_2O, *pD* = 3.14, 298 K), *δ*: 7.77 (t, 3 H, -NCH_2CCHC**H**$CHCC(=O)OH$, $^3J_{HH}$ = 7.8 Hz), 7.61 (d, 3 H, -$NCH_2CCHCHC$**H**$CC(=O)OH$, $^3J_{HH}$ = 7.8 Hz), 7.39 (d, 3 H, -NCH_2CC**H**$CHCHCC(=O)$-OH, $^3J_{HH}$ 7.8 Hz), 4.58 (s, 6 H, -NC**H$_2$**$CCHCHCHCC(=O)OH$), 3.84 (br s, 12 H, -NC**H$_2$**C**H$_2$**N-)

^{13}C{^{1}H} NMR (100 MHz, D_2O, *pD* = 3.14, 298 K), *δ*: 166.92 (-$NCH_2CCHCHCHC$**C**$(=O)OH$), 153.22 (-NCH_2**C**$CHCHCHCC(=O)OH$), 145.95 (-$NCH_2CCHCHCH$**C**$C(=O)OH$), 139.40 (-NCH_2CCH**C**$HCHCC(=O)$-OH), 127.28 (-NCH_2C**C**$HCHCHCC(=O)OH$), 125.09 (-NCH_2CCHCH**C**$HCC(=O)OH$), 59.99 (-N**C**$H_2CCHCHCHCC(=O)OH$), 57.81 (-N**C**H_2**C**H_2N-)

MS (ESI), *m/z*: 557.3 **[M + Na]$^+$**

HRMS (ESI), *m/z*: 535.2300 (Calculated for **[M+H]$^+$**, $C_{27}H_{31}N_6O_6$: 535.2300)

6.33. Gallium (III) complexation by H_3NO3PA

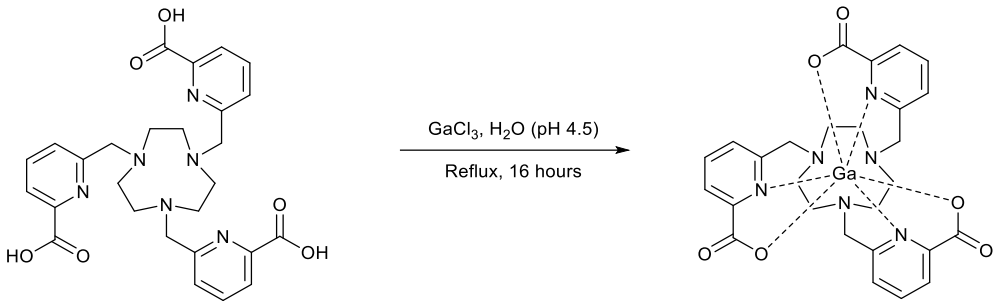

H_3NO3PA (29.5 mg, 55.2 µmol, 1 eq) was dissolved in water (4 mL) and $GaCl_3$ (24.1 mg, 136.5 µmol, 2.5 eq) added. The pH was adjusted to 4.5 and the solution heated to reflux for 16 h. The solution was dried to yield a white solid (48.4 mg, 80.5 µmol, 146%)

^{1}H NMR (400 MHz, D_2O, *pD* = 3.07, 298 K), *δ*: 8.37-7.49 (m, 9 H, -NCH_2CC**H**C**H**C**H**CC(=O)O-), 4.29-2.55 (m, -NC**H$_2$**CCHCHCHCC(=O)OH, -NC**H$_2$**C**H$_2$**N-)

^{1}H NMR (400 MHz, D_2O, *pD* = 3.07, 368 K), *δ*: 8.89-8.70 (br s, 6 H, -NCH_2CC**H**C**H**C**H**CC(=O)O-), 8.50-8.30 (br s, 3 H, -NCH_2CC**H**C**H**C**H**CC(=O)O-), 5.56-4.84 (br m, 6 H, -NC**H$_2$**CCHCHCHCC(=O)O-), 4.39-3.77 (br m, 12 H, -NC**H$_2$**C**H$_2$**N-)

MS (ESI), *m/z*: 601.3 **[^{69}Ga][M+H]$^+$**

HRMS (ESI), *m/z*: 601.1328(Calculated for **[^{69}Ga][M+H]$^+$** $C_{27}H_{28}{}^{69}GaN_6O_6$: 601.1321)

6.34. Synthesis of diethyl ((dibenzylamino)methyl)phosphonate (10)[244]

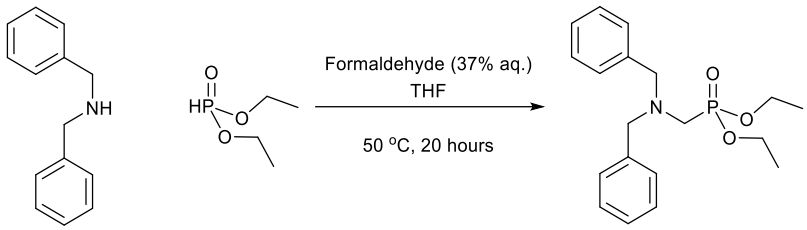

Diethyl phosphite (6.62 g, 6.18 mL, 0.048 mol, 1.2 eq) and dibenzylamine (7.88 g, 7.68 mL, 0.040 mol, 1 eq) were dissolved in tetrahydrofuran (20 mL). Formaldehyde solution (37%) (4.00 g, 3.67 mL, 0.059 mol, 1.2 eq) was added and the solution stirred at room temperature for 2.5 hours before heating to 50 °C for 20 hours. After cooling, the solvent was removed and the residue taken up in hexane (60 mL). The solution was washed with water (3 x 60 mL) and the organic layer was dried with magnesium sulfate before being concentrated to yield a clear oil (12.81 g, 0.037 mol, 92%).

^{1}H NMR (400 MHz, $CDCl_3$, 298 K), δ: 7.38 (br d, 4 H, $(C_6\mathbf{H_5}CH_2)_2NCH_2P(=O)(OCH_2CH_3)_2$, $^{3}J_{HH}$ = 7.1 Hz), 7.32 (br t, 4 H, $(C_6\mathbf{H_5}CH_2)_2NCH_2P(=O)(OCH_2CH_3)_2$, $^{3}J_{HH}$ = 7.1 Hz), 7.20 (t, 2 H, $(C_6\mathbf{H_5}CH_2)_2NCH_2P(=O)(OCH_2CH_3)_2$, $^{3}J_{HH}$ = 7.1 Hz), 4.06 (dt, 4 H, $(C_6H_5CH_2)_2NCH_2P(=O)(OC\mathbf{H_2}CH_3)_2$, $^{3}J_{PH}$ = 14.4 Hz, $^{3}J_{HH}$ = 7.2 Hz), 3.78 (br s, 4 H, $(C_6H_5C\mathbf{H_2})_2NCH_2P(=O)(OCH_2CH_3)_2$), 2.89 (d, 2 H, $(C_6H_5CH_2)_2NC\mathbf{H_2}P(=O)(OCH_2CH_3)_2$, $^{2}J_{PH}$ = 10.4 Hz), 1.29 (t, 6 H, $(C_6H_5CH_2)_2NCH_2P(=O)(OCH_2C\mathbf{H_3})_2$, $^{3}J_{HH}$ = 7.2 Hz)

^{13}C{^{1}H} NMR (100 MHz, $CDCl_3$, 298 K), δ: 138.84 (s, $(\mathbf{C_6}H_5CH_2)_2NCH_2P(=O)(OCH_2CH_3)_2$), 129.15 (s, $(\mathbf{C_6}H_5CH_2)_2NCH_2P(=O)(OCH_2CH_3)_2$), 128.33 (s, $(\mathbf{C_6}H_5CH_2)_2NCH_2P(=O)(OCH_2CH_3)_2$), 127.23 (s, $(\mathbf{C_6}H_5CH_2)_2NCH_2P(=O)(OCH_2CH_3)_2$), 71.82 (d, $(C_6H_5CH_2)_2NCH_2P(=O)(O\mathbf{C}H_2CH_3)_2$, $^{2}J_{PC}$ = 6.9 Hz), 59.39 (d, $(C_6H_5\mathbf{C}H_2)_2NCH_2P(=O)(OCH_2CH_3)_2$, $^{3}J_{PC}$ = 8.5 Hz), 48.40 (d, $(C_6H_5CH_2)_2N\mathbf{C}H_2P(=O)(O$-$CH_2CH_3)_2$, $^{1}J_{PC}$ = 159 Hz), 16.58 (d, $(C_6H_5CH_2)_2NCH_2P(=O)(OCH_2\mathbf{C}H_3)_2$, $^{3}J_{PC}$ = 6.1 Hz)

^{31}P{^{1}H} NMR (162 MHz, $CDCl_3$, 298 K), δ: 26.34 (s, $(C_6H_5CH_2)_2NCH_2\mathbf{P}(=O)(OCH_2CH_3)_2$)

MS (ESI), *m/z*: 348.5 **[M + H]$^{+}$**

6.35. Synthesis of diethyl (aminomethyl)phosphonate (**11**)[244]

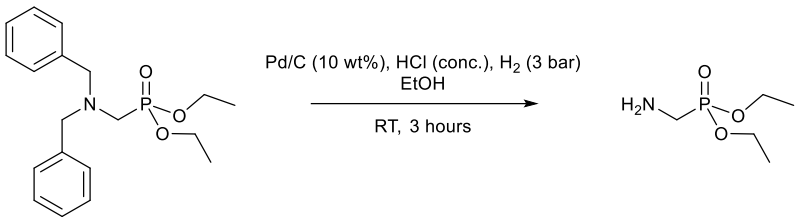

To a solution of **10** (12.00 g, 34.6 mmol, 1 eq) in ethanol (58 mL) was added concentrated hydrochloric acid (2.89 mL, 34.6 mmol, 1 eq) and Pd/C (10 wt%, 1.84 g, 1.7 mmol, 0.05 eq) and agitated under 3 bar hydrogen gas for 3 hours. The solution was neutralised with sodium hydroxide in water and filtered through celite to remove Pd/C. The solvent was removed and the residue taken up in diethyl ether, dried with magnesium sulfate and concentrated to yield a clear oil (3.48 g, 20.9 mmol, 60%).

^{1}H NMR (400 MHz, $CDCl_3$, 298 K), δ: 3.99 (m, 4 H, $H_2NCH_2P(=O)(OC\mathbf{H_2}CH_3)_2$), 3.04 (d, 2 H, $H_2NC\mathbf{H_2}P(=O)(OCH_2CH_3)_2$, $^{2}J_{PH}$ = 10.4 Hz), 1.35 (t, 6 H, $H_2NCH_2P(=O)(OCH_2C\mathbf{H_3})_2$, $^{3}J_{HH}$ = 7.1 Hz)

^{13}C{^{1}H} NMR (100 MHz, $CDCl_3$, 298 K), δ: 62.32 ($H_2NCH_2P(=O)(O\mathbf{C}H_2CH_3)_2$), 37.85 (d, $H_2N\mathbf{C}H_2P(=O)(OCH_2CH_3)_2$, $^{1}J_{PH}$ = 158 Hz), 16.52 ($(C_6H_5CH_2)_2NCH_2P(=O)(OCH_2\mathbf{C}H_3)_2$)

^{31}P{^{1}H} NMR (162 MHz, $CDCl_3$, 298 K), δ: 27.63 (s, $H_2NCH_2\mathbf{P}(=O)(OCH_2CH_3)_2$)

MS (ESI), *m/z*: 167.9 **[M + H]$^{+}$**

6.36. Synthesis of diethyl (6-methylpyridin -2-yl)phosphonate (**12**)

6.36.1 Palladium Catalysed Cross Coupling[278]

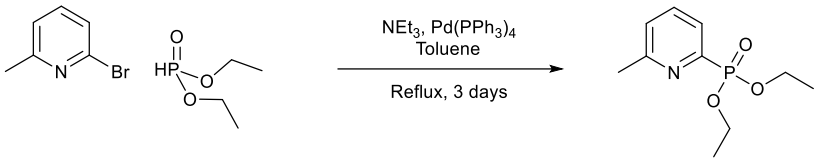

To diethyl phosphite (3.31 g, 3.09 mL, 24 mmol, 1.2 eq) was added toluene (30 mL, freeze-pump thaw degassed) under argon. 2-bromo-6-methylpyridine (3.44 g, 2.28 mL, 20 mmol, 1.0 eq) and triethylamine (7.07 g, 9.74 mL, 70 mmol, 3.5 eq) were added and argon bubbled through the solution for 1 hour at room temperature. Tetrakis(triphenylphosphine)palladium (0.51 g, 0.44 mmol, 0.02 eq) was added and the solution heated to reflux for 3 days. Starting material was still present by TLC. The solution was decanted and the solvent removed to give a crude yellow liquid. Purification by column chromatography (silica, dichloromethane/ethanol 0-2%) yielded an orange liquid (407 mg, 1.8 mmol, 9%). 1.72 g 2-bromo-6-methylpyridine was recovered (~50%).

6.36.2 Deoxylative phosphorylation of picoline-N-oxide[247]

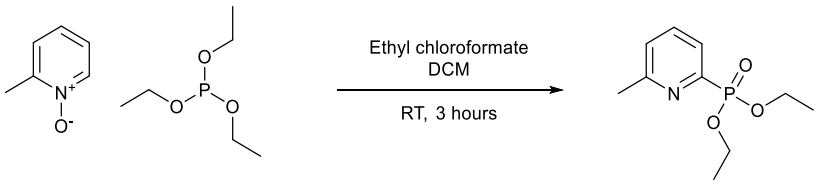

To 2-picoline-N-oxide (1.86 g, 13.7 mmol, 1 eq) in dichloromethane (anhydrous, 65 mL) was added ethylchloroformate (6.47 g, 5.68 mL, 48.1 mmol, 3.5 eq) with cooling in an ice bath. The solution was warmed to room temperature and stirred for 10 minutes. Triethylphosphite (9.91 g, 10.23 mL, 48.1 mmol, 3.5 eq) was added dropwise. The reaction was followed by TLC; after 2 hours N-oxopicoline remained. Additional ethyl chloroformate (1.00 mL) was added. After 90 minutes the reaction was diluted with dichloromethane (200 mL) and extracted with saturated potassium carbonate solution (300 mL), water (2 x 300 mL) and brine (300 mL). The organic layer was dried with magnesium sulfate and concentrated to a clear oil. Purification by column chromatography (silica, ethyl acetate) yielded a clear oil (3.11 g, 13.6 mmol, 99%).

*6.36.3 Diethyl (6-methylpyridin-2-yl)phosphonate (**12**)*

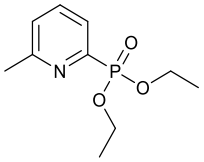

^{1}H NMR (400 MHz, $CDCl_3$, 298 K), δ: 7.74 (t, 1 H, $CH_3CCHC\mathbf{H}CHCP(=O)(OCH_2CH_3)_2$, $^{3}J_{HH}$ = 8.3 Hz), 7.64 (dd, 1 H, $CH_3CCHCHC\mathbf{H}CP(=O)(OCH_2CH_3)_2$, $^{3}J_{PH}$ = 16 Hz, $^{3}J_{HH}$ = 8.2 Hz), 7.25 (br d, 1 H, $CH_3CC\mathbf{H}CHCHCP(=O)(OCH_2CH_3)_2$, $^{3}J_{HH}$ = 8.3 Hz), 4.22 (m, 4 H, $CH_3CCHCHCHCP(=O)(OC\mathbf{H_2}CH_3)_2$, 2.60 (s, 3 H, $C\mathbf{H_3}CCHCHCHCP(=O)(OCH_2CH_3)_2$, 1.33 (t, 6 H, $CH_3CCHCHCHCP(=O)(OCH_2C\mathbf{H_3})_2$, $^{3}J_{HH}$ = 7.3 Hz)

^{1}H NMR (400 MHz, d_3-MeCN, 298 K), δ: 7.75 (dd, 1 H, $CH_3CCHCHC\mathbf{H}CP(=O)(OCH_2CH_3)_2$, $^{3}J_{PH}$ = 13.8 Hz, $^{3}J_{HH}$ = 7.0 Hz), 7.68 (t, 1 H, $CH_3CCHC\mathbf{H}CHCP(=O)(OCH_2CH_3)_2$, $^{3}J_{HH}$ = 7.0 Hz), 7.37 (br d, $CH_3CC\mathbf{H}CHCHCP(=O)(OCH_2CH_3)_2$, $^{3}J_{HH}$ = 7.0 Hz), 4.13 (dq, 4 H, $CH_3CCHCHCHCP(=O)(OC\mathbf{H_2}CH_3)_2$, $^{3}J_{PH}$ = 15.1 Hz, $^{3}J_{HH}$ = 7.2 Hz), 2.55 (s, 3 H, $C\mathbf{H_3}CCHCHCHCP(=O)(OCH_2CH_3)_2$), 1.28 (t, 6 H, $CH_3CCHCHCHCP(=O)(OCH_2C\mathbf{H_3})_2$, $^{3}J_{HH}$ = 7.1 Hz)

^{13}C{^{1}H} NMR (100 MHz, d_3-MeCN, 298 K), δ: 160.88 (d, $CH_3\mathbf{C}CHCHCHCP(=O)(OCH_2CH_3)_2$, $^{3}J_{PC}$ = 22.16 Hz), 152.51 (d, $CH_3CCHCHCH\mathbf{C}P(=O)(OCH_2CH_3)_2$, $^{1}J_{PC}$ = 225.4 Hz), 137.82 (d, $CH_3CCHCH\mathbf{C}HCP(=O)(OCH_2CH_3)_2$, $^{2}J_{PC}$ = 12.5 Hz), 127.18 (d, $CH_3C\mathbf{C}HCHCHCP(=O)(OCH_2CH_3)_2$, $^{4}J_{PC}$ = 3.9 Hz), 126.29 (d, $CH_3CCH\mathbf{C}HCHCP(=O)(OCH_2CH_3)_2$, $^{3}J_{PC}$ = 25.1 Hz), 63.84 (d, $CH_3CCHCHCHCP(=O)(O\mathbf{C}H_2CH_3)_2$, $^{2}J_{PC}$ = 5.8 Hz), 24.86 (s, $\mathbf{C}H_3CCHCHCHCP(=O)(OCH_2CH_3)_2$), 16.99 (d, $CH_3CCHCHCHCP(=O)(OCH_2\mathbf{C}H_3)_2$, $^{3}J_{PC}$ = 5.8 Hz)

^{31}P{^{1}H} NMR (162 MHz, d_3-MeCN, 298 K), δ: 11.14 (s, $CH_3CCHCHCHC\mathbf{P}(=O)(OCH_2CH_3)_{2)}$

MS (ESI), *m/z*: 230.1 **[M + H]$^{+}$**

HRMS (ESI), m/z: 230.0940 (Calculated for **[M+H]$^{+}$,** $C_{10}H_{17}N_1O_3P_1$: 230.0941)

6.37. Synthesis of diethyl (6-(bromomethyl)pyridin-2 -yl)phosphonate (**13**)[278]

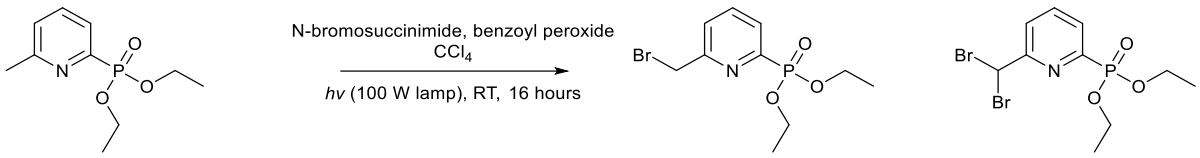

To **12** (3.21 g, 14.0 mmol, 1 eq) in carbon tetrachloride (50 mL) was added N-bromosuccinimide (2.99 g, 16.8 mmol, 1.2 eq) and dibenzoyl peroxide (1.69 g, 7.0 mmol, 0.5 eq). This was stirred under argon with irradiation from a 100 W lamp overnight. The solvent was removed under reduced pressure. The oil was taken up in dichloromethane (200 mL) and washed with dilute potassium carbonate solution (200 mL). The organic layer was collected, dried with magnesium sulfate and concentrated to yield an orange oil. Purification by column chromatography (silica, dichloromethane/methanol, 0-0.5%) yielded a pale yellow oil (822, 2.7 mmol, 19%).

*6.37.1 Diethyl (6-(bromomethyl)pyridin-2 -yl)phosphonate (**12**)*

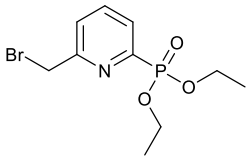

^{1}H NMR (400 MHz, $CDCl_3$, 298 K), δ: 7.88 (br t, 1 H, $BrCH_2CCHCHC\mathbf{H}CP(=O)(OCH_2CH_3)_2$, $^3J_{PH}$ = 7.8 Hz, $^3J_{HH}$ =7.8 Hz), 7.81 (td, 1 H, $BrCH_2CCHC\mathbf{H}CHCP(=O)(OCH_2CH_3)_2$, $^3J_{HH}$ = 7.8 Hz, $^4J_{PH}$ = 5.5 Hz), 7.61 (d, 1 H, $BrCH_2CC\mathbf{H}CHCHCP(=O)(OCH_2CH_3)_2$, $^3J_{HH}$ = 7.8 Hz), 4.61 (s, 2 H, $BrCH_2CCHCHCHCP(=O)(OCH_2CH_3)_2$), 4.32-4.20 (m, 4 H, $BrCH_2CCHCHCHCP(=O)(OCH_2CH_3)_2$), 1.37 (t, 6 H, $BrCH_2CCHCHCHCP(=O)(OCH_2CH_3)_2$, $^3J_{HH}$ = 7.1 Hz)

^{1}H NMR (400 MHz, d_3-MeCN, 298 K), δ: 7.90 (dd, 1 H, $BrCH_2CCHCHC\mathbf{H}CP(=O)(OCH_2CH_3)_2$, $^3J_{PH}$ = 13.8 Hz, $^3J_{HH}$ = 7.3 Hz), 7.8 (t, 1 H, $BrCH_2CCHC\mathbf{H}CHCP(=O)(OCH_2CH_3)_2$, $^3J_{HH}$ = 7.3 Hz), 7.65 (br d, 1 H, $BrCH_2CC\mathbf{H}CHCHCP(=O)(OCH_2CH_3)_2$, $^3J_{HH}$ = 7.3 Hz), 4.64 (s, 2 H, $BrC\mathbf{H_2}CCHCHCHCP(=O)(OCH_2CH_3)_2$), 4.15 (dq, 4 H, $BrCH_2CCHCHCHCP(=O)(OC\mathbf{H_2}CH_3)_2$, $^3J_{PH}$ = 14.0 Hz, $^3J_{HH}$ = 7.1 Hz), 1.29 (t, 6 H, $BrCH_2CCHCHCHCP(=O)(OCH_2C\mathbf{H_3})_2$, $^3J_{HH}$ = 7.1 Hz)

^{13}C{^{1}H} NMR (100 MHz, d_3-MeCN, 298 K), δ: 177.70 ($BrCH_2\mathbf{C}CHCHCHCP(=O)(OCH_2CH_3)_2$), 153.00 ($BrCH_2CCHCHCH\mathbf{C}P(=O)(OCH_2CH_3)_2$), 139.12 (d, $BrCH_2CCHCH\mathbf{C}HCP(=O)(OCH_2CH_3)_2$, $^2J_{PC}$ = 11.6 Hz), 128.38 (d, $BrCH_2CCH\mathbf{C}HCHCP(=O)(OCH_2CH_3)_2$, $^3J_{PC}$ = 25.0 Hz), 127.35 (d, $BrCH_2C\mathbf{C}HCHCHCP(=O)(OCH_2CH_3)_2$, $^4J_{PC}$ = 3.9 Hz), 64.17 (d, $BrCH_2CCHCHCHCP(=O)(O\mathbf{C}H_2CH_3)_2$, $^2J_{PC}$

= 5.8 Hz), 34.86 (s, Br**C**H_2CCHCHCHCP(=O)(OCH_2CH_3)$_2$), 17.0 ppm (d, $BrCH_2CCHCHCHCP(=O)(OCH_2$**C**$H_3)_2$, $^3J_{PC}$ = 6.7 Hz)

$^{31}P\{^1H\}$ NMR (162 MHz, d_3-MeCN, 298 K), δ: 10.10 ($BrCH_2CCHCHCHC$**P**(=O)(OCH_2CH_3)$_2$)

MS (ESI), *m/z*: 308.2 **[^{79}Br][M + H]$^+$**, 310.2 [**^{81}Br][M + H]$^+$**

HRMS (EI), m/z: 308.0043 (Calculated for **[^{79}Br][M+H]$^+$,** $C_{10}H_{16}{}^{79}Br_1N_1O_3P_1$: 308.0046)

6.37.2 Diethyl (6-(dibromomethyl)pyridin-2-yl)phosphonate

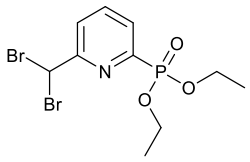

^{1}H NMR (400 MHz, $CDCl_3$, 298 K), δ: 8.04-7.87 (m, 3 H, Br_2CHCC**H**C**H**C**H**CP(=O)(OCH_2CH_3)$_2$), 6.73 (s, 1 H, Br_2C**H**CCHCHCHCP(=O)(OCH_2CH_3)$_2$), 4.34-4.18 (m, 4 H, $Br_2CHCCHCHCHCP(=O)(OC$**H$_2$**CH_3)$_2$), 1.37 (t, 6 H, $Br_2CHCCHCHCHCP(=O)(OCH_2C$**H$_3$**)$_2$, $^3J_{HH}$ = 7.1 Hz)

^{1}H NMR (400 MHz, d_3-MeCN, 298 K), δ: 7.98 (dd, 1 H, $Br_2CHCCHCHC$**H**CP(=O)(OCH_2CH_3)$_2$, $^3J_{PH}$ = 13.3 H, $^3J_{HH}$ = 7.6 Hz), 7.90-7.82 (m, 2 H, Br_2CHCC**H**C**H**CHCP(=O)(OCH_2CH_3)$_2$), 6.92 (s, 1 H, Br_2C**H**CCHCHCHCP(=O)(OCH_2CH_3)$_2$), 4.18 (dq, $Br_2CHCCHCHCHCP(=O)(OC$**H$_2$**CH_3)$_2$, $^3J_{PH}$ = 14.0 Hz, $^3J_{HH}$ = 7.1 Hz), 1.30 (t, $Br_2CHCCHCHCHCP(=O)(OCH_2C$**H$_3$**)$_2$, $^3J_{HH}$ = 7.1 Hz)

$^{13}C\{^1H\}$ NMR (100 MHz, d_3-MeCN, 298 K), δ: 160.46 (d, Br_2CH**C**CHCHCHCP(=O)(OCH_2CH_3)$_2$, $^3J_{PC}$ = 22.2 Hz), 153.04 (d, $Br_2CHCCHCHCH$**C**P(=O)(OCH_2CH_3)$_2$, $^1J_{PC}$ = 222.5 Hz), 139.89 (d, $Br_2CHCCHCH$**C**HCP(=O)(OCH_2CH_3)$_2$, $^2J_{PC}$ = 11.6 Hz), 129.68 (d, Br_2CHCCH**C**HCHCP(=O)(OCH_2CH_3)$_2$, $^3J_{PC}$ = 25.1 Hz), 124.87 (d, Br_2CHC**C**HCHCHCP(=O)(OCH_2CH_3)$_2$, $^4J_{PC}$ = 2.9 Hz), 64.43 (d, $Br_2CHCCHCHCHCP(=O)(O$**C**$H_2CH_3)_2$, $^2J_{PC}$ = 6.7 Hz), 42.70 (s, Br_2**C**HCCHCHCHCP(=O)(OCH_2CH_3)$_2$), 17.02 (d, $Br_2CHCCHCHCHCP(=O)(OCH_2$**C**$H_3)_2$, $^3J_{PC}$ = 6.7 Hz)

$^{31}P\{^1H\}$ NMR (162 MHz, d_3-MeCN, 298 K), δ: 9.28 (s, $Br_2CHCCHCHCHC$**P**(=O)(OCH_2CH_3)$_2$)

MS (ESI), *m/z*: 386.1 **[^{79}Br]$_2$[M + H]$^+$**, 388.1 **[^{79}Br][^{81}Br][M + H]$^+$**, 390.1 **[^{81}Br]$_2$[M + H]$^+$**

HRMS (ESI), *m/z*: 387.9131 (Calculated for **[^{79}Br][^{81}Br][M+H]$^+$**, $C_{10}H_{15}{}^{79}Br^{81}BrN_1O_3P_1$: 387.9131)

6.38. Synthesis of diethyl 6,6'-((((diethoxyphosphoryl)methyl)azanediyl)bis(methylene))dipicolinate (Et_4DPAP)

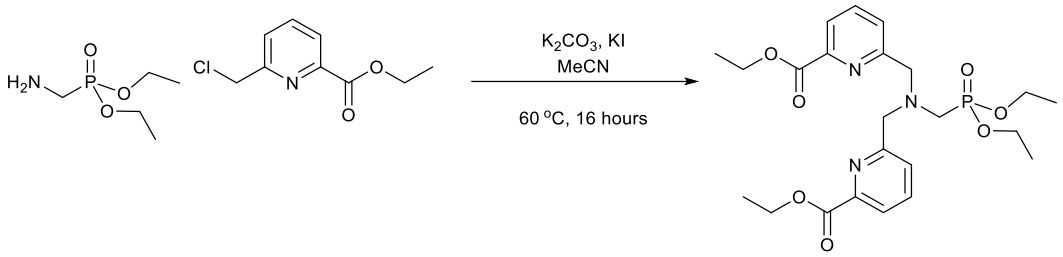

4 (0.991 g, 4.2 mmol, 2.1 eq), **10** (0.334 g, 2 mmol, 1 eq), potassium carbonate (1.05 g, 7.6 mmol, 3.8 eq), potassium iodide (0.697 g, 4.2 mmol, 2.21 eq) and acetonitrile (2.6 mL) and heated to 60 °C for 16 h. Water (10 mL) was added and extracted with dichloromethane (3 x 10 mL). The organic layers were combined and dried with magnesium sulfate and concentrated to yield an orange oil. This was purified by column chromatography (silica, dichloromethane/methanol 0-5%) to yield a yellow oil (614 mg, 1.25 mmol, 62%)

^{1}H NMR (400 MHz, d_6-DMSO, 298 K), δ: 7.94 (t, 2 H, -$NCH_2CCHC\mathbf{H}CHCC(=O)OCH_2CH_3$, $^3J_{HH}$ = 7.8 Hz), 7.89 (dd, 2 H, -$NCH_2CCHCHC\mathbf{H}CC(=O)OCH_2CH_3$, $^3J_{HH}$ = 7.8 Hz, $^4J_{HH}$ = 1.8 Hz), 7.77 (dd, 2 H, -$NCH_2CC\mathbf{H}CHCHCC(=O)OCH_2CH_3$, $^3J_{HH}$ = 7.8 Hz, $^4J_{HH}$ = 1.8 Hz), 4.30 (q, 4 H, -$NCH_2CCHCHCHCC(=O)OC\mathbf{H_2}CH_3$, $^3J_{HH}$ = 7.0 Hz), 3.96 (m, 8 H, -$NC\mathbf{H_2}CCHCHCHCC(=O)OCH_2CH_3$, -$NCH_2P(=O)(OC\mathbf{H_2}CH_3)_2$), 3.04 (d, 2 H, -$NC\mathbf{H_2}P(=O)(OCH_2CH_3)_2$, $^2J_{PH}$ = 10.1 Hz), 1.29 (t, 6 H, -$NCH_2CCHCHCHCC(=O)OCH_2C\mathbf{H_3}$, $^3J_{HH}$ = 7.1 Hz), 1.14 (t, 6 H, -$NCH_2P(=O)(OCH_2C\mathbf{H_3})_2$, $^3J_{HH}$ = 7.1 Hz)

^{13}C{^{1}H} NMR (100 MHz, d_6-DMSO, 298 K), δ: 165.25 (-$NCH_2CCHCHCHC\mathbf{C}(=O)OCH_2CH_3$), 159.70 (-$NCH_2\mathbf{C}CHCHCHCC(=O)OCH_2CH_3$), 147.50 (-$NCH_2CCHCHCH\mathbf{C}C(=O)OCH_2CH_3$), 138.43 (-$NCH_2CCH\mathbf{C}HCHCC(=O)OCH_2CH_3$), 126.95 (-$NCH_2C\mathbf{C}HCHCHCC(=O)OCH_2CH_3$), 123.87 (-$NCH_2CCHCH\mathbf{C}HCC(=O)OCH_2CH_3$), 61.45 (d, -$N\mathbf{C}H_2CCHCHCHCC(=O)OCH_2CH_3$, $^3J_{PC}$ = 5.8 Hz), 61.18 (s, -$NCH_2CCHCHCHCC(=O)O\mathbf{C}H_2CH_3$), 60.18 (d, -$NCH_2P(=O)(O\mathbf{C}H_2CH_3)_2$, $^2J_{PC}$ = 7.7 Hz) 49.05 (-$N\mathbf{C}H_2P(=O)(OCH_2CH_3)_2$, $^1J_{PC}$ = 183.4 Hz), 16.80 (-$NCH_2P(=O)(OCH_2\mathbf{C}H_3)_2$, $^3J_{PC}$ = 5.78 Hz), 14.67 (-$NCH_2CCHCHCHCC(=O)OCH_2\mathbf{C}H_3$)

^{31}P{^{1}H} NMR (162 MHz, d_6-DMSO, 298 K), δ: 25.50 (s, -$NCH_2\mathbf{P}(=O)(OCH_2CH_3)_2$)

MS (ESI), *m/z*: 494.5 **$[M+H]^+$**

HRMS (ESI), *m/z*: 494.2058 (Calculated for **$[M+H]^+$,** $C_{23}H_{33}N_3O_7P_1$: 393.2051)

6.39. Synthesis of 6,6'-(((phosphonomethyl)azanediyl)bis(methylene))dipicolinic acid (H_4DPAP)

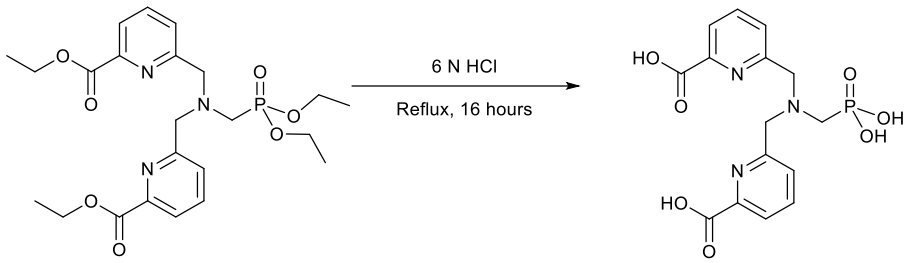

Et_4DPAP (174 mg, 0.35 mmol) was dissolved in 6 N HCl (10 mL). The solution was heated to reflux for 16 hours. After concentration to give a yellow oil, acetone was added to yield an off white solid (104 mg, 0.27 mmol, 78%).

^{1}H NMR (400 MHz, D_2O, *pD* = 7.14, 298 K), *δ*: 7.79-7.75 (m, 4 H, -NCH_2CCHC**H**C**H**CC(=O)OH), 7.43 (dd, 2 H, -NCH_2CC**H**CHCHCC(=O)OH, $^3J_{HH}$ = 6 Hz, $^4J_{HH}$ = 2.3 Hz), 4.77 (br s, overlaps with solvent peak, -NC**H_2**CCHCHCHCC(=O)OH), 3.44 (d, 2 H, -NC**H_2**P(=O)$(OH)_2$, $^2J_{PH}$ = 11.5 Hz)

^{13}C{^{1}H} NMR (100 MHz, D_2O, *pD* = 7.14, 298 K), *δ*: 172.15 (-$NCH_2CCHCHCHC$**C**(=O)OH), 152.72 (-NCH_2**C**CHCHCHCC(=O)OH), 150.94 (-$NCH_2CCHCHCH$**C**C(=O)OH), 138.82 (-NCH_2CCH**C**HCHCC(=O)-OH), 126.64 (-NCH_2C**C**HCHCHCC(=O)OH), 123.86 (-NCH_2CCHCH**C**HCC(=O)OH), 60.48 (-N**C**H_2CCH-CHCHCC(=O)OH), 54.20 (-N**C**H_2P(O)$(OH)_2$)

^{31}P{^{1}H} NMR (162 MHz, D_2O, *pD* = 7.14, 298 K), *δ*: 8.60 (-NCH_2**P**(=O)$(OH)_2$)

MS (ESI), *m/z*: 784.6 **[2M + Na]$^+$**

HRMS (ESI), *m/z*: 382.0799 (Calculated for **[M + H]$^+$,** $C_{15}H_{17}N_3O_7P_1$: 382.0799)

6.40. Gallium (III) complexation by H_4DPAP

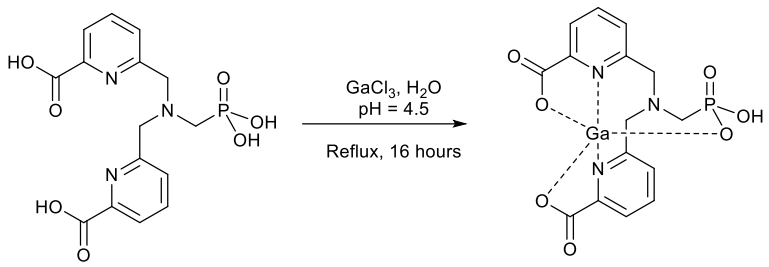

H_4DPAP (22 mg, 57.7 µmol) was added water (2 mL) and $GaCl_3$ (10.9 mg, 63.5 µmol, 1.1 eq). The pH was adjusted to 4.5 with NaOH. The suspension was heated to reflux for 16 hours before being concentrated to yield a white solid that was used without further purification (64.9 mg).

^{1}H NMR (400 MHz, D_2O, *pD* = 7.14, 298 K), *δ*: 8.19 (t, 2 H, -NCH_2CCHC**H**$CHCC(=O)O$-, $^{3}J_{HH}$ = 6.4 Hz), 8.13 (br d, 2 H, -$NCH_2CCHCHC$**H**$CC(=O)O$, $^{3}J_{HH}$ = 6.6 Hz), 7.76 (d, 2 H, -NCH_2CC**H**$CHCHCC(=O)O$-, $^{3}J_{HH}$ = 6.4 Hz), 4.51 (br s, 4 H, -NC**H$_2$**$CCHCHCHCC(=O)OH$), 2.64 (d, 2 H, -NC**H$_2$**$P(O)(OH)(O$-), $^{2}J_{PH}$ = 11.5 Hz)

^{13}C{^{1}H} NMR (100 MHz, D_2O, *pD* = 7.14, 298 K), *δ*: 152.77 (-NCH_2**C**$CHCHCHCC(=O)O$-), 152.72 (-$NCH_2CCHCHCH$**C**$C(=O)O$-) 141.84 (-NCH_2CCH**C**$HCHCC(=O)OH$), 126.38 (-NCH_2C**C**$HCHCHCC(=O)$-OH), 122.92 (-NCH_2CCHCH**C**$HCC(=O)OH$), 61.89 (-N**C**$H_2CCHCHCHCC(=O)O$-), 56.06 (d, -N**C**$H_2P(=O)(OH)(O$-), $^{1}J_{PC}$ = 146.4 Hz)

^{31}P{^{1}H} NMR (162 MHz, D_2O, *pD* = 7.14, 298 K), *δ*: 13.11 (-NCH_2**P**$(=O)(OH)_2$)

MS (ESI), *m/z*: 492.1 **[^{69}Ga][M+2Na-H]$^{+}$**, 494.1**[^{71}Ga][M+2Na-H]$^{+}$**

HRMS (ESI), *m/z*: 447.9819 (Calculated for **[M+H]$^{+}$,** $C_{15}H_{14}GaN_3O_7P_1$: 447.9820)

6.41. Synthesis of diethyl ((bis((6-(diethoxyphosphoryl)pyridine-2-yl)methyl)amino)methyl)phosphonate (Et_6DPPP)

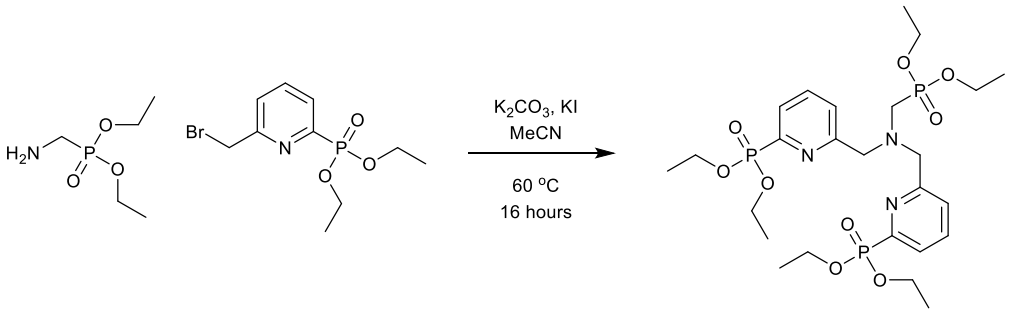

13 (164 mg, 0.53 mmol, 2.2 eq), **10** (40 mg, 0.24 mmol, 1 eq), potassium carbonate (167 mg, 1.21 mmol, 5 eq) and potassium iodide (88 mg, 0.53 mmol, 2.2 eq) were dissolved in acetonitrile (3 mL) and stirred at 60 °C for 16 hours. Water (10 mL) was added and the solution extracted with dichloromethane (3 x 10 mL). The combined organic layers were dried with magnesium sulfate and concentrated to yield a yellow oil. This oil was purified by column chromatography (silica, Dichloromethane/methanol 0-5%) to yield a yellow oil (19 mg, 0.03 mmol, 6%).

^{1}H NMR (400 MHz, $CDCl_3$, 298 K), *δ*:7.85-7.67 (m, 3 H, -NCH_2CC**H**C**H**C**H**$CP(=O)(OCH_2CH_3)_2$) , 4.30-4.15 (m, 8 H, -$NCH_2CCHCHCHCP(=O)(OC$**H$_2$**$CH_3)_2$), 4.12-4.08 (m, 8 H, -NC**H$_2$**$CCHCHCHCP(=O)(OCH_2CH_3)_2$, -$NCH_2P(=O)(OC$**H$_2$**$CH_3)_2$), 3.05 (d, 2 H, -$NC$**H$_2$**$P(=O)(OCH_2CH_3)_2$, $^2J_{PH}$ = 10.3 Hz), 1.34 (t, 12 H, -$NCH_2CCHCHCHCP(=O)(OCH_2C$**H$_3$**$)_2$, $^3J_{HH}$ = 7.0 Hz), 1.27 (t, 6 H, -$NCH_2P(=O)(OCH_2C$**H$_3$**$)_2$, $^3J_{HH}$ = 7.0 Hz)

^{13}C{^{1}H} NMR (100 MHz, $CDCl_3$, 298 K), *δ*: 159.96 (d, -NCH_2**C**$CHCHCHCP(=O)(OCH_2CH_3)_2$, $^3J_{PC}$ = 23.1 Hz), 151.11 (d, -$NCH_2CCHCHCH$**C**$P(=O)(OCH_2CH_3)_2$, $^1J_{PC}$ = 227.3 Hz), 136.77 (d, -NCH_2CCH**C**$HCHCP(=O)(OCH_2CH_3)_2$, $^3J_{PC}$ = 11.6 Hz), 126.50 (d, -NCH_2CCHCH**C**$HCP(=O)(OCH_2CH_3)_2$, $^2J_{PC}$ = 25.0 Hz), 125.99 (s, -NCH_2**C**$CHCHCHCP(=O)(OCH_2CH_3)_2$), 63.07 (d, -$NCH_2CCHCHCHCP(=O)(OC$**H$_2$**$CH_3)_2$, $^2J_{PC}$ = 5.8 Hz), 62.00 (d, -$NCH_2P(=O)(O$**C**$H_2CH_3)_2$, $^2J_{PC}$ = 6.9 Hz), 60.71 (s, -N**C**$H_2CCHCHCHCP(=O)(OCH_2CH_3)_2$), 49.29 (d, -N**C**$H_2P(=O)(OCH_2CH_3)_2$, $^1J_{PC}$ = 164.7 Hz), 16.48 (d, -$NCH_2P(=O)(OCH_2$**C**$H_3)_2$, $^3J_{PC}$ = 5.8 Hz), 16.33 (-$NCH_2CCHCHCHCP(=O)(OCH_2$**C**$H_3)_2$, $^3J_{PC}$ = 6.7 Hz)

^{31}P{^{1}H} NMR (162 MHz, $CDCl_3$, 298 K), *δ*: 25.91 (s, -NCH_2**P**$(=O)(OCH_2CH_3)_2$), 11.53 (s, -$NCH_2CCHCHCHC$**P**$(=O)(OCH_2CH_3)_2$)

MS (ESI), *m/z*: 622.9 **[M + H]$^+$**

HRMS (ESI), m/z: 622.2220 (Calculated for **[M + H]$^+$**, $C_{25}H_{43}N_3O_9P_3$: 622.2207)

6.42. Synthesis of ((bis((6-phosphonopyridin-2-yl)methyl)amino)methyl)phosphonic acid (H_6DPPP)

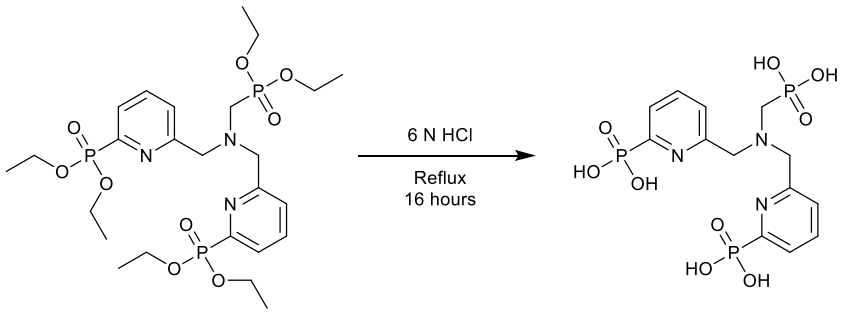

Et_6DPPP (40 mg, 64 µmol) was dissolved in 6 N HCl (4 mL). The solution was heated to reflux for 16 hours. The solution was concentrated to yield a yellow oil which was used without further purification (29 mg, 64 mmol, 100%).

^{1}H NMR (400 MHz, D_2O, pD = 6.1, 298 K), δ: 7.89-7.78 (m, 2 H, **py**), 7.74 (t, 1 H, **py**, $^3J_{HH}$ = 6.4 Hz), 7.62 (t, 1 H, **py**, $^3J_{HH}$ = 6.4 Hz), 7.43 (d, 1 H, **py**, $^3J_{HH}$ = 6.4 Hz), 7.31 (d, 1 H, **py**, $^3J_{HH}$ = 6.4 Hz), 4.67 (br s, 4 H, -NC**H$_2$**py), 3.16 (d, 2 H, -NC**H$_2$**P(=O)$(OH)_2$, $^2J_{PH}$ = 11.4 Hz)

^{31}P{^{1}H} NMR (162 MHz, D_2O, 298 K), δ: 10.15 (-NCH_2**P**(=O)$(OH)_2$), 7.11 (-py**P**(=O)$(OH)_2$)

MS (ESI), *m/z*: 451.8 **[M-H]**$^-$

6.43. Complexation of Ga(III) by H_6DPPP

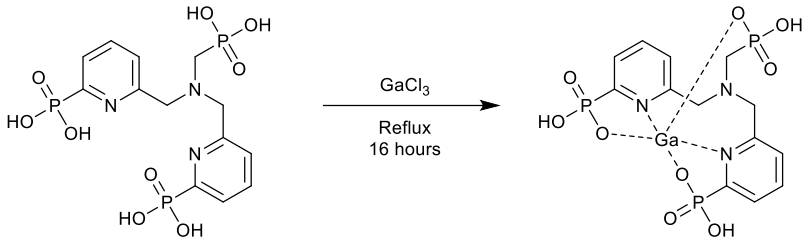

H_6DPPP (17 mg, 38 µmol) was dissolved in water (1 mL). $GaCl_3$ (7.3 mg, 31 µmol) in water (0.8 mL) was added and the pH adjusted to 4. The solution was heated to reflux for 16 hours. The solution was concentrated to yield a white solid (30 mg) that was used without further purification.

^{1}H NMR (400 MHz, D_2O, pD = 6.6, 298 K), *δ*: 8.37 (br s, 1 H, **py**), 8.03 (br s, 1 H, **py**), 7.94 (br s, 1 H, **py**), 7.86 (br s, 1 H, **py**), 7.71 (br s, 1 H, **py**), 7.45 (br s, 1 H, **py**), 4.50-4.22 (m, 3 H, -NC**H$_2$**py), 4.01 (br s, 1 H, -NC**H$_2$**py), 3.25 (br s, 1 H, -NC**H$_2$**P(=O)(O-)$_2$), 3.14 (br s, 1 H, -NC**H$_2$**P(=O)(O-)$_2$)

^{31}P{^{1}H} NMR (162 MHz, D_2O, pD = 6.6, 298 K), *δ*: 13.33 (-NCH$_2$**P**(=O)(O-)$_2$), 9.45 (-py**P**(=O)(O-)$_2$)

6.44. Synthesis of N1-benzyl-N2-(2-(benzylamino)ethyl)ethane-1,2-diamine (**14**)[255]

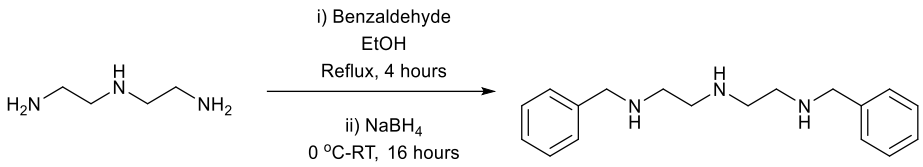

To diethylenetriamine (4.78 g, 5.0 mL, 46.3 mmol, 1 eq) in ethanol (50 mL) was added benzaldehyde (10.28 g, 9.9 mL, 96.8 mmol, 2 eq). The solution was heated to reflux for 4 hours. After cooling to 0 °C, sodium borohydride (12.26 g, 324.2 mmol, 7 eq) was added and the solution stirred at room temperature overnight. The solution was concentrated giving a yellow/white foamy solid. 1 M sodium hydroxide (250 mL) was added and extracted with chloroform (3 x 250 mL). The combined organic extracts were washed with 1 M sodium hydroxide (200 mL). After drying with magnesium sulfate, the organic layers were concentrated to approximately 300 mL. Concentrated hydrochloric acid (12.5 mL) was added with a large amount of white precipitate forming. This was allowed to cool before being collected on a sinter and washed with chloroform and diethyl ether. The white solid was dried on a high vacuum to yield a white solid (14.17 g, 29.3 mmol, 63%).

^{1}H NMR (400 MHz, D_2O, 298 K) *δ*: 7.44-7.37 (m, 10 H, NCH_2**Ph**), 4.21 (br s, 4 H, NC**H_2**Ph), 3.38-3.18 (m, 8 H, NC**H_2**C**H_2**N)

^{13}C{^{1}H} NMR (100 MHz, D_2O, 298 K) *δ*: 130.11 (NCH_2**Ph**), 129.89 (NCH_2**Ph**), 129.79 (NCH_2**Ph**), 129.34 (NCH_2**Ph**), 51.47 (N**C**H_2Ph), 43.61 (N**C**H_2**C**H_2N)

MS (ESI) *m/z*: 284.5 **[M+H]$^+$**

6.45. Synthesis of di-*tert*-butyl 2,2'-((((2-(*tert*-butoxy)-2-oxoethyl)azanediyl)bis(ethane-2,1-diyl))bis(benzylazanediyl))diacetate ($^{t}Bu_3Bn_2DT3A$)[256]

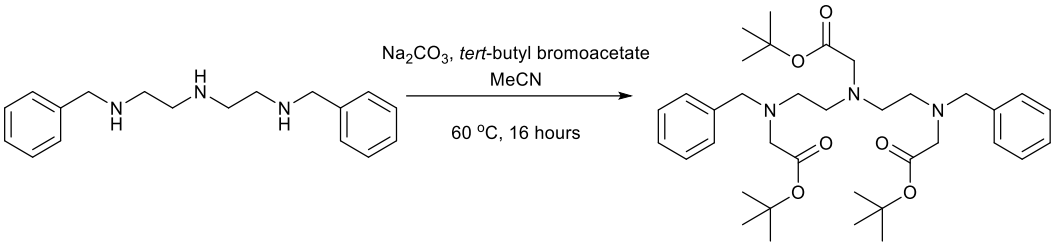

To **14** (6.06 g, 15.4 mmol, 1 eq) in acetonitrile (200 mL) was added sodium carbonate (13.08 g, 123.4 mmol, 8 eq). *Tert*-butyl bromoacetate (9.18 g, 7.0 mL, 47.1 mmol, 3.05 eq).was added slowly. The suspension was heated to 60 °C for 16 hours. The reaction was quenched by addition of water (1 L) and extracted with dichloromethane (3 x 1 L). The combined organic layers were dried with magnesium sulfate and concentrated to yield a yellow oil. Purification by column chromatography (silica, dichloromethane/triethylamine, 1%) yielded a yellow oil (4.56 g, 7.3 mmol, 47%)

^{1}H NMR (400 MHz, $CDCl_3$, 298 K) δ: 7.39-7.28 (m, 8 H, -NCH_2CC**H**C**H**CH), 7.23 (t, 2 H, -$NCH_2CCHCHC$**H**, $^{3}J_{HH}$ = 7.1 Hz), 3.78 (s, 4 H, -NC**H$_2$**Ph), 3.32 (s, 2 H, -NC**H$_2$**$C(=O)O^{t}Bu$), 3.23 (s, 4 H, $N(CH_2CH_2NC$**H$_2$**$C(=O)O^{t}Bu)_2$), 2.76 (br s, 8 H, -NC**H$_2$C H$_2$**N-), 1.46 (s, 18 H, $N(CH_2CH_2NCH_2C(=O)OC(C$**H$_3$**$)_3)_2$), 1.42 (s, 9 H, $NCH_2C(=O)OC(C$**H$_3$**$)_3$)

^{13}C{^{1}H} NMR (100 MHz, $CDCl_3$, 298 K) δ: 171.09 (-NCH_2**C**(**=**O)$O^{t}Bu$), 170.97 (-$N(CH_2CH_2NCH_2$**C**(**=**O)$O^{t}Bu)_2$), 139.21 (-NCH_2**C**$CHCHCH$), 129.08 (-NCH_2C**C**$HCHCH$), 128.30 (-NCH_2CCH**C**HCH), 127.08 (-NCH_2CCHCH**C**H), 80.81 (-C(=O)O**C**$(CH_3)_3$), 80.76 (-C(=O)O**C**$(CH_3)_3$), 58.42 (-N**C**H_2Ph), 56.05 (-N**C**$H_2C(=O)O^{t}Bu$), 55.23 (-$N(CH_2CH_2N$**C**$H_2C(=O)O^{t}Bu)_2$), 52.59 (-N**C**$H_2CH_2NCH_2$Ph), 52.04 (-NCH_2**C**H_2NCH_2Ph), 28.30 (-C(=O)OC(**C**$H_3)_3$), 28.25 (-C(=O)OC(**C**$H_3)_3$)

MS (ESI), *m/z*: 626.2 **[M+H]$^{+}$**

HRMS (ESI), m/z: 626.4168 (Calculated for **[M+H]$^{+}$**,$C_{36}H_{56}N_3O_6$: 626.4164)

6.46. Synthesis of 2,2'-((((carboxymethyl)azanediyl)bis(ethane-2,1-diyl))bis(benzylazanediyl))diacetic acid

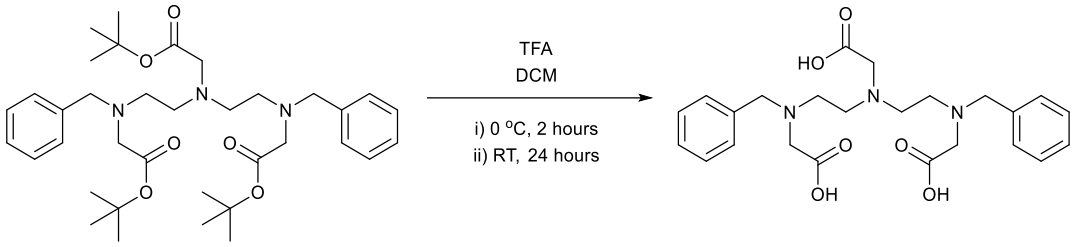

To $^{t}Bu_3Bn_2DT3A$ (2.710 g, 4.33 mmol, 1 eq) in dichloromethane (10 mL) at 0 °C was added trifluoroacetic acid (10 mL). The solution was stirred at 0 °C for 2 hours. The solution was allowed to warm to room temperature and stirred for 24 hours. The solution was concentrated and triturated with dichloromethane and ether to yield a white solid (2.00 g, 3.43 mmol, 79%).

^{1}H NMR (400 MHz, D_2O, 298 K) δ: 7.43 (br s, 10 H, -NCH_2***Ph***), 4.34 (s, 4 H, -NC***H$_2$***Ph), 3.90 (s, 4 H, $PhCH_2NC$***H$_2$***C(=O)OH), 3.18 (t, 4 H, -NCH_2C***H$_2$***NCH_2Ph, $^{3}J_{HH}$ = 5.9 Hz), 3.12 (s, 2 H, -NC***H$_2$***C(=O)OH), 2.79 (t, 4 H, -NC***H$_2$***CH_2NCH_2Ph, $^{3}J_{HH}$ = 5.9 Hz)

^{13}C{^{1}H} NMR (100 MHz, D_2O, 298 K) δ: 175.03 (-NCH_2**C**(=O)OH), 168.86 ($PhCH_2NCH_2$**C**(=O)OH), 131.20 (-NCH_2**Ph**), 130.52 (-NCH_2**Ph**), 129.48 (-NCH_2**Ph**), 128.41 (-NCH_2**Ph**), 59.44 (-N**C**H_2Ph), 54.19 (-N***C***H_2C(=O)OH, -$PhCH_2N$***C***H_2C(=O)OH), 51.21 (-NCH_2**C**H_2NCH_2Ph), 48.97 (-N**C**$H_2CH_2NCH_2Ph$)

MS (ESI) m/z: 458.8 **[M+H]$^{+}$**

HRMS (ESI), m/z: 458.2289 (Calculated for **[M+H]$^{+}$**, $C_{22}H_{32}N_3O_6$: 458.2286)

Elemental Analysis Found, %: C, 53.91, H, 5.44, N, 7.22 (Calculated for $(H_3Bn_2DT3A)(TFA)_{1.1}$, $C_{26.2}H_{32.1}F_{3.3}N_3O_{8.2}$, %: C, 53.98, H, 5.55, N, 7.21).

6.47. Ga(III) complexation by H_3Bn_2DT3A

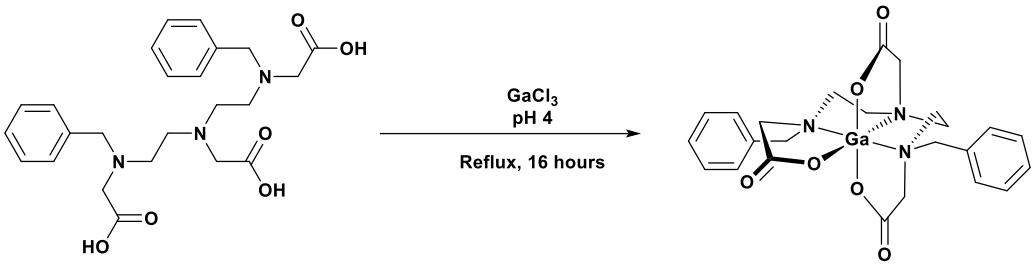

To H_3Bn_2DT3A (99 mg, 220 µmol) in water (10 mL) was added $GaCl_3$ (42 mg, 240 µmol). The pH was adjusted to 4 with NaOH and the solution heated to reflux for 16 hours. The solution was concentrated to yield a white/yellow solid (187 mg) which was used without further purification.

^{1}H NMR (400 MHz, D_2O, pD = 4.0, 298 K), *δ*: 7.50-7.28 (m, 10 H, -NCH$_2$**Ph**), 4.43-4.39 (m, 1 H, -NC**H$_2$**Ph), 4.27 (d, 1 H, -NC**H$_2$**C(=O)O-, $^2J_{HH}$ = 16 Hz), 4.17 (t, 1 H, -NC**H$_2$**Ph, $^2J_{HH}$ = 16 Hz), 4.05 (d, 1 H, -NC**H$_2$**Ph, $^2J_{HH}$ = 16 Hz), 3.95 (d, 1 H, -NC**H$_2$**Ph, $^2J_{HH}$ = 16 Hz, J = 3 Hz), 3.89 (d, 1 H, -NC**H$_2$**C(=O)O-, $^2J_{HH}$ = 19 Hz), 3.78 (t, 2 H, -NC**H$_2$**C(=O)O-, $^2J_{HH}$ = 13 Hz), 3.68-3.36 (m, 6 H, -NC**H$_2$**C**H$_2$**N-, -NC**H$_2$**C(=O)O-), 3.17 (dd, 1 H, -NC**H$_2$**C**H$_2$**N-, $^2J_{HH}$ = 17 Hz, $^3J_{HH}$ = 11 Hz), 3.11-3.09 (m, 1 H, -NC**H$_2$**C**H$_2$**N-), 2.90 (q, 1 H, -NC**H$_2$**C**H$_2$**N-, $^3J_{HH}$ = 5.5 Hz), 2.67 (quin, 1 H, -NC**H$_2$**C**H$_2$**N-, $^3J_{HH}$ = 6.4 Hz)

^{13}C{^{1}H} NMR (100 MHz, D_2O, pD = 4.0, 298 K), *δ*: 174.93 (-NCH$_2$**C**(=O)O-), 169.66 (-NCH$_2$**C**(=O)O-), 132.74 (**Ph**), 131.64 (**Ph**), 129.64 (**Ph**), 128.89 (**Ph**), 58.44 (-N**C**H$_2$Ph), 56.81 (-N**C**H$_2$C(=O)O-), 48.20 (-N**C**H$_2$**C**H$_2$N-)

^{1}H NMR (400 MHz, D_2O, pD = 6.8, 298 K), *δ*: 7.54-7.29 (m, 10 H, -NCH$_2$**Ph**), 4.31 (d, 1 H, NC**H$_2$**Ph, $^2J_{HH}$ = 17 Hz), 4.23 (d, 1 H, -NC**H$_2$**Ph, $^2J_{HH}$ = 13 Hz), 4.09 (d, 1 H, NC**H$_2$**C(=O)O-, $^2J_{HH}$ = 17 Hz), 3.99 (d, 1 H, NC**H$_2$**Ph, $^2J_{HH}$ = 13 Hz), 3.89-3.61 (m, 5 H, -NC**H$_2$**Ph, -NC**H$_2$**C(=O)O-, -NC**H$_2$**C**H$_2$**N-), 3.43 (br s, 4 H, -NC**H$_2$**C**H$_2$**N-, NC**H$_2$**C(=O)O-), 3.21 (t, 2 H, -NC**H$_2$**C**H$_2$**N-, $^2J_{HH}$ = 16 Hz), 3.11 (t, 2 H, -NC**H$_2$**C**H$_2$**N-, $^2J_{HH}$ = 15 Hz), 2.71 (br s, 1 H, -NC**H$_2$**C**H$_2$**N-)

^{13}C{^{1}H} NMR (100 MHz, D_2O, pD = 6.8, 298 K), *δ*: 175.15 (NCH$_2$**C**(=O)O-), 174.94 (NCH$_2$**C**(=O)O-), 132.74 (**Ph**), 131.64 (**Ph**), 129.42 (**Ph**), 128.88 (**Ph**), 57.28 (N**C**H$_2$Ph), 56.96 (-N**C**H$_2$C(=O)O-), 56.60 (-N**C**H$_2$C(=O)O-), 54.85 (-N**C**H$_2$**C**H$_2$N-), 49.49 (-N**C**H$_2$**C**H$_2$N-)

HRMS (ESI), *m/z*: 524.1734 (Calculated for **[^{69}Ga][M+H]$^+$**, $C_{24}H_{39}GaN_3O_6$: 524.1307)

6.48. Synthesis of 2-(benzylamino)ethan-1-ol (**15**)[263]

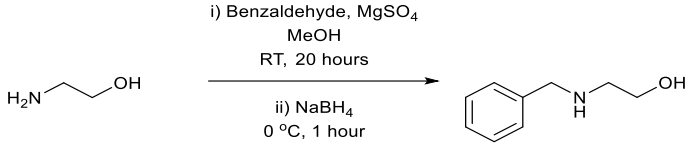

To 2-aminoethanol (10.0 g, 9.9 mL, 164 mmol, 1 eq) in methanol (120 mL) was added magnesium sulfate (39.4 g, 327 mmol, 2 eq). Benzaldehyde (17.4 g, 16.7 mL, 162 mmol, 1 eq) was added and the solution stirred at room temperature for 20 hours. The solution was cooled to 0 °C. Sodium borohydride (6.2 g, 167 mmol, 1 eq) was added portionwise slowly. Stirring was continued at 0 °C for 1 hour. The solution was filtered. Water and dichloromethane were added and the white solid that formed was filtered off. The organic layer was collected. The aqueous layer was extracted with dichloromethane. The combined extracts were dried and then taken up in ethyl acetate and washed with water. Following drying and concentration a colourless oil was obtained. (15.7 g, 104 mmol, 63%)

^{1}H NMR (400 MHz, $CDCl_3$, 298 K), δ: 7.35-7.28 (m, 5 H, -NCH_2**Ph**), 3.81 (s, 2 H, -NC**H_2**Ph), 3.66 (t, 2 H, -NCH_2C**H_2**OH, $^{3}J_{HH}$ = 5.5 Hz), 2.80 (t, 2 H, -NC**H_2**CH_2OH, $^{3}J_{HH}$ = 5.5 Hz), 2.36 (br s, 2 H, -N**H**, -O**H**)

^{13}C{^{1}H} NMR (100 MHz, $CDCl_3$, 298 K), δ: 139.85 (-NCH_2**C**CHCHCH), 128.47 (-NCH_2**Ph**), 128.09 (-NCH_2**Ph**), 127.10 (-NCH_2**Ph**), 60.88 (-NCH_2**C**H_2OH), 53.42 (-N**C**H_2CH_2OH), 50.41 (-N**C**H_2Ph)

MS (ESI), *m/z*: 152.1 **[M+H]$^{+}$**

6.49. Synthesis of *tert*-butyl N-benzyl-N-(2-hydroxyethyl)glycinate (16)[264]

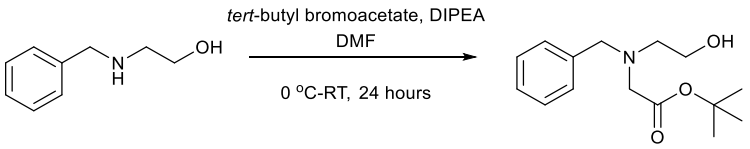

To ice cold **15** (15.7 g, 104 mmol, 1 eq) in dimethylformamide (100 mL) was added diisopropylethylamine (13.5 g, 18.1 mL, 104 mmol, 1 eq). *Tert*-butyl bromoacetate (20.3 g, 15.4 mL. 104 mmol, 1 eq) was added dropwise. The solution was allowed to warm to room temperature and stirring continued for 24 hours. The solvent was removed and the yellow residue taken up in dichloromethane (500 mL) and washed with water (3 x 200 mL) and brine (200 mL). The organic layer was dried with magnesium sulfate and concentrated to yield a yellow oil. Purification by column chromatography (silica, dichloromethane/methanol 0-10%) yielded a clear yellow oil (13.4 g, 50 mmol, 48%)

^{1}H NMR (400 MHz, $CDCl_3$, 298 K), δ: 7.35-7.32 (m, 5 H, -NCH_2**Ph**), 3.83 (s, 2 H, -NC**H_2**Ph), 3.60 (t, 2 H, -NCH_2C**H_2**OH, $^{3}J_{HH}$ = 5.5 Hz), 3.23 (s, 2 H, -NC**H_2**$C(=O)O^tBu$), 2.86 (t, 2 H, -NC**H_2**CH_2OH, $^{3}J_{HH}$ = 5.5 Hz), 1.45 (s, 9 H, -$NCH_2C(=O)OC(C$**H_3**$)_3$)

^{13}C{^{1}H} NMR (100 MHz, $CDCl_3$, 298 K), δ: 171.17 (-NCH_2**C**(**=**O)O^tBu), 138.35 (-NCH_2**C**$CHCHCH$), 128.87 (-NCH_2**Ph**), 128.42 (-NCH_2**Ph**), 127.33 (-NCH_2**Ph**), 81.36 (-$NCH_2C(=O)O$**C**$(CH_3)_3$), 58.87 (-NCH_2**C**H_2OH), 58.49 (-N**C**H_2Ph), 56.54 (-N**C**H_2CH_2OH), 55.32 (-N**C**$H_2C(=O)O^tBu$), 28.05 ($NCH_2C(=O)OC($**C**$H_3)_3$)

MS (ESI), *m/z*: 266.2 **[M+H]$^{+}$**

6.50. Synthesis of *tert*-butyl N-benzyl-N-(2-chloroethyl)glycinate (**17**)[265]

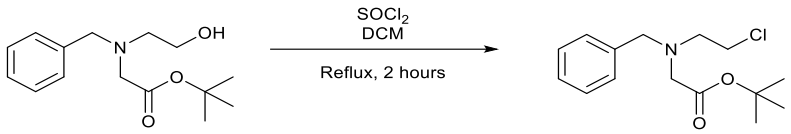

To **16** (7.7 g, 25 mmol, 1 eq) in dichloromethane (200 mL) was added thionyl chloride (6.0 g, 3.7 mL, 50 mmol, 2 eq). The solution was heated to reflux for 2 hours. Saturated sodium hydrogen carbonate (250 mL) was added. The organic layer was collected and the aqueous phase extracted with DCM (2 x 250 mL). The combined organic layers were dried with magnesium sulfate and concentrated to yield a yellow oil (6.1 g, 22 mmol, 85%).

^{1}H NMR (400 MHz, $CDCl_3$, 298 K), δ: 7.38-7.28 (m, 5 H, -NCH_2**Ph**), 3.89 (s, 2 H, -NC**H_2**Ph), 3.54 (t, 2 H, -NCH_2C**H_2**Cl, $^{3}J_{HH}$ = 6.0 Hz), 3.32 (s, 2 H, -NC**H_2**C(=O)O^{t}Bu), 3.08 (t, 2 H, -NC**H_2**CH_2Cl, $^{3}J_{HH}$ = 6.0 Hz), 1.48 (s, 9 H, -$NCH_2C(=O)OC(CH_3)_3$)

^{13}C NMR (100 MHz, $CDCl_3$, 298 K), δ: 170.68 (-NCH_2**C**(**=**O)$OC(CH_3)_3$), 138.85 (-NCH_2**C**CHCHCH), 128.77 (-NCH_2**Ph**), 128.35 (-NCH_2**Ph**), 127.24 (-NCH_2**Ph**), 81.12 (-$NCH_2C(=O)O$**C**$(CH_3)_3$), 58.23 (-N**C**H_2Ph), 55.78 (-N**C**H_2CH_2Cl), 55.41 (-N**C**H_2C(=O)O^{t}Bu), 42.28 (-NCH_2**C**H_2Cl), 28.19 (-$NCH_2C(=O)OC$(**C**$H_3)_3$)

MS (ESI), *m/z*: 284.2 **[^{35}Cl][M+H]$^{+}$**, 286.2 **[^{37}Cl][M+H]$^{+}$**

6.51. Synthesis of di-*tert*-butyl N,N-bis(2-(benzyl(2-(*tert*-butoxy)-2-oxoethyl)amino)ethyl)-L-glutamate ($^{t}Bu_4Bn_2DT3A.ga$)

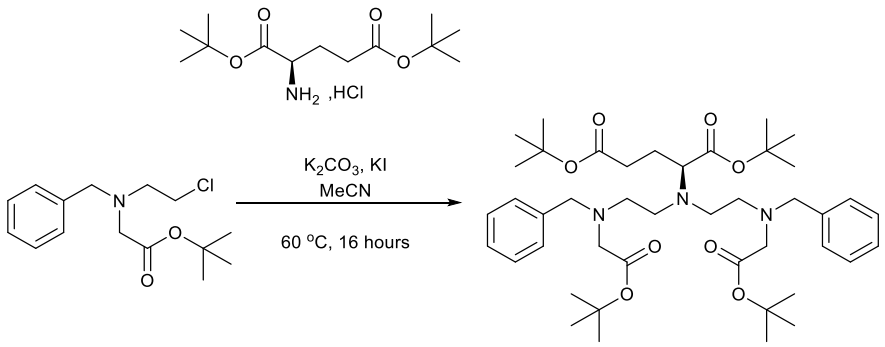

To **17** (2.0 g, 7.1 mmol, 2.1 eq) in acetonitrile (10 mL) was added di-*tert*-butyl glutamate hydrochloride (1.0 g, 3.4 mmol, 1 eq), potassium carbonate (2.3 g, 16.9 mmol, 5 eq) and potassium iodide (1.1 g, 7.1 mmol, 2.1 eq). The solution was heated to 60 °C for 16 hours. Water (15 mL) was added and extracted with dichloromethane (3 x 15 mL). The combined organic layers were dried with magnesium sulfate and concentrated to yield an orange oil. This was purified by column chromatography (silica, Hexane/Ethyl Acetate, 0-15%) yielding a clear oil (1.2 g, 1.6 mmol, 47%).

^{1}H NMR (400 MHz, $CDCl_3$, 298 K), δ: 7.34-7.28 (m, 8 H, -NCH_2**Ph**), 7.25-7.21 (m, 2 H, -NCH_2**Ph**), 3.75 (s, 4 H, -NC**H$_2$**Ph), 3.24 (dd, 1 H, -NC**H(**C(=O)O^{t}Bu)CH_2CH_2C(=O)^{t}Bu, $^{3}J_{HH}$ = 9.6, 6.0 Hz), 3.19 (s, 4 H, -NC**H$_2$**C(=O)O^{t}Bu), 2.78-2.61 (m, 8 H, -NC**H$_2$**C**H$_2$**N-), 2.30 (ddd, 1 H, -NCH(C(=O)O^{t}Bu)CH_2C**H$_2$**C(=O)O^{t}Bu, $^{2}J_{HH}$ = 16.5 Hz, $^{3}J_{HH}$ = 8.7, 6.0 Hz), 2.21 (ddd, 1 H, -NCH(C(=O)O^{t}Bu)CH_2C**H$_2$**C(=O)O^{t}Bu, $^{2}J_{HH}$ = 16.5 Hz, $^{3}J_{HH}$ = 8.7, 6.9 Hz), 1.91 (ddt, 1 H, -NCH(C(=O)O^{t}Bu)C**H$_2$**CH_2C(=O)O^{t}Bu, $^{2}J_{HH}$ = 13.2 Hz, $^{3}J_{HH}$ = 8.7, 6.0 Hz), 1.72 (dddd, 1 H, -NCH(C(=O)O^{t}Bu)C**H$_2$**CH_2C(=O)O^{t}Bu, $^{2}J_{HH}$ = 13.2 Hz, $^{3}J_{HH}$ = 9.6, 8.7, 6.0 Hz), 1.46 (s, 18 H, -C(=O)OC(C**H$_3$**)$_3$), 1.43 (s, 18 H, -C(=O)OC(C**H$_3$**)$_3$)

^{13}C{^{1}H} NMR (100 MHz, $CDCl_3$, 298 K), δ: 172.84 (-NCH(C(=O)O^{t}Bu)CH_2CH_2**C(=**O)O^{t}Bu), 172.32 (-NCH(**C(=**O)O^{t}Bu)CH_2CH_2C(=O)O^{t}Bu), 170.77 (-NCH_2**C(=**O)O^{t}Bu), 139.15 (-NCH_2**C**CHCHCH), 128.94 (-NCH_2**Ph**), 128.19 (-NCH_2**Ph**), 126.96 (-NCH_2**Ph**), 80.79 (-C(=O)O**C**$(CH_3)_3$), 80.65 (-C(=O)O**C**$(CH_3)_3$), 80.01 (-C(=O)O**C**$(CH_3)_3$), 63.41 (-N**C**H(C(=O)O^{t}Bu)CH_2CH_2C(=O)O^{t}Bu), 58.29 (-N**C**H_2Ph), 55.25 (-N**C**H_2C(=O)O^{t}Bu), 53.38 (-NCH_2**C**H_2NBn), 50.00 (-N**C**H_2CH_2NBn), 32.03 (-NCH(C(C=O)O^{t}Bu)CH_2**C**H_2C(=O)O^{t}Bu), 28.26 (-C(=O)OC(**C**$H_3)_3$), 28.20 (-C(=O)OC(**C**$H_3)_3$), 28.12 (-C(=O)OC(**C**$H_3)_3$), 25.05 (-NCH(C(=O)O^{t}Bu)**C**H_2CH_2C(=O)O^{t}Bu)

MS (ESI), *m/z*: 755.1 **[M + H]$^{+}$**

HRMS (ESI), *m/z*: 754.5000 (Calculated for **[M + H]$^{+}$**, $C_{43}H_{68}N_3O_8$: 754.5001)

6.52. Synthesis of N,N-bis(2-(benzyl(carboxymethyl)amino)ethyl)-L-glutamic acid ($H_4Bn_2DT3A.ga$)

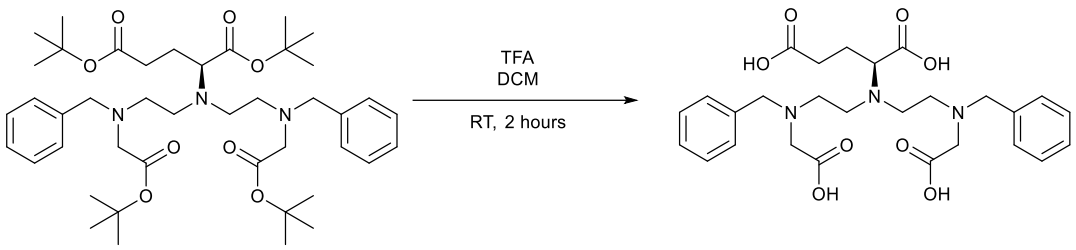

To $^{t}Bu_4Bn_2DT3A.ga$ (1.0 g, 1.3 mmol) in dichloromethane (10 mL) was added trifluoroacetic acid (10 mL). The solution was stirred at room temperature for 2 hours. The solution was concentrated. Dichloromethane (10 mL) and trifluoroacetic acid (10 mL) were added and stirring continued for 4 hours. The solution was concentrated and triturated with dichloromethane and ether to yield a white solid, collected by filtration (635 mg, 1.2 mmol, 92%).

^{1}H NMR (400 MHz, D_2O, pD = 4.1, 298 K), δ: 7.46 (br s, 10 H, -NCH$_2$**Ph**), 4.36 (d, 2 H, -NC**H**$_2$Ph, $^{2}J_{HH}$ = 13.8 Hz), 4.33 (d, 2 H, -NC**H**$_2$Ph, $^{2}J_{HH}$ = 13.8 Hz), 3.89 (s, 4 H, -NC**H**$_2$C(=O)OH), 3.18-3.05 (m, 4 H, -NCH$_2$**C**H$_2$N-), 2.93 (t, 1 H, -NC**H**(C(=O)OH)CH$_2$CH$_2$C(=O)OH, $^{3}J_{HH}$ = 6.9 Hz), 2.84-2.73 (m, 4 H, -N**C**H$_2$CH$_2$N-), 2.33 (dt, 1 H, -NCH(C(=O)OH)CH$_2$C**H**$_2$C(=O)OH, $^{2}J_{HH}$ = 17.0 Hz, $^{3}J_{HH}$ = 6.9 Hz), 2.24 (dt, 1 H, -NCH(C(=O)OH)CH$_2$C**H**$_2$C(=O)OH, $^{2}J_{HH}$ = 17.0 Hz, $^{3}J_{HH}$ = 6.9 Hz), 1.81 (dq, 1 H, -NCH(C(=O)OH)C**H**$_2$CH$_2$C(=O)OH, $^{2}J_{HH}$ = 14.0 Hz, $^{3}J_{HH}$ = 6.9 Hz), 1.57 (dq, 1 H, NCH(C(=O)OH)C**H**$_2$CH$_2$C(=O)OH, $^{2}J_{HH}$ = 14.0 Hz, $^{3}J_{HH}$ = 6.9 Hz)

^{13}C{^{1}H} NMR (100 MHz, D_2O, pD = 4.1, 298 K), δ: 177.13 (-NCH(C(=O)OH)CH$_2$CH$_2$**C**(=O)OH), 175.46 (-NCH(**C**(=O)OH)CH$_2$CH$_2$C(=O)OH), 168.94 (-NCH$_2$**C**(=O)OH), 131.15 (-NCH$_2$**Ph**), 130.64 (-NCH$_2$**Ph**), 129.62 (-NCH$_2$**Ph**), 128.61 (-NCH$_2$**Ph**), 61.58 (-N**CH**(C(=O)OH)CH$_2$CH$_2$C(=O)OH), 59.51 (-N**C**H$_2$Ph), 55.01 (-N**C**H$_2$C(=O)OH), 51.39 (-NCH$_2$**C**H$_2$NBn), 45.79 (-N**C**H$_2$CH$_2$NBn), 30.60 (-NCH(C(=O)OH)CH$_2$**C**H$_2$C(=O)OH), 22.91 (-NCH(C(=O)OH)**C**H$_2$CH$_2$C(=O)OH)

MS (ESI), *m/z*: 530.4 **[M+H]$^{+}$**

HRMS (ESI), *m/z*: 530.2500 (Calculated for **[M + H]$^{+}$**, $C_{27}H_{36}N_3O_8$: 530.2497)

6.53. Complexation of Ga(III) by $H_4Bn_2DT3A.ga$

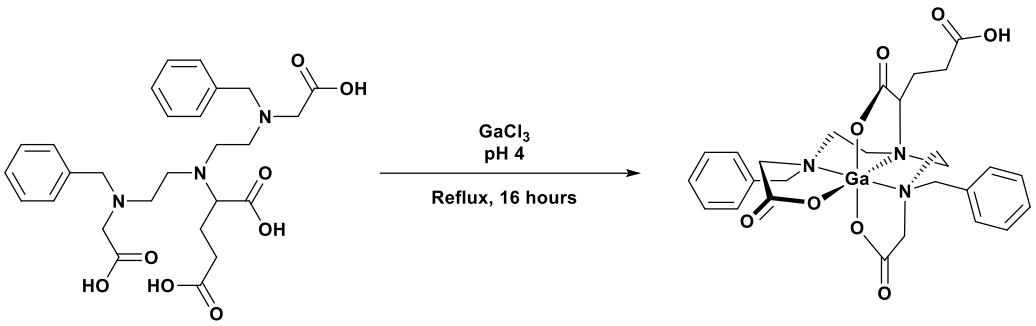

$H_4Bn_2DT3A.ga$ (15 mg, 25 µmol) was dissolved in water (5 mL) and $GaCl_3$ (4.9 mg, 28 µmol) added. The pH was adjusted to 4 and the solution heated to reflux for 16 hours. The solution was concentrated and the white solid (33 mg) dried and used without further purification.

^{1}H NMR (400 MHz, D_2O, pD = 3.8, 298 K), *δ*: 7.53-7.38 (m, 10 H, -NCH$_2$**Ph**), 5.41-4.44 (m, 2 H, -NC**H$_2$**Ph), 4.09 (dd, 1 H, -NC**H$_2$**C(=O)O-, $^2J_{HH}$ = 14.7, $^4J_{HH}$ = 2.8 Hz), 4.04-3.94 (m, 3 H, -NC**H$_2$**C(=O)O-, -NC**H$_2$**Ph), 3.94-3.65 (m, 3 H, -NC**H$_2$**C(=O)O-, -NC**H$_2$**C**H$_2$**N-), 3.61 (d, NC**H**(C(=O)O-)CH$_2$CH$_2$C(=O)OH, 1 H, $^3J_{HH}$ = 9.6 Hz), 3.29-2.95 (m, 5 H, -NC**H$_2$**C**H$_2$**N-), 2.86-2.63 (m, 3 H, -NCH(C(=O)O-)CH$_2$C**H$_2$**C(=O)OH, -NCH$_2$CH$_2$N-), 2.32 (dd, 1 H, -NC**H$_2$**C**H$_2$**N-. $^2J_{HH}$ = 13.1 Hz, $^3J_{HH}$ = 13.1 Hz), 2.04-1.87 (m, 2 H, -NCH(C(=O)O-)C**H$_2$**CH$_2$C(=O)OH)

^{13}C{^{1}H} NMR (100 MHz, D_2O, pD = 3.8, 298 K), *δ*: 175.39 (-**C**(=O)O-), 174.10 (-**C**(=O)O-), 169.49 (-**C**(=O)O-), 131.26 (-NCH$_2$**Ph**), 130.70 (-NCH$_2$**Ph**), 129.59 (-NCH$_2$**Ph**), 128.96 (-NCH$_2$**Ph**), 62.67 (-N**C**H(C(=O)O-)CH$_2$CH$_2$C(=O)OH)), 59.75 (-N**C**H$_2$Ph), 57.38 (-N**C**H$_2$C(=O)O-), 19.38 (NCH(C(=O)O-)C**H$_2$**CH$_2$C(=O)O-)

MS (ESI), *m/z*: 596.4 **[M+H]$^+$**

HRMS (ESI), *m/z*: 596.1533 (Calculated for **[^{69}Ga][M+H]$^+$**, $C_{27}H_{33}{}^{69}Ga_1N_3O_8$: 596.1518)

6.54. Synthesis of $H_3Bn_2DT3A.ga.PSMA$

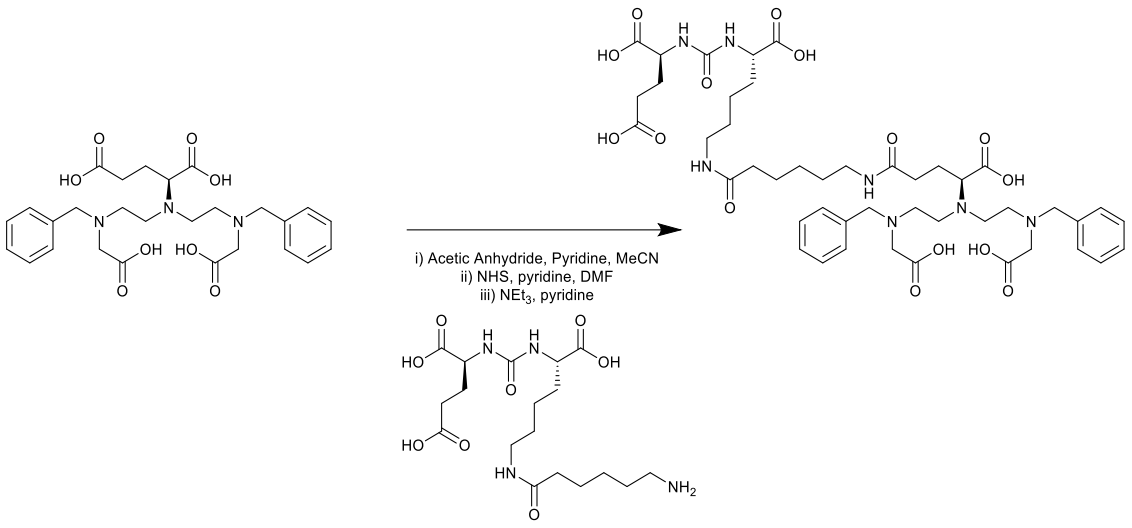

To $H_4Bn_2DT3A.ga$ (52.9 mg, 0.1 mmol, 2 eq) was added acetonitrile (2 mL), acetic anhydride (15.3 mg, 13.2 µL, 0.15 mmol, 3 eq) and pyridine (31.6 mg, 32.2 µL, 0.4 mmol, 8 eq). The suspension was stirred at room temperature under argon until dissolution and reaction were complete (30 minutes). Diethyl ether (4 mL) was added slowly producing a white precipitate. The precipitate was collected on a celite plug and washed with diethyl ether. The plug was dried with air. The product was eluted from the plug into the original round bottom flask with dimethylformamide (2 mL). N-hydroxysuccinimide (17.3 mg, 0.15 mmol, 3 eq) and pyridine (23.7 mg, 24.2 µL, 0.3 mmol, 6 eq) were added and the solution continued at room temperature under argon. After 2 hours further N-hydroxysuccinimide (6 eq) and pyridine (9 eq) in dimethylformamide (300 uL) were added and stirring continued. After 30 minutes, **9** (32.8 mg, 0.05 mmol, 1 eq) in dimethylformamide (200 µL) was added, followed by triethylamine (30.4 mg, 41.8 µL, 0.3 mmol, 6 eq). Stirring proceeded overnight under argon. The solution was concentrated under vacuum and purified by semi preparative HPLC (Acetonitrile + 0.1% TFA/Water + 0.1% TFA) to yield a clear oil (3.6 mg, 3.8 µmol, 7.6%).

^{1}H NMR (400 MHz, D_2O, 298 K), δ: 7.46-7.39 (m, 10 H, -NCH_2**Ph**), 4.35-4.28 (m, 4 H, -NC**H_2**Ph).4.15 (dd, 1 H, -NC(=O)NC**H**CH_2CH_2C(=O)OH, $^3J_{HH}$ = 9.2, 5.0 Hz), 4.06 (dd, 1 H, -NC(=O)NC**H**$CH_2CH_2CH_2CH_2$NC(=O)-, $^3J_{HH}$ = 8.7, 5.0 Hz), 3.87 (s, 4 H, -NC**H_2**C(=O)OH), 3.16-3.02 (m, 8 H, -NCH_2C**H_2**NCH_2Ph, -C**H_2**C(=O)NCH_2-), 2.91 (t, 1 H, -NC**H**(C(=O)OH)CH_2CH_2C(=O)N-, $^3J_{HH}$ = 6.9 Hz), 2.77 (br t, 4 H, -NC**H_2**CH_2NCH_2Ph, $^3J_{HH}$ = 6.0 Hz), 2.39 (t, 2 H, -NC(=O)NCHCH_2C**H_2**C(=O)OH, $^3J_{HH}$ = 7.1 Hz), 2.16-2.00 (m, 5 H, -NC(=O)NCHC**H_2**CH_2C(=O)OH, -CH_2C(=O)NC**H_2**-), 1.89-1.80 (m, 1 H, -NC(=O)NCHC**H_2**CH_2C(=O)OH), 1.80-1.66 (m, 2 H, -NC(=O)NCHC**H_2**$CH_2CH_2CH_2$NC(=O)-, -NCHC**H_2**CH_2C(=O)N-), 1.63-1.46 (m, 4 H, -NC(=O)NCHC**H_2**$CH_2CH_2CH_2$NC(=O)-, -NCH-C**H_2**CH_2C(=O)N-, -C**H_2**CH_2C(=O)N-), 1.44-1.36 (m, 4 H, -C**H_2**-), 1.32-1.16 (m, 4 H, -C**H_2**-)

$^{13}C\{^{1}H\}$ NMR (100 MHz, D_2O, 298 K), *δ*: 177.19 (-NC(=O)NCHCH$_2$CH$_2$**C**(**=**O)OH), 177.06 (-NC(=O)NCH(**C**(**=**O)OH)CH$_2$CH$_2$CH$_2$CH$_2$NC(=O)-), 176.72 (-CH$_2$**C**(=O)NCH$_2$-), 176.18 (-NC(=O)NCH(**C**(**=**O)OH)CH$_2$CH$_2$C(=O)N-), 175.38 (-NCH(**C**(**=**O)OH)), 174.61 (-CH$_2$**C**(=O)NCH$_2$-), 168.82 (-NCH$_2$C(=O)OH), 159.26 (-N**C**(=O)N-), 131.13 (-NCH$_2$**Ph**), 130.59 (-NCH$_2$**Ph**), 129.55 (-NCH$_2$**Ph**), 128.52 (-NCH$_2$**Ph**), 61.78 (-N**C**H(C(=O)OH)CH$_2$CH$_2$C(=O)N-), 59.41 (-N**C**H$_2$Ph), 54.82 (-N**C**H$_2$C(=O)OH), 53.15 (-NC(=O)N**C**HCH$_2$CH$_2$CH$_2$CH$_2$NC(=O)-), 52.50 (-NC(=O)N**C**HCH$_2$CH$_2$C(=O)-OH), 51.46 (-NCH$_2$**C**H$_2$NCH$_2$Ph), 45.77 (-N**C**H$_2$CH$_2$NCH$_2$Ph), 39.20 (-**C**H$_2$C(=O)NCH$_2$-), 38.87 (-**C**H$_2$C(=O)NCH$_2$-), 35.61 (-CH$_2$C(=O)N**C**H$_2$-), 32.33 (-CH$_2$C(=O)N**C**H$_2$-), 30.55 (-NC(=O)NCH-**C**H$_2$CH$_2$CH$_2$CH$_2$NC(=O)-), 29.98 (-NC(=O)NCHCH$_2$**C**H$_2$C(=O)OH), 27.99 (-**C**H$_2$-), 27.73 (-**C**H$_2$-), 26.21 (-NC(=O)NCH**C**H$_2$CH$_2$C(=O)OH), 25.47 (-**C**H$_2$CH$_2$C(=O)NCH$_2$-), 25.05 (-**C**H$_2$-), 23.93 (-NCH-**C**H$_2$CH$_2$C(=O)N-), 22.28 (-**C**H$_2$-)

HRMS (ESI), *m/z*: 944.4607 (Calculated for **[M + H]$^+$**, $C_{45}H_{66}N_7O_{15}$: 944.4611)

HPLC: Flow Rate: 3 ml min^{-1}. Solvent A: Acetonitrile + 0.1% TFA. Solvent B: Water + 0.1% trifluoroacetic acid. Gradient, ([Time / minutes] Solvent A: Solvent B): [0] 15:85, [5] 15:85, [15], 20:80, [25] 20:80. Retention time: 13 minutes

References

1 S. Dixon, *Diagnostic Imaging Dataset Annual Statistical Release 2016/17*, Leeds, 2017.

2 W. C. Röntgen, *Nature*, 1896, **53**, 274–276.

3 W. H. Sweet and G. L. Brownell, *Nucleonics*, 1954, **396**, 433–436.

4 W. H. Oldendorf, *Trans. Biomed. Electron.*, 1961, **8**, 68–72.

5 I. Donald, J. Macvigor and T. G. Brown, *Lancet*, 1957, **271**, 1188–1195.

6 P. C. Lauterbur, *Nature*, 1973, **242**, 117–118.

7 L. Jonsson, L. G. Larsson and I. Ragnhult, *Acta radiol.*, 1957, **47**, 217–228.

8 I. Rauscher, T. Maurer, K. Steiger, M. Schwaiger and M. Eiber, *Clin. Nucl. Med.*, 2017, **42**, 547–548.

9 H. Morais, *Clin. Med. Image Libr.*, 2017, **3**, 4–5.

10 C. J. C. dos S. Fernandes, M. S. Pessi, E. P. de Oliveira, D. Calderaro and R. de Souza, *Clin. Med. Image Libr.*, 2018, **4**, 3–4.

11 S. Arslan, *Clin. Med. Image Libr.*, 2017, **3**, 2–3.

12 G. J. R. Cook, G. K. Azad, B. P. Taylor, E. Lee, M. S. Morrison, S. Hughes, S. Morris, S. Rudman, S. Chowdhury and V. Goh, *Eur. J. Nucl. Med. Mol. Imaging*, 2018, **45**, 898–903.

13 N. J. Long and W.-T. Wong, *Chem. Mol. Imaging*, 2014, **24**, 408.

14 A. R. Kherlopian, T. Song, Q. Duan, M. A. Neimark, M. J. Po, J. K. Gohagan and A. F. Laine, *BMC Syst. Biol.*, 2008, **2**, 1–18.

15 J. Law, *Phys. Med. Biol.*, 2006, **51**, R155–R167.

16 E. C. Lin, *Mayo Clin. Proc.*, 2010, **85**, 1142–1146.

17 D. J. Brenner and E. J. Hall, *N. Engl. J. Med.*, 2007, **357**, 2277–2284.

18 D. A. Mankoff, *J. Nucl. Med.*, 2007, **48**, 18N, 21N.

19 M. L. Thakur and B. C. Lentle, *J. Nucl. Med.*, 2005, **46**, 11N–42N.

20 G. F. Knoll, *Radiation detection and measurement*, Wiley, Hoboken, New Jersey, 3rd ed., 2000.

21 P. W. Miller, N. J. Long, R. Vilar and A. D. Gee, *Angew. Chemie - Int. Ed.*, 2008, **47**, 8998–9033.

22 M. Partridge, A. Spinelli, W. Ryder and C. Hindorf, *Nucl. Instrum. Methods Phys. Res. A*, 2006, **568**, 933–936.

23 F. Wagner, Y. A. Hakami, G. Warnock, G. Fischer, M. W. Huellner and P. Veit-Haibach, *Mol. Imaging Biol.*, 2017, **19**, 795–803.

24 G. Audi, O. Bersillon, J. Blachot and A. H. Wapstra, *Nucl. Phys. A*, 2003, **729**, 3–128.

25 C. Champion and C. Le Loirec, *Phys. Med. Biol.*, 2007, **52**, 6605–6625.

26 A. K. Shukla and U. Kumar, *J. Med. Phys.*, 2006, **31**, 13–21.

27 H. Jadvar and J. A. Parker, in *Clinical PET and PET/CT*, Springer, London, 2005, pp. 45–67.

28 R. Hernandez, H. F. Valdovinos, Y. Yang, R. Chakravarty, H. Hong, T. E. Barnhart and W.

Cai, *Mol. Pharm.*, 2014, **11**, 2954–2961.

29 C. Vanasschen, M. Brandt, J. Ermert and H. H. Coenen, *Dalton Trans.*, 2016, **45**, 1315–1321.

30 P. Gawne, F. Man, J. Fonslet, R. Radia, J. Bordoloi, M. Cleveland, P. Jimenez-Royo, A. Gabizon, P. J. Blower, N. J. Long and R. T. M. de Rosales, *Dalton Trans.*, 2018, **47**, 9283–9293.

31 A. I. Jensen, G. W. Severin, A. E. Hansen, F. P. Fliedner, R. Eliasen, L. Parhamifar, A. Kjær, T. L. Andresen and J. R. Henriksen, *J. Control. Release*, 2018, **269**, 100–109.

32 A. L. Wooten, T. A. Aweda, B. C. Lewis, R. B. Gross and S. E. Lapi, *PLoS One*, 2017, **12**, 1–14.

33 J. P. Holland, M. J. Williamson and J. S. Lewis, *Mol. Imaging*, 2010, **9**, 1–20.

34 A. Luca, *EPJ web Conf.*, 2017, **146**, 8003.

35 T. J. Wadas, E. H. Wong, G. R. Weisman and C. J. Anderson, *Chem. Rev.*, 2010, **110**, 2858–2902.

36 Y. Zhang, H. Hong and W. Cai, *Curr. radiopharm.*, 2011, **4**, 131–139.

37 E. Boros, C. L. Ferreira, J. F. Cawthray, E. W. Price, B. O. Patrick, D. W. Wester, M. J. Adam and C. Orvig, *J. Am. Chem. Soc.*, 2010, **132**, 15726–15733.

38 S. S. Gambhir, *Nat. Rev. Cancer*, 2002, **2**, 683–693.

39 L. K. Shankar, J. M. Hoffman, S. Bacharach, M. M. Graham, J. Karp, A. A. Lammertsma, S. Larson, D. A. Mankoff, B. A. Siegel, A. Van den Abbeele, J. Yap and D. Sullivan, *J. Nucl. Med.*, 2006, **47**, 1059–1066.

40 G. Lappin and R. C. Garner, *Nat. Rev. Drug Discov.*, 2003, **2**, 233–240.

41 A. Bertoldo, G. Rizzo and M. Veronese, *Clin. Transl. Imaging*, 2014, **2**, 239–251.

42 D. Liu, P.-L. Khong, Y. Gao, U. Mahmood, B. Quinn, J. S. Germain, G. X. Xu and L. T. Dauer, *J. Nucl. Med.*, 2016, **57**, 907–912.

43 M. Rudin and R. Weissleder, *Nat. Rev. Drug Discov.*, 2003, **2**, 123–131.

44 A. J. Fischman, N. M. Alpert and R. H. Rubin, *Clin. Pharmacokinet.*, 2002, **41**, 581–602.

45 K. Ishiwata, W. Vaalburg, P. H. Elsinga, A. M. J. Paans and M. G. Woldring, *J. Nucl. Med.*, 1988, **29**, 1419–1427.

46 R. T. M. de Rosales, E. Arstad and P. J. Blower, *Target. Oncol.*, 2009, **4**, 183–97.

47 S. N. Reske, N. M. Blumstein, B. Neumaier, H.-W. Gottfried, F. Finsterbusch, D. Kocot, P. Möller, G. Glatting and S. Perner, *J. Nucl. Med.*, 2006, **47**, 1249–1254.

48 C. Solbach, M. Uebele, G. Reischl and H. J. MacHulla, *Appl. Radiat. Isot.*, 2005, **62**, 591–595.

49 A. B. Apolo, N. Pandit-Taskar and M. J. Morris, *J. Nucl. Med.*, 2008, **49**, 2031–2041.

50 C. A. Mathis, B. J. Lopresti and W. E. Klunk, *Nucl. Med. Biol.*, 2007, **34**, 809–822.

51 A. F. Shields, J. R. Grierson, B. M. Dohmen, H. J. Machulla, J. C. Stayanoff, J. M. Lawhorn-Crews, J. E. Obradovich, O. Muzik and T. J. Mangner, *Nat. Med.*, 1998, **4**, 1334–1336.

52 A. K. Buck, K. Herrmann, C. Shen, T. Dechow, M. Schwaiger and H. J. Wester, *Methods*, 2009, **48**, 205–215.

53 A. M. Groves, T. Win, S. Ben Haim and P. J. Ell, *Lancet Oncol.*, 2007, **8**, 822–830.

54 H. J. Wester, M. Herz, W. Weber, P. Heiss, R. Senekowitsch-Schmidtke, M. Schwaiger and G. Stöcklin, *J. Nucl. Med.*, 1999, **40**, 205–12.

55 L. R. Chervu and I. Sternlieb, *J. Nucl. Med.*, 1974, **15**, 1011–1013.

56 W. R. Harris and V. L. Pecoraro, *Biochemistry*, 1983, **22**, 292–299.

57 E. W. Price and C. Orvig, *Chem. Soc. Rev.*, 2014, **43**, 260–290.

58 S. J. Bogdanowich-Knipp, S. Chakrabarti, T. D. Williams, R. K. Dillman and T. J. Siahaan, *J. Pept. Res.*, 1999, **53**, 530–541.

59 Z. Cai, B. T. Y. Li, E. H. Wong, G. R. Weisman and C. J. Anderson, *Dalton Trans.*, 2015, **44**, 3945–3948.

60 M. D. Bartholomä, *Inorganica Chim. Acta*, 2012, **389**, 36–51.

61 M. Fani, J. P. André, H. R. Maecke, J. P. Andre and H. R. Maecke, *Contrast Media Mol. Imaging*, 2008, **3**, 53–60.

62 C. F. Ramogida, J. Pan, C. L. Ferreira, B. O. Patrick, K. Rebullar, D. T. T. Yapp, K.-S. Lin, M. J. Adam and C. Orvig, *Inorg. Chem.*, 2015, **54**, 4953–4965.

63 F. Zoller, P. J. Riss, F. P. Montforts, D. K. Kelleher, E. Eppard and F. Rösch, *Nucl. Med. Biol.*, 2013, **40**, 280–288.

64 B. P. Burke, N. Baghdadi, G. S. Clemente, N. Camus, A. Guillou, A. E. Kownacka, J. Domarkas, Z. Halime, R. Tripier and S. J. Archibald, *Faraday Discuss.*, 2014, **175**, 59–71.

65 B. P. Burke, N. Baghdadi, A. E. Kownacka, S. Nigam, G. S. Clemente, M. M. Al-Yassiry, J. Domarkas, M. Lorch, M. Pickles, P. Gibbs, R. Tripier, C. Cawthorne and S. J. Archibald, *Nanoscale*, 2015, **7**, 14889–14896.

66 S. Shi, B. C. Fliss, Z. Gu, Y. Zhu, H. Hong, H. F. Valdovinos, R. Hernandez, S. Goel, H. Luo, F. Chen, T. E. Barnhart, R. J. Nickles, Z. P. Xu and W. Cai, *Sci. Rep.*, 2015, **5**, 1–10.

67 S. Shi, C. Xu, K. Yang, S. Goel, H. F. Valdovinos, H. Luo, E. B. Ehlerding, C. G. England, L. Cheng, F. Chen, R. J. Nickles, Z. Liu and W. Cai, *Angew. Chemie - Int. Ed.*, 2017, **56**, 2889–2892.

68 S. Edmonds, A. Volpe, H. Shmeeda, A. C. Parente-Pereira, R. Radia, J. Baguña-Torres, I. Szanda, G. W. Severin, L. Livieratos, P. J. Blower, J. Maher, G. O. Fruhwirth, A. Gabizon and R. T. M. de Rosales, *ACS Nano*, 2016, **10**, 10294–10307.

69 P. Charoenphun, L. K. Meszaros, K. Chuamsaamarkkee, E. Sharif-Paghaleh, J. R. Ballinger, T. J. Ferris, M. J. Went, G. E. D. Mullen and P. J. Blower, *Eur. J. Nucl. Med. Mol. Imaging*, 2014, **42**, 278–287.

70 M. J. Welch, M. L. Thakur, R. E. Coleman, M. Patel, B. A. Siegel and M. M. Ter-Pogossian, *J. Nucl. Med.*, 1977, **18**, 558–562.

71 J. L. Dearling, J. S. Lewis, D. W. McCarthy, M. J. Welch and P. J. Blower, *Chem. Commun.*, 1998, 2531–2532.

72 M. A. Deri, B. M. Zeglis, L. C. Francesconi and J. S. Lewis, *Nucl. Med. Biol.*, 2013, **40**, 3–14.

73 B. Gutfilen, S. A. L. Souza and G. Valentini, *Drug Des. Devel. Ther.*, 2018, **12**, 3235–3245.

74 S. R. Banerjee and M. G. Pomper, *Appl. Radiat. Isot.*, 2013, **76**, 2–13.

75 J. R. Ballinger and K. K. Solanki, *Nucl. Med. Commun.*, 2011, **32**, 1109–1112.

76 F. Rosch, *Appl. Radiat. Isot.*, 2013, **76**, 24–30.

77 J. Seemann, E. Eppard, B. P. Waldron, T. L. Ross and F. Roesch, *Appl. Radiat. Isot.*, 2015, **98**, 54–59.

78 N. S. Loktionova, A. N. Belozub, D. V. Filosofov, K. P. Zhernosekov, T. Wagner, A. Türler and F. Rösch, *Appl. Radiat. Isot.*, 2011, **69**, 942–946.

79 W. A. P. Breeman, M. Jong, E. Blois, B. F. Bernard, M. Konijnenberg, E. P. Krenning, M. De Jong, E. De Blois, B. F. Bernard, M. Konijnenberg and E. P. Krenning, *Eur. J. Nucl. Med. Mol. Imaging*, 2005, **32**, 478–485 8p.

80 G.-J. Meyer, H. Maecke, J. Schuhmacher, W. H. Knapp, M. Hofmann, H. Mäcke, J. Schuhmacher, W. H. Knapp and M. Hofmann, *Eur. J. Nucl. Med. Mol. Imaging*, 2004, **31**, 1097–1104.

81 D. Mueller, I. Klette, R. P. Baum, M. Gottschaldt, M. K. Schultz and W. A. P. Breeman, *Bioconjug. Chem.*, 2012, **23**, 1712–1717.

82 K. P. Zhernosekov, D. V. Filosofov, R. P. Baum, P. Aschoff, H. Bihl, A. A. Razbash, M. Jahn, M. Jennewein and F. Rosch, *J. Nucl. Med.*, 2007, **48**, 1741–1748.

83 R. Vis, J. Lavalaye and E. M. W. van de Garde, *EJNMMI Res.*, 2015, **5**, 27.

84 M. D. Bartholomä, A. S. Louie, J. F. Valliant and J. Zubieta, *Chem. Rev.*, 2010, **110**, 2903–2920.

85 M. Lin, G. J. Waligorski and C. G. Lepera, *Appl. Radiat. Isot.*, 2018, **133**, 1–3.

86 F. Alves, V. H. P. Alves, S. J. C. Do Carmo, A. C. B. Neves, M. Silva and A. J. Abrunhosa, *Mod. Phys. Lett. A*, 2017, **32**, 1740013.

87 G. Bandoli, A. Dolmella, F. Tisato, M. Porchia and F. Refosco, *Coord. Chem. Rev.*, 2009, **253**, 56–77.

88 Y. Li, A. E. Martell, R. D. Hancock, J. H. Reibenspies, C. J. Anderson and M. J. Welch, *Inorg. Chem.*, 1996, **35**, 404–414.

89 E. Wong, P. Caravan, S. Liu, S. J. Rettig and C. Orvig, *Inorg. Chem.*, 1996, **35**, 715–724.

90 S. V. Govindan, R. B. Michel, G. L. Griffiths, D. M. Goldenberg and M. J. Mattes, *Nucl. Med. Biol.*, 2005, **32**, 513–519.

91 Y. Z. Sun, C. J. Anderson, T. S. Pajeau, D. E. Reichert, R. D. Hancock, R. J. Motekaitis, A. E. Martell and M. J. Welch, *J. Med. Chem.*, 1996, **39**, 458–470.

92 K. Plössl, R. Chandra, W. Qu, B. P. Lieberman, M.-P. P. Kung, R. Zhou, B. Huang and H. F. Kung, *Nucl. Med. Biol.*, 2008, **35**, 83–90.

93 J. Notni and H. J. Wester, *J. Label. Compd. Radiopharm.*, 2018, **61**, 141–153.

94 I. Velikyan, *Molecules*, 2015, **20**, 12913–12943.

95 I. Kayani, J. B. Bomanji, A. Groves, G. Conway, S. Gacinovic, T. Win, J. Dickson, M. Caplin and P. J. Ell, *Cancer*, 2008, **112**, 2447–2455.

96 B. Oronsky, P. C. Ma, D. Morgensztern and C. A. Carter, *Neoplasia*, 2017, **19**, 991–1002.

97 S. Adams, R. Baum, T. Rink, K. Usadel and G. Hör, *Eur. J. Nucl. Med.*, 1998, **25**, 79–83.

98 T. A. Hope, E. K. Bergsland, M. F. Bozkurt, M. Graham, A. P. Heaney, K. Herrmann, J. R. Howe, M. H. Kulke, P. L. Kunz, J. Mailman, L. May, D. C. Metz, C. Millo, S. O'Dorisio, D. L. Reidy-Lagunes, M. C. Soulen and J. R. Strosberg, *J. Nucl. Med.*, 2017, **59**, 66–74.

99 A. Afshar-Oromieh, U. Haberkorn, M. Eder, M. Eisenhut and C. M. Zechmann, *Eur. J. Nucl. Med. Mol. Imaging*, 2012, **39**, 1085–1086.

100 R. L. Siegel, K. D. Miller and A. Jemal, *CA. Cancer J. Clin.*, 2017, **67**, 7–30.

101 K. Kopka, M. Benešová, C. Bařinka, U. Haberkorn and J. Babich, *J. Nucl. Med.*, 2017, **58**, 17S–26S.

102 G. J. Stasiuk and N. J. Long, *Chem. Commun.*, 2013, **49**, 2732–2746.

103 Z. Liu, Y. Yan, S. Liu, F. Wang and X. Chen, *Bioconjugate Chem.*, 2009, **20**, 1016–1025.

104 J. Simecek, J. Notni, T. G. Kapp, H. Kessler and H. J. Wester, *Mol. Pharm.*, 2014, **11**, 1687–1695.

105 J. Simecek, M. Schulz, J. Notni, J. Plutnar, V. Kubicek, J. Havlickova and P. Hermann, *Inorg. Chem.*, 2012, **51**, 577–590.

106 C. L. Ferreira, E. Lamsa, M. Woods, Y. Duan, P. Fernando, C. Bensimon, M. Kordos, K. Guenther, P. Jurek and G. E. Kiefer, *Bioconjugate Chem.*, 2010, **21**, 531–536.

107 D. M. Weekes, C. F. Ramogida, M. de G. Jaraquemada-Peláez, B. O. Patrick, C. Apte, T. I. Kostelnik, J. F. Cawthray, L. Murphy and C. Orvig, *Inorg. Chem.*, 2016, **55**, 12544–12558.

108 M. Fani, L. Del Pozzo, K. Abiraj, R. Mansi, M. L. Tamma, R. Cescato, B. Waser, W. A. Weber, J. C. Reubi and H. R. Maecke, *J. Nucl. Med.*, 2011, **52**, 1110–1118.

109 R. A. Dumont, F. Deininger, R. Haubner, H. R. Maecke, W. A. Weber and M. Fani, *J. Nucl. Med.*, 2011, **52**, 1276–1284.

110 M. Weineisen, M. Schottelius, J. Simecek, R. P. Baum, A. Yildiz, S. Beykan, H. R. Kulkarni, M. Lassmann, I. Klette, M. Eiber, M. Schwaiger and H.-J. Wester, *J. Nucl. Med.*, 2015, **56**, 1169–1176.

111 Z. Varasteh, B. Mitran, U. Rosenström, I. Velikyan, M. Rosestedt, G. Lindeberg, J. Sörensen, M. Larhed, V. Tolmachev and A. Orlova, *Nucl. Med. Biol.*, 2015, **42**, 446–454.

112 C. M. Kang, S. M. Kim, H. J. Koo, M. S. Yim, K. H. Lee, E. K. Ryu and Y. S. Choe, *Eur. J. Nucl. Med. Mol. Imaging*, 2013, **40**, 198–206.

113 X. Gu, G. Cai, R. Zhang, M. Jiang, Y. Zhou, D. Pan, Y. Xu and H. Huang, *J. Radioanal. Nucl. Chem.*, 2015, **303**, 777–782.

114 G. Amouroux, J. Pan, S. Jenni, C. Zhang, Z. Zhang, N. Hundal-jabal, N. Colpo, Z. Liu, F. Benard and K.-S. Lin, *Mol. Pharm.*, 2015, **12**, 2879–2888.

115 M. Eder, S. Knackmuss, F. Le Gall, U. Reusch, V. Rybin, M. Little, U. Haberkorn, W. Mier and M. Eisenhut, *Eur. J. Nucl. Med. Mol. Imaging*, 2010, **37**, 1397–1407.

116 M. Braeuer, N. Anizan, A. Habenicht, D. Diallo, S. Mohanta, F. Hyafil, Z. Qin, Z. Varasteh, S. G. Nekolla, K. Steiger, J. Vigne, Y. Li, D. Le Guludec, D. R. Vera, R. Aid-Launais, Y. Döring, M. Schwaiger and J.-E. Fabre, *EJNMMI Res.*, , DOI:10.1186/s13550-017-0287-y.

117 I. Velikyan, G. J. Beyer and B. Långström, *Bioconjug. Chem.*, 2004, **15**, 554–560.

118 M. Peez-Malo, G. Szabo, E. Eppard, A. Vagner, I. Toh, A. Maiocchi, E. Hyun Suh, Z. Kovas, Z. Baranyai and F. Ro, *Inorg. Chem.*, 2018, **57**, 6107–6117.

119 E. Eppard, M. Wuttke, P. L. Nicodemus and F. Rosch, *J. Nucl. Med.*, 2014, **55**, 1023–1028.

120 C. L. Ferreira, D. T. T. Yapp, D. Mandel, R. K. Gill, E. Boros, M. Q. Wong, P. Jurek and G. E. Kiefer, *Bioconjug. Chem.*, 2012, **23**, 2239–2246.

121 V. Kubíček, J. Havlíčková, J. Kotek, G. Tircsó, P. Hermann, É. Tóth and I. Lukeš, *Inorg. Chem.*, 2010, **49**, 10960–10969.

122 R. Delgado, Y. Sun, R. J. Motekaitis and A. E. Martell, *Inorg. Chem.*, 1993, **32**, 3320–

3326.

123 I. Velikyan, H. Maecke and B. Langstrom, *Bioconjug. Chem.*, 2008, **19**, 569–573.

124 Z. Liu, G. Niu, F. Wang and X. Chen, *Eur. J. Nucl. Med. Mol. Imaging*, 2009, **36**, 1483–1494.

125 K. P. Eisenwiener, M. I. M. Prata, I. Buschmann, H. W. Zhang, A. C. Santos, S. Wenger, J. C. Reubi and H. R. Macke, *Bioconjugate Chem.*, 2002, **13**, 530–541.

126 K. Pohle, J. Notni, J. Bussemer, H. Kessler, M. Schwaiger and A. J. Beer, *Nucl. Med. Biol.*, 2012, **39**, 777–784.

127 J. Notni, J. Simecek and H. J. Wester, *ChemMedChem*, 2014, **9**, 1107–1115.

128 J. Notni, J. Simecek, P. Hermann and H. J. Wester, *Chem. Eur. J.*, 2011, **17**, 14718–14722.

129 J. Šimeček, O. Zemek, P. Hermann, H. J. Wester and J. Notni, *ChemMedChem*, 2012, **7**, 1375–1378.

130 J. Šimeček, O. Zemek, P. Hermann, J. Notni and H.-J. Wester, *Mol. Pharm.*, 2014, **11**, 3893–3903.

131 J. Simecek, P. Hermann, H. J. Wester and J. Notni, *ChemMedChem*, 2013, **8**, 95–103.

132 V. Kubíček, Z. Böhmová, R. Ševčíková, J. Vaněk, L. Přemysl, Z. Poláková, R. Michalicová, J. Kotek and P. Hermann, *Inorg. Chem.*, 2018, **57**, 3061–3072.

133 E. T. Clarke and A. E. Martell, *Inorganica Chim. Acta*, 1991, **181**, 273–280.

134 J. Notni, K. Pohle and H. J. Wester, *Nucl. Med. Biol.*, 2013, **40**, 33–41.

135 Z. Baranyai, D. Reich, A. Vagner, M. Weineisen, I. Toth, H.-J. H.-J. Wester, J. Notni, A. Vágner, M. Weineisen, I. Tóth, H.-J. H.-J. Wester and J. Notni, *Dalton Trans.*, 2015, **44**, 11137–11146.

136 J. Notni, P. Hermann, I. Dregely and H. J. Wester, *Chem. - A Eur. J.*, 2013, **19**, 12602–12606.

137 F. A. Rojas-Quijano, G. Tircsõ, E. Tircsõné Benyõ, Z. Baranyai, H. Tran Hoang, F. K. Kálmán, P. K. Gulaka, V. D. Kodibagkar, S. Aime, Z. Kovács and A. D. Sherry, *Chem. - A Eur. J.*, 2012, **18**, 9669–9676.

138 G. Máté, J. Šimeček, M. Pniok, I. Kertész, J. Notni, H. J. Wester, L. Galuska and P. Hermann, *Molecules*, 2015, **20**, 13112–13126.

139 A. Schmidtke, T. Läppchen, C. Weinmann, L. Bier-Schorr, M. Keller, Y. Kiefer, J. P. Holland and M. D. Bartholomä, *Inorg. Chem.*, 2017, **56**, 9097–9110.

140 T. Läppchen, Y. Kiefer, J. P. Holland and M. D. Bartholomä, *Nucl. Med. Biol.*, 2018, **60**, 45–54.

141 M. T. Ma, O. C. Neels, D. Denoyer, P. Roselt, J. A. Karas, D. B. Scanlon, J. M. White, R. J. Hicks and P. S. Donnelly, *Bioconjugate Chem.*, 2011, **22**, 2093–2103.

142 M. Bhadwal, T. Das, H. Dev Sarma and S. Banerjee, *Mol. Imaging Biol.*, 2015, **17**, 111–118.

143 F. Bryden, H. Savoie, E. V Rosca and R. W. Boyle, *Dalton Trans.*, 2015, **44**, 4925–4932.

144 Y. Fazaeli, A. R. Jalilian, M. M. Amini, K. Ardaneh, A. Rahiminejad, F. Bolourinovin, S. Moradkhani and A. Majdabadi, *Nucl. Med. Mol. Imaging*, 2012, **46**, 20–26.

145 C. Zhai, G. M. Franssen, M. Petrik, P. Laverman, D. Summer, C. Rangger, R. Haubner, H. Haas and C. Decristoforo, *Mol. Imaging Biol.*, 2016, **18**, 758–767.

146 M. Petrik, H. Haas, G. Dobrozemsky, C. Lass-Flörl, A. Helbok, M. Blatzer, H. Dietrich and C. Decristoforo, *J. Nucl. Med.*, 2010, **51**, 639–645.

147 P. A. Knetsch, C. Zhai, C. Rangger, M. Blatzer, H. Haas, P. Kaeopookum, R. Haubner and C. Decristoforo, *Nucl. Med. Biol.*, 2015, **42**, 115–122.

148 M. Petrik, G. M. Franssen, H. Haas, P. Laverman, C. Hörtnagl, M. Schrettl, A. Helbok, C. Lass-Flörl and C. Decristoforo, *Eur. J. Nucl. Med. Mol. Imaging*, 2012, **39**, 1175–1183.

149 M. Petrik, G. M. Franssen, H. Haas, P. Laverman, C. Hörtnagl, M. Schrettl, A. Helbok, C. Lass-Flörl and C. Decristoforo, *Eur. J. Nucl. Med. Mol. Imaging*, 2012, **39**, 1175–1183.

150 M. Petrik, C. Zhai, Z. Novy, L. Urbanek, H. Haas and C. Decristoforo, *Mol. Imaging Biol.*, 2016, **18**, 344–352.

151 C. Zhai, D. Summer, C. Rangger, H. Haas, R. Haubner and C. Decristoforo, *J. Label. Compd. Radiopharm.*, 2015, **58**, 209–214.

152 M. Benešová, M. Schäfer, U. Bauder-Wäst, A. Afshar-Oromieh, C. Kratochwil, W. Mier, U. Haberkorn, K. Kopka and M. Eder, *J. Nucl. Med.*, 2015, **56**, 914–920.

153 M. Weineisen, J. Simecek, M. Schottelius, M. Schwaiger and H.-J. Wester, *EJNMMI Res.*, 2014, **4**, 63.

154 M. Guleria, T. Das, J. Amirdhanayagam, H. D. Sarma and A. Dash, *Cancer Biother. Radiopharm.*, 2018, **33**, 1–9.

155 S. Y. Yap, T. W. Price, H. Savoie, R. W. Boyle and G. J. Stasiuk, *Chem. Commun.*, 2018, **54**, 7952–7954.

156 T. W. Price, J. Greenman and G. J. Stasiuk, *Dalton Trans.*, 2016, **45**, 15702–15724.

157 R. J. Motekaitis, A. E. Martell and M. J. Welch, *Inorg. Chem.*, 1990, **29**, 1463–1467.

158 M. Eder, O. Neels, M. Müller, U. Bauder-Wüst, Y. Remde, M. Schäfer, U. Hennrich, M. Eisenhut, A. Afshar-Oromieh, U. Haberkorn and K. Kopka, *Pharmaceuticals*, 2014, **7**, 779.

159 M. Eder, A. V. Krivoshein, M. Backer, J. M. Backer, U. Haberkorn and M. Eisenhut, *Nucl. Med. Biol.*, 2010, **37**, 405–412.

160 M. Schäfer, U. Bauder-Wüst, K. Leotta, F. Zoller, W. Mier, U. Haberkorn, M. Eisenhut and M. Eder, *EJNMMI Res*, 2012, **2**, 23.

161 S. Ray Banerjee, Z. Chen, M. Pullambhatla, A. Lisok, J. Chen, R. C. Mease and M. G. Pomper, *Bioconjug. Chem.*, 2016, **27**, 1447–1455.

162 Z. Zha, J. Song, S. R. Choi, Z. Wu, K. Ploessl, M. Smith and H. Kung, *Bioconjug. Chem.*, 2016, **27**, 1314–1323.

163 M. Eder, M. Schäfer, U. Bauder-Wüst, W. E. Hull, C. Wängler, W. Mier, U. Haberkorn and M. Eisenhut, *Bioconjug. Chem.*, 2012, **23**, 688–697.

164 J. Schuhmacher, G. Klivényi, R. Matys, M. Stadler, T. Regiert, H. Hauser, J. Doll, W. Maier-Borst and M. Zöller, *Cancer Res.*, 1995, **55**, 115–123.

165 J. Schuhmacher, G. Klivenyi, W. E. Hull, R. Matys, H. Hauser, H. Kalthoff, W. H. Schmiegel, W. Maier-Borst and S. Matzku, *Nucl. Med. Biol.*, 1992, **19**, 809–824.

166 S. Migliari, A. Sammartano, M. Scarlattei, G. Serreli, C. Ghetti, C. Cidda, G. Baldari, O. Ortenzia and L. Ru, *ACS Omega*, 2017, **2**, 7120–7126.

167 C. F. Ramogida, J. F. Cawthray, E. Boros, C. L. Ferreira, B. O. Patrick, M. J. Adam and C. Orvig, *Inorg. Chem.*, 2015, **54**, 2017–2031.

168 E. Boros, C. L. Ferreira, D. T. T. Yapp, R. K. Gill, E. W. Price, M. J. Adam and C. Orvig, *Nucl. Med. Biol.*, 2012, **39**, 785–794.

169 G. A. Bailey, E. W. Price, B. M. Zeglis, C. L. Ferreira, E. Boros, M. J. Lacasse, B. O. Patrick, J. S. Lewis, M. J. Adam and C. Orvig, *Inorg. Chem.*, 2012, **51**, 12575–12589.

170 E. Boros, C. L. Ferreira, B. O. Patrick, M. J. Adam and C. Orvig, *Nucl. Med. Biol.*, 2011, **38**, 1165–1174.

171 C. F. Ramogida, L. Murphy, J. F. Cawthray, J. D. Ross, M. J. Adam and C. Orvig, *J. Inorg. Biochem.*, 2016, **162**, 253–262.

172 C. F. Ramogida, D. Schindler, C. Schneider, Y. L. K. Tan, S. Huh, C. L. Ferreira, M. J. Adam and C. Orvig, *RSC Adv.*, 2016, **6**, 103763–103773.

173 B. P. Waldron, D. Parker, C. Burchardt, D. S. Yufit, M. Zimny and F. Roesch, *Chem. Commun.*, 2013, **49**, 579–581.

174 L. Manzoni, L. Belvisi, D. Arosio, M. P. Bartolomeo, A. Bianchi, C. Brioschi, F. Buonsanti, C. Cabella, C. Casagrande, M. Civera, M. De Matteo, L. Fugazza, L. Lattuada, F. Maisano, L. Miragoli, C. Neira, M. Pilkington-Miksa and C. Scolastico, *ChemMedChem*, 2012, **7**, 1084–1093.

175 J. Pfister, D. Summer, C. Rangger, M. Petrik, E. von Guggenberg, P. Minazzi, G. B. Giovenzana, L. Aloj and C. Decristoforo, *EJNMMI Res.*, 2015, **5**, 1–11.

176 E. Von Guggenberg, C. Rangger, J. Sosabowski, P. Laverman, J. C. Reubi, I. J. Virgolini and C. Decristoforo, *Mol. Imaging Biol.*, 2012, **14**, 366–375.

177 A. Vágner, C. D'Alessandria, G. Gambino, M. Schwaiger, S. Aime, A. Maiocchi, I. Tóth, Z. Baranyai and L. Tei, *ChemistrySelect*, 2016, **1**, 163–171.

178 Z. Baranyai, F. Uggeri, A. Maiocchi, G. B. Giovenzana, C. Cavallotti, A. Takács, I. Tóth, I. Bányai, A. Bényei, E. Brucher and S. Aime, *Eur. J. Inorg. Chem.*, 2013, 147–162.

179 J. Seemann, B. P. Waldron, F. Roesch and D. Parker, *ChemMedChem*, 2015, **10**, 1019–1026.

180 B. A. Nock, A. Kaloudi, J. Nagel, J.-P. Sinnes, F. Roesch and T. Maina, *Dalton Trans.*, 2017, **46**, 14584–14590.

181 J. Seemann, B. Waldron, D. Parker and F. Roesch, *EJNMMI Radiopharm. Chem.*, 2016, **1**, 1–12.

182 J. Greiser, C. Kühnel, H. Görls, W. Weigand and M. Freesmeyer, *Dalton Trans.*, 2018, **47**, 9000–9007.

183 R. Cusnir, C. Imberti, R. C. Hider, P. J. Blower and M. T. Ma, *Int. J. Mol. Sci.*, 2017, **18**, 4–7.

184 D. J. Berry, Y. M. Ma, J. R. Ballinger, R. Tavare, A. Koers, K. Sunassee, T. Zhou, S. Nawaz, G. E. D. Mullen, R. C. Hider and P. J. Blower, *Chem. Commun.*, 2011, **47**, 7068–7070.

185 M. T. Ma, C. Cullinane, K. Waldeck, P. Roselt, R. J. Hicks and P. J. Blower, *EJNMMI Res.*, 2015, **5**, 1–11.

186 C. Imberti, S. Y. A. A. Terry, C. Cullinane, F. Clarke, G. H. Cornish, N. K. Ramakrishnan, P. Roselt, A. P. Cope, R. J. Hicks, P. J. Blower and M. T. Ma, *Bioconjug. Chem.*, 2017, **28**, 481–495.

187 M. T. Ma, C. Cullinane, C. Imberti, J. Baguña Torres, S. Y. A. A. Terry, P. Roselt, R. J. Hicks, P. J. Blower, J. Baguna Torres, S. Y. A. A. Terry, P. Roselt, R. J. Hicks and P. J. Blower, *Bioconjug. Chem.*, 2016, **27**, 309–318.

188 S. Nawaz, G. E. D. Mullen, K. Sunassee, J. Bordoloi, P. J. Blower and J. R. Ballinger, *EJNMMI Res.*, 2017, **7**, 86–95.

189 J. D. Young, V. Abbate, C. Imberti, L. K. Meszaros, M. T. Ma, S. Y. A. Terry, R. C. Hider, G. E. Mullen and P. J. Blower, *J. Nucl. Med.*, 2017, **58**, 1270–1277.

190 T. Derlin, S. Schmuck, C. Juhl, J. Zörgiebel, S. M. Schneefeld, A. C. A. Walte, K. Hueper, C. A. von Klot, C. Henkenberens, H. Christiansen, J. T. Thackeray, T. L. Ross and F. M. Bengel, *Eur. J. Nucl. Med. Mol. Imaging*, 2018, **45**, 913–922.

191 T. Derlin, S. Schmuck, C. Juhl, S. Teichert, J. Zörgiebel, H. J. Wester, S. M. Schneefeld, A. C. A. Walte, J. T. Thackeray, T. L. Ross and F. M. Bengel, *Mol. Imaging Biol.*, 2018, **20**, 650–658.

192 M. S. Hofman, P. Eu, P. Jackson, E. Hong, D. Binns, A. Iravani, D. Murphy, C. Mitchell, S. Siva, R. J. Hicks, J. D. Young, P. Blower and G. E. Mullen, *J. Nucl. Med.*, 2017, **59**, 625–631.

193 F. Silva, M. P. C. Campello, L. Gano, C. Fernandes, I. C. Santos, I. Santos, J. R. Ascenso, M. Joao Ferreira and A. Paulo, *Dalton Trans.*, 2015, **44**, 3342–3355.

194 R. L. Arrowsmith, P. A. Waghorn, M. W. Jones, A. Bauman, S. K. Brayshaw, Z. Hu, G. Kociok-Kohn, T. L. Mindt, R. M. Tyrrell, S. W. Botchway, J. R. Dilworth and S. I. Pascu, *Dalton Trans.*, 2011, **40**, 6238–6252.

195 I. S. Alam, R. L. Arrowsmith, F. Cortezon-Tamarit, F. Twyman, G. Kociok-Köhn, S. W. Botchway, J. R. Dilworth, L. Carroll, E. O. Aboagye and S. I. Pascu, *Dalton Trans.*, 2016, **45**, 144–155.

196 C. J. Anderson and M. J. Welch, *Chem. Rev.*, 1999, **99**, 2219–2234.

197 O. Thews, M. Zimny, E. Eppard, M. Piel, N. Bausbacher, V. Nagel and F. Rösch, *Mol. Imaging Biol.*, 2014, **16**, 802–812.

198 M. Fellner, W. Dillenburg, H.-G. Buchholz, N. Bausbacher, M. Schreckenberger, F. Renz, F. Rösch and O. Thews, *Mol. Imaging Biol.*, 2011, **13**, 985–994.

199 M. Picchio, C. Crivellaro, G. Giovacchini, L. Gianolli and C. Messa, *Q J Nucl Med Mol Imaging*, 2009, **53**, 245–268.

200 T. Maurer, M. Eiber, M. Schwaiger and J. E. Gschwend, *Nat. Rev. Urol.*, 2016, **13**, 226–235.

201 B. Baur, C. Solbach, E. Andreolli, G. Winter, H.-J. J. Machulla and S. N. Reske, *Pharmaceuticals*, 2014, **7**, 517–529.

202 A. Afshar-Oromieh, A. Malcher, M. Eder, M. Eisenhut, H. G. Linhart, B. A. Hadaschik, T. Holland-Letz, F. L. Giesel, C. Kratochwil, S. Haufe, U. Haberkorn and C. M. Zechmann, *Eur. J. Nucl. Med. Mol. Imaging*, 2013, **40**, 486–495.

203 A. Afshar-Oromieh, H. Hetzheim, C. Kratochwil, M. Benesova, M. Eder, O. C. Neels, M. Eisenhut, W. Kubler, T. Holland-Letz, F. L. Giesel, W. Mier, K. Kopka and U. Haberkorn, *J. Nucl. Med.*, 2015, **56**, 1697–1705.

204 D. Satpati, A. Shinto, K. K. Kamaleshwaran, S. Sane and S. Banerjee, *Mol. Imaging Biol.*, 2016, **18**, 420–427.

205 E. Farkas, J. Nagel, B. P. Waldron, D. Parker, I. Tóth, E. Brücher, F. Rösch and Z. Baranyai, *Chem. - A Eur. J.*, 2017, **23**, 10358–10371.

206 S. Liu, *Adv. Drug Deliv. Rev.*, 2008, **60**, 1347–1370.

207 E. Boros and A. B. Packard, *Chem. Rev.*, 2018, **119**, 870–901.

208 A. Nonat, P. H. H. Fries, J. Pécaut and M. Mazzanti, *Chem. - A Eur. J.*, 2007, **13**, 8489–8506.

209 G. J. Stasiuk, S. Tamang, D. Imbert, C. Gateau, P. Reiss, P. Fries and M. Mazzanti, *Dalton Trans.*, 2013, **42**, 8197.

210 A. Forgács, R. Pujales-Paradela, M. Regueiro-Figueroa, L. Valencia, D. Esteban-Gómez, M. Botta and C. Platas-Iglesias, *Dalton Trans.*, 2017, **46**, 1546–1558.

211 M. Khannam, T. Weyhermüller, U. Goswami and C. Mukherjee, *Dalton Trans.*, 2017, **46**, 10426–10432.

212 P. L. de Sousa, J. B. Livramento, L. Helm, A. E. Merbach, W. Même, B. T. Doan, J. C. Beloeil, M. I. M. Prata, A. C. Santos, C. F. G. C. Geraldes and É. Tóth, *Contrast Media Mol. Imaging*, 2008, **3**, 78–85.

213 B. Hacht, *Bull. - Korean Chem. Soc.*, 2008, **29**, 372–376.

214 H. V. T. T. Luong and J. C. Liu, *Sep. Purif. Technol.*, 2014, **132**, 115–119.

215 K. Hagvall, P. Persson and T. Karlsson, *Geochim. Cosmochim. Acta*, 2014, **146**, 76–89.

216 S. L. Madsen, M. J. Welch, R. J. Motekaitis and A. E. Martell, *Int. J. Radiat. Appl. Instrumentation. Part B. Nucl. Med. Biol.*, 1992, **19**, 431–444.

217 R. Delgado, M. Do Carmo Figueira, S. Quintino, M. D. Figueira and S. Quintino, *Talanta*, 1997, **45**, 451–462.

218 A. M. Nonat, C. Gateau, P. H. Fries, L. Helm and M. Mazzanti, *Eur. J. Inorg. Chem.*, 2012, **2012**, 2049–2061.

219 A. Albert, *Biochem. J.*, 1952, **50**, 690–698.

220 J. C. Cassatt and R. G. Wilkins, *J. Am. Chem. Soc.*, 1968, **90**, 6045–6050.

221 M. I. Tsionou, C. E. Knapp, C. A. Foley, C. R. Munteanu, A. Cakebread, C. Imberti, T. R. Eykyn, J. D. Young, B. M. Paterson, P. J. Blower and M. T. Ma, *RSC Adv.*, 2017, **7**, 49586–49599.

222 M. Felber, M. Bauwens, J. M. J. M. Mateos, S. Imstepf, F. M. Mottaghy and R. Alberto, *Chem. - A Eur. J.*, 2015, **21**, 6090–6099.

223 T. W. Price, J. Gallo, V. Kubíček, Z. Böhmová, T. J. Prior, J. Greenman, P. Hermann and G. J. Stasiuk, *Dalton Trans.*, 2017, **46**, 16973–16982.

224 Y. Bretonnière, M. Mazzanti, J. Pécaut, F. A. Dunand and A. E. Merbach, *Inorg. Chem.*, 2001, **40**, 6737–6745.

225 A. Pellissier, Y. Bretonnière, N. Chatterton, J. Pécaut, P. Delangle and M. Mazzanti, *Inorg. Chem.*, 2007, **46**, 3714–3725.

226 G. Nocton, A. Nonat, C. Gateau and M. Mazzanti, *Helv. Chim. Acta*, 2009, **92**, 2257–2273.

227 C. Gateau, M. Mazzanti, J. Pécaut, F. A. Dunand, L. Helm, J. Pecaut, F. A. Dunand and L. Helm, *Dalton Trans.*, 2003, **12**, 2428–2433.

228 N. H. Evans, R. Carr, M. Delbianco, R. Pal, D. S. Yufit and D. Parker, *Dalton Trans.*, 2013, **42**, 15610.

229 N. Wartenberg, O. Raccurt, E. Bourgeat-Lami, D. Imbert and M. Mazzanti, *Eur. J. Inorg. Chem.*, 2013, **9**, 1493–1498.

230 A. Guillou, L. M. P. Lima, M. Roger, D. Esteban-Gómez, R. Delgado, C. Platas-Iglesias, V. Patinec and R. Tripier, *Eur. J. Inorg. Chem.*, 2017, **2017**, 2435–2443.

231 J. Notni, P. Hermann, J. Havlíčková, J. Kotek, V. Kubíček, J. Plutnar, N. Loktionova, P. J. Riss, F. Rösch and I. Lukeš, *Chem. - A Eur. J.*, 2010, **16**, 7174–7185.

232 J. Simecek, J. Notni, V. Kubicek and P. Hermann, *Nucl. Med. Biol.*, 2010, **37**, 679.

233 D. Zhang, B. Bousquet, J. C. Mulatier, D. Pitrat, M. Jean, N. Vanthuyne, L. Guy, J. P. Dutasta and A. Martinez, *J. Org. Chem.*, 2017, **82**, 6082–6088.

234 H. Wang, Z. Xin, R. Xiang, S. Liu, X. Gao and C. Li, *Chinese J. Chem.*, 2016, **34**, 757–762.

235 X. Zeng, D. Coquière, A. Alenda, E. Garrier, T. Prangé, Y. Li, O. Reinaud, I. Jabin, D. Coquiére, A. Alenda, E. Garrier, T. Prangé, Y. Li, O. Reinaud and I. Jabin, *Chem. - A Eur. J.*, 2006, **12**, 6393–6402.

236 Y. Bretonnière, M. Mazzanti, J. Pécaut, F. A. Dunand and A. E. Merbach, *Chem. Commun.*, 2001, 621–622.

237 W. Raphael, PhD thesis, L'Universite Joseph Fourier-Grenoble 1, 1999.

238 B. P. Burke, G. S. Clemente and S. J. Archibald, *J. Label. Compd. Radiopharm.*, 2014, **57**, 239–243.

239 T. W. Price, J. Greenman and G. J. Stasiuk, *Dalton Trans.*, 2016, **45**, 15702–15724.

240 Y. Bretonnière, M. Mazzanti, J. Pecaut, F. A. Dunand and A. E. Merbach, *Dalton Trans.*, 2003, **40**, 6737–6745.

241 M. Audras, L. Berthon, C. Berthon, D. Guillaumont, T. Dumas, M. C. Illy, N. Martin, I. Zilbermann, Y. Moiseev, Y. Ben-Eliyahu, A. Bettelheim, S. Cammelli, C. Hennig and P. Moisy, *Inorg. Chem.*, 2017, **56**, 12248–12259.

242 G. J. Stasiuk, H. Smith, M. Wylezinska-Arridge, J. L. Tremoleda, W. Trigg, S. K. Luthra, V. M. Iveson, F. N. E. Gavins and N. J. Long, *Chem. Commun.*, 2013, **49**, 564–566.

243 M. Roger, L. M. P. Lima, M. Frindel, C. Platas-Iglesias, J.-F. F. Gestin, R. Delgado, V. Patinec and R. Tripier, *Inorg. Chem.*, 2013, **52**, 5246–5259.

244 V. Bjornstad and K. Undheim, *Synth. Commun.*, 2009, **39**, 1793–1800.

245 G. Keglevich and E. Bálint, *Molecules*, 2012, **17**, 12821–12835.

246 J. W. Walton, R. Carr, N. H. Evans, A. M. Funk, A. M. Kenwright, D. Parker, D. S. Yufit, M. Botta, S. De Pinto and K.-L. L. Wong, *Inorg. Chem.*, 2012, **51**, 8042–8056.

247 S. J. Lee, H. S. Kim, H. W. Yang, B. W. Yoo and C. M. Yoon, *Bull. Korean Chem. Soc.*, 2014, **35**, 2155–2158.

248 E. Boros, C. L. Ferreira, J. F. Cawthray, E. W. Price, B. O. Patrick, D. W. Wester, M. J. Adam and C. Orvig, *J. Am. Chem. Soc.*, 2010, **132**, 15726–15733.

249 W. Jung, Y. K. Chung, D. M. Shin and S. Kim, 2002, **1267**, 1263–1267.

250 D. A. Moore, P. E. Fanwick and M. J. Welch, *Inorg. Chem.*, 1990, **29**, 672–676.

251 C. T. Yang, Y. Li and S. Liu, *Inorg. Chem.*, 2007, **46**, 8988–8997.

252 J. Y. Lee, J. M. Jeong, Y. J. Kim, H. J. Jeong, Y. S. Lee, D. S. Lee and J. K. Chung, *Nucl. Med. Biol.*, 2014, **41**, 210–215.

253 R. Chakravarty, S. Chakraborty, A. Dash and M. R. A. Pillai, *Nucl. Med. Biol.*, 2013, **40**, 197–205.

254 L. Wei, X. Zhang, F. Gallazzi, Y. Miao, X. Jin, M. W. Brechbiel, H. Xu, T. Clifford, M. J. Welch, J. S. Lewis and T. P. Quinn, *Nucl. Med. Biol.*, 2009, **36**, 345–354.

255 G. Gros and J. Hasserodt, *European J. Org. Chem.*, 2015, **2015**, 183–187.

256 E. W. Price, J. F. Cawthray, G. A. Bailey, C. L. Ferreira, E. Boros, M. J. Adam and C. Orvig, *J. Am. Chem. Soc.*, 2012, **134**, 8670–8683.

257 M. D. National Institute of Standards and Technology: Gaithersburg, 2003.

258 J. Costa, R. Ruloff, L. Burai, L. Helm and A. E. Merbach, *J. Am. Chem. Soc.*, 2005, **127**, 5147–5157.

259 T. J. McMurry, C. G. Pippin, C. Wu, K. A. Deal, M. W. Brechbiel, S. Mirzadeh and O. A. Gansow, *J. Med. Chem.*, 1998, **41**, 3546–3549.

260 D. T. Guranda, G. A. Ushakov, P. G. Yolkin and V. K. Švedas, *J. Mol. Catal. B Enzym.*, 2012, **74**, 48–53.

261 C. H. Arrowsmith, H. X. Guo and A. J. Kresge, *J. Am. Chem. Soc.*, 1994, **116**, 8890–8894.

262 B. Drahoš, V. Kubíček, C. S. Bonnet, P. Hermann, I. Lukeš and É. Tóth, *Dalton Trans.*, 2011, **40**, 1945–1951.

263 R. Hemelaere, J. Desroches and J. F. Paquin, *Org. Lett.*, 2015, **17**, 1770–1773.

264 G. Bechara, N. Leygue, C. Galaup, B. Mestre-Voegtlé and C. Picard, *Tetrahedron*, 2010, **66**, 8594–8604.

265 F. Couty, B. Drouillat and F. Lemée, *European J. Org. Chem.*, 2011, **2011**, 794–801.

266 S. A. Kularatne, Z. Zhou, J. Yang, C. B. Post and P. S. Low, *Mol. Pharm.*, 2009, **6**, 790–800.

267 T. Liu, Y. Toriyabe, M. Kazak and C. E. Berkman, *Biochemistry*, 2008, **47**, 12658–12660.

268 M. Zhou, Z. Diwu, N. Panchuk-Voloshina and R. P. Haugland, *Anal. Biochem.*, 1997, **253**, 162–168.

269 Y.-C. Cheng and W. H. Prusoff, *Biochem. Pharmacol.*, 1973, **22**, 3099–3108.

270 C. Rojas, S. T. Frazier, J. Flanary and B. S. Slusher, *Anal. Biochem.*, 2002, **310**, 50–54.

271 A. Bevilacqua, R. I. Gelb, W. B. Hebard and L. J. Zompa, *Inorg. Chem.*, 1987, **26**, 2699–2706.

272 P. K. Glasoe and F. A. Long, *J. Phys. Chem.*, 1960, **64**, 188–190.

273 P. Táborský, P. Lubal, J. Havel, J. Kotek, P. Hermann and I. Lukeš, *Collect. Czech. Chem. Commun.*, 2005, **70**, 1909–1942.

274 M. Försterová, I. Svobodová, P. Lubal, P. Táborský, J. Kotek, P. Hermann and I. Lukeš, *Dalton Trans.*, 2007, **0**, 535–549.

275 M. Kývala, P. Lubal and I. Lukeš, *Spanish-Italian Mediterr. Congr. Thermodyn. Met. Complexes (SIMEC 98)*, 1998.

276 M. Kývala and I. Lukeš, *Int. Conf. Chemom. '95*, 1995, 63.

277 X. Li, C. Zhan, Y. Wang and J. Yao, *Chem. Commun.*, 2008, 2444–2446.

278 J. W. Walton, D. Bari, D. Parker, G. Pescitelli, L. Di Bari, D. Parker, G. Pescitelli, H. Puschmann and D. S. Yufit, *Chem. Commun.*, 2011, **47**, 12289–12291.

Chapter 7 Appendix 1 – Potentiometric Data

Table 7.1: Protonation constants (pK_a) of ligands and stability constants (logK_{ML}) complexes (T = 25 °C, I = 0.1 M NMe_4Cl). Charges are omitted.

	H_3Dpaa	H_4Dpaa.ga	H_3Dpaa.dab	H_3Bn_2DT3A
pK_1	7.38(2)	7.17(1)	11.35(1)	9.70(1)
pK_2	3.73(2)	4.67(2)	5.39(2)	7.48(1)
pK_3	2.82(2)	3.92(2)	3.77(3)	3.34(1)
pK_4	-	2.75(2)	2.69(3)	1.50(2)
pK_5	-	-	-	1.40(2)
Ga + L = [Ga(L)]	18.53(5)	18.36(3)	22.08(1)	18.25(3)
[Ga(HL)] = [Ga(L)] + H	1.0(2)	4.04(3)	5.40(2)	2.73(3)
[Ga(L)] = [Ga(L)(OH)] + H	4.41(2)	5.27(1)	-	5.32(2)
[Ga(L)(OH)] = [Ga(L)$(OH)_2$] + H	9.63(8)	-	-	8.21(2)
Cu+ L = [Cu(L)]	10.85(1)	14.52(7)	19.1(1)	18.9(1)
[Cu(HL)] = [Cu(L)] + H	3.38(1)	4.54(7)	5.0(1)	2.8(1)
[Cu(H_2L)] = [Cu(HL)] + H	-	3.10(7)	2.8(1)	-
[Cu(L)] = [Cu(L)(OH)] + H	9.86(2)	10.52(7)	12.5(1)	-
[Cu(L)(OH)] = [Cu(L)$(OH)_2$] + H	12.00(2)	-	-	-
Zn + L = [Zn(L)]	11.93(3)	13.38(7)	15.8(1)	14.12(3)
[Zn(HL)] = [Zn(L)] + H	2.33(4)	4.65(7)	6.8(1)	4.16(1)
[Zn(H_2L)] = [Zn(HL)] + H	-	1.77(8)	1.8(1)	-
[Zn(L)] = [Zn(L)(OH)] + H	11.27(3)	12.24(7)	12.2(1)	12.06(4)
[Zn(L)(OH)] = [Zn(L)$(OH)_2$] + H	-	-	-	-

Table 7.2: Overall protonation constants of ligands and stability constants (logβ) of complexes. (T = 25 °C, I = 0.1 M NMe_4Cl). Charges are omitted.

	H_3Dpaa	H_4Dpaa.ga	H_3Dpaa.dab	H_3Bn_2DT3A
HL	7.38(2)	7.17(1)	11.35(1)	9.70(1)
H_2L	11.11(2)	11.84(2)	16.74(2)	17.18(1)
H_3L	13.93(2)	15.76(2)	20.51(3)	20.52(1)
H_4L	-	18.51(2)	23.20(3)	22.02(2)
H_5L	-	-	-	23.42(2)
[Ga(L)]	18.53(5)	18.36(3)	22.08(1)	18.25(3)
[Ga(HL)]	19.5(2)	22.40(3)	27.48(2)	20.98(3)
[Ga(L)(OH)]	14.12(2)	13.09(1)	-	12.93(2)
[Ga(L)$(OH)_2$]	4.49(8)	-	-	4.72(2)
[Cu(L)]	10.85(1)	14.52(7)	19.1(1)	18.9(1)
[Cu(HL)]	14.23(1)	19.06(7)	24.1(1)	21.7(1)
[Cu(H_2L)]	-	22.16(7)	26.9(1)	-
[Cu(L)(OH)]	0.99(2)	4.00(7)	6.6(1)	-
[Cu(L)$(OH)_2$]	-11.01(2)	-	-	-
[Zn(L)]	11.93(3)	13.38(7)	15.8(1)	14.12(3)
[Zn(HL)]	14.26(4)	18.03(7)	22.6(1)	18.28(1)
[Zn(H_2L)]	-	19.80(8)	24.3(1)	-
[Zn(L)(OH)]	0.66(3)	1.14(7)	3.6(1)	2.06(4)

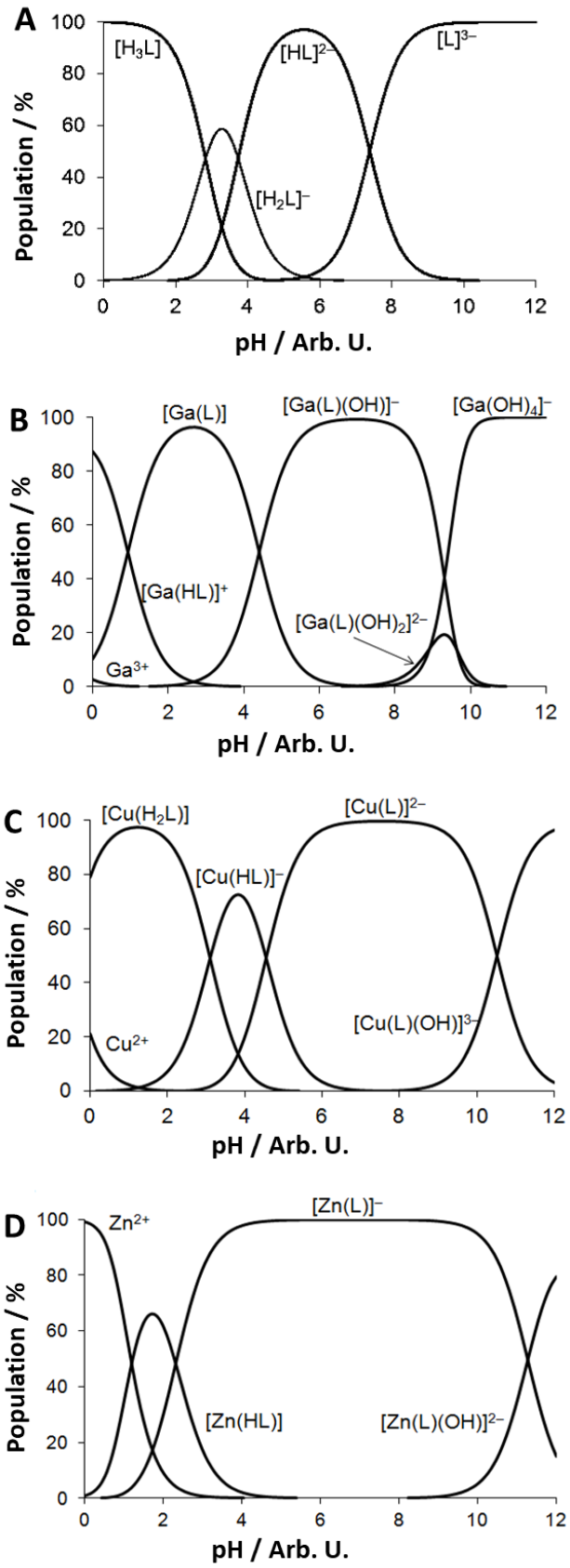

Figure 7.1: Distribution diagrams for A) H_3Dpaa, B) Ga(III)-Dpaa, C) Cu(II)-Dpaa, D) Zn(II)-Dpaa. (T = 25 °C, I = 0.1 M NMe_4Cl, *[L]* = *[M]* = 4 μM)

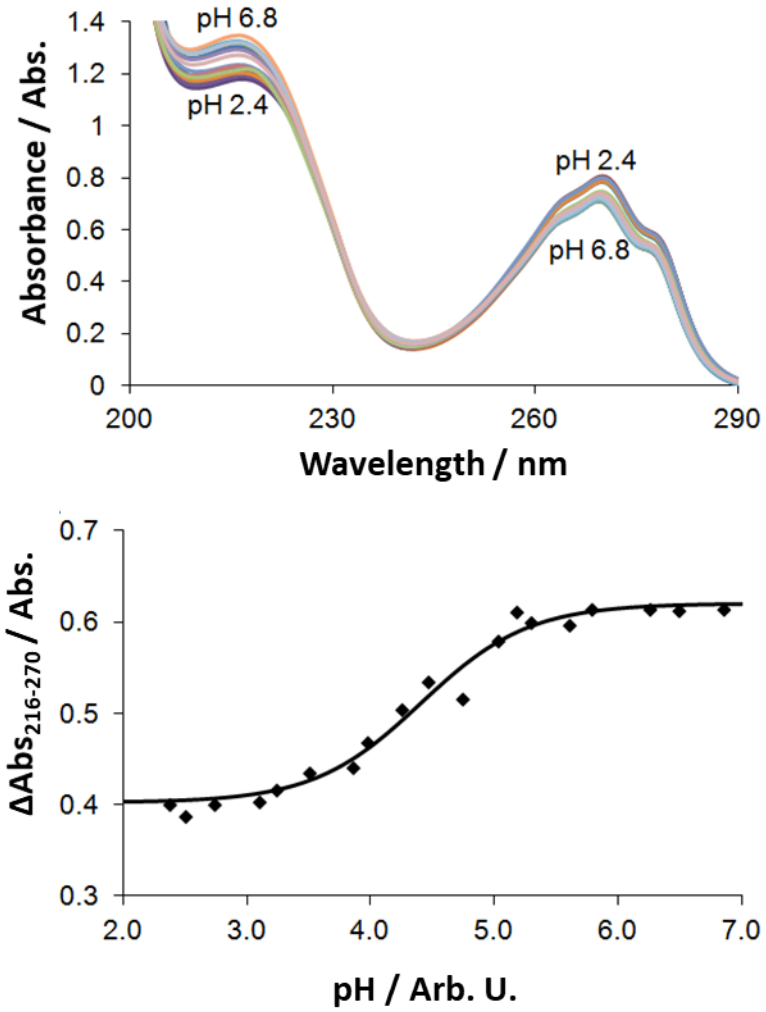

Figure 7.2: UV-Vis titration of Ga(III)-Dpaa system. Top: UV-Vis spectra variation with pH. Bottom: Difference of absorbance, ΔAbs = Abs_{216nm} – $Abs_{270\ nm}$, used to evaluate results. The line corresponds to the best fit. (T = 25 °C, *[L]* = *[M]* = 0.1 mM.

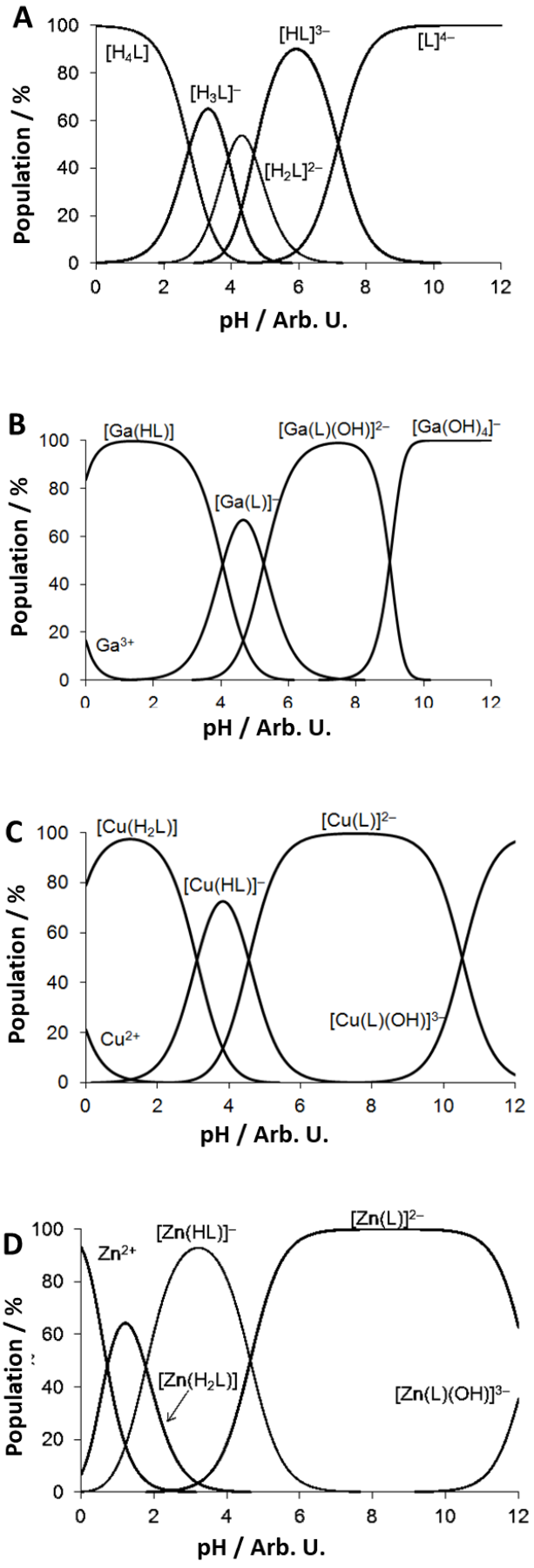

Figure 7.3: Distribution diagrams for A) H_4Dpaa.ga, B) Ga(III)-Dpaa.ga, C) Cu(II)-Dpaa.ga, D) Zn(II)-Dpaa.ga. (T = 25 °C, I = 0.1 M NMe_4Cl, *[L]* = *[M]* = 4 µM)

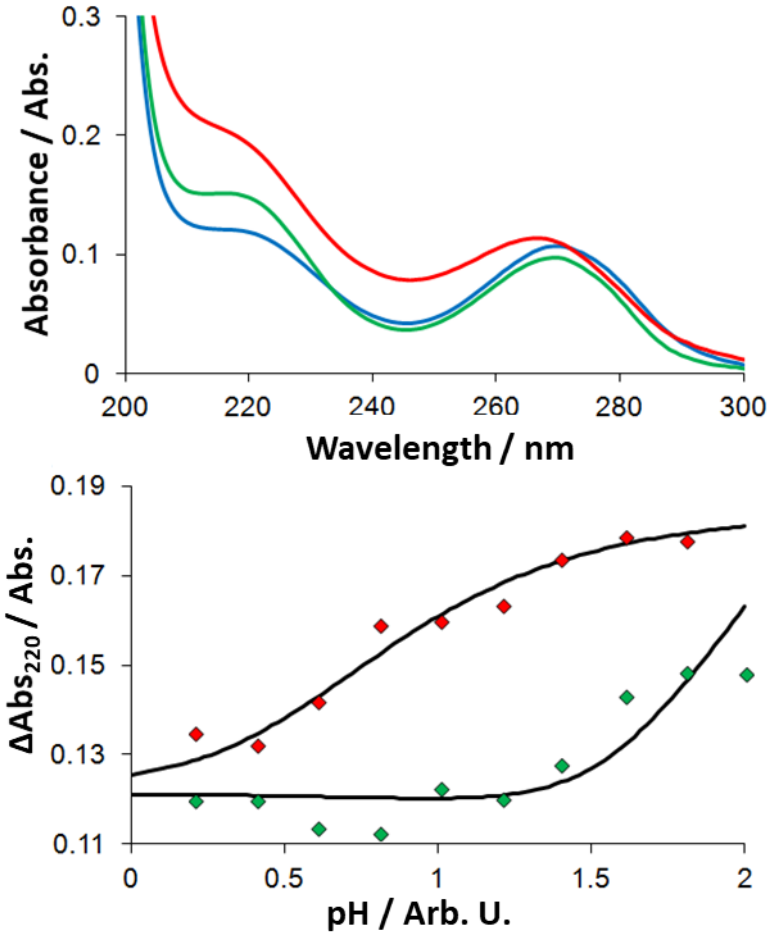

Figure 7.4: UV-Vis titration of M-Dpaa.ga system. Top: UV-Vis spectra of H_4Dpaa.ga (blue), Cu(II)-Dpaa.ga (red), Zn(II)-Dpaa.ga (green). Bottom: Difference of absorbance, ΔAbs used to evaluate results. The line corresponds to the best fit. (T = 25 °C, *[L]* = *[M]* = 0.01 mM)

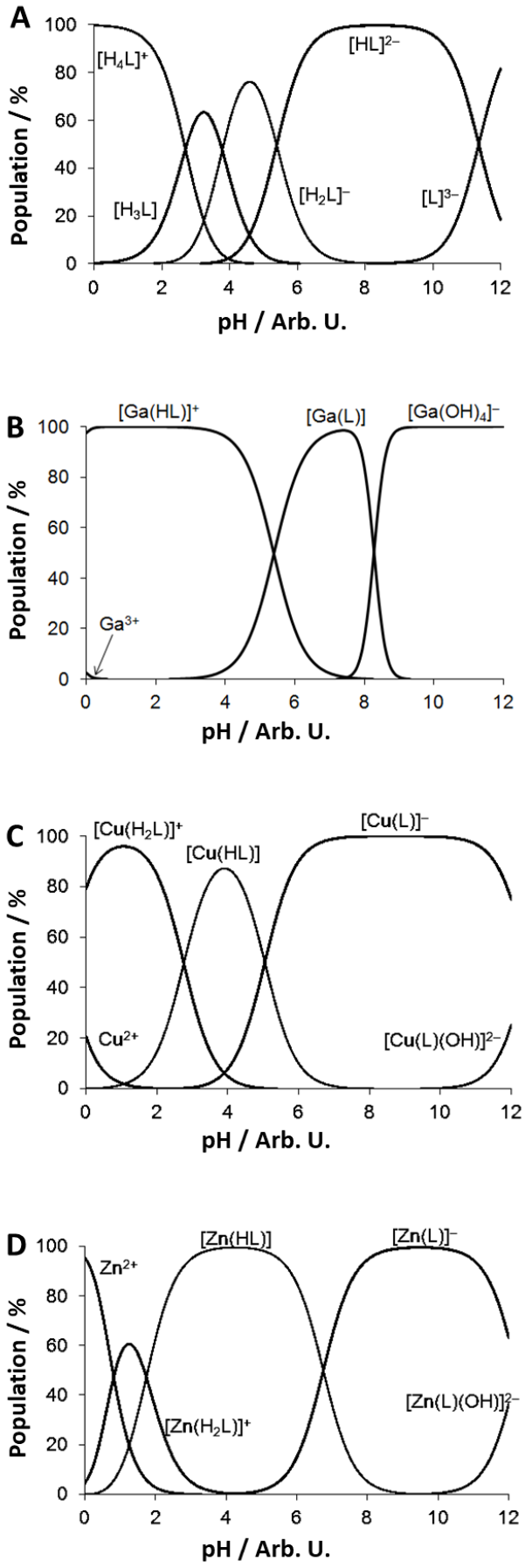

Figure 7.5: Distribution diagrams for A) H_3Dpaa.dab, B) Ga(III)-Dpaa.dab, C) Cu(II)-Dpaa.dab, D) Zn(II)-Dpaa.dab. (*T* = 25 °C, *I* = 0.1 M NMe_4Cl, *[L]* = *[M]* = 4 μM)

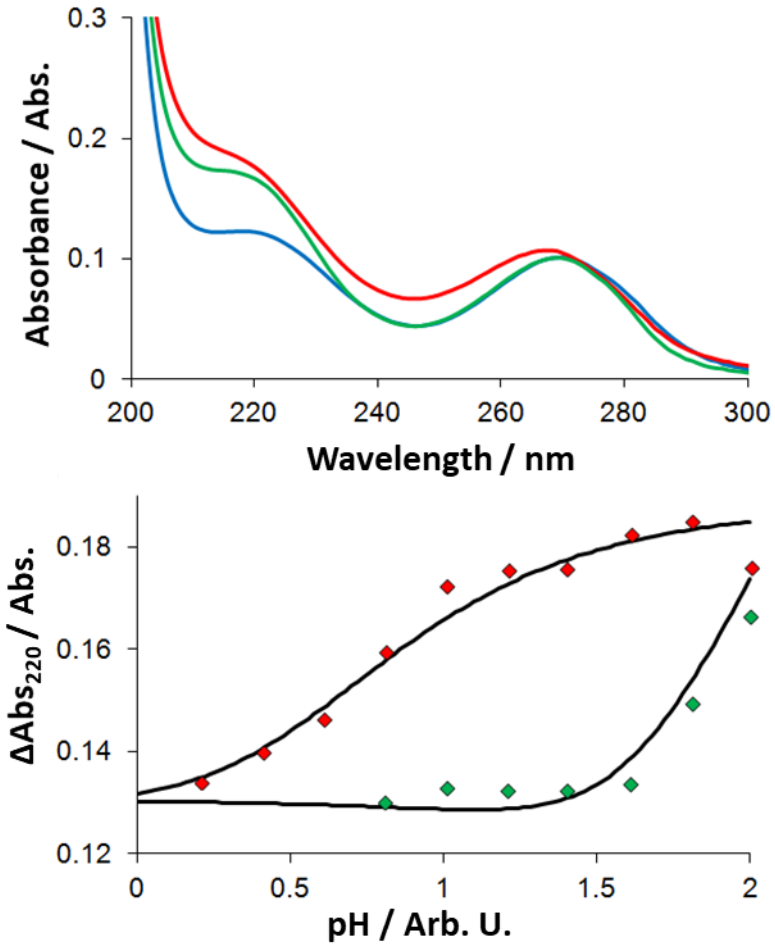

Figure 7.6: UV-Vis titration of M-Dpaa.dab system. Top: UV-Vis spectra of H_4Dpaa.dab (blue), Cu(II)-Dpaa.dab (red), Zn(II)-Dpaa.dab (green). Bottom: Difference of absorbance, ΔAbs used to evaluate results. The line corresponds to the best fit. (T = 25 °C, *[L]* = *[M]* = 0.01 mM)

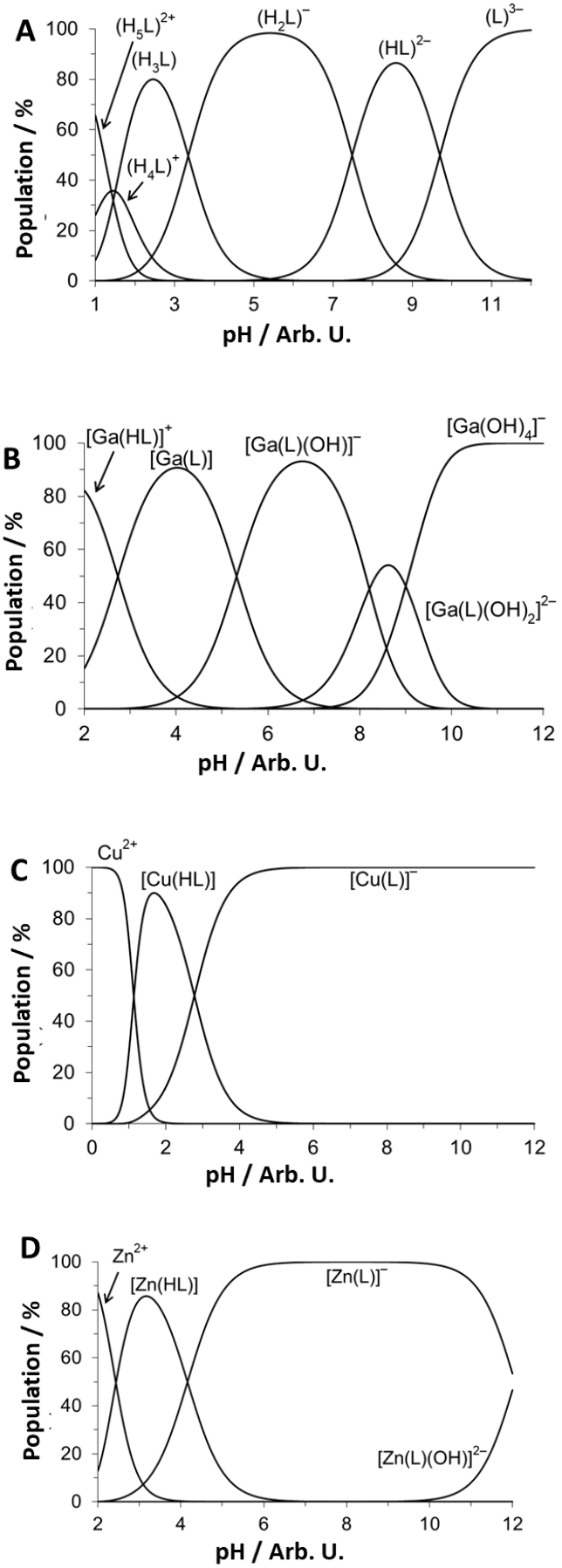

Figure 7.7: Distribution diagrams for A) H_3Bn_2DT3A, B) Ga(III)-Bn_2DT3A, C) Cu(II)-Bn_2DT3A, D) Zn(II)-Bn_2DT3A. (T = 25 °C, I = 0.1 M NMe_4Cl, *[L]* = 4μM, *[M]* = 2 μM).

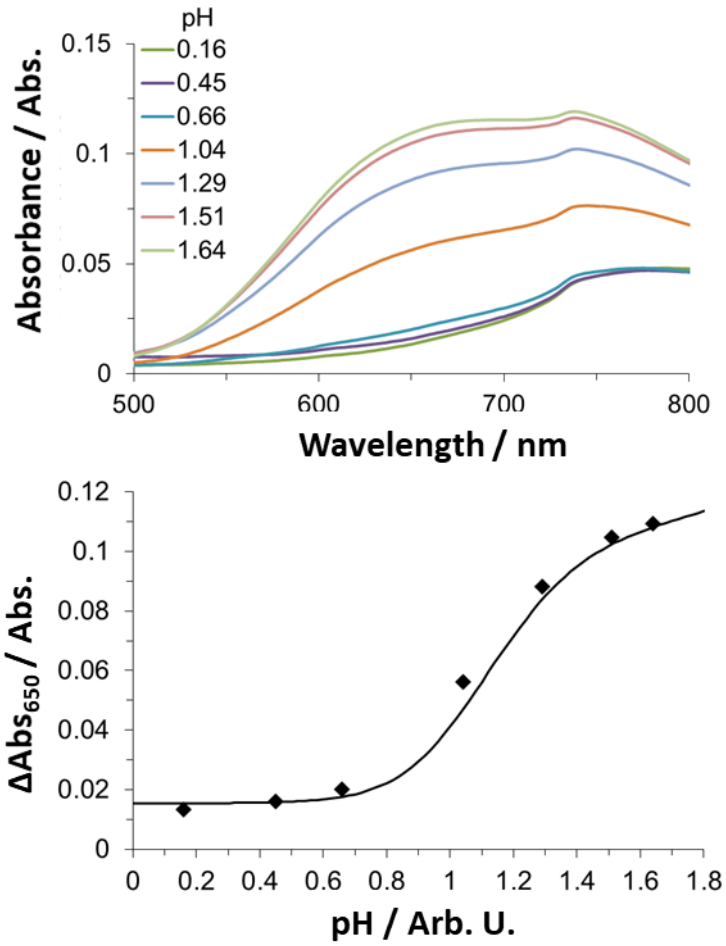

Figure 7.8: UV-Vis titration of Cu(II)-Bn_2DT3A system. Top: UV-Vis spectra variation with pH. Bottom: Difference of absorbance at 650 nm, ΔAbs, used to evaluate results. The line corresponds to the best fit. (*T* = 25 °C, *[L]* = *[M]* = 0.01 mM)

Chapter 8 Appendix 2 – Crystal Structure Data

8.1. [Ga(Dpaa)(H_2O)]

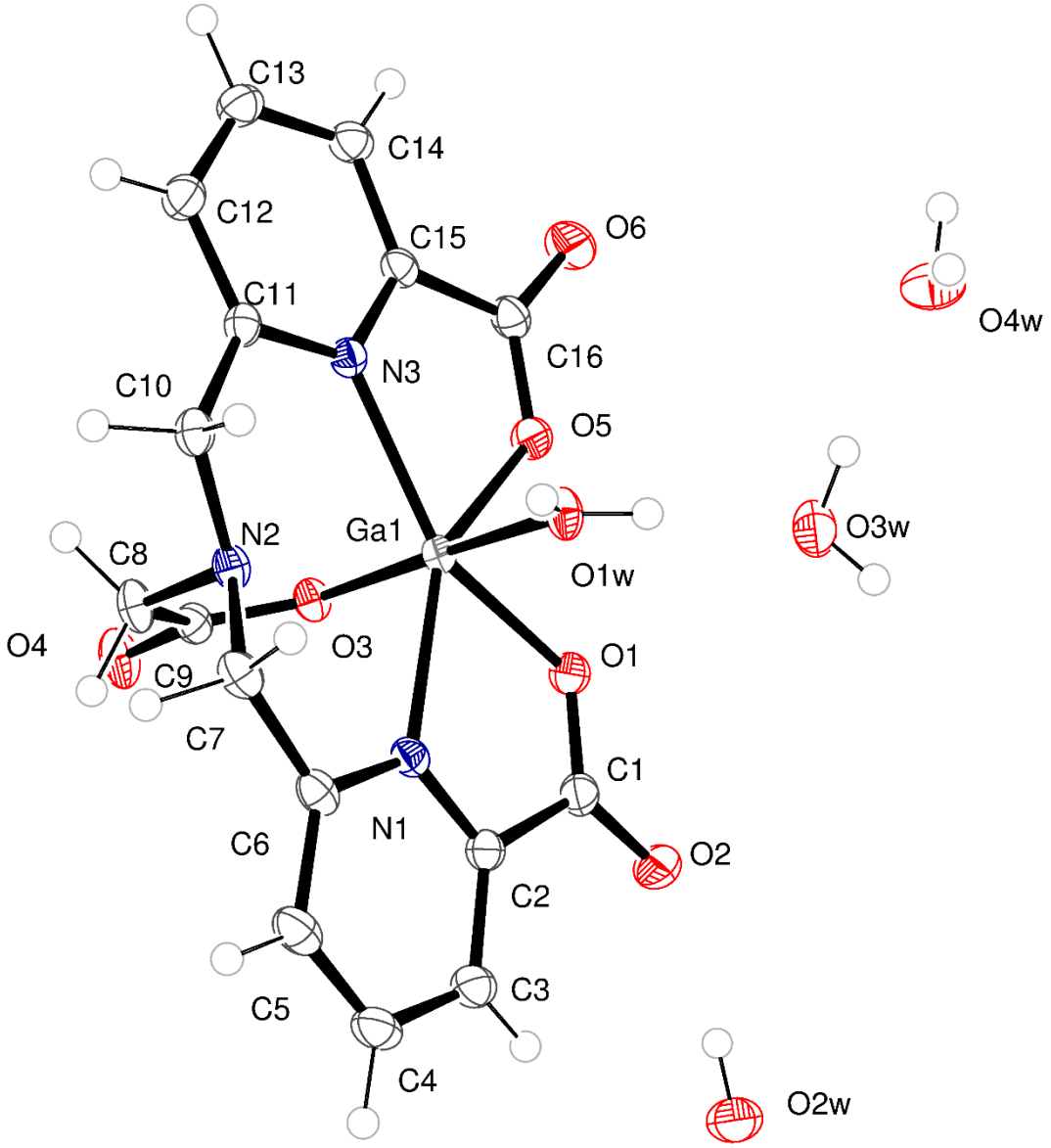

Figure 8.1: ORTEP representation of molecular structure of [Ga(Dpaa)(H_2O)] obtained by single crystal X-ray crystallography (drawn at 30% certainty).

Table 8.1: Crystal data and structure refinement for [Ga(Dpaa)(H_2O)]. CCDC Reference: 1549314

Identification code	[Ga(Dpaa)(H_2O)]	
Empirical formula	C32 H40 Ga2 N6 O20	
Formula weight	968.14	
Temperature	100(2) K	
Wavelength	0.6889 Å	
Crystal system	Triclinic	
Space group	P -1	
Unit cell dimensions	a = 7.06810(10) Å	α = 93.6180(10)°.
	b = 8.21920(10) Å	β = 93.7920(10)°.
	c = 15.9952(2) Å	γ = 91.9130(10)°.
Volume	924.69(2) $Å^3$	
Z	1	
Density (calculated)	1.739 Mg/m^3	
Absorption coefficient	1.425 mm^{-1}	
F(000)	496	
Crystal size	0.040 × 0.005 × 0.005 mm^3	
Theta range for data collection	1.239 to 36.179°.	
Index ranges	-11 ≤ h ≤ 12, -13 ≤ k ≤ 13, -27 ≤ l ≤ 27	
Reflections collected	20701	
Independent reflections	8614 [R(int) = 0.0570]	
Completeness to theta = 24.415°	99.4 %	
Refinement method	Full-matrix least-squares on F^2	
Data / restraints / parameters	8614 / 18 / 304	
Goodness-of-fit on F^2	1.010	
Final R indices [I>2sigma(I)]	R1 = 0.0425, wR2 = 0.1063	
R indices (all data)	R1 = 0.0491, wR2 = 0.1099	
Extinction coefficient	none	
Largest diff. peak and hole	1.606 and -0.543 $e.Å^{-3}$	

Table 8.2: Atomic coordinates (x 10^4) and equivalent isotropic displacement parameters ($Å^2$x 10^3) for [Ga(Dpaa)(H_2O)]. U(eq) is defined as one third of the trace of the orthogonalized U^{ij} tensor.

	x	y	z	U(eq)		x	y	z	U(eq)
C(16)	2172(2)	2325(2)	746(1)	20(1)	C(1)	2081(2)	2278(2)	3892(1)	20(1)
C(15)	2469(2)	4046(2)	508(1)	17(1)	N(3)	2742(2)	5132(1)	1166(1)	15(1)
C(14)	2432(2)	4480(2)	-316(1)	21(1)	N(2)	2635(2)	7123(1)	2530(1)	16(1)
C(13)	2655(2)	6128(2)	-457(1)	23(1)	N(1)	2785(2)	5075(1)	3729(1)	16(1)
C(12)	2957(2)	7258(2)	225(1)	22(1)	O(5)	2021(2)	2180(1)	1532(1)	20(1)
C(11)	3021(2)	6715(2)	1036(1)	17(1)	O(6)	2071(2)	1185(1)	209(1)	30(1)
C(10)	3490(2)	7824(2)	1805(1)	18(1)	O(3)	-144(1)	4541(1)	2377(1)	17(1)
C(8)	595(2)	7459(2)	2537(1)	20(1)	O(4)	-2468(1)	6249(1)	2513(1)	26(1)
C(9)	-749(2)	5983(2)	2476(1)	17(1)	O(1)	2047(2)	2141(1)	3096(1)	20(1)
C(7)	3663(2)	7737(2)	3323(1)	19(1)	O(2)	1853(2)	1125(1)	4346(1)	28(1)
C(6)	3167(2)	6642(2)	3991(1)	19(1)	Ga(1)	2501(1)	4089(1)	2391(1)	14(1)
C(5)	3131(2)	7157(2)	4838(1)	24(1)	O(1W)	5177(1)	3798(1)	2459(1)	20(1)
C(4)	2705(2)	6028(2)	5411(1)	25(1)	O(2W)	1706(2)	427(2)	5999(1)	32(1)
C(3)	2364(2)	4395(2)	5138(1)	23(1)	O(3W)	6426(2)	973(2)	2665(1)	28(1)
C(2)	2423(2)	3980(2)	4285(1)	18(1)	O(4W)	8643(2)	186(2)	1407(1)	30(1)

Table 8.3: Bond lengths for [Ga(Dpaa)(H_2O)].

Bond Length / Å					
C(16)-O(6)	1.2275(17)	C(8)-H(8A)	0.99	C(1)-O(2)	1.2437(18)
C(16)-O(5)	1.2822(18)	C(8)-H(8B)	0.99	C(1)-O(1)	1.2692(18)
C(16)-C(15)	1.500(2)	C(9)-O(4)	1.2462(17)	N(3)-Ga(1)	2.2017(12)
C(15)-N(3)	1.3358(17)	C(9)-O(3)	1.2774(16)	N(1)-Ga(1)	2.2354(11)
C(15)-C(14)	1.386(2)	C(7)-N(2)	1.4713(18)	O(5)-Ga(1)	2.0229(10)
C(14)-C(13)	1.393(2)	C(7)-C(6)	1.492(2)	O(3)-Ga(1)	1.9173(10)
C(14)-H(14)	0.940(15)	C(7)-H(7A)	0.99	O(1)-Ga(1)	2.0441(10)
C(13)-C(12)	1.388(2)	C(7)-H(7B)	0.99	Ga(1)-O(1W)	1.9109(10)
C(13)-H(13)	0.950(16)	C(6)-N(1)	1.3414(18)	O(1W)-H(1A)	0.826(16)
C(12)-C(11)	1.397(2)	C(6)-C(5)	1.395(2)	O(1W)-H(1B)	0.809(16)
C(12)-H(12)	0.931(16)	C(5)-C(4)	1.385(2)	O(2W)-H(2A)	0.829(16)
C(11)-N(3)	1.3405(17)	C(5)-H(5)	0.967(16)	O(2W)-H(2B)	0.871(16)
C(11)-C(10)	1.4965(19)	C(4)-C(3)	1.392(2)	O(3W)-H(3A)	0.867(16)
C(10)-N(2)	1.4808(18)	C(4)-H(4)	0.937(15)	O(3W)-H(3B)	0.831(16)
C(10)-H(10A)	0.99	C(3)-C(2)	1.390(2)	O(4W)-H(4A)	0.829(16)
C(10)-H(10B)	0.99	C(3)-H(3)	0.911(16)	O(4W)-H(4B)	0.848(16)
C(8)-N(2)	1.4776(17)	C(2)-N(1)	1.3343(18)		
C(8)-C(9)	1.5098(19)	C(2)-C(1)	1.502(2)		

Table 8.4: Bond Angles for [Ga(Dpaa)(H_2O)]

Bond Angle / °					
O(6)-C(16)-O(5)	124.73(14)	O(4)-C(9)-O(3)	122.15(13)	C(7)-N(2)-C(8)	110.99(11)
O(6)-C(16)-C(15)	120.70(14)	O(4)-C(9)-C(8)	116.59(12)	C(7)-N(2)-C(10)	110.64(11)
O(5)-C(16)-C(15)	114.56(12)	O(3)-C(9)-C(8)	121.25(12)	C(8)-N(2)-C(10)	111.30(11)
N(3)-C(15)-C(14)	122.95(13)	N(2)-C(7)-C(6)	108.37(11)	C(2)-N(1)-C(6)	119.95(12)
N(3)-C(15)-C(16)	113.68(12)	N(2)-C(7)-H(7A)	110	C(2)-N(1)-Ga(1)	114.45(9)
C(14)-C(15)-C(16)	123.36(13)	C(6)-C(7)-H(7A)	110	C(6)-N(1)-Ga(1)	125.47(10)
C(15)-C(14)-C(13)	118.02(14)	N(2)-C(7)-H(7B)	110	C(16)-O(5)-Ga(1)	122.08(9)
C(15)-C(14)-H(14)	121	C(6)-C(7)-H(7B)	110	C(9)-O(3)-Ga(1)	122.95(9)
C(13)-C(14)-H(14)	121	H(7A)-C(7)-H(7B)	108.4	C(1)-O(1)-Ga(1)	122.55(9)
C(12)-C(13)-C(14)	119.16(14)	N(1)-C(6)-C(5)	120.79(14)	O(1W)-Ga(1)-O(3)	175.40(4)
C(12)-C(13)-H(13)	120.4	N(1)-C(6)-C(7)	115.27(12)	O(1W)-Ga(1)-O(5)	92.32(5)
C(14)-C(13)-H(13)	120.4	C(5)-C(6)-C(7)	123.92(13)	O(3)-Ga(1)-O(5)	92.23(4)
C(13)-C(12)-C(11)	119.20(14)	C(4)-C(5)-C(6)	119.19(14)	O(1W)-Ga(1)-O(1)	91.66(4)
C(13)-C(12)-H(12)	120.4	C(4)-C(5)-H(5)	120.4	O(3)-Ga(1)-O(1)	90.08(4)
C(11)-C(12)-H(12)	120.4	C(6)-C(5)-H(5)	120.4	O(5)-Ga(1)-O(1)	75.92(4)
N(3)-C(11)-C(12)	121.16(13)	C(5)-C(4)-C(3)	119.71(14)	O(1W)-Ga(1)-N(3)	89.19(5)
N(3)-C(11)-C(10)	115.85(12)	C(5)-C(4)-H(4)	120.1	O(3)-Ga(1)-N(3)	91.36(4)
C(12)-C(11)-C(10)	122.92(13)	C(3)-C(4)-H(4)	120.1	O(5)-Ga(1)-N(3)	74.95(4)
N(2)-C(10)-C(11)	109.13(11)	C(2)-C(3)-C(4)	117.59(14)	O(1)-Ga(1)-N(3)	150.87(4)
N(2)-C(10)-H(10A)	109.9	C(2)-C(3)-H(3)	121.2	O(1W)-Ga(1)-N(1)	88.30(5)
C(11)-C(10)-H(10A)	109.9	C(4)-C(3)-H(3)	121.2	O(3)-Ga(1)-N(1)	88.09(4)
N(2)-C(10)-H(10B)	109.9	N(1)-C(2)-C(3)	122.71(14)	O(5)-Ga(1)-N(1)	149.89(4)
C(11)-C(10)-H(10B)	109.9	N(1)-C(2)-C(1)	113.18(12)	O(1)-Ga(1)-N(1)	73.97(4)
H(10A)-C(10)-H(10B)	108.3	C(3)-C(2)-C(1)	124.12(14)	N(3)-Ga(1)-N(1)	135.16(4)
N(2)-C(8)-C(9)	115.99(11)	O(2)-C(1)-O(1)	124.78(14)	Ga(1)-O(1W)-H(1A)	124.1(16)
N(2)-C(8)-H(8A)	108.3	O(2)-C(1)-C(2)	119.63(14)	Ga(1)-O(1W)-H(1B)	122.6(16)
C(9)-C(8)-H(8A)	108.3	O(1)-C(1)-C(2)	115.59(12)	H(1A)-O(1W)-H(1B)	113.1(19)
N(2)-C(8)-H(8B)	108.3	C(15)-N(3)-C(11)	119.45(12)	H(2A)-O(2W)-H(2B)	106.0(18)
C(9)-C(8)-H(8B)	108.3	C(15)-N(3)-Ga(1)	114.25(9)	H(3A)-O(3W)-H(3B)	99.6(17)
H(8A)-C(8)-H(8B)	107.4	C(11)-N(3)-Ga(1)	126.19(9)	H(4A)-O(4W)-H(4B)	102.3(18)

Table 8.5: Anisotropic displacement parameters ($Å^2 x\ 10^3$) for [Ga(Dpaa)(H_2O)]. The anisotropic displacement factor exponent takes the form: $-2\pi^2[h^2a^{*2}U_{11} + ... + 2\ h\ k\ a^*\ b^*\ U_{12}]$

	U_{11}	U_{22}	U_{33}	U_{23}	U_{13}	U_{12}
C(16)	20(1)	18(1)	20(1)	-3(1)	0(1)	2(1)
C(15)	14(1)	18(1)	17(1)	-1(1)	1(1)	2(1)
C(14)	0(1)	25(1)	17(1)	0(1)	0(1)	3(1)
C(13)	22(1)	28(1)	19(1)	5(1)	1(1)	3(1)
C(12)	22(1)	21(1)	23(1)	5(1)	3(1)	2(1)
C(11)	14(1)	16(1)	20(1)	2(1)	1(1)	2(1)
C(10)	17(1)	14(1)	23(1)	1(1)	1(1)	-1(1)
C(8)	13(1)	15(1)	30(1)	-2(1)	0(1)	2(1)
C(9)	14(1)	19(1)	19(1)	1(1)	1(1)	2(1)
C(7)	17(1)	17(1)	22(1)	-5(1)	-1(1)	-1(1)
C(6)	14(1)	20(1)	21(1)	-4(1)	0(1)	2(1)
C(5)	1(1)	26(1)	23(1)	-8(1)	-1(1)	3(1)
C(4)	3(1)	34(1)	17(1)	-5(1)	-1(1)	7(1)
C(3)	20(1)	30(1)	19(1)	2(1)	2(1)	6(1)
C(2)	15(1)	21(1)	18(1)	2(1)	1(1)	4(1)
C(1)	20(1)	19(1)	22(1)	4(1)	5(1)	4(1)
N(3)	16(1)	14(1)	16(1)	0(1)	0(1)	1(1)
N(2)	13(1)	15(1)	21(1)	-1(1)	0(1)	1(1)
N(1)	15(1)	18(1)	16(1)	-1(1)	1(1)	2(1)
O(5)	26(1)	15(1)	19(1)	-1(1)	1(1)	0(1)
O(6)	43(1)	20(1)	24(1)	-8(1)	2(1)	0(1)
O(3)	14(1)	16(1)	21(1)	-1(1)	0(1)	1(1)
O(4)	13(1)	21(1)	44(1)	-1(1)	2(1)	1(1)
O(1)	24(1)	15(1)	20(1)	2(1)	3(1)	0(1)
O(2)	39(1)	22(1)	24(1)	8(1)	8(1)	2(1)
Ga(1)	13(1)	13(1)	16(1)	0(1)	1(1)	1(1)
O(1W)	13(1)	18(1)	30(1)	3(1)	2(1)	3(1)
O(2W)	45(1)	30(1)	22(1)	2(1)	4(1)	0(1)
O(3W)	26(1)	23(1)	36(1)	4(1)	5(1)	6(1)
O(4W)	35(1)	33(1)	21(1)	0(1)	2(1)	-7(1)

Table 8.6: Hydrogen coordinates ($x\ 10^4$) and isotropic displacement parameters ($Å^2\ x\ 10^3$) for [Ga(Dpaa)(H_2O)].

	x	y	z	U(eq)		x	y	z	U(eq)
H(14)	2263(3)	3685(13)	-766(7)	25	H(4)	2645(2)	6360(6)	5979(9)	30
H(13)	2600(2)	6474(6)	-1014(9)	27	H(3)	2112(5)	3627(14)	5506(7)	28
H(12)	3115(3)	8364(19)	143(2)	26	H(1A)	5670(30)	2910(20)	2506(15)	47(2)
H(10A)	4884	7947	1916	22	H(1B)	5940(30)	4560(20)	2481(15)	47(2)
H(10B)	2988	8916	1720	22	H(2A)	1890(30)	640(30)	5511(11)	47(2)
H(8A)	257	8134	2062	24	H(2B)	580(30)	-40(30)	5978(14)	47(2)
H(8B)	391	8116	3061	24	H(3A)	7220(30)	910(30)	2277(12)	47(2)
H(7A)	3299	8864	3475	23	H(3B)	7110(30)	670(30)	3066(11)	47(2)
H(7B)	5047	7749	3261	23	H(4A)	9690(30)	680(30)	1470(14)	47(2)
H(5)	3401(5)	8288(19)	5022(3)	28	H(4B)	8600(30)	-170(30)	896(11)	47(2)

8.2. [Ga(Dpaa.ga)(H_2O)]

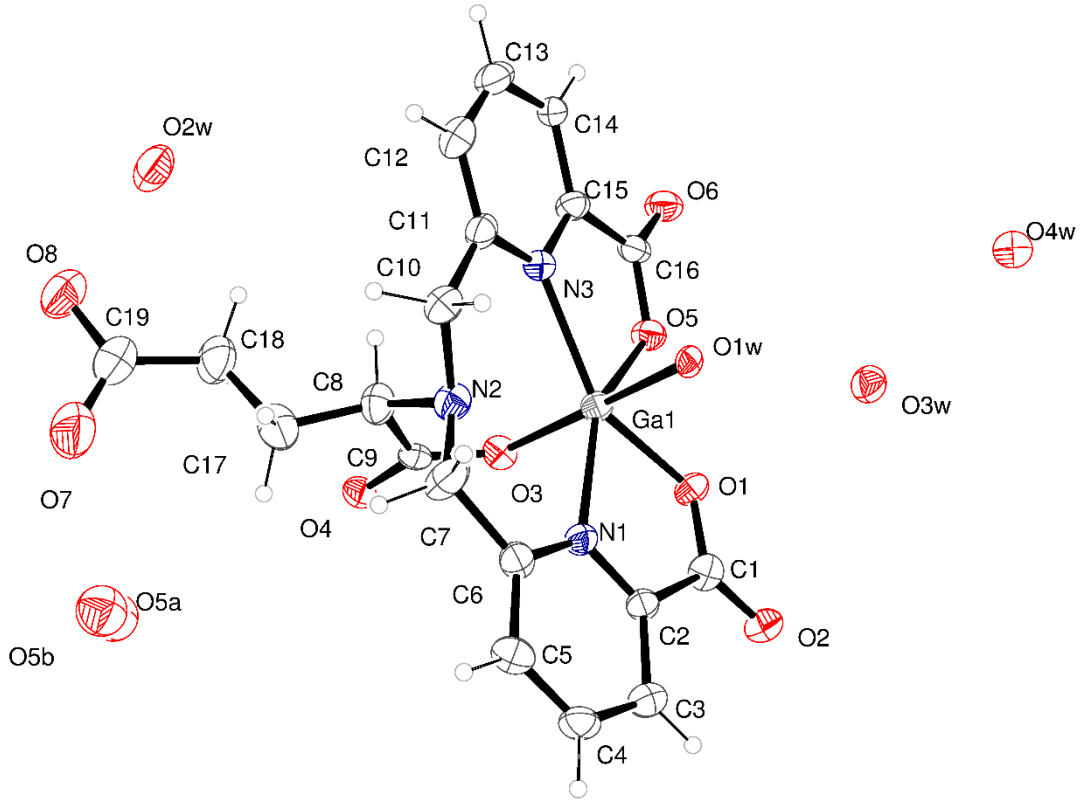

Figure 8.2: ORTEP representation of molecular structure of [Ga(Dpaa.ga)(H_2O)] obtained by single crystal X-ray crystallography (Drawn at 30% certainty).

The structure presented above was determined using synchrotron radiation (λ = 0.6889 Å) and a data collection that lasted 12 minutes in total. The structure determination confirms the chemical connectivity and the binding of gallium, although the fit parameters are only moderately good (R1 = 0.1133 for data with I > 2σI). The crystal examined was found to suffer from damage in the X-ray beam; this causes a loss of intensity in the X-ray scattering and always leads to poor quality of fit of the model to data. Interestingly in this case, a total of 70 minutes X-ray scattering data were collected from one crystal and it is possible to refine the structure using all of the data (70 minutes). This gives a hint as to the mode of decomposition of the compound in the X-ray beam. The structure refined from all data is shown below. The major portion of the ligand is unchanged, but two key changes are observed. There is loss of water (O5a/O5b) and the ligand starts to decompose. There is evidence that this decomposition involves loss of the arm containing unbound carboxylate and in particular with loss of CO_2. In the structure refinement the carboxylate O7-C19-O8 is 34% occupied and C17 & C18 are 58% occupied. The decomposition of the ligand and loss of water is accompanied by fracture of the crystal and loss of scattered intensity

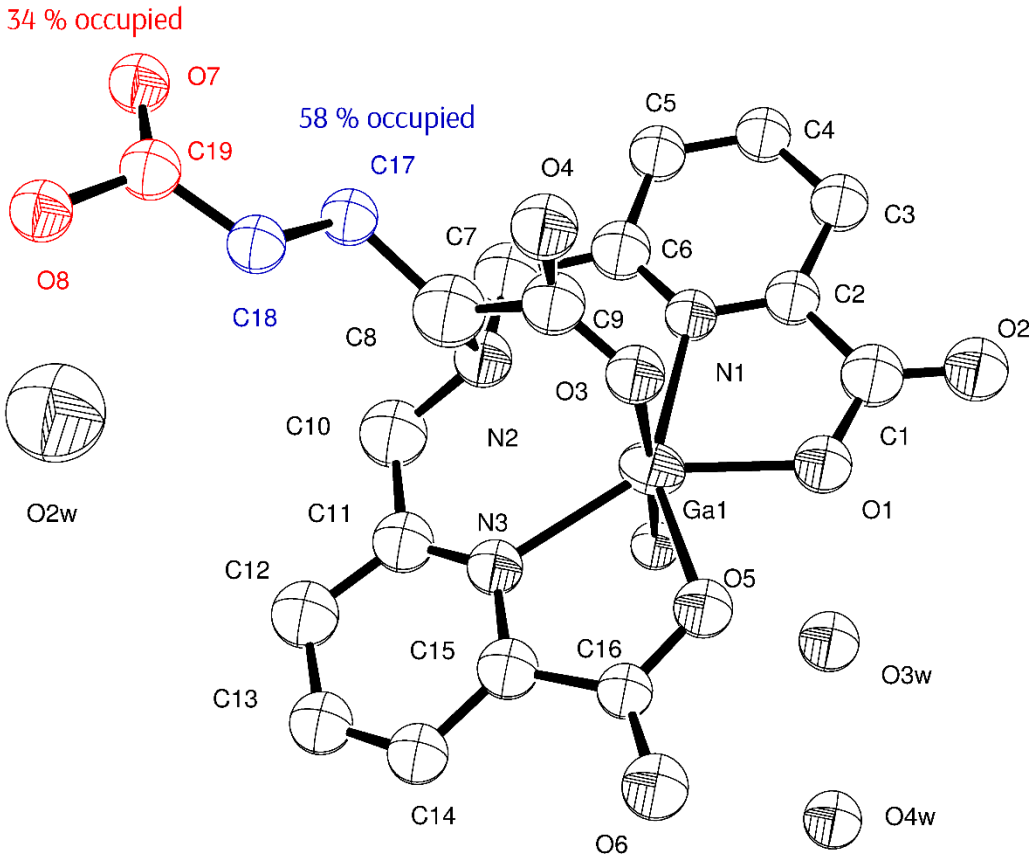

Figure 8.3: ORTEP representation of decomposed form of [Ga(Dpaa.ga)(H_2O)]. (Hydrogen atoms have been omitted for clarity. Atoms are drawn at the 30% probability level.)

Table 8.7: Crystal data and structure refinement for [Ga(Dpaa.ga)(H_2O)]. CCDC Reference: 1530703

Identification code	[Ga(Dpaa.ga)(H_2O)]
Empirical formula	C19 H15 Ga N3 O12.87
Formula weight	561.02
Temperature	100(2) K
Wavelength	0.6889 Å
Crystal system	Orthorhombic
Space group	P c c n
Unit cell dimensions	a = 20.7850(12) Å α= 90°.
	b = 30.2224(18) Å β= 90°.
	c = 7.2085(6) Å γ = 90°.
Volume	4528.2(5) $Å^3$
Z	8
Density (calculated)	1.646 Mg/m^3
Absorption coefficient	1.186 mm^{-1}
F(000)	2272
Crystal size	0.060 × 0.005 × 0.005 mm^3
Theta range for data collection	1.152 to 24.835°.
Index ranges	-18 ≤ h ≤ 25, -34 ≤ k ≤ 36, -5 ≤ l ≤ 8
Reflections collected	12211
Independent reflections	4251 [R(int) = 0.2109]
Completeness to theta = 24.415°	98.70%
Refinement method	Full-matrix least-squares on F2
Data / restraints / parameters	4251 / 0 / 324
Goodness-of-fit on F^2	1.009
Final R indices [I>2sigma(I)]	R1 = 0.1133, wR2 = 0.2750
R indices (all data)	R1 = 0.1749, wR2 = 0.3333
Extinction coefficient	none
Largest diff. peak and hole	2.429 and -1.265 e.$Å^{-3}$

Table 8.8: Atomic coordinates (x 10^4) and equivalent isotropic displacement parameters ($Å^2$x 10^3) for [Ga(Dpaa.ga)(H_2O)]. U(eq) is defined as one third of the trace of the orthogonalized U^{ij} tensor.

	x	y	z	U(eq)		x	y	z	U(eq)
C(1)	6833(5)	6659(3)	8618(14)	42(2)	N(1)	5723(3)	6848(3)	8318(11)	37(2)
C(2)	6315(5)	7008(3)	8454(13)	37(2)	N(2)	4577(4)	6459(3)	8383(12)	46(2)
C(3)	6463(5)	7467(3)	8481(15)	46(2)	N(3)	4926(4)	5646(2)	7676(12)	38(2)
C(4)	5939(6)	7744(3)	8382(15)	49(3)	O(1)	6620(3)	6261(2)	8593(9)	38(2)
C(5)	5329(6)	7583(3)	8255(15)	49(3)	O(2)	7410(3)	6767(2)	8770(10)	47(2)
C(6)	5236(5)	7120(3)	8225(14)	43(2)	O(3)	5507(3)	6175(2)	10931(9)	39(2)
C(7)	4567(5)	6919(4)	8010(20)	64(4)	O(4)	4892(3)	6364(2)	13293(9)	42(2)
C(8)	4385(5)	6323(4)	10379(15)	52(3)	O(5)	6103(3)	5528(2)	8674(10)	42(2)
C(9)	4965(5)	6307(3)	11585(14)	38(2)	O(6)	6035(4)	4791(2)	8491(10)	50(2)
C(10)	4139(5)	6216(4)	7094(15)	45(2)	O(7)	2659(6)	6738(5)	13270(30)	159(8)
C(11)	4325(5)	5732(4)	7111(14)	44(2)	O(8)	2399(5)	6009(4)	13643(19)	103(4)
C(12)	3916(5)	5410(4)	6575(15)	51(3)	Ga(1)	5684(1)	6128(1)	8297(1)	35(1)
C(13)	4119(6)	4975(4)	6611(16)	57(3)	O(1W)	5774(3)	6136(2)	5594(8)	31(1)
C(14)	4723(5)	4869(3)	7168(13)	40(2)	O(2W)	2697(4)	5262(3)	12728(18)	86(3)
C(15)	5120(5)	5220(3)	7721(14)	40(2)	O(3W)	6908(3)	6035(2)	4157(10)	48(2)
C(16)	5802(5)	5159(3)	8327(13)	39(2)	O(4W)	7175(3)	5538(2)	1058(10)	45(2)
C(17)	3813(6)	6555(5)	11190(17)	63(3)	O(5A)	3527(10)	7313(7)	15090(30)	86
C(18)	3424(6)	6189(5)	12280(20)	73(4)	O(5B)	3183(13)	7538(9)	13380(40)	86
C(19)	2811(7)	6314(6)	13080(30)	96(5)					

Table 8.9: Bond lengths for [Ga(Dpaa)(H_2O)].

Bond Length / Å					
C(1)-O(2)	1.248(12)	C(8)-N(2)	1.549(14)	C(16)-O(6)	1.217(12)
C(1)-O(1)	1.280(12)	C(8)-H(8)	1	C(16)-O(5)	1.304(11)
C(1)-C(2)	1.512(14)	C(9)-O(4)	1.252(11)	C(17)-C(18)	1.577(19)
C(2)-N(1)	1.324(12)	C(9)-O(3)	1.284(11)	C(17)-H(17A)	0.99
C(2)-C(3)	1.424(14)	C(10)-N(2)	1.495(13)	C(17)-H(17B)	0.99
C(3)-C(4)	1.376(16)	C(10)-C(11)	1.513(15)	C(18)-C(19)	1.45(2)
C(3)-H(3)	0.95	C(10)-H(10A)	0.99	C(18)-H(18A)	0.99
C(4)-C(5)	1.361(16)	C(10)-H(10B)	0.99	C(18)-H(18B)	0.99
C(4)-H(4)	0.95	C(11)-N(3)	1.339(13)	C(19)-O(8)	1.32(2)
C(5)-C(6)	1.414(14)	C(11)-C(12)	1.349(15)	C(19)-O(7)	1.33(2)
C(5)-H(5)	0.95	C(12)-C(13)	1.379(18)	N(1)-Ga(1)	2.180(8)
C(6)-N(1)	1.304(13)	C(12)-H(12)	0.95	N(3)-Ga(1)	2.192(7)
C(6)-C(7)	1.526(15)	C(13)-C(14)	1.355(16)	O(1)-Ga(1)	2.000(6)
C(7)-N(2)	1.414(14)	C(13)-H(13)	0.95	O(3)-Ga(1)	1.939(7)
C(7)-H(7A)	0.99	C(14)-C(15)	1.402(13)	O(5)-Ga(1)	2.028(7)
C(7)-H(7B)	0.99	C(14)-H(14)	0.95	Ga(1)-O(1W)	1.958(6)
C(8)-C(9)	1.488(15)	C(15)-N(3)	1.351(12)		
C(8)-C(17)	1.499(16)	C(15)-C(16)	1.494(14)		

Table 8.10: Bond Angles for [Ga(Dpaa.ga)(H_2O)]

Bond Angle / °					
O(2)-C(1)-O(1)	125.3(9)	N(2)-C(10)-C(11)	108.4(8)	C(19)-C(18)-H(18B)	107.8
O(2)-C(1)-C(2)	120.7(9)	N(2)-C(10)-H(10A)	110	C(17)-C(18)-H(18B)	107.8
O(1)-C(1)-C(2)	114.0(8)	C(11)-C(10)-H(10A)	110	H(18A)-C(18)-H(18B)	107.2
N(1)-C(2)-C(3)	123.8(9)	N(2)-C(10)-H(10B)	110	O(8)-C(19)-O(7)	119.3(15)
N(1)-C(2)-C(1)	114.5(8)	C(11)-C(10)-H(10B)	110	O(8)-C(19)-C(18)	120.7(17)
C(3)-C(2)-C(1)	121.7(9)	H(10A)-C(10)-H(10B)	108.4	O(7)-C(19)-C(18)	120.0(15)
C(4)-C(3)-C(2)	114.9(10)	N(3)-C(11)-C(12)	122.3(10)	C(6)-N(1)-C(2)	119.8(9)
C(4)-C(3)-H(3)	122.6	N(3)-C(11)-C(10)	115.4(9)	C(6)-N(1)-Ga(1)	126.8(7)
C(2)-C(3)-H(3)	122.6	C(12)-C(11)-C(10)	122.3(10)	C(2)-N(1)-Ga(1)	113.5(6)
C(5)-C(4)-C(3)	121.6(10)	C(11)-C(12)-C(13)	119.3(11)	C(7)-N(2)-C(10)	110.8(9)
C(5)-C(4)-H(4)	119.2	C(11)-C(12)-H(12)	120.4	C(7)-N(2)-C(8)	115.9(10)
C(3)-C(4)-H(4)	119.2	C(13)-C(12)-H(12)	120.4	C(10)-N(2)-C(8)	106.8(8)
C(4)-C(5)-C(6)	118.8(10)	C(14)-C(13)-C(12)	120.9(10)	C(11)-N(3)-C(15)	118.2(8)
C(4)-C(5)-H(5)	120.6	C(14)-C(13)-H(13)	119.5	C(11)-N(3)-Ga(1)	127.1(7)
C(6)-C(5)-H(5)	120.6	C(12)-C(13)-H(13)	119.5	C(15)-N(3)-Ga(1)	114.4(6)
N(1)-C(6)-C(5)	121.1(10)	C(13)-C(14)-C(15)	116.8(10)	C(1)-O(1)-Ga(1)	121.8(6)
N(1)-C(6)-C(7)	117.5(9)	C(13)-C(14)-H(14)	121.6	C(9)-O(3)-Ga(1)	123.3(6)
C(5)-C(6)-C(7)	121.3(9)	C(15)-C(14)-H(14)	121.6	C(16)-O(5)-Ga(1)	122.3(6)
N(2)-C(7)-C(6)	111.0(9)	N(3)-C(15)-C(14)	122.5(9)	O(3)-Ga(1)-O(1W)	172.7(3)
N(2)-C(7)-H(7A)	109.4	N(3)-C(15)-C(16)	114.1(8)	O(3)-Ga(1)-O(1)	93.7(3)
C(6)-C(7)-H(7A)	109.4	C(14)-C(15)-C(16)	123.3(9)	O(1W)-Ga(1)-O(1)	90.6(3)
N(2)-C(7)-H(7B)	109.4	O(6)-C(16)-O(5)	125.0(9)	O(3)-Ga(1)-O(5)	90.9(3)
C(6)-C(7)-H(7B)	109.4	O(6)-C(16)-C(15)	121.2(9)	O(1W)-Ga(1)-O(5)	95.9(3)
H(7A)-C(7)-H(7B)	108	O(5)-C(16)-C(15)	113.9(8)	O(1)-Ga(1)-O(5)	75.4(3)
C(9)-C(8)-C(17)	115.5(10)	C(8)-C(17)-C(18)	105.8(11)	O(3)-Ga(1)-N(1)	85.8(3)
C(9)-C(8)-N(2)	110.0(8)	C(8)-C(17)-H(17A)	110.6	O(1W)-Ga(1)-N(1)	89.5(3)
C(17)-C(8)-N(2)	116.2(10)	C(18)-C(17)-H(17A)	110.6	O(1)-Ga(1)-N(1)	76.2(3)
C(9)-C(8)-H(8)	104.5	C(8)-C(17)-H(17B)	110.6	O(5)-Ga(1)-N(1)	151.1(3)
C(17)-C(8)-H(8)	104.5	C(18)-C(17)-H(17B)	110.6	O(3)-Ga(1)-N(3)	96.5(3)
N(2)-C(8)-H(8)	104.5	H(17A)-C(17)-H(17B)	108.7	O(1W)-Ga(1)-N(3)	82.7(3)
O(4)-C(9)-O(3)	120.7(9)	C(19)-C(18)-C(17)	117.9(13)	O(1)-Ga(1)-N(3)	148.9(3)
O(4)-C(9)-C(8)	118.1(9)	C(19)-C(18)-H(18A)	107.8	O(5)-Ga(1)-N(3)	75.1(3)
O(3)-C(9)-C(8)	120.4(9)	C(17)-C(18)-H(18A)	107.8	N(1)-Ga(1)-N(3)	133.8(3)

Table 8.11: Anisotropic displacement parameters ($Å^2 x\ 10^3$) for [Ga(Dpaa.ga)(H_2O)]. The anisotropic displacement factor exponent takes the form: $-2\pi^2[h^2a^{*2}U_{11} + ... + 2\ h\ k\ a^*\ b^*\ U_{12}]$

	U_{11}	U_{22}	U_{33}	U_{23}	U_{13}	U_{12}
C(1)	45(5)	40(5)	41(6)	13(5)	-2(4)	4(5)
C(2)	42(5)	29(5)	40(5)	4(4)	5(4)	-2(4)
C(3)	50(6)	44(6)	44(6)	3(5)	-4(5)	-8(5)
C(4)	64(7)	30(5)	55(7)	3(5)	3(5)	-5(5)
C(5)	60(6)	39(5)	47(6)	3(5)	-8(5)	6(5)
C(6)	47(5)	41(5)	43(6)	2(5)	4(5)	2(5)
C(7)	41(6)	46(6)	106(11)	15(7)	-1(6)	-5(5)
C(8)	48(6)	64(7)	43(6)	2(5)	6(5)	0(5)
C(9)	44(5)	23(4)	47(6)	-3(4)	1(5)	-2(4)
C(10)	41(5)	50(6)	46(6)	8(5)	-5(4)	-3(4)
C(11)	39(5)	58(7)	36(5)	-3(5)	5(4)	-11(5)
C(12)	42(5)	59(7)	52(7)	12(5)	2(5)	-4(5)
C(13)	51(6)	72(8)	48(7)	-9(6)	0(5)	-26(6)
C(14)	38(5)	45(6)	38(5)	-9(4)	6(4)	-10(4)
C(15)	46(6)	34(5)	42(5)	0(4)	3(4)	-9(4)
C(16)	49(6)	32(5)	37(5)	-6(4)	1(4)	-3(4)
C(17)	56(7)	83(9)	49(7)	-10(6)	-12(6)	14(6)
C(18)	43(6)	89(10)	86(10)	0(8)	-2(6)	7(6)
C(19)	59(8)	101(13)	129(16)	-15(11)	10(9)	-11(9)
N(1)	37(4)	32(4)	43(5)	1(4)	2(4)	-2(3)
N(2)	42(5)	54(5)	42(5)	2(4)	-4(4)	-3(4)
N(3)	37(4)	35(4)	43(5)	-5(4)	2(4)	-3(3)
O(1)	39(3)	37(4)	40(4)	10(3)	-1(3)	-6(3)
O(2)	42(4)	44(4)	54(5)	4(3)	-7(3)	-6(3)
O(3)	46(4)	40(4)	31(3)	5(3)	-3(3)	3(3)
O(4)	46(4)	44(4)	34(4)	-6(3)	-2(3)	-1(3)
O(5)	42(3)	36(4)	47(4)	-3(3)	-3(3)	0(3)
O(6)	56(4)	39(4)	55(5)	-5(3)	-1(4)	-6(3)
O(7)	92(9)	96(10)	290(20)	-46(11)	74(11)	-7(7)
O(8)	70(7)	87(8)	153(11)	-5(7)	28(6)	-22(6)
Ga(1)	36(1)	33(1)	36(1)	2(1)	-1(1)	-1(1)
O(1W)	35(3)	30(3)	27(3)	6(3)	8(2)	-3(2)
O(2W)	50(5)	55(5)	154(10)	7(6)	20(6)	-3(4)
O(3W)	42(4)	60(4)	42(4)	-3(4)	0(3)	-7(3)
O(4W)	46(4)	43(4)	45(4)	3(3)	-6(3)	1(3)

Table 8.12: Hydrogen coordinates (x 10^4) and isotropic displacement parameters (Å^2 x 10^3) for [Ga(Dpaa.ga)(H_2O)].

	x	y	z	U(eq)		x	y	z	U(eq)
H(3)	6892	7575	8561	55	H(12)	3493	5481	6176	61
H(4)	6004	8055	8403	59	H(13)	3832	4747	6241	69
H(5)	4972	7779	8188	58	H(14)	4869	4571	7182	48
H(7A)	4266	7067	8868	77	H(17A)	3545	6686	10196	75
H(7B)	4412	6968	6725	77	H(17B)	3952	6793	12041	75
H(8)	4247	6007	10264	62	H(18A)	3347	5939	11416	87
H(10A)	4179	6337	5823	55	H(18B)	3703	6077	13287	87
H(10B)	3687	6251	7500	55					

8.3. H_4Dpaa.ga

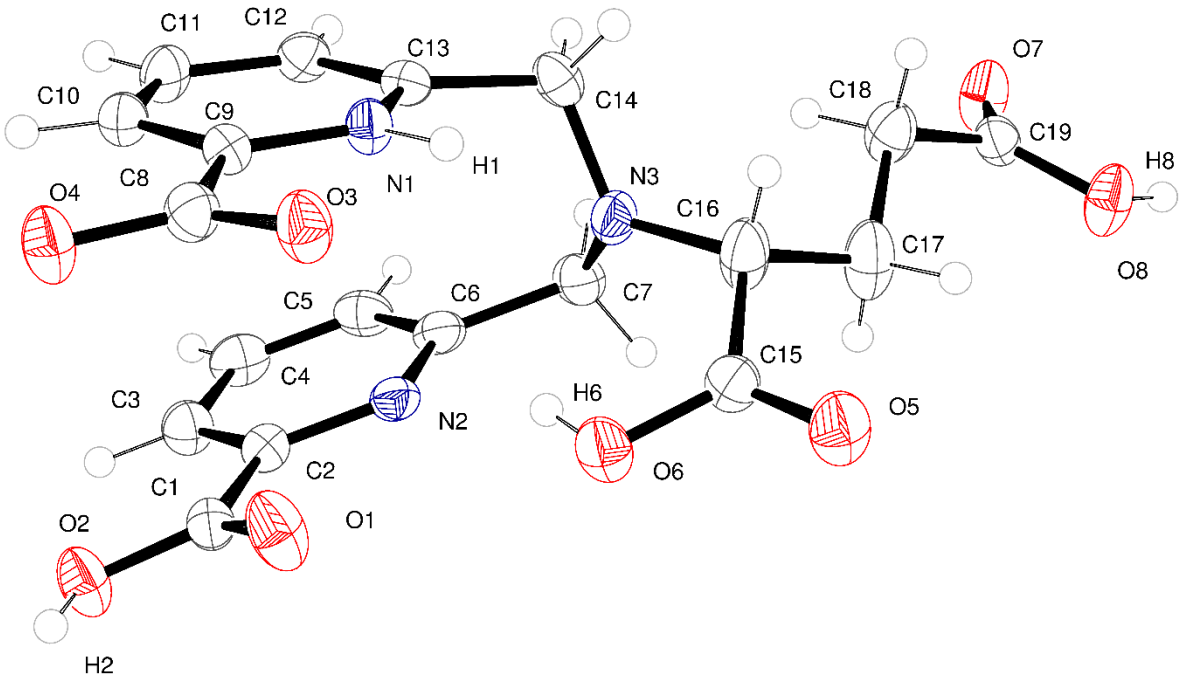

Figure 8.4: ORTEP representation of molecular structure of H_4Dpaa.ga obtained by single crystal X-ray crystallography (drawn at 30% certainty).

Table 8.13: Crystal data and structure refinement for H_4Dpaa.ga. CCDC Reference: 1530704

Identification code	H_4Dpaa.ga
Empirical formula	C19 H19 N3 O8
Formula weight	417.37
Temperature	150(2) K
Wavelength	0.71073 Å
Crystal system	Monoclinic
Space group	P 21/n
Unit cell dimensions	a = 7.0852(6) Å α = 90°. b = 32.290(4) Å β = 94.108(7)°. c = 7.6786(6) Å γ = 90°.
Volume	1752.2(3) Å3
Z	4
Density (calculated)	1.582 Mg/m^3
Absorption coefficient	0.125 mm^{-1}
F(000)	872
Crystal size	0.275 x 0.130 x 0.056 mm^3
Theta range for data collection	1.261 to 25.550°.
Index ranges	-8<=h<=8, -38<=k<=38, -9<=l<=9
Reflections collected	9845
Independent reflections	3229 [R(int) = 0.0571]
Completeness to theta = 25.42°	99.90%
Refinement method	Full-matrix least-squares on F^2
Data / restraints / parameters	3229 / 0 / 275
Goodness-of-fit on F^2	0.792
Final R indices [I>2sigma(I)]	R1 = 0.0440, wR2 = 0.0727
R indices (all data)	R1 = 0.1003, wR2 = 0.0804
Extinction coefficient	n/a
Largest diff. peak and hole	0.400 and -0.220 e.$Å^{-3}$

Table 8.14: Atomic coordinates (x 10^4) and equivalent isotropic displacement parameters ($Å^2$x 10^3) for H_4Dpaa.ga. U(eq) is defined as one third of the trace of the orthogonalized U^{ij} tensor.

	x	y	z	U(eq)		x	y	z	U(eq)
C(1)	1513(4)	4436(1)	2417(4)	27(1)	C(16)	3186(4)	2812(1)	4732(5)	41(1)
C(2)	3301(4)	4230(1)	1922(3)	25(1)	C(17)	3562(4)	2391(1)	4062(5)	44(1)
C(3)	4688(4)	4440(1)	1097(4)	30(1)	C(18)	5511(4)	2226(1)	4632(4)	33(1)
C(4)	6338(4)	4236(1)	748(4)	33(1)	C(19)	6014(4)	1821(1)	3864(4)	27(1)
C(5)	6534(4)	3826(1)	1251(4)	31(1)	N(1)	4192(3)	3897(1)	6672(3)	23(1)
C(6)	5097(4)	3633(1)	2064(4)	27(1)	N(2)	3491(3)	3829(1)	2417(3)	25(1)
C(7)	5238(4)	3189(1)	2690(4)	33(1)	N(3)	4540(3)	3137(1)	4406(3)	27(1)
C(8)	1982(4)	4445(1)	7410(4)	26(1)	O(1)	419(3)	4271(1)	3318(3)	41(1)
C(9)	3868(3)	4308(1)	6779(3)	23(1)	O(2)	1335(2)	4814(1)	1763(3)	35(1)
C(10)	5250(4)	4575(1)	6304(4)	26(1)	O(3)	909(2)	4175(1)	7944(2)	32(1)
C(11)	6903(4)	4423(1)	5693(4)	29(1)	O(4)	1723(2)	4829(1)	7333(2)	33(1)
C(12)	7164(4)	3999(1)	5566(3)	26(1)	O(5)	-134(2)	2712(1)	4654(3)	40(1)
C(13)	5775(4)	3734(1)	6063(3)	23(1)	O(6)	761(2)	3326(1)	3803(3)	34(1)
C(14)	5845(3)	3270(1)	5831(4)	26(1)	O(7)	7582(3)	1747(1)	3406(3)	37(1)
C(15)	1145(4)	2946(1)	4378(4)	28(1)	O(8)	4639(2)	1548(1)	3749(3)	37(1)

Table 8.15: Bond lengths for H_4Dpaa.ga.

Bond Lengths / Å					
C(1)-O(1)	1.202(3)	C(8)-O(4)	1.255(3)	C(15)-C(16)	1.516(3)
C(1)-O(2)	1.320(3)	C(8)-C(9)	1.520(4)	C(16)-N(3)	1.456(3)
C(1)-C(2)	1.505(4)	C(9)-N(1)	1.348(3)	C(16)-C(17)	1.482(4)
C(2)-N(2)	1.351(3)	C(9)-C(10)	1.374(3)	C(16)-H(16)	1
C(2)-C(3)	1.385(4)	C(10)-C(11)	1.382(4)	C(17)-C(18)	1.516(3)
C(3)-C(4)	1.385(4)	C(10)-H(10)	0.95	C(17)-H(17A)	0.99
C(3)-H(3)	0.95	C(11)-C(12)	1.386(3)	C(17)-H(17B)	0.99
C(4)-C(5)	1.382(4)	C(11)-H(11)	0.95	C(18)-C(19)	1.488(3)
C(4)-H(4)	0.95	C(12)-C(13)	1.379(3)	C(18)-H(18A)	0.99
C(5)-C(6)	1.380(4)	C(12)-H(12)	0.95	C(18)-H(18B)	0.99
C(5)-H(5)	0.95	C(13)-N(1)	1.353(3)	C(19)-O(7)	1.212(3)
C(6)-N(2)	1.347(3)	C(13)-C(14)	1.509(3)	C(19)-O(8)	1.312(3)
C(6)-C(7)	1.513(4)	C(14)-N(3)	1.446(3)	N(1)-H(1)	0.95(2)
C(7)-N(3)	1.450(3)	C(14)-H(14A)	0.99	O(2)-H(2)	0.84
C(7)-H(7A)	0.99	C(14)-H(14B)	0.99	O(6)-H(6)	0.84
C(7)-H(7B)	0.99	C(15)-O(5)	1.209(3)	O(8)-H(8)	0.84
C(8)-O(3)	1.246(3)	C(15)-O(6)	1.327(3)		

Table 8.16: Bond Angles for [Ga(Dpaa)(H_2O)]

Bond Angles / °					
O(1)-C(1)-O(2)	125.6(2)	N(1)-C(9)-C(8)	117.6(2)	C(15)-C(16)-H(16)	103.6
O(1)-C(1)-C(2)	122.5(2)	C(10)-C(9)-C(8)	124.1(2)	C(16)-C(17)-C(18)	113.9(2)
O(2)-C(1)-C(2)	111.9(2)	C(9)-C(10)-C(11)	120.3(2)	C(16)-C(17)-H(17A)	108.8
N(2)-C(2)-C(3)	122.6(2)	C(9)-C(10)-H(10)	119.9	C(18)-C(17)-H(17A)	108.8
N(2)-C(2)-C(1)	114.9(2)	C(11)-C(10)-H(10)	119.9	C(16)-C(17)-H(17B)	108.8
C(3)-C(2)-C(1)	122.4(2)	C(10)-C(11)-C(12)	119.7(2)	C(18)-C(17)-H(17B)	108.8
C(2)-C(3)-C(4)	119.3(2)	C(10)-C(11)-H(11)	120.2	H(17A)-C(17)-H(17B)	107.7
C(2)-C(3)-H(3)	120.3	C(12)-C(11)-H(11)	120.2	C(19)-C(18)-C(17)	115.8(2)
C(4)-C(3)-H(3)	120.3	C(13)-C(12)-C(11)	119.5(2)	C(19)-C(18)-H(18A)	108.3
C(5)-C(4)-C(3)	118.2(3)	C(13)-C(12)-H(12)	120.2	C(17)-C(18)-H(18A)	108.3
C(5)-C(4)-H(4)	120.9	C(11)-C(12)-H(12)	120.2	C(19)-C(18)-H(18B)	108.3
C(3)-C(4)-H(4)	120.9	N(1)-C(13)-C(12)	118.7(2)	C(17)-C(18)-H(18B)	108.3
C(6)-C(5)-C(4)	119.7(3)	N(1)-C(13)-C(14)	117.5(2)	H(18A)-C(18)-H(18B)	107.4
C(6)-C(5)-H(5)	120.1	C(12)-C(13)-C(14)	123.6(2)	O(7)-C(19)-O(8)	122.7(2)
C(4)-C(5)-H(5)	120.1	N(3)-C(14)-C(13)	111.1(2)	O(7)-C(19)-C(18)	122.5(2)
N(2)-C(6)-C(5)	122.7(2)	N(3)-C(14)-H(14A)	109.4	O(8)-C(19)-C(18)	114.8(2)
N(2)-C(6)-C(7)	114.8(2)	C(13)-C(14)-H(14A)	109.4	C(9)-N(1)-C(13)	123.5(2)
C(5)-C(6)-C(7)	122.5(2)	N(3)-C(14)-H(14B)	109.4	C(9)-N(1)-H(1)	118.2
N(3)-C(7)-C(6)	112.3(2)	C(13)-C(14)-H(14B)	109.4	C(13)-N(1)-H(1)	118.2
N(3)-C(7)-H(7A)	109.1	H(14A)-C(14)-H(14B)	108	C(6)-N(2)-C(2)	117.5(2)
C(6)-C(7)-H(7A)	109.1	O(5)-C(15)-O(6)	119.8(2)	C(14)-N(3)-C(7)	114.3(2)
N(3)-C(7)-H(7B)	109.1	O(5)-C(15)-C(16)	120.5(2)	C(14)-N(3)-C(16)	118.6(2)
C(6)-C(7)-H(7B)	109.1	O(6)-C(15)-C(16)	119.7(2)	C(7)-N(3)-C(16)	120.8(2)
H(7A)-C(7)-H(7B)	107.9	N(3)-C(16)-C(17)	117.6(2)	C(1)-O(2)-H(2)	109.5
O(3)-C(8)-O(4)	128.1(2)	N(3)-C(16)-C(15)	113.3(2)	C(15)-O(6)-H(6)	109.5
O(3)-C(8)-C(9)	118.1(2)	C(17)-C(16)-C(15)	113.1(2)	C(19)-O(8)-H(8)	109.5
O(4)-C(8)-C(9)	113.7(2)	N(3)-C(16)-H(16)	103.6		
N(1)-C(9)-C(10)	118.3(2)	C(17)-C(16)-H(16)	103.6		

Table 8.17: Anisotropic displacement parameters ($Å^2 x\ 10^3$) for H_4Dpaa.ga. The anisotropic displacement factor exponent takes the form: $-2\pi^2[h^2a^{*2}U_{11} + ... + 2\ h\ k\ a^*\ b^*\ U_{12}]$

	U_{11}	U_{22}	U_{33}	U_{23}	U_{13}	U_{12}
C(1)	25(2)	21(1)	34(2)	1(1)	-1(1)	0(1)
C(2)	25(2)	24(1)	27(2)	-1(1)	0(1)	-2(1)
C(3)	28(2)	29(1)	33(2)	0(1)	4(1)	0(1)
C(4)	24(2)	44(2)	31(2)	2(1)	6(1)	-5(1)
C(5)	24(2)	39(2)	28(2)	-3(1)	1(1)	7(1)
C(6)	23(2)	29(1)	28(2)	-5(1)	-4(1)	3(1)
C(7)	37(2)	26(2)	36(2)	-5(1)	-5(2)	9(1)
C(8)	27(2)	24(2)	28(2)	-3(1)	3(1)	2(1)
C(9)	24(2)	21(1)	24(2)	1(1)	0(1)	1(1)
C(10)	30(2)	23(1)	26(2)	1(1)	0(1)	-2(1)
C(11)	25(2)	27(2)	34(2)	1(1)	5(1)	-7(1)
C(12)	19(1)	29(2)	30(2)	-1(1)	2(1)	2(1)
C(13)	22(1)	25(1)	22(2)	1(1)	0(1)	2(1)
C(14)	24(1)	25(1)	31(2)	6(1)	5(1)	5(1)
C(15)	24(2)	25(1)	35(2)	-4(1)	3(1)	4(1)
C(16)	24(2)	24(1)	73(3)	2(2)	5(2)	-2(1)
C(17)	29(2)	25(2)	79(3)	0(2)	15(2)	0(1)
C(18)	30(2)	25(1)	46(2)	-7(1)	4(2)	2(1)
C(19)	24(2)	24(1)	32(2)	6(1)	3(1)	0(1)
N(1)	20(1)	20(1)	31(1)	0(1)	4(1)	0(1)
N(2)	20(1)	25(1)	29(1)	-3(1)	-4(1)	2(1)
N(3)	23(1)	22(1)	38(2)	0(1)	1(1)	-3(1)
O(1)	32(1)	33(1)	59(2)	15(1)	19(1)	4(1)
O(2)	32(1)	25(1)	50(1)	7(1)	12(1)	7(1)
O(3)	26(1)	24(1)	46(1)	4(1)	7(1)	-1(1)
O(4)	33(1)	21(1)	48(1)	1(1)	10(1)	3(1)
O(5)	25(1)	34(1)	62(2)	5(1)	9(1)	0(1)
O(6)	22(1)	29(1)	53(1)	7(1)	7(1)	3(1)
O(7)	28(1)	27(1)	59(2)	-8(1)	18(1)	-2(1)
O(8)	29(1)	23(1)	61(2)	-7(1)	13(1)	-2(1)

Table 8.18: Hydrogen coordinates (x 10^4) and isotropic displacement parameters ($Å^2$ x 10^3) for H_4Dpaa.ga.

	x	y	z	U(eq)		x	y	z	U(eq)
H(3)	4511	4722	774	36	H(16)	3324	2776	6029	49
H(4)	7307	4373	178	39	H(17A)	3420	2397	2770	53
H(5)	7653	3678	1039	37	H(17B)	2598	2199	4466	53
H(7A)	4501	3010	1847	40	H(18A)	6462	2433	4329	40
H(7B)	6576	3099	2727	40	H(18B)	5604	2198	5920	40
H(10)	5068	4866	6395	32	H(1)	3250(20)	3712(5)	7047(10)	28
H(11)	7855	4609	5362	34	H(2)	336	4922	2079	53
H(12)	8291	3892	5139	31	H(6)	1775	3448	3621	51
H(14A)	7145	3186	5595	32	H(8)	5038	1325	3351	56
H(14B)	5519	3133	6923	32					

8.4. [Ga(Tpaa)]

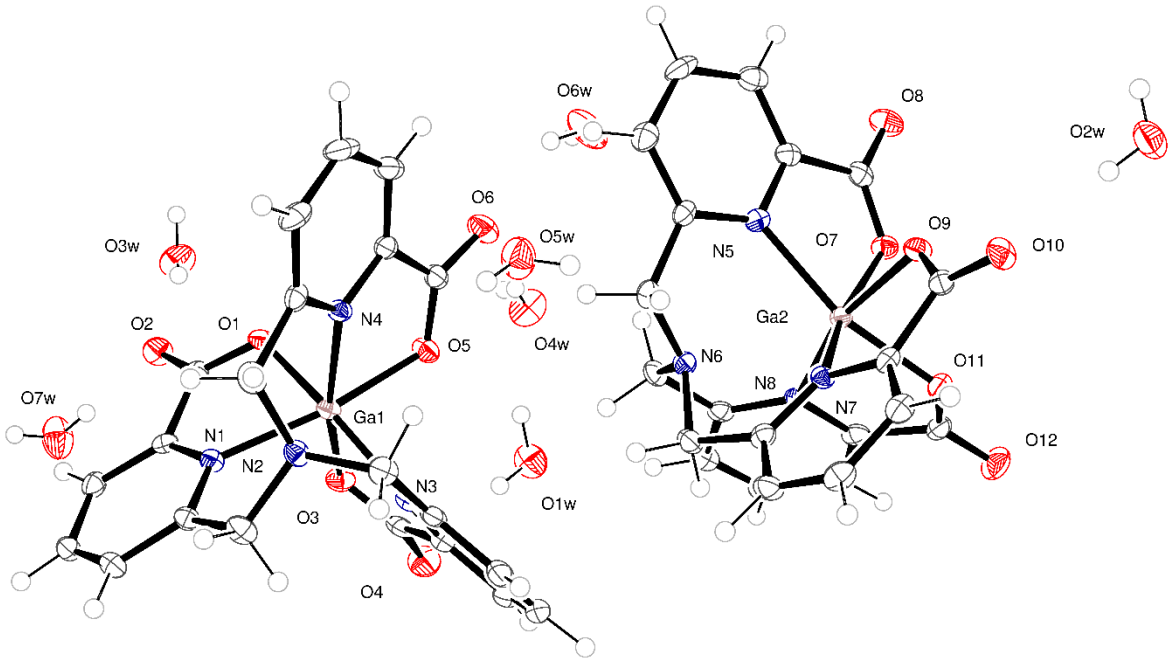

Figure 8.5: ORTEP representation of molecular structure of [Ga(Tpaa)] obtained by single crystal X-ray crystallography (drawn at 30% certainty).

Table 8.19: Crystal data and structure refinement for [Ga(Tpaa)]. CCDC Reference: 1878045

Identification code	[Ga(Tpaa)]
Empirical formula	C42 H44 Ga2 N8 O19
Formula weight	1104.29
Temperature	150(2) K
Wavelength	0.71073 Å
Crystal system	Monoclinic
Space group	P 21
Unit cell dimensions	a = 11.5621(5) Å α = 90°. b = 12.6405(4) Å β = 99.100(4)°. c = 15.2889(7) Å γ = 90°.
Volume	2206.36(16) $Å^3$
Z	2
Density (calculated)	1.662 Mg/m^3
Absorption coefficient	1.313 mm^{-1}
F(000)	1132
Crystal size	0.430 x 0.150 x 0.120 mm^3
Theta range for data collection	1.784 to 29.183°.
Index ranges	-15<=h<=15, -15<=k<=17, -14<=l<=20
Reflections collected	23251
Independent reflections	9173 [R(int) = 0.0330]
Completeness to theta = 25.242°	98.20%
Absorption correction	Semi-empirical from equivalents
Max. and min. transmission	0.883 and 0.870
Refinement method	Full-matrix least-squares on F^2
Data / restraints / parameters	9173 / 24 / 684
Goodness-of-fit on F2	0.847
Final R indices [I>2sigma(I)]	R1 = 0.0269, wR2 = 0.0473
R indices (all data)	R1 = 0.0357, wR2 = 0.0483
Absolute structure parameter	0.455(8)
Extinction coefficient	n/a
Largest diff. peak and hole	0.410 and -0.359 $e.Å^{-3}$

Table 8.20: Atomic coordinates (x 10^4) and equivalent isotropic displacement parameters ($Å^2$x 10^3) for [Ga(Tpaa)]. U(eq) is defined as one third of the trace of the orthogonalized U^{ij} tensor.

	x	y	z	U(eq)		x	y	z	U(eq)
Ga(1)	8236(1)	127(1)	7496(1)	14(1)	O(10)	3539(2)	7798(2)	8234(2)	22(1)
O(1)	8102(2)	-1234(2)	8169(2)	17(1)	O(11)	2013(2)	5631(2)	6447(2)	18(1)
O(2)	8541(2)	-2956(2)	8093(2)	23(1)	O(12)	629(2)	5482(2)	5254(2)	30(1)
O(3)	7368(2)	-687(2)	6466(2)	20(1)	N(5)	3540(2)	3937(2)	8542(2)	15(1)
O(4)	6092(2)	-465(2)	5222(2)	29(1)	N(6)	4792(2)	3520(2)	7283(2)	15(1)
O(5)	6630(2)	477(2)	7764(2)	19(1)	N(7)	4484(2)	5583(2)	7136(2)	14(1)
O(6)	5659(2)	833(2)	8877(2)	26(1)	N(8)	2643(2)	3666(2)	6394(2)	15(1)
N(1)	9732(2)	-662(2)	7278(2)	15(1)	C(31)	1496(3)	4164(3)	8610(3)	18(1)
N(2)	10065(2)	1390(2)	7543(2)	16(1)	C(32)	2720(2)	3894(3)	9077(3)	16(1)
N(3)	8024(2)	1284(2)	6515(2)	17(1)	C(33)	2972(3)	3579(3)	9946(3)	22(1)
N(4)	8643(2)	946(2)	8665(2)	15(1)	C(34)	4110(3)	3283(3)	10275(3)	25(1)
C(1)	8682(2)	-2010(3)	7921(3)	17(1)	C(35)	4936(3)	3265(3)	9715(3)	22(1)
C(2)	9635(3)	-1715(3)	7389(3)	15(1)	C(36)	4631(2)	3583(3)	8846(3)	16(1)
C(3)	10385(3)	-2419(3)	7089(3)	19(1)	C(37)	5457(2)	3549(3)	8173(3)	18(1)
C(4)	11268(2)	-2013(3)	6651(3)	19(1)	C(38)	4233(3)	2514(3)	7009(3)	18(1)
C(5)	11403(2)	-939(3)	6587(3)	18(1)	C(39)	3160(2)	2729(3)	6333(3)	17(1)
C(6)	10620(2)	-260(3)	6914(2)	16(1)	C(40)	2723(3)	2016(3)	5669(3)	21(1)
C(7)	10725(3)	917(3)	6896(3)	21(1)	C(41)	1734(3)	2283(3)	5071(3)	26(1)
C(8)	9538(3)	2412(3)	7278(3)	20(1)	C(42)	1253(3)	3277(3)	5117(3)	22(1)
C(9)	8531(3)	2239(3)	6541(3)	18(1)	C(43)	1736(3)	3955(3)	5774(3)	19(1)
C(10)	8151(3)	2986(3)	5891(3)	24(1)	C(44)	1392(2)	5117(3)	5819(2)	18(1)
C(11)	7238(3)	2739(3)	5226(3)	25(1)	C(45)	5388(3)	4016(3)	6620(3)	18(1)
C(12)	6759(3)	1735(3)	5182(3)	24(1)	C(46)	5334(2)	5207(3)	6719(2)	16(1)
C(13)	7182(3)	1017(3)	5845(3)	18(1)	C(47)	6145(3)	5888(3)	6429(3)	20(1)
C(14)	6831(2)	-134(3)	5831(2)	20(1)	C(48)	6076(3)	6966(3)	6588(3)	20(1)
C(15)	10628(3)	1301(3)	8449(3)	20(1)	C(49)	5240(3)	7335(3)	7068(3)	19(1)
C(16)	9709(2)	1280(3)	9054(3)	17(1)	C(50)	4461(3)	6620(3)	7341(3)	15(1)
C(17)	9899(3)	1604(3)	9921(3)	23(1)	C(51)	3580(2)	6890(3)	7937(3)	17(1)
C(18)	8977(3)	1606(3)	10405(3)	26(1)	O(1W)	3932(2)	-260(2)	5823(2)	34(1)
C(19)	7866(3)	1323(3)	9988(3)	23(1)	O(2W)	2045(2)	9094(2)	9061(2)	33(1)
C(20)	7734(3)	1002(3)	9129(3)	17(1)	O(3W)	6894(2)	-4243(3)	8730(2)	34(1)
C(21)	6572(3)	743(3)	8556(3)	19(1)	O(4W)	3882(2)	-106(3)	7588(2)	37(1)
Ga(2)	2981(1)	4796(1)	7392(1)	13(1)	O(5W)	8280(2)	3898(3)	9174(2)	35(1)
O(7)	1444(2)	4452(2)	7802(2)	18(1)	O(6W)	3431(2)	913(3)	9520(2)	41(1)
O(8)	667(2)	4051(2)	9013(2)	27(1)	O(7W)	8958(2)	-4914(3)	7130(2)	41(1)
O(9)	2965(2)	6107(2)	8128(2)	18(1)					

Table 8.21: Bond lengths for [Ga(Tpaa)].

Bond Lengths / Å					
Ga(1)-O(3)	2.012(3)	C(12)-H(12)	0.95	C(35)-H(35)	0.95
Ga(1)-O(5)	2.013(2)	C(13)-C(14)	1.510(6)	C(36)-C(37)	1.511(5)
Ga(1)-O(1)	2.022(3)	C(15)-C(16)	1.514(5)	C(37)-H(37A)	0.99
Ga(1)-N(4)	2.054(3)	C(15)-H(15A)	0.99	C(37)-H(37B)	0.99
Ga(1)-N(1)	2.068(3)	C(15)-H(15B)	0.99	C(38)-C(39)	1.509(5)
Ga(1)-N(3)	2.083(3)	C(16)-C(17)	1.372(6)	C(38)-H(38A)	0.99
O(1)-C(1)	1.279(4)	C(17)-C(18)	1.390(6)	C(38)-H(38B)	0.99
O(2)-C(1)	1.240(5)	C(17)-H(17)	0.95	C(39)-C(40)	1.392(5)
O(3)-C(14)	1.276(4)	C(18)-C(19)	1.388(5)	C(40)-C(41)	1.388(5)
O(4)-C(14)	1.233(4)	C(18)-H(18)	0.95	C(40)-H(40)	0.95
O(5)-C(21)	1.269(5)	C(19)-C(20)	1.359(6)	C(41)-C(42)	1.381(6)
O(6)-C(21)	1.238(4)	C(19)-H(19)	0.95	C(41)-H(41)	0.95
N(1)-C(6)	1.343(4)	C(20)-C(21)	1.519(5)	C(42)-C(43)	1.371(5)
N(1)-C(2)	1.349(5)	Ga(2)-O(11)	1.985(2)	C(42)-H(42)	0.95
N(2)-C(15)	1.439(5)	Ga(2)-O(9)	2.006(3)	C(43)-C(44)	1.526(6)
N(2)-C(8)	1.458(5)	Ga(2)-O(7)	2.023(2)	C(45)-C(46)	1.515(6)
N(2)-C(7)	1.469(5)	Ga(2)-N(8)	2.080(3)	C(45)-H(45A)	0.99
N(3)-C(13)	1.340(5)	Ga(2)-N(5)	2.081(3)	C(45)-H(45B)	0.99
N(3)-C(9)	1.340(5)	Ga(2)-N(7)	2.093(3)	C(46)-C(47)	1.396(5)
N(4)-C(16)	1.350(4)	O(7)-C(31)	1.280(5)	C(47)-C(48)	1.388(5)
N(4)-C(20)	1.361(4)	O(8)-C(31)	1.227(4)	C(47)-H(47)	0.95
C(1)-C(2)	1.515(5)	O(9)-C(51)	1.279(4)	C(48)-C(49)	1.384(5)
C(2)-C(3)	1.371(5)	O(10)-C(51)	1.238(4)	C(48)-H(48)	0.95
C(3)-C(4)	1.404(5)	O(11)-C(44)	1.281(4)	C(49)-C(50)	1.386(5)
C(3)-H(3)	0.95	O(12)-C(44)	1.223(4)	C(49)-H(49)	0.95
C(4)-C(5)	1.372(5)	N(5)-C(32)	1.347(5)	C(50)-C(51)	1.509(5)
C(4)-H(4)	0.95	N(5)-C(36)	1.350(4)	O(1W)-H(1B)	0.90(2)
C(5)-C(6)	1.397(5)	N(6)-C(37)	1.453(5)	O(1W)-H(1A)	0.86(2)
C(5)-H(5)	0.95	N(6)-C(45)	1.455(5)	O(2W)-H(2A)	0.78(2)
C(6)-C(7)	1.493(6)	N(6)-C(38)	1.457(4)	O(2W)-H(2B)	0.80(2)
C(7)-H(7A)	0.99	N(7)-C(46)	1.340(4)	O(3W)-H(3A)	0.81(2)
C(7)-H(7B)	0.99	N(7)-C(50)	1.349(5)	O(3W)-H(3B)	0.81(2)
C(8)-C(9)	1.502(5)	N(8)-C(39)	1.337(4)	O(4W)-H(4A)	0.82(2)
C(8)-H(8A)	0.99	N(8)-C(43)	1.348(5)	O(4W)-H(4B)	0.79(2)
C(8)-H(8B)	0.99	C(31)-C(32)	1.520(4)	O(5W)-H(5A)	0.80(2)
C(9)-C(10)	1.391(5)	C(32)-C(33)	1.373(6)	O(5W)-H(5B)	0.83(2)
C(10)-C(11)	1.380(6)	C(33)-C(34)	1.383(5)	O(6W)-H(6B)	0.82(2)
C(10)-H(10)	0.95	C(33)-H(33)	0.95	O(6W)-H(6A)	0.80(2)
C(11)-C(12)	1.382(6)	C(34)-C(35)	1.380(6)	O(7W)-H(7C)	0.79(2)
C(11)-H(11)	0.95	C(34)-H(34)	0.95	O(7W)-H(7D)	0.83(2)
C(12)-C(13)	1.390(5)	C(35)-C(36)	1.380(5)		

Table 8.22: Bond Angles for [Ga(Tpaa)]

Bond Angles / °					
O(3)-Ga(1)-O(5)	84.78(10)	C(13)-C(12)-H(12)	120.9	C(35)-C(34)-H(34)	120.3
O(3)-Ga(1)-O(1)	83.93(11)	N(3)-C(13)-C(12)	121.4(3)	C(33)-C(34)-H(34)	120.3
O(5)-Ga(1)-O(1)	86.36(10)	N(3)-C(13)-C(14)	114.5(3)	C(34)-C(35)-C(36)	119.7(3)
O(3)-Ga(1)-N(4)	162.94(9)	C(12)-C(13)-C(14)	123.8(3)	C(34)-C(35)-H(35)	120.2
O(5)-Ga(1)-N(4)	78.72(10)	O(4)-C(14)-O(3)	125.8(4)	C(36)-C(35)-H(35)	120.2
O(1)-Ga(1)-N(4)	90.69(12)	O(4)-C(14)-C(13)	119.3(3)	N(5)-C(36)-C(35)	120.7(3)
O(3)-Ga(1)-N(1)	87.35(11)	O(3)-C(14)-C(13)	114.8(3)	N(5)-C(36)-C(37)	115.6(3)
O(5)-Ga(1)-N(1)	163.82(11)	N(2)-C(15)-C(16)	109.6(2)	C(35)-C(36)-C(37)	123.7(3)
O(1)-Ga(1)-N(1)	78.77(11)	N(2)-C(15)-H(15A)	109.8	N(6)-C(37)-C(36)	109.9(2)
N(4)-Ga(1)-N(1)	107.52(11)	C(16)-C(15)-H(15A)	109.8	N(6)-C(37)-H(37A)	109.7
O(3)-Ga(1)-N(3)	78.91(12)	N(2)-C(15)-H(15B)	109.8	C(36)-C(37)-H(37A)	109.7
O(5)-Ga(1)-N(3)	89.11(10)	C(16)-C(15)-H(15B)	109.8	N(6)-C(37)-H(37B)	109.7
O(1)-Ga(1)-N(3)	162.58(10)	H(15A)-C(15)-H(15B)	108.2	C(36)-C(37)-H(37B)	109.7
N(4)-Ga(1)-N(3)	104.91(12)	N(4)-C(16)-C(17)	121.0(3)	H(37A)-C(37)-H(37B)	108.2
N(1)-Ga(1)-N(3)	103.22(11)	N(4)-C(16)-C(15)	114.6(3)	N(6)-C(38)-C(39)	108.6(3)
C(1)-O(1)-Ga(1)	114.6(2)	C(17)-C(16)-C(15)	124.4(3)	N(6)-C(38)-H(38A)	110
C(14)-O(3)-Ga(1)	116.0(2)	C(16)-C(17)-C(18)	119.7(3)	C(39)-C(38)-H(38A)	110
C(21)-O(5)-Ga(1)	116.2(2)	C(16)-C(17)-H(17)	120.1	N(6)-C(38)-H(38B)	110
C(6)-N(1)-C(2)	120.7(3)	C(18)-C(17)-H(17)	120.1	C(39)-C(38)-H(38B)	110
C(6)-N(1)-Ga(1)	126.7(2)	C(19)-C(18)-C(17)	119.2(4)	H(38A)-C(38)-H(38B)	108.3
C(2)-N(1)-Ga(1)	111.6(2)	C(19)-C(18)-H(18)	120.4	N(8)-C(39)-C(40)	120.7(3)
C(15)-N(2)-C(8)	116.2(3)	C(17)-C(18)-H(18)	120.4	N(8)-C(39)-C(38)	116.1(3)
C(15)-N(2)-C(7)	114.4(3)	C(20)-C(19)-C(18)	118.3(3)	C(40)-C(39)-C(38)	123.2(3)
C(8)-N(2)-C(7)	114.3(3)	C(20)-C(19)-H(19)	120.8	C(41)-C(40)-C(39)	119.3(3)
C(13)-N(3)-C(9)	120.8(3)	C(18)-C(19)-H(19)	120.8	C(41)-C(40)-H(40)	120.4
C(13)-N(3)-Ga(1)	111.2(2)	C(19)-C(20)-N(4)	122.8(3)	C(39)-C(40)-H(40)	120.4
C(9)-N(3)-Ga(1)	127.6(2)	C(19)-C(20)-C(21)	125.1(3)	C(42)-C(41)-C(40)	119.0(4)
C(16)-N(4)-C(20)	118.7(3)	N(4)-C(20)-C(21)	111.9(3)	C(42)-C(41)-H(41)	120.5
C(16)-N(4)-Ga(1)	127.5(2)	O(6)-C(21)-O(5)	125.5(3)	C(40)-C(41)-H(41)	120.5
C(20)-N(4)-Ga(1)	113.0(2)	O(6)-C(21)-C(20)	118.9(4)	C(43)-C(42)-C(41)	119.1(4)
O(2)-C(1)-O(1)	125.7(3)	O(5)-C(21)-C(20)	115.6(3)	C(43)-C(42)-H(42)	120.5
O(2)-C(1)-C(2)	118.8(3)	O(11)-Ga(2)-O(9)	85.11(10)	C(41)-C(42)-H(42)	120.5
O(1)-C(1)-C(2)	115.4(3)	O(11)-Ga(2)-O(7)	85.30(10)	N(8)-C(43)-C(42)	121.8(3)
N(1)-C(2)-C(3)	121.9(3)	O(9)-Ga(2)-O(7)	85.26(10)	N(8)-C(43)-C(44)	114.1(3)
N(1)-C(2)-C(1)	113.1(3)	O(11)-Ga(2)-N(8)	79.20(12)	C(42)-C(43)-C(44)	123.8(3)
C(3)-C(2)-C(1)	124.9(3)	O(9)-Ga(2)-N(8)	164.02(10)	O(12)-C(44)-O(11)	126.5(4)
C(2)-C(3)-C(4)	118.0(4)	O(7)-Ga(2)-N(8)	90.41(10)	O(12)-C(44)-C(43)	119.7(3)
C(2)-C(3)-H(3)	121	O(11)-Ga(2)-N(5)	162.98(10)	O(11)-C(44)-C(43)	113.7(3)
C(4)-C(3)-H(3)	121	O(9)-Ga(2)-N(5)	89.19(11)	N(6)-C(45)-C(46)	109.1(3)
C(5)-C(4)-C(3)	119.7(3)	O(7)-Ga(2)-N(5)	78.24(10)	N(6)-C(45)-H(45A)	109.9
C(5)-C(4)-H(4)	120.2	N(8)-Ga(2)-N(5)	105.00(12)	C(46)-C(45)-H(45A)	109.9
C(3)-C(4)-H(4)	120.2	O(11)-Ga(2)-N(7)	90.03(11)	N(6)-C(45)-H(45B)	109.9
C(4)-C(5)-C(6)	119.7(3)	O(9)-Ga(2)-N(7)	78.09(10)	C(46)-C(45)-H(45B)	109.9
C(4)-C(5)-H(5)	120.2	O(7)-Ga(2)-N(7)	163.03(11)	H(45A)-C(45)-H(45B)	108.3
C(6)-C(5)-H(5)	120.2	N(8)-Ga(2)-N(7)	104.75(11)	N(7)-C(46)-C(47)	120.8(3)

N(1)-C(6)-C(5)	119.8(3)	N(5)-Ga(2)-N(7)	104.49(11)	N(7)-C(46)-C(45)	116.4(3)
N(1)-C(6)-C(7)	117.1(3)	C(31)-O(7)-Ga(2)	116.80(19)	C(47)-C(46)-C(45)	122.8(3)
C(5)-C(6)-C(7)	123.1(3)	C(51)-O(9)-Ga(2)	117.2(2)	C(48)-C(47)-C(46)	119.3(3)
N(2)-C(7)-C(6)	109.9(3)	C(44)-O(11)-Ga(2)	117.4(2)	C(48)-C(47)-H(47)	120.4
N(2)-C(7)-H(7A)	109.7	C(32)-N(5)-C(36)	119.1(3)	C(46)-C(47)-H(47)	120.4
C(6)-C(7)-H(7A)	109.7	C(32)-N(5)-Ga(2)	112.4(2)	C(49)-C(48)-C(47)	119.3(3)
N(2)-C(7)-H(7B)	109.7	C(36)-N(5)-Ga(2)	127.7(2)	C(49)-C(48)-H(48)	120.4
C(6)-C(7)-H(7B)	109.7	C(37)-N(6)-C(45)	113.7(3)	C(47)-C(48)-H(48)	120.4
H(7A)-C(7)-H(7B)	108.2	C(37)-N(6)-C(38)	115.9(3)	C(48)-C(49)-C(50)	118.8(4)
N(2)-C(8)-C(9)	108.7(3)	C(45)-N(6)-C(38)	114.4(3)	C(48)-C(49)-H(49)	120.6
N(2)-C(8)-H(8A)	110	C(46)-N(7)-C(50)	119.9(3)	C(50)-C(49)-H(49)	120.6
C(9)-C(8)-H(8A)	110	C(46)-N(7)-Ga(2)	127.8(2)	N(7)-C(50)-C(49)	121.7(3)
N(2)-C(8)-H(8B)	110	C(50)-N(7)-Ga(2)	111.8(2)	N(7)-C(50)-C(51)	113.6(3)
C(9)-C(8)-H(8B)	110	C(39)-N(8)-C(43)	119.8(3)	C(49)-C(50)-C(51)	124.5(3)
H(8A)-C(8)-H(8B)	108.3	C(39)-N(8)-Ga(2)	128.7(2)	O(10)-C(51)-O(9)	125.3(3)
N(3)-C(9)-C(10)	120.1(3)	C(43)-N(8)-Ga(2)	111.4(2)	O(10)-C(51)-C(50)	120.0(3)
N(3)-C(9)-C(8)	115.9(3)	O(8)-C(31)-O(7)	126.6(3)	O(9)-C(51)-C(50)	114.5(3)
C(10)-C(9)-C(8)	123.9(3)	O(8)-C(31)-C(32)	118.8(4)	H(1B)-O(1W)-H(1A)	94(2)
C(11)-C(10)-C(9)	119.4(4)	O(7)-C(31)-C(32)	114.6(3)	H(2A)-O(2W)-H(2B)	113(4)
C(11)-C(10)-H(10)	120.3	N(5)-C(32)-C(33)	122.5(3)	H(3A)-O(3W)-H(3B)	105(3)
C(9)-C(10)-H(10)	120.3	N(5)-C(32)-C(31)	113.4(3)	H(4A)-O(4W)-H(4B)	111(4)
C(10)-C(11)-C(12)	119.9(4)	C(33)-C(32)-C(31)	124.0(3)	H(5A)-O(5W)-H(5B)	105(3)
C(10)-C(11)-H(11)	120.1	C(32)-C(33)-C(34)	118.3(3)	H(6B)-O(6W)-H(6A)	106(3)
C(12)-C(11)-H(11)	120.1	C(32)-C(33)-H(33)	120.8	H(7C)-O(7W)-H(7D)	107(3)
C(11)-C(12)-C(13)	118.2(4)	C(34)-C(33)-H(33)	120.8		
C(11)-C(12)-H(12)	120.9	C(35)-C(34)-C(33)	119.4(4)		

Table 8.23: Anisotropic displacement parameters ($Å^2 x\ 10^3$) for [Ga(Tpaa)]. The anisotropic displacement factor exponent takes the form: $-2\pi^2[h^2a^{*2}U_{11} + ... + 2\ h\ k\ a^*\ b^*\ U_{12}]$

	U_{11}	U_{22}	U_{33}	U_{23}	U_{13}	U_{12}
Ga(1)	16(1)	14(1)	13(1)	-1(1)	4(1)	-1(1)
O(1)	22(1)	16(2)	15(2)	0(1)	8(1)	-2(1)
O(2)	26(1)	18(2)	27(2)	3(1)	9(1)	-4(1)
O(3)	25(1)	19(1)	16(2)	-4(1)	4(1)	-3(1)
O(4)	27(1)	35(2)	24(2)	-7(1)	-2(1)	-2(1)
O(5)	15(1)	24(2)	18(2)	-4(1)	4(1)	-1(1)
O(6)	23(1)	29(2)	29(2)	-1(1)	13(1)	0(1)
N(1)	15(1)	15(2)	15(2)	-1(1)	4(1)	-1(1)
N(2)	18(1)	13(2)	19(2)	-2(1)	5(1)	0(1)
N(3)	19(1)	19(2)	14(2)	-3(1)	7(1)	2(1)
N(4)	19(1)	13(2)	13(2)	-1(1)	4(1)	1(1)
C(1)	18(1)	17(2)	14(2)	-2(2)	-1(1)	-1(1)
C(2)	17(1)	18(2)	10(2)	1(2)	1(1)	-2(1)
C(3)	23(2)	14(2)	17(2)	0(2)	0(1)	3(1)
C(4)	17(1)	24(2)	16(2)	-2(2)	3(1)	4(1)
C(5)	16(1)	21(2)	19(2)	-3(2)	5(1)	-1(1)
C(6)	14(1)	18(2)	17(2)	1(2)	5(1)	-1(1)
C(7)	21(2)	17(2)	26(2)	0(2)	11(1)	-5(1)
C(8)	23(2)	16(2)	22(2)	-1(2)	5(1)	-3(1)
C(9)	23(2)	15(2)	17(2)	0(2)	12(1)	2(1)
C(10)	30(2)	19(2)	25(2)	2(2)	14(2)	7(1)
C(11)	33(2)	25(2)	20(2)	7(2)	12(2)	12(1)
C(12)	25(2)	33(2)	14(2)	-1(2)	4(1)	7(2)
C(13)	18(1)	20(2)	16(2)	-1(2)	7(1)	3(1)
C(14)	20(1)	27(2)	15(2)	-7(2)	7(1)	1(1)
C(15)	20(1)	16(2)	24(2)	-6(2)	1(1)	-3(1)
C(16)	19(1)	12(2)	18(2)	1(2)	0(1)	2(1)
C(17)	31(2)	21(2)	15(2)	-1(2)	-6(2)	-2(1)
C(18)	45(2)	21(2)	12(2)	2(2)	4(2)	0(2)
C(19)	35(2)	18(2)	17(2)	2(2)	10(2)	3(1)
C(20)	23(2)	12(2)	17(2)	4(2)	7(1)	3(1)
C(21)	23(2)	15(2)	20(2)	3(2)	9(1)	3(1)
Ga(2)	15(1)	13(1)	13(1)	0(1)	3(1)	0(1)
O(7)	17(1)	21(2)	17(1)	0(1)	4(1)	-2(1)
O(8)	22(1)	34(2)	27(2)	-1(1)	13(1)	-4(1)
O(9)	22(1)	16(2)	16(2)	-2(1)	6(1)	-2(1)
O(10)	28(1)	13(1)	26(2)	-5(1)	6(1)	-1(1)
O(11)	20(1)	16(1)	17(2)	2(1)	1(1)	1(1)
O(12)	32(1)	32(2)	23(2)	4(1)	-7(1)	7(1)
N(5)	18(1)	13(2)	14(2)	0(1)	2(1)	-2(1)
N(6)	16(1)	14(2)	16(2)	1(1)	4(1)	0(1)
N(7)	15(1)	14(2)	13(2)	-1(1)	2(1)	-1(1)
N(8)	16(1)	15(2)	13(2)	-1(1)	5(1)	0(1)
C(31)	22(2)	11(2)	21(2)	-4(2)	6(1)	-2(1)
C(32)	21(1)	12(2)	15(2)	-3(2)	4(1)	-3(1)
C(33)	30(2)	18(2)	19(2)	-2(2)	8(2)	-3(1)

C(34)	37(2)	23(2)	14(2)	7(2)	-1(2)	-2(1)
C(35)	24(2)	19(2)	21(2)	-2(2)	-2(2)	0(1)
C(36)	20(1)	11(2)	16(2)	0(1)	-1(1)	-1(1)
C(37)	14(1)	18(2)	21(2)	2(2)	1(1)	2(1)
C(38)	22(2)	12(2)	21(2)	-3(2)	7(1)	1(1)
C(39)	19(1)	18(2)	16(2)	2(2)	8(1)	-3(1)
C(40)	25(2)	16(2)	23(2)	-2(2)	9(1)	-5(1)
C(41)	28(2)	31(2)	18(2)	-6(2)	5(2)	-11(1)
C(42)	20(2)	29(2)	18(2)	0(2)	3(1)	-5(1)
C(43)	16(1)	26(2)	17(2)	3(2)	6(1)	-3(1)
C(44)	18(1)	21(2)	17(2)	5(2)	3(1)	1(1)
C(45)	19(2)	17(2)	20(2)	0(2)	8(1)	2(1)
C(46)	13(1)	19(2)	15(2)	2(2)	1(1)	-1(1)
C(47)	18(1)	26(2)	18(2)	1(2)	8(1)	0(1)
C(48)	20(1)	20(2)	21(2)	4(2)	3(1)	-6(1)
C(49)	22(2)	17(2)	18(2)	-1(2)	-1(1)	-2(1)
C(50)	17(1)	13(2)	14(2)	2(2)	-1(1)	-1(1)
C(51)	17(1)	20(2)	13(2)	-2(2)	-3(1)	2(1)
O(1W)	27(1)	36(1)	37(2)	-5(2)	4(1)	-2(1)
O(2W)	38(1)	24(2)	39(2)	-5(2)	15(1)	4(1)
O(3W)	35(1)	31(2)	35(2)	10(2)	7(1)	-10(1)
O(4W)	37(1)	31(2)	39(2)	1(2)	-1(1)	-10(1)
O(5W)	24(1)	36(2)	46(2)	10(2)	10(1)	2(1)
O(6W)	32(1)	41(2)	55(2)	-18(2)	21(1)	-8(1)
O(7W)	36(1)	33(2)	51(2)	-15(2)	-4(1)	6(1)

Table 8.24: Hydrogen coordinates (x 10^4) and isotropic displacement parameters (Å^2 x 10^3) for [Ga(Tpaa)].

	x	y	z	U(eq)		x	y	z	U(eq)
H(3)	10309	-3158	7175	22	H(40)	3099	1354	5624	25
H(4)	11771	-2480	6401	23	H(41)	1394	1789	4637	31
H(5)	12025	-659	6320	22	H(42)	596	3488	4699	27
H(7A)	11560	1123	7038	25	H(45A)	5006	3805	6020	22
H(7B)	10416	1183	6295	25	H(45B)	6215	3781	6700	22
H(8A)	10127	2882	7075	24	H(47)	6738	5618	6125	24
H(8B)	9257	2752	7788	24	H(48)	6597	7444	6371	24
H(10)	8516	3660	5904	28	H(49)	5200	8065	7208	23
H(11)	6940	3258	4800	30	H(1B)	4130(30)	-180(40)	6414(16)	50
H(12)	6157	1541	4712	29	H(1A)	4640(20)	-240(40)	5720(30)	50
H(15A)	11160	1910	8603	24	H(2A)	2310(40)	8640(30)	8800(30)	50
H(15B)	11100	645	8528	24	H(2B)	1960(40)	8930(40)	9549(19)	50
H(17)	10657	1825	10191	28	H(3A)	7330(40)	-3750(30)	8670(30)	50
H(18)	9106	1800	11013	31	H(3B)	6830(40)	-4240(40)	9253(18)	50
H(19)	7214	1352	10296	27	H(4A)	4410(30)	170(30)	7930(30)	55
H(33)	2381	3564	10312	26	H(4B)	3740(40)	-680(20)	7750(30)	55
H(34)	4320	3093	10880	30	H(5A)	8940(20)	3950(30)	9090(40)	52
H(35)	5712	3034	9927	26	H(5B)	7990(30)	4480(20)	9050(30)	52
H(37A)	5967	4182	8240	21	H(6B)	3120(30)	340(30)	9380(40)	62
H(37B)	5962	2914	8274	21	H(6A)	4120(20)	830(40)	9530(30)	62
H(38A)	4008	2146	7528	21	H(7C)	9610(20)	-5080(40)	7320(30)	62
H(38B)	4784	2056	6749	21	H(7D)	8810(40)	-4380(30)	7400(30)	62

8.5. [Ga(Bn$_2$DT3A)]

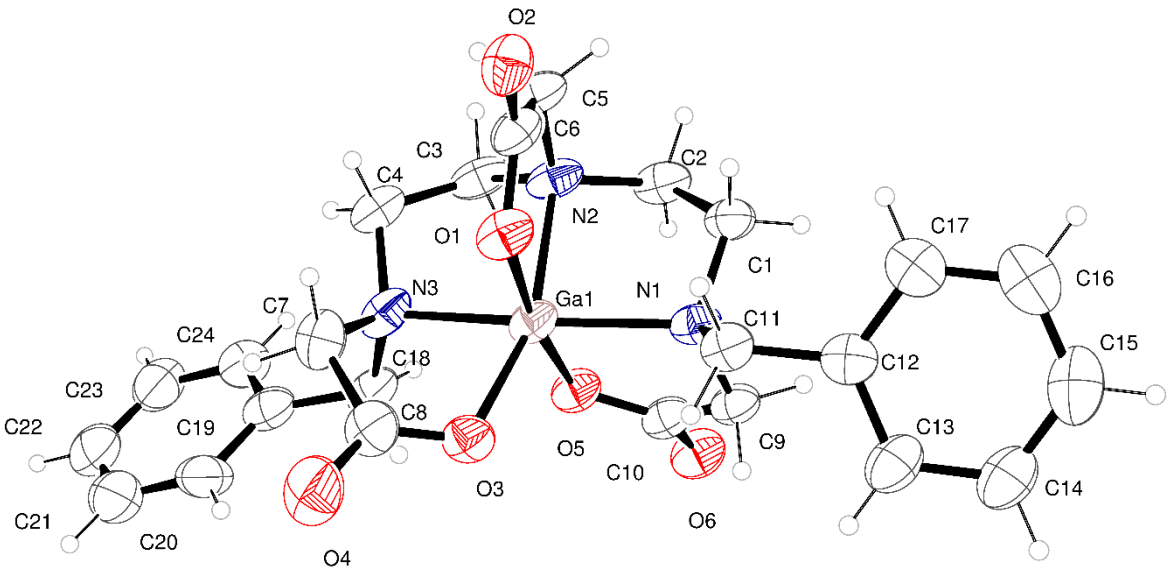

Figure 8.6: ORTEP representation of molecular structure of [Ga(Bn$_2$DT3A)] obtained by single crystal X-ray crystallography (drawn at 30% certainty).

Table 8.25: Crystal data and structure refinement for [Ga(Bn_2DT3A)]. CCDC Reference: 1864389

Identification code	[Ga(Bn_2DT3A)]
Empirical formula	C24 H28 Ga N3 O6.33
Formula weight	529.55
Temperature	100(2) K
Wavelength	1.54186 Å
Crystal system	Trigonal
Space group	R 3 :H
Unit cell dimensions	a = 24.5666(5) Å α = 90°.
	b = 24.5666(5) Å β = 90°.
	c = 10.0351(2) Å γ = 120°.
Volume	5245.0(2) $Å^3$
Z	9
Density (calculated)	1.509 Mg/m^3
Absorption coefficient	2.027 mm^{-1}
F(000)	2472
Crystal size	0.200 x 0.150 x 0.100 mm^3
Theta range for data collection	4.873 to 69.572°.
Index ranges	-29<=h<=21, -22<=k<=29, -9<=l<=12
Reflections collected	15590
Independent reflections	3910 [R(int) = 0.0264]
Completeness to theta = 67.686°	99.70%
Absorption correction	Semi-empirical from equivalents
Max. and min. transmission	0.6268 and 0.0495
Refinement method	Full-matrix least-squares on F2
Data / restraints / parameters	3910 / 1 / 287
Goodness-of-fit on F2	1.102
Final R indices [I>2sigma(I)]	R1 = 0.0758, wR2 = 0.1849
R indices (all data)	R1 = 0.0771, wR2 = 0.1870
Absolute structure parameter	0.00(4)
Extinction coefficient	n/a
Largest diff. peak and hole	1.830 and -0.447 e.$Å^{-3}$

Table 8.26: Atomic coordinates (x 10^4) and equivalent isotropic displacement parameters ($Å^2$x 10^3) for [Ga(Bn_2DT3A)]. U(eq) is defined as one third of the trace of the orthogonalized U^{ij} tensor.

	x	Y	z	U(eq)		x	y	z	U(eq)
Ga(1)	1528(1)	3313(1)	5106(1)	60(1)	C(9)	2121(3)	2696(4)	3771(9)	63(2)
O(1)	813(3)	3344(3)	4254(7)	69(1)	C(10)	2375(4)	2850(4)	5188(9)	65(2)
O(2)	-222(3)	2855(3)	3958(7)	77(2)	C(11)	1457(4)	2891(4)	2242(8)	66(2)
O(3)	2056(3)	4170(3)	4503(6)	68(1)	C(12)	1500(2)	2502(3)	1108(5)	68(2)
O(4)	2180(6)	5108(5)	4732(11)	115(3)	C(13)	2060(2)	2733(3)	405(7)	84(2)
O(5)	2173(3)	3160(3)	5868(6)	65(1)	C(14)	2097(3)	2402(4)	-682(6)	90(3)
O(6)	2750(3)	2709(4)	5581(8)	83(2)	C(15)	1573(4)	1840(4)	-1065(6)	100(4)
N(1)	1524(3)	2693(3)	3632(7)	60(1)	C(16)	1013(3)	1609(2)	-362(7)	94(3)
N(2)	796(3)	2529(4)	6013(7)	67(2)	C(17)	977(2)	1940(3)	724(6)	80(2)
N(3)	1561(4)	3794(4)	6896(8)	73(2)	C(18)	2176(4)	4022(5)	7666(10)	76(2)
C(1)	982(3)	2062(3)	4028(10)	66(2)	C(19)	2334(3)	4504(3)	8789(6)	78(2)
C(2)	889(4)	2004(4)	5523(10)	73(2)	C(20)	2633(3)	5144(3)	8515(8)	100(4)
C(3)	902(4)	2677(5)	7471(9)	76(2)	C(21)	2817(3)	5575(2)	9553(11)	114(5)
C(4)	1007(4)	3335(5)	7713(9)	75(2)	C(22)	2702(4)	5366(4)	10865(9)	126(6)
C(5)	177(4)	2438(5)	5558(10)	73(2)	C(23)	2403(4)	4726(4)	11139(6)	104(4)
C(6)	245(4)	2906(4)	4490(8)	66(2)	C(24)	2219(3)	4295(3)	10101(7)	85(2)
C(7)	1545(6)	4328(5)	6335(11)	82(2)	O(1W)	3450(20)	6290(20)	13840(50)	153(14)
C(8)	1952(5)	4551(5)	5081(11)	79(2)					

Table 8.27: Bond lengths for [Ga(Bn_2DT3A)].

Bond Lengths / Å					
Ga(1)-O(3)	1.937(5)	C(1)-H(1B)	0.99	C(13)-H(13)	0.95
Ga(1)-O(5)	1.960(5)	C(2)-H(2A)	0.99	C(14)-C(15)	1.39
Ga(1)-O(1)	1.987(5)	C(2)-H(2B)	0.99	C(14)-H(14)	0.95
Ga(1)-N(2)	2.077(6)	C(3)-C(4)	1.523(16)	C(15)-C(16)	1.39
Ga(1)-N(1)	2.120(7)	C(3)-H(3A)	0.99	C(15)-H(15)	0.95
Ga(1)-N(3)	2.129(8)	C(3)-H(3B)	0.99	C(16)-C(17)	1.39
O(1)-C(6)	1.288(11)	C(4)-H(4A)	0.99	C(16)-H(16)	0.95
O(2)-C(6)	1.214(10)	C(4)-H(4B)	0.99	C(17)-H(17)	0.95
O(3)-C(8)	1.231(12)	C(5)-C(6)	1.518(12)	C(18)-C(19)	1.537(13)
O(4)-C(8)	1.243(13)	C(5)-H(5A)	0.99	C(18)-H(18A)	0.99
O(5)-C(10)	1.291(11)	C(5)-H(5B)	0.99	C(18)-H(18B)	0.99
O(6)-C(10)	1.202(10)	C(7)-C(8)	1.528(15)	C(19)-C(20)	1.39
N(1)-C(9)	1.472(8)	C(7)-H(7A)	0.99	C(19)-C(24)	1.39
N(1)-C(1)	1.507(9)	C(7)-H(7B)	0.99	C(20)-C(21)	1.39
N(1)-C(11)	1.512(10)	C(9)-C(10)	1.522(13)	C(20)-H(20)	0.95
N(2)-C(5)	1.492(10)	C(9)-H(9A)	0.99	C(21)-C(22)	1.39
N(2)-C(3)	1.498(13)	C(9)-H(9B)	0.99	C(21)-H(21)	0.95
N(2)-C(2)	1.500(13)	C(11)-C(12)	1.522(10)	C(22)-C(23)	1.39
N(3)-C(7)	1.445(12)	C(11)-H(11A)	0.99	C(22)-H(22)	0.95
N(3)-C(4)	1.503(12)	C(11)-H(11B)	0.99	C(23)-C(24)	1.39
N(3)-C(18)	1.532(13)	C(12)-C(13)	1.39	C(23)-H(23)	0.95
C(1)-C(2)	1.513(14)	C(12)-C(17)	1.39	C(24)-H(24)	0.95
C(1)-H(1A)	0.99	C(13)-C(14)	1.39		

Table 8.28: Bond Angles for [Ga(Bn_2DT3A)]

Bond Angle / °					
O(3)-Ga(1)-O(5)	99.4(3)	N(2)-C(2)-H(2B)	109.9	N(1)-C(11)-H(11B)	108.3
O(3)-Ga(1)-O(1)	87.1(3)	C(1)-C(2)-H(2B)	109.9	C(12)-C(11)-H(11B)	108.3
O(5)-Ga(1)-O(1)	172.0(3)	H(2A)-C(2)-H(2B)	108.3	H(11A)-C(11)-H(11B)	107.4
O(3)-Ga(1)-N(2)	160.9(3)	N(2)-C(3)-C(4)	109.3(7)	C(13)-C(12)-C(17)	120
O(5)-Ga(1)-N(2)	93.4(2)	N(2)-C(3)-H(3A)	109.8	C(13)-C(12)-C(11)	119.2(5)
O(1)-Ga(1)-N(2)	81.5(3)	C(4)-C(3)-H(3A)	109.8	C(17)-C(12)-C(11)	120.7(5)
O(3)-Ga(1)-N(1)	108.8(3)	N(2)-C(3)-H(3B)	109.8	C(14)-C(13)-C(12)	120
O(5)-Ga(1)-N(1)	81.2(3)	C(4)-C(3)-H(3B)	109.8	C(14)-C(13)-H(13)	120
O(1)-Ga(1)-N(1)	92.3(2)	H(3A)-C(3)-H(3B)	108.3	C(12)-C(13)-H(13)	120
N(2)-Ga(1)-N(1)	87.0(3)	N(3)-C(4)-C(3)	108.7(7)	C(13)-C(14)-C(15)	120
O(3)-Ga(1)-N(3)	80.9(3)	N(3)-C(4)-H(4A)	110	C(13)-C(14)-H(14)	120
O(5)-Ga(1)-N(3)	88.1(3)	C(3)-C(4)-H(4A)	110	C(15)-C(14)-H(14)	120
O(1)-Ga(1)-N(3)	97.6(3)	N(3)-C(4)-H(4B)	110	C(16)-C(15)-C(14)	120
N(2)-Ga(1)-N(3)	85.4(3)	C(3)-C(4)-H(4B)	110	C(16)-C(15)-H(15)	120
N(1)-Ga(1)-N(3)	166.5(2)	H(4A)-C(4)-H(4B)	108.3	C(14)-C(15)-H(15)	120
C(6)-O(1)-Ga(1)	119.9(5)	N(2)-C(5)-C(6)	112.6(7)	C(15)-C(16)-C(17)	120
C(8)-O(3)-Ga(1)	113.4(6)	N(2)-C(5)-H(5A)	109.1	C(15)-C(16)-H(16)	120
C(10)-O(5)-Ga(1)	119.5(6)	C(6)-C(5)-H(5A)	109.1	C(17)-C(16)-H(16)	120
C(9)-N(1)-C(1)	110.2(5)	N(2)-C(5)-H(5B)	109.1	C(16)-C(17)-C(12)	120
C(9)-N(1)-C(11)	110.7(6)	C(6)-C(5)-H(5B)	109.1	C(16)-C(17)-H(17)	120
C(1)-N(1)-C(11)	113.1(7)	H(5A)-C(5)-H(5B)	107.8	C(12)-C(17)-H(17)	120
C(9)-N(1)-Ga(1)	106.6(5)	O(2)-C(6)-O(1)	125.3(8)	N(3)-C(18)-C(19)	118.3(6)
C(1)-N(1)-Ga(1)	103.9(5)	O(2)-C(6)-C(5)	119.4(8)	N(3)-C(18)-H(18A)	107.7
C(11)-N(1)-Ga(1)	112.1(5)	O(1)-C(6)-C(5)	115.2(6)	C(19)-C(18)-H(18A)	107.7
C(5)-N(2)-C(3)	112.1(7)	N(3)-C(7)-C(8)	109.7(8)	N(3)-C(18)-H(18B)	107.7
C(5)-N(2)-C(2)	110.6(8)	N(3)-C(7)-H(7A)	109.7	C(19)-C(18)-H(18B)	107.7
C(3)-N(2)-C(2)	116.5(6)	C(8)-C(7)-H(7A)	109.7	H(18A)-C(18)-H(18B)	107.1
C(5)-N(2)-Ga(1)	110.4(5)	N(3)-C(7)-H(7B)	109.7	C(20)-C(19)-C(24)	120
C(3)-N(2)-Ga(1)	103.8(5)	C(8)-C(7)-H(7B)	109.7	C(20)-C(19)-C(18)	120.9(6)
C(2)-N(2)-Ga(1)	102.7(4)	H(7A)-C(7)-H(7B)	108.2	C(24)-C(19)-C(18)	118.9(6)
C(7)-N(3)-C(4)	118.0(7)	O(3)-C(8)-O(4)	123.6(10)	C(21)-C(20)-C(19)	120
C(7)-N(3)-C(18)	109.5(8)	O(3)-C(8)-C(7)	117.6(8)	C(21)-C(20)-H(20)	120
C(4)-N(3)-C(18)	110.8(7)	O(4)-C(8)-C(7)	118.7(10)	C(19)-C(20)-H(20)	120
C(7)-N(3)-Ga(1)	99.4(6)	N(1)-C(9)-C(10)	111.9(6)	C(22)-C(21)-C(20)	120
C(4)-N(3)-Ga(1)	105.9(6)	N(1)-C(9)-H(9A)	109.2	C(22)-C(21)-H(21)	120
C(18)-N(3)-Ga(1)	112.7(5)	C(10)-C(9)-H(9A)	109.2	C(20)-C(21)-H(21)	120
N(1)-C(1)-C(2)	111.8(7)	N(1)-C(9)-H(9B)	109.2	C(21)-C(22)-C(23)	120
N(1)-C(1)-H(1A)	109.2	C(10)-C(9)-H(9B)	109.2	C(21)-C(22)-H(22)	120
C(2)-C(1)-H(1A)	109.2	H(9A)-C(9)-H(9B)	107.9	C(23)-C(22)-H(22)	120
N(1)-C(1)-H(1B)	109.2	O(6)-C(10)-O(5)	124.9(9)	C(24)-C(23)-C(22)	120
C(2)-C(1)-H(1B)	109.2	O(6)-C(10)-C(9)	120.8(8)	C(24)-C(23)-H(23)	120
H(1A)-C(1)-H(1B)	107.9	O(5)-C(10)-C(9)	114.3(7)	C(22)-C(23)-H(23)	120
N(2)-C(2)-C(1)	109.0(6)	N(1)-C(11)-C(12)	115.9(6)	C(23)-C(24)-C(19)	120
N(2)-C(2)-H(2A)	109.9	N(1)-C(11)-H(11A)	108.3	C(23)-C(24)-H(24)	120
C(1)-C(2)-H(2A)	109.9	C(12)-C(11)-H(11A)	108.3	C(19)-C(24)-H(24)	120

Table 8.29: Anisotropic displacement parameters ($Å^2 x\ 10^3$) for [Ga(Bn_2DT3A)]. The anisotropic displacement factor exponent takes the form: $-2\pi^2[h^2a^{*2}U_{11} + ... + 2\ h\ k\ a^*\ b^*\ U_{12}]$

	U_{11}	U_{22}	U_{33}	U_{23}	U_{13}	U_{12}
Ga(1)	61(1)	68(1)	59(1)	20(1)	14(1)	40(1)
O(1)	67(3)	84(3)	75(3)	24(3)	5(3)	52(3)
O(2)	90(4)	94(4)	73(4)	-5(3)	-10(3)	65(4)
O(3)	73(3)	62(3)	68(3)	21(2)	11(2)	34(2)
O(4)	157(8)	94(5)	121(7)	37(5)	38(6)	82(6)
O(5)	60(2)	77(3)	67(3)	13(2)	6(2)	41(2)
O(6)	72(3)	103(5)	95(5)	10(4)	-2(3)	59(4)
N(1)	48(3)	61(3)	73(4)	18(3)	8(2)	29(2)
N(2)	53(3)	84(4)	70(4)	34(3)	19(3)	39(3)
N(3)	79(4)	99(5)	61(4)	18(3)	20(3)	60(4)
C(1)	54(3)	57(3)	89(6)	14(3)	12(3)	28(3)
C(2)	59(4)	75(4)	91(6)	33(4)	15(4)	39(4)
C(3)	59(4)	111(6)	65(5)	35(5)	19(3)	48(4)
C(4)	65(4)	113(6)	62(4)	12(4)	11(3)	55(4)
C(5)	54(4)	95(6)	82(6)	22(5)	14(3)	46(4)
C(6)	57(4)	89(5)	65(5)	1(4)	1(3)	47(4)
C(7)	100(6)	95(6)	72(5)	0(5)	-7(5)	66(6)
C(8)	90(5)	77(5)	84(6)	18(4)	6(5)	53(5)
C(9)	50(3)	68(4)	78(5)	13(3)	10(3)	35(3)
C(10)	59(4)	74(4)	69(5)	18(4)	11(3)	39(3)
C(11)	66(4)	68(4)	69(5)	14(3)	5(3)	38(3)
C(12)	64(4)	74(4)	75(5)	12(4)	-8(3)	40(3)
C(13)	77(5)	116(7)	81(6)	0(5)	1(4)	64(6)
C(14)	88(6)	123(8)	92(7)	3(6)	2(5)	77(6)
C(15)	135(10)	126(9)	90(7)	-19(6)	-32(7)	103(9)
C(16)	114(8)	81(5)	98(7)	-4(5)	-37(7)	56(6)
C(17)	82(5)	80(5)	87(6)	7(4)	-18(5)	47(4)
C(18)	72(4)	95(6)	79(6)	18(4)	21(4)	56(4)
C(19)	59(4)	95(6)	90(6)	9(5)	8(4)	46(4)
C(20)	64(5)	78(6)	150(12)	18(6)	23(6)	29(4)
C(21)	87(7)	93(7)	171(15)	5(9)	13(8)	54(6)
C(22)	77(7)	127(10)	177(17)	-43(11)	6(8)	54(7)
C(23)	90(7)	133(10)	96(8)	-20(7)	0(5)	61(7)
C(24)	79(5)	97(6)	81(6)	4(5)	6(4)	44(5)

Table 8.30: Hydrogen coordinates (x 10^4) and isotropic displacement parameters ($Å^2$ x 10^3) for [Ga(Bn_2DT3A)].

	x	y	z	U(eq)		x	y	z	U(eq)
H(1A)	1061	1727	3706	79	H(11A)	1789	3334	2111	79
H(1B)	593	2001	3598	79	H(11B)	1047	2873	2181	79
H(2A)	517	1594	5747	87	H(13)	2418	3117	667	101
H(2B)	1261	2027	5958	87	H(14)	2480	2560	-1162	108
H(3A)	1273	2654	7773	91	H(15)	1598	1614	-1808	120
H(3B)	532	2366	7984	91	H(16)	656	1225	-624	113
H(4A)	628	3353	7453	90	H(17)	594	1783	1205	96
H(4B)	1090	3442	8670	90	H(18A)	2525	4206	7015	91
H(5A)	-48	2482	6332	88	H(18B)	2169	3648	8057	91
H(5B)	-80	2006	5204	88	H(20)	2712	5287	7618	120
H(7A)	1704	4673	6996	98	H(21)	3022	6012	9366	136
H(7B)	1107	4208	6110	98	H(22)	2828	5660	11575	151
H(9A)	2435	3010	3153	75	H(23)	2324	4583	12036	125
H(9B)	2057	2278	3521	75	H(24)	2014	3858	10288	102

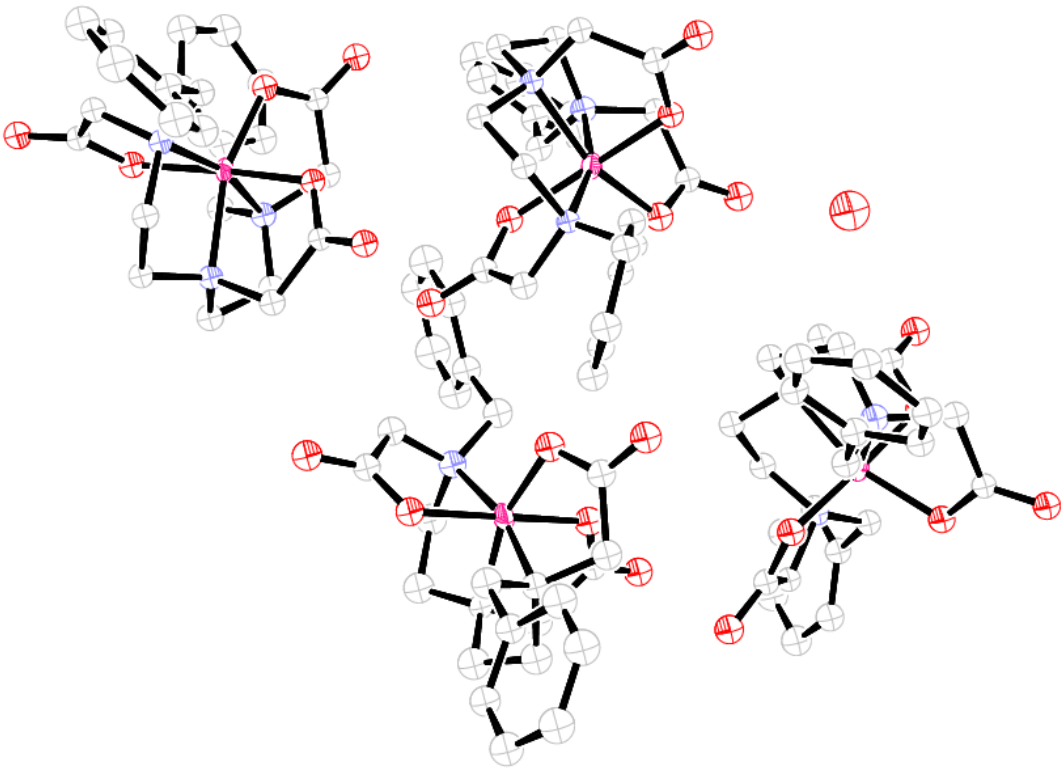

Figure 8.7: ORTEP representation of molecular structure of [Ga(Bn_2DT3A)] obtained by single crystal X-ray crystallography of crystal grown at pH 5.3 (drawn at 30% certainty).

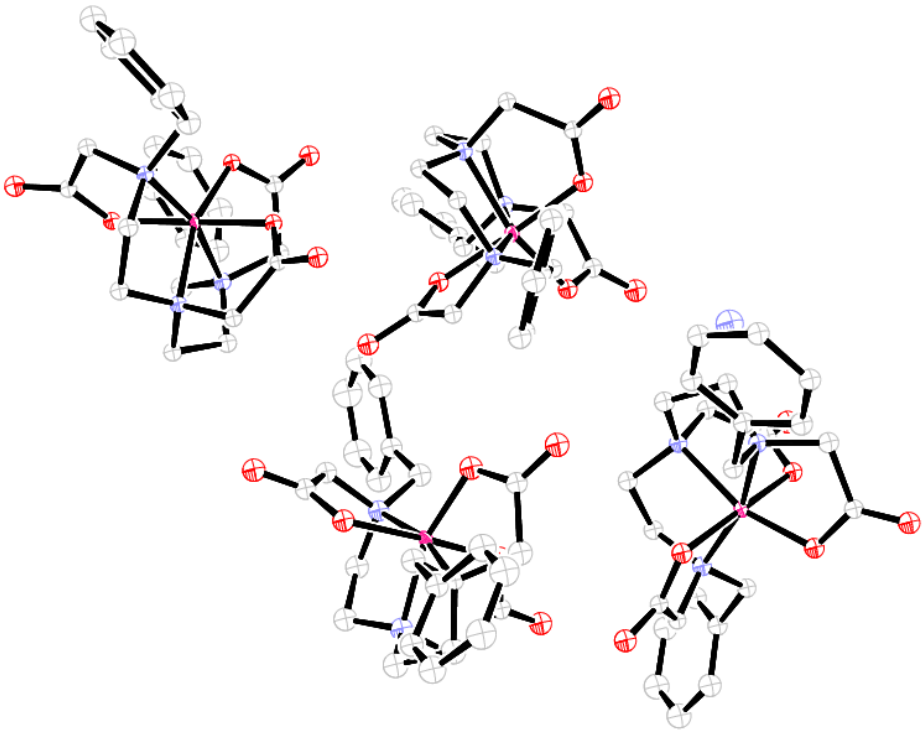

Figure 8.8: ORTEP representation of molecular structure of [Ga(Bn_2DT3A)] obtained by single crystal X-ray crystallography of crystal grown at pH 6.8(drawn at 30% certainty).

Chapter 9 Appendix 3 – *In vivo* investigation of [^{68}Ga][Ga(Bn_2DT3A)]

9.1. Experimental Methods

9.1.1 Preparation of [^{68}Ga][Ga(Bn_2DT3A)]

H_3Bn_2DT3A (500 µM) in 0.1 M phosphate buffer (1 mL, pH 7.8) was added to dried [^{68}Ga]$GaCl_3$ and the solution shook at room temperature for 15 minutes.

The solution was purified by semi-preparative HPLC and the isolated fraction (200 µL) diluted with water (2 mL) and trapped on an Oasis Hydrophilic-Lipophilic Balanced cartridge. The cartridge was washed with water (2 mL) and dried with argon. The activity was eluted with ethanol (500 µL) and dried at 99 °C under argon for 10 minutes. The dried activity was resuspended in PBS (200 µL) and passed through a sterile filter before use.

9.1.2 Preparation of [^{68}Ga][Ga(Citrate)]

To dried [^{68}Ga]$GaCl_3$ was added sodium citrate in water (1 mM, 1 mL). The solution was shook for 15 minutes at room temperature. The pH was adjusted to 7 with sodium hydroxide and the solution passed through a sterile filter before use.

9.1.3 Measurement of octanol-PBS partition coefficient

[^{68}Ga][Ga(Bn_2DT3A)] in PBS (10 µL) was added to PBS (90 µL) and octanol (100 µL). The solution was shook for 15 minutes at room temperature before being separated by centrifugation at 15 krpm for 10 minutes. The layers were separated and their activity measured with a gamma counter.

The partition coefficient determined was $\log D_{octanol/PBS}$(pH 7.4) = -2.91 +/- 0.07

9.1.4 In vivo experiments

A male Sprague Dawley rat (500 g) was induced using isoflurane (5%) and anesthatised state maintained with isoflurane (3%) in oxygen (1 L min^{-1}). The solution of [^{68}Ga][Ga(Bn_2DT3A)] (2-4 MBq) in PBS was administered *via* tail vein injection.

Whole body PET data acquisition (2 or 3 bed positions, 23 or 66 minute dynamic scan) was synchronised with radiotracer *i.v.* injection (2-4 MBq, 200 µL), a CT scan (40 kV, 140 µA, 360 projections, 8 shots) was acquired following each PET scan to show anatomical co-registration; temperature and respiration were monitored throughout the scan. PET-CT imaging data were acquired on a Sedecal SuperArgus 2R PET scanner. PET data were reconstructed using 3D Ordered Subset Expectation Maximisation (OSEM3D) algorithm with 16 subsets and 2 iterations and corrections for randoms, scatter and attenuation. Images were normalised using the

injected dose and animal weight to give Standardised Uptake Values (SUV). Data was analysed using AMIDE software.

Following recovery the urine was collected; a portion of urine (300 µL) was added to a solution of acetonitrile + 0.1% TFA (600 µL). The suspension was sonicated and pelleted at 14 krpm at 5 ^{o}C for 5 minutes. The supernatant was analysed by HPLC.

HPLC Gradient, [time / minutes, %A, %B]: Solvent A: Water + 0.1% TFA, Solvent B: Methanol + 0.1% TFA. [0, 95, 5], [3, 95, 5], [18, 5, 95], [25, 5, 95], [26, 95, 5], [30, 95, 5]

9.2. [^{68}Ga][Ga(Citrate)] – 3 bed positions

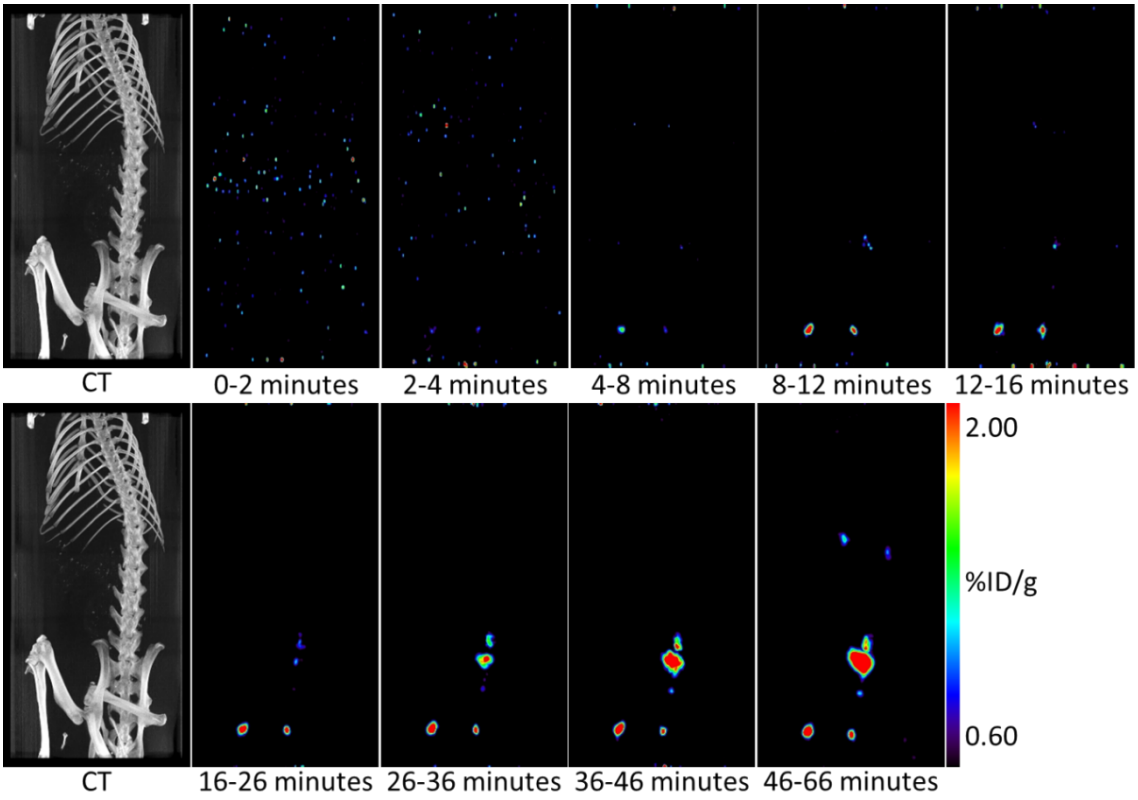

Figure 9.1: Coronal PET and CT scans of male rat injected with [^{68}Ga][Ga(Citrate)].

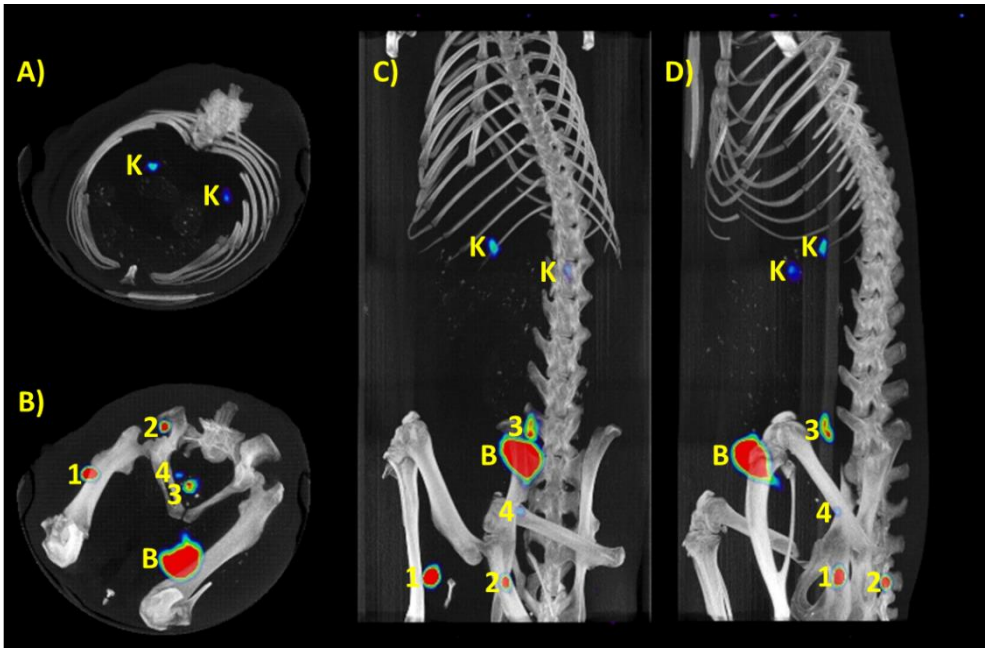

Figure 9.2: PET-CT fused scans of a rat 46-66 minutes after injection with [^{68}Ga][Ga(Citrate)]. A) Transverse projection of upper abdomen. B) Transverse projection of lower abdomen. C) Coronal projection. D) Sagittal projection. Areas of increased uptake are annotated. K = kidneys, B = bladder.

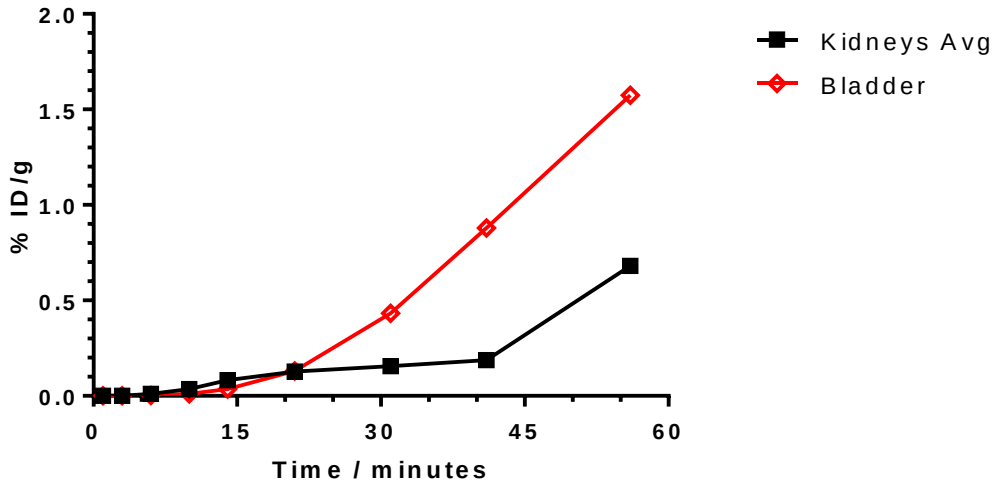

Figure 9.3: Activity time curves for selected organs.

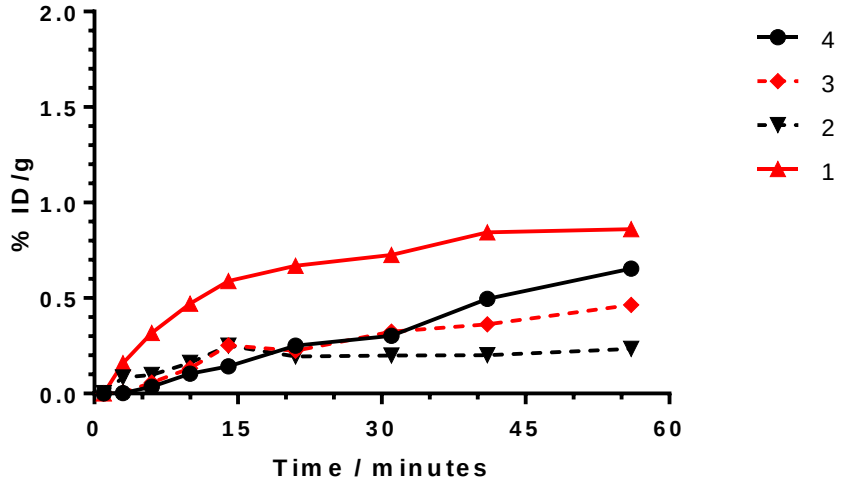

Figure 9.4: Activity-time curves for additional regions of increased uptake.

9.3. [^{68}Ga][Ga(Citrate)] – 3 bed positions

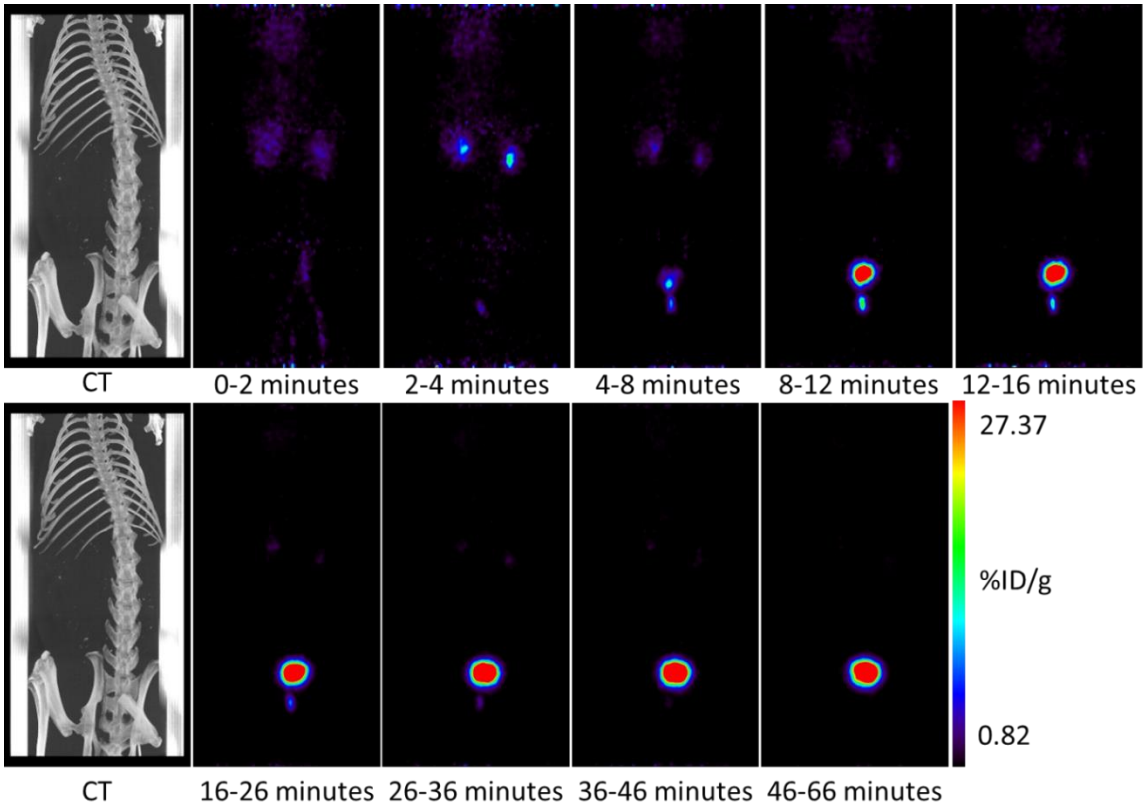

Figure 9.5: Coronal PET and CT scans of male rat injected with [^{68}Ga][Ga(Citrate)].

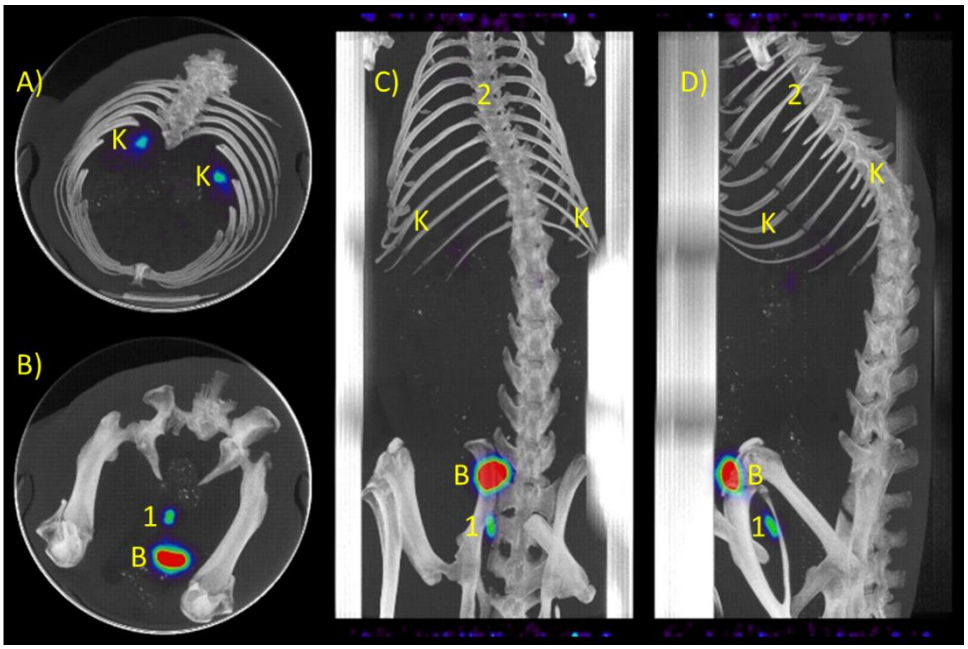

Figure 9.6: Fused PET-CT scans of a rat after injection with [^{68}Ga][Ga(Citrate)]. A) Transverse projection of upper abdomen 2-4 minutes after injection. B) Transverse projection of lower abdomen 12-16 minutes post injection. C) Coronal projection 12-16 minutes post injection. D) Sagittal projection 12-16 minutes post injection. Areas of increased uptake are annotated. K = kidneys, B = bladder.

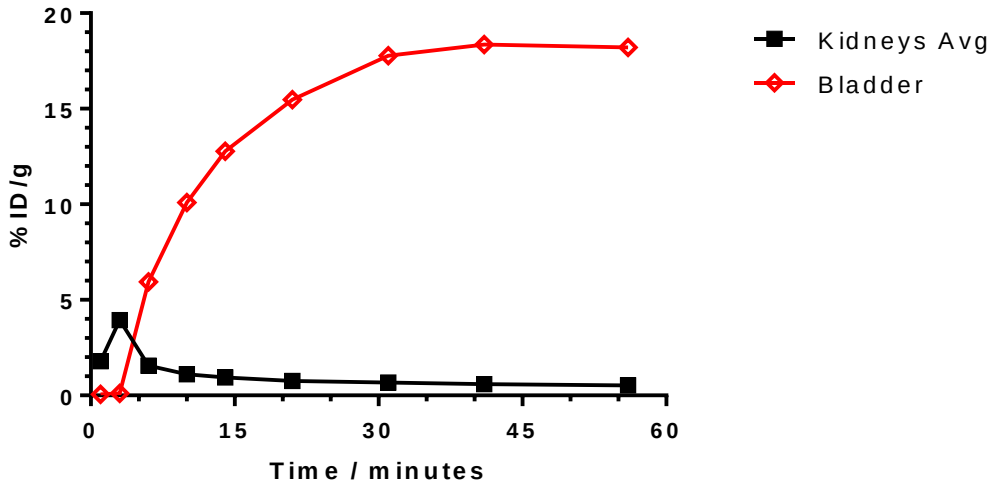

Figure 9.7: Activity time curves for selected organs.

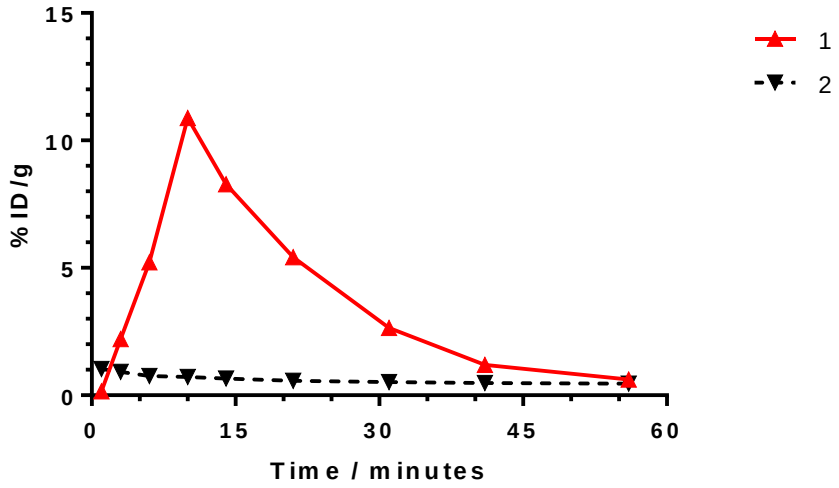

Figure 9.8: Activity-time curves for additional regions of increased uptake.

9.4. [^{68}Ga][Ga(Bn$_2$DT3A)] – 2 bed positions

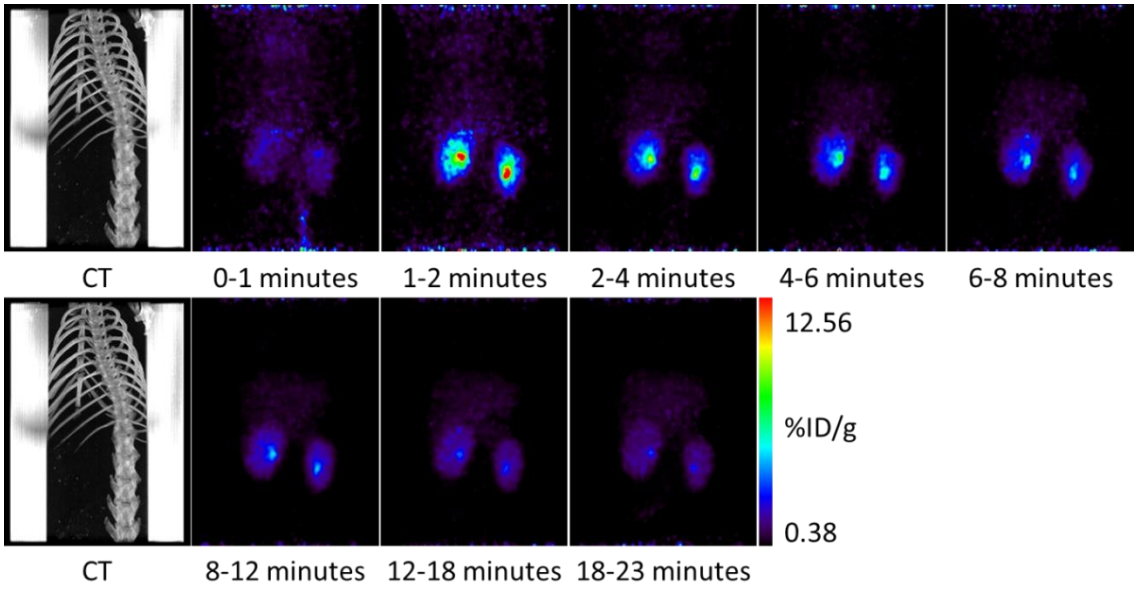

Figure 9.9: Coronal PET and CT scans of male rat injected with [^{68}Ga][Ga(Bn$_2$DT3A)].

Figure 9.10: Fusion PET-CT scans of rat injected with [^{68}Ga][Ga(Bn$_2$DT3A)] 18-23 minutes post injection.

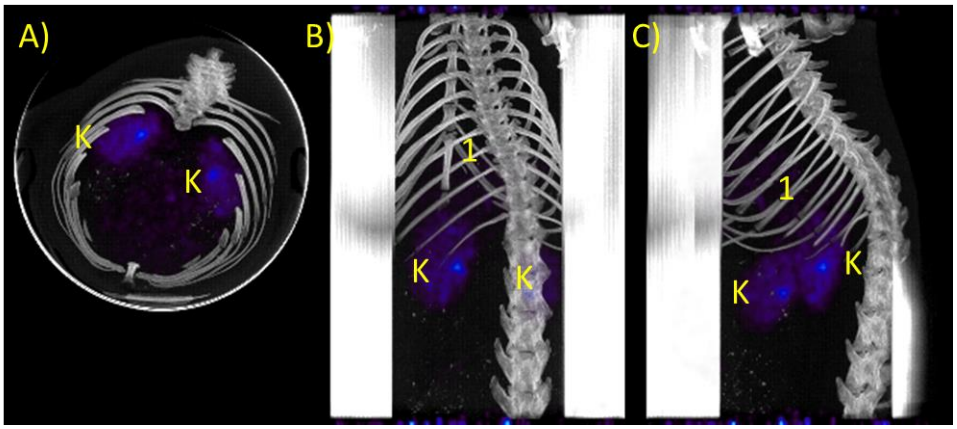

A) Transverse projection. B) Coronal projection. C) Sagittal projection. Areas of increased uptake are annotated. K = kidneys.

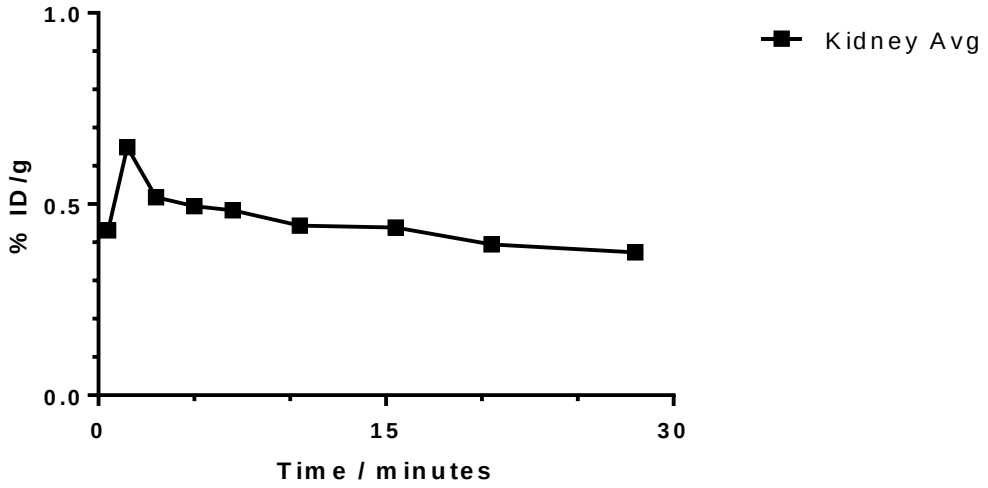

Figure 9.11: Activity time curves for selected organs.

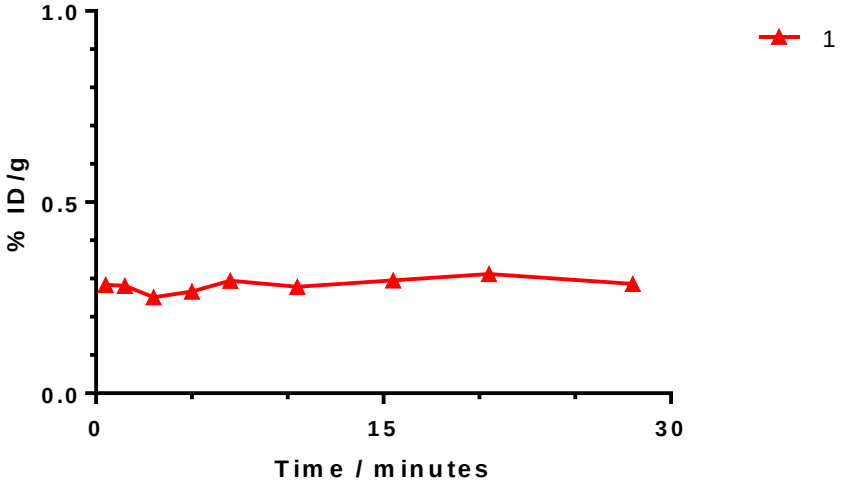

Figure 9.12: Activity-time curves for additional regions of increased uptake.

9.5. [^{68}Ga][Ga(Bn$_2$DT3A)] – 3 bed positions

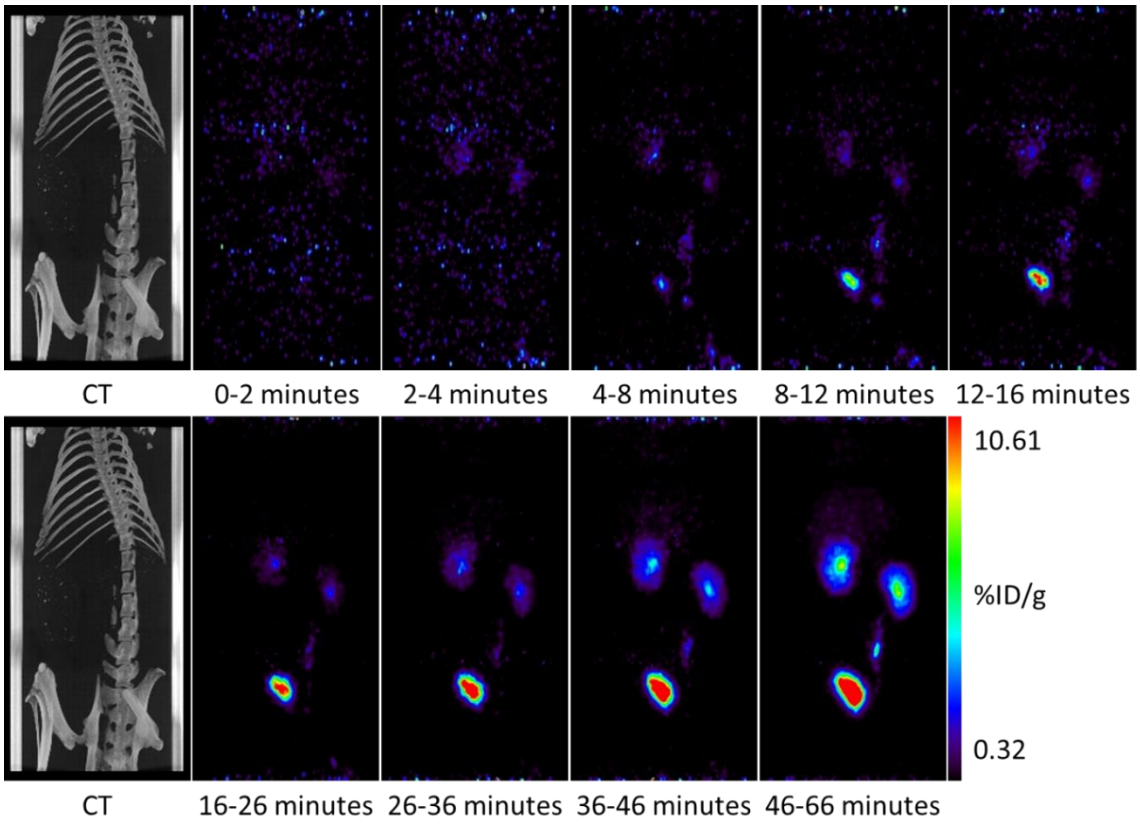

Figure 9.13: Coronal PET and CT scans of male rat injected with [^{68}Ga][Ga(Bn$_2$DT3A)].

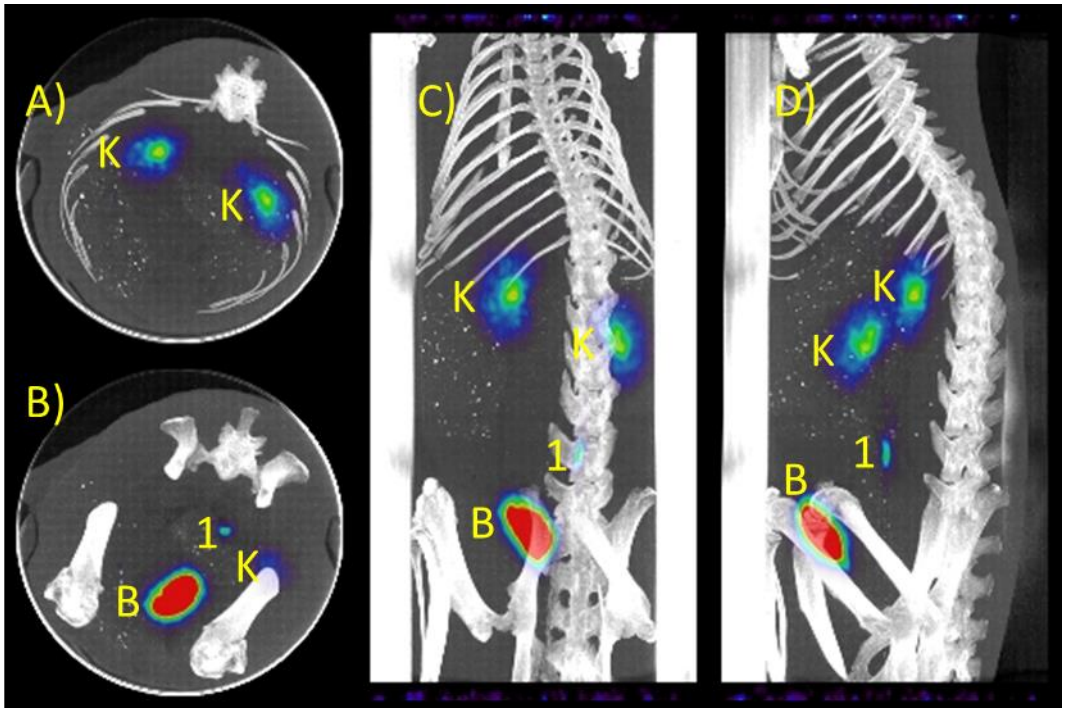

Figure 9.14: Fused PET-CT scans of a rat 46-66 minutes post injection with [^{68}Ga][Ga(Bn$_2$DT3A)]. A) Transverse projection of upper abdomen. B) Transverse projection of lower abdomen. C) Coronal projection. D) Sagittal projection. Areas of increased uptake are annotated. K = kidneys, B = bladder.

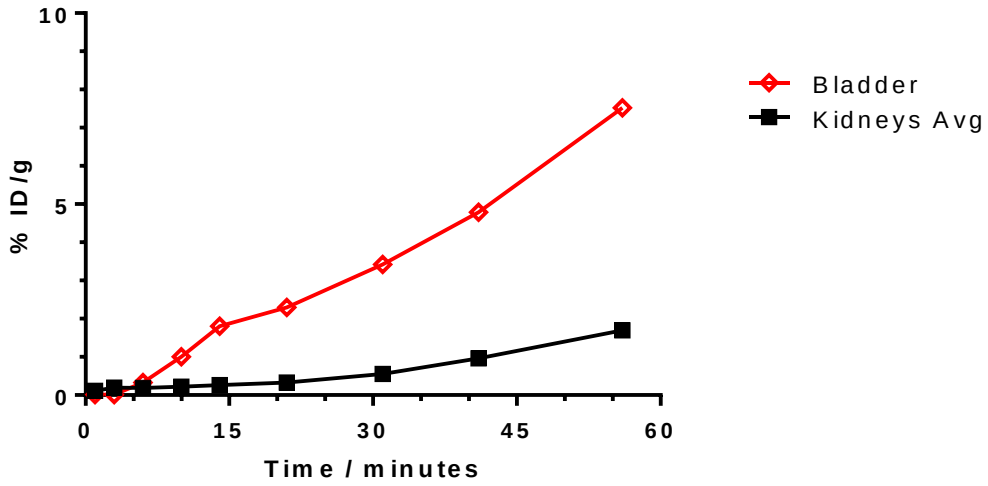

Figure 9.15: Activity time curves for selected organs.

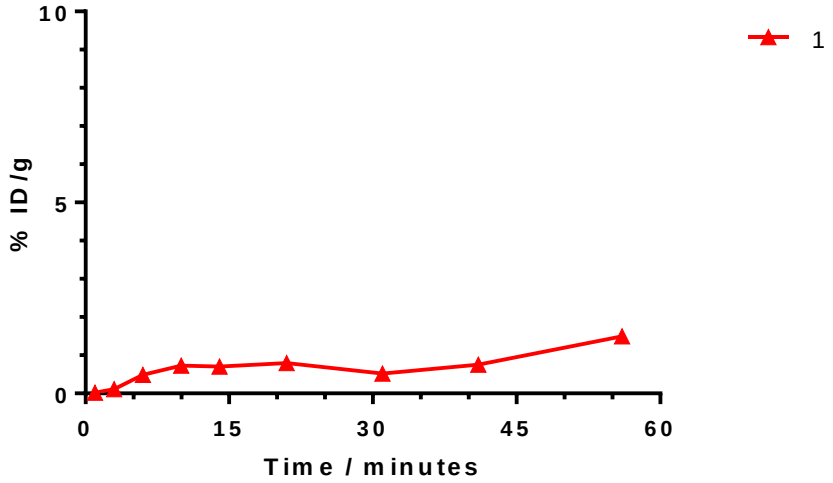

Figure 9.16: Activity-time curves for additional regions of increased uptake.

9.6. [^{68}Ga][Ga(Bn$_2$DT3A)] – 3 bed positions

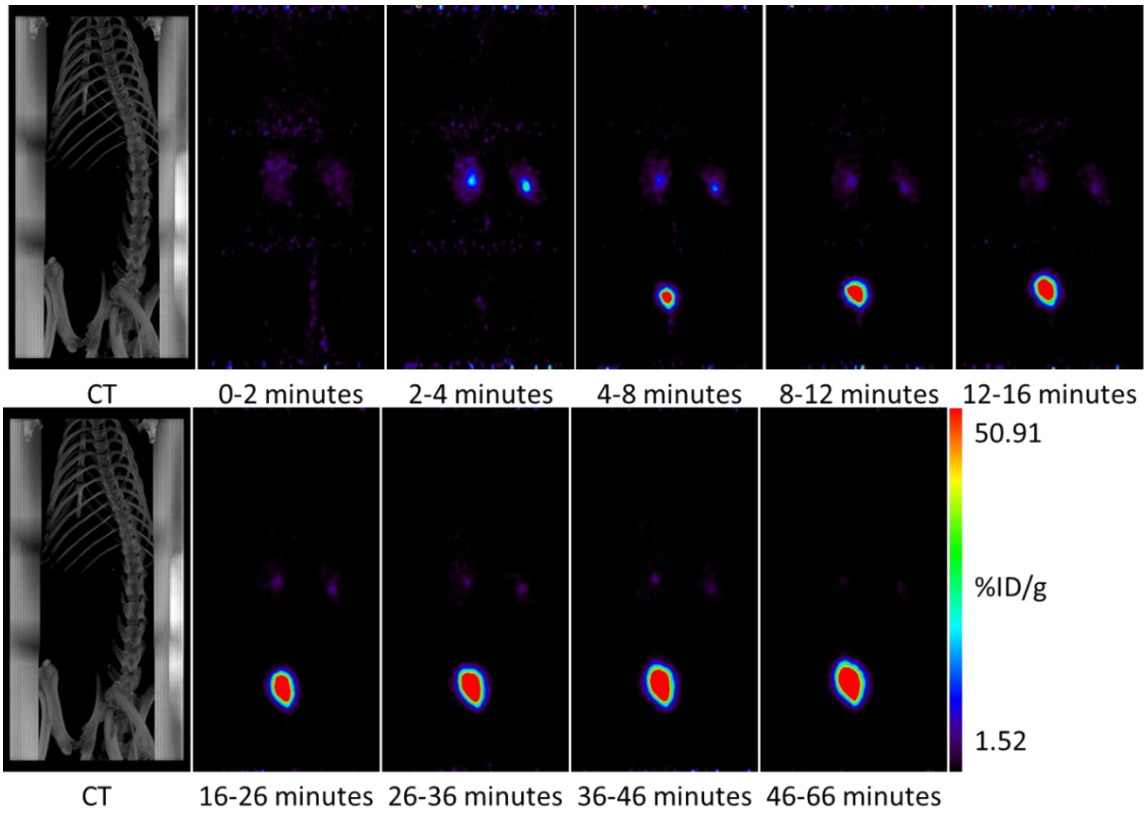

Figure 9.17: Coronal PET and CT scans of male rat injected with [^{68}Ga][Ga(Bn$_2$DT3A)].

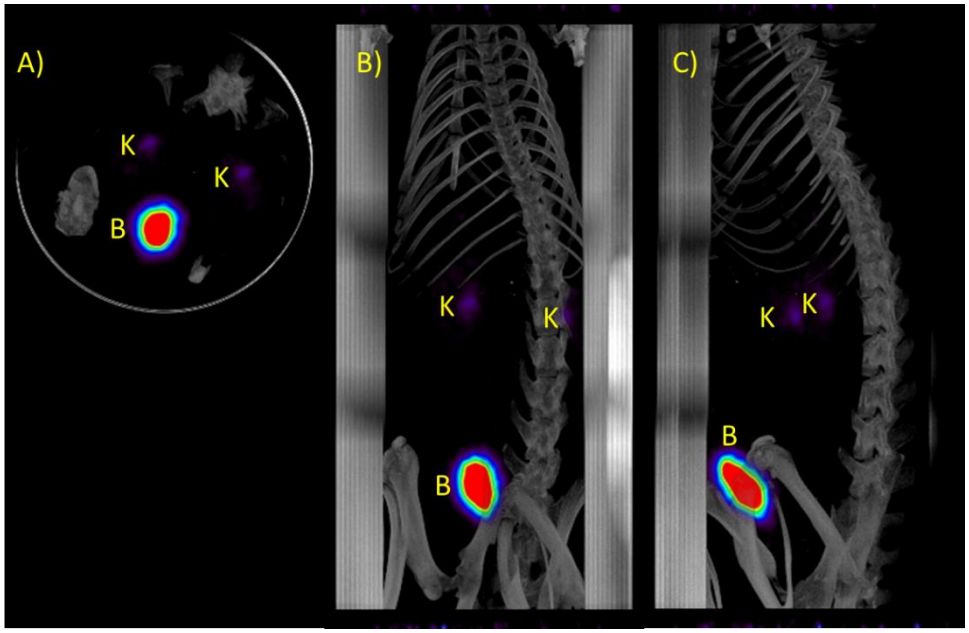

Figure 9.18: Fused PET-CT scans of a rat 36-46 minutes post injection with [^{68}Ga][Ga(Bn$_2$DT3A)]. A) Transverse projection of upper abdomen. B) Transverse projection of lower abdomen. C) Coronal projection. D) Sagittal projection. Areas of increased uptake are annotated. K = kidneys, B = bladder.

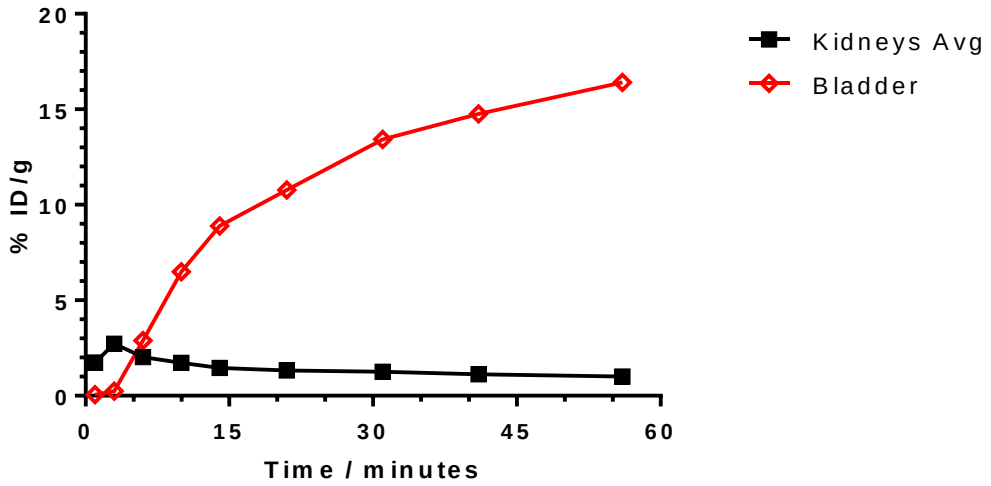

Figure 9.19: Activity time curves for selected organs.

9.7. Metabolite analysis

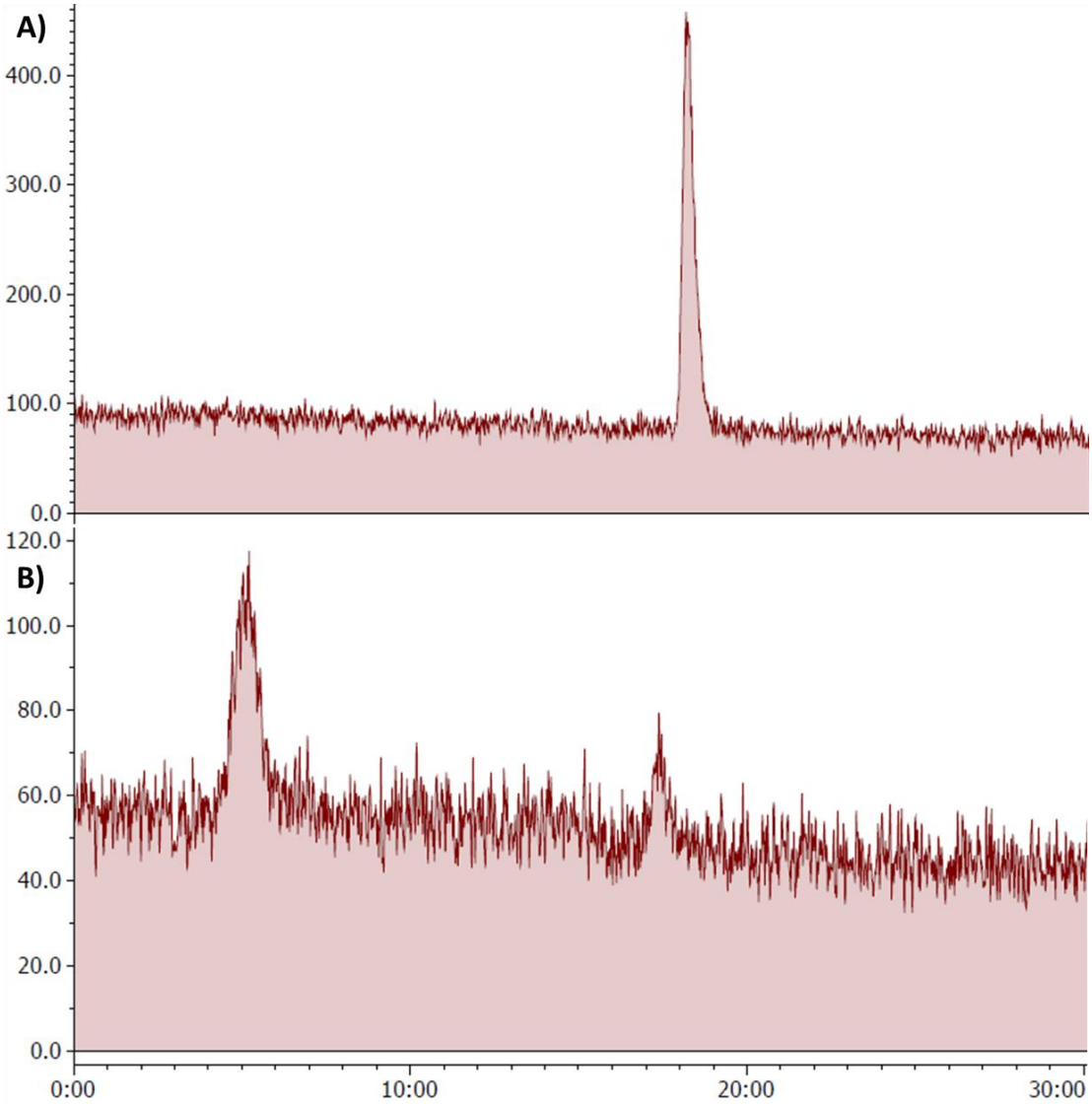

Figure 9.20: Radio-HPLC of A) [^{68}Ga][Ga(Bn_2DT3A)] formulation prior to administration to rat B) urine following imaging.

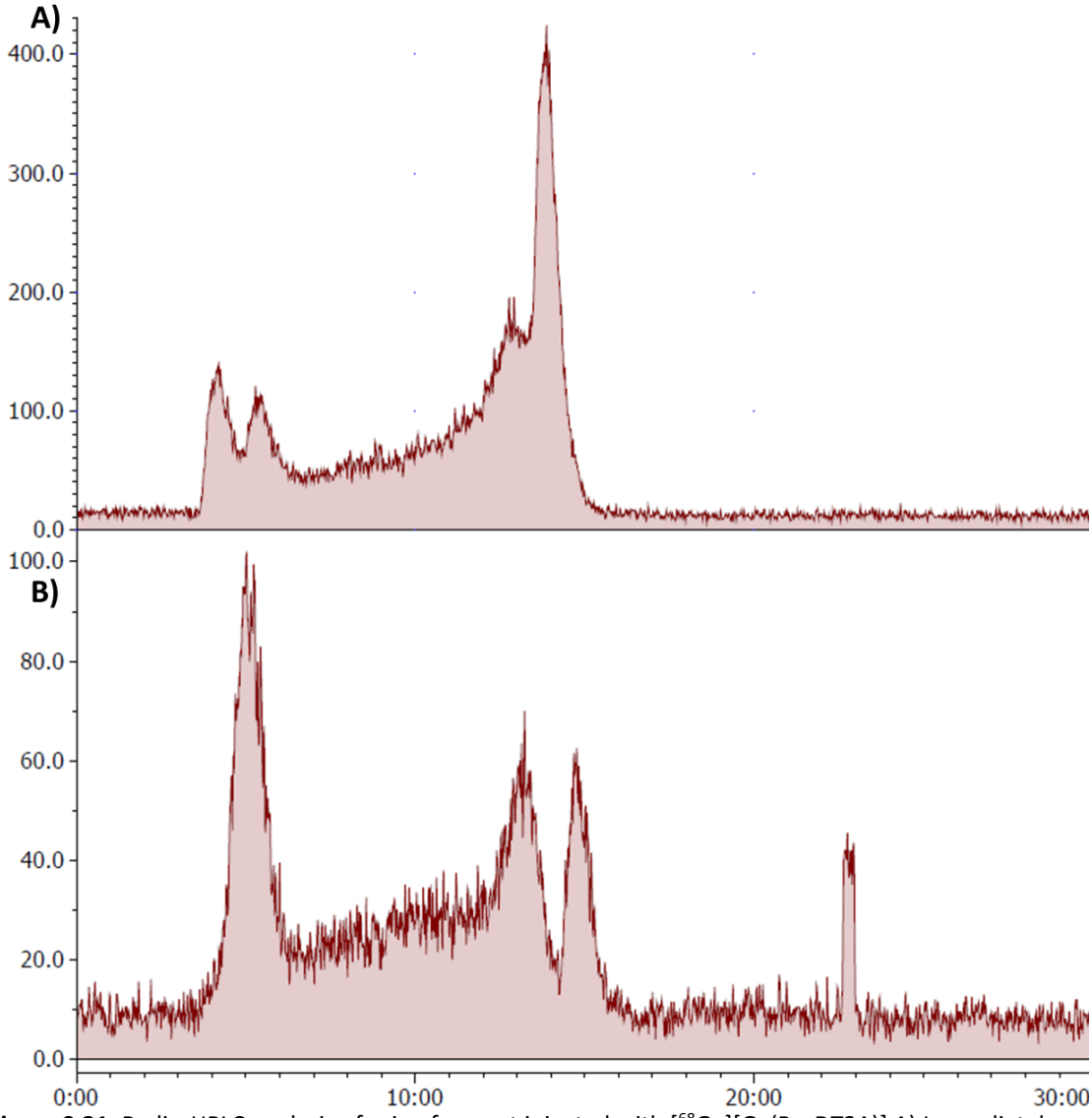

Figure 9.21: Radio-HPLC analysis of urine from rat injected with [^{68}Ga][Ga(Bn$_2$DT3A)] A) Immediately following pelleting, B) 1 hour later.

Chapter 10 Appendix 4 – Investigation of ^{68}Ga serum species

^{68}Ga was concentrated as previously described (Experimental methods 6.3.1). To dried ^{68}Ga (approximately 9 MBq) was added 100 µL of the desired analyte. This solution was incubated for 30 minutes at 37 ^{o}C before being analysed by TLC in three eluents on alumina backed silica gel plates (Experimental methods 6.3.1).

Analytes:

- 98% Acetone, 2% 0.1 N HCl
- Sodium carbonate (100 mM) in water
- 1 mM Sodium citrate (1 mM) in water
- Foetal bovine serum
- A*po*-transferrin (1 mg ml^{-1}) and sodium carbonate (100 mM) in water
- Water (pH 6)

Eluents:

- 0.1 M Sodium citrate in water (pH 5)
- Water (pH 5)
- 0.1 M Sodium acetate (pH 5)

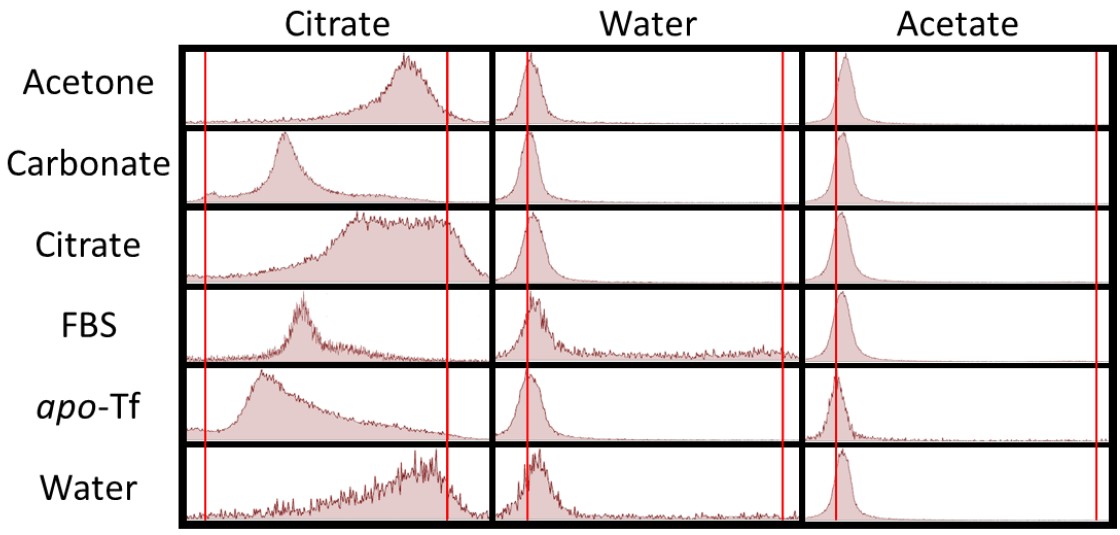

Figure 10.1: radio-TLC results for different combinations of ^{68}Ga, analyte and eluate. Baseline and solvent front indicated by red lines.